Chunfei Li

Nonlinear Optics

Principles and Applications

上海交通大學出版社
SHANGHAI JIAO TONG UNIVERSITY PRESS

Springer

Nonlinear Optics

Chunfei Li

Nonlinear Optics

Principles and Applications

上海交通大學出版社
SHANGHAI JIAO TONG UNIVERSITY PRESS

Springer

Chunfei Li
Harbin Institute of Technology
Harbin
China

ISBN 978-981-10-1487-1 ISBN 978-981-10-1488-8 (eBook)
DOI 10.1007/978-981-10-1488-8

Jointly published with Shanghai Jiao Tong University Press, Shanghai, China

Library of Congress Control Number: 2016947471

© Shanghai Jiao Tong University Press, Shanghai and Springer Nature Singapore Pte Ltd. 2017
This work is subject to copyright. All rights are reserved by the Publishers, whether the whole or part of the material is concerned, specifically the rights of translation, reprinting, reuse of illustrations, recitation, broadcasting, reproduction on microfilms or in any other physical way, and transmission or information storage and retrieval, electronic adaptation, computer software, or by similar or dissimilar methodology now known or hereafter developed.
The use of general descriptive names, registered names, trademarks, service marks, etc. in this publication does not imply, even in the absence of a specific statement, that such names are exempt from the relevant protective laws and regulations and therefore free for general use.
The publishers, the authors and the editors are safe to assume that the advice and information in this book are believed to be true and accurate at the date of publication. Neither the publishers nor the authors or the editors give a warranty, express or implied, with respect to the material contained herein or for any errors or omissions that may have been made.

Printed on acid-free paper

This Springer imprint is published by Springer Nature
The registered company is Springer Science+Business Media Singapore Pte Ltd.

Preface

Nonlinear Optics is one of subdisciplines of Modern Optics, it has an important academic status in the Modern Optics as same as the Laser Physics.

Laser Physics studies on the principle of laser devices and properties of laser, the main research contents include the stimulated radiation theory, optical resonant cavity theory, laser propagation theory, laser coherence theory, laser frequency spectrum, laser spatial mode, and laser power property.

Nonlinear Optics studies on various kinds of nonlinear effects in the interaction between laser and matter. The research contents include two aspects: one is studying in the laser how to change the macroscopic parameters of matter (susceptibility, dielectric coefficient, refractive index, absorption coefficient, etc.) and the microscopic structure of matter, thereby to realize "controlling matter by laser"; other one is studying in the pump laser induced matter change how to effect the parameters of the signal light propagating in the matter (frequency, power, wave vector, phase, pulse width, frequency spectrum, group velocity, propagation direction, etc.), thereby to realize "controlling light with light."

In short, Laser Physics studies the laser generation method; and Nonlinear Optics studies the laser controlling method, the two courses are basics of laser application. Therefore, the optics specialized graduate students must study Nonlinear Optics, besides study Laser Physics.

Nonlinear optics was established soon after the invention of laser in 1960. It has half a century of development history; its research field has been continuously developed in depth and breadth. Now the nonlinear optics has gained extensive applications. For example, it has been widely used in laser technology in order to change the frequency of the laser, compress the pulse width of laser, and achieve the tunable power and frequency of laser; the nonlinear optics has been used to make various optoelectronic devices, such as laser, optical amplifier, optical modulator, optical storage, optical display, and optical switches, which are widely used in the optoelectronic technology and photonic technology; the nonlinear optics has made important contribution to the development of optical fiber communication, space optical communication, and nonlinear optical communications (optical

soliton communication, optical chaotic communication, and optical quantum communication, etc.); the nonlinear optics has been used to study the optical logic, optical router, optical switching, optical interconnection, optical wavelength conversion, wavelength division multiplexing, and time division multiplexing technology and to promote the digital optical information processing, the all-optical computer, and the all-optical network technology; in addition, the nonlinear optics has been used to make the nonlinear optical fiber sensors to promote the development of the optical sensing technology; using the phase conjugation principle for the compensation of the waveform distortion of light; using the nonlinear optical limiting technology to against the blinding laser weapons; using the nonlinear optical principle to develop the spectral analysis technology with high spatial resolution and high temporal resolution, which has been applied to the analysis of material composition and hyperfine energy level structure of atom and molecule; using the multiphoton absorption effect for high-precision laser processing of nanoscale materials and devices; and the nonlinear optics is a powerful tool for study of new materials, such as surface, interface and low dimension materials, nano materials, and chiral materials; it is a necessary tool for measuring the nonlinear optical parameters of materials. Therefore, to master the basic knowledge of the nonlinear optics is necessary for scientists and engineers working in the field of the optoelectronic technology, the photonic technology, and the optical information technology.

Up to now, the published books on nonlinear optics have many versions in the world. These books have made important contributions to the related research and teaching works. But due to historical reasons, most of the existing books on nonlinear optics are old in the content, too deep in the theory, too many mathematical formulas, less actual application, or the unit and symbol are confusing, the readability is not good, and they are not suitable to directly use as short-term teaching materials.

This book attempts using "light wave" and "photon" the two kinds of physical images, clearly, deeply, and systematically to expound the basic principles of nonlinear optics. On the one hand, using the first order nonlinear wave equations in frequency domain and in "slowly variation amplitude" approximation and the classical polarization model in interaction between light and electric dipoles; on the other hand, using the rate equation theory based on photon excited energy-level transition in molecular system, as well as the photonic energy conservation and momentum conservation principle, to explain various nonlinear optical effects. The book uses the practical unit system, achieving the unity of symbol and unit. In the book, the author gives the strict mathematical derivation to basic theory, in the same time, pays attention to the experimental verification and the practical application. The book tries to reflect the latest progress in the research of nonlinear optics.

In order to make this book more refined, in the treatment of the second-order nonlinear optical effects, the author uses approximate method to transfer the problem of anisotropic medium into the problem of isotropic medium, avoiding the tedious description of crystal optics and complex tensor operation. Then all of the second-order nonlinear optical effects can be condensed into one chapter,

in order to have more space to focus on the third-order nonlinear optical effects. In this way, the teachers may finish the course teaching in 60 class hours, and the readers mastered certain optics and mathematics knowledge may study the book himself.

The author has been engaged in the research of nonlinear optics for more than 30 years, published about 300 academic papers and 5 books in the field of nonlinear optics. This book contains the author's achievements in research of nonlinear optics, for example, the optical bistability and optical instability in Chap. 8; the excited-state nonlinear optics and optical limiting in Chap. 7; the all-optical switches in Chap. 10; the spatial self-phase modulation in Chap. 5; the spatial optical soliton in Chap. 9; and the measurements of nonlinear optical parameters (such as Z-scan) in some chapters. So this book is also a review of author's research works.

The author engaged in the teaching graduate-student course "nonlinear optics" for many years. The writing of this book is based on his teaching material for course. The author hopes that the book can be a popular textbook for graduate students studying on the optics professional, but also can be used as a reference book for scientific and technical personnel working in the field of optoelectronic technology, photonic technology, optical information technology, and nonlinear optical material technology.

I sincerely thank my original Ph.D. graduate students and Master graduate students who did many contributions to this book. Heartfelt thank to the professors and colleagues who gave me support and encouragement in my research and teaching works. I am also thankful to the teachers and readers who use this book and would like to offer the valuable comments to me for modifying the book in the near future.

Guangzhou Chunfei Li
December 2015

Contents

1 Introduction 1
1.1 Importance of Nonlinear Optics 1
1.1.1 Status of Nonlinear Optics in Modern Physics 1
1.1.2 Status of Nonlinear Optics in Modern Optics 2
1.1.3 Nonlinear Optics Is a Basis of Photonic Technology 3
1.2 Physical Meaning of Nonlinear Optics 5
1.2.1 Phenomenon Related with High-Order Polarization. . . . 5
1.2.2 Nonlinear Response of Medium to the Optical Field 6
1.2.3 Parameters of Medium Are Function of Optical Field 7
1.3 Research Content of Nonlinear Optics 8
1.3.1 Typical Nonlinear Optical Effects 8
1.3.2 Two Kinds of Nonlinear Optical Effects 13
1.3.3 Nonlinear Optical Materials. 14
1.4 Development History of Nonlinear Optics 15
1.4.1 Brief History of Nonlinear Optics 15
1.4.2 Development Tendency of Nonlinear Optics 16
1.5 Applications of Nonlinear Optics 17
1.5.1 Application in Laser Technology. 18
1.5.2 Application in Information Technology. 18
1.5.3 Application in Material Technology 19
References. 21

2 Polarization Theory of Nonlinear Medium 23
2.1 Wave Equations of Nonlinear Medium. 23
2.1.1 Maxwell's Equations for Nonlinear Medium. 23
2.1.2 Time-Domain Wave Equation in Anisotropic Nonlinear Medium. 25

2.1.3 Time-Domain Wave Equation in Isotropic Nonlinear Medium . . . 26
2.1.4 Frequency-Domain Wave Equation in Anisotropic Nonlinear Medium . . . 28
2.1.5 Frequency-Domain Wave Equation in Isotopic Nonlinear Medium . . . 28
2.2 Polarization and Susceptibility of Nonlinear Medium . . . 30
2.2.1 Frequency-Domain Expressions of Polarization and Susceptibility . . . 30
2.2.2 Degeneration Factor of Polarization . . . 34
2.2.3 Symmetry of Susceptibility Tensor . . . 37
2.3 Real Part and Imaginary Part of Susceptibility . . . 40
2.3.1 Relation Between Real Part and Imaginary Part of Susceptibility (K–K Relation) . . . 40
2.3.2 Physical Significance of Real Part and Imaginary Part of Susceptibility . . . 41
2.3.3 Relation Between Nonlinear Refractive Index and Nonlinear Absorption Coefficient . . . 45
Appendix A: Derivation of K–K Relation . . . 46
Appendix B: Two Systems of Units . . . 48
I. Fundamental Formula . . . 49
II. Conversion of Two Unit Systems . . . 49
References . . . 49

3 Optical Three-Wave Coupling Processes . . . 51
3.1 Three-Wave Coupled Equations . . . 51
3.1.1 Review of Second-Order Nonlinear Optics Effects in Isotopic Medium . . . 51
3.1.2 Approximate Description of Second-Order Nonlinear Optics Effect in Anisotropic Medium . . . 53
3.1.3 Three-Wave Coupled Equations in Anisotropic Medium . . . 55
3.2 Optical Second-Harmonic Generation . . . 57
3.2.1 Small Signal Approximation . . . 58
3.2.2 High Fundamental Wave Consumption . . . 61
3.2.3 Phase Matching Technology . . . 64
3.2.4 Experimental Facilities for Second Harmonic Generation . . . 69
3.3 Optical Sum Frequency, Difference Frequency and Parameter Amplification . . . 71
3.3.1 Optical Sum Frequency and Frequency Up-Conversion . . . 71
3.3.2 Optical Difference Frequency and Frequency Down-Conversion . . . 75

3.3.3 Optical Parametric Amplification 78
3.3.4 Comparison of Four Kinds of Three-Wave Mixing Processes and Experimental Facilities 79
3.4 Optical Parametric Oscillator 81
3.4.1 Threshold Value Equations of Optical Parametric Oscillation 81
3.4.2 Double Resonant Parametric Oscillator 83
3.4.3 Singly Resonant Parametric Oscillator 85
References 88

4 Optical Four-Wave Coupling Process 89
4.1 Introduction to Third-Order Nonlinear Optical Effects 89
4.2 Optical Third Harmonic and Optical Four-Wave Mixing 91
4.2.1 Optical Third Harmonic 91
4.2.2 Optical Four-Wave Mixing 94
4.2.3 Degenerated Four-Wave Mixing 95
4.3 Optical Phase Conjugation 97
4.3.1 Definition and Characteristic of Optical Phase Conjugation 97
4.3.2 Optical Phase Conjugation in Four-Wave Mixing Process 99
4.3.3 Application of Optical Phase Conjugation 105
References 107

5 Optical Kerr Effect and Self-focusing 109
5.1 Optical Kerr Effect 109
5.1.1 Self-phase Modulation Optical Kerr Effect 111
5.1.2 Cross-Phase Modulation Optical Kerr Effect 114
5.1.3 Optical-Kerr-Effect Induced Birefringence 116
5.2 Self-focusing of Light Beam 119
5.2.1 Steady State Self-focusing 119
5.2.2 Dynamic State Self-focusing 127
5.2.3 Self-phase Modulation Based on Self-focusing 132
5.3 Z-scan Measurement of Nonlinear Optical Parameter 135
5.3.1 Experimental Method of Z-scan Measurement 135
5.3.2 Theoretical Calculation of Z-scan Measurement 138
5.3.3 Other Z-scan Technologies 143
References 146

6 Nonlinear Stimulated Scattering 149
6.1 Introduction to Light Scattering 149
6.1.1 Classification of Light Scattering 149
6.1.2 Stimulated Radiation Light Scattering Characteristics 151

6.2 Stimulated Raman Scattering 152
6.2.1 Physical Picture of Stimulated Raman Scattering 152
6.2.2 Classical Theory of Stimulated Raman Scattering 157
6.2.3 Experiments of Stimulated Raman Scattering 163
6.3 Stimulated Brillouin Scattering 164
6.3.1 Physical Picture of Stimulated Brillouin Scattering 164
6.3.2 Classical Theory of Stimulated Brillouin Scattering . . . 167
6.3.3 Experiments of Stimulated Brillouin Scattering 172
References 175

7 Nonlinear Absorption and Refraction of Light 177
7.1 Single-Photon Absorption and Two-Photon Absorption 177
7.1.1 Light-Intensity Transmission Equations 177
7.1.2 Single-Photon Nonlinear Absorption and Refraction 180
7.1.3 General Theory of Two-Photon Absorption 183
7.1.4 Two-Photon Absorption and Refraction in Semiconductor 186
7.2 Saturable Absorption and Reverse Saturable Absorption 193
7.2.1 Molecular-Energy-Level Model of Saturable Absorption 193
7.2.2 Relation Between Saturable Absorption and Three-Order Nonlinear Absorption 199
7.2.3 Molecular-Energy-Level Mode of Reverse Saturable Absorption 200
7.2.4 Application of Reverse Saturable Absorption in All-Optical Limiting 206
7.3 Saturable Refraction and Reverse Saturable Refraction 207
7.3.1 Description of Saturable Refraction and Reverse Saturable Refraction 207
7.3.2 Physical Significance of Sign Symbol of Nonlinear Refraction Coefficient 211
References 214

8 Optical Bistability and Its Instability 215
8.1 Introduction to Optical Bistability 215
8.1.1 Basic Conception of Optical Bistability 215
8.1.2 Classification of Optical Bistable Device 217
8.2 Optical Bistable Device 219
8.2.1 Principle of F–P Etalon Intrinsic Optical Bistable Device 219
8.2.2 Principle of Electro-Optical Hybrid Optical Bistable Device 229
8.2.3 Application of Optical Bistable Devices 235

8.3 Optical Instability of Optical Bistability 237
8.3.1 Stability Analysis of Optical Bistability. 237
8.3.2 Instability of Optical Bistability. 242
References. 250

9 Propagation of Light Pulse in Fiber and Optical Soliton 251
9.1 Nonlinear Schrodinger Equation 251
9.1.1 Helmholtz Equation. 252
9.1.2 Derivation of Frequency-Domain Wave Equation in Fiber 255
9.1.3 Derivation of Nonlinear Schrodinger Equation 257
9.2 Group Velocity Dispersion and Self-phase Modulation 260
9.2.1 Pulse Propagation Excluding Dispersion and Nonlinearity. 262
9.2.2 Influence of Dispersion to Pulse Propagation 262
9.2.3 Influence of Self-phase Modulation to Pulse Propagation 266
9.2.4 Combined Action of Dispersion and Self-phase Modulation 268
9.3 Time Soliton and Space Soliton 272
9.3.1 Time Soliton 272
9.3.2 Space Soliton. 276
References. 278

10 All-Optical Switch Based on Nonlinear Optics 279
10.1 Summarization of All-Optical Switch 279
10.1.1 Research Direction of All-Optical Switch 279
10.1.2 Classification of All-Optical Switch. 284
10.2 Nonlinear Optical Coupler All-Optical Switch 289
10.2.1 Symmetric Coupler Under Low Incident Power 290
10.2.2 Symmetric Coupler All-Optical Switch in Self-phase Modulation. 293
10.2.3 Asymmetric Coupler All-Optical Switch in Cross-Phase Modulation 296
10.3 Nonlinear Sagnac Interferometer All-Optical Switch. 300
10.3.1 Symmetric Sagnac Interferometer in Low Incident Power 300
10.3.2 Sagnac Interferometer All-Optical Switch with a Non-3 dB Coupler 305
10.3.3 Sagnac Interferometer All-Optical Switch in Cross-Phase Modulation 307
10.3.4 Sagnac Interferometer All-Optical Switch with a Optical Amplifier 309

10.4 Nonlinear M–Z Interferometer All-Optical Switch 311
10.4.1 M–Z Interferometer All-Optical Switch with Different Arm Materials. 311
10.4.2 M–Z Interferometer All-Optical Switch with Different Arm Lengths. 313
10.5 Nonlinear Ring Resonator All-Optical Switch 314
10.5.1 All-Optical Switch in a M–Z Interferometer Coupled with a SCRR. 315
10.5.2 All-Optical Switch in a DCRR 321
10.6 Nonlinear Fiber Grating All-Optical Switch 325
10.6.1 Single Nonlinear FBG All-Optical Switch. 326
10.6.2 Single Nonlinear LPFG All-Optical Switch. 334
10.6.3 Nonlinear Fiber Connected LPFG-Pair All-Optical Switch 339
10.6.4 Nonlinear Fiber Connected FBG-Pair Optical Bistable Switch 348
10.7 Nanoscale All-Optical Switches 355
10.7.1 Nano-waveguide Interferometer All-Optical Switches 357
10.7.2 Photonic Crystal All-Optical Switch 363
10.7.3 Surface Plasmon Polariton All-Optical Switch. 372
10.7.4 Silicon Nano-waveguide Resonant Cavity All-Optical Switch. 382
References. 384

About the Author

Chunfei Li graduated from Harbin Institute of Technology (HIT), China, in 1961, where he majored in Physics and Electronics. Since 1969 he was employed by the Physics Department of HIT as a teaching assistant. From 1962 to 1965, he visited Jilin University to study Theoretical Physics. In 1965, he returned to Physics Department of HIT, where he was successively promoted to be Lecturer (1978), Associate Professor (1982), and Full Professor (1985). From 1985 to 1998, he served as chairman of Physics Department in HIT. After that he is the director of the Institute of Advanced Optics in HIT. Since 2004, he is a professor invited specially at South China Normal University in Guangzhou.

From 1987 to 1989, Prof. Li was invited to be one of 70 members of the Chinese High Technology Specialist Committee, working in the group of information technology to preside over the research programs on optoelectronic devices in China.

Since 1979, Prof. Li began his research work on nonlinear optics, especially, optical bistability. He was invited by Prof. Hyatt Gibbs to work in his group at the Optical Sciences Center, University of Arizona, respectively, in 1982, 1984, and 1996. In the following years, Prof. Li expanded his research work in China to optical bistability, optical instability, excited-state nonlinear optics, optical limiting, nonlinear fiber optics, chiral nonlinear optics, all-optical switches, and nanophotonics. He was one of pioneers in these research fields in China.

In the past 35 years, Prof. Li accomplished more than 300 papers published in famous international and domestic journals and 5 books: "*Nonlinear Optics*", "*Nonlinear Optics Principles and Applications*," "*Principles of All-Optical Switch*", "*All-Optical Switch Based on Nonlinear Optics*" and "*Photonics Technology and Application*" published by Chinese Publishing Houses. Because of his remarkable research works, he was awarded 4 science prizes by the Chinese Government, respectively in 1987, 1996, 2000 and 2008.

Professor Li is a fellow of Chinese Optical Society and international member of OSA and SPIE. He was an editor serving for two Chinese journals: "*ACTA OPTICA SINICA*" and "*ACTA PHOTONICA SINICA*" and one international journal: "*Nonlinear Optical Physics and Materials*."

As a supervisor, Prof. Li has tutored about 40 Ph.D. graduate students and 40 Master graduate students. He lectured courses for graduate students on "*Nonlinear Optics*," "*Laser Physics*," and "*Principles of Optical Switches*."

In the past 35 years, as a short-term visiting professor, Prof. Li has invited to work in a number of world-level research groups at University of Arizona, UC Santa Barbara, UC Los Angeles, University of Southern California, University of South Alabama, Penn State University, Tokyo University, University of Queensland, and so on.

Professor Li has rich experience in the international and domestic conferences. He was one of International Chairs of the First Conference on Nonlinear Optics at Hawaii, USA, in 1990. He was a Program Committee Member of the Conference on Optical Computing at Edinburgh, UK, in 1994 and an invited speaker in many international conferences. He has chaired 3 conferences on nonlinear optics in China, at Guangzhou in 1991; at Nanjing in 1993; and at Harbin in 1995, and has chaired 8th Photonic Conference at Nanchang in 2012.

Abstract

This book systematically describes the basic principles of nonlinear optics by using the concise classical polarization theory and physical conception of photons. The book briefly explains the second-order nonlinear optical effects, emphatically discusses the third-order nonlinear optical effects, and introduces the recent research progress and application of nonlinear optics, including optical bistability, optical chaos, optical soliton, excited-state nonlinear optics, all-optical switch, nonlinear optical limiting, and Z-scan measuring technology, which are contained in the author's research results.

This book can be a textbook for optics professional graduate students in physics and electronics departments or a reference book for science and technology personnel working in the area of laser, optoelectronic, optical communication, or optical material technologies.

Chapter 1
Introduction

This chapter discusses the importance of nonlinear optics in physics, optics and photonics technology, the physical meaning of nonlinear optics, the research contents, the research history and the development trend of nonlinear optics, and the situation and prospect of application of nonlinear optics.

1.1 Importance of Nonlinear Optics

1.1.1 Status of Nonlinear Optics in Modern Physics

As is well-known,the modern physics was found on two headstones of the quantum physics and the relativity physics in the early 20th century. The quantum physics studies the movement theory of microscopic particles including molecules, atoms, nucleons and elemental particles; the relativity physics studies the movement theory of high speed object near light velocity and the gravitational interaction among objects with big quality. Because the quantum theory is found on the corpuscular property of light, and the relativity theory is found on the principle of constancy of light velocity, so the optics is the basic of quantum theory and relativity theory.

Some people think that the nonlinear physics founded in the latter half of the 20th century also is a headstone of the modern physics. The nonlinear physics is study of the nonlinear relationship between action and reaction (response) of objects under a strong interaction. These phenomena contain in different fields of physics, to form the nonlinear mechanics, nonlinear acoustics, nonlinear thermodynamics, nonlinear electromagnetism, and nonlinear optics, respectively. Nonlinear optics is one of branches of the nonlinear physics.

© Shanghai Jiao Tong University Press,
Shanghai and Springer Nature Singapore Pte Ltd., 2017

C. Li, *Nonlinear Optics*, DOI 10.1007/978-981-10-1488-8_1

1.1.2 Status of Nonlinear Optics in Modern Optics

Since the invention of laser in 1960, the modern optics was born. We call the optics based on the common light source with the spontaneous radiation as traditional optics; and the optics based on the laser source with the stimulated radiation as modern optics (we can call it as Photonics). In the latter half of the 20th century, the modern optics developed very quickly, surround the laser research and application to generate several subdisciplines of modern optics. Table 1.1 lists a number of relatively mature subdisciplines of modern optics and their research object and main application [1].

Among the subdisciplines of modern optics, the laser physics and the nonlinear optics are most important. The laser physics mainly studies the principle of laser devices and properties of laser; and nonlinear optics studies various nonlinear effects in the interaction between laser and matter. There are two aspects: one is that the pump light induces the change of matter's macroscopic parameters (susceptibility, dielectric coefficient, refractive index, absorption coefficient, etc.) or the change of matter's microscopic structure, to realize "controlling matter by light";

Table 1.1 Research object and main application of subdisciplines of modern optics (Photonics)

Subdisciplines	Research object	Main application
Laser physics	Laser device theory and properties of laser	Design of different types of laser devices with different parameters of output laser beams. Laser induces strong field and extreme physical environment; laser control particles and cell. Using laser for illumination, measuring, display, sensing, communication and laser processing
Nonlinear optics	Interaction between laser and matter	Light pulse compress, frequency conversion, elimination of distortion in transmission medium, nonlinear communications, all-optical switch, optical storage, slow light, high resolution spectrum analyze, and digital optical information processing
Fourier optics	Fourier optics theory and optical information processing	Holography, holographic storage, optical picture processing, simulation optical computing, and information safety
Guided wave optics	Light transmission and control in fiber and planar waveguide	Light transmission in fiber and planer waveguides; dispersion, loss, polarization, and power control, active and passive waveguide devices, coupling between fiber and device
Quantum optics	Non-classical optical phenomena	Using squeezed state to suppress the noise in optical communication; using quantum entangled state for quantum secrecy communication, quantum storage, quantum computing and quantum information processing

the other one is that the change of matter induces the change of parameters of the signal light propagating in the matter (frequency, power, wavevector, phase, pulsewidth, frequency spectrum, group velocity, propagation direction, etc.), thereby the "Controlling light with light" can be realized. In short, the laser physics studies the laser generation method; and the nonlinear optical studies the laser controlling method. Both are the basis of laser application. Therefore, the optics specialized graduate students must study nonlinear optics, besides study laser physics.

1.1.3 Nonlinear Optics Is a Basis of Photonic Technology

Figure 1.1 gives a comparison of development roadmaps of photonics and electronics; we find both have spectacular similarity [1].

Optics was founded after Newton published a book "Optics" to summary the achievement of geometrical optics in 1704, and Fresnel used the Huygens-Fresnel principle to explain the wave optics phenomena in 1818. Electromagnetism was founded after Coulomb established the Coulomb law in 1785 and Maxwell summarized the electromagnetic field theory in l873.

Electromagnetism and Optics are subdisciplines of physics, both born in 18–19th century. Electrotechnology was generated due to the application of Electromagnetism; and Engineering Optics was generated due to the application of Optics.

In 1906 human invented electronic valve to solve the problem of "Controlling electrons", then the Elections start established. However, in that time the electronic valve is the vacuum electronic valve, so the electronics was called "Vacuum electronic valve electronics". Utile in 1948 the semiconductor transistor was invented; the "Solid state electronics" was born.

Since 1960 the micrometer semiconductor integrated circuit was invented, the "Microelectronics" and "Microelectronic technology" were generated. The next

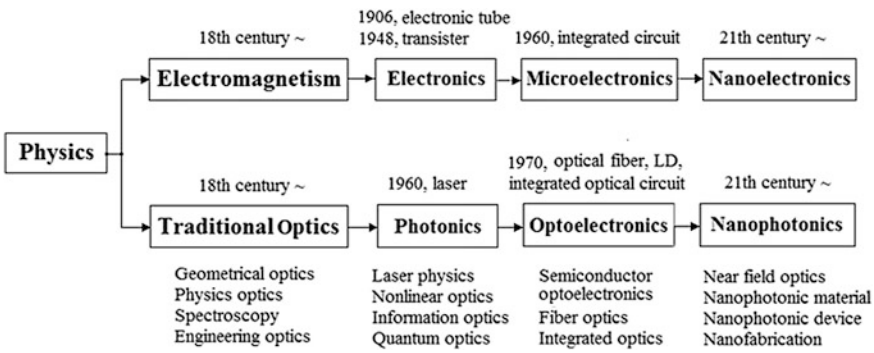

Fig. 1.1 Comparison between two development roadmaps of photonics and electronics

step of electronics should be "Nanoelectronics" and "Nanoelectronic technology". The nanoelectronic devices, such as nanotube and graphite devices will be used. Due to the inherent limitation in the bandwidth, capability, transmission speed, etc. the electronic technology meets a bottleneck for further developing; it cannot satisfy the requirement of current modern science and technology. Therefore developing photonic science and technology is necessary tendency.

The traditional optics start from 18th century is based on the nature light source. Since 1960 the invention of laser, the modern optics based the stimulated radiation light source was born. The appearance of the different lasers, such as gases, solid, dye, semiconductor and chemical lasers and their widespread application formed a new "Laser technology".

Laser is a generator of photons at same state. So that the born of laser means the born of photonics. Photonics is a science to study photon's generation, transmission, control, detect, display, storage, and interaction with matter, it is the core content of modern optics.

After laser born, over 10 years development, it appeared low-loss silica fiber, room temperature heterojunction semiconductor laser diode, and various semiconductor photoelectrical integrated devices and waveguide devices, for instance, lasers, optical amplifiers, modulators, detectors, optical switch and grating sensors, and different fibers, these devices have micrometer size. Therefore, the photonics in this stage can call Microphotonics (corresponding to Microelectronics). Because the main feature of Microphotonics are "controlling light with electricity" for the devices and "optical and electrical hybrid" for the systems, so the photonics in this stage can also be called as "Optoelectronics", the corresponding technology is optoelectronic technology. The optoelectronic technology contains following four parts: the information optoelectronic technology; the energy optoelectronic technology; the material optoelectronic technology and the biomedical optoelectronic technology. All of these technologies are related to the interaction between laser and matter, so nonlinear optics is a basis of optoelectronic technology.

The next stage of photonics is "Nanophotonics". In that stage will adopt the nanophotonic technology and the combinative ultrafast-photonic technology, the target of Nanophotonics is to realize the "Controlling light with light", namely the all-optical technology. Because photons are not charged, it cannot directly realize "Controlling light with light" by interaction between photons similar to electrons in the transistor. The only way is use nonlinear optics method indirectly to realize "Controlling light with light". That is through a pump light to change the parameters of medium or the micro-stricture of medium to control the frequency, amplitude, phase, polarization, or group speed of the signal light, which is propagating in the medium. Up to now, using nonlinear optics method people can control the frequency (or wavelength) of the signal light, but cannot control the amplitude (or power) of the signal light, that means the all-optical switches cannot be made. The all-optical switching is a basic technology for optical digital information processing. The all-optical switch is a basic device of all-optical communication and all-optical computer in the future.

In the latter half of 20th century, laser source problem has well solved, but the laser controlling problem is not solved, this is an important problem to be solved. For this purpose, nonlinear optics will give play to key action. In short, the nonlinear optics is an important basis of photonics and its applications.

1.2 Physical Meaning of Nonlinear Optics

What is the nonlinear optics? We can explain his physical meaning from the viewpoint of that the light induces the polarization of medium.

1.2.1 Phenomenon Related with High-Order Polarization

When a common light with an electrical field strength (or amplitude) $\boldsymbol{E}$ irradiates the medium, under the action of light electrical field, the electric charge of molecule and atom in the medium occurs overall or relative displacement, induced a secondary light electrical field, which is described by a physical quantity-electric polarization $\boldsymbol{P}$, the induced polarization depends linearly on the electrical field amplitude, the relationship between $\boldsymbol{P}$ and $\boldsymbol{E}$ is

$$\boldsymbol{P} = \varepsilon_0 \boldsymbol{\chi}^{(1)} \cdot \boldsymbol{E}, \tag{1.2.1}$$

where the constant of proportionality $\boldsymbol{\chi}^{(1)}$ is the linear susceptibility, which is a complex number tensor for the anisotropic medium; ε_0 is the dielectric coefficient in the vacuum.

If the incident light is a laser, its intensity is much higher than common light in several orders of magnitude. We can make the expansion of electric polarization into a power series of light electrical field amplitude, the relationship between $\boldsymbol{P}$ and $\boldsymbol{E}$ for the anisotropic medium is

$$\boldsymbol{P} = \varepsilon_0 \boldsymbol{\chi}^{(1)} \cdot \boldsymbol{E} + \varepsilon_0 \boldsymbol{\chi}^{(2)} : \boldsymbol{EE} + \varepsilon_0 \boldsymbol{\chi}^{(3)} \vdots \boldsymbol{EEE} + \cdots, \tag{1.2.2}$$

where $\boldsymbol{\chi}^{(1)}$ is linear susceptibility, $\boldsymbol{\chi}^{(2)}$ and $\boldsymbol{\chi}^{(3)}$ are the second- and third-order nonlinear susceptibilities, respectively. $\boldsymbol{\chi}^{(1)}$, $\boldsymbol{\chi}^{(2)}$ and $\boldsymbol{\chi}^{(3)}$ are second-, third- and fourth-rank tensors, respectively. The symbols "$\cdot$", ":" and "$\vdots$" are denoted second-, third- and fourth-rank tensor multiplication operations, respectively. In the right side of Eq. (1.2.2), the first item is linear polarization, the second item, third item, and so on are high-order nonlinear polarizations, so Eq. (1.2.2) can be denoted by electric polarizations:

$$\begin{aligned} \boldsymbol{P} &= \boldsymbol{P}^{(1)} + \boldsymbol{P}^{(2)} + \boldsymbol{P}^{(3)} + \cdots \\ &= \boldsymbol{P}_L + \boldsymbol{P}_{NL}, \end{aligned} \tag{1.2.3}$$

where first item is linear polarization, which is denoted by

$$\boldsymbol{P}_L = \boldsymbol{P}^{(1)}, \tag{1.2.4}$$

the following items are high-order nonlinear polarization, which is denoted by

$$\boldsymbol{P}_{NL} = \boldsymbol{P}^{(2)} + \boldsymbol{P}^{(3)} + \cdots. \tag{1.2.5}$$

In short, nonlinear optics studies the phenomenon related with the high-order nonlinear polarization of the medium.

1.2.2 Nonlinear Response of Medium to the Optical Field

Now we suppose the medium is an isotopic homogeneous medium, in Eq. (1.2.2), the $\boldsymbol{\chi}$ can be written to the scalar quantity, $\boldsymbol{P}$ and $\boldsymbol{E}$ are the vector quantities, then Eq. (1.2.2) can be expressed as

$$\begin{aligned} \boldsymbol{P} &= \varepsilon_0\chi^{(1)}\boldsymbol{E} + \varepsilon_0\chi^{(2)}|\boldsymbol{E}|\boldsymbol{E} + \varepsilon_0\chi^{(3)}|\boldsymbol{E}|^2\boldsymbol{E} + \cdots \\ &= \boldsymbol{P}^{(1)} + \boldsymbol{P}^{(2)} + \boldsymbol{P}^{(3)} + \cdots, \end{aligned} \tag{1.2.6}$$

The linear polarization, second-order nonlinear polarization and third-order nonlinear polarization can be expressed as

$$\boldsymbol{P}^{(1)} = \varepsilon_0\chi^{(2)}\boldsymbol{E}, \tag{1.2.7}$$

$$\boldsymbol{P}^{(2)} = \varepsilon_0\chi^{(2)}|\boldsymbol{E}|\boldsymbol{E}, \tag{1.2.8}$$

$$\boldsymbol{P}^{(3)} = \varepsilon_0\chi^{(3)}|\boldsymbol{E}|^2\boldsymbol{E}. \tag{1.2.9}$$

We can see that in the case of linear polarization, the polarization of medium is proportional to the field strength; however in the case of second-order nonlinear polarization, the polarization of medium is proportional to the square of field strength; in the case of third-order nonlinear polarization, the polarization of medium is proportional to the triple of field strength. In conclusion, in the nonlinear polarization case, the polarization of medium is not proportional to the field strength.

Therefore, Nobel laureate Bloembergen [2], an authoritative scholar in nonlinear optics, gave a strict scientific definition of nonlinear optics: “If the response of matter to the impressed electromagnetic field is not a linear function of the

impressed electromagnetic field strength, this optical phenomenon belongs to the field of nonlinear optics".

It is worth noting that the definition said the electromagnetic field, namely the light field, which is composed by electrical field and magnetic field. Actually, the light magnetic field also has effect to the magnetic polarization of the medium. Especially in the material composed by asymmetry chiral molecules the effect is stronger. However, for the common materials, the effect of light magnetic field to the medium is very weak, it can be ignored. Therefore, in the general nonlinear optics books, people only consider the contribution of light electrical field to the nonlinear optical effects of the medium.

1.2.3 Parameters of Medium Are Function of Optical Field

If we only consider the linear optical effect and third-order nonlinear optical effect, the total polarization of the medium is

$$\boldsymbol{P} = \varepsilon_0(\chi^{(1)} + \chi^{(3)}|\boldsymbol{E}|^2)\boldsymbol{E} = \varepsilon_0(\chi^{(1)} + \Delta\chi^{(1)})\,\boldsymbol{E}, \tag{1.2.10}$$

where

$$\Delta\chi^{(1)} = \chi^{(3)}|\boldsymbol{E}|^2 \propto \chi^{(3)}\boldsymbol{I} \tag{1.2.11}$$

is the variation quantity of first-order susceptibility induced by the electrical field of impressed light, which is proportional to the square of light field amplitude, i.e., the light intensity $\boldsymbol{I}$.

Because the third-order nonlinear susceptibility is a complex number, it can be written to real and imaginary two parts:

$$\chi^{(3)} = \chi^{(3)\prime} + i\chi^{(3)\prime\prime}. \tag{1.2.12}$$

In Chap. 2 we will prove that, the reflective index and the absorption coefficient of the medium also can be divided into linear and nonlinear two parts:

$$n = n_0 + \Delta n, \tag{1.2.13}$$

$$\alpha = \alpha_0 + \Delta\alpha, \tag{1.2.14}$$

where n_0 is the linear reflective index; Δn is the nonlinear reflective index; α_0 is the linear absorption coefficient; $\Delta\alpha$ is the nonlinear absorption coefficient. And the nonlinear reflective index is related with the real part of susceptibility; the nonlinear absorption coefficient is related with the imaginary party of susceptibility; and both are proportional to the light intensity $I \propto |E|^2$:

$$\Delta n \propto (\chi^{(3)\prime})I, \tag{1.2.15}$$

$$\Delta\alpha \propto (\chi^{(3)\prime\prime})I. \tag{1.2.16}$$

In conclusion, for the third-order nonlinear effect, the variation of susceptibility, the reflective index and the absorption coefficient are all linearly related with light intensity; in other word, they are the function of optical field amplitude. Therefore, we can generally say that the nonlinear optical phenomenon is the phenomenon in which the variation of optical parameters of the medium is the function of the optical field amplitude.

1.3 Research Content of Nonlinear Optics

1.3.1 Typical Nonlinear Optical Effects

What is difference between nonlinear optics and linear optics? The basic difference has two: firstly, the light sources of both are different: the linear optics is used the incoherent and low power nature light; the nonlinear optics is used the coherent and high power laser. Secondly, in the case of linear optics, the optical parameters of the medium are independent with the light field; but in the case of nonlinear optics, the parameters of medium, such as refractive index, absorption coefficient, susceptibility, etc. are the function of the light electrical field amplitude.

Now we list the following 10 nonlinear optical effects to further explain the difference between the nonlinear optics and the linear optics.

1. **Optical Kerr Effect**

When a laser beam passes through a medium, the refractive index of the medium will be changed. The variation quantity is proportional to the light intensity, that is

$$n = n_0 + n_2 I, \tag{1.3.1}$$

where n_0 is the linear refractive index of medium. I is light intensity in medium. n_2 is the nonlinear refraction coefficient. n_2 can be positive or negative, it depends on the medium. So the refractive index of medium can be increased or decreased with increase of light intensity. However, in the linear optics case, when the light beam passes though the medium, the refractive index of medium cannot be changed. It will keep the constant n_0.

2. **Self-focusing and Self-defocusing**

When a Gaussian-type laser beam passes through a medium, due to the radial distribution of light intensity is ununiformed, the Kerr effect induced the refractive index in radial direction is gradually changed, to form a like-convex lens

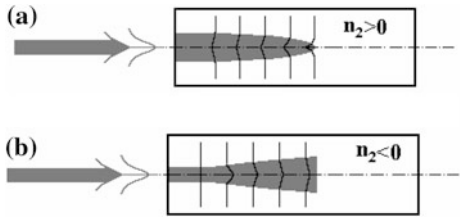

Fig. 1.2 Nonlinear refraction phenomena: **a** self-focusing; **b** self-defocusing

(for $n_2 > 0$) effect or a like-concave lens effect (for $n_2 < 0$), so that the transverse dimension of light beam in the medium becomes small and small, i.e., self-focusing, or becomes large and large, i.e., self-defocusing. These two nonlinear refraction effects are show in Fig. 1.2.

However, in the linear optics case, the refractive index not changes with light intensity, so the self-focusing and self-defocusing cannot occur.

3. **Nonlinear Absorption**

In the condition of resonance interaction between laser and medium, the absorption coefficient of medium α can be changed with increase of light intensity until saturation. The absorption-coefficient change is different for different material: if α decreases with increase of light intensity, i.e., the saturation absorption as shown in Fig. 1.3a; if α increase with increase of light intensity, i.e., the reverse saturation absorption, as shown in Fig. 1.3b.

In the linear optics case, the light passes though the medium, the absorption coefficient cannot be change with the light intensity; it is a constant of α_0.

4. **Multiwave Mixing**

In nonlinear optics, when a number of laser beams transmit in the medium, it is possible occurrence of the energy (or frequency) interconversion among the laser beams, in the same time the light with new frequency will be generated. This is the multiwave mixing effect. Usually we can see the three-wave mixing or the four-wave mixing. For example, two light beams at same frequency input a nonlinear crystal in the same time to produce a new light beam at the double frequency. This is optical frequency-doubled effect as shown in Fig. 1.4a. In the another

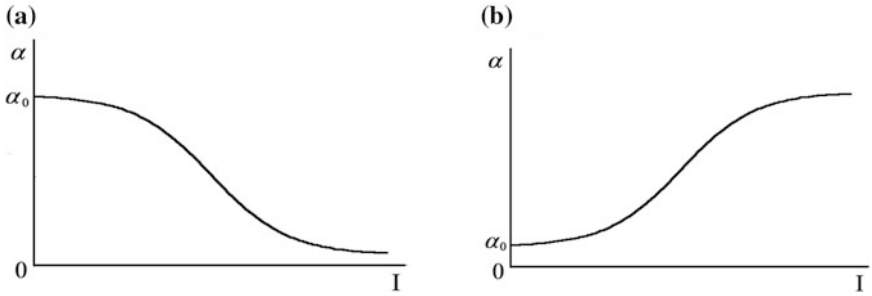

Fig. 1.3 Nonlinear absorption phenomena: **a** saturable absorption; **b** revers saturable absorption

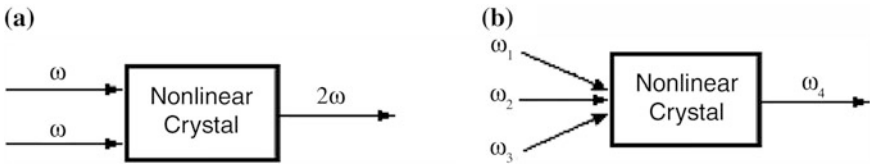

Fig. 1.4 Multiwave mixing phenomena: **a** optical frequency doubling; **b** four-wave mixing

example, when three lights at different frequency input a nonlinear crystal, it is possible to produce a new light at the frequency that is the sum of the frequencies of three input beams, the four-wave mixing is shown in Fig. 1.4b.

However in the linear optics case, when a number of light beams cross transport in the medium, the light beams cannot reciprocally interchange their energies; even cannot produce a new light.

5. **Phase Conjugation**

When a number of laser beams transmit in the medium, they could mutual transfer their phase signals, and it is possible to lead the phases of two beams become a conjugation relation. Figure 1.5 shows that when we input a signal light $(\boldsymbol{E}_\mathrm{p})$ at frequency ω into a nonlinear medium, and at the same time reversely input two strong-power pump lights $(\boldsymbol{E}_1$ and $\boldsymbol{E}_2)$ into the medium, in the reverse direction of signal light can produce a new light at same frequency ω, with an amplitude that is the conjugated amplitude of the signal light. The new light is called the conjugated light $(\boldsymbol{E}_\mathrm{c})$. The conjugated two lights $\boldsymbol{E}_\mathrm{p}$ and $\boldsymbol{E}_\mathrm{c}$ are expressed in the right side of Fig. 1.5.

However in the linear optics case, a number of light beams transit in the medium, they cannot mutually transfer their phase signals and the phase conjugation effect cannot appear.

6. **Stimulated Raman Scattering**

A laser beam inputs the medium and interacts with the molecules of medium to generate a series of stimulated-radiation scattered lights at different frequencies, this is stimulated Raman scattering. The spectrogram of stimulated Raman scattering is shown in Fig. 1.6. The longer dotted line at the center of spectrum is the incident laser. The spectral lines in both sides are multi-order scattering lights. The lights at lower frequency in the left side are called Stokes scattering lights; the lights at higher frequency in the right side are called anti-Stokes scattering lights.

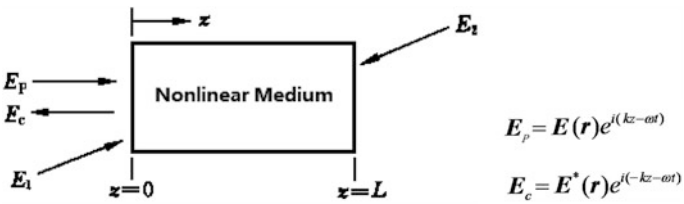

Fig. 1.5 Schematic diagram of phase conjugation effect

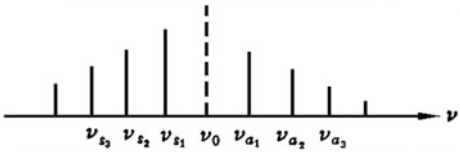

Fig. 1.6 Stimulated Raman scattering spectrogram

The common light interacting with molecules also can generate the scattering lights at different frequencies, but these scattering lights are just common lights. And only appear the first-order stokes scattering light and the first-order anti-stokes scattering light, without multi-order scattering phenomenon.

7. **Optical Bistability**

A laser beam with the intensity I_{i0} inputs into an F–P optical cavity containing a nonlinear medium, it can produce two possible transmitted light intensities I_{t1} and I_{t2}, such device is the optical bistable device. The characteristic curve of optical bistability is shown in Fig. 1.7.

However in the case of linear optics, when a common light passes through an F–P cavity, the transmitted light intensity is a linear function of the incident light intensity only.

8. **Nonlinear Optical Limiting**

A laser beam passes through an optical device containing a nonlinear material; its transmittance may decreases with increase of optical intensity. When the light intensity is strong enough, the transmittance can reduce to the zero, as shown in Fig. 1.8. This is the characteristic curve of a nonlinear optical limiter. The slop of the curve is the transmittance $T = \frac{dP_T}{dP_I}$, which changes with the incident power P_I. When $P_I = 0, T = T_0$, T_0 is linear transmittance. When $P_I = P_{I0}, T = 0$, the transmitted power P_T is limited below P_{T0}.

However in the case of linear optics, when a light beam passes through the material, the transmittance is a constant; it cannot be changed with the light intensity.

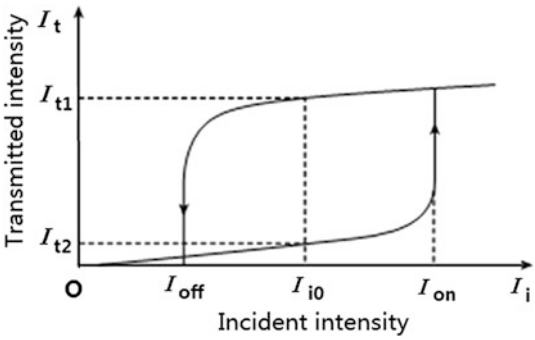

Fig. 1.7 Characteristic *curve* of the optical bistability

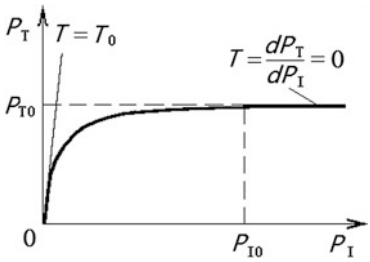

Fig. 1.8 Characteristic *curve* of nonlinear optical limiting

9. **Optical Soliton**

When a common light pulse takes a long-distance transmission in the optical fiber, its pulsewidth will be broaden with increase of the transmission distance due to the dispersion of fiber, as shown in Fig. 1.9a. However, if it is a laser pulse, and transmission fiber is selected by an anomalous dispersion fiber, the pulsewidth can keep a constant, that is because the nonlinear self-phase modulation counteracting the group dispersion of fiber to form a time optical soliton, as shown in Fig. 1.9b.

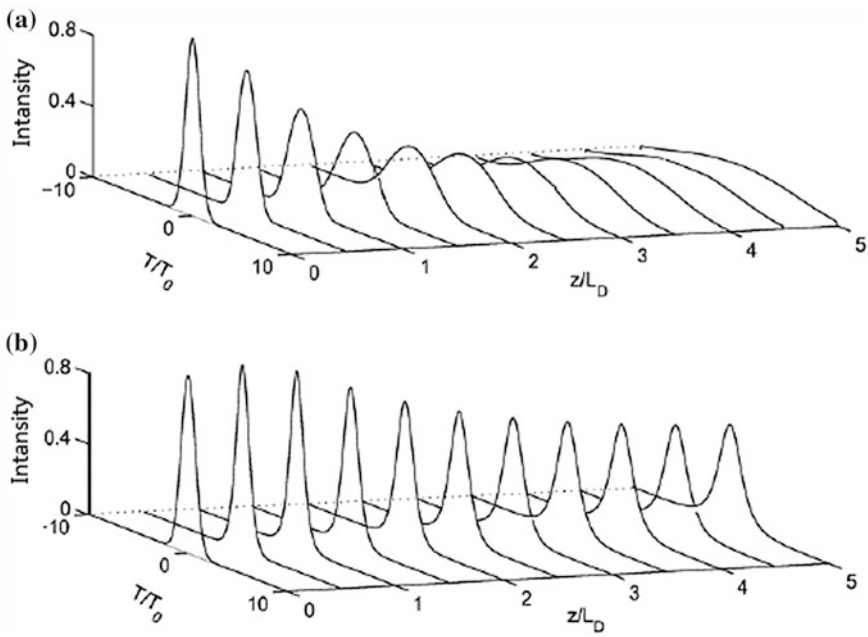

Fig. 1.9 The formation of time optical soliton in the fiber: **a** the dispersion of common light pulse makes the pulsewidth broaden; **b** the self-phase modulation of laser pulse balances the dispersion, to keep the pulsewidth as a constant

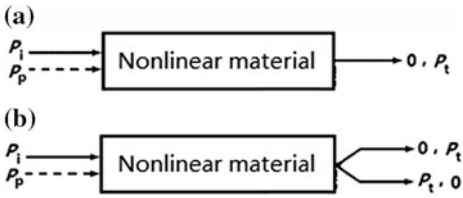

Fig. 1.10 Schematic diagram of all-optical switches: **a** intensity-type all-optical switch; **b** space-type all-optical switch

10. **All-optical Switch**

Because the photon is not charged, it cannot use a light directly to control the intensity or direction of the other light. However, in the nonlinear optics case, we can use a strong laser (pump light) to change the optical parameter of the medium, and then realize the controlling of the signal light passing through the medium, changing its intensity or propagation direction as shown in Fig. 1.10a, b, respectively. In the figure, P_P is the power of the pump light, P_i and P_t are the input and output powers of the signal light, respectively.

1.3.2 Two Kinds of Nonlinear Optical Effects

According to the difference of energy conversion process we can divide the nonlinear optics into two kinds: the passive nonlinear optics and the active nonlinear optics.

1. **Passive Nonlinear Optics**

The feature of the passive nonlinear optics is that in the nonlinear optical process, as a result the energy exchange between light and medium is nonoccurrence; however the energy exchange among the light fields at different frequencies is occurrence, in addition the light field at a new frequency may produce. All the lights including the original lights and the produced new light in the mixing process obey the energy conservation law and the momentum conservation law. The passive nonlinear optical process includes, for example, the frequency doubling, three-wave mixing, parameter processing, four-wave mixing, phase conjugation, etc. in which, the frequency doubling and the four-wave mixing have shown in Fig. 1.4.

2. **Active Nonlinear Optics**

The feature of the active nonlinear optics is that the energy exchange between light and medium is occurrence; and the change of optical parameter of medium is associated with the light electrical field amplitude, for example, the nonlinear absorption (saturable absorption, reverse saturable absorption, two-photon absorption, etc.); the nonlinear refraction (optical Kerr effect, self-focusing and self-defocusing, saturable refraction and reverse saturable refraction, two-photon refraction, etc.); the nonlinear scattering (stimulated Raman scattering, stimulated

Brillouin scattering, etc.), optical bistability and optical limiting, etc. The most of these active nonlinear optical processes have explained in above section.

1.3.3 Nonlinear Optical Materials

The nonlinear optical materials with different nonlinear mechanisms have many kinds. Table 1.2 lists some typical nonlinear optical materials and their nonlinear optical mechanisms.

What kind material is good nonlinear material? According to requirements of the device made by nonlinear materials, which should be:

1. The material has large nonlinear refraction coefficient n_2;
2. The material has low linear absorption coefficient α_0, with high optical transparency;
3. The material has short response time to impressed light field;
4. The material has simple and low-cost fabrication processing.

However, above requirements are contradicted with each other. the materials with strong nonlinearity often has large absorption loss, for instance, the compound semiconductors have the strong nonlinearity, but they work in the large absorption spectrum area; and the materials with strong nonlinearity usually have slow response time, for example, the liquid crystals have strong nonlinearity, but they have slow response time, because its response is rely on the molecular rotation; the materials with high transparency and fast response time often have low nonlinearity, such as silicon and silica, because they have symmetrical molecular structure. Therefore, the selection of material should comprehensively consider the material properties and the requirements of device.

Table 1.2 Nonlinear optical materials and nonlinear mechanisms (or structures)

Nonlinear optical material	Nonlinear mechanism (or structure)
Semiconductor	Electron or exciton mechanism
Organic and polymer	Electron or molecular polarization
Electro-optical crystal	External electro-optical effect
Photorefractive material	Internal electro-optical effect
Liquid crystal	Molecular orientation polarization
Cluster material(C_{60}, etc.)	Molecular polarization
Chiral molecule material	Molecular electric moment and magnetic moment
Quantum confinement (quantum well, quantum wire, quantum dot)	Semiconductor with periodic alternative large and low energy gap structure
Photonic crystal (1D, 2D and 3D)	Dielectrics with periodic alternative high and low refractive index structure
Surface plasmon polaritons	Meter-dielectric interface nano structure

1.4 Development History of Nonlinear Optics

1.4.1 Brief History of Nonlinear Optics

The development history of nonlinear optics can be divided into the following several stages:

1. **Initial Foundation Stage of Nonlinear Optics**

Before laser invention, there are several theory predictions of the nonlinear optical phenomenon, for example, 1931 Goeppert and Mayer theoretically predicted the two-photon absorption; 1956 Buckingham proposed the theory of Kerr effect. However, in that time it is difficult to experimentally verify these theory predictions.

Since laser invention in 1960, scientists carried through a series of experimental studied and found a lot of nonlinear optical effects. In 1965 Nobel praise winner Bloembergen [3] has written a book "Nonlinear Optical Phenomena" to summarize the research achievements in that period time, and then founded the new discipline "Nonlinear optics". So from 1961 to 1965 is the initial foundation stage of nonlinear optics. The important events in this stage are:

1961, the discovery of frequency doubling in ruby laser by Franken et al. [4];

1962–1964, the discovery of stimulated Raman scattering and stimulated Brillouin scattering [5–7];

1962–1965, the discovery of sum frequency, difference frequency, parametric oscillation, four-wave mixing [8–10];

1963–1966, the discovery of saturable absorption, two photon absorption [11, 12];

1962–1964, the discovery of self-focusing and self-phase modulation [13, 14];

1965, Bloembergen [3] published the book "Nonlinear Optical Phenomena".

2. **Mature Stage of Nonlinear Optics**

After 1965, the scientists discovered many new nonlinear optical effects in experiments and made the theoretical explains. In 1984 the famous professor Shen [15] published a book "The Principles of Nonlinear Optics" to summary the research achievements in that period time. From 1965 to 1984 for near 20 years is mature stage of nonlinear optics. The significative events in this stage are:

1962–1975, the discovery of transient-state coherent optics effects (photon-echo, optical nutation, self-inductance transparency, etc.) [16];

1963–1983, the discovery of degenerate four-wave mixing and optical phase conjugation [17–19];

1964–1974, the study of optical Kerr effect and the verification by the experiment [20, 21];

1975–1985, the discovery of optical bistability and optical chaos [22, 23];

1972–1987, the study of nonlinear optical properties in fiber and optical soliton [24–26];

1984, Professor Shen [15] published the book "The Principles of Nonlinear Optics".

3. **Application Development Stage of Nonlinear Optics**

After 1984 scientists continually found many new nonlinear optical phenomena, the theory of nonlinear optics became more mature. The application of nonlinear optics has a large development, especially in the applications of the laser science and technology, the information science and technology and the material science and technology. Since 1984–2015 for 30 years is the application development stage of nonlinear optics. The major events in this stage are:

1982–1998, the study of nonlinear optical properties of semiconductor quantum confinement materials [27, 28];

1985–1989, the discovery of high efficient nonlinear optical crystal materials BBO and LBO [29, 30];

1985–1991, the study of nonlinear optical properties of organic and polymer [31, 32];

1987–1995, the discovery of reverse saturable absorption and optical limiting effects [33–35];

1979–1993, the study of photorefractive effect and its nonlinear optical theory [36, 37];

1985–1997, the application in quantum optics (squeezed state and quantum entanglement, etc.) [38, 39];

1985–1999, the application in nonlinear interferometer-type all-optical switches [40–42];

1984–2001, the application in optical fiber communication, optical soliton communication and nonlinear communication, etc. [43, 44];

1979–2002, the application in photonic crystal [45, 46];

1995–2005, the application in chiral molecular materials [47, 48];

1995–2006, the application in light speed controlling (slow light and fast light) [49–52];

2006–2015, the application in surface plasmon polaritons technology [53, 54].

1.4.2 Development Tendency of Nonlinear Optics

In this half of century, the nonlinear optics continually and rapidly developed in depth and breadth, its development tendency displayed on the several respects: the study objects, the study in time and space scales, and the nonlinear optical materials.

1. **Study Objects**

The development tendency of the nonlinear optics study is from strong light source to the weak light source; from the resonance area to the non-resonance area; from

the fundamental state-excited state transition to the excited state-excited state transition; from the two-energy mode to the multi-energy mode; from the local area to the non-local area, etc.

2. **Space Scale**

For different space scale of material system, the law of interaction between light and material is different. It needs use different theory to study. The macroscopic scale system should use the wave optics theory; the microscopic scale system should use the quantum optics theory; now the studied heat point is turned to the nano-scale material system, in the nano-scale material system we should use the near-field optics theory. However, the nonlinear optics theory in the nano-scale system is not mature yet, it needs further development.

3. **Time Scale**

The study of nonlinear optics is developed from the steady-state process to the quasi-steady-state process, and to the transient-state (dynamic state) process; the different process should use different theory. To study the steady-state process based on the continues light or the quasi-steady-state process based on the microsecond-pulsed light, we can use the steady-state nonlinear wave equations, which are not contained the time derivative; but to study the transient-state process based on the nanosecond, picosecond or femtosecond short-pulsed light, we should use nonlinear wave equations contained first-order or second-order derivatives.

4. **Nonlinear Optical Material**

From the inorganic material to the organic material; from the amorphous material to the crystalline material; from the symmetric material to the asymmetric material (chiral material); from the homogenous material to the composite material; form the high dimensional material to the low dimensional material, such as 3D balk, 2D surface and thin film, ID line, and OD particle; from macroscopic material to nano-structure material, such as semiconductor quantum well, quantum line, and quantum dot; 3D, 2D, and 1D photonic crystal; metal-dialectic intersurface; nanotube, nano sphere and nano cluster, etc.

1.5 Applications of Nonlinear Optics

What are the applications of nonlinear optics? From the current point of view, the applications of nonlinear optics mainly have following three aspects: in the laser technology; in the information technology and in the materials technology [55].

1.5.1 Application in Laser Technology

1. **New Laser Device**

Based on the principles of nonlinear optics, scientists have made various new type laser devices, such as the ultrashort pulsed lasers, the wavelength or power tunable lasers, the stimulated Raman laser, the nonlinear fiber laser, the soliton laser, the terahertz laser, the nanoscale laser, etc. In addition, the nonlinear optics also can use for the laser mode selection, the laser power stabilization and the laser parameter measurement, etc.

2. **Laser Pulse Compression**

The Q-switching and mode-locking technologies are based on the nonlinear optics. These technologies are used for compression of the laser pulsewidth to generate the picosecond, femtosecond and attosecond ultrashort pulsed lasers.

3. **Laser Frequency Conversion**

Using nonlinear optical technologies, such as the frequency doubling; sum frequency; difference frequency; parametric amplification and oscillation; third harmonic generation; four-wave mixing; stimulated scattering, etc., the various laser-frequency conversions are realized.

4. **Laser Transportation**

The important application in adaptive optical technology is based on the optical phase conjugation of nonlinear optics, for example, the compensation of the light beam distortion in the laser atmospheric transmission; also can be used to solve the problem of light beam distortion in laser nuclear fusion, etc.

5. **Laser Protection**

It has significance in militarily to protect the laser blind weapons, which are using the laser pulses to damage the human eye and the photodetectors. The nonlinear optical limiters based on the principle of nonlinear optics are advantageous in compare with the linear optical limiters.

1.5.2 Application in Information Technology

1. **Optical Communication**

In currant optical communication including the fiber optical communication and the space optical communication, there are many technologies based on nonlinear optics, for instance, the semiconductor laser, Raman optical amplifier, optical modulator, self-focusing lens, optical switch, wavelength convertor, optical delayer, optical add drop multiplexer, optical switching, optical cross connect, etc. Novel

optical communication technology, for example, the coherent optical communication, optical soliton communication, optical chaos communication, optical quantum communication, and future all-optical communication are all associated with nonlinear optics.

2. **Optical Computing**

The digital optical information processing is the development direction of future information processing technology. The key technologies used in future optical computer, such as the all-optical computer, optical logic gate, optical number arithmetic device, 3D two-photon optical storage, optical amplifier, all-optical switch, optical clock-signal generator, etc., they all establish on the basis of nonlinear optics.

3. **Optical Sensing**

The distributed fiber sensor based on Raman and Brillouin fibers is a new type fiber sensing technology. In order to realize all-optical sensing network (internet of things), the all-optical switch made by nonlinear fiber grating is a key device. In the laser remote sensing technology, the nonlinear optics also plays an important role.

1.5.3 Application in Material Technology

1. **High Resolution Spectrum Analysis**

Taking advantage of ultrafast laser pulse excited stimulated Raman scattering, four-wave mixing, second harmonics, two-photon absorption, etc. nonlinear optical effects, people have developed the nonlinear spectrum analysis technology with high space resolution and high time resolution, extensively used to analyze and measure the state and structure of the atoms and molecules, the hyperfine structure of energy level, and change of physical and chemical cluster structure, activity of biological cell, etc. The combination of the nonlinear spectrum technology and the near-field optical microscopy forms imaginable near-field spectrum technology, to be used for analyzing state change of nano-structure, the luminescence process of matter and chemical reaction process, etc.

2. **Micromachining of Material**

The laser direct writing high precision processing by using multiphoton absorption (such as two-photon absorption) and multiphoton ionization has been used in the preparation of nanometer materials and the process of nano structure. In order to improve the luminous efficiency of solid light-emitting devices (LED) and the absorption efficiency of solar cells, to make microstructure graphics on the surface of the device with a laser micro machining method is an effective measure.

3. **Investigation of New Material**

The nonlinear optics method can be used for investigation of the following materials: the surface, intersurface, cluster etc. low dimensional materials; the quantum well, quantum line and quantum dot, etc. quantum confinement materials; 1D, 2D and 3D photonic crystal materials; the surface plasmon polariton material; the nanosphere, nanocavity, nanotube etc. nanoscale materials; the negative refractive index materials; the chiral materials; the biologic cell materials, etc. and measuring the nonlinear optical parameters of these new materials.

At present the applications of nonlinear optics in laser technology include the laser device technology, the laser frequency conversion technology, the laser transmission technology, etc. are comparative maturity, however, the laser protection technology (nonlinear limiter) is not well maturity; in the application of material technology, the extensive application is high resolution nonlinear spectrum analysis technology. The laser microprocessor technology has had a lager progress. In respect of nonlinear parameter measuring, Z-scan technology has had larger development, but the measurement accuracy and the stability should be enhanced. In the respect of information technology application, nonlinear optics has big potential. But the optical digital processing technology, such as all-optical switch and its application in all-optical communication, all-optical computer and all-optical sensing network, is still in foundational research stage. We hope after the research of nanometer devices obtains a great progress in the near future, it will have a successful application.

In shout, nonlinear optics is the basis of nowadays and future photonic technology, it will powerfully promote the information photonic technology, the energy photonic technology, the material photonic technology and the biologic technology development in an all-around way.

Review Questions of Chapter 1

1. What is the important significance to study nonlinear optics?
2. Take examples to explain what is the difference between linear optics and nonlinear optics?
3. What are relationships between the polarization of medium and the electrical field amplitude of incident light in two-order and three-order nonlinear optical effects?
4. What is difference between the passive nonlinear optics and the active nonlinear optics?
5. How many kinds of the nonlinear optical materials there are? What is their nonlinear mechanism?
6. Please introduce the development stages of nonlinear optics. What is the development trend of nonlinear optics?
7. To compare the development processes of photonics and electronics, what are their similarities and differentia?
8. Why nonlinear optics is an important basis of photonics? What are the mature applications and the development potential?

References

1. S. Liu, C. Li, *Photonics: Technology and Application* (Guangdong Science and Technology Publishing house, Guangzhou, China, 2006)
2. N. Bloembergen, *Nonlinear Spectroscopy, Proceedings* (North-Holland, Amsterdam, 1977)
3. N. Bloembergen, *Nonlinear Optics* (Benjamin, New York, 1965)
4. P.A. Franken, C.W. Hill et al., Generation of optical harmonics. Phys. Rev. Lett. **7**(4), 118–119 (1961)
5. G. Eckhardt, R.W. Hellwarth et al., Stimulated Raman scattering from organic liquids. Phys. Rev. Lett. **9**(11), 455–457 (1962)
6. E. Garmire, E. Pandarese, C.H. Townes, Coherently driven molecular vibrations and light modulation. Phys. Rev. Lett. **11**(4), 160–163 (1963)
7. R.Y. Chiao, C.H. Townes, B.P. Stoicheff, Stimulated Brillouin scattering and coherent generation of intense hypersonic waves. Phys. Rev. Lett. **12**(21), 592–595 (1964)
8. N. Bloembergen, J. Ducuing, Experimental verification of optical laws of non-linear reflection. Phys. Lett. **6**(1), 5–6 (1963)
9. S.A. Akhmanov, A.I. Kovrigin, M.M. Strukov, Frequency dependence of threshold of optical breakdown in air. JETP Lett. **1**(1), 25–29 (1965)
10. J.A. Giordmaine, R.C. Miller, Tunable coherent parametric oscillation in $LiNbO_3$ at optical frequencies. Phys. Rev. Lett. **14**(24), 973–976 (1965)
11. A. Szoke, A. Javan, Isotope shift and saturation behavior of the 1.15-μ transition of Ne. Phys. Rev. Lett. **10**(12), 521–524 (1963)
12. W.F. Kosonocky, S.E. Harrison, Saturation of absorption and fluorescence in solutions of phthalocyanines. J. Appl. Phys. **37**(13), 4789–4797 (1966)
13. G.A. Askaryan, Interaction between laser radiation and oscillating surfaces. Sov. Phys. JETP **15**(6), 1161–1162 (1962)
14. M.J. Hercher, Laser-induced damage in transparent media. J. Opt. Soc. Am. **54**(4), 563–569 (1964)
15. Y.R. Shen, *The Principles of Nonlinear Optics* (Wiley, New York, 1984)
16. B.I. Stepanov, E.V. Ivakin et al., Recording two-dimensional and three-dimensional dynamic holograms in transparent substances. Sov. Phys. Doklady **16**, 46 (1971)
17. A. Yariv, D.M. Pepper, Amplified reflection, phase conjugation, and oscillation in degenerate four-wave mixing. Opt. Lett. **1**(1), 16–18 (1977)
18. L. Allen, J.H. Eberly, *Optical Resonance and Two-level Atoms* (Wiley, New York, 1975)
19. R.A. Fisher (ed.), *Optical Phase Conjugation* (Academic Press, New York, 1963)
20. P.D. Maker, R.W. Terhune, C.M. Savage, Intensity-dependent changes in the refractive index of liquids. Phys. Rev. Lett. **12**(18), 507–509 (1964)
21. G.K.L. Wong, Y.R. Shen, Transient self-focusing in a nematic liquid crystal in the isotropic phase. Phys. Rev. A **10**(4), 1277–1284 (1974)
22. S.L. McCall, H.M. Gibbs, T.N.C. Venkatesan, Optical transistor and bistability (A). J. Opt. Soc. Am. **65**, 1184 (1975)
23. H.M. Gibbs, *Optical Bistability: Controlling Light with Light* (Academic Press, 1985)
24. R.H. Stolen, E.P. Ippen, A.R. Tynes, Raman oscillation in glass optical waveguide. Appl. Phys. Lett. **20**(2), 62–64 (1972)
25. L.F. Mollenauer, R.H. Stolen, The soliton laser. Opt. Lett. **9**(1), 13–15 (1984)
26. V.M. Mitev, L.M. Kovechev, Soliton shaping by stimulated Raman process in silica optical fibers. Opt. Commun. **63**(6), 421–424 (1987)
27. D.A.B. Miller, D.S. Chemla et al., Large room temperature optical nonlinearity in $GaAs/Ga_{1-x}Al_x$ As multiple quantum well structures. Appl. Phys. Lett. **41**(8), 679–681 (1982)
28. H. Haug (ed.), *Optical Nonlinearities and Instability in Semiconductors* (Academic Press, 1998)
29. C.T. Chen, B.C. Wu, J. Aidong, A new-type ultraviolet SHG crystal β-BaB_2O_4. Sci. Sin **B28**, 235–243 (1985)

30. C.T. Chen, Y.C. Wu, J. Aidong, New nonlinear-optical crystal: LiB_3O_5. J. Opt. Soc. Am. B **6** (4), 616–621 (1986)
31. D.J. Williams, D.S. Chemla, J. Zuss (eds.), *Nonlinear Optical Properties of Organic Molecules and Crystals*, vol. 1 (Academic Press, New York, 1987)
32. P.N. Prasad, K.J. Williams, *Introduction to Nonlinear Optical Effects and Polymers* (Wiley, New York, 1991)
33. R. Adair, L.L. Chase, S.A. Payne, Nonlinear refractive-index measurements of glasses using three-wave frequency mixing. J. Opt. Soc. Am. B **4**(6), 875–881 (1987)
34. L.W. Tutt, S.W. McCahon, Reverse saturable absorption in metal cluster compounds. Opt. Lett. **15**(12), 700–702 (1990)
35. Chunfei Li, Jinhai Si, Miao Yang et al., Excited-state nonlinear absorption in multi-energy-level molecular systems. Phys. Rev. A **51**(1), 569–575 (1995)
36. N.V. Kukhtarev, V.B. Markov, et al., Holographic storage in electrooptic crystals. II. Beam coupling—light amplification. Ferroelectries **22**(1), 961–964 (1978)
37. P. Yeh, *Introduction to Photorefractive Nonlinear Optics* (Wiley, New York, 1993)
38. R.E. Slusher, L.W. Hollberg et al., Observation of squeezed states generated by four-wave mixing in an optical cavity. Phys. Rev. Lett. **55**(22), 2409–2412 (1985)
39. D. Bouwmeester, J.-W. Pan et al., Experimental quantum teleportation. Nature **90**(11), 575–579 (1997)
40. H.M. Gibbs, *Optical Bistability: Controlling Light with Light* (Academic Press, New York, 1985)
41. M.G. Kane, W. Glesk, J.P. Sokoloff, P.R. Prucnal, Asymmetric optical loop mirror: analysis of all-optical switch. Applied Opt. **33**(29), 6833–6841 (1994)
42. J.E. Heebner, R.W. Boyd, Enhanced all-optical switching by use of nonlinear fiber ring resonator. Opt. Lett. **24**, 847–849 (1999)
43. W. Zhao, E. Bourkoff, Propagation properties of dark solitons. Opt. Lett. **14**(13), 703–705 (1989)
44. G.P. Agrawal, *Application of Nonlinear Fiber Optics* (Academic Press, New York, 2001)
45. H.G. Winful et al., Theory of bistability in nonlinear distributed feedback structures. Appl. Phys. Lett. **35**(5), 379–381 (1979)
46. R.E. Slusher, B.J. Eggleton (eds.) *Nonlinear Photonic Crystals* (Springer, New York, 2002)
47. J.J. Maki, A. Persoons, Surface second-harmonic generation from chiral materials. Phys. Rev. B **51**(3), 1425–1434 (1995)
48. X. Wang, J. Li, C. Li, Three-coupled-oscillator model for nonlinear optical response of chiral molecules with tripod-like structure. Chem. Phys. **320**(1), 37–44 (2005)
49. V. Hau, S.E. Harris, Z. Dutton, C.H. Behroozi, Light speed reduction to 17 metres per second in an ultracold atomic gas. Nature **397**(18), 594–598 (1999)
50. K. Olga, Y. Rostovtsev, M.O. Scully, Stopping light via hot atoms. Phys. Rev. Lett. **86**(4), 628–631 (2001)
51. M.S. Bigelow, N.N. Lepeshkin, R.W. Boyd, Superluminal and slow light propagation in a room temperature solid. Science **301**, 200–202 (2003)
52. C.J. Chang-Hasnain, S.L. Chuang, Slow and fast light in semiconductor quantum-well and quantum-dot devices. J. Light-wave Technol. **24**(12), 4642–4654 (2006)
53. G.A. Wurtz, R. Pollard, A.V. Zayats, Optical bistability in nonlinear surface-plasmon polaritonic crystals. Phys. Rev. Lett. **97**(5), 057402-1–057402-4 (2006)
54. M. Kauranen, A.V. Zayats, Nonlinear plasmonics. Nat. Photon. **6**, 737 (2012)
55. E. Garmire, Nonlinear optics in daily life. Opt. Express **21**(25), 30532–30544 (2013)

Chapter 2
Polarization Theory of Nonlinear Medium

This chapter starting from the Maxwell's equations deduces different forms of nonlinear wave equations for the light propagation in the isotropic and anisotropic nonlinear mediums, and in the time and frequency domains; gives the frequency-domain expressions of the polarization and susceptibility of the nonlinear medium; defines the degenerate factor of polarization; introduces the symmetries of nonlinear susceptibility; discusses the relationship between the real part and the imaginary part of susceptibility (K–K relation); points out that the physical meanings of the real part and the imaginary part of third-order nonlinear susceptibility are the nonlinear refractive index and nonlinear absorption coefficient respectively; finally introduces the two kinds of unit systems in nonlinear optics.

2.1 Wave Equations of Nonlinear Medium

2.1.1 Maxwell's Equations for Nonlinear Medium

Under the action of the laser, a medium appears the nonlinear optical effect, which is called the nonlinear medium. When a light wave, as an electromagnetic wave, propagates in the nonlinear medium, it obeys the law depended on the Maxwell equations, in general which can be written as

$$\nabla \times \boldsymbol{E} = -\frac{\partial \boldsymbol{B}}{\partial t}, \tag{2.1.1}$$

$$\nabla \times \boldsymbol{H} = \frac{\partial \boldsymbol{D}}{\partial t} + \boldsymbol{J}, \tag{2.1.2}$$

$$\nabla \cdot \boldsymbol{D} = \rho, \tag{2.1.3}$$

© Shanghai Jiao Tong University Press,
Shanghai and Springer Nature Singapore Pte Ltd., 2017

C. Li, *Nonlinear Optics*, DOI 10.1007/978-981-10-1488-8_2

$$\nabla \cdot \boldsymbol{B} = 0. \tag{2.1.4}$$

It also has the following matter equations:

$$\boldsymbol{D} = \varepsilon_0 \boldsymbol{E} + \boldsymbol{P}, \tag{2.1.5}$$

$$\boldsymbol{B} = \mu_0(\boldsymbol{H} + \boldsymbol{M}), \tag{2.1.6}$$

$$\boldsymbol{J} = \sigma \boldsymbol{E}, \tag{2.1.7}$$

where $\boldsymbol{E}$ and $\boldsymbol{H}$ are denoted the electric field strength and the magnetic field strength, respectively; $\boldsymbol{D}$ and $\boldsymbol{B}$ are denoted the electric induction strength and the magnetic induction strength, respectively; $\boldsymbol{P}$ and $\boldsymbol{M}$ are denoted the electric polarization and magnetic polarization, respectively. For non-ferromagnetic material, the magnetization phenomenon is very week, we can let $\boldsymbol{M} = 0$; ε_0 and μ_0 are denoted the vacuum electric coefficient and the vacuum permeability, respectively; $\boldsymbol{\sigma}$ is the conductivity, strictly speaking, it is a second-order tensor in the anisotropic medium, here approximately is a scalar; $\boldsymbol{J}$ is the conduction current density; $\boldsymbol{\rho}$ is the free charge density, both can be connected each other through the law of conservation of charge:

$$\nabla \cdot \boldsymbol{J} + \frac{\partial \rho}{\partial \boldsymbol{t}} = 0. \tag{2.1.8}$$

For the metal and semiconductor, the conduction current density $\boldsymbol{J}$ and the free charge density $\boldsymbol{\rho}$ these two quantities cannot be neglected, but for the insulator medium, we can assume they are inexistence, then do not consider Eq. (2.1.8). Because the conductivity $\boldsymbol{\sigma}$ is related to the absorption, assuming the linear absorption coefficient is $\boldsymbol{\alpha}$, and then we have relationship $\alpha = \mu_0 \sigma c/n$, so Eq. (2.1.7) should be reserved.

If a strong light (laser) acts on the nonlinear medium, the relationship between $\boldsymbol{P}$ and $\boldsymbol{E}$ is nonlinear, the medium induced $\boldsymbol{P}$ can be spread out into a power series of $\boldsymbol{E}$:

$$\boldsymbol{P} = \varepsilon_0 \boldsymbol{\chi}^{(1)} \cdot \boldsymbol{E} + \varepsilon_0 \boldsymbol{\chi}^{(2)} : \boldsymbol{EE} + \varepsilon_0 \boldsymbol{\chi}^{(3)} \vdots \boldsymbol{EEE} + \cdots, \tag{2.1.9}$$

where $\boldsymbol{\chi}^{(\mathrm{n})}$ is n-order electric susceptibility ($n = 1, 2, 3, \ldots$), which is a $n + 1$-order tensor.

The polarization $\boldsymbol{P}$ can be divided into the linear and nonlinear two parts. The nonlinear part is just the sum of high-order terms of polarization, which is called as nonlinear polarization noted by $\boldsymbol{P}_{\mathbf{NL}}$, that is

$$\boldsymbol{P}_{NL} = \boldsymbol{\varepsilon}_0 \boldsymbol{\chi}^{(2)} : \boldsymbol{EE} + \varepsilon_0 \boldsymbol{\chi}^{(3)} \vdots \boldsymbol{EEE} + \ldots = \boldsymbol{P}^{(2)} + \boldsymbol{P}^{(3)} + \cdots. \tag{2.1.10}$$

Then Eq. (2.1.9) can be expressed as

$$\boldsymbol{P} = \varepsilon_0 \boldsymbol{\chi}^{(1)} \cdot \boldsymbol{E} + \boldsymbol{P}_{NL}. \tag{2.1.11}$$

Substituting Eq. (2.1.11) into Eq. (2.1.5), we obtain

$$\boldsymbol{D} = \varepsilon_0 \boldsymbol{E} + \varepsilon_0 \chi^{(1)} \cdot \boldsymbol{E} + \boldsymbol{P}_{NL} = \boldsymbol{\varepsilon} \cdot \boldsymbol{E} + \boldsymbol{P}_{NL}, \tag{2.1.12}$$

where

$$\boldsymbol{\varepsilon} = \boldsymbol{\varepsilon}_0 (1 + \boldsymbol{\chi}^{(1)}) \tag{2.1.13}$$

is the linear dielectric coefficient; in which $\boldsymbol{\chi}^{(1)}$ is linear susceptibility. In the anisotropic medium, $\boldsymbol{\chi}^{(1)}$ and $\boldsymbol{\varepsilon}$ are complex-number second-order tensors. Here we only consider the electric dipole moment approximate, and neglected the action of the electric quadrupole moment and the magnetism dipole moment.

Therefore, Maxwell equations in anisotropic, nonlinear, nonmagnetic medium can be simplified [1] as

$$\nabla \times \boldsymbol{E} = -\mu_0 \frac{\partial \boldsymbol{H}}{\partial t}, \tag{2.1.14}$$

$$\nabla \times \boldsymbol{H} = \frac{\partial \boldsymbol{D}}{\partial t} + \sigma \boldsymbol{E}, \tag{2.1.15}$$

$$\boldsymbol{D} = \boldsymbol{\varepsilon} \cdot \boldsymbol{E} + \boldsymbol{P}_{NL}. \tag{2.1.16}$$

2.1.2 Time-Domain Wave Equation in Anisotropic Nonlinear Medium

In both sides of Eq. (2.1.14) carrying on $\nabla\times$ operation, then substituting Eq. (2.1.15) into it, and using Eq. (2.1.16), finally we obtain

$$\nabla \times \nabla \times \boldsymbol{E} + \mu_0 \sigma \frac{\partial \boldsymbol{E}}{\partial t} + \mu_0 \frac{\partial^2 \boldsymbol{\varepsilon} \cdot \boldsymbol{E}}{\partial t^2} = -\mu_0 \frac{\partial^2 \boldsymbol{P}_{NL}}{\partial t^2}. \tag{2.1.17}$$

This is wave equation for describing the transportation of the light wave in the anisotropic nonlinear medium. In comparison with the linear wave equation, this equation is only added an item on the right side, equivalent to exist a secondary wave source related with polarization $\boldsymbol{P}_{NL}$. The second item on the left is associated with the absorption loss of the medium.

Suppose the medium is lossless, i.e., $\sigma = 0$, and using the formula $c = 1/\sqrt{\mu_0\varepsilon_0}$, then Eq. (2.1.17) can be written to

$$[\nabla \times (\nabla\times) + \frac{1}{\varepsilon_0 c^2}\frac{\partial^2}{\partial t^2}\boldsymbol{\varepsilon}\cdot]\,\boldsymbol{E}(\boldsymbol{r},t) = -\frac{1}{\varepsilon_0 c^2}\frac{\partial^2}{\partial t^2}\boldsymbol{P}_{NL}(\boldsymbol{r},t). \tag{2.1.18}$$

This is time-domain wave equation in the non-absorption anisotropic nonlinear medium.

The light field strength $\boldsymbol{E}$ and nonlinear polarization $\boldsymbol{P}_{NL}$ in Eqs. (2.1.17) and (2.1.18) are the function of the time and position. In order to solve the equation and find the optical field strength $\boldsymbol{E}$, we mast firstly find out the nonlinear polarization $\boldsymbol{P}_{NL}$.

2.1.3 Time-Domain Wave Equation in Isotropic Nonlinear Medium

Assuming that the nonlinear medium is an non-absorption, homogeneous, isotopic medium, in Eq. (2.1.18) $\nabla \cdot \boldsymbol{E} = 0$, then $\nabla \times \nabla \times \boldsymbol{E} = \nabla(\nabla \cdot \boldsymbol{E}) - \nabla^2\boldsymbol{E} = -\nabla^2\boldsymbol{E}$; the original $\boldsymbol{\varepsilon}$ is a tensor, if the light wave with the amplitude of $\boldsymbol{E}$ is a plane wave and a transverse wave, its component paralleled to propagation direction can be neglected, so the tensor $\boldsymbol{\varepsilon}$ can be written to scalar quantity $\boldsymbol{\varepsilon}$. Using formula $n = \sqrt{\varepsilon/\varepsilon_0}$, thus Eq. (2.1.18) becomes

$$\nabla^2\boldsymbol{E}(\boldsymbol{r},t) - \frac{n^2}{c^2}\frac{\partial^2}{\partial t^2}\boldsymbol{E}(\boldsymbol{r},t) = \frac{1}{\varepsilon_0 c^2}\frac{\partial^2}{\partial t^2}\boldsymbol{P}_{NL}(\boldsymbol{r},t). \tag{2.1.19}$$

This is a time-domain wave equation for the plane light wave propagates in a non-absorption and isotopic nonlinear medium, which is an inhomogeneous second-order differential equation, it is difficulty to solve, in general, it needs approximately simplification treatment, the slow amplitude approximation is an used way. By using this method, the second-order differential equation will become a first-order differential equation.

In order to simplify, assuming a monochromic plane wave field propagates along z-direction, and the light field strength and the nonlinear polarization are denoted as a product of amplitude factor and phase factor, respectively:

$$\boldsymbol{E}(\mathrm{r},t) = \boldsymbol{E}(z,t)e^{i(kz-\omega t)}, \tag{2.1.20}$$

$$\boldsymbol{P}_{NL}(\boldsymbol{r},t) = \boldsymbol{P}_{NL}(z,t)e^{i(k'z-\omega t)}. \tag{2.1.21}$$

Substituting Eqs. (2.1.20) and (2.1.21) into Eq. (2.1.19), in which the various items have following differential coefficients of $\boldsymbol{E}(z,t)$ and $\boldsymbol{P}_{NL}(z,t)$, respectively:

$$\nabla^2\boldsymbol{E}(z,t) = \left[\left(\frac{\partial^2}{\partial z^2} + i2k\frac{\partial}{\partial z} - k^2\right)|\boldsymbol{E}(z,t)|\right]e^{i(kz-\omega t)}, \tag{2.1.22}$$

$$\frac{\partial^2}{\partial t^2}\boldsymbol{E}(z,t) = \left[\left(\frac{\partial^2}{\partial t^2} - i2\omega\frac{\partial}{\partial t} - \omega^2\right)|\boldsymbol{E}(z,t)|\right]e^{i(kz-\omega t)}, \tag{2.1.23}$$

$$\frac{\partial^2}{\partial t^2}\boldsymbol{P}_{NL}(z,t) \cong -\omega^2|\boldsymbol{P}_{NL}(z,t)|e^{i(k'z-\omega t)}. \tag{2.1.24}$$

Suppose the variation of field strength is very slow in the space distant within the scope of light wavelength and within the time scope of optical frequency; i.e., satisfy the following space and time conditions of the slowly varying field amplitude approximation [2]

$$\left|\frac{\partial^2\boldsymbol{E}(z,t)}{\partial z^2}\right| << \left|k\frac{\partial\boldsymbol{E}(z,t)}{\partial z}\right| \text{ and } \left|\frac{\partial^2\boldsymbol{E}(z,t)}{\partial t^2}\right| << \left|\omega\frac{\partial\boldsymbol{E}(z,t)}{\partial t}\right|. \tag{2.1.25}$$

Substituting Eqs. (2.1.22)–(2.1.24) into Eq. (2.1.19), using the slowly varying amplitude approximation condition of Eq. (2.1.25), omitting the items with second-order differential coefficients for the space and time, and using $k = (\omega/c)n$ and $v = c/n$, therefore, we obtain the following Eq. [3]:

$$\frac{\partial\boldsymbol{E}(z,t)}{\partial z} + \frac{1}{v}\frac{\partial\boldsymbol{E}(z,t)}{\partial t} = \frac{i\omega}{2\varepsilon_0 cn}\boldsymbol{P}_{NL}(z,t)e^{i\Delta kz}, \tag{2.1.26}$$

where $\Delta k = k' - k$, k and k' are the wave vectors of original light field and polarization field, respectively. Equation (2.1.26) is the time-domain wave equation when the monochromic plane light wave propagates in non-absorption and isotopic nonlinear medium, and the optical field strength $\boldsymbol{E}(z,t)$ satisfies the space and time slowly varying amplitude approximation condition. If the light wave is a continuous wave, or a light pulse with a wide pulse width, in Eq. (2.1.26) $v = c/n$ is the phase velocity of light wave; if the light wave is a short pulse (for example is a picosecond pulse), it is not a monochromic wave, we can regard as a wave packet, the form of time-domain nonlinear wave equation is same as Eq. (2.1.26), in which optical field amplitude $\boldsymbol{E}(z,t)$ should express as an integral of time. In this case, the group velocity of wave pocket should denoted by $v = d\omega/dk$.

2.1.4 Frequency-Domain Wave Equation in Anisotropic Nonlinear Medium

The anisotropic-medium time-domain nonlinear wave Eq. (2.1.18) can be changed to frequency-domain formation. For this purpose we should pass through Fourier transform, to spread $\boldsymbol{E}(\boldsymbol{r},t)$ and $\boldsymbol{P}_{NL}(\boldsymbol{r},t)$ into the sum of multiple monochromic plane waves, and write each monochromic wave to be the product of amplitude and phase two factors, then we have

$$\boldsymbol{E}(\boldsymbol{r},t)=\sum_i \boldsymbol{E}_i(\mathbf{k}_i,\omega_i)=\sum_i \boldsymbol{E}_i e^{\mathrm{i}(\mathbf{k}_i\boldsymbol{r}-\omega_i t)}, \tag{2.1.27}$$

$$\begin{aligned}\boldsymbol{P}_{NL}(\boldsymbol{r},t)&=\sum_{n\geq 2}\boldsymbol{P}^{(n)}(\boldsymbol{r},t)=\sum_{n\geq 2}\sum_i \boldsymbol{P}_i^{(n)}(\boldsymbol{k}_i',\omega_i)\\&=\sum_i \boldsymbol{P}_i^{NL}(\boldsymbol{k}_i',\omega_i)=\sum_i \boldsymbol{P}_i^{NL}(\boldsymbol{k}_i',\omega_i)e^{\mathrm{i}(\boldsymbol{k}_i'\boldsymbol{r}-\omega_i t)},\end{aligned} \tag{2.1.28}$$

where ω is the angular frequency of light wave, $\boldsymbol{k}$ and $\boldsymbol{k}'$ are wave vectors of the light field and the polarization field of the monochromic plane wave, respectively. To substitute Eqs. (2.1.27) and (2.1.28) into Eq. (2.1.18), and omit the summation mark and ordinal number i, we can obtain

$$[\nabla\times(\nabla\times)-\frac{\omega^2}{\varepsilon_0 c^2}\boldsymbol{\varepsilon}\cdot]\boldsymbol{E}(\boldsymbol{k},\omega)=\frac{\omega^2}{\varepsilon_0 c^2}\boldsymbol{P}_{NL}(\boldsymbol{k}',\omega). \tag{2.1.29}$$

This is the frequency-domain wave equation for the monochromic plane wave propagating in a non-absorption anisotropic nonlinear medium.

2.1.5 Frequency-Domain Wave Equation in Isotopic Nonlinear Medium

Assuming that the medium is isotopic and homogeneous; $\boldsymbol{E}(\boldsymbol{k},\omega)$ is denoted the light field strength of the monochromic plane wave, which is a transverse wave, i.e., the component paralleled to $\boldsymbol{K}$ can be neglected, so that in wave Eq. (2.1.29) $\nabla\cdot\boldsymbol{E}=0$, and $\nabla\times\nabla\times\boldsymbol{E}=-\nabla^2\boldsymbol{E}$, the tensor $\boldsymbol{\varepsilon}$ can be written to the scalar $\boldsymbol{\varepsilon}$, further using the relations $k=k_0 n$, $k_0=\omega/c$ and $n=\sqrt{\varepsilon/\varepsilon_0}$, then we obtain

$$\nabla^2\boldsymbol{E}(\boldsymbol{k},\omega)+k^2\boldsymbol{E}(\boldsymbol{k},\omega)=-\frac{k_0^2}{\varepsilon_0}\boldsymbol{P}_{NL}(\boldsymbol{k}',\omega). \tag{2.1.30}$$

This is frequency-domain wave equation for the monochromic plane wave propagating in a non-absorption isotopic nonlinear medium. This is an

inhomogeneous second-order differential equation, it is difficult to directly solve. We can take a simplified deal with by using the slowly varying amplitude approximate method as follows.

Considering that the monochrome plane wave propagates along z-direction, its amplitude varies with z, but no change with time. The light field strength and nonlinear polarization are respectively denoted by

$$\boldsymbol{E}(\boldsymbol{k},\ \omega) = \boldsymbol{E}(z,\ \omega)e^{\mathrm{i}(kz-\omega t)}, \tag{2.1.31}$$

$$\boldsymbol{P}_{NL}(\boldsymbol{k},\omega) = \boldsymbol{P}_{NL}(z,\ \omega)e^{i(k\prime z-\omega t)}. \tag{2.1.32}$$

where $\boldsymbol{k}$ and $\boldsymbol{k}'$ are wave vectors of the original light field and polarization field respectively. $\boldsymbol{E}(z,\ \omega)$ and $\boldsymbol{P}_{NL}(z,\ \omega)$ denote the field amplitudes and nonlinear polarization respectively. Substituting Eqs. (2.1.31) and (2.1.32) into Equation (2.1.30), the first item of left of Eq. (2.1.30) is

$$\nabla^2\boldsymbol{E}(z,\omega) = \left(\frac{\partial^2}{\partial z^2} + i2k\frac{\partial}{\partial z} - k^2\right)\boldsymbol{E}(z,\ \omega)e^{i(kz-\omega t)}. \tag{2.1.33}$$

So the items containing coefficient k^2 in Eq. (2.1.30) can be eliminated, Eq. (2.1.30) becomes

$$\left(\frac{\partial^2}{\partial z^2} + i2k\frac{\partial}{\partial z}\right)\boldsymbol{E}(z,\omega)e^{i(kz-\omega t)} = -\frac{k_0^2}{\varepsilon_0}\boldsymbol{P}_{NL}(z,\ \omega)(z)e^{i(k'z-\omega t)}. \tag{2.1.34}$$

Suppose that the light field strength satisfies the space slowly varying field amplitude approximation condition:

$$\left|\frac{\partial^2\boldsymbol{E}(z,\omega)}{\partial z^2}\right| << \left|k\frac{\partial\boldsymbol{E}(z,\omega)}{\partial z}\right|, \tag{2.1.35}$$

the items having second derivative of light field strength in Eq. (2.1.34) can be omitted, and to combine the exponent factors in both side of equation, Eq. (2.1.34) can be written to

$$\frac{\partial\boldsymbol{E}(z,\omega)}{\partial z} = \frac{ik_0^2}{2\varepsilon_0 k}\boldsymbol{P}_{NL}(z,\omega)e^{\mathrm{i}\Delta kz}, \tag{2.1.36}$$

where

$$\Delta k = k' - k, \tag{2.1.37}$$

where $\boldsymbol{k}$ and k' are wave vectors of the original light field and the polarization field, respectively.

Because $k = (\omega/c)n$ and $k_0 = \omega/c$, then Eq. (2.1.36) also can be expressed as

$$\frac{\partial \boldsymbol{E}(z,\omega)}{\partial z} = \frac{i\omega}{2\varepsilon_0 cn}\boldsymbol{P}_{NL}(z,\omega)e^{i\Delta kz}. \tag{2.1.38}$$

Equation (2.1.38) is a frequency-domain wave equation for a monochromic plane light wave propagating along z-direction in the isotopic, uniform and lossless nonlinear medium under the condition of slowly varying amplitude approximation. It is a first-order differential equation, relatively easy to be solved. If know the nonlinear polarization $\boldsymbol{P}_{NL}(z,\omega)$, we can obtain the solution of light field strength $\boldsymbol{E}(z,\omega)$. In this book, all of the investigative nonlinear optical processes will describe and explain by using this simple first-order differential equation.

Firstly, using the nonlinear coupling wave equations we can solve the multi-wave mixing nonlinear optical problem. Generally speaking, for n-order nonlinear polarization effect, we can list $n+1$ nonlinear coupling wave Equations similar to Eq. (2.1.38), simultaneous solving these $n+1$ equations, we can find the $n+1$ light field strengths with different frequency, thus obtain the law of energy mutual transformation among these light fields.

For example, for the second-order nonlinear optical effect, there are 2 original light fields at two different frequencies and 1 new generated polarization field, it requires 3 coupling wave equations, we can simultaneous solve these 3 coupling wave equations to obtain the 3 field strengths; For the third-order nonlinear optical effect, there are 3 original light fields and 1 new generated polarization field, it requires 4 coupling equations, then we can simultaneous solve out the 4 field strengths.

If existing absorption in the medium, according to Eq. (2.1.17), $\sigma \neq 0$, we can obtain the slowly varying amplitude approximation frequency-domain wave equation considering the absorption for the propagation of the monochromatic light wave along z-direction:

$$\frac{\partial \boldsymbol{E}(z,\omega)}{\partial z} + \frac{\alpha}{2}\boldsymbol{E}(z,\omega) = \frac{i\omega}{2\varepsilon_0 cn}\boldsymbol{P}_{NL}(z,\omega)e^{i\Delta kz}, \tag{2.1.39}$$

where $\alpha = \mu_0 \sigma c/n$ is the linear absorption coefficient of medium.

2.2 Polarization and Susceptibility of Nonlinear Medium

2.2.1 Frequency-Domain Expressions of Polarization and Susceptibility

1. **Frequency-Domain Expressions in Anisotropic Medium**

Under the action of light field, the polarization phenomenon is generated in an anisotropic medium. What is relationship between the polarization $\boldsymbol{P}$ and the light

electric field strength $\boldsymbol{E}$? At first, we are going to investigate the causal relationship in time between $\boldsymbol{P}$ and $\boldsymbol{E}$ [4], and then discuss the frequency-domain expressions of polarization $\boldsymbol{P}$ and susceptibility $\boldsymbol{\chi}$ in the case of the linear optics and different order nonlinear optics phenomena.

(1) **In Linear Polarization Case**

The induced electric polarization of medium $d\boldsymbol{P}^{(1)}(t)$ at the moment t is generated by the light electric filed strength $\boldsymbol{E}(t_1)$ before the moment $t_1 = t - dt_1$, $d\boldsymbol{P}^{(1)}(t)$ and $\boldsymbol{E}(t_1)$ has the following direct-ratio relation in the time interval dt_1:

$$d\boldsymbol{P}^{(1)}(t) = \varepsilon_0 \boldsymbol{\chi}^{(1)}(t - t_1) \cdot \boldsymbol{E}(t_1) dt_1. \tag{2.2.1}$$

Considering the contribution of $\boldsymbol{E}(t_1)$ to $\boldsymbol{P}^{(1)}(t)$ in all time before the moment t, we have

$$\boldsymbol{P}^{(1)}(t) = \int_{-\infty}^{\infty} \varepsilon_0 \boldsymbol{\chi}^{(1)}(t - t_1) \cdot \boldsymbol{E}(t_1) dt_1. \tag{2.2.2}$$

Actual, when $t_1 < t$, $\boldsymbol{E}(t_1)$ has no contribution to $\boldsymbol{P}^{(1)}(t)$, i.e., $\boldsymbol{\chi}^{(1)}(t - t_1) = 0$.

In order to further get the relationship between $\boldsymbol{P}$ and $\boldsymbol{E}$ in the frequency-domain, we take the Fourier transform of $\boldsymbol{E}(t_1)$ and $\boldsymbol{P}^{(1)}(t)$, i.e.,

$$\boldsymbol{E}(t_1) = \int_{-\infty}^{\infty} \boldsymbol{E}(\omega) e^{-i\omega t_1} d\omega, \tag{2.2.3}$$

$$\boldsymbol{P}^{(1)}(t) = \int_{-\infty}^{\infty} \boldsymbol{P}(\omega)^{(1)} e^{-i\omega t} d\omega. \tag{2.2.4}$$

To substitute Eqs. (2.2.3) and (2.2.4) into Eq. (2.2.2), and eliminate the integral sign, we obtain the frequency-domain expression:

$$\boldsymbol{P}^{(1)}(\omega) = \varepsilon_0 \boldsymbol{\chi}^{(1)}(\omega) \cdot \boldsymbol{E}(\omega), \tag{2.2.5}$$

where

$$\boldsymbol{\chi}^{(1)}(\omega) = \int_{-\infty}^{\infty} \boldsymbol{\chi}^{(1)}(t - t_1) e^{i\omega(\mathrm{t}-\mathrm{t}_1)} dt_1. \tag{2.2.6}$$

where $\boldsymbol{\chi}^{(1)}(\omega)$ is a linear polarization tensor, it is a second-order tensor with 9 tensor elements, that is

$$\boldsymbol{\chi}^{(1)}(\omega) = \begin{bmatrix} \chi_{11}^{(1)}(\omega) & \chi_{12}^{(1)}(\omega) & \chi_{13}^{(1)}(\omega) \\ \chi_{21}^{(1)}(\omega) & \chi_{22}^{(1)}(\omega) & \chi_{23}^{(1)}(\omega) \\ \chi_{31}^{(1)}(\omega) & \chi_{32}^{(1)}(\omega) & \chi_{33}^{(1)}(\omega) \end{bmatrix}. \tag{2.2.7}$$

In the rectangular coordinate system, the every element of linear polarization tensor can be expressed by its index, i.e.,

$$\boldsymbol{\chi}^{(1)}(\omega) = \begin{bmatrix} XX & XY & XZ \\ YX & YY & YZ \\ ZX & ZY & ZZ \end{bmatrix}. \tag{2.2.8}$$

(2) **In Nonlinear Polarization Case**

As mention in the previous section, the polarization $\boldsymbol{P}$ can spread as the power series of $\boldsymbol{E}$, in the frequency domain the $\boldsymbol{P}$ can be expressed as

$$\boldsymbol{P}(\omega) = \boldsymbol{P}^{(\mathbf{1})}(\omega) + \boldsymbol{P}^{(\mathbf{2})}(\omega) + \boldsymbol{P}^{(\mathbf{3})}(\omega) + \cdots. \tag{2.2.9}$$

Similar to Eqs. (2.2.5) and (2.2.6), the second-order nonlinear polarization and the second-order nonlinear susceptibility can be expressed as

$$\boldsymbol{P}^{(2)}(\omega) = \varepsilon_0 \boldsymbol{\chi}^{(2)}(\omega; \omega_1, \omega_2) : \boldsymbol{E}(\omega_1)\boldsymbol{E}(\omega_2), \tag{2.2.10}$$

$$\boldsymbol{\chi}^{(2)}(\omega) = \int_{-\infty}^{\infty} \boldsymbol{\chi}^{(2)}(t - t_1, t - t_2) e^{i[\omega_1(t-t_1) + \omega_2(t-t_2)]} dt_1 dt_2. \tag{2.2.11}$$

$\boldsymbol{\chi}^{(2)}$ is called second-order polarization tensor, it is a third-order tensor with 27 tensor elements:

$$\boldsymbol{\chi}^{(2)}(\omega) = \begin{bmatrix} XXX & XYY & XZZ & XYZ & XZY & XZX & XXZ & XXY & XYZ \\ YXX & YYY & YZZ & YYZ & YZY & YZX & YXZ & YXY & YYZ \\ ZXX & ZYY & ZZZ & ZYZ & ZZY & ZZX & ZXZ & ZXY & ZYZ \end{bmatrix}. \tag{2.2.12}$$

In a similar way, the third-order nonlinear polarization and the third-order nonlinear susceptibility can be expressed as respectively

$$\boldsymbol{P}^{(3)}(\omega) = \varepsilon_0 \boldsymbol{\chi}^{(3)}(\omega; \omega_1, \omega_2, \omega_3) \vdots \boldsymbol{E}(\omega_1)\boldsymbol{E}(\omega_2)\boldsymbol{E}(\omega_3), \tag{2.2.13}$$

$$\boldsymbol{\chi}^{(3)}(\omega) = \int_{-\infty}^{\infty} \boldsymbol{\chi}^{(3)}(t-t_1, t-t_2, t-t_3) e^{i[\omega_1(t-t_1)+\omega_2(t-t_2)+\omega_3(t-t_3)]} dt_1 dt_2 dt_3. \tag{2.2.14}$$

$\boldsymbol{\chi}^{(3)}$ is called third-order polarization tensor, it is a four-order tensor with 81 tensor elements.

In the similar way, n-order nonlinear polarization and n-order nonlinear susceptibility can be expressed as

$$\boldsymbol{P}^{(n)}(\omega) = \varepsilon_0 \boldsymbol{\chi}^{(n)}(\omega; \omega_1, \omega_2, \ldots, \omega_n) \vdots \boldsymbol{E}(\omega_1)\boldsymbol{E}(\omega_2), \ldots, \boldsymbol{E}(\omega_n), \tag{2.2.15}$$

where $\boldsymbol{\chi}^{(n)}$ is a n+1-order tensor, sign of "$\vdots$" is denoted the multiplication of n +1-order tensor.

$$\boldsymbol{\chi}^{(n)}(\omega) = \int_{-\infty}^{\infty} \boldsymbol{\chi}^{(n)}(t-t_1, t-t_2, \ldots, t - t_n) e^{i[\omega_1(t-t_1)+\omega_2(t-t_2)+\ldots+\omega_n(t-t_n)]} dt_1 dt_2 \ldots dt_n. \tag{2.2.16}$$

It is worth noting that in the bracket of above every order susceptibility is inserted a semicolon, according to the regulation of this book, after the semicolon are original light fields at the frequencies of $\omega_1, \omega_2, \ldots, \omega_n$; before the semicolon is the polarization field at the frequency of ω. According to the energy conservation law, the frequency of polarization field is the sum of frequencies of all original fields:

$$\omega = \omega_1 + \omega_2 + \cdots + \omega_n. \tag{2.2.17}$$

2. **Rectangular Coordinate Frequency-Domain Expressions in Anisotropic Medium**

Below we provide the frequency-domain expressions by rectangular coordinate component for each order polarizations in anisotropic medium. The polarization-filed frequency ω is a sum of the original-field frequencies, $\omega = \omega_1 + \omega_2 + \omega_3 + \cdots$.

$$P_\mu^{(1)}(\omega) = \sum_\alpha \varepsilon_0 \chi_{\mu\alpha}^{(1)}(\omega; \omega) E_\alpha(\omega), \tag{2.2.17}$$

$$P_\mu^{(2)}(\omega) = \sum_{\alpha\beta} \varepsilon_0 \chi_{\mu\alpha\beta}^{(2)}(\omega; \omega_1, \omega_2) E_\alpha(\omega_1) E_\beta(\omega_2), \tag{2.2.18}$$

$$P_{\mu}^{(3)}(\omega) = \sum_{\alpha\beta\gamma} \varepsilon_0 \chi_{\mu\alpha\beta\gamma}^{(3)}(\omega; \omega_1, \omega_2, \omega_3) E_{\alpha}(\omega_1) E_{\beta}(\omega_2) E_{\gamma}(\omega_3), \tag{2.2.19}$$

$$P_{\mu}^{(n)}(\omega) = \sum_{\alpha\beta\gamma} \varepsilon_0 \chi_{\mu\alpha\beta\gamma}^{(n)}(\omega; \omega_1, \omega_2, \ldots, \omega_n) E_{\alpha}(\omega_1) E_{\beta}(\omega_2) \ldots E_{\gamma}(\omega_n), \tag{2.2.20}$$

式中 $\mu, \alpha, \beta, \gamma, \ldots = x, y, z$.

3. **Frequency-Domain Expressions in Isotopic Medium**

For uniform isotopic nonlinear medium, the light field strength $\boldsymbol{E}(\omega)$ and the polarization $\boldsymbol{P}(\omega)$ are complex number vectors, and the susceptibility $\boldsymbol{\chi}$ is a complex number scalar. The each-order polarization can be expressed as follows.

Linear polarization:

$$\boldsymbol{P}^{(1)}(\omega) = \varepsilon_0 \boldsymbol{\chi}^{(1)}(\omega; \omega) \boldsymbol{E}(\omega). \tag{2.1.21}$$

Second-order nonlinear polarization:

$$\boldsymbol{P}^{(2)}(\omega) = \varepsilon_0 \boldsymbol{\chi}^{(2)}(\omega; \omega_1, \omega_2) \boldsymbol{E}(\omega_1) \boldsymbol{E}(\omega_2). \tag{2.1.22}$$

Third-order nonlinear polarization:

$$\boldsymbol{P}^{(3)}(\omega) = \varepsilon_0 \boldsymbol{\chi}^{(3)}(\omega; \omega_1, \omega_2, \cdots \omega_3) \boldsymbol{E}(\omega_1) \boldsymbol{E}(\omega_2) \boldsymbol{E}(\omega_3). \tag{2.1.23}$$

The n-order nonlinear polarization:

$$\boldsymbol{P}^{(n)}(\omega) = \varepsilon_0 \boldsymbol{\chi}^{(n)}(\omega; \omega_1, \omega_2, \ldots, \omega_n) \boldsymbol{E}(\omega_1) \boldsymbol{E}(\omega_2) \ldots \boldsymbol{E}(\omega_n). \tag{2.1.24}$$

When you write the the expressions of polarization, you should determine the frequences of each light field participated in the designated nonlinear optical process and write out correct susceptibility expressions. If in the incident light electric fields having conjugate complex number of field, we should add a minus sign in the front of corresponding frequency inside the bracket of susceptibility.

2.2.2 Degeneration Factor of Polarization

Assuming the incident light field is consisted by a series monochromic plane waves at frequencies $\omega_1, \omega_2, \cdots \omega_n$. The electric field strength of each monochromic plane wave at frequency $\omega_i (i = 1, 2, 3 \cdots)$ is a complex number, in general it can be written to a sum of complex number and its conjugate complex number (c.c). Therefore the total incident light electric field strength $\boldsymbol{E}(\boldsymbol{r}, t)$ can be expressed as

$$\boldsymbol{E}(\boldsymbol{r},t) = \sum_{\mathrm{i}} \boldsymbol{E}(\omega_{\mathrm{i}}) e^{-i(\omega_{\mathrm{i}} t - \boldsymbol{k}_i \cdot \boldsymbol{r})} + c.c.. \tag{2.2.25}$$

The n-order polarization at the frequency of $\omega = \omega_1 + \omega_2 + \cdots + \omega_n$ is induced by n original light fields at frequencies of $\omega_1, \omega_2, \cdots, \omega_n$. Actually, the original light fields may include several light fields at the same frequency, i.e., existing the frequency degeneracy. Because the frequency degeneracy and the symmetry of susceptibility, in the rectangular coordinate component expression for the anisotropic nonlinear medium should add a coefficient D, which is called degeneration factor, so the rectangular coordinate component expression of n-order polarization is given by

$$P_{\mu}^{(n)}(\omega) = D \sum_{\alpha\beta\cdots\gamma} \varepsilon_0 \boldsymbol{\chi}_{\mu\alpha\beta\cdots\gamma}^{(n)}(\omega; \omega_1, \omega_2, \omega_3, \cdots, \omega_n) E_{\alpha}(\omega_1) E_{\beta}(\omega_2) \cdots E_{\gamma}(\omega_n), \tag{2.2.26}$$

For the isotopic nonlinear medium, if all the light fields propagate along the z-direction, the n-order polarization expression in the frequency degeneracy case also need add the degeneration factor, namely

$$\boldsymbol{P}^{(n)}(z,\omega) = D\varepsilon_0 \boldsymbol{\chi}^{(n)}(\omega; \omega_1, \omega_2, \ldots, \omega_n) \boldsymbol{E}(z,\omega_1) \boldsymbol{E}(z,\omega_2) \ldots \boldsymbol{E}(z,\omega_n), \tag{2.2.27}$$

It can be proved that, if the light field strength is expressed as Eq. (2.2.25), the formula of degeneration factor is given by [5]

$$D = \frac{n!}{m!}, \tag{2.2.28}$$

where n is the order number of nonlinear polarization, m is the frequency degenerate number of original light fields. In this book the light field strength is all expressed as Eq. (2.2.25), so the Eq. (2.2.28) is used to calculate the degeneration factor in this book.

In some literature, considering the relation $\boldsymbol{E}(t) = \boldsymbol{E}_0 \cos \omega t = \frac{1}{2}\boldsymbol{E}_0(e^{\mathrm{i}\omega t} + e^{-\mathrm{i}\omega t})$, the light field strength is expressed as

$$\boldsymbol{E}(\boldsymbol{r},t) = \frac{1}{2} \sum_{\mathrm{i}} \boldsymbol{E}(\omega_{\mathrm{i}}) e^{-i(\omega_{\mathrm{i}} t - \boldsymbol{k}_i \cdot \boldsymbol{r})} + c.c. \tag{2.2.29}$$

It can be proved that in this case the formula of degeneration factor should be written to

$$D = 2^{1-n} \left(\frac{n!}{m!} \right). \tag{2.2.30}$$

Same as above, here n is the order number of nonlinear polarization, m is the frequency degenerate number of original light fields.

Table 2.1 list the susceptibility expressions and corresponding two kinds of degeneration factors for various nonlineal optical effects. In the susceptibility expressions, after the semicolon are the frequencies of the incident (original) light fields, $\omega_1, \omega_2, \cdots, \omega_n$; before the semicolon is the frequency of the generated (polarization) field $\omega = \omega_1 + \omega_2 + \cdots + \omega_n$, the negative frequency delegates that its light field is a conjugate complex of the light field at positive frequency.

Table 2.1 Susceptibility expressions and two kinds of degeneration factors for nonlineal optical effects

Nonlinear optical process	Order (n)	Susceptibility	$D = n!/m!$	$D = 2^{1-n}(n!/m!)$
Linear absorption	1	$\chi^{(1)}(\omega;\omega)$	1	1
Linear refraction	1	$\chi^{(1)}(\omega;\omega)$	1	1
Electrooptical effect	2	$\chi^{(2)}(\omega;\omega,0)$	2	1
Frequency doubling effect	2	$\chi^{(2)}(2\omega;\omega,\omega)$	1	1/2
Sum frequency effect	2	$\chi^{(2)}(\omega_3;\omega_1,\omega_2)$	2	1
Difference frequency effect	2	$\chi^{(2)}(\omega_2;\omega_3,-\omega_1)$	2	1
Triple frequency harmonic	3	$\chi^{(3)}(3\omega;\omega,\omega,\omega)$	1	1/4
Single-photon nonlinear refraction	3	$\chi^{(3)}(\omega;\omega,-\omega,\omega)$	3	3/4
Single-photon nonlinear absorption	3	$\chi^{(3)}(\omega;\omega,-\omega,\omega)$	3	3/4
Two-photon nonlinear absorption	3	$\chi^{(3)}(\omega_1;\omega_2,-\omega_2,\omega_1)$	6	3/2
Self-phase modulation optical Kerr effect	3	$\chi^{(3)}(\omega;\omega,-\omega,\omega)$	3	3/4
Cross-phase modulation optical Kerr effect	3	$\chi^{(3)}(\omega;\omega_{\mathrm{p}},-\omega_p,\omega)$	6	3/2
Four wave mixing	3	$\chi^{(3)}(\omega_4;\omega_1,\omega_2,\omega_3)$	6	3/2
Degenerate four wave mixing	3	$\chi^{(3)}(\omega;\omega,-\omega,\omega)$	3	3/4
Degenerate four wave mixing back phase conjugation	3	$\chi^{(3)}(\omega_c;\omega_1,-\omega_2,\omega_p)$	6	3/2
Degenerate four wave mixing forward phase conjugation	3	$\chi^{(3)}(\omega_c;\omega_1,\omega_2,-\omega_p)$	6	3/2
Stoks stimulated Raman scattering	3	$\chi^{(3)}(\omega_{\mathrm{s}};\omega_{\mathrm{p}},-\omega_p,\omega_s)$	6	3/2
Anti-stoks stimulated Raman scattering	3	$\chi^{(3)}(\omega_{as};\omega_p,\omega_p,-\omega_s)$	3	3/4

2.2.3 Symmetry of Susceptibility Tensor

There are some universal symmetric relationships among tensor elements of nonlinear susceptibility tensor. These symmetric relationships reflect the real-number character of polarization and the symmetry of medium structure. If you want to know the certification of these symmetries in detail, you can refer to relater reference materials [4, 6–8]. Here we just give a brief introduction.

1. **Authenticity Condition**

Linear susceptibility tensor of medium can be expressed as the form of Eq. (2.2.6):

$$\boldsymbol{\chi}^{(1)}(\omega) = \int_{-\infty}^{\infty} \boldsymbol{\chi}^{(1)}(t - t_1) e^{i\omega(t-t_1)} dt_1.$$

Taking its conjugate complex number, we obtain

$$\boldsymbol{\chi}^{(1)*}(\omega) = \int_{-\infty}^{\infty} \boldsymbol{\chi}^{(1)}(t - t_1) e^{-i\omega(\mathrm{t}-\mathrm{t}_1)} dt_1 = \boldsymbol{\chi}^{(1)}(-\omega). \tag{2.2.31}$$

In a similar way, we can prove that the tensor elements of each-order nonlinear susceptibility have following characteristics:

$$\boldsymbol{\chi}_{ijk}^{(2)*}(\omega; \omega_1, \omega_2) = \boldsymbol{\chi}_{jki}^{(2)}(\omega_1; -\omega_2, \omega) = \boldsymbol{\chi}_{kji}^{(2)}(\omega_2; -\omega_1, \omega), \tag{2.2.32}$$

$$\begin{aligned} \boldsymbol{\chi}_{ijkl}^{(3)*}(\omega; \omega_1, \omega_2, \omega_3) &= \boldsymbol{\chi}_{jkli}^{(3)}(\omega_1; -\omega_2, -\omega_3, \omega) \\ &= \boldsymbol{\chi}_{kijl}^{(3)}(\omega_2; \omega, -\omega_1, -\omega_3) \\ &= \boldsymbol{\chi}_{lijk}^{(3)}(\omega_3; \omega, -\omega_1, -\omega_2), \\ &\ldots\ldots \end{aligned} \tag{2.2.33}$$

Above relationships guarantee the characteristics that the each susceptibility is a real number, so it is called the authenticity condition. If the frequency of original optical field is far from the resonance frequency of medium, the medium is know as non-dispersion and lossless, we can remove out the symbol of conjugate complex number "$*$" in Eqs. (2.2.32)–(2.2.33).

1. **Symmetry of Intrinsic Substitution**

It can be proved that susceptibility tensor has following intrinsic symmetry of frequency substitution: if do not change the location of polarization-field frequency, when the sequence of any two frequencies of original optical field mutually

interchanges, corresponding two tensor elements are same. For example, for second-order and third-order nonlinear effects we have:

$$\chi_{ijk}^{(2)}(\omega;\omega_m,\omega_n) = \chi_{ikj}^{(2)}(\omega;\omega_n,\omega_m), \tag{2.2.34}$$

$$\begin{aligned}\chi_{ijkl}^{(3)}(\omega;\omega_m,\omega_n,\omega_q) &= \chi_{ikjl}^{(3)}(\omega;\omega_n,\omega_m,\omega_q)\\ &= \chi_{ijlk}^{(3)}(\omega;\omega_m,\omega_q,\omega_n)\\ &= \chi_{ilkj}^{(3)}(\omega;\omega_q,\omega_n,\omega_m).\end{aligned} \tag{2.2.35}$$

2. **Symmetry of Complete Substitution**

If the frequency of original optical field far from the resonance frequency of medium, the medium is know as non-dispersion and lossless, there is the symmetry of complete substitution, i.e., the frequency of the polarization field can interchange place with any frequency of original field, for example, the second-order and the third-order nonlinear optical effects have:

$$\chi_{ijk}^{(2)}(\omega;\omega_m,\omega_n) = \chi_{jik}^{(2)}(\omega_m;\omega,\omega_n) = \chi_{kji}^{(2)}(\omega_n;\omega_m,\omega), \tag{2.2.36}$$

$$\begin{aligned}\chi_{ijkl}^{(3)}(\omega;\omega_m,\omega_n,\omega_q) &= \chi_{jikl}^{(3)}(\omega_m;\omega,\omega_n,\omega_q)\\ &= \chi_{kjil}^{(3)}(\omega_n;\omega_m,\omega,\omega_q)\\ &= \chi_{ljki}^{(3)}(\omega_q;\omega_m,\omega_n,\omega).\end{aligned} \tag{2.2.37}$$

In the above tensor elements of susceptibility, interchange the frequency in any order, the numerical value of tensor elements keeps no change; this feature is called complete-substitution symmetry.

3. **Time Reversion Symmetry**

According to the real number character of nonlinear polarization, it is can be proved that any tensor element possesses following characteristic:

$$\chi_{ll_1l_2\cdots l_n}^{(n)}(\omega;\omega_1,\omega_2,\ldots,\omega_n) = \chi_{ll_1l_2\cdots l_n}^{(n)}(-\omega;-\omega_1,-\omega_2,\ldots,-\omega_n). \tag{2.2.38}$$

4. **Spatial Structure Symmetry**

We mentioned previous, the susceptibility is a 3-D space tensor. In which $\boldsymbol{\chi}^{(1)}$ is a second-order tensor, with 9 tensor elements; $\boldsymbol{\chi}^{(2)}$ is a third-order tensor, with 27 tensor elements; $\boldsymbol{\chi}^{(3)}$ is a four-order tensor, with 81 tensor elements. Because the structure of nonlinear medium (such as nonlinear crystal) has symmetry (rotate symmetry and translation symmetry, etc.), it makes the part of tensor elements to be zero, and there exists specific relationships among some tensor elements, to lead

total number of independent tensor elements of nonlinear susceptibility tensor depletes.

According to the symmetry of the crystal, the crystal can be divided into 7 systems of crystallization: triclinic crystal system, monoclinic crystal system, orthorhombic crystal system, quadratic crystal system, trigonal crystal system, hexagonal crystal system, cubic crystal system (or isotopic medium). People already found the susceptibility tensor form of these 7 crystal systems and their 32 crystal classes. Visible, the symmetry is higher; the number of the non-zero tensor element and independent tensor element is less.

For example, for second-order tensor $\boldsymbol{\chi}^{(1)}$, its orthorhombic crystal system and cubic crystal system (or isotopic medium) only have 3 and 1 independent tensor element respectively:

$$\boldsymbol{\chi}^{(1)}(\omega) = \begin{bmatrix} XX & 0 & 0 \\ 0 & YY & 0 \\ 0 & 0 & ZZ \end{bmatrix}, \qquad \boldsymbol{\chi}^{(1)}(\omega) = \begin{bmatrix} XX & 0 & 0 \\ 0 & XX & 0 \\ 0 & 0 & XX \end{bmatrix}.$$

Orthorhombic crystal system Cubic crystal system and isotopic medium

For another example, for third-order tensor $\boldsymbol{\chi}^{(2)}$, its crystal class 222 (D_2) of orthorhombic crystal system and crystal class $\overline{4}3m$ (T_d) of cubic crystal system, they only have 6 and 1 independent tensor element respectively:

$$\boldsymbol{\chi}^{(2)}(\omega) = \begin{bmatrix} 0 & 0 & 0 & \mathrm{XYZ} & \mathrm{XZY} & 0 & 0 & 0 & 0 \\ 0 & 0 & 0 & 0 & 0 & YZX & YXZ & 0 & 0 \\ 0 & 0 & 0 & 0 & 0 & 0 & 0 & ZXY & ZYZ \end{bmatrix}$$

Crystal class 222 (D_2) of orthorhombic crystal system

$$\boldsymbol{\chi}^{(2)}(\omega) = \begin{bmatrix} 0 & 0 & 0 & XYZ & XYZ & 0 & 0 & 0 & 0 \\ 0 & 0 & 0 & 0 & 0 & XYZ & XYZ & 0 & 0 \\ 0 & 0 & 0 & 0 & 0 & 0 & 0 & XYZ & XYZ \end{bmatrix}$$

Crystal class $\overline{4}3m$ (T_d) of cubic crystal system

Now we study the characteristics of susceptibility of the medium with centre (inversion) symmetry, So called centre symmetry, it is $\boldsymbol{P}$ and $\boldsymbol{E}$ should change to revers direction under inverse conversion of coordinate $\{x, y, z\} \to \{-x, -y, -z\}$ to keep the formula of polarization invariability. That is to say, for the following general formula of n-order polarization:

$$\boldsymbol{P}^{(n)}(\omega) = \varepsilon_0 \boldsymbol{\chi}^{(n)}(\omega; \omega_1, \omega_2, \ldots, \omega_n) \vdots \boldsymbol{E}(\omega_1)\boldsymbol{E}(\omega_2)\ldots\boldsymbol{E}(\omega_n), \tag{2.2.39}$$

when making conversion of coordinates $\{x, y, z\} \to \{-x, -y, -z\}$, in left side of formula the vector $\boldsymbol{P}$ becomes $-\boldsymbol{P}$, and in the right side of formula every vector $\boldsymbol{E}$ becomes $-\boldsymbol{E}$, so the Eq. (2.2.39) becomes

$$\boldsymbol{P}'^{(n)}(\omega) = (-1)^{n+1}[\varepsilon_0 \boldsymbol{\chi}'^{(n)}(\omega; \omega_1, \omega_2, \ldots, \omega_n) \vdots \boldsymbol{E}'(\omega_1)\boldsymbol{E}'(\omega_2)\ldots\boldsymbol{E}'(\omega_n)]. \tag{2.2.40}$$

In order to maintain the form of Eq. (2.2.40) same as that of Eq. (2.2.39), we should require that when $n = 2, 4, \ldots$ (even number), $\boldsymbol{P}'^{(n)} = 0$, i.e., $\boldsymbol{\chi}'^{(n)}(\omega; \omega_1, \omega_2, \ldots, \omega_n) = 0$. Namely even-order susceptibility is zero for the medium with centre symmetry. If we only consider the nonlinear effect up to third-order, for the medium with centre symmetry, it is nonexistence of second-order nonlinear effect, only existence of third-order nonlinear effect.

2.3 Real Part and Imaginary Part of Susceptibility

2.3.1 Relation Between Real Part and Imaginary Part of Susceptibility (K–K Relation)

The susceptibility $\chi(\omega)$ is a function of frequency, in general it is a complex number, can be expressed as

$$\chi(\omega) = \chi'(\omega) + i\chi''(\omega). \tag{2.3.1}$$

Between the real part and the imaginary part of linear susceptibility has following relationships (the derivation of the formula see Appendix 2.A):

$$\chi'(\omega) = \frac{1}{\pi} P.V. \int_{-\infty}^{\infty} \frac{\chi''(\omega')}{\omega' - \omega} d\omega', \tag{2.3.2}$$

$$\chi''(\omega) = -\frac{1}{\pi} P.V. \int_{-\infty}^{\infty} \frac{\chi'(\omega')}{\omega' - \omega} d\omega', \tag{2.3.3}$$

The integral in Eqs. (2.3.2) and (2.3.3) is Cauchy's principle value integral, namely when integral removing the singular point $\omega' = \omega$. Equations (2.3.2) and (2.3.3) are famous *Kramers-Kronig* dispersion relation, in short K–K relation [9, 10]. From K–K relation we can see that as long as know any one of the real part and the imaginary part of the susceptibility as a function of frequency, we can through above relationship to find out another one.

According to the substitution symmetry of susceptibility $\chi(-\omega) = \chi^*(\omega)$ and Eq. (2.3.1), we can rewrite the K–K relation to be:

$$\chi'(\omega) = \frac{2}{\pi} P.V. \int_0^\infty \frac{\omega' \chi''(\omega')}{\omega'^2 - \omega^2} d\omega'', \tag{2.3.4}$$

$$\chi''(\omega) = -\frac{2\omega}{\pi} P.V. \int_0^\infty \frac{\chi'(\omega')}{\omega'^2 - \omega^2} d\omega'. \tag{2.3.5}$$

Because integral just in positive frequency range, the K–K relations as form of Eqs. (2.3.4) and (2.3.5) are more accord with the physical significance.

K–K relation is derived from the linear susceptibility, for the linear optical system it is always correct, but only a part of processes in nonlinear optical system comply with K–K relation. For instance, second harmonic effect, third harmonic effect, four-wave mixing (except degenerate four-wave mixing), cross-phase modulation Kerr effect (except self-phase modulation Kerr effect) etc. (see Ref. [10]).

2.3.2 Physical Significance of Real Part and Imaginary Part of Susceptibility

1. **Relation of Linear Susceptibility with Linear Refractive Index and Linear Absorption Coefficient**

Now we investigate that a monochrome plane wave at frequency of ω propagates in an isotopic medium along z-direction to generate the polarization. Suppose the light field denoted by

$$\boldsymbol{E}(z, \omega) = \boldsymbol{E}(z) e^{\mathrm{i}(kz - \omega t)} + c.c., \tag{2.3.6}$$

where $\boldsymbol{k}$ is a complex number wave vector, its real part k' is related with the refractive index of medium; the imaginary part k'' is related with the absorption coefficient of medium, namely

$$k = k' + ik'' = k_0 n_0 + i\frac{\alpha_0}{2}, \tag{2.3.7}$$

where $k_0 = \omega/c$ is the wave vector in vacuum; n_0 and α_0 are linear refractive index and linear absorption of medium respectively (α_0 is absorption coefficient for light power, so it is divided by 2).

Considering the linear polarization effect in far from the resonance situation, using the definition of electric induction strength, we obtain

$$\boldsymbol{D} = \varepsilon_0 \boldsymbol{E} + \boldsymbol{P}^{(1)} = \varepsilon_0 \boldsymbol{E} + \varepsilon_0 \chi^{(1)}(\omega)\boldsymbol{E} = [\varepsilon_0 + \varepsilon_0 \chi^{(1)}(\omega)]\boldsymbol{E} = \varepsilon \boldsymbol{E}, \tag{2.3.8}$$

where ε_0 is the dielectric coefficient in vacuum; $\varepsilon = \varepsilon_0 + \varepsilon_0 \chi^{(1)}(\omega)$ is the complex linear dielectric coefficient of medium; $\chi^{(1)}(\omega)$ is complex linear susceptibility of medium, which can be divided into the real and the imaginary two parts: $\chi^{(1)}(\omega) = \chi^{(1)\prime}(\omega) + i\chi^{(1)\prime\prime}(\omega)$. Using relation $\varepsilon' = \varepsilon_0[1 + \chi^{(1)\prime}(\omega)]$, then $\boldsymbol{\varepsilon}$ can be expressed as

$$\varepsilon = \varepsilon_0 + \varepsilon_0 \chi^{(1)\prime}(\omega) + i\varepsilon_0 \chi^{(1)\prime\prime}(\omega) = \varepsilon' + i\varepsilon_0 \chi^{(1)\prime\prime}(\omega) = \varepsilon'[1 + i\frac{\varepsilon_0}{\varepsilon'}\chi^{(1)\prime\prime}(\omega)]. \tag{2.3.9}$$

To use the linear refractive index $n_0 = \sqrt{\varepsilon'/\varepsilon_0}$, Eq. (2.3.9) can be written as

$$\varepsilon = n_0^2 \varepsilon_0 [1 + i\frac{\chi^{(1)\prime\prime}(\omega)}{n_0^2}]. \tag{2.3.10}$$

Further use complex linear refractive index $n = \sqrt{\varepsilon/\varepsilon_0}$ and light velocity in vacuum $c = 1/\sqrt{\mu_0 \varepsilon_0}$, the complex wave vector of medium can be written as

$$k = \frac{\omega}{c} n = \omega\sqrt{\mu_0 \varepsilon}. \tag{2.3.11}$$

Substituting Eq. (2.3.10) into Eq. (2.3.11), we obtain

$$k = k_0 n_0 \left(1 + i\frac{\chi^{(1)\prime\prime}(\omega)}{n_0^2}\right)^{\frac{1}{2}}, \tag{2.3.12}$$

In the bracket of left of Eq. (2.3.12), the model of second item is much smaller than 1, so the bracket factor can be spread to Taylor's series, after that approximately taking front two items, we obtain

$$k \approx k_0 n_0 \left[1 + i\frac{\chi^{(1)\prime\prime}(\omega)}{2n_0^2}\right] = k_0 n_0 + i\frac{k_0}{2n_0}\chi^{(1)\prime\prime}(\omega). \tag{2.3.13}$$

To compare the Eq. (2.3.13) with Eq. (2.3.7), and use of $n_0 = \sqrt{\varepsilon'/\varepsilon_0}$ and $\varepsilon' = \varepsilon_0[1 + \chi^{(1)\prime}(\omega)]$, we obtain

$$n_0 = [1 + \chi^{(1)\prime}(\omega)]^{\frac{1}{2}} \approx 1 + \frac{1}{2}\chi^{(1)\prime}(\omega), \tag{2.3.14}$$

$$\alpha_0 = \frac{k_0}{n_0}\chi^{(1)\prime\prime}(\omega) = \frac{\omega}{cn_0}\chi^{(1)\prime\prime}(\omega). \tag{2.3.15}$$

We can see that, the linear reflective index and the linear absorption coefficient of the medium are linearly related with the real part and the imaginary part of first-order susceptibility, respectively.

2. **Relation of Third-Order Nonlinear Susceptibility with Nonlinear Refractive Index and Nonlinear Absorption Coefficient**

We suppose the medium is a third-order nonlinear medium; the input laser is monochromatic plane wave as expressed by Eq. (2.3.6), the light field $\boldsymbol{E}(z)$ can be solved by using the slowly varying amplitude approximation nonlinear wave Eq. (2.1.38). Here let $\Delta k = k' - k = 0$. Equation (2.1.38) becomes

$$\frac{\partial \boldsymbol{E}(z)}{\partial z} = \frac{i\omega}{2\varepsilon_0 cn_0}\boldsymbol{P}_{\mathrm{NL}}(z). \tag{2.3.16}$$

The third-order nonlinear polarization (for example, Kerr effect) can be expressed as

$$\boldsymbol{P}_{NL}(z) = \boldsymbol{P}^{(3)}(z) = 3\varepsilon_0\chi^{(3)}(\omega)|\boldsymbol{E}(z)|^2\boldsymbol{E}(z). \tag{2.3.17}$$

Using $\chi^{(3)} = \chi^{(3)\prime}(\omega) + i\chi^{(3)\prime\prime}(\omega)$, Eq. (2.3.17) becomes

$$\boldsymbol{P}_{\mathrm{NL}}(z) = 3\varepsilon_0[\chi^{(3)\prime}(\omega)|\boldsymbol{E}(z)|^2 + i\chi^{(3)\prime\prime}(\omega)|\boldsymbol{E}(z)|^2]\boldsymbol{E}(z). \tag{2.3.18}$$

Substituting Eq. (2.3.18) into Eq. (2.3.16), we obtain

$$\frac{\partial \boldsymbol{E}(z)}{\partial z} = \frac{i3\omega}{2cn_0}[\chi^{(3)\prime}(\omega)|\boldsymbol{E}(z)|^2 + i\chi^{(3)\prime\prime}(\omega)|\boldsymbol{E}(z)|^2]\boldsymbol{E}(z). \tag{2.3.19}$$

Using $I = \frac{1}{2}\varepsilon_0 cn_0|\boldsymbol{E}(z)|^2$, Eq. (2.3.19) becomes

$$\frac{\partial \boldsymbol{E}(z)}{\partial z} = i3\left[k_0\frac{\chi^{(3)\prime}(\omega)}{\varepsilon_0 cn_0^2}I + i\frac{\omega\chi^{(3)\prime\prime}(\omega)}{\varepsilon_0 c^2 n_0^2}I\right]\boldsymbol{E}(z). \tag{2.3.20}$$

Setting

$$k_{NL} = 3k_0\frac{\chi^{(3)\prime}(\omega)}{\varepsilon_0 cn_0^2}I + i3\frac{\omega\chi^{(3)\prime\prime}(\omega)}{\varepsilon_0 c^2 n_0^2}I, \tag{2.3.21}$$

Equation (2.3.20) becomes

$$\frac{\partial \boldsymbol{E}(z)}{\partial z} = ik_{NL}\boldsymbol{E}(z). \tag{2.3.22}$$

The solution of Eq. (2.3.22) is

$$\boldsymbol{E}(z) = \boldsymbol{E}(0)e^{ik_{NL}z}. \tag{2.3.23}$$

From the definition Eq. (2.3.6) of light field

$$\boldsymbol{E}(z,\omega) = \boldsymbol{E}(z)e^{i(kz-\omega t)} = \boldsymbol{E}(0)e^{ik_{NL}z}e^{i(kz-\omega t)} = \boldsymbol{E}(0)e^{ik_T z}e^{-i\omega t} \tag{2.3.24}$$

where $k_T = k + k_{NL}$ is the total wave vector, it is a complex number, can be divided into the real part and the imaginary part, the real part is corresponding to the total refractive index n; the imaginary part is corresponding to the total absorption α:

$$k_T = k_T' + ik_T'' = n + i\frac{\alpha}{2}. \tag{2.3.25}$$

The each of total refractive index and total absorption coefficient can be divided into linear and nonlinear two parts, namely

$$n = n_0 + \Delta n, \tag{2.3.26}$$

$$\alpha = \alpha_0 + \Delta\alpha. \tag{2.3.27}$$

Substituting Eqs. (2.3.26) and (2.3.27) into Eq. (2.3.25), we obtain

$$k_T = k_0 n_0 + k_0 \Delta n + i\frac{\alpha_0}{2} + i\frac{\Delta\alpha}{2}. \tag{2.3.28}$$

Using Eq. (2.3.21), the total wave vector can be written to the sum of linear and nonlinear two parts:

$$k_T = k + k_{NL} = k_0 n_0 + i\frac{\alpha_0}{2} + 3k_0\frac{\chi^{(3)\prime}(\omega)}{\varepsilon_0 c n_0^2}I + i3\frac{\omega\chi^{(3)\prime\prime}(\omega)}{\varepsilon_0 c^2 n_0^2}I. \tag{2.3.29}$$

To compare Eqs. (2.3.28) and (2.3.29), then we obtain the expressions of nonlinear refractive index Δn and the nonlinear absorption coefficient $\Delta\alpha$:

$$\Delta n = \frac{3}{\varepsilon_0 c n_0^2}\chi^{(3)\prime}(\omega)I, \tag{2.3.30}$$

$$\Delta\alpha = \frac{6\omega}{\varepsilon_0 c^2 n_0^2}\chi^{(3)\prime\prime}(\omega)I. \tag{2.3.31}$$

From Eqs. (2.3.30) to (2.3.31) we can see that for the third-order nonlinear medium, its nonlinear refractive index depends on the real part of third-order susceptibility and is proportional to the light intensity; its nonlinear absorption coefficient depends on the imaginary part of third-order susceptibility and is also proportional to the light intensity.

2.3.3 Relation Between Nonlinear Refractive Index and Nonlinear Absorption Coefficient

If K–K relation is applicative to a certain third-order nonlinear process, from Eqs. (2.3.30) and (2.3.31) we can obtain the relation between the real part of susceptibility $\chi^{(3)\prime}(\omega)$ and the nonlinear refractive index $\Delta n(\omega)$, and the relation between the imaginary part of susceptibility $\chi^{(3)\prime\prime}(\omega)$ and the nonlinear absorption coefficient $\Delta\alpha(\omega)$, respectively. Substituting them into Eq. (2.3.4) of K–K relation, thus we get the relation between the nonlinear refractive index $\Delta n(\omega)$ and the nonlinear absorption coefficient $\Delta\alpha(\omega)$:

$$\Delta n(\omega) = \frac{c}{\pi} P.V. \int_0^\infty \frac{\Delta\alpha(\omega')}{\omega'^2 - \omega^2} d\omega'. \tag{2.3.32}$$

Because the nonlinear refractive index of medium is very difficult to measure directly, often pass through measuring nonlinear absorption coefficient to indirectly determine the nonlinear refractive index. If measured the linear absorption spectrum of a nonlinear medium and its nonlinear absorption spectrum under a high power light, from the difference of these two spectrums to obtain $\Delta\alpha(\omega')$, then we can using Eq. (2.3.32) to calculate the nonlinear refractive index at the frequency of ω, $\Delta n(\omega)$. Then we can also use Eq. (2.3.30) to reversely calculate the real part of the third-order susceptibility at that frequency $\chi^{(3)\prime}(\omega)$.

Review Questions of Chapter 2

1. From Maxwell equations to deduce the time-domain wave equation for the light wave propagates in the anisotropic nonlinear medium and the isotopic nonlinear medium.
2. To deduce frequency-domain wave equation for the monochromic plane light wave in the anisotropic nonlinear medium and the isotopic nonlinear medium.
3. To deduce the steady-state wave equation and dynamic equation for monochromic plane light wave in isotopic medium under the slowly-varying-amplitude approximation.
4. Write down the general frequency-domain expression of nonlinear polarization. What is degeneration factor? List several examples of second and third-order nonlinear effects, and write their nonlinear polarization expressions (including degeneration factors).

5. What kinds of symmetries do the nonlinear polarization tensor has? Why the mediums with centre symmetry have no the second-order nonlinearity, only have the third-order nonlinearity?
6. Write down the expression of relation between real part and imaginary part of linear susceptibility (K–K relation). What high order nonlinear processes can apply K–K relation?
7. For linear medium, what are the relationships of the refractive index and absorption coefficient with the real part and the imaginary part of the susceptibility respectively? For third-order nonlinear medium, what is the relationship between the nonlinear refractive index and the nonlinear absorption coefficient?
8. In nonlinear optics, there are two systems of units: International system (MKS//SI) and Gaussian system (mgs/esu). How to distinguish the basic formula in these two systems and how to convert the units between two systems?

Appendix A: Derivation of K–K Relation [9, 10]

K–K relation is obtained at first from linear system. Firstly we consider the mathematic property of linear susceptibility. The light frequency can be regard as a complex number quantity, in the complex number plane of frequency ω' we integral to linear susceptibility $\chi^{(1)}(\omega')$ as follows.

$$\int_{-\infty}^{\infty} \frac{\chi^{(1)}(\omega')d\omega}{\omega' - \omega}. \tag{2.A.1}$$

Considering there is a singular point at point of $\omega' = \omega$. In order to avoid that singular point, we integral along a loop on the upper half of ω' complex number plane $(\omega' \geq 0)$, as shown in Fig. 2.1; then take the limitation of $R \to \infty, \quad \varepsilon \to 0$, the integral of Eq. (2.A.1) can be finished. According to Cauchy's theorem, because it has no singular point on the closed loop, the integral should be zero. We can explain physically like this: for the real frequency ω, the susceptibility $\chi(\omega)$ is measurable, so that it is limited, the integral to it is convergent.

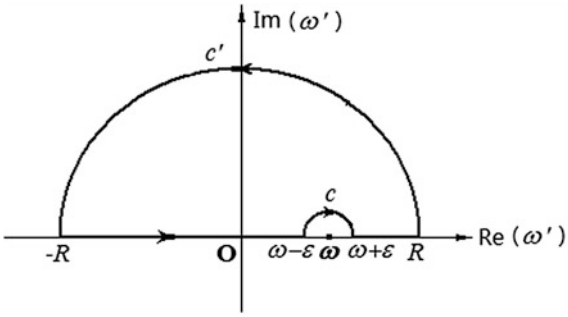

Fig. 2.1 Field of integration used for derivation of K–K relation

The integral of loop can be divided into following four segments: the semicircle c′ around the original point from $-\boldsymbol{R}$ to $\boldsymbol{R}$; the semicircle c around point ω from $\omega-\varepsilon$ to $\omega+\varepsilon$; and the two straight lines along the real axis of ω': from $-\boldsymbol{R}$ to $\omega-\varepsilon$ and from $\omega+\varepsilon$ to $\boldsymbol{R}$, i.e.,

$$\int_{c'} \frac{\chi^{(1)}(\omega')}{\omega'-\omega} d\omega' + \int_{c} \frac{\chi^{(1)}(\omega')}{\omega'-\omega} d\omega' + \left[\int_{-R}^{\omega-\varepsilon} \frac{\chi^{(1)}(\omega') d\omega'}{\omega'-\omega} + \int_{\omega+\varepsilon}^{R} \frac{\chi^{(1)}(\omega') d\omega'}{\omega'-\omega} \right] = 0. \tag{2.A.2}$$

For the first item, the integral of c′ tends to zero with $|R| \to \infty$, that is because when $|R| \to \infty$, $|\omega'|$ increases, $\chi(\omega')/|\omega'|$ tens to zero. For the second item, in the integral of $\boldsymbol{c}$, assuming $\omega' = \omega + \varepsilon e^{\mathrm{i}\varphi}$, when $\varepsilon \to 0$, the integral becomes

$$\lim_{\varepsilon\to 0} \int_{c} \frac{\chi^{(1)}(\omega')}{\omega'-\omega} d\omega' = \lim_{\varepsilon\to 0} \int_{\pi}^{0} \frac{\chi^{(1)}(\omega+\varepsilon \mathrm{e}^{\mathrm{i}\varphi}) i e^{\mathrm{i}\varphi}}{\varepsilon e^{\mathrm{i}\varphi}} d\varphi = -i\pi\chi^{(1)}(\omega). \tag{2.A.3}$$

For the third item, when $R \to \infty$, it is Cauchy-principal-value integral:

$$\left[\int_{-\infty}^{\omega-\varepsilon} \frac{\chi^{(1)}(\omega') d\omega'}{\omega'-\omega} + \int_{\omega+\varepsilon}^{\infty} \frac{\chi^{(1)}(\omega') d\omega}{\omega'-\omega} \right] = P.V. \int_{-\infty}^{\infty} \frac{\chi^{(1)}(\omega') d\omega'}{\omega'-\omega}. \tag{2.A.4}$$

In the condition of $R \to \infty, \quad \varepsilon \to 0$, substituting Eqs. (2.A.3) and (2.A.4) into Eq. (2.A.2), we obtain

$$\chi^{(1)}(\omega) = -\frac{i}{\pi} P.V. \int_{-\infty}^{\infty} \frac{\chi^{(1)}(\omega')}{\omega'-\omega} d\omega'. \tag{2.A.5}$$

To substrate $\chi^{(1)}(\omega) = \chi^{(1)\prime}(\omega) + i\chi^{(1)\prime\prime}(\omega)$ and $\chi^{(1)}(\omega') = \chi^{(1)\prime}(\omega') + i\chi^{(1)\prime\prime}(\omega')$ into Eq. (2.A.5) respectively, and the real part and imaginary part respectively equal, then we obtain K–K relation expressions as same as Eqs. (2.3.2) and (2.3.3) in the case of linear polarization.

$$\chi^{(1)\prime}(\omega) = \frac{1}{\pi} P.V. \int_{-\infty}^{\infty} \frac{\chi^{(1)\prime\prime}(\omega')}{\omega'-\omega} d\omega', \tag{2.A.6}$$

$$\chi^{(1)\prime\prime}(\omega) = -\frac{1}{\pi} P.V. \int_{-\infty}^{\infty} \frac{\chi^{(1)\prime}(\omega')}{\omega'-\omega} d\omega'. \tag{2.A.7}$$

According to $\chi^{(1)}(-\omega') = \chi^{(1)}(\omega')^*$, $\chi^{(1)\prime}(\omega')$ is the even function of ω', i.e., $\chi^{(1)\prime}(-\omega') = \chi^{(1)\prime}(\omega')$; and $\chi^{(1)\prime\prime}(\omega')$ is odd function of ω', i.e., $\chi^{(1)\prime\prime}(-\omega') = -\chi^{(1)\prime\prime}(\omega')$, therefore Eqs. (2.A.6) and (2.A.7) can be written as

$$\begin{aligned}\chi^{(1)\prime}(\omega) &= \frac{1}{\pi}P.V.\left[\int_{-\infty}^{0}\frac{\chi^{(1)\prime\prime}(\omega')}{\omega'-\omega}d\omega' + \int_{0}^{\infty}\frac{\chi^{(1)\prime\prime}(\omega')}{\omega'-\omega}d\omega'\right] \\ &= \frac{1}{\pi}P.V.\left[\int_{0}^{\infty}\frac{\chi^{(1)\prime\prime}(\omega')}{\omega'+\omega}d\omega' + \int_{0}^{\infty}\frac{\chi^{(1)\prime\prime}(\omega')}{\omega'-\omega}d\omega'\right] \\ &= \frac{2}{\pi}P.V.\int_{0}^{\infty}\frac{\omega'\chi^{(1)\prime\prime}(\omega')}{(\omega'^2-\omega^2)}d\omega',\end{aligned} \tag{2.A.8}$$

$$\begin{aligned}\chi^{(1)\prime\prime}(\omega) &= -\frac{1}{\pi}P.V.\left[\int_{-\infty}^{0}\frac{\chi^{(1)\prime}(\omega')}{\omega'-\omega}d\omega' + \int_{0}^{\infty}\frac{\chi^{(1)\prime}(\omega')}{\omega'-\omega}d\omega'\right] \\ &= \frac{1}{\pi}P.V.\left[\int_{0}^{\infty}\frac{\chi^{(1)\prime}(\omega')}{\omega'+\omega}d\omega' - \int_{0}^{\infty}\frac{\chi^{(1)\prime}(\omega')}{\omega'-\omega}d\omega'\right] \\ &= -\frac{2\omega}{\pi}P.V.\int_{0}^{\infty}\frac{\chi^{(1)\prime}(\omega')}{(\omega'^2-\omega^2)}d\omega'.\end{aligned} \tag{2.A.9}$$

Thus we have proved the K–K relation expressions (2.3.4) and (2.3.5) in the linear polarization.

Appendix B: Two Systems of Units [11]

There are two different unit systems commonly used in nonlinear optics: one is the international system (System International, SI), or called the practical unit system to use the units of Meter, Kilogram and Second (i.e., MKS system); other one is the Gaussian system to use the units of centimeter, gram and second (i.e., cgs system). This unit system also can be called the electrostatic unit system (i.e., esu system). In short, there are two unit systems in nonlinear optics: International system (MKS/SI) and Gaussian system (cgs/esu). This book only uses the international unit system.

Here we briefly review these two unit systems and the conversion between two systems.

I. Fundamental Formula

Electric displacement formula:

MKS/SI unit system $\boldsymbol{D} = \varepsilon_0 \boldsymbol{E} + \boldsymbol{P}$

cgs/esu unit system $\boldsymbol{D} = \boldsymbol{E} + 4\pi \boldsymbol{P}$

Susceptibility formula:

MKS/SI unit system $\boldsymbol{P}(t) = \varepsilon_0[\boldsymbol{\chi}^{(1)}\boldsymbol{E}(t) + \boldsymbol{\chi}^{(2)}\boldsymbol{E}^2(t) + \boldsymbol{\chi}^{(3)}\boldsymbol{E}^3(t) + \cdots]$

cgs/es unit system $\boldsymbol{P}(t) = \boldsymbol{\chi}^{(1)}\boldsymbol{E}(t) + \boldsymbol{\chi}^{(2)}\boldsymbol{E}^2(t) + \boldsymbol{\chi}^{(3)}\boldsymbol{E}^3(t) + \cdots$

II. Conversion of Two Unit Systems

Electric field strength $\boldsymbol{E}(SI) = 3 \times 10^4 \boldsymbol{E}(esu)$

Linear susceptibility $\boldsymbol{\chi}^{(1)}(SI) = 4\pi \boldsymbol{\chi}^{(1)}(esu)$

Second-order susceptibility

$$\boldsymbol{\chi}^{(2)}(SI) = \frac{4\pi}{3 \times 10^4}\boldsymbol{\chi}^{(2)}(esu) = 4.189 \times 10^{-4}\boldsymbol{\chi}^{(2)}(esu)$$

Third-order susceptibility

$$\boldsymbol{\chi}^{(3)}(SI) = \frac{4\pi}{(3 \times 10^4)^2}\boldsymbol{\chi}^{(3)}(esu) = 1.40 \times 10^{-8}(esu)$$

n-order susceptibility

$$\boldsymbol{\chi}^{(n)}(SI) = \frac{4\pi}{(c \times 10^{-4})^{n-1}}\boldsymbol{\chi}^{(n)}(esu),\ \mathrm{c} = 3 \times 10^8$$

References

1. N. Bloembergen, *Nonlinear Optics* (Benjamin, NY, 1965)
2. J.A. Armstrong, N. Bloembergen et al., Interactions between light waves in a nonlinear dielectric. Phys. Rev. **127**(6), 1918–1939 (1962)
3. S.A. Akhmanov, A.S. Chirkin, K. Drabovich, Nonstationary nonlinear optical effects and ultrashort light pulse formation. IEEE J. Quant. Electr. **4**(10), 598–605 (1968)
4. P.N. Butcher, *Nonlinear Optical Phenomenon* (Ohio State University Press, Columbus, 1965)
5. P.D. Maker, R.W. Terhune, Study of optical effects due to an induced polarization third order in the electric field strength. Phys. Rev. A **137**(3A), 801–818 (1965)
6. Y.R. Shen, Permutation symmetry of nonlinear susceptibilities and energy relation. Phys. Rev. **167**(3), 818–821 (1968)

7. D.A. Kleinman, Nonlinear dielectric polarization in optical media. Phys. Rev. **126**(6), 1977–1979 (1962)
8. J.F. Nye, *Physical Properties of Crystals* (Oxford University Press, London, 1957)
9. A. Yariv, *Quantum Electronics*, 2nd edn. Appendix A (Wiley, 1975)
10. R.W. Boyd, *Nonlinear Optics*, 3rd edn. (Academic Press Inc., 2008
11. R.W. Boyd, *Nonlinear Optics*, *Appendix C*, 3rd Edn. (Academic Press Inc. 2008)

Chapter 3
Optical Three-Wave Coupling Processes

This chapter uses a reformed first-order frequency-domain wave equation for the isotopic medium to approximately describe the second-order nonlinear optics effects in the anisotropic medium. At first, the three-wave coupling equations are deduced, then based on these equations, several typical second-order nonlinear optics effects are studied: optical frequency doubling, sum frequency, difference frequency, and optical parameter amplification and parameter oscillation. The power conversion efficiency formulas for these effects are given. Finally, the basic concepts of phase matching are introduced based on the frequency doubling effect.

3.1 Three-Wave Coupled Equations

3.1.1 Review of Second-Order Nonlinear Optics Effects in Isotopic Medium

Firstly we discuss the second-order nonlinear optics effect in general, it contains what specific effects, and we will give the polarizations of these effects in the isotopic material.

Assuming that the incident light electrical fields consisted by two monochromatic light fields at the different frequencies and with same propagation direction, the total electrical field strength can be expressed as

$$\boldsymbol{E}(t) = \sum_{n=1,.2} \boldsymbol{E}_n e^{-i\omega_n t} + c.c. = \boldsymbol{E}_1 e^{-i\omega_1 t} + \boldsymbol{E}_2 e^{-i\omega_2 t} + c.c. \tag{3.1.1}$$

In the isotopic medium without center symmetry, the second-order nonlinear polarization is

© Shanghai Jiao Tong University Press,
Shanghai and Springer Nature Singapore Pte Ltd., 2017

C. Li, *Nonlinear Optics*, DOI 10.1007/978-981-10-1488-8_3

$$\boldsymbol{P}^{(2)}(t) = \varepsilon_0 \chi^{(2)} \boldsymbol{E}^2(t). \tag{3.1.2}$$

Substituting Eq. (3.1.1) into Eq. (3.1.2), after combination of the items with same frequency component, we obtain:

$$\begin{aligned}\boldsymbol{P}^{(2)}(t) = \varepsilon_0 \chi^{(2)} [(&\boldsymbol{E}_1^2 e^{-i2\omega_1 t} + \boldsymbol{E}_2^2 e^{-i2\omega_2 t} + 2\boldsymbol{E}_1 \boldsymbol{E}_2 e^{-i(\omega_1+\omega_2)t} + 2\boldsymbol{E}_1 \boldsymbol{E}_2^* e^{-i(\omega_1-\omega_2)t}) \\ &+ 2(\boldsymbol{E}_1 \boldsymbol{E}_1^* + \boldsymbol{E}_2 \boldsymbol{E}_2^*)] + c.c.\end{aligned} \tag{3.1.3}$$

The Eq. (3.1.3) can be summarized by a simple formula, that is

$$\boldsymbol{P}^{(2)}(t) = \sum_i \boldsymbol{P}^{(2)}(\omega_i) e^{-i\omega_i t} + c.c, \tag{3.1.4}$$

where i takes the positive integer. The polarization $\boldsymbol{P}^{(2)}(\omega_i)$ corresponds to the different second-order nonlinear optics effect with different susceptibility $\chi^{(2)}(\omega_i)$, which is

$$\boldsymbol{P}^{(2)}(\omega_i) = D\varepsilon_0 \chi^{(2)}(\omega_i) \boldsymbol{E}(\omega_1) \boldsymbol{E}(\omega_2), \tag{3.1.5}$$

where ω_i is the frequency of polarization field composed by two original monochromic fields at frequencies of ω_1 and ω_2 in different modes. Form Eq. (3.1.3) we can see that ω_i has five modes: $2\omega_1$, $2\omega_2$, $\omega_1 + \omega_2$, $\omega_1 - \omega_2$ and 0. For second-order nonlinearity, $n = 2$, the degeneration factor is $D = n!/m! = 2/m!$. When $m = 1$, $D = 2$; when $m = 2$, $D = 1$. Therefore, corresponding to the different ω_i, the second-order nonlinear optics effects and corresponding polarizations are respectively:

Optical frequency doubling

$$\boldsymbol{P}(2\omega_1) = \varepsilon_0 \chi^{(2)}(2\omega_1) \boldsymbol{E}_1^2, \tag{3.1.6}$$

Optical frequency doubling

$$\boldsymbol{P}(2\omega_2) = \varepsilon_0 \chi^{(2)}(2\omega_2) \boldsymbol{E}_2^2, \tag{3.1.7}$$

Optical sum frequency

$$\boldsymbol{P}(\omega_1 + \omega_2) = 2\varepsilon_0 \chi^{(2)}(\omega_1 + \omega_2) \boldsymbol{E}_1 \boldsymbol{E}_2, \tag{3.1.8}$$

Optical difference frequency

$$\boldsymbol{P}(\omega_1 - \omega_2) = 2\varepsilon_0 \chi^{(2)}(\omega_1 - \omega_2) \boldsymbol{E}_1 \boldsymbol{E}_2^*, \tag{3.1.9}$$

Optical rectification

$$\boldsymbol{P}(0) = 2\varepsilon_0\chi^{(2)}(0)(\boldsymbol{E}_1\boldsymbol{E}_1^* + \boldsymbol{E}_2\boldsymbol{E}_2^*). \tag{3.1.10}$$

3.1.2 Approximate Description of Second-Order Nonlinear Optics Effect in Anisotropic Medium

In general, the medium with the second-order nonlinear optical effect is not isotopic, it is anisotropic, such as the crystal medium. However, for describing the second-order nonlinear effect in the crystal medium should using tensor calculation method, it is complicated, and needs take up a larger space. This chapter we present a method that using the slowly-varying-amplitude approximated frequency-domain first-order wave equation for the isotropic medium to approximately describe the second-order nonlinear optical effects in the anisotropic medium. For simplicity, we suppose that the medium is far from the resonance area, and the absorption loss can be neglected.

The characteristic of light propagation in the anisotropic medium is: the propagation direction of light wave ($\boldsymbol{k}$) is different with the direction of energy flow ($\boldsymbol{I} = \boldsymbol{E} \times \boldsymbol{H}$), there is an included angle α between both. Because the electric induction strength $\boldsymbol{D}$ in the medium is perpendicular to the propagation direction of the light; and the electrical field strength $\boldsymbol{E}$ is perpendicular the direction of energy flow, so there is an included angle α between $\boldsymbol{D}$ and $\boldsymbol{E}$. Actually α is small, $\alpha < 3°$ for the most of crystals.

Considering a monochromic plane wave propagates along z direction in an anisotropic medium, Suppose its wave vector $\boldsymbol{k}$ is along z direction; and there is an included angle α between $\boldsymbol{k}$ and the energy flow $\boldsymbol{I} = \boldsymbol{E} \times \boldsymbol{H}$. The electric induction strength $\boldsymbol{D}$ is along x direction; the magnetic field strength $\boldsymbol{H}$ is along y direction, which is perpendicular to the plane consisted by $\boldsymbol{D}$, $\boldsymbol{E}$ and $\boldsymbol{k}$, as shown in Fig. 3.1 [1].

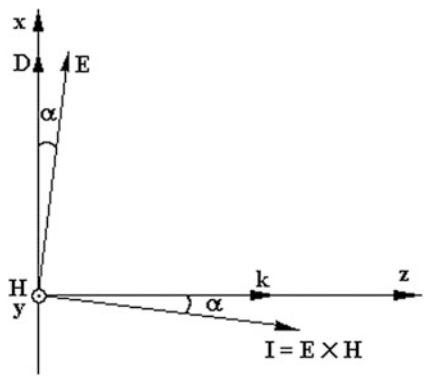

Fig. 3.1 Relationship among electromagnetic wave vectors E, D, H, k, and $\boldsymbol{I} = \boldsymbol{E} \times \boldsymbol{H}$, when the monochromic plane light wave propagates in an anisotropic medium

Suppose the frequency of above monochromic plane wave is ω, the light electrical field strength is expressed as a product of amplitude and phase:

$$\boldsymbol{E}(z,\omega) = \boldsymbol{E}(z)e^{i(kz-\omega t)} = \hat{\boldsymbol{e}}E(z)e^{i(kz-\omega t)}, \tag{3.1.6}$$

where $\hat{\boldsymbol{e}}$ is the unit vector along the electrical field direction. The polarization corresponding to the light electrical field strength is

$$\boldsymbol{P}_{NL}(z,\omega) = \boldsymbol{P}_{NL}(z)e^{i(k'z-\omega t)}. \tag{3.1.7}$$

The each of $\boldsymbol{E}(z,\omega)$ and $\boldsymbol{P}_{NL}(z,\omega)$ can be written to the vector sum of two orthogonal components, i.e., the horizontal component perpendicular to $\boldsymbol{k}$ (noted by $\boldsymbol{T}$) and the longitudinal component parallel to $\boldsymbol{k}$ (noted by S):

$$\boldsymbol{E}(z,\omega) = \boldsymbol{E}_T(z,\omega) + \boldsymbol{E}_S(z,\omega), \tag{3.1.8}$$

$$\boldsymbol{P}_{NL}(z,\omega) = \boldsymbol{P}_{NL}^T(z,\omega) + \boldsymbol{P}_{NL}^S(z,\omega). \tag{3.1.9}$$

The horizontal component of field amplitude abides by following frequency-domain wave equation for isotropic medium in the condition of slowly-varying-amplitude approximation:

$$\frac{\partial \boldsymbol{E}_T(z)}{\partial z} = \frac{i\omega}{2\varepsilon_0 cn}\boldsymbol{P}_{NL}^T(z)e^{i\Delta kz}. \tag{3.1.10}$$

To make the dot product of the unit vector $\hat{\boldsymbol{e}}$ in the two sides of Eq. (3.1.10) respectively, and using

$$\hat{\boldsymbol{e}} \cdot \boldsymbol{E}_T = E_T \cos\alpha = E\cos^2\alpha$$

and

$$\boldsymbol{P}_{NL}^T \approx \boldsymbol{P}_{NL},$$

then we obtain

$$\frac{\partial E(z)}{\partial z} = \frac{i\omega}{2\varepsilon_0 cn\cos^2\alpha}\hat{\boldsymbol{e}} \cdot \boldsymbol{P}_{NL}(z)e^{i\Delta kz}. \tag{3.1.11}$$

If take $\cos^2\alpha \approx 1$ approximately, Eq. (3.1.11) becomes

$$\frac{\partial E(z)}{\partial z} = \frac{i\omega}{2\varepsilon_0 cn}\hat{\boldsymbol{e}} \cdot \boldsymbol{P}_{NL}(z)e^{\mathrm{i}\Delta kz}, \tag{3.1.12}$$

where $\Delta k = k' - k$, k is the wave vector of original light field, k' is the wave vector of polarization field. This is the slowly-varying-amplitude-approximation

frequency-domain wave equation for propagation of the light field amplitude of the monochromic plane wave in the anisotropic medium. The difference between this equation and the slowly-varying-amplitude- approximation frequency-domain wave equation in isotropic medium is replaced $P_{NL}(z)$ by $\hat{\boldsymbol{e}} \cdot \boldsymbol{P}_{NL}(z)$.

3.1.3 Three-Wave Coupled Equations in Anisotropic Medium

In general case, two light wave fields $\boldsymbol{E}(\omega_1, \boldsymbol{k}_1)$ and $\boldsymbol{E}(\omega_2, \boldsymbol{k}_2)$ with different incident directions interact with a nonlinear crystal medium, to induce a new light wave field $\boldsymbol{E}(\omega_3, \boldsymbol{k}_3)$. The three-wave coupling process is shown in Fig. 3.2.

This three-waves coupling process can use the photon concept to describe. The three photons at different frequency ω_1, ω_2 and ω_3 should meet the following energy conservation law:

$$\hbar\omega_3 = \hbar\omega_1 + \hbar\omega_2. \tag{3.1.13}$$

If we want to realize the optimum coupling of three photons, the three photons also need satisfy the momentum conservation law as follows

$$\hbar\boldsymbol{k}_3 = \hbar\boldsymbol{k}_1 + \hbar\boldsymbol{k}_2. \tag{3.1.14}$$

To describe this process by using optical wave concept, the frequencies of three waves should satisfy the relationship: $\omega_3 = \omega_1 + \omega_2$. Here we just talk about sum frequency process. Actually there are difference processes, which satisfy the relationship $\omega_1 = \omega_3 - \omega_2$ and $\omega_2 = \omega_3 - \omega_1$.

Assuming that three monochromic plane waves at frequencies ω_1, ω_2, ω_3 propagate in the anisotropic medium, they all along z direction, to generate a sum frequency or two difference frequency nonlinear effects, their second-order nonlinear polarizations can be expressed as respectively:

$$\boldsymbol{P}^{(2)}(z, \omega_1) = D\varepsilon_0\boldsymbol{\chi}^{(2)}(\omega_1; -\omega_2, \omega_3) : \boldsymbol{E}^*(z, \omega_2)\boldsymbol{E}(z, \omega_3), \tag{3.1.15}$$

$$\boldsymbol{P}^{(2)}(z, \omega_2) = D\varepsilon_0\boldsymbol{\chi}^{(2)}(\omega_2; \omega_3, -\omega_1) : \boldsymbol{E}(z, \omega_3)\boldsymbol{E}^*(z, \omega_1), \tag{3.1.16}$$

$$\boldsymbol{P}^{(2)}(z, \omega_3) = D\varepsilon_0\boldsymbol{\chi}^{(2)}(\omega_3; \omega_1, \omega_2) : \boldsymbol{E}(z, \omega_1)\boldsymbol{E}(z, \omega_2), \tag{3.1.17}$$

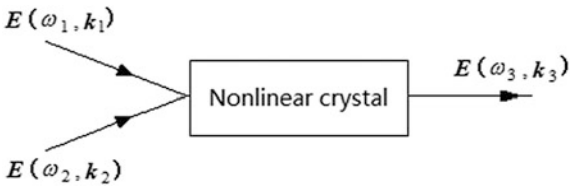

Fig. 3.2 Schematic diagram of the three-wave coupling process

where D is the degeneration factor, if two original lights are at different frequencies, $D = 2$; if two original lights are at same frequency, $D = 1$.

If denoting the three light fields respectively to be $\boldsymbol{E}(z, \omega_1) = \hat{\boldsymbol{e}}_1 E_1$, $E(\mathrm{z}, \omega_2) = \hat{\boldsymbol{e}}_2 E_2$, and $E(\mathrm{z}, \omega_3) = \hat{\boldsymbol{e}}_3 E_3$, then we have

$$\boldsymbol{P}_1^{(2)}(z) = D\varepsilon_0 \boldsymbol{\chi}^{(2)}(\omega_1; -\omega_2, \omega_3) : \hat{\boldsymbol{e}}_2 \hat{\boldsymbol{e}}_3 E_2^* E_3, \tag{3.1.18}$$

$$\boldsymbol{P}_2^{(2)}(z) = D\varepsilon_0 \boldsymbol{\chi}^{(2)}(\omega_2; \omega_3, -\omega_1) : \hat{\boldsymbol{e}}_3 \hat{\boldsymbol{e}}_1 E_3 E_1^*, \tag{3.1.19}$$

$$\boldsymbol{P}_3^{(2)}(z) = D\varepsilon_0 \boldsymbol{\chi}^{(2)}(\omega_3; \omega_1, \omega_2) : \hat{\boldsymbol{e}}_1 \hat{\boldsymbol{e}}_2 E_1 E_2. \tag{3.1.20}$$

In the frequency-domain wave Eq. (3.1.12), if setting $\boldsymbol{P}_{NL} = \boldsymbol{P}^{(2)}$, then substituting Eqs. (3.1.18)–(3.1.20) into Eq. (3.1.12), then we obtain following equations:

$$\frac{\partial E_1(z)}{\partial z} = \frac{i\omega_1}{2cn_1} D\hat{\boldsymbol{e}}_1 \cdot \boldsymbol{\chi}^{(2)}(\omega_1; -\omega_2, \omega_3) : \hat{\boldsymbol{e}}_2 \hat{\boldsymbol{e}}_3 E_2^* E_3 e^{\mathrm{i}\Delta kz}, \tag{3.1.21}$$

$$\frac{\partial E_2(z)}{\partial z} = \frac{i\omega_2}{2cn_2} D\hat{\boldsymbol{e}}_2 \cdot \boldsymbol{\chi}^{(2)}(\omega_2; \omega_3, -\omega_1) : \hat{\boldsymbol{e}}_3 \hat{\boldsymbol{e}}_1 E_3 E_1^* e^{\mathrm{i}\Delta kz}, \tag{3.1.22}$$

$$\frac{\partial E_3(z)}{\partial z} = \frac{i\omega_3}{2cn_3} D\hat{\boldsymbol{e}}_3 \cdot \boldsymbol{\chi}^{(2)}(\omega_3; \omega_1, \omega_2) : \hat{\boldsymbol{e}}_1 \hat{\boldsymbol{e}}_2 E_1 E_2 e^{-\mathrm{i}\Delta kz}. \tag{3.1.23}$$

According to the frequency substitution symmetry of susceptibility, three nonlinear susceptibilities are equal, namely

$$\begin{aligned} \hat{\boldsymbol{e}}_1 \cdot \boldsymbol{\chi}^{(2)}(\omega_1; -\omega_2, \omega_3) : \hat{\boldsymbol{e}}_2 \hat{\boldsymbol{e}}_3 &= \hat{\boldsymbol{e}}_2 \cdot \boldsymbol{\chi}^{(2)}(\omega_2; \omega_3, -\omega_1) : \hat{\boldsymbol{e}}_3 \hat{\boldsymbol{e}}_1 \\ &= \hat{\boldsymbol{e}}_3 \cdot \boldsymbol{\chi}^{(2)}(\omega_3; \omega_1, \omega_2) : \hat{\boldsymbol{e}}_1 \hat{\boldsymbol{e}}_2 = \boldsymbol{\chi}_{eff}^{(2)}, \end{aligned} \tag{3.1.24}$$

here $\chi_{eff}^{(2)}$ is a real number, it is called the efficient nonlinear susceptibility, which is used for measurement of the coupling strength among three waves. To omit the corner mark *eff*, i.e., $\chi_{eff}^{(2)} = \chi^{(2)}$, the three components of susceptibility can be written to the following scalar forms:

$$\chi^{(2)}(\omega_1; -\omega_2, \omega_3) = \hat{\boldsymbol{e}}_1 \cdot \boldsymbol{\chi}^{(2)}(\omega_1; -\omega_2, \omega_3) : \hat{\boldsymbol{e}}_2 \hat{\boldsymbol{e}}_3, \tag{3.1.25}$$

$$\chi^{(2)}(\omega_2; \omega_3, -\omega_1) = \hat{\boldsymbol{e}}_2 \cdot \boldsymbol{\chi}^{(2)}(\omega_2; \omega_3, -\omega_1) : \hat{\boldsymbol{e}}_3 \hat{\boldsymbol{e}}_1, \tag{3.1.26}$$

$$\chi^{(2)}(\omega; \omega_1, \omega_2) = \hat{\boldsymbol{e}}_3 \cdot \boldsymbol{\chi}^{(2)}(\omega_3; \omega_1, \omega_2) : \hat{\boldsymbol{e}}_1 \hat{\boldsymbol{e}}_2. \tag{3.1.27}$$

Therefore, the wave Eqs. (3.1.21)–(3.1.23) can be written to

$$\frac{\partial E_1(z)}{\partial z} = i\frac{D\omega_1}{2cn_1}\chi^{(2)}(\omega_1; -\omega_2, \omega_3)E_2^*(z)E_3(z)e^{i\Delta kz}, \tag{3.1.28}$$

$$\frac{\partial E_2(z)}{\partial z} = i\frac{D\omega_2}{2cn_2}\chi^{(2)}(\omega_2; \omega_3, -\omega_1)E_3(z)E_1^*(z)e^{i\Delta kz}, \tag{3.1.29}$$

$$\frac{\partial E_3(z)}{\partial z} = i\frac{D\omega_3}{2cn_3}\chi^{(2)}(\omega_3; \omega_1, \omega_2)E_1(z)E_2(z)e^{-i\Delta kz}, \tag{3.1.30}$$

where Δk is phase mismatch factor, which can be expressed as

$$\Delta k = k_1 + k_2 - k_3. \tag{3.1.31}$$

The meaning of Δ k for different processes are different: for difference frequency process described by Eq. (3.1.28) is $\Delta k = k_1 - (k_3 - k_2)$; for difference frequency process described by Eq. (3.1.29) is $\Delta k = k_2 - (k_3 - k_1)$; for sum frequency process described by Eq. (3.1.30) is $-\Delta k = k_3 - (k_1 + k_2)$. If the three wave is phase matched, then $\Delta k = 0$, it is equivalent to that the three photons satisfy the momentum conservation law.

3.2 Optical Second-Harmonic Generation

Optical second harmonic generation, i.e., optical frequency doubling, is a special case of three wave mixing processes. That is one of nonlinear optical phenomena, which found at the earliest. The experimental setup for studying the frequency doubling in 1961 by Franken et al. is shown in Fig. 3.3 [2]. The ruby laser (at the wavelength λ_1 = 694.3 nm) passed through a quartz crystal to produce the frequency doubling light (at the wavelength λ_2 = 347.15 nm). Two light beams are separated by a prism.

Now the application of optical frequency doubling has been mature. For example, it is used to transform from infrared laser at the wavelength of 1.06 μm generated by a Nd:YAG laser to the green laser at the wavelength of 532 nm.

Considering a monochromic plane light wave at frequency ω passes through a nonlinear crystal with length of L to produce a frequency doubling light at frequency 2ω, as shown in Fig. 3.4.

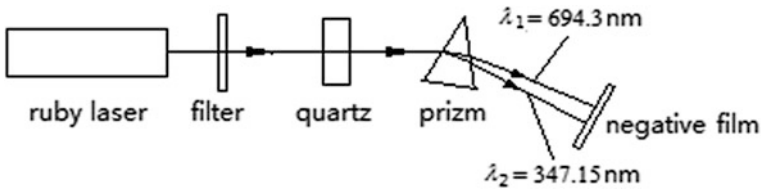

Fig. 3.3 Experimental facility of frequency doubling by Franken et al.

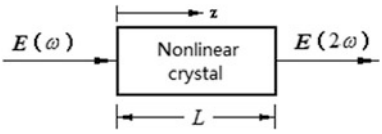

Fig. 3.4 Schematic diagram of the frequency doubling process

Suppose the crystal does no absorption for these two lights, now we are going to calculate the intensity of the frequency doubling light transmitted from crystal and the efficiency of frequency doubling conversion, i.e., the ratio between the power of frequency doubling light and the power of fundamental frequency light.

We can use three wave coupled Eqs. (3.1.28)–(3.1.30) to deal with second harmonic generation problems. We suppose the fundamental frequency is $\omega_1 = \omega_2 = \omega$, and the second harmonic frequency is $\omega_3 = 2\omega$. When establishing the wave equation of fundamental frequency light filed, we should set the degeneration factor to be $D = 2$; and when establishing the wave equation of frequency doubling optical field, setting the degeneration factor to be $D = 1$.

We will study following two kinds of optical frequency doubling effects: one is the case of low conversion efficiency without the fundamental frequency light loss (the small signal approximation); another one is the case of high conversion efficiency having the fundamental frequency light loss.

3.2.1 Small Signal Approximation

If the fundamental frequency light is very weak, only a small part of incident fundamental frequency light energy convert to the frequency doubling light energy, i.e., the frequency doubling conversion efficiency is very low. In this case the outputted frequency doubling light power is much smaller than the incident fundamental frequency light power, it can be regard that the amplitude of fundamental frequency light is a constant approximately:

$$E_2(z) = E_1(z) \approx E_1(0). \tag{3.2.1}$$

So when applying Eqs. (3.1.28)–(3.1.30), we can write that

$$\frac{\partial E_1(z)}{\partial z} = 0, \tag{3.2.2}$$

$$\frac{\partial E_2(z)}{\partial z} = 0, \tag{3.2.3}$$

$$\frac{\partial E_3(z)}{\partial z} = \frac{i(2\omega)}{2cn_3}\chi^{(2)}(2\omega;\ \omega,\ \omega)E_1^2(0)e^{-i\Delta kz}, \tag{3.2.4}$$

where

$$\Delta k = 2k_1 - k_3. \tag{3.2.5}$$

We assume that the length of crystal is L, and use boundary condition: $E_1(0)$ = constant, $E_3(0) = 0$, directly taking integral of Eq. (3.2.4), and using $\int_0^L e^{-i\Delta kz}dz = \frac{i}{\Delta k}(e^{-i\Delta kL} - 1)$ to obtain the frequency doubling optical field amplitude outputted from the crystal:

$$E_3(L) = -\frac{\omega\chi^{(2)}}{cn_3\Delta k}E_1^2(0)(e^{-i\Delta kL} - 1). \tag{3.2.6}$$

According to usual practice, we introduce the frequency doubling coefficient d to replace the second-order nonlinear susceptibility $\chi^{(2)}$ [3]:

$$d = \frac{\chi^{(2)}}{2}, \tag{3.2.7}$$

and set $n_1 = n_\omega$, $n_3 = n_{2\omega}$, then Eq. (3.2.6) becomes

$$E_3(L) = -\frac{2\omega d}{cn_{2\omega}\Delta k}E_1^2(0)(e^{-i\Delta kL} - 1). \tag{3.2.8}$$

Using frequency multiplication formula of trigonometric function, from Eq. (3.2.8) we can obtain

$$\begin{aligned} |E_3(L)|^2 &= E_3(L)\cdot E_3(L)^* = \left(\frac{2\omega d}{cn_{2\omega}\Delta k}\right)^2 |E_1(0)|^4 \cdot 4\sin^2(\Delta kL/2) \\ &= \frac{4\omega^2 d^2 L^2}{c^2 n_{2\omega}^2}|E_1(0)|^4 \cdot \frac{\sin^2(\Delta kL/2)}{(\Delta kL/2)^2} = \frac{4\omega^2 d^2 L^2}{c^2 n_{2\omega}^2}|E_1(0)|^4 \mathrm{sinc}^2\left(\frac{\Delta kL}{2}\right). \end{aligned}$$

Using the relation between the intensity and the amplitude for the fundamental frequency light and the frequency doubling light:

$$I_1(0) = \frac{1}{2}\varepsilon_0 cn_\omega |E_1(0)|^2, \tag{3.2.9}$$

$$I_3(L) = \frac{1}{2}\varepsilon_0 cn_{2\omega} |E_3(L)|^2, \tag{3.2.10}$$

we can obtain the relationship between the intensity of outputted frequency doubling light and the intensity of incident fundamental light:

$$I_3(L) = \frac{8\omega^2 d^2 L^2}{\varepsilon_0 n_{2\omega} n_\omega^2 c^3} I_1^2(0) \mathrm{sinc}^2\left(\frac{\Delta kL}{2}\right), \tag{3.2.11}$$

where the relationship between the function $\mathrm{sinc}^2(\Delta kL/2)$ and $\Delta kL/2$ is shown in Fig. 3.5.

The optical frequency doubling efficiency is defined as the ratio of the outputted frequency doubling light power $P_3(L)$ with the inputted fundamental frequency light power $P_1(0)$:

$$\eta = \frac{P_3(L)}{P_1(0)} = \frac{I_3(L)}{I_1(0)} = \frac{8\omega^2 d^2 L^2}{\varepsilon_0 n_{2\omega} n_\omega^2 c^3} \frac{P_1(0)}{S} \mathrm{sinc}^2\left(\frac{\Delta kL}{2}\right). \tag{3.2.12}$$

The above equation has been used $I_1 = P_1/S$, were S is the cross sectional area of incident fundamental frequency light beam.

From Eq. (3.2.12) we can see that, under small signal condition (the loss of fundamental wave is omitted), the frequency doubling process has following properties:

1. When $\Delta k = 0$, $\sin c^2(\Delta kL/2) = 1$, $n_{2\omega} = n_\omega = n$, the frequency doubling conversion efficiency η takes the maximum:

$$\eta = \frac{8\omega^2 d^2 L^2}{\varepsilon_0 n^3 c^3} \cdot \frac{P_1(0)}{S}. \tag{3.2.13}$$

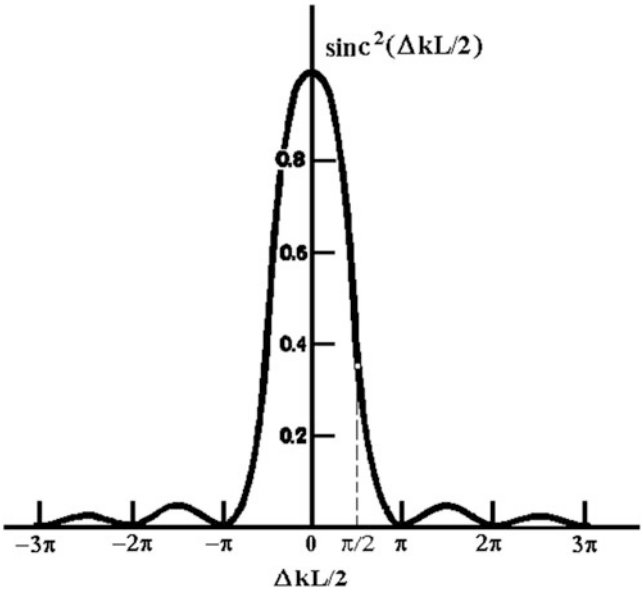

Fig. 3.5 Relationship between function $\mathrm{sinc}^2(\Delta kL/2)$ and $\Delta kL/2$

As you see that the frequency doubling conversion efficiency is proportional to the power of incident fundamental frequency light; is proportional to the frequency doubling coefficient of crystal d and the length of crystal L, and is reverse proportional to the cross sectional area of incident fundamental frequency light S. Therefore, we can used following measures to enhance the frequency doubling efficiency: to select the nonlinear crystal with high frequency doubling coefficient and a longer size; to use the high power fundamental frequency light and the focused fundamental frequency light beam.

2. When $\Delta k \neq 0$, for a certain wave vector mismatch factor Δk, the length of crystal L is equal to so called the coherence length:

$$L_c = \frac{\pi}{\Delta k}, \tag{3.2.14}$$

we have $\frac{\Delta k L_c}{2} = \frac{\pi}{2}$ at the location of imaginary line in Fig. 3.5. If $L < L_c$, there is higher frequency doubling conversion efficiency; if $L > L_c$, the frequency doubling conversion efficiency goes down quickly, after that making a periodic variation with a small amplitude.

3.2.2 High Fundamental Wave Consumption

In high conversion efficiency case, the foundational frequency wave amplitude cannot regard as a constant, the small signal approximation is not applicable. Below we consider the case that the phase matching condition is satisfied ($\Delta k = 0$), i.e., $n_1 = n_2 = n_3 = n$. For the foundational frequency light at $\omega_1 = \omega_2 = \omega$, and $E_1 = E_2$, the degeneration factor is $D = 2$; for the frequency doubling light at $\omega_3 = 2\omega$, the degeneration factor is $D = 1$; replacing the frequency doubling coefficient d to the susceptibility $\chi^{(2)} = 2d$, in this case the three coupling Eqs. (3.1.28)–(3.1.30) becomes the two coupling equations:

$$\frac{\partial E_1(z)}{\partial z} = \frac{i2\omega d}{cn} E_1^*(z) E_3(z), \tag{3.2.15}$$

$$\frac{\partial E_3(z)}{\partial z} = \frac{i2\omega d}{cn} E_1^2(z). \tag{3.2.16}$$

Taking conjugate complex number and multiplying by $E_1(z)$ on the two sides of Eq. (3.2.15), and then multiplying by $E_3^*(z)$ on the two sides of Eq. (3.2.16), finally adding the two equations, then we obtain:

$$\frac{\partial}{\partial z}(|E_1(z)|^2 + |E_3(z)|^2) = 0. \tag{3.2.17}$$

Namely $|E_1(z)|^2 + |E_3(z)|^2 = |E_1(0)|^2 + |E_3(0)|^2$. Because when $z = 0$, $E_3(0) = 0$ and $E_1(0) \neq 0$, then we have

$$|E_1(z)|^2 + |E_3(z)|^2 = |E_1(0)|^2 = \text{constant}. \tag{3.2.18}$$

Visible, at any z-coordinate point in the crystal, the sum of the intensity of foundational frequency light and the intensity of frequency doubling light is equal to the intensity of foundational frequency light at the start point, that is to say, the production of frequency doubling light comes at the expense of the consumption of fundamental frequency light.

Taking module on the both sides of Eq. (3.2.16), then substituting the $|E_1(z)|^2$ obtained from Eq. (3.2.18) into it, and giving a definition of

$$\kappa = \frac{2\omega d}{cn}, \tag{3.2.19}$$

then we obtain

$$\frac{d(|E_3(z)/E_1(0)|)}{dz} = \kappa|E_1(0)|\left[1 - (|E_3(z)/E_1(0)|)^2\right]. \tag{3.2.20}$$

Setting $|E_3(z)/E_1(0)| = v$, making the separation of variables to Eq. (3.2.20), integral on both sides of it, and using integral formula

$$\int \frac{dv}{1 - v^2} = \tanh^{-1} v, \tag{3.2.21}$$

then we obtain the formula for the frequency doubling light field amplitude:

$$|E_3(z)| = |E_1(0)| \tanh(\kappa|E_1(0)|z). \tag{3.2.22}$$

Now we set the hyperbolic tangent function $\tanh(\kappa|E_1(0)|z) = \tanh x = a$, substitute Eq. (3.2.22) into Eq. (3.2.18), and use the relation between the hyperbolic secant function and the hyperbolic tangent function $\text{sech}x = \sqrt{1 - a^2}$, then obtain the formula for the fundamental frequency light field amplitude:

$$|E_1(z)| = |E_1(0)|\text{sech}(\kappa|E_1(0)|z). \tag{3.2.23}$$

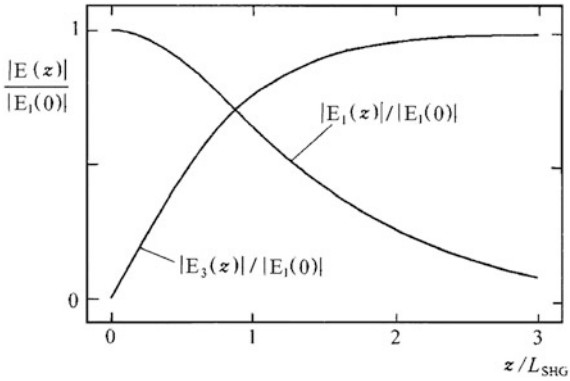

Fig. 3.6 Under the phase matched condition, the curves of the frequency doubling light relative amplitude $|E_3(z)|/|E_1(0)|$ and the foundational frequency light relative amplitude $|E_1(z)|/|E_1(0)|$ versus the relative coordinate z/L_{SHG} along the length direction of crystal

Making a definition of the efficient frequency doubling length:

$$L_{SHG} = [\kappa|E_1(0)|]^{-1} = \left[\frac{2\omega d}{cn}|E_1(0)|\right]^{-1}, \tag{3.2.24}$$

then Eqs. (3.2.22) and (3.2.23) can be written as

$$|E_3(z)| = |E_1(0)|\tanh(z/L_{SHG}), \tag{3.2.25}$$

$$|E_1(z)| = |E_1(0)|\mathrm{sech}(z/L_{SHG}). \tag{3.2.26}$$

Figure 3.6 shows the curves of $|E_3(z)|/|E_1(0)|$ and $|E_1(z)|/|E_1(0)|$ as the function of z/L_{SHG}.

We can see that, under the phase matching condition, the foundational frequency light continually transforms to the frequency doubling light with the increase of the crystal length coordinate. In the theory, when the frequency doubling crystal length achieves to the two times of efficient frequency doubling length, $E_3(z)$ will tend to $E_1(0)$, namely near the frequency doubling conversion efficiency of 100 %. However, in practice, there are many restrictions, such as the absorption and the diffraction of the materials, the reflection from crystal end face, and the laser beam is not monochromic plane wave, etc. For the KDP crystal with length of $L = 2L_{SHG} = 2\,cm$, the frequency doubling conversion efficiency is less than 60 %.

Utilizing the amplitude-intensity relation of Eqs. (3.2.9) and (3.2.10), from Eq. (3.2.25) we can obtain the frequency doubling conversion efficiency formula under the condition of high fundamental wave consumption:

$$\eta = \frac{P_3(L)}{P_1(0)} = \frac{n_{2\omega}}{n_\omega}\frac{|E_3(L)|^2}{|E_1(0)|^2} = \frac{n_{2\omega}}{n_\omega}\tanh^2\frac{L}{L_{SHG}}. \tag{3.2.27}$$

According to Eq. (3.2.24), $(L/L_{SHG})^2 \propto I_1(0)$, in the case of small signal approximation, there is the approximate relation:

$$\tanh^2(L/L_{SHG}) \approx (L/L_{SHG})^2. \tag{3.2.28}$$

For $\Delta k = 0$, $n_{2\omega} = n_\omega = n$ is required, then Eq. (3.2.27) changes to Eq. (3.2.13), which is the frequency doubling conversion efficiency formula for the small signal approximation.

3.2.3 Phase Matching Technology

When the frequency doubling light and the fundamental frequency light are collinear, the phase matching condition is $\Delta k = k_3 - 2k_1 = 0$, or $2k_1 = k_3$, i.e., $2k_\omega = k_{2\omega}$. From wave vector formulas $k_\omega = (\omega/c)n_\omega$ and $k_{2\omega} = (2\omega/c)n_{2\omega}$ we obtain

$$n_\omega = n_{2\omega}. \tag{3.2.29}$$

Namely, the phase matching condition requires that the refractive index for the frequency doubling light is equal to the refractive index for the fundamental frequency light in the crystal.

How to realize that the fundamental frequency light and the frequency doubling light induce the same refractive index in an identical crystal? In general, we can use the birefringence characteristic of the anisotropic crystal to realize it.

The light at any frequency ω propagates in the anisotropic crystal, besides the direction of optical axis, generally there exists two orthogonal polarization directions with different refractive index, namely $n_\perp(\omega) \neq n_\parallel(\omega)$, such as the situation of o light and e light. However, for two light beams at different frequency (such as the fundamental frequency light at ω and the frequency doubling light at 2ω), it is possible to find a propagation direction that its two orthogonal polarization directions have same refractive index, i.e., $n_\perp(\omega) = n_\parallel(\omega')$, in this way the phase matching condition can be satisfied.

Previous we have talk about that there are 7 crystal systems in the nature, in which 6 crystal systems are belong to anisotropic crystal; only one - cubic crystal system is belong to isotropic crystal. The 6 anisotropic crystals can be divided into two kinds: the uniaxial crystal and the biaxial crystal. The trigonal crystal system, the tetragonal crystal system, and the hexagonal crystal system are belong to the uniaxial crystal; the triclinic crystal system, the monoclinic crystal system and the orthorhombic crystal system are belong to the biaxial crystal. The classification of crystal is shown in Table 3.1.

Table 3.1 Classification of crystal

Classification of crystal		Crystal system
Anisotropic crystal	Uniaxial crystal	Trigonal, tetragonal, hexagonal
	Biaxial crystal	Triclinic, monoclinic, orthorhombic
Isotropic crystal		Cubic

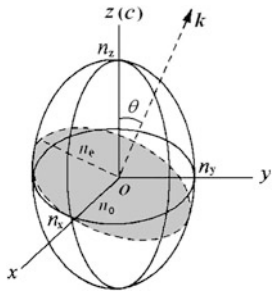

Fig. 3.7 Refractive index ellipsoid of the positive uniaxial crystal

In order to describe the law of light wave propagation in the anisotropic medium, one can use the refractive-index ellipsoid method. We can establish an equation in the principal axis coordinate system O*xyz*:

$$\frac{x^2}{n_x^2} + \frac{y^2}{n_y^2} + \frac{z^2}{n_z^2} = 1. \tag{3.2.30}$$

The index ellipsoid described by this equation is shown in Fig. 3.7. In which n_x, n_y, n_z are the half axis length of rectangular coordinates axis x, y, z, respectively, which are called the principal refractive index.

For the isotropic cubic crystal, $n_x = n_y = n_z = n_0$, Eq. (3.2.30) becomes

$$x^2 + y^2 + z^2 = n_0^2. \tag{3.2.31}$$

This is a ball with radius of n_0, so no matter the light propagation along any direction, the refractive index always is same.

For anisotropic crystal, in general there exists one or two special optical axis directions, the light wave propagates along the optical axis direction without birefringence. The crystal only has one optical axis, which is called the uniaxial crystal. If selecting z-axis as the optical axis c, then $n_x = n_y = n_o$, $n_z = n_e \neq n_o$, the refractive index ellipsoid equation is

$$\frac{x^2}{n_o^2} + \frac{y^2}{n_o^2} + \frac{z^2}{n_e^2} = 1, \tag{3.2.32}$$

where n_o is the refractive index of ordinary light (o light); n_e is the refractive index of extraordinary light (e light). This is an index ellipsoid, its rotation axis is z-axis.

There are two kinds of uniaxial crystals: if $n_o > n_e$, it is a negative uniaxial crystal; if $n_e > n_o$, it is a positive uniaxial crystal. Figure 3.7 shows a refractive index ellipsoid of positive uniaxial crystal.

In Fig. 3.7, wave vector $\boldsymbol{k}$ denotes the propagation direction of light wave, the intersection angle between $\boldsymbol{k}$ and optical axis c is θ. A cross section passing through the original point and perpendicular to $\boldsymbol{k}$ intersects with the ellipsoid to form a ellipse-shape intersecting line. The length of two half axis of the ellipsoid are just refractive indexes n_o and n_e corresponding to two orthogonal polarization states. Visible, the polarization direction of the ordinary light (0 light) is perpendicular to the plane consisted with the optical axis c and wave vector $\boldsymbol{k}$; and the polarization direction of the extraordinary light (e light) is just in that plane.

The refractive index of extraordinary light n_e is a function of intersection angle θ of the optical axis c and the wave vector $\boldsymbol{k}$, It is not difficult to prove that the following formula is satisfied:

$$\frac{1}{n_e^2(\theta)} = \frac{\sin^2\theta}{n_e^2} + \frac{\cos^2\theta}{n_o^2}. \tag{3.2.33}$$

When $\boldsymbol{k}$ is along the optical axis direction, $\theta = 0$, $n_e(0^0) = n_o$; when k is perpendicular to the optical axis direction, $\theta = 90^0$, $n_e(90^0) = n_e$.

We can through adjusting the interaction angle θ between the crystal optical axis c and the incident light wave vector $\boldsymbol{k}$ to change the refractive index of crystal $n_e(\theta)$, to lead the frequency doubling effect satisfying the phase matching condition $\Delta\boldsymbol{k} = 0$. This is called as angle phase matching method [3, 4]. Meanwhile, we also can through varying the temperature of crystal to change refractive index of crystal $n_e(\theta)$, to realize $\Delta\boldsymbol{k} = 0$, this is called the temperature phase matching method.

Now we discuss the so called first phase matching condition, in this condition, two fundamental frequency lights take the same polarization direction. In general, the polarization state of fundamental frequency light is selected with higher refractive index. Namely for negative uniaxial crystal ($n_o > n_e$), taking the fundamental frequency light as o polarization state, the frequency doubling light as e polarization state; for positive uniaxial crystal ($n_e > n_o$), taking the fundamental frequency light as e polarization state, the frequency doubling light as o polarization state.

The phase matching condition for the negative uniaxial crystal is

$$n_{\mathrm{o}}^{\omega} = n_e^{\omega}(\theta_m). \tag{3.2.34}$$

Figure 3.8 draws a refractive index surface diagram in the negative uniaxial crystal when the phase matching between the fundamental frequency light and the frequency doubling light are sufficed. The solid line are the o light index ball and the e light index ellipsoid for the fundamental frequency light at frequency of ω; the imaginary line are o light index ball and the e light index ellipsoid for the frequency doubling light at frequency of 2 ω. We can see that there is a point of intersection between the o light index surface of fundamental wave and the e light index surface

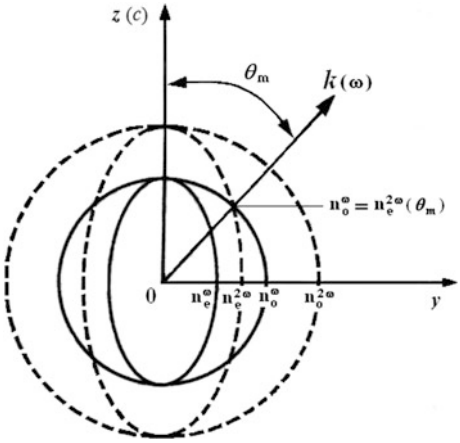

Fig. 3.8 In negative uniaxial axis crystal, the fundamental frequency light and the frequency doubling light matched refractive-index surface diagram. The *solid line* are the o light index ball and the e light index ellipsoid for the fundamental frequency light at frequency ω; the *imaginary line* are the o light index ball and the e light index ellipsoid for the frequency doubling light at frequency 2ω

of frequency doubling wave, the intersection point corresponded the intersection angle between the wave vector and optical axis θ_m satisfies Eq. (3.2.34), θ_m is just phase matching angle. In the figure, n_o^{ω}, n_e^{ω} and $n_o^{2\omega}$, $n_e^{2\omega}$ are two principal refractive indexes of the fundamental frequency light and the frequency doubling light, respectively.

Substituting Eq. (3.2.34) into Eq. (3.2.33), we can obtain the formula of the phase matching angle of negative uniaxial crystal θ_m:

$$\sin^2\theta_m = \frac{\left(n_o^{\omega}\right)^{-2} - \left(n_o^{2\omega}\right)^{-2}}{\left(n_e^{2\omega}\right)^{-2} - \left(n_o^{2\omega}\right)^{-2}}. \tag{3.2.35}$$

For example, in negative uniaxial crystal KDP, using the ordinary light of ruby laser at frequency of 0.6943 μm as the fundamental frequency, under the phase matching condition, the matching angle is $\theta_m = 50.4°$, the extraordinary light of frequency doubling wave at frequency of 0.3471 μm can be obtained.

The phase matching condition of the positive uniaxial crystal is

$$n_o^{2\omega} = n_e^{\omega}(\theta_m). \tag{3.2.36}$$

Figure 3.9 draws a refractive index surface diagram in positive uniaxial crystal when the phase matching between the fundamental frequency light and the frequency doubling light are sufficed. Visible, there is an intersection point between the fundamental wave e light refractive-index surface and the frequency doubling wave o light refractive-index surface. The intersection point corresponded intersection angle between the wave vector and the optical axis θ_m satisfies Eq. (3.2.34), θ_m is just the phase matching angle.

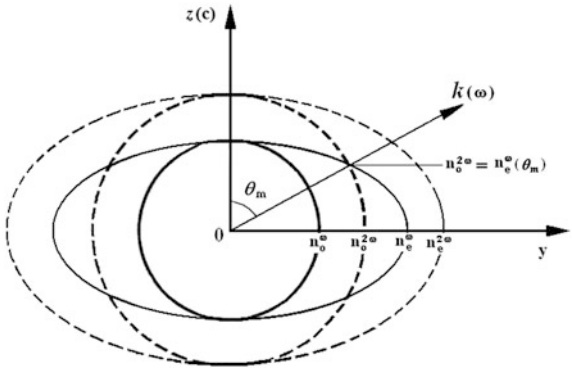

Fig. 3.9 In positive uniaxial crystal, the fundamental frequency light and the frequency doubling light matched refractive-index surface diagram. The *solid line* are the o light index ball and the e light index ellipsoid for the fundamental frequency light at frequency ω; the *imaginary line* are the o light index ball and the e light index ellipsoid for the frequency doubling light at frequency 2ω

Substituting Eq. (3.2.36) into Eq. (3.2.33), in same way the possible uniaxial crystal phase matching angle θ_m formula can be obtain:

$$\sin^2\theta_m = \frac{\left(n_o^{2\omega}\right)^{-2} - \left(n_o^{\omega}\right)^{-2}}{\left(n_e^{\omega}\right)^{-2} - \left(n_o^{\omega}\right)^{-2}}. \tag{3.2.37}$$

In above phase matching condition, two fundamental frequency lights take same polarization direction, we call the first class phase match. In which, the polarization characteristic of negative uniaxial crustal is denoted by symbol o + o → e; the polarization characteristic of positive uniaxial crustal is denoted by symbol e + e → o. their phase matching condition are list in the Table 3.2.

Actually, the phase matching condition also exists second class phase matching scheme, that is taking perpendicular propagation directions of two foundational frequency lights: one is o light, another one is e light. Its polarization characteristics for negative uniaxial crystal is o + e → e; for positive uniaxial crystal is o + e → o. Their phase matching condition is also listed Table 3.2. About the

Table 3.2 Phase matching condition of uniaxial crystal

Crystal type	First class phase match		Second class phase match	
	Polarization characteristic	Phase matching condition	Polarization characteristic	Phase matching condition
Negative uniaxial crystal	o + e → e	$n_o^{\omega} = n_e^{2\omega}(\theta_m)$	o + o → e	$\frac{1}{2}\left[n_o^{\omega}(\theta_m) + n_e^{\omega}\right] = n_o^{2\omega}(\theta_m)$
Positive uniaxial crystal	o + e → o	$n_o^{2\omega} = n_e^{\omega}(\theta_m)$	e + e → o	$\frac{1}{2}\left[n_o^{\omega} + n_e^{\omega}(\theta_m)\right] = n_o^{2\omega}$

deduction of second class phase matching condition, reader can refer to the related reference material, here we do not give unnecessary details.

Except for the uniaxial crystal phase matching condition, there is the biaxial crystal phase matching condition, if you want to know the knowledge in this aspect, please also refer to the related reference material.

3.2.4 Experimental Facilities for Second Harmonic Generation

Figure 3.10 gives several schematic diagrams of typical experimental facilities, these facilities are composed by three parts: the nonlinear optical crystal, the fundamental wave source, and the phase matching system.

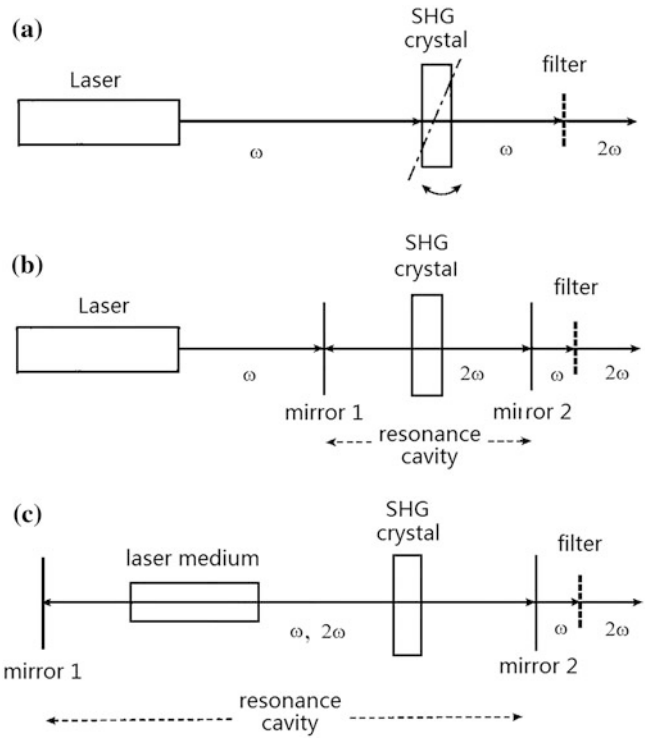

Fig. 3.10 Typical experimental facilities for the optical second harmonic generation **a** single-pass mode; **b** external cavity mode; **c** intracavity mode

1. **Nonlinear Optical Crystal**

Generally people use the artificial growth bulk or flake-like high quality crystal, the optical axis of crystal relative to the incident fundamental wave has a certain matching angle. To reduce the reflection loss, it can plate the antireflection coating on crystal two parallel end surface. According to the different methods of phase matching, the nonlinear crystal is divided into the following three categories:

(1) Angle tuning phase matching crystal: KDP, ADP, KTP, $LiIO_3$, BBO, LBO etc. Frequency doubling of the incidence laser at the near infrared or visible wavelength, to produce the visible light or near ultraviolet light, the efficiency can reach 30 and 50 %.
(2) Temperature tuning phase matching crystal: $LiNbO_3$, $KNbO_3$, Ba_2NaNbO_{15} etc. They have better optical transmission property in the spectrum region 0.4-5μm, it can be used to produce near-infrared frequency doubling light, the efficiency is higher than 50 %.
(3) Semiconductor crystal for producing infrared second harmonic wave, such as Ag_3AsS_3, $AgGaSe_2$, $CdGeAs_2$, CdSe, GaSe, etc. These crystals have high second-order nonlinear susceptibility, in the wide infrared spectrum region have better transmittance.

2. **Fundamental Wave Optical Source**

Mostly people adopt the solid pulse lasers as the optical sources, such as Nd-glass laser, Nd-doped Gamet laser, Ruby laser, etc. The CW solid and liquid laser can also be used for continuous frequency doubling light output. In order to enhance the frequency doubling conversion efficiency, the focusing light passing through the crystal also can be used.

3. **Phase Matching System**

According to the different nonlinear crystals and experimental conditions, the different phase matching, exciting and coupling methods can be used. Figure 3.10a shows a usually used the mode that the light beam single-pass through the crystal, it is suitable to the angle phase matching method. Figure 3.10b showed equipment is suitable to temperature phase matching frequency doubling crystal, the crystal inserts into the resonance cavity, let's lower power fundamental light multiple-pass through the crystal, to enhance the convention efficiency. It also can insert the frequency doubling crystal into the fundamental wave laser cavity, as shown in Fig. 3.10c, because the light intensity inside laser cavity is much stronger than outputted light intensity outside the cavity, in benefit of enhancement of conversion efficiency.

3.3 Optical Sum Frequency, Difference Frequency and Parameter Amplification

3.3.1 Optical Sum Frequency and Frequency Up-Conversion

Now we discuss the coupled Eqs. (3.1.28)–(3.1.30), which will be used for the sum frequency and difference frequency processes. In order to simplify the equations, we define a set of new light electric field amplitudes A_i and nonlinear coefficient κ, which are

$$A_i(z) = \sqrt{\frac{n_i}{\omega_i}} E_i(z) \quad (i = 1, 2, 3), \tag{3.3.1}$$

$$\kappa = \frac{\chi^{(2)}}{2c} \sqrt{\frac{\omega_1 \omega_2 \omega_3}{n_1 n_2 n_3}} = \frac{d}{c} \sqrt{\frac{\omega_1 \omega_2 \omega_3}{n_1 n_2 n_3}}, \tag{3.3.2}$$

where d is the frequency doubling coefficient. So the coupled Eqs. (3.1.28)–(3.1.30) are simplified as

$$\frac{\partial A_1(\mathrm{z})}{\partial \mathrm{z}} = iD\kappa A_2^*(z) A_3(z) e^{i\Delta kz}, \tag{3.3.3}$$

$$\frac{\partial A_2(\mathrm{z})}{\partial \mathrm{z}} = iD\kappa A_3(z) A_1^*(z) e^{i\Delta kz}, \tag{3.3.4}$$

$$\frac{\partial A_3(\mathrm{z})}{\partial \mathrm{z}} = iD\kappa A_1(z) A_2(z) e^{-i\Delta kz}, \tag{3.3.5}$$

where $\Delta k = k_1 + k_2 - k_3 = 0$.

Now we discuss the sum frequency process. There are three photons at different frequency joining this process. According to Eqs. (3.1.13) and (3.1.14), they satisfy following the energy and momentum conservation relations, respectively:

$$\omega_3 = \omega_1 + \omega_2, \tag{3.3.6}$$

$$\boldsymbol{k}_3 = \boldsymbol{k}_1 + \boldsymbol{k}_2. \tag{3.3.7}$$

The optical sum frequency can be used for the frequency upconversion [5, 6], that is an effective means to produce shorter wavelength coherent radiation. For example, using crystal Ag_3AsS_3 as a sum frequency crystal, a 1.06-wavelength YAG laser as the pumping light (ω_2), to convert the 10.6 μm-wavelength CO_2 infrared light (ω_1) into the 96 μm-wavelength visible light (ω_3). That is because the detection of middle and far infrared light must use the refrigerant detector, the detection of visible light can use the room temperature fast detector.

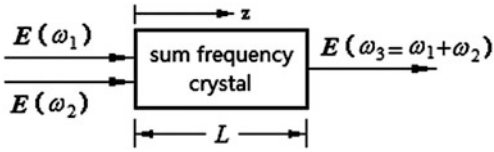

Fig. 3.11 Schematic diagram of the collinear optical sum frequency process

Assuming that the three waves at ω_1, ω_2 and ω_3 participated in sum frequency process collinearly propagate in the nonlinear crystal, all along z-direction, as shown in Fig. 3.11, we will used coupled Eqs. (3.3.3)–(3.3.5) to calculate the variation of field amplitudes of the sum frequency light (ω_3) and the signal light (ω_1) with the coordinate axis z.

We suppose that the intensity of pump light ω_2 is strong enough, so that its amplitude does not change in the sum frequency process, i.e., it is a constant:

$$A_2(z) \approx A_2(0) = \text{constant}. \tag{3.3.8}$$

Thus the three coupled Eqs. (3.3.3)–(3.3.5) becomes two. Considering the frequency without degeneration, taking $D = 2$; and to defied a sum-frequency nonlinear coefficient κ_{SF}, it is two times of the original nonlinear coefficient κ, i.e.,

$$\kappa_{SF}=2\kappa, \tag{3.3.9}$$

Therefore the two coupled equations for sum frequency process are given by

$$\frac{\partial A_1(z)}{\partial z} = i\kappa_{SF}A_2(0)A_3(z)e^{i\Delta kz}, \tag{3.3.10}$$

$$\frac{\partial A_3(z)}{\partial z} = i\kappa_{SF}A_1(z)A_2(0)e^{-i\Delta kz}. \tag{3.3.11}$$

We further define g_{SF} is the sum frequency gain factor (suppose it is a real number):

$$g_{SF} = \kappa_{SF}A_2(0) = \frac{2d}{c}\sqrt{\frac{\omega_1\omega_3}{n_1n_3}}\boldsymbol{E}_2(0), \tag{3.3.12}$$

Under phase matching condition, i.e., $\Delta k = 0$, Eqs. (3.3.10) and (3.3.11) are simplified to

$$\frac{\partial A_1(z)}{\partial z} = ig_{SF}A_3(z), \tag{3.3.13}$$

$$\frac{\partial A_3(z)}{\partial z} = ig_{SF}A_1(z). \tag{3.3.14}$$

Then making derivation of two side of Eq. (3.3.14), and substituting Eq. (3.3.13) into it, we obtain

$$\frac{d^2A_3(z)}{dz^2} + g_{SF}^2 A_3(z) = 0. \tag{3.3.15}$$

The general solution of Eq. (3.3.15) is

$$A_3(z) = C_1 \cos(g_{SF}z) + C_2 \sin(g_{SF}z). \tag{3.3.16}$$

To take $z = 0$ in Eq. (3.3.16), and use boundary condition $A_3(0) = 0$, obtain $C_1 = 0$. Equation (3.3.16) becomes

$$A_3(z) = C_2 \sin(g_{SF}z). \tag{3.3.17}$$

Then we substitute Eq. (3.3.17) into (3.3.14), after derivation, set $z = 0$ to get $C_2 = iA_1(0)$. So from Eq. (3.3.16) to obtain

$$A_3(z) = iA_1(0) \sin(g_{SF}z). \tag{3.3.18}$$

Further substituting Eq. (3.3.18) into (3.3.14), after derivation to obtain

$$A_1(z) = A_1(0) \cos(g_{SF}z), \tag{3.3.19}$$

To take mode square of above two amplitudes $A_3(z)$ and $A_1(z)$ respectively, then add together, we obtain

$$|A_1(z)|^2 + |A_3(z)|^2 = |A_1(0)|^2. \tag{3.3.20}$$

Using relations

$$I_1 = \frac{1}{2}\varepsilon_0 c n_1 |E_1|^2 = \frac{1}{2}\varepsilon_0 c \omega_1 |A_1|^2, \tag{3.3.21}$$

$$I_3 = \frac{1}{2}\varepsilon_0 c n_3 |E_3|^2 = \frac{1}{2}\varepsilon_0 c \omega_3 |A_3|^2, \tag{3.3.22}$$

we obtain

$$\left(\frac{\omega_1}{\omega_3}\right) I_3(z) + I_1(z) = I_1(0). \tag{3.3.23}$$

We can see that because the intensity of incident signal $I_1(0)$ is a constant, the increase of light intensity $I_3(z)$ is the price of the decrease of light intensity $I_1(z)$. From Eq. (3.3.19) to obtain $|\boldsymbol{A}_1|^2$, then use Eqs. (3.3.21) and (3.3.23), we obtain

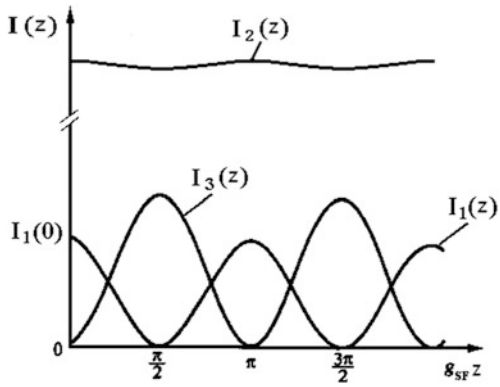

Fig. 3.12 In the phase match sum frequency process the *curves* of variation of intensities of two light beams at ω_1 and ω_3 with the distance $g_{SF}z$

$$I_3(z) = \frac{\omega_3}{\omega_1} I_1(0) \sin^2(g_{SF}z). \tag{3.3.24}$$

If the length of crystal is L, the conversion efficiency of sum frequency is

$$\eta = \frac{I_3(L)}{I_1(0)} = \frac{\omega_3}{\omega_1} \sin^2(g_{SF}L). \tag{3.3.25}$$

Figure 3.12 shows that in sum frequency process, under phase matching condition, the curves of variation of light intensities of two beams at frequency ω_1 and ω_3 with distance z.

Figure 3.12 can be explained as follows:in the beginning the intensity of light wave at ω_1 drop off gradually, its energy transfers to the light wave at ω_3 . When the propagation distance increases to $g_{SF}z = \pi/2$, the conversion efficiency reaches to maximum. In this case, $\eta > 1$, that is due to except all $I_1(0)$ converts to $I_3(z)$ at this point, actually there is a small part light coming from pump light $I_2(z)$ at ω_2 . It can be proved that the sum of three light intensities remains unchanged, i.e., $I_1 + I_2 + I_3 = constant$. After the intensity of light wave at ω_3 reaches the peak, it will pass through the difference frequency with the pump light at ω_2 to send its energy back to the light at $\omega_1 = \omega_3 - \omega_2$. Therefore, the periodic oscillation situation will appear.

If the intensity of pump light $I_2(z)$ at frequency ω_2 is very small, from gain factor definition Eq. (3.3.12) we can know that g_{SF} is also very small, so in the efficiency Eq. (3.3.25) we have

$$\sin^2(g_{SF}L) \approx (g_{SF}L)^2, \tag{3.3.26}$$

This is the case of small signal approximation. Therefore we obtain the frequency conversion efficiency formula in the case of the small signal approximation and $\Delta k = 0$:

$$\eta \approx \frac{\omega_3}{\omega_1} g_{SF}^2 L^2 = \frac{8\omega_3^2 d^2 L^2 I_2(0)}{\varepsilon_0 n_1 n_2 n_3 c^3}. \tag{3.3.27}$$

It can be proved, in the case of the small signal approximation and $\Delta k \neq 0$, the frequency conversion efficiency formula becomes

$$\eta \approx \frac{\omega_3}{\omega_1} g_{SF}^2 L^2 = \frac{8\omega_3^2 d^2 L^2 I_2(0)}{\varepsilon_0 n_1 n_2 n_3 c^3} \mathrm{sinc}^2(\Delta kL/2). \tag{3.3.28}$$

We can see that Eq. (3.3.28) is only an oscillation factor more than Eq. (3.3.27).

3.3.2 Optical Difference Frequency and Frequency Down-Conversion

In the optical difference frequency process, according to the energy and momentum conservation laws, the frequencies and wave vectors are required to satisfy the following relations:

$$\omega_2 = \omega_3 - \omega_1, \tag{3.3.29}$$

$$\boldsymbol{k}_2 = \boldsymbol{k}_3 - \boldsymbol{k}_1. \tag{3.3.30}$$

Figure 3.13 is a schematic diagram of the optical difference frequency process in the z-direction collinear propagation case. To utilize this process can realize frequency down-conversion: using the difference frequency of two visible laser (ω_3 and ω_1) to obtain an infrared laser ($\omega_2 = \omega_3 - \omega_1$) output. For example using $LiNbO_3$ as a difference frequency crystal, and a 532 nm-wavelength YAG frequency doubled laser (ω_3) as a pump laser, it makes difference frequency with a tunable dye laser (ω_1) with the wavelength range of 575–650 nm, the result of difference frequency can obtain a tunable infrared laser (ω_2) output with the wavelength range of 3.40–5.65 μm [7].

Assuming that the intensity of the pump light at frequency ω_3 is strong enough, so that its intensity can be regarded do not change in the difference frequency process, we have

$$A_3(z) \approx A_3(0), \tag{3.3.31}$$

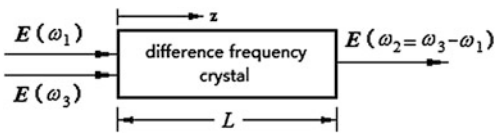

Fig. 3.13 Schematic diagram of optical difference frequency or frequency down-conversion process

Suppose $A_3(0)$ is a real number, and taking $D = 2$ for the difference frequency process, then three coupled Eqs. (3.3.3)–(3.3.5) become two equations:

$$\frac{\partial A_1(z)}{\partial z} = i\kappa_{DF} A_2^*(z) A_3(0) e^{i\Delta kz}, \tag{3.3.32}$$

$$\frac{\partial A_2(z)}{\partial z} = i\kappa_{DF} A_1^*(z) A_3(0) e^{i\Delta kz}, \tag{3.3.33}$$

where κ_{DF} is the nonlinear coupling coefficient of difference frequency, the relationship between κ_{DF} and κ is

$$\kappa_{DF} = 2\kappa. \tag{3.3.34}$$

Under the case of $\Delta k = 0$, Eqs. (3.3.32) and (3.3.33) are simplified as

$$\frac{\partial A_1(z)}{\partial z} = i g_{DF} A_2^*(z), \tag{3.3.35}$$

$$\frac{\partial A_2(z)}{\partial z} = i g_{DF} A_1^*(z), \tag{3.3.36}$$

where g_{DF} is defined as the gain coefficient of difference frequency:

$$g_{DF} = \kappa_{DF} A_3(0) = \frac{2d}{c}\sqrt{\frac{\omega_1\omega_2}{n_1 n_2}} \boldsymbol{E}_3(0). \tag{3.3.37}$$

Making derivation of two side of Eq. (3.3.35), and substituting the conjugate Eq. (3.3.36) into it, then we obtain

$$\frac{d^2 A_1(z)}{dz^2} - g_{DF}^2 A_1(z) = 0. \tag{3.3.38}$$

The general solution of Eq. (3.3.38) is

$$A_1(z) = D_1 \sinh(g_{DF} z) + D_2 \cosh(g_{DF} z). \tag{3.3.39}$$

To utilize the bounder condition at $z = 0: A_2(0) = 0$ and $A_1(0) \neq 0$, from Eqs. (3.3.39) to (3.3.36), we obtain the following field amplitudes:

$$A_1(z) = A_1(0)\cosh(g_{DF} z), \tag{3.3.40}$$

$$A_2^*(z) = -iA_1(0)\sinh(g_{DF} z). \tag{3.3.41}$$

Figure 3.14 draws the variation of two field amplitudes with z. from the figure we can see that the difference frequency generation field at frequency ω_2 and the

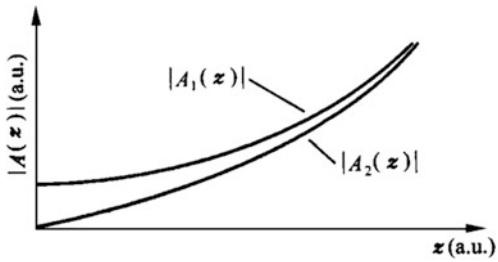

Fig. 3.14 Characteristics of the variation of field amplitude $|A_1(z)|$ and $|A_2(z)|$ with z

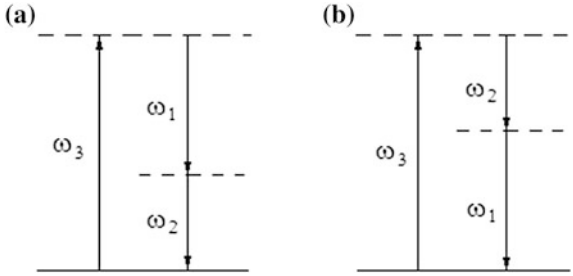

Fig. 3.15 Explanation of difference frequency characteristics: **a** the signal filed ω_1 excites to generate the difference frequency filed $\omega_2 = \omega_3 - \omega_1$; **b** the difference frequency filed ω_2 excites to generation the new signal field ω_1

signal field at ω_1 monotonously increase at the same time in the nonlinear interaction, it is total different with the sum frequency appeared oscillation.

Following figure of the energy level transition is used for explaining the reason of the difference frequency generation field and the signal filed monotonously increase at the same time.

Figure 3.15a shows the signal field ω_1 excites to generate the difference frequency field $\omega_2 = \omega_3 - \omega_1$, Fig. 3.15b shows the difference frequency field ω_2 excites to generate the signal field ω_1, the new signal field ω_1 again enhances the generation of the new difference frequency field ω_2, such repetition, to lead the two fields exponentially growth.

From Eqs. (3.3.40) to (3.3.41) we obtain the amplitude square formulas:

$$|A_1(z)|^2 = |A_1(0)|^2 \cosh^2(gz), \tag{3.3.42}$$

$$|A_2(z)|^2 = |A_1(0)|^2 \sinh^2(gz). \tag{3.3.43}$$

If the length of crystal is L, from Eq. (3.3.43) and relationships

$$I_1 = \frac{1}{2}\varepsilon_0 c n_1 |E_1|^2 = \frac{1}{2}\varepsilon_0 c \omega_1 |A_1|^2, \tag{3.3.44}$$

$$I_2 = \frac{1}{2}\varepsilon_0 c n_2 |E_2|^2 = \frac{1}{2}\varepsilon_0 c \omega_2 |A_2|^2, \tag{3.3.45}$$

we obtain the difference frequency conversion efficiency formula under $\Delta k = 0$:

$$\eta = \frac{I_2(L)}{I_1(0)} = \frac{\omega_2}{\omega_1}\sinh^2(g_{DF}L). \tag{3.3.46}$$

In small signal case, the pump light $E_3(0)$ is small, from Eq. (3.3.37) g_{DF} is also small, so that in Eq. (3.3.46) we have

$$\sinh^2(g_{DF}L) \approx (g_{DF}L)^2, \tag{3.3.47}$$

Therefore, under the small signal and $\Delta k = 0$ case the difference frequency conversion efficiency is

$$\eta \approx \frac{\omega_2}{\omega_1}(g_{DF}L)^2 = \frac{8\omega_2^2 d^2 L^2 I_3(0)}{\varepsilon_0 n_1 n_2 n_3 c^3}. \tag{3.3.48}$$

3.3.3 *Optical Parametric Amplification*

In the process similar to the difference frequency, the pump light energy gradually transfers to the signal light with the increase of propagation distance, leads the signal light to amplify, and in the same time generates the idler frequency light, this process is similar to the parametric amplification in microwave waveband, so it is called the optical parametric amplification (OPA) [8]. Suppose that the pump light at the frequency of $\omega_3 = \omega_p$ with the amplitude $E_3 = E_p$; the signal light at the frequency of $\omega_1 = \omega_s$ with the amplitude $E_1 = E_s$; the idler light at the frequency of $\omega_2 = \omega_i$ with the amplitude $E_2 = E_i$, the optical parametric amplification process is shown in Fig. 3.16.

We can regard the gain coefficient of difference frequency g_{DF} as the gain coefficient of parametric amplification g, which is described by Eq. (3.3.37).

In the beginning, $I_1(0) \neq 0$ and $I_2(0) = 0$. If the pump light filed $E_3(0)$ is very strong, we have $gz >> 1$, so that

$$\sinh gz = \frac{e^{gz} - e^{-gz}}{2} \approx \frac{1}{2}e^{gz}, \quad \text{and } \cosh gz = \frac{e^{gz} + e^{-gz}}{2} \approx \frac{1}{2}e^{gz},$$

then Eqs. (3.3.42) and (3.3.43) becomes

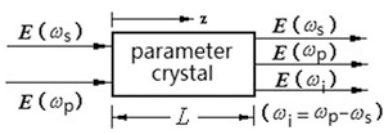

Fig. 3.16 Schematic diagram of optical parametric amplification process

$$|A_1(z)|^2 \approx \frac{1}{4}|A_1(0)|^2 e^{2gz}, \tag{3.3.50}$$

$$|A_2(z)|^2 \approx \frac{1}{4}|A_1(0)|^2 e^{2gz}. \tag{3.3.51}$$

That means that in this case, the intensity of idler light is equal to the intensity of signal light.

According to Eq. (3.3.50), the magnification of parametric amplification M for signal light is defined as

$$M = \frac{I_1(z)}{I_1(0)} = \frac{|A_1(z)|^2}{|A_1(0)|^2} \approx \frac{1}{4}e^{2gz}. \tag{3.3.45}$$

Because the gain coefficient of parametric amplification g is proportional to the pump light filed amplitude $E_3(0)$, form Eq. (3.3.45) we can see that the magnification of parametric amplifier exponentially enhances with increase of $E_3(0)$. Due to g is proportional to $d \propto \chi^{(2)}$, so that the second-order nonlinear susceptibility decides the ability of parametric amplification.

3.3.4 Comparison of Four Kinds of Three-Wave Mixing Processes and Experimental Facilities

1. **Comparison of Characteristics of Four Kinds of Three-Wave Mixing Processes**

Previous we introduced 4 kinds of three-wave mixing processes: the second harmonic generation (SHG), the sum frequency generation (SFG), the difference frequency generation (DFG) and the optical parametric amplification (OPA), as shown in Fig. 3.17.

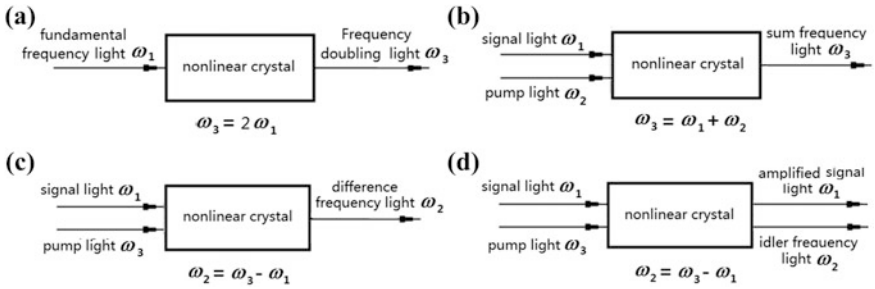

Fig. 3.17 Three-wave mixing processes: **a** second harmonic generation; **b** sum frequency generation; **c** difference frequency generation; **d** optical parametric amplification

The second harmonic is a particular case of the sum frequency $\omega_3 = \omega_1 + \omega_2$, both are belong to the case that the energy of two low-frequency light fields transfer to that of a high-frequency light field, i.e., the frequency up-conversion; the optical parametric amplification is particular case of the difference frequency, both are belong to the case that the energy of two high-frequency light fields transfer to that of a low-frequency light field, i.e., the frequency down-conversion. The difference of both is that the difference frequency pays attention to the generation of the difference frequency light at $\omega_2 = \omega_3 - \omega_1$, however the optical parametric amplification pays attention to the amplification of the signal light at ω_1 (the light at ω_2 regards as the idler-frequency light). For the three processes: the frequency doubling, the sum frequency and the difference frequency, the power conversion efficiency η needs to be studied. For the parametric amplification, the magnification M is instead of η. The pump light is different in above 4 different processes: in second harmonic process, it is the fundamental frequency light at ω_1; in sum frequency process, it is the light at ω_2; in difference frequency process and parametric amplification process, it is the light at ω_3.

2. Experimental Facilities of Three-Wave Mixing Process

Above four kinds of optical three-wave mixing processes have similar generation mechanism, the requirements of the nonlinear crystal materials and the phase matching condition are the same.

The common requirements of nonlinear crystals are (1) piezo-electric crystal without center symmetry; (2) the phase match in certain way is satisfied, for example the angle match or the temperature match. The propagation directions of three waves can be different, but should satisfy the momentum conservation condition; (3) the crystal materials have good optical transparency for the two incident lights and one generated light.

To three-wave mixing experimental systems we have following same requirements: (1) two incident light sources at different frequencies; (2) the facilities to realize angle match or temperature match; (3) the dispersion element and absorption element (prism, grating and filter, etc.) used for separating the transmitted lights at different frequencies.

As an example, Fig. 3.18 gives a typical three-wave mixing (such as sum frequency) experimental setup.

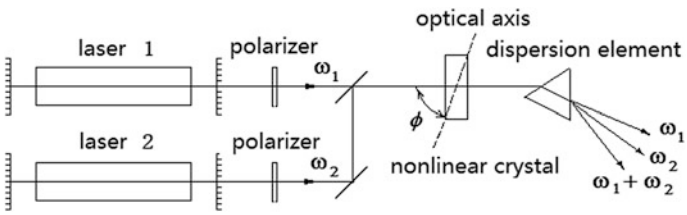

Fig. 3.18 Typical experimental setup for three-wave mixing (sum frequency)

3.4 Optical Parametric Oscillator

Because the amplification factor of the single pass through the nonlinear crystal in the optical parametric amplification is small, in order to enhance the energy conversion efficiency, we can place the parametric amplifier into a resonant cavity, the lights at frequency ω_s (and ω_i) oscillates in the cavity to be enhanced, when the energy of pump light at frequency ω_p over a certain threshold value, the gain of the nonlinear interaction overcomes the intracavity loss, then a stable light beam at frequency of ω_s (and ω_i) can be outputted from the cavity, this device is called the optical parametric oscillator (OPO) [9, 10].

In comparison of the parametric oscillator with the laser oscillator, the similarities is that both can generate the coherent light output; the difference is that the gain in the cavity of optical parametric oscillator is generated by the nonlinear effect, not by the population inversion; and the gain is in one way, the returning light cannot be enhanced, only be wastage.

3.4.1 Threshold Value Equations of Optical Parametric Oscillation

In order to deduce the optical parametric oscillation threshold value equation, suppose the length of crystal is L, two ends of crystal is fabricated to be spherical mirrors with the equal radius of curvature, their amplitude reflectivity are r_1 and r_2 for the signal light at frequency ω_1 and the idler light at frequency ω_2, respectively; the intensity reflectivity are $R_1 = |r_1|^2$ and $R_2 = |r_2|^2$, respectively; and the pump light at frequency ω_3 is transparent, as shown in Fig. 3.19.

Suppose the pump light intensity in the cavity is independent of propagation distance, the signal light electrical field and the idler light electrical field on the plane at any position z in the cavity can be expressed by a matrix $\tilde{A}(z)$:

$$\tilde{\boldsymbol{A}}(z) = \begin{vmatrix} A_1(z)e^{ik_1 z} \\ A_2^*(z)e^{-ik_2 z} \end{vmatrix}. \tag{3.4.1}$$

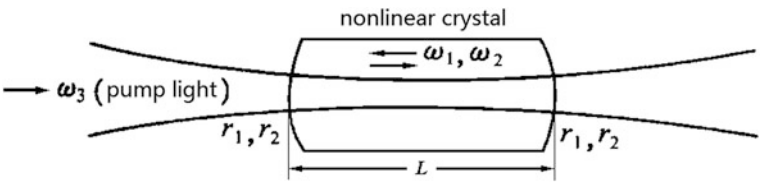

Fig. 3.19 Schematic diagram of the parametric oscillator with crystal structure

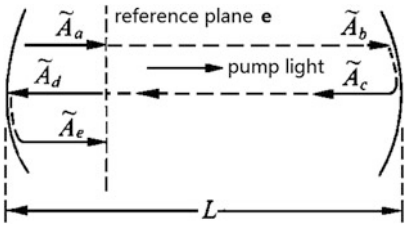

Fig. 3.20 The signal light and the idler light satisfy the self-consistent condition

Considering that under the excitation of pump light ω_3, at $z = 0$ the spontaneous radiation of the signal light at ω_1 and the idler light at ω_2 are produced in the meantime, namely $A_1(0) \neq 0$ and $A_2(0) \neq 0$, the solutions of coupled Eqs. (3.3.32) and (3.3.33) in difference frequency process are

$$A_1(z) = A_1(0)\cosh(gz) + iA_2^*(0)\sinh(gz), \tag{3.4.2}$$

$$A_2^*(z) = A_2^*(0)\cosh(gz) - iA_1(0)\sinh(gz). \tag{3.4.3}$$

The optical field amplitude at $z = L$ is

$$\tilde{\boldsymbol{A}}(L) = \begin{vmatrix} e^{ik_1L}\cosh(gL) & ie^{ik_1L}\sinh(gL) \\ -\,ie^{-k_2L}\sinh(gL) & e^{-k_2L}\cosh(gL) \end{vmatrix} \tilde{\boldsymbol{A}}(0). \tag{3.4.4}$$

The stable oscillation requires satisfying the self-consistent condition that after the light propagation for a round trip in the cavity $\tilde{\boldsymbol{A}}(z)$ is invariable, as shown in Fig. 3.20.

At the reference plane e, it should have

$$\tilde{\boldsymbol{A}}_e(z) = \tilde{\boldsymbol{A}}_a(z), \tag{3.4.5}$$

$\tilde{\boldsymbol{A}}_e(z)$ is obtained from $\tilde{\boldsymbol{A}}_a(z)$ multiplies the following 4 matrixes: the parametric amplification matrix for the light propagation from left to right, the reflection matrix at the end of right, the propagation matrix from right to left without gain, and the reflection matrix at the end of left, namely

$$\tilde{\boldsymbol{A}}_e = \begin{vmatrix} r_1 & 0 \\ 0 & r_2^* \end{vmatrix} \begin{vmatrix} e^{\mathrm{i}k_1L} & 0 \\ 0 & e^{-\mathrm{i}k_2L} \end{vmatrix} \begin{vmatrix} r_1 & 0 \\ 0 & r_2^* \end{vmatrix} \begin{vmatrix} e^{\mathrm{i}k_1L}\cosh(gL) & ie^{\mathrm{i}k_1L}\sinh(gL) \\ -ie^{-\mathrm{i}k_2L}\sinh(gL) & e^{-\mathrm{i}k_2L}\cosh(gL) \end{vmatrix} \tilde{\boldsymbol{A}}_a. \tag{3.4.6}$$

That is

$$\tilde{\boldsymbol{A}}_e = \begin{vmatrix} r_1^2\cosh(gL)e^{\mathrm{i}2k_1L} & ir_1^2\sinh(gL)e^{\mathrm{i}2k_1L} \\ -i(r_2^*)^2\sinh(gL)e^{-\mathrm{i}2k_2L} & (r_2^*)^2\cosh(gL)e^{-\mathrm{i}2k_2L} \end{vmatrix} \tilde{\boldsymbol{A}}_a = \boldsymbol{M}\tilde{\boldsymbol{A}}_a \tag{3.4.7}$$

The following self-consistent condition should be satisfied:

$$\tilde{\boldsymbol{A}}_e = \tilde{\boldsymbol{A}}_a = \boldsymbol{I}\tilde{\boldsymbol{A}}_a = \boldsymbol{M}\tilde{\boldsymbol{A}}_a$$

or

$$(\boldsymbol{M} - \boldsymbol{I})\tilde{\boldsymbol{A}}_a = 0, \tag{3.4.8}$$

where $\boldsymbol{I}$ is an unit matrix. If $\tilde{\boldsymbol{A}}_a$ has nonzero solution, it requires the determinant $|\boldsymbol{M} - \boldsymbol{I}| = 0$, so we obtain

$$[r_1^2 \cosh(gL)e^{i2k_1L} - 1][(r_2^*)^2 \cosh(gL)e^{-i2k_2L} - 1] = r_1^2(r_2^*)^2 \sinh^2(gL)e^{-i2(k_2-k_1)L}. \tag{3.4.9}$$

Equation (3.4.9) is called the parametric oscillation threshold equation, i.e. the starting oscillation condition of the parametric oscillator.

There are two kinds of optical parameter oscillators: one parameter oscillator allows signal light (ω_s) and idler light (ω_i) together oscillation and output, which is called the Double Resonant Oscillator (DRO); another one only allows the signal light (ω_s) oscillation and output, which is called the Singly Resonant Oscillator (SRO). Below we will introduce their working principles respectively.

3.4.2 Double Resonant Parametric Oscillator

Figure 3.21 shows the schematic diagram of the double resonant oscillator, in which the three light beams are collinear. The nonlinear crystal is inserted into the optical cavity consisted of two spherical reflectors. The signal light and the idler light are two longitudinal modes of resonant cavity, and the resonant cavity for the

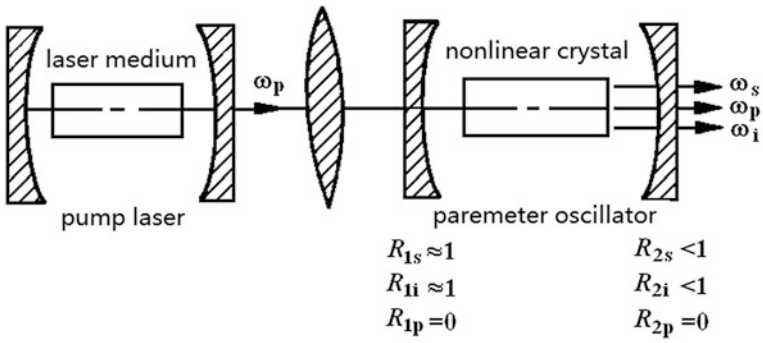

Fig. 3.21 Schematic diagram of collinear double resonant oscillator

pump light is transparent. So that the reflectivity of two spherical reflectors at front and back of the cavity for the signal light, the idler light and the pump light are $R_{1s} \approx 1$, $R_{1i} \approx 1$, $R_{1p} = 0$ and $R_{2s} < 1$, $R_{2i} < 1$, $R_{2p} = 0$, respectively.

Considering two cavity mirrors have the reflection loss and phase shift at the same time for the two lights at $\omega_1 = \omega_s$ and $\omega_2 = \omega_i$, we set

$$r_1^2 = R_1 e^{-i\phi_1}, \tag{3.4.10}$$

$$(r_2^*)^2 = R_2 e^{i\phi_2}, \tag{3.4.11}$$

where ϕ_1 and ϕ_2 are two cavity mirrors induced phase shifts. Substituting Eqs. (3.4.10) and (3.4.11) into Eq. (3.4.9), we obtain the threshold equation:

$$\begin{aligned}&[R_1 \cosh(gL) e^{i(2k_1 L - \phi_1)} - 1][R_2 \cosh(gL) e^{-i(2k_2 L - \phi_2)} - 1] \\ &\quad = R_1 R_2 \sinh^2(gL) e^{-i[2(k_2 - k_1)L - (\phi_2 - \phi_1)]}.\end{aligned} \tag{3.4.12}$$

When satisfying the phase condition:

$$\begin{aligned}2k_1 L - \phi_1 &= 2m\pi \\ 2k_2 L - \phi_2 &= 2n\pi\end{aligned} \quad (m, n \text{ is the integer}), \tag{3.4.13}$$

the exponents in two factors on left side of Eq. (3.4.12) are positive real numbers, in this case the corresponding gain is minimum, i.e., the threshold gain is $g = g_t$. The Eq. (3.4.13) denoted two light beams at frequency of ω_1 and ω_2 are laser longitudinal modes of the resonant cavity.

Using $\cosh^2 x - \sinh^2 x = 1$ and phase condition Eq. (3.4.13), the threshold Eq. (3.4.12) becomes

$$(R_1 + R_2)\cosh(g_t L) - R_1 R_2 = 1. \tag{3.4.14}$$

When $g_t L$ is smaller, After series expansion of $\cosh(g_t L)$ and approximately taking the front two items, we obtain

$$\cosh(g_t L) \approx 1 + \frac{(g_t L)^2}{2}, \tag{3.4.15}$$

Substituting Eq. (3.4.15) into Eq. (3.4.14), we obtain

$$(g_t L)^2 = \frac{2(1 - R_1)(1 - R_2)}{R_1 + R_2}. \tag{3.4.16}$$

Assuming $R_1 \approx R_2 \approx 1$, $R_1 + R_2 \approx 2$, then

$$(g_t L)^2 = (1 - R_1)(1 - R_2). \tag{3.4.17}$$

Therefore, the threshold condition of double resonant parametric oscillator is

$$(g_t L)_{DRO} = \sqrt{(1 - R_1)(1 - R_2)}. \tag{3.4.18}$$

Substituting Eq. (3.4.18) into Eq. (3.3.48) for the difference frequency conversion efficiency, then we obtain the pump light intensity threshold of double resonant parametric oscillator:

$$(I_{3t})_{DRO} = \frac{\varepsilon_0 n_1 n_2 n_3 c^3}{8\omega_1 \omega_2 d^2 L^2}(1 - R_1)(1 - R_2). \tag{3.4.19}$$

As an example, the $LiNbO_3$ crystal based double resonant parametric oscillator, to take the single pass loss of cavity is 2%, $\lambda_1 = \lambda_2 = 1\,\mu\text{m}$, $(1 - R_1) = (1 - R_2) = 2 \times 10^{-2}$, $d = 5 \times 10^{-12}\,\text{m/V}$, $n_1 \approx n_2 \approx n_3 \approx 2$, the estimated oscillation threshold intensity is $I_{3t} = 1.2 \times 10^3\,\text{W/cm}^2$. It is equivalently the output intensity of a common CW laser.

Although the pump light intensity threshold of the double resonant parametric oscillator is lower, its requirement for the stability of the resonant cavity is very high, and the length of cavity is easy effected by temperature variation and vibratory.

3.4.3 Singly Resonant Parametric Oscillator

The use of non-collinear phase matching technology to separate the directions of three light beams is shown in Fig. 3.22. It only allows the wave vector $\boldsymbol{k}_s$ of signal light at ω_s along the cavity axis direction, and making the signal light resonance with the resonant cavity. But the $\boldsymbol{k}_p$ of pump light and $\boldsymbol{k}_i$ of idler light are not along the cavity axis direction. The wave vectors of three light beams must satisfy following phase matching condition:

$$\boldsymbol{k}_p = \boldsymbol{k}_s + \boldsymbol{k}_i. \tag{3.4.20}$$

Now we start from the threshold Eq. (3.4.9) to deduce the threshold condition of the singly resonant parametric oscillator. For the singly resonant parametric oscillator, $r_2^* = 0$, Eq. (3.4.9) is simplified as

$$r_1^2 \cosh(gL) e^{i2k_1 L} = 1. \tag{3.4.21}$$

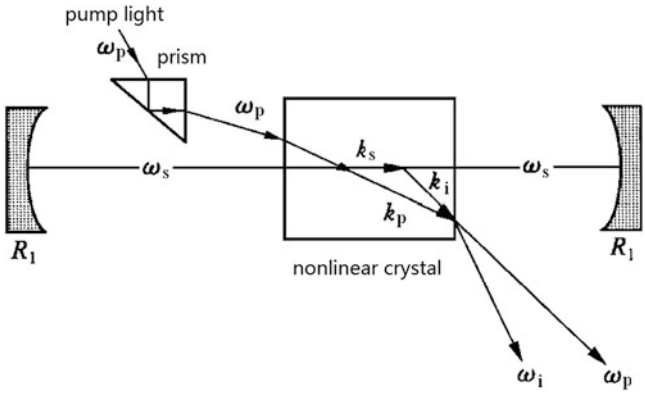

Fig. 3.22 Schematic diagram of non-collinear phase match in the singly resonant parametric oscillator

Setting $r_1^2 = R_1 e^{-i\phi_1}$, and substituting it into Eq. (3.4.21), then we obtain the phase condition:

$$2k_1 L - \phi_1 = 2m\pi, \tag{3.4.22}$$

Equation (3.4.21) then is

$$R_1 \cosh(g_t L) = 1. \tag{3.4.23}$$

Because $g_t L$ is very small, Eq. (3.4.23) can approximately simplify to

$$R_1\left(1 + \frac{g_t^2 L^2}{2}\right) = 1. \tag{3.4.24}$$

Taking $R_1 \approx 1$, then

$$(g_t L)_{SRO} = \sqrt{2(1 - R_1)}. \tag{3.4.25}$$

We substitute Eq. (3.4.24) into Eq. (3.3.48) for the difference frequency conversion efficiency, then obtain the pump light intensity threshold of singly resonant parametric oscillator:

$$(I_{3t})_{SRO} = \frac{\varepsilon_0 n_1 n_2 n_3 c^3}{8\omega_1 \omega_2 d^2 L^2} 2(1 - R_1). \tag{3.4.26}$$

To compare the pump light threshold intensity formula (3.4.26) for the singly resonant parametric oscillator and the formula (3.4.19) for the double resonant parametric oscillator, we obtain

$$\frac{(I_{3t})_{SRO}}{(I_{3t})_{DRO}} = \frac{[(g_t L)_{SRO}]^2}{[(g_t L)_{DRO}]^2} = \frac{2}{1 - R_2}. \tag{3.4.27}$$

where $1 - R_2$ can be regard as the cavity mirror loss of idler light at frequency ω_2. If the loss is 2 %, then the threshold of singly resonant parametric oscillator is higher than the threshold of double resonant parametric oscillator about 100 times. Even though the starting threshold of singly resonant parametric oscillator is higher, however its requirement in respect of resonant cavity stability is much lower.

Optical parametric oscillation (OPO) can be used to obtain wavelength tunable laser in a wide wavelength region. It not only can obtain the visible and infrared steady-state continuous wave, but also can obtain the picosecond or femtosecond ultrashort pulse laser, it has extensive application in the optical spectrum technology. There are many kinds of nonlinear crystal used for OPO, more good crystals mainly include KTP, BBO and LBO, they have not only larger second-order nonlinear coefficient and much higher optical damage threshold, but also wide transparent wavelength range, for example, BBO can reach 2500–190 nm; LBO can reach 3000–160 nm.

Review Questions of Chapter 3

1. Please deduce slowly-varying-amplitude approximation wave equation for describing the propagation of the monochromic plane wave in anisotropic medium and the three-wave mixing equations for describing the second-order nonlinear optics processes.
2. In fundamental wave small signal approximation condition, from three-wave mixing equations, please find out the frequency doubling wave intensity conversion efficiency formula. In order to enhance the frequency doubling efficiency, what measures you can adopt?
3. In high fundamental wave consumption condition, from three-wave mixing equations, please find out the law of variation of the frequency doubling field amplitude and fundamental frequency field amplitude with the propagation distance, and find out frequency doubling wave intensity conversion efficiency formula.
4. When the frequency doubling light and fundamental frequency light collinearly propagate, what is the refractive-index phase matching condition of frequency doubling crystal? Please discuss the phase matching conditions of negative uniaxial crystal and positive uniaxial crystal in the first- class phase matching condition and the second-class phase matching condition.
5. From three-wave mixing equations to deduce the coupling equations between the sum frequency light field and the signal light field, and the intensity conversion efficiency formula.

6. From three-wave mixing equations to deduce the coupling equations between the difference frequency light field and the signal light field, and the intensity conversion efficiency formula.
7. What is optical parameter amplification? Please deduce the magnification formula of parameter amplification. The parameter amplification process has what different physical meaning in comparison with the sum frequency and difference frequency processes?
8. What is optical parametric oscillator? Please discuss the working principles of the double resonant parametric oscillator and the singly resonant parametric oscillator, please deduce the pump light intensity threshold formula of these two parameter oscillators, and point out the advantages and disadvantages of both parameter oscillators.

References

1. A. Yariv, P. Yeh, *Optical Waves in Crystals* (Wiley, New York, 1984)
2. P.A. Franken, C.W. Hill et al., Generation of optical harmonics. Phys. Rev. Lett. **7**(4), 118–119 (1961)
3. F. Zernike, J.E. Midwinter, *Applied Nonlinear Optics* (Wiley, New York, 1973)
4. M.V. Hobden, Phase-Matched Second-Harmonic generation in biaxial crystals. Appl. Phys. **38** (11), 4365–4372 (1967)
5. C.L. Tang (ed.), *Quantum Electronics: a treatise* (Academic press, New York, 1975)
6. R.W. Boyd, C.H. Townes, An infrared upconverter for astronomical imaging. Appl. Phys. Lett. **31**(7), 440–442 (1977)
7. L.S. Goldberg, Narrow-bandwidth tunable infrared difference-frequency generation at high repetition rates in $LiIO_3$. Appl. Opt. **14**(3), 653–655 (1975)
8. S.A. Akhmanov, A.I. Kovrigin, M.M. Strukov, Frequency dependence of threshold of optical breakdown in air. JETP Lett. **1**, 25–29 (1965)
9. J.A. Giordmaine, R.C. Miller, Tunable coherent parametric oscillation in $LiNbO_3$ at optical frequencies. Phys. Rev. Lett. **14**(24), 973–976 (1965)
10. C.L. Tang, L.K. Cheng, *Fundamentals of optical parametric processes and oscillators* (Harwood Academic, New York, 1996)

Chapter 4
Optical Four-Wave Coupling Process

In this chapter we will start to study the third-order nonlinear optical phenomena. Because susceptibility $\chi^{(3)}$ is much smaller than $\chi^{(2)}$, the third-order nonlinear effect is much weaker than second-order nonlinear effect. However all mediums are common existence of the third-order nonlinear effect. This chapter mainly discuss the passive third-order nonlinear optics phenomena, in which the energy exchange only happens among light waves, these phenomena include the third harmonic, four-wave mixing and phase conjugation, etc. Subsequent chapters will discuss active third-order nonlinear optics phenomena, in which existing the energy exchange between light and medium, these phenomena include the optical Kerr effect, stimulated light scattering, nonlinear absorption and refraction, optical bistability, optical soliton, and nonlinear all-optical switch, etc.

4.1 Introduction to Third-Order Nonlinear Optical Effects

At first we generally discuss which specific nonlinear optical effects does the third-order nonlinear optical process contain?

Suppose that the incident light field $\boldsymbol{E}(t)$ is consisted of three monochromatic light fields at different frequencies propagating along a same direction:

$$\boldsymbol{E}(t) = \boldsymbol{E}_1(\omega_1)e^{-i\omega_1 t} + \boldsymbol{E}_2(\omega_1)e^{-i\omega_2 t} + \boldsymbol{E}_3(\omega_1)e^{-i\omega_3 t} + c.c. \tag{4.1.1}$$

The corresponding time-domain third-order nonlinear polarization in the isotropic medium is expressed as

$$\boldsymbol{P}^{(3)}(t) = \varepsilon_0 \chi^{(3)} \boldsymbol{E}^3(t). \tag{4.1.2}$$

© Shanghai Jiao Tong University Press,
Shanghai and Springer Nature Singapore Pte Ltd., 2017

C. Li, *Nonlinear Optics*, DOI 10.1007/978-981-10-1488-8_4

Substituting Eq. (4.1.1) into Eq. (4.1.2), and combining the items with the same frequency, we obtain

$$\boldsymbol{P}^{(3)}(t) = \sum_i \boldsymbol{P}^{(3)}(\omega_i)e^{-i\omega_i t}, \tag{4.1.3}$$

where i is the positive integer, $\boldsymbol{\omega}_i$ contains all kinds of frequency components, which is the frequency of polarization field composed of frequencies of three monochromatic light fields $\boldsymbol{\omega}_1, \boldsymbol{\omega}_2, \boldsymbol{\omega}_3$ in different way.

For different third-order nonlinear optical effect, there is different susceptibility $\chi^{(3)}(\omega_i)$ corresponding to the nonlinear polarization in the frequency domain:

$$\boldsymbol{P}^{(3)}(\omega_i) = D\varepsilon_0\chi^{(3)}(\omega_i)\boldsymbol{E}(\omega_1)\boldsymbol{E}(\omega_2)\boldsymbol{E}(\omega_3), \tag{4.1.4}$$

where D is degeneration factor, for the third-order nonlinear effect, $n = 3$, if taking the degeneracy of m, then $D = n!/m! = 6/m!$. There are three values: when $m = 1$, $D = 6$; when $m = 2$, $D = 3$; when $m = 3$, $D = 1$. Below is a list of several typical third-order nonlinear optical effects, their polarization field frequency ω_i is equal to the combination of following different incident field frequency:

Third harmonic

$$(\boldsymbol{\omega}_1 + \boldsymbol{\omega}_1 + \boldsymbol{\omega}_1) \quad D = 1$$

Four wave mixing

$$(\boldsymbol{\omega}_1 + \boldsymbol{\omega}_2 + \boldsymbol{\omega}_3) \quad D = 6$$

Degenerate four wave mixing

$$(\boldsymbol{\omega}_1 - \boldsymbol{\omega}_1 + \boldsymbol{\omega}_1) \quad D = 3$$

Four wave mixing phase conjugation

$$(\boldsymbol{\omega}_1 + \boldsymbol{\omega}_2 - \boldsymbol{\omega}_3) \quad D = 6$$

Self-phase modulation optical Kerr effect

$$(\boldsymbol{\omega}_1 - \boldsymbol{\omega}_1 + \boldsymbol{\omega}_1) \quad D = 3$$

(Self-focusing, saturable absorption)
Cross phase modulation optical Kerr effect

$$(\boldsymbol{\omega}_2 - \boldsymbol{\omega}_2 + \boldsymbol{\omega}_1) \quad D = 6$$

(Two photon absorption)
Stocks Raman scattering

$$(\boldsymbol{\omega}_1 - \boldsymbol{\omega}_1 + \boldsymbol{\omega}_2) \quad D = 6$$

Anti-Stocks Raman scattering

$$(\boldsymbol{\omega}_1 + \boldsymbol{\omega}_1 - \boldsymbol{\omega}_2) \quad D = 3$$

In above third-order nonlinear optics phenomena, former 4 kinds belong to the passive nonlinear effects; later 4 kinds belong to the active nonlinear effects.

In general the passive third-order nonlinear optics process is a four-wave coupling process, there is the interaction of 4 light fields, which includes three extraneous light fields $E(\omega_1), E(\omega_2), E(\omega_3)$ and one polarization light field $E(\omega_i)$, in principle we need establish 4 nonlinear coupling equations to simultaneously solve these 4 light field amplitudes.

If some nonlinear optics process exists the small signal approximation, namely its polarization field is much weaker than the pump light field, in this case its nonlinear conversion efficiency is not high, we can regard that the pump light amplitude is unchangeable with the change of propagation distance in the nonlinear process, so we can omit the equation of that pump light field. In this way the number of the coupling equations can be reduced.

4.2 Optical Third Harmonic and Optical Four-Wave Mixing

4.2.1 Optical Third Harmonic

Optical third harmonic generation is a third-order nonlinear optics effect that the original light field at the frequency ω inputs the medium and generates a polarization light field at the frequency 3ω.

The principle of optical third harmonic effect is shown in Fig. 4.1. The three foundational frequency lights inputted into the third-order nonlinear medium are at the same frequency, namely, $\boldsymbol{\omega}_1 = \boldsymbol{\omega}_2 = \boldsymbol{\omega}_3 = \boldsymbol{\omega}$. According to the principle of conservation of energy, the frequency of new generated third harmonic light is $\boldsymbol{\omega}_1 + \boldsymbol{\omega}_2 + \boldsymbol{\omega}_3 = 3\boldsymbol{\omega}$.

Considering that, in the third harmonic effect, the foundational frequency light field $E(z, \omega)$ and the third harmonic light field $E(z, 3\omega)$ both are monochromic

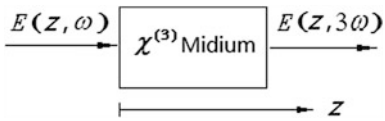

Fig. 4.1 Schematic diagram of optical third harmonic effect

plane waves propagating along z direction, the medium is non-absorption isotropic medium, we only consider the small signal approximation case, and the foundational frequency light field amplitude has no change in the z direction, i.e.

$$E(z,\omega) = E(0,\omega) = constant. \tag{4.2.1}$$

So we can omit 3 equations related 3 foundational frequency light field, only need consider the slowly-varying-amplitude approximation nonlinear wave equation corresponding to the third harmonic light field. If we adopt following notations:$E_{3\omega}(z) = E(z,3\omega)$,$E_{\omega}(z) = E(z,\omega)$, $P^{(3)}_{3\omega}(z) = P^{(3)}(z,3\omega)$, and $D = 1$, the wave equation can be written as

$$\frac{\partial E_{3\omega}(z)}{\partial z} = i\frac{3\omega}{2\varepsilon_0 c n_{3\omega}} P^{(3)}_{3\omega}(z) e^{-i\Delta k z}, \tag{4.2.2}$$

where the nonlinear polarization of third harmonic effect

$$P^{(3)}_{3\omega}(Z) = \varepsilon_0 \chi^{(3)}(3\omega;\omega,\omega,\omega) E^3_{\omega}(Z). \tag{4.2.3}$$

Substituting Eq. (4.2.3) into Eq. (4.2.2), we obtain

$$\frac{\partial E_{3\omega}(Z)}{\partial z} = i\frac{3\omega}{2c n_{3\omega}} \chi^{(3)}(3\omega;\omega,\omega,\omega) E^3_{\omega}(Z) e^{-i\Delta k z}, \tag{4.2.4}$$

where

$$\Delta k = k_{3\omega} - 3k_{\omega} = \frac{3\omega}{c}(n_{3\omega} - n_{\omega}). \tag{4.2.5}$$

In Eq. (4.2.4), $\chi^{(3)}(3\omega;\omega,\omega,\omega)$ and $E_{\omega}(z) = E_{\omega}(0)$ are constant, we can make the equation variables separation, and then directly integrate to solve it. Setting the length of crystal is L, the result of integration is

$$E_{3\omega}(L) = -\frac{3\omega}{2c n_{3\omega}\Delta k} \chi^{(3)} E^3_{\omega}(0)(e^{-i\Delta k L} - 1). \tag{4.2.6}$$

To fine $|E_{3\omega}(L)|^2 = E_{3\omega}(L) \cdot E^*_{3\omega}(L)$, and use the intensity equations:

$$I_{3\omega}(L) = \frac{1}{2}\varepsilon_0 c n_{3\omega} |E_{3\omega}(L)|^2, \tag{4.2.7}$$

$$I_{\omega}(0) = \frac{1}{2}\varepsilon_0 c n_{\omega} |E_{\omega}(0)|^2, \tag{4.2.8}$$

we obtain the outputted intensity of the third harmonic light:

$$I_{3\omega}(L) = \frac{9\omega^2 L^2}{\varepsilon_0^2 c^4 n_\omega^3 n_{3\omega}} \left|\chi^{(3)}\right|^2 I_\omega^3(0) sinc^2\left(\frac{\Delta kL}{2}\right). \tag{4.2.9}$$

where the shape of function $\mathrm{sinc}^2(\Delta kL/2)$ is same as that of the frequency doubling under small signal approximation as shown in Fig. 3.5. The power conversion efficiency of the third harmonic light is

$$\eta = \frac{P_{3\omega}(L)}{P_\omega(0)} = \frac{9\omega^2 L^2}{\varepsilon_0^2 c^4 n_{3\omega} n_\omega^3} \left|\chi^{(3)}\right|^2 \left(\frac{P_\omega(0)}{S}\right)^2 sinc^2\left(\frac{\Delta kL}{2}\right). \tag{4.2.10}$$

If we define a coherent length $L_c = \pi/\Delta k$, it has $(\Delta kL_c/2) = \pi/2$. When $L \geq L_c$, the third harmonic efficiency drops down quickly.

Under phase matching condition, i.e. $\Delta k = 0$, $n_{3\omega} = n_\omega$, in this case there is a maximum of the third harmonic conversion efficiency:

$$\eta = \frac{9\omega^2 L^2}{\varepsilon_0^2 c^4 n_\omega^4 S^2} \left|\chi^{(3)}\right|^2 (P_\omega(0))^2 \tag{4.2.11}$$

where $P_\omega(0)$ is the foundational frequency light power, S is the cross sectional area of incident foundational frequency light beam.

After the discovery of the frequency doubling effect by using the ruby laser inputted in the quartz crystal soon, people found the third harmonic effect in some transparent nonlinear crystals. In general nonlinear crystal material, the second-order susceptibility of $\left|\chi^{(2)}\right|$ is about $10^{-3} \sim 10^{-8}$ esu, but the third order susceptibility $\left|\chi^{(3)}\right|$ is only $10^{-12} \sim 10^{-15}$ esu,so the third harmonic effect is much weaker than the second harmonic effect.

The solid crystal material is generally difficult to meet the requirement of phase matching condition, so it is hard to realize the third harmonic effect. In addition, for the common solid crystal, the ability to withstand the laser damage is very low, only the calcite crystal has stronger ability to withstand the laser damage due to it has birefringence characteristic. So the calcite crystal was used to get better third harmonic light, however its third harmonic conversion efficiency is low, the highest conversion efficiency is only 3×10^{-6}.

Researches show that the alkali metal steam has very strong nonlinear resonant enhancement effect in the visible light region, thus it has larger third-order susceptibility and stronger third harmonic conversion efficiency. In addition, the ultimate strength of the laser damage resistance of gas medium is higher than that of solid medium in several orders of magnitude, so the gas medium are often used to produce third harmonic. For example, using YAG laser at wavelength of 1.06 μm as the foundational frequency light, it is very easy to observe the third harmonic laser at wavelength of 355 nm in sodium steam. When the incident light power reaches to 300 MW, the third harmonic conversion efficiency can achieve 3.7 % [1–3].

4.2.2 Optical Four-Wave Mixing

Now we consider the frequency mixing of 4 light waves at different frequency in the third-order nonlinear medium, as shown in Fig. 4.2, where we set the incident light field amplitudes are $\boldsymbol{E}_2 = \boldsymbol{E}(\boldsymbol{r}, \omega_2), \boldsymbol{E}_1 = \boldsymbol{E}(\boldsymbol{r}, \omega_1)$ and $\boldsymbol{E}_3 = \boldsymbol{E}(\boldsymbol{r}, \omega_3)$, and the polarization light field amplitude is $\boldsymbol{E}_4 = \boldsymbol{E}(\boldsymbol{r}, \omega_4)$.

In the optical four-wave mixing process, if the phase matching condition is satisfied, the relations of energy and momentum conservation of photons are respectively:

$$\omega_4 = \omega_1 + \omega_2 + \omega_3, \tag{4.2.12}$$

$$\boldsymbol{k}_4 = \boldsymbol{k}_1 + \boldsymbol{k}_2 + \boldsymbol{k}_3 \tag{4.2.13}$$

The third-order nonlinear polarization generated by polarization field at frequency ω_4 in the medium is

$$\boldsymbol{P}^{(3)}(\boldsymbol{r}, \omega_4) = 6\varepsilon_0 \boldsymbol{\chi}^{(3)}(\omega_4;\omega_1,\omega_2,\omega_3)\boldsymbol{E}(\boldsymbol{r}, \omega_1)\boldsymbol{E}(\boldsymbol{r}, \omega_2)\boldsymbol{E}(\boldsymbol{r}, \omega_3). \tag{4.2.14}$$

Assuming 4 waves are the monochromic plane waves, and all waves propagate along z direction, the first-order coupling wave equation corresponding to the light field at frequency ω_4 is

$$\frac{\partial E(z, \omega_4)}{\partial z} = i\frac{\omega_4}{2\varepsilon_0 c n_4} P^{(3)}(z, \omega_4) e^{-i\Delta k z}. \tag{4.2.15}$$

Substituting the z-direction expression of Eq. (4.2.14) into Eq. (4.2.15), then the equation is written to

$$\frac{\partial E(z, \omega_4)}{\partial z} = i\frac{3\omega_4}{c n_4} \chi^{(3)}(\omega_4; \omega_1, \omega_2, \omega_3) E(z, \omega_1) E(z, \omega_2) E(z, \omega_3) e^{-i\Delta k z}, \tag{4.2.16}$$

where

$$\Delta k = k_4 - (k_1 + k_2 + k_3). \tag{4.2.17}$$

In the same way we can write other 3 coupling equations corresponding to the light waves at frequencies of ω_1, ω_2 and ω_3.

In the four wave mixing, for the 3 original light field frequencies:ω_1, ω_2 and ω_3, except above compound mode of $\omega_4 = \omega_1 + \omega_2 + \omega_3$, there are other compound modes, for example it can exist the following process: the difference frequency

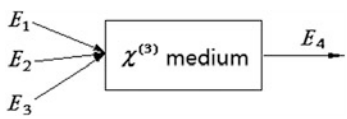

Fig. 4.2 schematic diagram of optical four-wave mixing

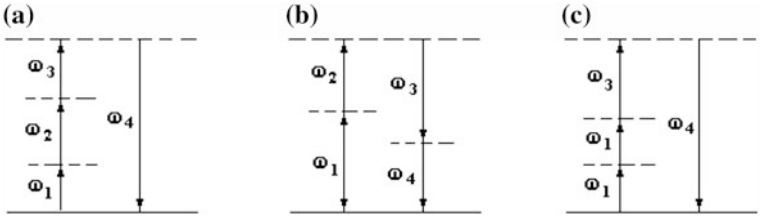

Fig. 4.3 The Energy-level diagrams for 3 kinds of four-wave mixing processes: **a** $\omega_4 = \omega_1 + \omega_2 + \omega_3$; **b** $\omega_4 = \omega_1 + \omega_2 - \omega_3$; **c** $\omega_4 = 2\omega_1 + \omega_3$

$\omega_4 = \omega_1 + \omega_2 - \omega_3$ and the sum frequency $\omega_4 = 2\omega_1 + \omega_3$ $(\omega_1 = \omega_2)$. We can explain above 3 processes by the 3 energy level diagrams as shown in Fig. 4.3 [4, 5].

4.2.3 Degenerated Four-Wave Mixing

The four-wave mixing process in the situation of 4 waves at same frequency is called the degenerated four-wave mixing [6], the relationship of 4 frequencies is

$$\omega_1 = \omega_2 = \omega_3 = \omega_4 = \omega. \tag{4.2.18}$$

The energy conservation condition for the degenerated four-wave mixing is

$$\omega = \omega - \omega + \omega. \tag{4.2.19}$$

In this process, the third-order susceptibility is denoted by $\boldsymbol{\chi}^{(3)}(\omega; \omega, -\omega, \omega)$, the degeneration factor is $D = 3$, and then the nonlinear polarization is expressed as

$$\boldsymbol{P}^{(3)}(\boldsymbol{r}, \omega) = 3\varepsilon_0 \boldsymbol{\chi}^{(3)}(\omega; \omega, -\omega, \omega)\boldsymbol{E}^2(\boldsymbol{r}, \omega)\boldsymbol{E}^*(\boldsymbol{r}, \omega). \tag{4.2.20}$$

In general case, 4 wave vectors of degenerated four-wave mixing could have different directions. However, it must obey the momentum conservation relation in the phase matching case:

$$\boldsymbol{k}_4 = \boldsymbol{k}_1 - \boldsymbol{k}_2 + \boldsymbol{k}_3. \tag{4.2.21}$$

Now we consider a special degenerated four-wave mixing case, that is existing two pairs of wave vectors, each of them has two wave vectors with reverse direction: one pair of $\boldsymbol{k}$ and $-\boldsymbol{k}$ are wave vectors of two pump lights with reverse direction; another one pair of $\boldsymbol{k}'$ and $-\boldsymbol{k}'$ are wave vectors of mutual conjugated signal lights, if the former is a probe light, the latter is called the phase conjugation light of the probe light, as shown in Fig. 4.4a. These four light waves satisfy the

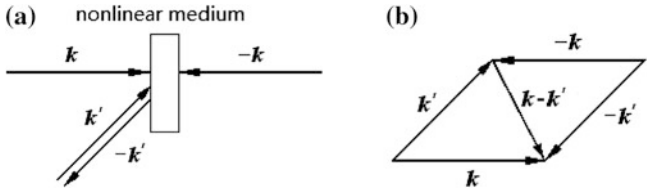

Fig. 4.4 Schematic diagram of degenerated four–wave mixing: **a** the configuration of the two pump lights, the probe light and the conjugated light; **b** the momentum-conservation vector relation

relation of momentum conservation as show in Eq. (4.2.21). If setting $\boldsymbol{k}_1 = \boldsymbol{k}, \boldsymbol{k}_2 = \boldsymbol{k}', \boldsymbol{k}_3 = -\boldsymbol{k}, \boldsymbol{k}_4 = -\boldsymbol{k}'$ Eq. (4.2.21) becomes

$$-\boldsymbol{k}' = \boldsymbol{k} - \boldsymbol{k}' + (-\boldsymbol{k}). \tag{4.2.22}$$

Then the wave vectors of these 4 light waves satisfy the momentum-conservation vector relation as shown in Fig. 4.4b. Equation (4.2.22) can be written to

$$\boldsymbol{k}' + (-\boldsymbol{k}') = \boldsymbol{k} + (-\boldsymbol{k}). \tag{4.2.23}$$

That is to say, no matter what the angle between signal light and pump light is, these two pairs of light automatically satisfy the phase matching condition.

It is worth noting that, such degenerated four-wave mixing nonlinear process is similar to typical holography process (or grating forming process), both can generate the phase conjugation light. The holography process is shown in Fig. 4.5.

In the degenerated four-wave mixing, $\boldsymbol{k}'$ can be regard as the object light, $\boldsymbol{k}$ is the reference light, two lights mutually interfere to generate and record a hologram (form a grating), as shown in Fig. 4.5a. If using the reference light $\boldsymbol{k}$ to irradiate the hologram, and blocking the object light $\boldsymbol{k}'$, from the reverse direction of the object light, i.e. the direction of $-\boldsymbol{k}'$, we can see the virtual image of object (the reflected light of grating), as shown in Fig. 4.5b; if under the irradiation of another reference light $-\boldsymbol{k}$, from the direction of $-\boldsymbol{k}'$, we can see the pseudoscopic image (the

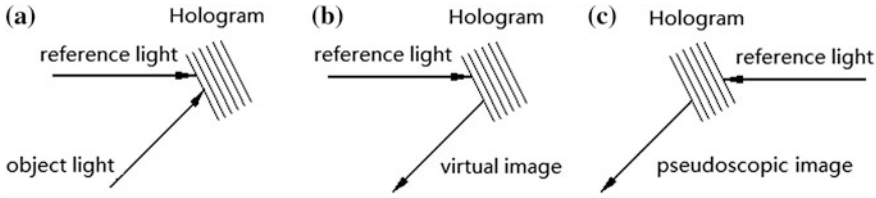

Fig. 4.5 The holography process: **a** the hologram records; **b** the virtual image reappears; **c** the pseudoscopic image reappears

scattered light of the grating), as shown in Fig. 4.5c. The pseudoscopic image is the phase conjugated light of the original object light.

Although both of the holography process and the degenerated four-wave mixing process all can generate the phase conjugated light, but the holography has the basic difference from the four-wave mixing: at first, the holography has the record and reproduce two processes. These two processes are paragraphing in the time. However the phase conjugated light and the signal light in the four-wave mixing are appeared at the same time in the same nonlinear process. Secondly, the frequency of the reference light and the frequency of the object light in the holography should be the same; otherwise it cannot obtain the stable hologram. But in the four-wave mixing, the pump light and the signal light can be different frequencies. In addition, in the holography, the polarization directions of the reference light and the object light cannot be mutual orthogonal; otherwise the hologram cannot be recorded. However, in the four-wave mixing, when the polarization directions of the pump light and the signal light are orthogonal, one can also obtain the phase conjugated light, due to the tensor characteristic of third-order susceptibility.

In next section we will give a strict definition of the optical phase conjugation.

4.3 Optical Phase Conjugation

4.3.1 Definition and Characteristic of Optical Phase Conjugation

A light wave at the frequency ω propagates along z direction, its field amplitude can generally be expressed as a complex number, which is an amplitude factor multiplied by a phase factor, and then adding its conjugation complex number, namely

$$\boldsymbol{E}(\boldsymbol{r},t) = \boldsymbol{E}(\boldsymbol{r})e^{i(kz-\omega t)} + c.c. \tag{4.3.1}$$

If this light field inputs into a system, its outputted-light-field amplitude $\mathbf{E}^*(\mathbf{r})$ is the conjugated complex number of the original inputted-light-field amplitude E(r), then the outputted light wave is called the phase conjugated wave of the inputted light wave, its field amplitude can be expressed as

$$\boldsymbol{E}_c(\boldsymbol{r},t) = \boldsymbol{E}^*(\boldsymbol{r})e^{i(\pm kz-\omega t)} + c.c. \tag{4.3.2}$$

When taking the negative sign at the front of the wave vector k, it is corresponding to the case of the backward phase conjugation of the original light wave, its light field amplitude is the complex phase conjugation of the original light field amplitude, but the propagation direction of phase conjugated wave is the reverse propagation direction of the original light wave, and its space distribution of the

wavefront is totally the same as the space distribution of wavefront of the original light wave.

When taking the positive sign at the front of the wave vector k, it is corresponding to the case of the forward phase conjugation of the original light wave, its light field amplitude is the complex phase conjugation of the original light field amplitude, the propagation direction of phase conjugated wave is the same as the propagation direction of the original light wave, but its space distribution of the wavefront is relative to the space distribution of wavefront of the original light wave into the mirror symmetry [6, 7].

To utilize the characteristic of the backward phase conjugation can make the phase conjugated reflective mirror; and to utilize the characteristic of the forward phase conjugation can make the phase conjugated transmitting mirror,what is the difference between these phase conjugated mirrors and the common planar reflective and transmitting mirrors? Figure 4.6a, b draw up a spherical wave sent by a point light source, which is reflected by the phase conjugated reflective mirror based on the backward phase conjugation and transmitted by the phase conjugated transmitting mirror based on the forward phase conjugation, respectively. The propagation direction of former is contrary to the propagation direction of the original wave, but the wave fronts of two waves are the same. The propagation direction of latter is consistent with the propagation direction of the original wave, but the wave fronts of two waves are made a relation of mirror image symmetry. Figure 4.1c, d also draw up the action of corresponding common reflective mirror and transmitting mirror to the spherical wave sent by a point light source, it is clear that they have a big difference in compared with the phase conjugated reflective mirror and the phase conjugated transmitting mirror.

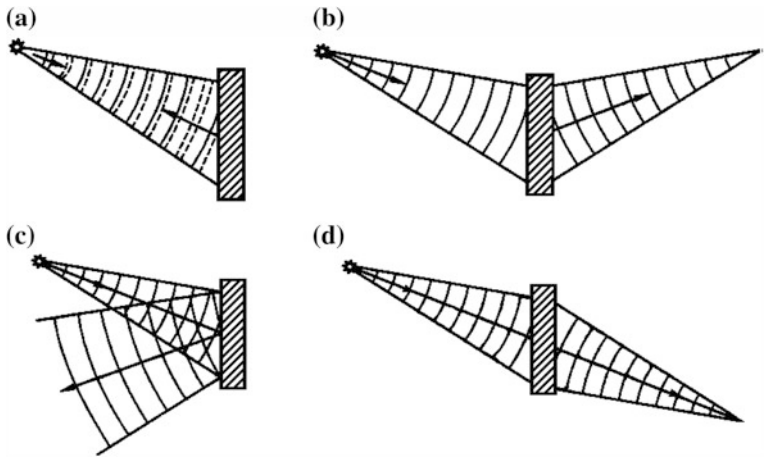

Fig. 4.6 Comparison of the action of phase conjugation mirrors and common planar mirrors to the light wave of point light source: **a** the phase conjugation reflective mirror; **b** the phase conjugation transmitting mirror; **c** the common planar reflective mirror; **d** the common planar transmitting mirror

Now we go back to discuss the backward phase conjugation [taking negative sign in front of the k in the phase conjugation light field expression (4.3.2)]. Now we write down the complete expressions of the original wave field and the phase conjugation wave field, respectively:

$$\boldsymbol{E}(\boldsymbol{r},t) = \boldsymbol{E}(\boldsymbol{r})e^{i(kz-\omega t)} + \boldsymbol{E}^*(\boldsymbol{r})e^{i(-kz+\omega t)}, \tag{4.3.3}$$

$$\boldsymbol{E}_c(\boldsymbol{r},t) = \boldsymbol{E}^*(\boldsymbol{r})e^{i(-kz-\omega t)} + \boldsymbol{E}(\boldsymbol{r})e^{i(kz+\omega t)}. \tag{4.3.4}$$

To compare above two equations, we can see that

$$\boldsymbol{E}_c(\boldsymbol{r},t) = \boldsymbol{E}(\boldsymbol{r},-t). \tag{4.3.5}$$

Therefore the backward phase conjugation light wave is called the time reversal of the original light wave, the space distribution of wavefront of the back phase conjugation light wave is the same as that of the original light wave, and only the propagation direction of the backward phase conjugation light wave is opposite to the original light wave.

4.3.2 Optical Phase Conjugation in Four-Wave Mixing Process

1. **Backward Phase Conjugation and Forward Phase Conjugation in Four-Wave Mixing**

Though the four-wave mixing to realize the phase conjugation, in general, there are a pair of pump lights and a pair of signal lights. The pump light $\boldsymbol{E}_1$ or $\boldsymbol{E}_2$ has stronger power in comparison with the signal light. Two signal lights are the probe light $\boldsymbol{E}_\mathrm{p}$ and the phase conjugation light $\boldsymbol{E}_c$. The four-wave-mixing phase conjugation satisfies following the energy conservation and momentum conservation relations:

$$\omega_c = \omega_1 + \omega_2 - \omega_p, \tag{4.3.6}$$

$$\boldsymbol{k}_c = \boldsymbol{k}_1 + \boldsymbol{k}_2 - \boldsymbol{k}_p. \tag{4.3.7}$$

Under the conditions of energy conservation and momentum conservation, the polarization expression of the phase conjugation signal light field $\boldsymbol{E}_c(\boldsymbol{r},\omega_c)$ is (D = 6):

$$\boldsymbol{P}_c^{(3)}(\boldsymbol{r},\omega_\mathrm{c}) = 6\varepsilon_0\boldsymbol{\chi}^{(3)}(\omega_c;\omega_1,\omega_2,-\omega_p)\boldsymbol{E}_1(\boldsymbol{r},\omega_1)\boldsymbol{E}_2(\boldsymbol{r},\omega_2)\boldsymbol{E}_P^*(\boldsymbol{r},\omega_p). \tag{4.3.8}$$

The 4 light fields joined four-wave mixing phase conjugation have two geometry configurations: the backward phase conjugation and the forward phase conjugation.

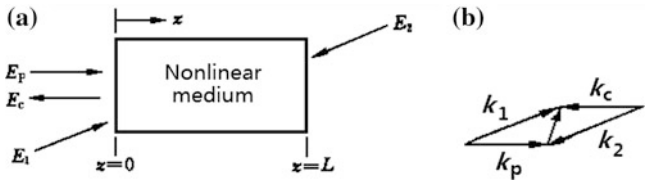

Fig. 4.7 The backward four-wave mixing phase conjugation: **a** the geometry configuration of 4 light fields; **b** the relation of wave vectors under the momentum conservation

For the backward phase conjugation, the pump lights $\boldsymbol{E}_1$ and $\boldsymbol{E}_2$ are separated in the two sides of the nonlinear medium, with reversed propagation directions (with reversed wave vectors); the probe signal light $\boldsymbol{E}_p$ and the conjugate signal light $\boldsymbol{E}_c$ are located at one side of the medium, also with reversed propagation directions (with reversed wave vectors), the geometry configuration of 4 light fields is shown in Fig. 4.7a. The wave vectors of 4 light fields satisfy the momentum conservation relation, namely $\boldsymbol{k}_c = (\boldsymbol{k}_1 - \boldsymbol{k}_p) + \boldsymbol{k}_2$, as shown in Fig. 4.7b.

For the forward phase conjugation, the pump light $\boldsymbol{E}_1$ and $\boldsymbol{E}_2$ are located at the same side of the nonlinear medium, with the same propagation direction; the probe signal light $\boldsymbol{E}_p$ and conjugated signal light $\boldsymbol{E}_c$ are located at two sides of the medium, into a mirror image each other, its geometry configuration of 4 light fields is shown in Fig. 4.8a. The wave vectors of 4 light fields satisfy the momentum conservation principle, namely $\boldsymbol{k}_c = (\boldsymbol{k}_1 + \boldsymbol{k}_2) - \boldsymbol{k}_p$, as shown in Fig. 4.8b.

2. **Backward Phase Conjugation in Degenerated Four-Wave Mixing**

Now we study the backward phase conjugation based on the degenerated four-wave mixing. In the case of the degenerated four-wave mixing, the probe light $\boldsymbol{E}_p(\boldsymbol{r})$, the conjugation light $\boldsymbol{E}_c(\boldsymbol{r})$, the pump lights $\boldsymbol{E}_1(\boldsymbol{r})$ and $\boldsymbol{E}_2(\boldsymbol{r})$ are at the same frequency:

$$\omega_p = \omega_c = \omega_1 = \omega_2 = \omega. \tag{4.3.9}$$

Thus the degenerated four-wave mixing based backward phase conjugation has the relations of wave vectors: $\boldsymbol{k}_2 = -\boldsymbol{k}_1$ and $\boldsymbol{k}_c = -\boldsymbol{k}_p$. From the momentum

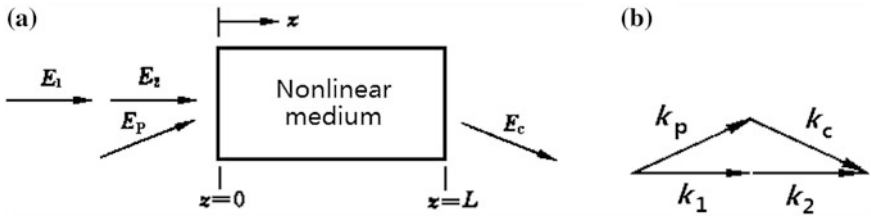

Fig. 4.8 The forward four-wave mixing phase conjugation: **a** the geometry configuration of 4 light fields; **b** the relation of wave vectors under the momentum conservation

conservation formula (4.3.7) we can see that the phase conjugation condition of this nonlinear process is automatically satisfied.

Now we start discuss the propagation characteristic of the conjugation light in the nonlinear medium. We assume that the nonlinear medium is isotropic, non-absorption, and far from the resonance; the process satisfies the phase matching condition, $\Delta \boldsymbol{k} = 0$; This is in small signal approximation case, the pump light is much stronger than the signal light, so $\boldsymbol{E}_1(\boldsymbol{r})$ and $\boldsymbol{E}_2(\boldsymbol{r})$ have no decay in z direction, we can only consider the coupling equations for two signal lights. And assuming $\boldsymbol{E}_p(\boldsymbol{r})$ propagates along the z direction; $\boldsymbol{E}_c(\boldsymbol{r})$ propagates along the –z direction, using polarization Eq. (4.3.8), we obtain following two nonlinear coupling wave equations:

$$\frac{dE_p(z)}{dz} = i\frac{3\omega}{nc}\chi^{(3)}E_1E_2E_c^*(z), \tag{4.3.10}$$

$$\frac{dE_c(z)}{dz} = -i\frac{3\omega}{nc}\chi^{(3)}E_1E_2E_p^*(z), \tag{4.3.11}$$

where $\chi^{(3)} = \chi^{(3)}(\omega_c; \omega_1, \omega_2, -\omega_p) = \chi^{(3)}(\omega_p; \omega_1, \omega_2, -\omega_c)$ is third-order nonlinear susceptibility of medium, in the far from resonance case it is a real number.

To define the gain coefficient:

$$g = \frac{3\omega}{nc}\chi^{(3)}E_1E_2. \tag{4.3.12}$$

g is a real number. Equations (4.3.10) and (4.3.11) are simplified as

$$\frac{dE_p(z)}{dz} = igE_c^*(z), \tag{4.3.13}$$

$$\frac{dE_c(z)}{dz} = -igE_p^*(z). \tag{4.3.14}$$

Setting the length of the medium is L, and considering the following boundary condition: the light field E_p is inputted from the surface at $z = 0$ where $E_p(0) \neq 0$, and outputted from the surface at $z = L$ where $E_p(L) \neq 0$; the light field E_c is reflected by the surface at $z = L$ where $E_c(L) = 0$, then outputted from the surface at $z = 0$ where $E_c(0) \neq 0$. The solutions of Eqs. (4.2.13) and (4.2.14) are

$$E_p(z) = \frac{\cos[g(z-L)]}{\cos(gL)}E_p(0), \tag{4.3.15}$$

$$E_c(z) = -i\frac{\sin[g(z-L)]}{\cos(gL)}E_p^*(0). \tag{4.3.16}$$

So the light field amplitudes at the two end surfaces of medium are respectively:

$$E_p(L) = \frac{1}{\cos(gL)} E_P(0), \tag{4.3.17}$$

$$E_c(0) = i\ \tan(gL) E_p^*(0), \tag{4.3.18}$$

where $E_p(L)$ is the outputted probe light amplitude from the surface at $z = L$; $E_c(0)$ is the outputted conjugation light amplitude from the surface at $z = 0$. They all are produced from $E_p(0)$, the former is the transmitted light of $E_p(0)$; the latter is its reflected light, both of them are amplified in the nonlinear process. Form Eq. (4.3.18) we can see, at $z = 0$, the conjugated light amplitude $E_c(0)$ is proportional to the conjugate complex number of probe light amplitude $E_p^*(0)$, but their propagation directions are opposite.

We define the power transmitted coefficient and the power reflected coefficient of phase conjugation, respectively:

$$T = \frac{|E_p(L)|^2}{|E_p(0)|^2} = \sec^2(gL), \tag{4.3.19}$$

$$R = \frac{|E_c(0)|^2}{|E_p(0)|^2} = \tan^2(gL). \tag{4.3.20}$$

From Eqs. (4.2.17)–(4.2.20) we can obtain the following conclusions:

(1) The process produced signal light $E_c(0)$ is the phase conjugation wave of original probe light $E_p(0)$. The reflectivity R increases with the increase of gL. Form Eq. (4.2.12) we can see, $\chi^{(3)}$ of the medium and the pump light amplitudes E_1 and E_2 are larger, g is larger, in order to produce high phase conjugation reflectivity, we need select the material with large $\chi^{(3)}$ and the high power pump light.

(2) When $\frac{1}{4}\pi < gL < \frac{3}{4}\pi$, due to $\tan(gL) > 1$, $R > 1$, this means that through the four-wave mixing process, the phase conjugation light is amplified. At same time, the transmittance of the probe light $T \geq 1$, so the probe light is also amplified.

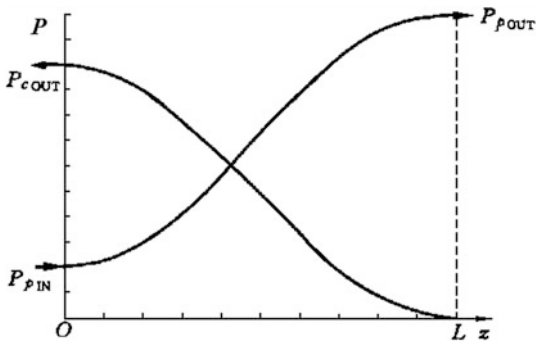

Fig. 4.9 Amplification action of the probe light and the phase conjugation light in degenerated four-wave mixing backward phase conjugation process

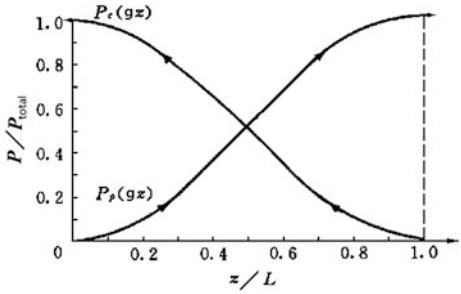

Fig. 4.10 Power distributions of the probe light and the phase conjugation light in the medium when the oscillation condition $gL = \pi/2$ is satisfied

Figure 4.9 gives the curves of that the probe light power and the phase conjugation light power vary with increase of z when R and T both are greater than 1.

(3) When $gL = \pi/2$, $R \to \infty$, $T \to \infty$, the non-cavity self-oscillation in the medium is produced. In this case the signal light don't need input into the medium, the energy comes from the pump light, there are outputted signal light and phase conjugation light, it just likes a parameter oscillator. In this case the light power distribution is shown in Fig. 4.10.

Early stage the amplification and oscillation phenomena of degenerated four-wave mixing backward phase conjugation wave had observed in the CS_2 liquid and sodium steam. The experimental facility is shown in Fig. 4.11 [8].

3. Other Phase Conjugation Situation

Above study only consider the small signal situation. In the high conversion efficiency case, the variation of pump light with change of the distance has to consider, in this case we need simultaneous solve the 4 coupling equations. In above study we also ignored the pump light induced refractive-index change and absorption in the medium; moreover, the study is only based on the non-resonance condition. The strict study should consider these factors.

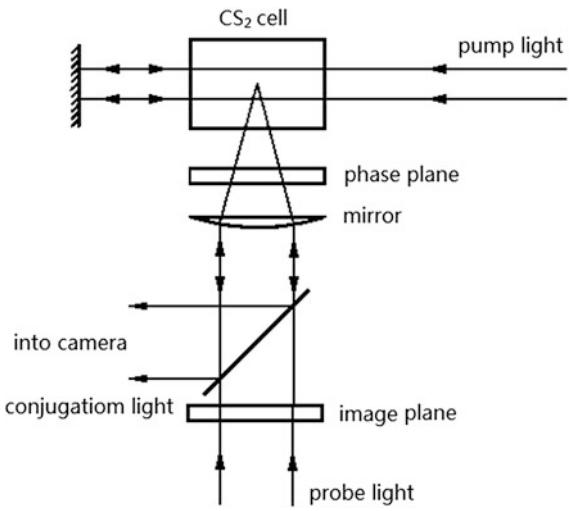

Fig. 4.11 Experimental facility for study degenerated four-wave mixing backward phase conjugation process

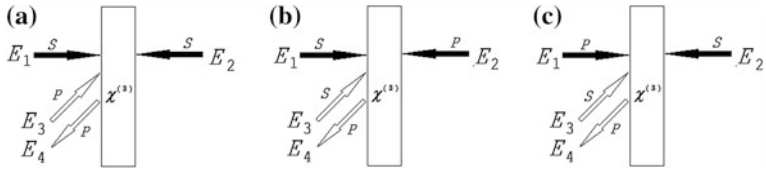

Fig. 4.12 3 Different light polarization combinations for degenerated four-wave mixing backward phase conjugation

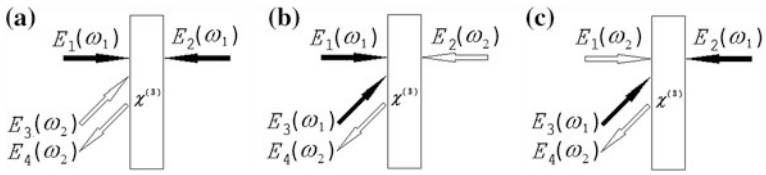

Fig. 4.13 Two group frequency configurations for the part degenerated four-wave mixing phase conjugation

It's worth noting that, above deduction of the formulas for the four-wave mixing phase conjugation implies the assumption that the 4 light waves participated in the process all have the same frequency and polarization direction. Actually, in the degenerated four-wave mixing phase conjugation, 4 light beams at the same frequency can have different polarization directions (the vertical polarization *s* or the parallel polarization *p*). Figure 4.12 shows the 3 kinds of combinations with the orthogonal polarization directions: (a) is the case that two pump lights have a same polarization direction, and two signal lights have another same polarization direction, these two polarization directions are orthogonal. (b) and (c) are the cases that each of pump light-signal light group has a same polarization direction, the two groups have the orthogonal polarization directions. All above three cases can realize the phase conjugation.

Not only complete degenerated four-wave mixing can realize the phase conjugation, but also the part degenerated four-wave mixing composited by two pair of lights at different frequency can realize the phase conjugation. Figure 4.13 shows three phase conjugation configurations at two different frequencies.

There are many methods to realize phase conjugation, except the four-wave mixing, the method of three-wave mixing, stimulated scattering, and backward laser emission etc. can also be used to generate the phase conjugation wave [9].

4.3.3 Application of Optical Phase Conjugation

1. **Wavefront Distortion Compensation**

The conjugate reflected mirror based on the backward phase conjugation principle can automatically compensate the wavefront distortion, which is formed when the light pass through the irregular disturbance medium [10]. Figure 4.14 gives a comparison of different actions to the wavefront distortion in the medium by a phase conjugation mirror and a common reflected mirror. After a parallel plane wave passing though the distortion medium, it is then reflected by a common reflected mirror or a phase conjugation mirror, respectively, the common reflected mirror plays a roll of increasing the wavefront distortion; but the phase conjugation mirror has an action that compensates or offsets the wavefront distortion. In the figure, the real line is the wavefront of incident wave; the dotted line is the wavefront of reflected wave.

2. **Measurement of Susceptibility**

Now we introduce a method for measuring third-order susceptibility by a degenerated four-wave mixing backward phase conjugation experiment [11]. If from the experiment to measure the data of light-wave amplitudes: E_1, E_2, E_c and E_p, and know the laser wavelength λ, the length of nonlinear medium L, and the refractive index of medium n, using the following reflectivity formula (4.3.20) and gain coefficient formula (4.3.12):

$$R = \frac{|E_c(0)|^2}{|E_p(0)|^2} = \tan^2(gL),$$

$$g = \frac{3\omega}{nc}\chi^{(3)}E_1E_2,$$

we can calculate the value of the third-order susceptibility $\chi^{(3)}$.

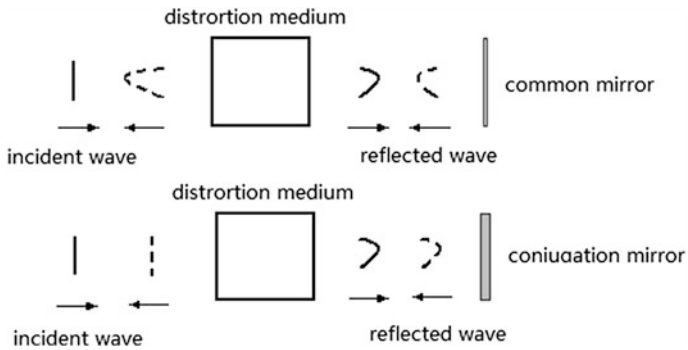

Fig. 4.14 Comparison of the distortion-compensation action of phase conjugation mirror and the distortion-enhancement action of common reflected mirror

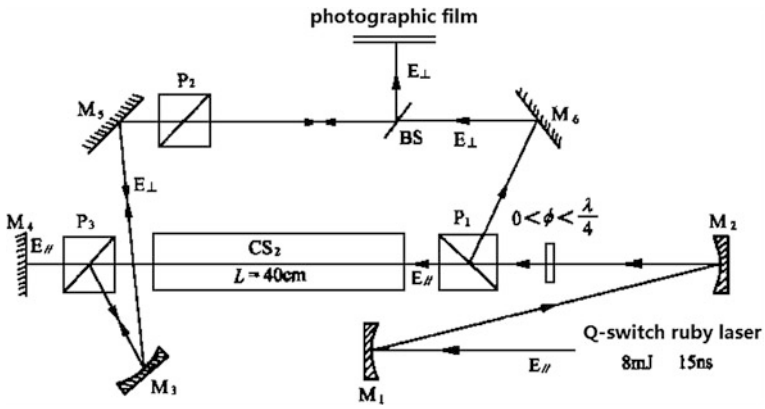

Fig. 4.15 Experimental setup for measuring $\chi^{(3)}$ based on degenerated four-wave mixing phase conjugation using a polarization separation technique

Here we introduce a degenerated four-wave mixing backward phase conjugation experiment based on the light polarization separation technique with a high measurement accuracy, in the experiment the 4 light beams collinearly propagate in the medium CS_2, because the polarization directions of signal lights and pump lights are orthogonal, we can separate out the conjugated signal lights from the pump lights. Figure 4.15 gives an experimental setup in detail.

A parallel polarization light send by a Q-switch pulsed ruby laser, it passes through the reflected mirrors M_1 and M_2, a wave pate, two Glan prisms (polarization beam splitter) P_1 and P_3, and the reflected mirror M_4, to form two pump lights E_1 and E_2 with the reversed propagation direction and the paralleled polarization direction. The light reflected from P_1 with the vertical polarization passes through M_6, P_2, M_5 and M_3, then reflected into the medium CS_2 by P_3, to form the incident signal light E_c with the vertical polarization. The conjugated signal light E_P with the reverse propagation direction relative to the signal light and the vertical polarization passes through P_3, M_3, M_5, P_2 and the beam splitter BS is finally measured by a photographic film.

Review Questions of Chapter 4

1. Which are passive third-order nonlinear optics effects? Write down their nonlinear susceptibility formulae.
2. Please derive the third harmonic effect power conversion efficiency formula in small signal approximation case.
3. What is four-wave mixing effect? Write down its polarization expression and slowly-varying amplitude-approximation frequency-domain wave equation
4. What is degenerated four-wave mixing? What kind phase matching condition it satisfies? To compare with the holography, what identical or different characteristics do they have?

5. How to define the phase conjugation? What characteristic does it has? Which methods can be used for realizing the phase conjugation?
6. Give out the polarization expression of four-wave-mixing phase conjugation. What is difference between back phase conjugation and forward phase conjugation? What kind energy and momentum conservation relations do they have to meet?
7. Establish the signal light and the conjugated light coupled wave equations for the back phase conjugation process based on the degenerated four-wave mixing. Discuss the transmission characteristic of phase conjugation wave in the medium.
8. What are applications of optical phase conjugation? Draw a picture to explain the action of phase conjugation in compensation of the wavefront distortion. How to use degenerated four-wave mixing phase conjugation method to measure the third-order susceptibility of nonlinear medium $\chi^{(3)}$?

References

1. J.F. Young, G.C. Bjorklund et al., Third-harmonic generation in phase-matched Rb vapor. Phys. Rev. Lett. **27**(23), 1551–1553 (1971)
2. R.B. Miles, S.E. Harris, Optical third-harmonic generation in alkali metal vapors. IEEE J. Quant. Electr. **9**(4), 470–484 (1973)
3. D.M. Bloom, G.W. Bekkers et al., Third harmonic generation in phase-matched alkali metal vapors. Appl. Phys. Lett. **26**(12), 687–689 (1975)
4. Y.R. Shen, *The Principles of Nonlinear Optics* (Wiley, 1984)
5. J.L. Oudar, Y.R. Shen, Nonlinear spectroscopy by multi resonant four-wave mixing. Phys. Rev. A **22**(3), 1141–1158 (1980)
6. R.A. Fisher (ed.), *Optical Phase Conjugation* (Academic Press, New York, 1963)
7. A. Yariv, Phase conjugate optics and real-time holography. IEEE J. Quant. Electr. **14**(9), 650–660 (1978)
8. D.M. Pepper et al., Observation of amplified phase-conjugate reflection and optical parametric oscillation by degenerate four-wave mixing in a transparent medium. Appl. Phys. Lett. **33**(1), 41–44 (1978)
9. G.S. He, S.H. Liu, *Highlight Optics* (Science Press, Beijing, China, 2011)
10. C.R. Giuliano, Applications of optical phase conjugation. Phys. Today **34**(4), 27–37 (1981)
11. S.X. Qian, G.M. Wang, *Principle and Development of Nonlinear Optics* (Fudan University Press, Shanghai, China, 2000)

Chapter 5
Optical Kerr Effect and Self-focusing

In this chapter, firstly we will study light intensity induced medium refractive-index change phenomenon, i.e., optical Kerr effect. Mainly study on the self-phase modulation optical Kerr effect, the cross-phase modulation optical Kerr effect, and related light induced birefringence effect. Secondly, we will study the self-focusing effect induced by transverse strength inhomogeneous distribution of Gaussian beam, including steady-state and dynamic self-focusing, time and space self-phase modulation phenomena. Finally, we will introduce Z-scan technology for measuring nonlinear parameters of materials, including experimental method and theoretical calculation method.

5.1 Optical Kerr Effect

Optical Kerr effect and electro-optics Kerr effect are two effects with different physical mechanism. The electro-optics Kerr effect is a phenomenon that the linear polarized light passing through a transparent medium applied a static electric field becomes an elliptically polarized light. This effect arises from the electrical field induced birefringence in the medium. The incident light is divided into two components with orthogonal polarization directions (o light and e light), which have different reflective index in the medium. The reflective-index difference between two lights Δn is proportional to the external static electric field strength $\boldsymbol{E}_0$, i.e., $\Delta n \propto |\boldsymbol{E}_0|$, this effect belongs to second-order nonlinear optics effect, its nonlinear susceptibility is denoted as $\chi^{(2)}(\omega;\omega,0)$.

The optical Kerr effect discussed in this section is a phenomenon that the refractive-index change of medium is directly induced by the light electric field of incident light. The magnitude of refractive-index change is proportional to the square of light electric filed strength or the light intensity, i.e., $\Delta n \propto |\boldsymbol{E}|^2 \propto I$. This effect belongs to three-order nonlinear optics effect [1–6], its nonlinear

© Shanghai Jiao Tong University Press,
Shanghai and Springer Nature Singapore Pte Ltd., 2017

C. Li, *Nonlinear Optics*, DOI 10.1007/978-981-10-1488-8_5

susceptibility is denoted as $\chi^{(3)}(\omega;\omega,-\omega,\omega)$. Sometimes the optical Kerr effect is simply called Kerr effect. The medium with optical Kerr effect is called Kerr medium.

We suppose a light beam propagates in the medium, the optical Kerr effect makes the refractive-index change of the medium Δn, and the phase change of the light for the propagation distance L is

$$\Delta\phi = k_0 \Delta n L = \frac{2\pi L}{\lambda_0}\Delta n, \tag{5.1.1}$$

where λ_0 and k_0 are the wavelength and the wave vector of signal light in the vacuum. That is to say, when a light passes through a medium, the refractive-index change of medium can modulate the light phase. The phase change quantity is proportional to the refractive-index change quantity. So we can through the detection of light phase change $\Delta\phi$ to determine the refractive-index change of the medium Δn. According to the different phase modulation method, the optical Kerr effect can be classified into following two types.

1. **Self-phase Modulation Optical Kerr Effect**

If a high-power signal light inputs alone into the nonlinear medium, only rely on its own light intensity to generate the optical Kerr effect, namely to make the refractive-index change of the medium, thereby modulating the phase of the light own, this process that using the single light beam to generate the optical Kerr effect and to realize its own phase modulation is called self-phase modulation (SPM) optical Kerr effect, also called self-action optical Kerr effect.

2. **Cross-phase Modulation Optical Kerr Effect**

If a weak-power signal light together with a high-power pump light both input the nonlinear medium, the pump light generates the optical Kerr effect to make the refractive-index change of the medium and induces the phase modulation of the signal light. Such using the mutual action of the signal light and the pump light to produce the optical Kerr effect and the phase modulation process is called cross-phase modulation (XPM) optical Kerr effect, also called mutual-action optical Kerr effect. Sometime this method for producing the optical Kerr effect is called the pump-probe method.

In the XPM optical Kerr effect, the pump light and the signal light can take different frequency (or different polarization direction). In general, the frequency of pump light is chose in high absorption area of the medium; the frequency of signal light is chose in transparent area of the medium.

Figure 5.1 shows two light-path graphs for SPM optical Kerr effect and XPM optical Kerr effect respectively.

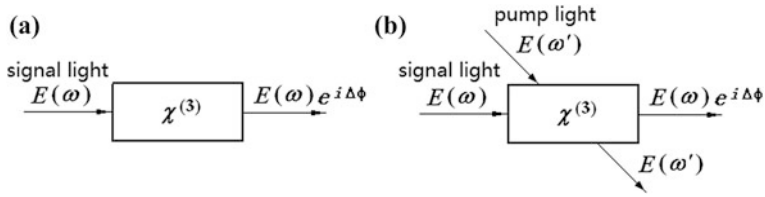

Fig. 5.1 Schematic diagrams of two kinds of optical Kerr effects: **a** SPM optical Kerr effect; **b** XPM optical Kerr effect

5.1.1 Self-phase Modulation Optical Kerr Effect

Assuming in the SPM optical Kerr effect case, a strong light at the frequency ω with the electric field strength $\boldsymbol{E}(\omega)$ propagates in the isotropic medium, and interacts with the medium to generate the third–order nonlinear polarization:

$$\boldsymbol{P}^{(3)}(\omega) = 3\varepsilon_0\chi^{(3)}(\omega;\omega,-\omega,\omega)|\boldsymbol{E}(\omega)|^2\boldsymbol{E}(\omega). \tag{5.1.2}$$

If we only study the first-order and the third-order nonlinear processes in SPM optical Kerr effect, and only study the light induced refractive-index change, we can only take the real number part of the nonlinear susceptibility, and then the light induced polarization is

$$\begin{aligned}\boldsymbol{P}(\omega) &= \boldsymbol{P}^{(1)}(\omega) + \boldsymbol{P}^{(3)}(\omega)\\ &= \varepsilon_0\chi^{(1)\prime}\boldsymbol{E}(\omega) + 3\varepsilon_0\chi^{(3)\prime}(\omega;\omega,-\omega,\omega)|\boldsymbol{E}(\omega)|^2\boldsymbol{E}(\omega).\end{aligned} \tag{5.1.3}$$

According to the relations between the electric induction strength and the electric field strength, $\boldsymbol{D} = \varepsilon_0\boldsymbol{E} + \boldsymbol{P}$ and $\boldsymbol{D} = \varepsilon\boldsymbol{E}$, we obtain the relation of the dielectric coefficient with the polarization and electric field strength, that is

$$\varepsilon = \varepsilon_0 + \boldsymbol{P}(\omega)/\boldsymbol{E}(\omega) \tag{5.1.4}$$

Substituting the Eq. (5.1.3) into the Eq. (5.1.4), we obtain

$$\varepsilon = \varepsilon_0\left(1 + \chi^{(1)\prime} + 3\chi^{(3)\prime}(\omega;\omega,-\omega,\omega)|\boldsymbol{E}(\omega)|^2\right), \tag{5.1.5}$$

where ε_0 is dielectric coefficient of medium in the vacuum. Using formulae $n = \sqrt{\varepsilon/\varepsilon_0}$ and $n_0^2 = 1 + \chi^{(1)\prime}$, we obtain

$$n = n_0\sqrt{1 + \frac{3\chi^{(3)\prime}}{n_0^2}|\boldsymbol{E}(\omega)|^2} \approx n_0 + \frac{3\chi^{(3)\prime}}{2n_0}|\boldsymbol{E}(\omega)|^2. \tag{5.1.6}$$

In Eq. (5.1.6), considering the later item in root sign is much small than 1, so after Taylor series expansion it is possible to take the linear approximation. The first item of right side of formula is a linear refractive index, second item is nonlinear refractive index, i.e., $n = n_0 + \Delta n$, therefore, the nonlinear refractive index is

$$\Delta n = \frac{3\chi^{(3)\prime}(\omega;\omega,-\omega,\omega)}{2n_0}|\boldsymbol{E}(\omega)|^2. \tag{5.1.7}$$

If we set

$$\bar{n}_2 = \frac{3\chi^{(3)\prime}(\omega;\omega,-\omega,\omega)}{2n_0}, \tag{5.1.8}$$

then Eq. (5.1.7) becomes

$$\Delta n = \bar{n}_2|\boldsymbol{E}(\omega)|^2. \tag{5.1.9}$$

Visibly, the nonlinear refractive index is proportional to the square of field amplitude; the ratio coefficient $\bar{n}_2$ is called nonlinear refraction coefficient, which is proportional to the real number part of the third-order susceptibility,

In order to express the relation between Δn and I, using the formula $I = \frac{1}{2}\varepsilon_0 c n_0|\boldsymbol{E}(\omega)|^2$, Eq. (5.1.9) can be written to

$$\Delta n = \frac{3\chi^{(3)\prime}(\omega;\omega,-\omega,\omega)}{\varepsilon_0 c n_0^2}I. \tag{5.1.10}$$

If we set

$$n_2 = \frac{3\chi^{(3)\prime}(\omega;\omega,-\omega,\omega)}{\varepsilon_0 c n_0^2}, \tag{5.1.11}$$

Equation (5.1.10) becomes

$$\Delta n = n_2 I. \tag{5.1.12}$$

Visibly, in the SPM optical Kerr effect, the refractive-index change (nonlinear refractive index) is proportional to the light intensity, and the ratio coefficient n_2 is also called nonlinear refraction coefficient, which is proportional to the real part of the third-order susceptibility.

To compare Eqs. (5.1.8) and (5.1.11), the relationship between two nonlinear refraction coefficients n_2 and $\bar{n}_2$ is

$$n_2 = \left(\frac{2}{\varepsilon_0 c n_0}\right)\bar{n}_2. \tag{5.1.13}$$

In SPM optical Kerr effect, the total refractive index of the medium is

$$n = n_0 + n_2 I. \tag{5.1.14}$$

Usually the unit of the light intensity I is $\mathrm{W/cm^2}$, so the unit of n_2 is $\mathrm{cm^2/W}$. Using Eq. (5.1.11), we can give the unit conversion relationship between n_2 (the unit is $\mathrm{cm^2/W}$) and $\chi^{(3)}$(the unit is esu):

$$n_2\left(\frac{\mathrm{cm^2}}{\mathrm{W}}\right) = \frac{4\times 10^{-2}}{n_0^2}\chi^{(3)}(\mathrm{esu}). \tag{5.1.15}$$

In above SPM optical Kerr effect, the refractive-index change of the medium generated by light intensity I will induce the phase change of the light propagating in the medium. Setting the propagation distance of light is L, the refractive-index change of the medium is Δn, and then the phase change of the light $\Delta\phi$ is expressed by Eq. (5.1.1). Substituting Eq. (5.1.12) into Eq. (5.1.1), we can obtain the phase change of the light, which is

$$\Delta\phi = \frac{2\pi L}{\lambda_0}\Delta n = \frac{2\pi L}{\lambda_0} n_2 I = \frac{2\pi L n_2}{\lambda_0 S} P. \tag{5.1.16}$$

Here $I = P/S$, where P is the power of the incident light; S is the effective cross section of light beam. We can see that the light (at frequency of λ_0) interacts with a nonlinear medium (such as an optical waveguide with n_2, S and L), the phase change of the light is proportional to its power.

There are many physical mechanisms of refractive-index change induced by optical Kerr effect; Table 5.1 lists the numerical values of nonlinear refraction coefficient n_2, nonlinear susceptibility $\chi^{(3)}$ and response time τ of the medium in several typical physical process of the optical Kerr effect (in room temperature).

Table 5.1 shows that the nonlinear refraction coefficient of Kerr medium is larger, the response time of medium slower, vice versa. For example, the liquid crystal and CS_2 belong to the same molecular orientation mechanism; the nonlinear refraction coefficient of liquid crystal is larger than that of CS_2 in 10 orders of magnitude. But the response time of the liquid crystal is slower than that of CS_2 in 10–12 orders of magnitude. The Si and dye belong to the same thermal mechanism, the nonlinear refraction coefficient of Si is lower than that of the dye in one order of magnitude, but the respond time is faster than that of the dye in one order of magnitude. However, the case of semiconductor is rather different. Although the semiconductors belonging different exciton nonlinear mechanisms such as free exciton, bound exciton, biexciton etc.; they have different n_2, but their response time usually are in nanosecond or sub-nanosecond order of magnitude. HgCdTe is

Table 5.1 Physical mechanisms and parameters of several typical optical Kerr effects [7]

Physical mechanism	$n_2(\mathrm{cm}^2/\mathrm{W})$	$\chi^{(3)}(\mathrm{esu})$	$\tau(\mathrm{s})$
Electronic polarization	10^{-16}	10^{-14}	10^{-15}
Electrostriction	10^{-14}	10^{-12}	10^{-9}
Molecular orientation (CS_2)	10^{-13}	10^{-11}	10^{-12}
Saturation atomic absorption	10^{-10}	10^{-9}	10^{-8}
Biexciton (CuCl)	10^{-10}	10^{-8}	10^{-9}
Semiconductor doped-glass (CdSe)	10^{-10}	10^{-8}	10^{-8}
In-valence band transition (HgCdTe)	10^{-8}	10^{-6}	10^{-12}
Two- photon (InSb)	10^{-7}	10^{-5}	10^{-8}
Thermal effect (Si)	10^{-7}	10^{-5}	10^{-4}
Thermal effect (dye)	10^{-6}	10^{-4}	10^{-3}
Bound exciton (CdS)	10^{-5}	10^{-4}	10^{-8}
Free exciton (GaAs)	10^{-4}	10^{-4}	10^{-9}
Free exciton (GaAs/AlGaAs MQW)	10^{-4}	10^{-2}	10^{-8}
Molecular orientation (nematic liquid crystal)	10^{-3}	10^{-1}	1

based on the mechanism of in-valence band transition, its n_2 value is moderation, but the response time is higher, it reaches to picosecond.

5.1.2 Cross-Phase Modulation Optical Kerr Effect

In the case of XPM optical Kerr effect, we consider a weak signal light at frequency ω with the electric field strength $\boldsymbol{E}(\omega)$ and a strong pump light frequency at frequency ω' with the electric field strength $\boldsymbol{E}(\omega')$ simultaneously propagate in an isotropic medium, the interaction of pump lights with the medium generates the third-order nonlinear polarization for the signal-light frequency, which is

$$\boldsymbol{P}^{(3)}(\omega) = 6\varepsilon_0\chi^{(3)}(\omega;\omega',-\omega',\omega)|\boldsymbol{E}(\omega')|^2\boldsymbol{E}(\omega). \tag{5.1.17}$$

If we only consider the first-order linear effect and the third-order nonlinear effects, the total nonlinear polarization is

$$\boldsymbol{P}(\omega) = \varepsilon_0\chi^{(1)\prime}\boldsymbol{E}(\omega) + 6\varepsilon_0\chi^{(3)\prime}(\omega;\omega',-\omega',\omega)|\boldsymbol{E}(\omega')|^2\boldsymbol{E}(\omega). \tag{5.1.18}$$

Repeating the previous calculation, we can obtain the dielectric coefficient:

$$\varepsilon = \varepsilon_0\left(1 + \chi^{(1)\prime} + 6\chi^{(3)\prime}(\omega;\omega',-\omega',\omega)|\boldsymbol{E}(\omega')|^2\right). \tag{5.1.19}$$

Finally, we obtain the total refractive index $n = n_0 + \Delta n$, in which the nonlinear refractive index is

$$\Delta n = \frac{3\chi^{(3)\prime}(\omega;\omega',-\omega',\omega)}{n_0}|\boldsymbol{E}(\omega')|^2. \tag{5.1.20}$$

Setting:

$$\bar{n}_2^{(cross)} = \frac{3\chi^{(3)\prime}(\omega;\omega',-\omega',\omega)}{n_0}, \tag{5.1.21}$$

Equation (5.1.20) becomes

$$\Delta n = \bar{n}_2^{(cross)}|\boldsymbol{E}(\omega')|^2. \tag{5.1.22}$$

To use intensity formula for the pump light $I_\mathrm{p} = \frac{1}{2}\varepsilon_0 c n_0 |\boldsymbol{E}(\omega')|^2$, the Eq. (5.1.20) can be written to

$$\Delta n = \frac{6\chi^{(3)\prime}(\omega;\omega',-\omega',\omega)}{\varepsilon_0 c n_0^2} I_p. \tag{5.1.23}$$

Setting:

$$n_2^{(\mathrm{cross})} = \frac{6\chi^{(3)\prime}(\omega;\omega',-\omega',\omega)}{\varepsilon_0 c n_0^2}, \tag{5.1.24}$$

then we have

$$\Delta n = n_2^{(cross)} I_p. \tag{5.1.25}$$

Visible, in the XPM optical Kerr effect, the refractive-index change of medium is proportional to the intensity of the pump light, and the ratio coefficient $n_2^{(cross)}$ is the nonlinear refraction coefficient for the XPM optical Kerr effect, which is proportional to the real part of the third-order nonlinear susceptibility.

Because in the common case $\omega' \neq \omega$, the third-order susceptibility $\chi^{(3)\prime}(\omega;\omega',-\omega',\omega)$ is different with $\chi^{(3)\prime}(\omega;\omega,-\omega,\omega)$, however, if we only consider non-resonance case, and assume the dispersion effects at two different frequencies can be neglected, then we have

$$\chi^{(3)\prime}(\omega;\omega',-\omega',\omega) \approx \chi^{(3)\prime}(\omega;\omega,-\omega,\omega), \tag{5.1.26}$$

To compare Eqs. (5.1.24) and (5.1.11), we have

$$n_2^{(\text{cross})} = 2n_2. \tag{5.1.27}$$

Way the nonlinear refraction coefficient induced by XPM Kerr effect is 2 times of the nonlinear refraction coefficient induced by SPM Kerr effect? That is because the difference of degeneration factors in two cases is 2 times. Substituting Eq. (5.1.27) into Eq. (5.1.25), then we get

$$\Delta n = 2n_2 I_p. \tag{5.1.28}$$

This is the refractive-index change of the medium receptive by the signal light at the frequency ω under the action of the pump light. This refractive-index change is proportional to the intensity of the pump light; the ratio coefficient is two times of the nonlinear refraction coefficient in the SPM Kerr effect. For the signal light, the total refractive index in XPM Kerr effect is

$$n = n_0 + 2n_2 I_p. \tag{5.1.29}$$

If the propagation distance of the signal light in the medium is $\boldsymbol{L}$, the phase change of signal light induced by the pump light is

$$\Delta\phi = \frac{2\pi}{\lambda_0}\Delta nL = \frac{2\pi L(2n_2 I_\text{p})}{\lambda_0} = \frac{4\pi L n_2}{\lambda_0 S} P_P. \tag{5.1.30}$$

where P_P is the power of the pump light, S is the effective cross section of the signal beam. Visible, the phase change of the signal light is proportional to the power of the pump light.

5.1.3 Optical-Kerr-Effect Induced Birefringence

When a polarized pump light passes through the isotropic nonlinear medium, the optical Kerr effect will induce different refractive-index changes in different transverse directions perpendicular to the propagation direction of the pump light. It equivalently changes an isotropic medium to be an anisotropic birefringence medium (such as uniaxial crystal). In this time if we let a linear polarized signal light passes through medium along the direction of pump light, this linear polarized light will become an elliptic polarization light, its o light and e light components have different refractive index. Now we study this light-induced birefringence effect.

Assuming a frequency ω monochromic signal light $E(\omega)$ and a frequency ω' monochromic pump light $E(\omega')$ together propagate along z direction, but their polarization directions are different: the polarization direction of the pump light is

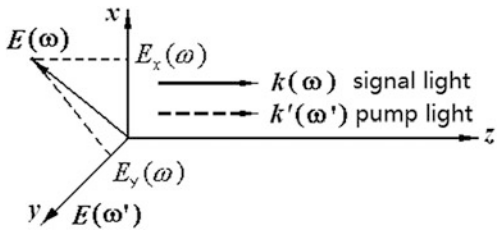

Fig. 5.2 Propagation direction and polarization direction of the signal light at ω and the pump light at ω'

along y direction; the polarization direction of the signal light is along any direction in $x-y$ plane. $E(\omega)$ has two components in x and y directions respectively: $E_x(z,\omega)$ and $E_y(z,\omega)$, as shown in Fig. 5.2.

Under the action of the pump light, the components $E_x(z,\omega)$ and $E_y(z,\omega)$ of signal light generate the nonlinear polarizations in x and y directions respectively

$$P_x^{(3)}(z,\omega) = 6\varepsilon_0\chi_{xxyy}^{(3)}(\omega;\omega',-\omega',\omega)|E(\omega')|^2E_x(z,\omega), \tag{5.1.31}$$

$$P_y^{(3)}(z,\omega) = 6\varepsilon_0\chi_{yyyy}^{(3)}(\omega;\omega',-\omega',\omega)|E(\omega')|^2E_y(z,\omega). \tag{5.1.32}$$

Setting the wave-vector difference of lights $E_x(z,\omega)$ and $E_y(z,\omega)$ is $\Delta k = 0$, the nonlinear coupling wave equations in x and y direction respectively are (D = 6)

$$\frac{dE_x(z,\omega)}{dz} = i\frac{3\omega}{cn_\omega}\chi_{xxyy}^{(3)}(\omega;\omega',-\omega',\omega)|E(\omega')|^2E_x(z,\omega), \tag{5.1.33}$$

$$\frac{dE_y(z,\omega)}{dz} = i\frac{3\omega}{cn_\omega}\chi_{yyyy}^{(3)}(\omega;\omega',-\omega',\omega)|E(\omega')|^2E_y(z,\omega). \tag{5.1.34}$$

Assuming the pump light $E(\omega')$ without change in z direction in the process, we can solve the signal light amplitudes in x and y directions respectively, namely

$$E_x(z,\omega) \propto \exp\left\{ik_0\left[\frac{3}{n_\omega}\chi_{xxyy}^{(3)}(\omega;\omega',-\omega',\omega)|E(\omega')|^2\right]z\right\} = e^{ik_0\Delta n_\perp}, \tag{5.1.35}$$

$$E_y(z,\omega) \propto \exp\left\{ik_0\left[\frac{3}{n_\omega}\chi_{yyyy}^{(3)}(\omega;\omega',-\omega',\omega)|E(\omega')|^2\right]z\right\} = e^{ik_0\Delta n_\parallel}. \tag{5.1.36}$$

$\Delta n_\perp$ and $\Delta n_\parallel$ in Eqs. (5.1.35) and (5.1.36) are the nonlinear refractive indexes in x and y directions respectively (or the refractive-index changes of o light and e light), $\Delta n_\perp$ and $\Delta n_\parallel$ are respectively

$$\Delta n_\perp = \frac{3}{n_\omega}\chi_{xxyy}^{(3)}(\omega;\omega',-\omega',\omega)|\boldsymbol{E}(\omega')|^2, \tag{5.1.37}$$

$$\Delta n_{\parallel} = \frac{3}{n_{\omega}} \chi^{(3)}_{yyyy}(\omega; \omega', -\omega', \omega) |\boldsymbol{E}(\omega')|^2. \tag{5.1.38}$$

Visible, two refractive index changes in orthogonal polarization directions are all proportional to the intensity of the pump light.

This strength of light-induced birefringence generated by the pump light can be measure by using the Kerr coefficient defined by the following formula:

$$K_{\omega'}(\omega) = \frac{\Delta n_{\parallel}(\omega) - \Delta \mathrm{n}_{\perp}(\omega)}{\lambda |E(\omega')|^2}. \tag{5.1.39}$$

Substituting Eqs. (5.1.37) and (5.1.38) into Eq. (5.1.39), and using the formula $k_0 = \frac{\omega}{c} = \frac{2\pi}{\lambda_0} = \frac{2\pi n_{\omega}}{\lambda}$, we can obtain the relationship between the Kerr coefficient and the difference of two third-order susceptibilities:

$$K_{\omega'}(\omega) = \frac{3\omega}{2\pi c} \left(\chi^{(3)}_{\mathrm{yyyy}} - \chi^{(3)}_{\mathrm{xxyy}} \right). \tag{5.1.40}$$

When the signal light passes through the medium for length of L, the phase difference between above o light and e light is

$$\Delta\phi = \frac{2\pi}{\lambda_0} (\Delta n_{\parallel} - \Delta n_{\perp}) L = \frac{2\pi L K_{\omega'}(\omega)}{n_{\omega}} |E(\omega')|^2. \tag{5.1.41}$$

Using the intensity formula of the pump light $I_{\mathrm{p}} = \frac{1}{2} \varepsilon_0 c n_{\omega'} |\boldsymbol{E}(\omega')|^2$, we obtain

$$\Delta\phi = \frac{4\pi L K_{\omega'}(\omega)}{\varepsilon_0 c n_{\omega'} n_{\omega}} I_{\mathrm{p}}. \tag{5.1.42}$$

Visible, the phase difference between o light and e light of the signal light is proportional to the intensity of the pump light.

When the power of pump light is strong enough to lead $\Delta\phi = \pi$, it corresponds to the rotation angle of the polarization plane of signal light $\varphi = \Delta\phi/2 = 90°$. So that we can design a nonlinear polarization type all-optical switch to control the intensity of a signal light by using a pump light, as shown in Fig. 5.3.

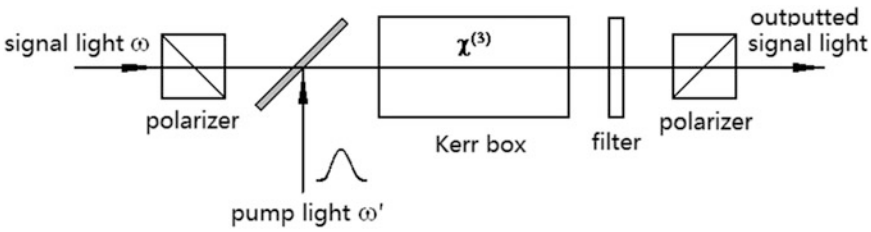

Fig. 5.3 A nonlinear polarization-type Kerr box all-optical switching device based on the cross-phase modulation optical Kerr effect

In Fig. 5.3 the container installing the nonlinear organic liquid (for example, Nitrobenzene etc.) is called the Kerr box. The signal light comes from a He–Ni laser; the pump light source can use a YAG picosecond laser. Two polarizers are placed mutual orthogonally. The filter is used for stopping the pump light, which only allow the signal light passing through. If without the pump light, the signal light cannot pass through the device (off-state); if adding the pump light, the polarization plane of signal light is rotated 90°, so the signal light passes through the device (on-state). According to Eq. (5.1.41), in the condition of $\Delta\phi = \pi$, the threshold intensity of the pump light for optical switching is

$$I_{\mathrm{p}} = \frac{\varepsilon_0 c n_{\omega'} n_{\omega}}{4LK_{\omega'}(\omega)}. \tag{5.1.43}$$

So the Kerr coefficient larger and the length of Kerr box longer, the required intensity of pump light for optical switching lower.

The advantage of such polarization-type optical switch based on optical Kerr effect is having faster switching speed. The disadvantage is need higher pump-light power, due to small $K_{\omega'}(\omega)$ of Kerr materials; in addition, the polarizers should expend a half of intensity of signal light, and the absorption and dispersion of Kerr box also wear down the intensity of signal light.

5.2 Self-focusing of Light Beam

5.2.1 Steady State Self-focusing

1. **Self-focusing of Light Beam and Diffraction of Light Beam**

When a single mode laser propagates in the nonlinear medium, because the laser beam has Gaussian-type transverse intensity distribution, i.e., the intensity at the center is much stronger than the intensity at the edge. The optical Kerr effect will lead that the refractive-index distribution in the medium becomes non-uniform along the radial direction. In this case, the nonlinear medium plays a role similar to a lens; the profile size of the light beam will be continuously changed: convergence or divergence, as shown in Fig. 5.4.

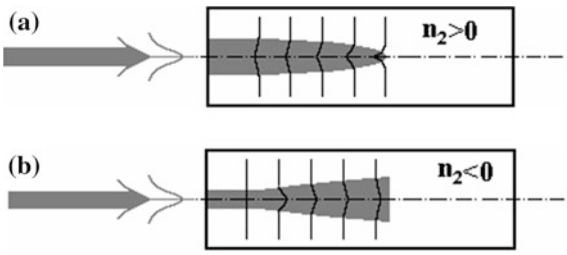

Fig. 5.4 A Gaussian-type laser beam propagates in the nonlinear medium, continuously changes the transverse profile size: **a** self-focusing ($n_2 > 0$); **b** self-defocusing ($n_2 < 0$)

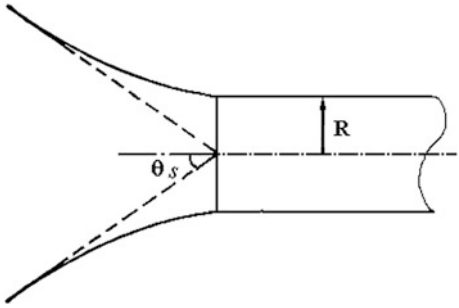

Fig. 5.5 The convergence action to the Gaussian light beam by self-focusing lens effect in the medium

As mention above that the refractive-index change Δn is proportional to the light intensity I, i.e., $\Delta n = n_2 I$, the ratio coefficient n_2 is nonlinear refraction coefficient. When $n_2 > 0$, the medium shows the plus lens effect, the light beam is focused, it is called self-focusing; when $n_2 < 0$, the medium shows the concave lens effect, the light beam is defocused, it is called self-defocusing.

For the self-focusing case, the intensity of Gaussian light beam is gradually degenerative along radial direction of the medium from axes to edge of the beam. So that the refractive index of the medium $n = n_0 + n_2 I$ is also gradually decreasing along the radial direction. The area near the input end of the medium can be approximately regard as a fiber self-focusing lens, as shown in Fig. 5.5.

The greatest numerical aperture on the input end face of fiber self-focusing lens can be calculated by the formula:

$$NA = n_0 \sin\theta_s = \sqrt{n^2(0) - n^2(R)}, \tag{5.2.1}$$

where θ_S is largest convergence angle, n_0 is the linear refractive index of medium. $n(0)$ is total refractive index on the center axis of light beam, $n(0) = n_0 + \Delta n$, where Δn is the light field induced refractive-index change. $n(R)$ is the total refractive index at the edge of light beam, where light field is zero, so $\Delta n = 0$, then $n(R) \approx n_0$. In addition, Δn is much smaller than n_0, i.e., $\Delta n^2 \ll n_0 \Delta n$, Δn^2 can be neglected, thus from Eq. (5.2.1) we can obtain:

$$n_0 \sin\theta_s \approx \sqrt{(n_0 + \Delta n)^2 - n_0^2} \approx \sqrt{2 n_0 \Delta n}. \tag{5.2.2}$$

In general the convergence angle is very small, approximately $\sin\theta_s^2 \approx \theta_s^2$, so from Eq. (5.2.2), we obtain the relationship between the self-focusing convergence angle and the nonlinear refractive index induced by the laser:

$$\theta_s^2 \approx \frac{2\Delta n}{n_0}. \tag{5.2.3}$$

On the other hand, if the incident surface is located at the beam waist of Gaussian light beam, the diffraction of Gaussian beam is shown in Fig. 5.6.

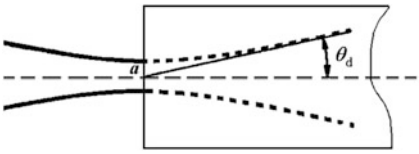

Fig. 5.6 The diffraction of the Gaussian light beam

As we known that the diffraction angle of Gaussian light beam approximately is

$$\theta_d \approx \frac{\lambda}{\pi a n_0} = \frac{2}{ka}, \tag{5.2.4}$$

where n_0 is the linear refractive index of medium, k is the wave vector of light, a is the radius of the beam waist.

According to Eqs. (5.2.3) and (5.2.4), the square of ratio between the convergence angle of self-focusing and the diffraction angle of laser is

$$\frac{\theta_s^2}{\theta_d^2} = \frac{1}{4}\left(\frac{2\Delta n}{n_0}\right) / \left(\frac{1}{k^2 a^2}\right). \tag{5.2.5}$$

We can see that in the self-focusing process, on the one hand, the strong light via optical Kerr effect to increase Δn, so that to enhance the convergent ability of light beam; on the other hand, the strong light leads the shrink of spot radius at focus point of light beam, to enhance the divergence ability of light beam, namely, in self-focusing process, there is a competition between the self-focusing and the diffraction. Later we will prove that as long as satisfying the condition:

$$\frac{2\Delta n}{n_0} \geq \frac{1}{k^2 a^2} \text{ or } \theta_s \geq \frac{\theta_d}{2}, \tag{5.2.6}$$

the self-focusing will always stronger than the diffraction, until the other nonlinear effects (for example, the stimulated scattering, two-photon absorption, photoinduced breakdown, etc.) terminate the self-focusing process. If both the convergence action of the laser self-focusing and the divergence action of the laser diffraction achieve a balance, namely $\theta_s = \theta_d/2$, a self-trapping effect will be appeared. The stable self-trapping process is just the space optical soliton effect.

Considering $\Delta n = n_2 I$, according to Eq. (5.2.6), the laser intensity required for producing self-focusing will be:

$$I \geq \frac{n_0}{2 n_2 k^2 a^2}. \tag{5.2.7}$$

Form Eq. (5.2.7) we can see, the nonlinear refraction coefficient of medium n_2 larger (self-focusing action larger), and the beam waist radius of laser a larger (diffraction action smaller), the laser intensity required for generating self-focusing smaller. Using Eq. (5.2.7) we can quantitatively estimate the light intensity required

for generating self-focusing. For example, setting $n_2 = 10^{-13}\,\mathrm{cm}^2/\mathrm{W}$, $a \approx 1\,\mathrm{mm}$, $k = 2 \times 10^4\ \mathrm{cm}^{-1}$, we calculate to get the incident light power required for generating self-focusing exceed 1 MW/cm^2.

2. **Steady-state Theory of Self-Focusing**

If the response time of medium is much shorter than the pulsewidth of incident laser, the theory of self-focusing can dear with by the steady-state method [8]. Below we introduce the paraxial steady-state theory of self-focusing. From the nonlinear wave Eq. 2.1.17), assuming $\sigma = 0$(neglecting the loss of light), we obtain

$$\nabla \times \nabla \times \boldsymbol{E} + \mu_0 \frac{\partial^2 \boldsymbol{\varepsilon}.\boldsymbol{E}}{\partial t^2} = -\mu_0 \frac{\partial^2 \boldsymbol{P}_{NL}}{\partial t^2}. \tag{5.2.8}$$

We assume that the medium is isotropic, so $\nabla \cdot \boldsymbol{E} = 0$, in Eq. (5.2.8), $\nabla \times \nabla \times \boldsymbol{E} = \nabla(\nabla \cdot \boldsymbol{E}) - \nabla^2 \boldsymbol{E} = -\nabla^2 \boldsymbol{E}$, and ε is a scalar. Using the formulae $c = 1/\sqrt{\varepsilon_0 \mu_0}$ and $n_0 = \sqrt{\varepsilon/\varepsilon_0}$, the wave Eq. (5.2.8) can be written to the following scalar form:

$$\left(\nabla_\perp^2 \boldsymbol{E} + \frac{\partial^2 \boldsymbol{E}}{\partial z^2}\right) - \frac{n_0}{c^2}\frac{\partial^2 \boldsymbol{E}}{\partial t^2} = \frac{\varepsilon_0}{c^2}\frac{\partial^2 \boldsymbol{P}_{NL}}{\partial t^2}. \tag{5.2.9}$$

where

$$\nabla_\perp^2 = \frac{\partial^2}{\partial x^2} + \frac{\partial^2}{\partial y^2}. \tag{5.2.10}$$

For the Kerr medium, using Eq. (5.1.7), to write $\boldsymbol{P}_{NL}$ in the right side of Eq. (5.2.9) to be

$$\boldsymbol{P}_{\boldsymbol{NL}} = 3\varepsilon_0 \chi^{(3)} |\boldsymbol{E}|^2 \boldsymbol{E} = 2\varepsilon_0 n_0 \Delta n \boldsymbol{E}. \tag{5.2.11}$$

Then the wave Eq. (5.2.9) becomes

$$\nabla_\perp^2 \boldsymbol{E} + \frac{\partial^2 \boldsymbol{E}}{\partial z^2} - \frac{n_0^2}{c^2}\frac{\partial^2 \boldsymbol{E}}{\partial t^2} = \left(\frac{2\Delta n}{n_0}\right)\frac{n_0^2}{c^2}\frac{\partial^2 \boldsymbol{E}}{\partial t^2}. \tag{5.2.12}$$

Suppose $\boldsymbol{E}$ is the light electric field strength of a monochromic plane wave at frequency ω propagated along z direction:

$$\boldsymbol{E}(z,t) = \tilde{\boldsymbol{E}}(z,t) e^{-i(\omega t - kz)}, \tag{5.2.13}$$

where $\tilde{\boldsymbol{E}}(z,t)$ is the complex amplitude of light electric field, $k = k_0 n_0 = n_0 \omega / c$; n_0 is the linear refractive index of the medium. Substituting Eq. (5.2.13) into Eq. (5.2.12), the second item of left of Eq. (5.2.12) becomes

$$\begin{aligned}\frac{\partial^2 \boldsymbol{E}}{\partial z^2} &= 2ik\frac{\partial \tilde{\boldsymbol{E}}}{\partial z}e^{-i(\omega s-kz)} - k^2\tilde{\boldsymbol{E}}e^{-i(\omega t-kz)} - \frac{\partial^2 \tilde{\boldsymbol{E}}}{\partial z^2}e^{-i(\omega t-kz)} \\ &\approx 2ik\frac{\partial \tilde{\boldsymbol{E}}}{\partial z}e^{-i(\omega t-kz)} - k^2\tilde{\boldsymbol{E}}e^{-i(\omega t-kz)}.\end{aligned} \tag{5.2.14}$$

In Eq. (5.2.14), assuming the complex amplitude $\tilde{\boldsymbol{E}}$ is a slowly-varying-approximation function of z, so the items containing $\frac{\partial^2 \tilde{\boldsymbol{E}}}{\partial z^2}$ are neglected.

In Eq. (5.2.12), the third item of left side and the item of right side both contain:

$$\begin{aligned}\frac{n_0^2}{c^2}\frac{\partial^2 \boldsymbol{E}}{\partial t^2} &= \frac{n_0^2}{c^2}\left[-\omega^2\tilde{\boldsymbol{E}}e^{-i(\omega t-kz)} - 2i\omega\frac{\partial \tilde{\boldsymbol{E}}}{\partial \boldsymbol{t}}e^{-i(\omega t-kz)} + \frac{\partial^2 \tilde{\boldsymbol{E}}}{\partial \boldsymbol{t}^2}e^{-i(\omega t-kz)}\right] \\ &\approx -k^2\tilde{\boldsymbol{E}}e^{-i(\omega t-kz)}.\end{aligned} \tag{5.2.15}$$

In Eq. (5.2.15), the items containing $\frac{\partial \tilde{\boldsymbol{E}}}{\partial t}$ and $\frac{\partial^2 \tilde{\boldsymbol{E}}}{\partial t^2}$ can be neglected due to the steady state reason.

To substitute Eqs. (5.2.14) and (5.2.15) into Eq. (5.2.12), and to eliminate the phase factors in the two sides of the equation, the equation becomes

$$\nabla_\perp^2\tilde{\boldsymbol{E}} + 2ik\frac{\partial \tilde{\boldsymbol{E}}}{\partial z} = -2k^2\frac{\Delta n}{n_0}\tilde{\boldsymbol{E}}. \tag{5.2.16}$$

This is a parabolic-type steady-state self-focusing wave equation (here $\tilde{\boldsymbol{E}}$ is independent of the time).

In general, the light wave is not a planar wave, in order to reflect the geometric difference between the actual wave front and the plane wave front, introduce a phase function $S(r, x)$, where r is the radial coordinate, the complex amplitude $\tilde{\boldsymbol{E}}$ can be expressed as

$$\tilde{\boldsymbol{E}} = \boldsymbol{E}_0(r,z)e^{ikS(r,z)}. \tag{5.2.17}$$

where $\boldsymbol{E}_0(r,z)$ is the amplitude function of light field, $kS(r,x) = \varphi$ is the phase of light field. $\boldsymbol{E}_0(r,z)$ and $S(r,x)$ are axis-symmetric real number. To substitute Eq. (5.2.17) into Eq. (5.2.16), then Eq. (5.2.16) is divided into the real part and the imaginary part two coupling equations:

$$\frac{\partial \boldsymbol{E}_0^2}{\partial z} + \nabla_\perp \cdot (\boldsymbol{E}_0^2\nabla_\perp S) = 0, \tag{5.2.18}$$

$$\frac{\partial S}{\partial z} + \frac{1}{2}(\nabla_\perp S)^2 = \frac{\nabla_\perp^2 \boldsymbol{E}_0}{2k^2\boldsymbol{E}_0} + \frac{\Delta n}{n_0}. \tag{5.2.19}$$

Equation (5.2.18) describes the energy change of the light. Using light intensity formula $I = \frac{1}{2}\varepsilon_0 n_0 c \boldsymbol{E}_0^2(r,z)$ and power formula $P = \int_0^\infty I(r,z) 2\pi r dr$, we integral the Eq. (5.2.18) on the whole cross section, obtain $\frac{\partial P}{\partial z} = 0$. This indicate that in the propagation process P is no change with z, the energy conservation is kept. For the Gaussian light beam, the light power at every point on the z axis is equal to the power of beam waist at $z = 0$. Assuming the field strength at that point is $\boldsymbol{E}_0 = \boldsymbol{E}_{0m} e^{-\frac{r^2}{2a_0^2}}$, and we have $\boldsymbol{E}_0^2 = \boldsymbol{E}_{0m}^2$, where a_0 is the radius of the beam waist. The cross sectional area is $A = \pi a_0^2$, thus the total power passing through any cross section of light beam P is giving by

$$P = IA = \frac{1}{2}\varepsilon_0 n_0 c \boldsymbol{E}_{0m}^2 \cdot \pi a_0^2. \tag{5.2.20}$$

Equation (5.2.19) describes the change of light wave front. The first item of right side is the action of diffraction, the second item is the action of optical nonlinearity. When $\Delta n = 0$, it is the sphere wave mode; if $\Delta n \neq 0$, it is the approximate sphere wave, only the curvature center of sphere changes along the z axis. This equation can be approximately solved in the near axis condition. The solution form of Eq. (5.2.19) can be written to

$$\boldsymbol{E}_0(r,z) = \boldsymbol{E}_{0m} \frac{a_0}{a(z)} e^{-\frac{r^2}{2a(z)^2}}, \tag{5.2.21}$$

$$S(r,z) = \frac{r^2}{2R(z)} + \phi(z), \tag{5.2.22}$$

where r is radial coordinate, $a(z)$ is the radius of light beam, $R(z)$ is the radius of wave front. When $R \to \infty$, $S = \phi(z)$, it is a plane wave.

$\Delta n / n_0$ in Eq. (5.2.19) can be calculated approximately as follows: because $r^2 \ll a(z)^2$, $\left(e^{-\frac{r^2}{2a^2}}\right)^2 = e^{-\frac{r^2}{a^2}} \approx 1 - \frac{r^2}{a^2}$; and according to Eq. (5.1.8), $\Delta n = \bar{n}_2 |\boldsymbol{E}_0|^2 \approx \bar{n}_2 \boldsymbol{E}_{0m}^2$, therefore,

$$\frac{\Delta n}{n_0} = \frac{\bar{n}_2 |\boldsymbol{E}_0|^2}{n_0} \approx \frac{\bar{n}_2 \boldsymbol{E}_{0m}^2}{n_0} \cdot \frac{a_0^2}{a^2} e^{-\frac{r^2}{a^2}} \approx \frac{\bar{n}_2 \boldsymbol{E}_{0m}^2}{n_0} \cdot \frac{a_0^2}{a^2}\left(1 - \frac{r^2}{a^2}\right). \tag{5.2.23}$$

Substituting Eqs. (5.2.21)–(5.2.23) into Eq. (5.2.19), we can obtain following two equations:

$$\frac{d\phi}{dz} = -\frac{1}{k^2 a^2} + \frac{B}{k^2 a^2}, \tag{5.2.24}$$

$$\left(1 - \frac{dR}{dz}\right) = R^2(1 - 2B) \cdot \frac{1}{k^2 a^4}, \tag{5.2.25}$$

where

$$B = \frac{k^2 a_0^2 \bar{n}_2 \boldsymbol{E}_{0m}^2}{2n_0} \approx \frac{k^2 a_0^2 \Delta n}{2n_0}. \tag{5.2.26}$$

Using the cylindrical coordinate system, we replace x, y, z by r, φ, z, and $\nabla_\perp = \frac{\partial}{\partial r}$, $\nabla_\perp^2 = \left(\frac{\partial^2}{\partial r^2} + \frac{1}{r}\frac{\partial}{\partial r}\right)$. Substituting Eqs. (5.2.21) and (5.2.22) into Eq. (5.2.18), we can obtain

$$\frac{da(z)}{dz} = \frac{a(z)}{R(z)}. \tag{5.2.27}$$

To make the derivation of Eq. (5.2.27) on both sides to z, and use Eq. (5.2.25), we can obtain

$$\frac{d^2 a}{dz^2} = \left(1 - \frac{dR}{dz}\right) \cdot \frac{a}{R^2} = (1 - 2B) \cdot \frac{1}{k^2 a^3}.$$

On the two side of above equation times $2\frac{da}{dz}$, and integral of it to get

$$\left(\frac{da}{dz}\right)^2 = (2B - 1) \cdot \frac{1}{k^2 a^2} + C.$$

The integration constant C is determined by initial condition $R(0) = R_0$, $a(0) = a_0$, $\phi(0) = 0$, then we obtain:

$$C = \left(\frac{a_0}{R_0}\right)^2 + (1 - 2B) \cdot \frac{1}{k^2 a_0^2}.$$

Finally, Eq. (5.2.27) becomes

$$\frac{a^2(z)}{a_0^2} = (1 - 2B)\frac{z^2}{k^2 a_0^4} + \left(1 + \frac{z}{R_0}\right)^2. \tag{5.2.28}$$

This is the light beam radius variation law in the isotropic nonlinear medium and for the paraxial approximate solution.

If incident light is a plane wave, $R_0 \to \infty$, Eq. (5.2.28) is simplified as

$$\frac{a^2(z)}{a_0^2} = (1 - 2B)\frac{z^2}{k^2 a_0^4} + 1. \tag{5.2.29}$$

It is thus clear that when $B > \frac{1}{2}$, $a(z) < a_0$, the light beam is convergence, that is self-focusing case. Light beam forms a focal spot at the focus point $z = z_f$, at that

point $a(z_f) = 0$. When $B < \frac{1}{2}$, $a(z) > a_0$, light beam is divergence, this is self-defocusing case. When $B = \frac{1}{2}$, $a(z) = a_0$, keeping the radius of light beam no change, it is the self-trapping case.

Therefore, B determines the law of light beam propagation. According to Eq. (5.2.26), B also can be denoted

$$B = \frac{\Delta n/n_0}{1/k^2 a_0^2}. \tag{5.2.30}$$

Visible, the physical meaning of B is the ratio of light induced refractive–index change and light diffraction. When $B = \frac{1}{2}$, namely $\frac{2\Delta n}{n_0} = \frac{1}{k^2 a_0^2}$. From Eq. (5.2.6), we get $\theta_s = \frac{1}{2}\theta_d$, this equivalently to achieve a balance between the nonlinear action and the diffraction action.

In general case, let $a(z_f) = 0$, from Eq. (5.2.28) can calculate to get the location of self-focusing focal point z_f:

$$\frac{1}{z_f} = -\frac{1}{R_0} \pm \frac{1}{ka_0^2}\sqrt{2B - 1}. \tag{5.2.31}$$

This formula can rewrite to the form denoted by the light power. According to Eqs. (5.2.30), (5.2.20) and $k = (\omega/c)n_0$, than get

$$B = \frac{\omega^2 \bar{n}_2}{\varepsilon_0 \pi c^3} P. \tag{5.2.32}$$

The power for $B = \frac{1}{2}$ is defined as the critical power P_c, from Eq. (5.2.32), the P_c is given by

$$P_c = \frac{\varepsilon_0 \pi c^3}{2\omega^2 \bar{n}_2}. \tag{5.2.33}$$

Visible, the nonlinearity of material stronger, the threshold power for generating the self-focusing lower.

Because $P/P_0 = 2B$, Eq. (5.2.31) can rewrite to be

$$\frac{1}{z_f} = -\frac{1}{R_0} \pm \frac{1}{ka_0^2}\sqrt{\frac{P}{P_c} - 1}. \tag{5.2.34}$$

Now we discuss the variation law of cross-section size of focal light beam with the propagation distance in different input wave front cases.

(1) When the incident light is a plane wave, $R_0 \to \infty, P > P_c$, the focal length of self-focusing z_f is a positive value:

$$z_f = \frac{ka_0^2}{\sqrt{P/P_c - 1}}, \tag{5.2.35}$$

Where a_0 is smaller and P is larger, z_f is smaller, so the focal length is shorter.

(2) When the incident light is convergent, i.e., $R_0 < 0$, then the focal length z_f satisfies:

$$\frac{1}{z_f} = \frac{1}{|R_0|} \pm \frac{1}{ka_0^2}\sqrt{\frac{P}{P_c} - 1}. \tag{5.2.36}$$

If the incident wave is weak convergent, i.e., $|R|_0 > ka_0^2/\sqrt{P/P_c - 1}$, the second item in the right side of Eq. (5.2.36) takes sign "+", in this case it only has one focal point moving toward the incident direction;

If the incident wave is strong convergent, i.e., $|R_0| < ka_0^2/\sqrt{P/P_c - 1}$, the second item in the right side of Eq. (5.2.36) takes sign "±", namely there exist two focal points.

(3) When the incident light is divergent, i.e., $R_0 > 0$, the focal length z_f satisfies:

$$\frac{1}{z_f} = -\frac{1}{|R_0|} \pm \frac{1}{ka_0^2}\sqrt{\frac{P}{P_c} - 1}. \tag{5.2.37}$$

The condition that the light beam gradually transfer from divergent to convergent is $z_f > 0$, namely $R_0 > ka_0^2/\sqrt{P/P_c - 1}$. This shows that for the certain incident light power, only when the divergence of the incident light is not too big, it is possible to form the self-focusing in the medium. Figure 5.7 gives the pictures of the variation of self-focusing light spot size with z in different input conditions.

5.2.2 Dynamic State Self-focusing

If the incident laser is a short pulsed, we have to consider the variation of light-beam parameters with time. The dynamic state self-focusing can be divided into two situations: one is the quasi stable state self-focusing, in this case the laser pulsewidth is much longer than the response time of medium for inducing the change of refractive index, for example, the laser pulsewidth is 10^{-9} s (such as ns laser pulse), the response time of medium is 10^{-12} s (such as ps molecular

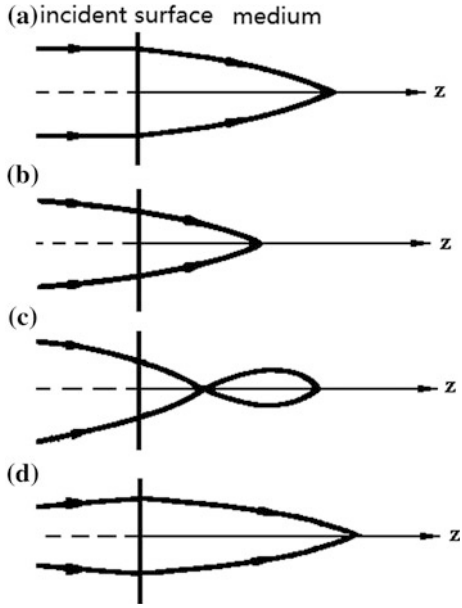

Fig. 5.7 In the steady-state condition, pictures of variation of self-focusing light spot with z under different input condition: **a** parallel light incidence; **b** weak convergent light incidence; **c** strong convergent light incidence; **d** weak divergent light incidence

relaxation time). The other one is the transient state self-focusing, in this case the laser pulsewidth is close to or shorter than the response time of medium.

1. **Quasi Stable State Self-focusing**

For quasi stable state self-focusing, it cannot fully neglect the variation of amplitude with time, when solving the wave Eq. (5.2.8), we can neglect second derivative of time $\frac{\partial^2 \mathrm{E}}{\partial t^2}$, but should remain the first derivative of time $\frac{\partial \mathrm{E}}{\partial t}$. In the meantime we still remain the slow-variation condition of $\boldsymbol{E}$ with z coordinate. Then Eq. (5.2.12) becomes

$$\nabla_{\perp}^2 \boldsymbol{E} + i2k\left(\frac{\partial}{\partial z} + \frac{1}{v}\frac{\partial}{\partial t}\right)\boldsymbol{E} = -2k^2\frac{\Delta n}{n_0}\boldsymbol{E}, \tag{5.2.38}$$

here $v = \frac{\partial \omega}{\partial k}$ is group velocity. Let us introduce two new independent variables:

$$t' = t - z/v \text{ and } z' = z, \tag{5.2.39}$$

and use of derivation formula for composite function, as a result we get

$$\begin{aligned}\frac{\partial E'(z',t')}{\partial z} &= \frac{\partial}{\partial z}E\left(z, t = t' + \frac{z}{v}\right) = \frac{\partial E(z,t)}{\partial z} + \frac{\partial E(z,t)}{\partial t}\cdot\frac{\partial t}{\partial z} \\ &= \frac{\partial E(z,t)}{\partial z} + \frac{\partial E(z,t)}{\partial t}\cdot\frac{1}{v}.\end{aligned} \tag{5.2.40}$$

So Eq. (5.2.38) is rewritten to

$$\nabla_{\perp}^{2}\boldsymbol{E}' + i2k\frac{\partial \boldsymbol{E}'}{\partial z} = -2k^{2}\frac{\Delta n}{n_0}\boldsymbol{E}'. \tag{5.2.41}$$

To compare Eq. (5.2.41) and steady-state self-focusing wave Eq. (5.2.16), one can see these two equations have same form. The form of solved self-focusing focal length formula is also similar. But only the focal length is the function of the time. In the plane wave incidence case, the self-focusing focal length is

$$z_f'(z', t') = \frac{ka_0^2}{\sqrt{[P(z', t')/P_c] - 1}}. \tag{5.2.42}$$

If still using z and t as variables, above equation can be expressed as

$$z_{\mathrm{f}}(z, t) = z_{\mathrm{f}}'(z', t') = \frac{ka_0^2}{\sqrt{[P(z, t - z/v)/P_c] - 1}}. \tag{5.2.43}$$

Visible, in dynamic self-focusing case, the self-focusing focal length is changed with time. z_f at t moment is induced by light power at $t - z/v$ moment.

Above solution comes from the paraxonic approximation, the strict numerical solution gives the relationship of z_f and P, that is

$$z_f(t) = \frac{K}{\sqrt{P(t')} - 0.852\sqrt{P_c}}, \tag{5.2.44}$$

where the constant K and the critical power P_c both can be experimentally determined.

For example, a picosecond laser pulse inputs CS_2 to produce the self-focusing. The variation of incident pulse power with time $P(t)$ is shown in Fig. 5.8b, using Eq. (5.2.44) the calculated curve of the variation of self-focusing focal point position with time $z_{\mathrm{f}}(t)$ is shown in Fig. 5.8a, it is a U shaped curve [9].

Assuming that the half maximum width of light pulse is 1 *ns*, the peak power is $P_{\max}$=P_{D} = 42.5 kW, the self-focusing threshold power is P_c = 8 kW, and K = 11.6 cm/kW$^{1/2}$, the length of sample cell is L = 30 cm. The every point on the pulse waveform successively starts from the time moment of t_A, t_B, t_C, t_D, t_D and t_E, with power value of P_A, P_B, P_C, P_D, and P_E respectively (they are all larger than the critical power value P_c). The lights with velocity of c/n_0 (the slope of imaginary line) propagate in the medium, on point A, B, C, D, E in 20 cm medium length to form the self-focusing focal points, respectively.

The first arrived focal point is point C (position z_B), then move along two sub-lines of U shape path. The velocity of the focal point is determined by the slop of U shape line: the moving velocity of focal point moving along first sub-line C–B—A is from lager than light velocity until equal to light velocity c/n_0: the velocity

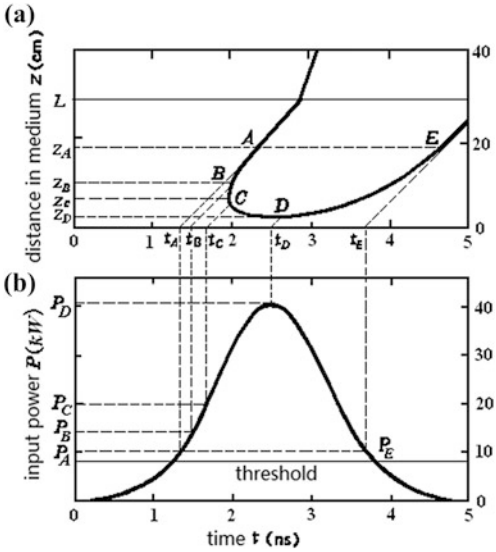

Fig. 5.8 Track of focal point for quasi stable state self-focusing: **a** the input light power waveform; **b** the variation of focal point location with time

of point C is ∞, the velocity of point B is faster than light velocity, the velocity of point A is just light velocity. For the focal point moving along second sub-line C–D–E: the velocity of point C is—∞, the velocity of point D is zero, the velocity of point E is recovered to light velocity. From C to D is back up along reverse direction of incident light, point D is corresponding to the maximum of pulse power $P_{\max}$, having shortest focal length. After that go ahead along direction of incident light from point D arrive at point E. Here we assume point A and point E is located between the end surfaces of sample cell (in 20 cm). If the light power in sample cell not lower than the threshold power, the two focal points starting from these two points will move ahead remaining the light velocity of medium c/n_0, until to the end of sample cell $z = L$, then output with light velocity in vacuum c. This bifocal moving image have been proved in experiments.

After the focal point $z_f = z_c$ and before output from the end surface one can observe the filament induced by self-focusing focal point movement, as shown in Fig. 5.9. By using the stripe camera one can shoot the diameter of the filament, which is basic equal to the diameter of focal point.

A large number of experiments found that, when a single mode light pulse inputs the transparent medium, one can see that the self-focusing of light beam makes the light beam shrink, then generates a filament with diameter about 10 μm keeping the diameter variation about 20 %, it is sustainable for several centimeter; for

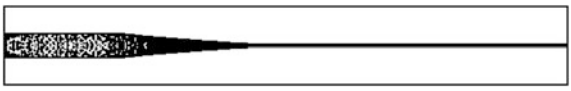

Fig. 5.9 the phenomenon of the filament induced by the dynamic self-focusing

multimode pulse, it will break up into many filaments. All of these filaments are track of movement of dynamic self-focusing focal point with time.

It's worth noting that the moving velocity of self-focusing focal point exceeds the light velocity, it not violates special relativity, because the focal point at different moment comes from self-focusing of different part of incident pulse that exceeds the self-focusing threshold, so that the movement of focal point not representative the energy transmitting process in which the whole light pulse signal enters the medium. The propagation velocity of light pulse must describe by the group velocity, the group velocity never exceed the light velocity.

2. **Transient State Self-focusing**

Above dynamic self-focusing analysis is established on the hypothesis that the response of medium to the light field is instant, namely when laser intensity reaches self-focusing threshold light intensity, the action of light field immediately induce refractive-index change, the self-focusing phenomenon immediately happens. But in the case that the laser pulsewidth is shorter to (or close to) the response time to the refractive-index change of medium, the refractive-index change Δn has a certain delay time to the action of laser. This makes that when laser pulse propagates in the medium, its wavefront becomes the horn shape [10]. This transient self-focusing phenomena can use Fig. 5.10 to make qualitatively explain.

Figure 5.10a gives the curves of laser pulse power variation with time. In which *a*–*f* denotes each moments at that moment the power satisfies the threshold condition. When the part *a* of pulse firstly inputs, because the power is weaker and the medium too later response to the light field, Δn is too small, the light is almost linearly diffracted. When the part *b* of pulse inputs, Δn becomes larger, but it is not enough to induce the self-focusing, the light beam is still diffracted, however the diffracted angle is smaller. When the part *c* of pulse inputs, Δn generated by the parts *a* and *b* is big

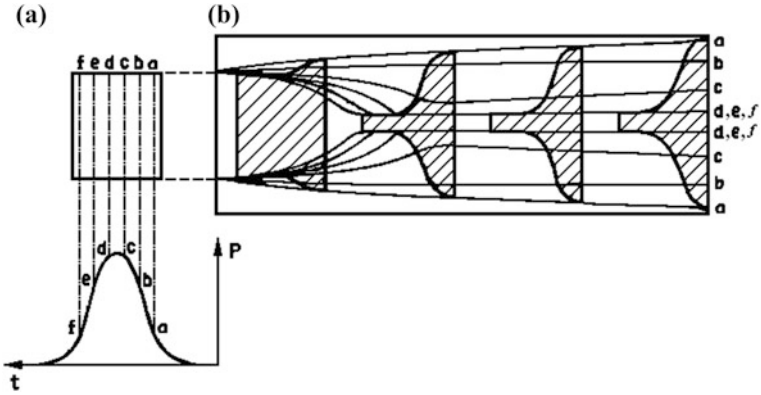

Fig. 5.10 The laser pulse forms a horn shape propagation in the transient self-focusing process: **a** the *curve* of laser pulse power variation with time; **b** the ray of light and the wave front of different part of light pulse in the medium

enough, it overcomes the diffraction to lead the light rays convergent toward to the center. When the parts *d, e, f* of pulse input, although the light power gradually becomes smaller, the refractive-index change Δn generated by pervious pulse parts is accumulated to be big enough. It overcomes the diffraction of light to induce the self-focusing, and lead the focus maintaining a longer time. If connecting the wavefront of light pulse at *a–f* every moments in the same time, then the horn-shape transverse outline of pulse laser can be obtained as shown in Fig. 5.10b. the diameter of horn-shape neck is about several microns, it can keep the shape no change, this is called the dynamic self-tripping. This horn-shape wavefront figure can be observed in the Kerr medium by using the picosecond pulse laser source.

5.2.3 Self-phase Modulation Based on Self-focusing

The self-focusing process based on the interaction between the strong light and the medium contains abundant physical phenomena. If incident light is a pulse light, its light intensity changes with time, the phase of the light also changes with time. To lead the frequency of light happens the peak and valley of periodic change (frequency chirp effect) and the frequency spectrum broadening of outputted light, this phenomenon that the phase modulation to the light frequency by self-focusing is called time self-phase modulation. Self-focusing also can make the phase periodic change on the cross section of light beam, to generate peak and valley of ring-shape intensity distribution on the cross section of light beam. This phenomenon that phase modulation to the light intensity space distribution by self-focusing is called space self-phase modulation. We are going to introduce these two effects below.

1. **Time Self-phase Modulation**

The experiments found that a laser pulse with narrow line width (0.1–1 cm^{-1}), after self-focusing, the outputted light from the filament area have very strong frequency spectrum broaden. For nanosecond pulse, the broaden is about dozens wave number (cm^{-1}); for picosecond pulse, the broaden can reach above several thousand wave number; for sub-femtosecond pulse, even can broaden to be white continues spectrum. These self-focusing light spectrum line self-broaden effect arises from the self-phase modulation of self-focusing light. it can be explained using the following physical model [11, 12].

The light field of the incident laser pulse can be denoted as

$$E(z,\tau) = E_0(z,\tau)e^{i\phi(z,\tau)}, \tag{5.2.45}$$

where $\tau = t - (z/v)$, $v$is the group velocity of light pulse. $E_0(z,t)$ is the amplitude, $\phi(z,t)$ is the phase. The light pulse propagates in the self-focusing filament, the amplitude loss can be neglected, so the light power density is $|E(z,\tau)|^2 = |E(\tau)|^2$ at the any z point. According to Kerr effect, the refractive-index change of medium induced

by light power is $\Delta n(\tau) = \bar{n}_2|E(\tau)|^2$. The light beam passes through the self-focusing filament for distance of L and induces the following phase change (phase shift):

$$\Delta\phi(\tau) = \frac{\omega}{c}\Delta n(\tau)L = \frac{\omega}{c}\bar{n}_2|E(\tau)|^2 L. \tag{5.2.46}$$

So the phase change of the light is proportional to light pulse power density.

According to the Fourier analysis principle, the light filed phase change leads the frequency movement (frequency broadening), which is

$$\Delta\omega(\tau) = -\frac{\partial\Delta\phi(\tau)}{\partial\tau}, \tag{5.2.47}$$

where $\Delta\omega = \omega(\tau) - \omega_0$ is the frequency movement induced by self-phase modulation, ω_0 is the center frequency of light pulse, $\omega(\tau)$ is the frequency at moment τ.

The light filed amplitude in the frequency domain is a function of frequency movement, it can be obtain from Fourier transform:

$$E(\Delta\omega, z) = \frac{1}{2\pi}\int_{-\infty}^{\infty} E(z,\tau)e^{i\Delta\omega\tau}d\tau. \tag{5.2.48}$$

The corresponding frequency spectrum distribution of light intensity is

$$I(\Delta\omega, z) \propto |E(\Delta\omega, z)|^2. \tag{5.2.49}$$

If the incident light pulse is a Gaussian-type laser pulse with pulsewidth about 2 ps. Because $\Delta\phi(\tau) \propto |E(\tau)|^2$, the phase shift $\Delta\phi$ is also Gaussian symmetric as shown in the upper graph of Fig. 5.11. Using Eq. (5.2.47) calculated frequency shift chirp curve is shown in the middle graph of Fig. 5.11. The negative and positive two peaks of $\Delta\omega(\tau)$ are corresponding to two inflection points of Gaussian-type phase curve, respectively. By using Eqs. (5.2.48) and (5.2.49) calculated frequency spectrum distribution curve of light power is shown in the lower graph of Fig. 5.11. It is visible that the power spectrum relative to laser frequency ω_0 is symmetric. The right side is $\Delta\omega = \omega - \omega_0$, the left side is $-\Delta\omega = \omega - \omega_0$, the total width of frequency spectrum intruding the right and left sides is about 300 cm^{-1}.

On the curve of $\Delta\omega(\tau)$, there are many pairs of symmetric points with same slope, the frequencies of two corresponding points are the same, but the phases are different, it seems exist two point sources with same frequency and different phase, sending out two light waves and to interfere each other, result in the spectrogram of light power broadening with frequency. Whether the constructive interference or the destructive interference is dependent on the phase difference, therefore on the outputted spectrum occurs the peak-valley half-period oscillation structure. the interference number in right or left side is depended on integer near $|\Delta\phi|_{max}/2\pi$. Figure 5.11 points out that the maximum phase shift is 80 π, so the number of interference peak is at most of 40, as shown in lower picture of Fig. 5.11.

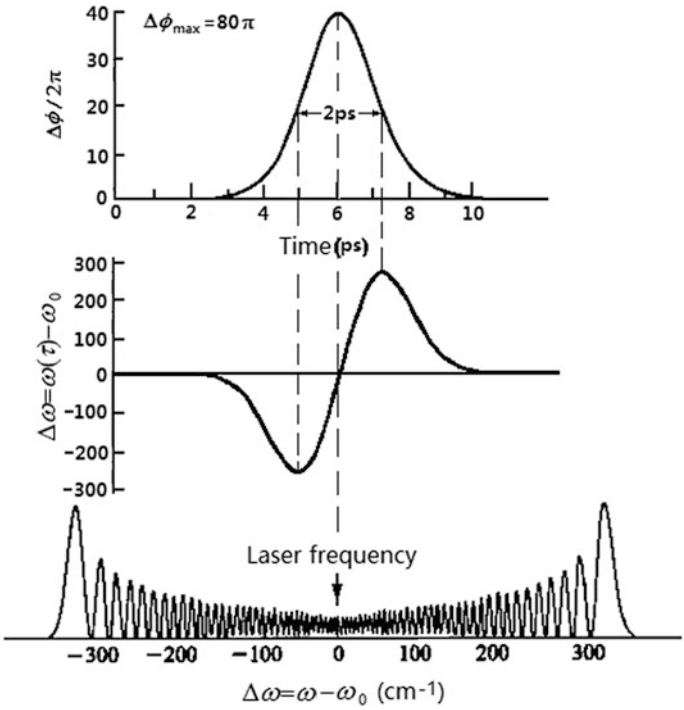

Fig. 5.11 The phase modulation and self-broadening power spectrum of light pulse in the self-focusing medium [13]

Because $|\Delta\omega|_{max} = \left|\frac{\partial\Delta\phi}{\partial\tau}\right|_{max}$, the maximum of frequency spectrum width is generated by the interference of two lights from two inflection points located at maximum slope of $\Delta\phi(\tau)$, so that the widest peak is located at right and left farthest ends. The slope near the center of $\Delta\phi(\tau)$ curve is minimum, where the spectrum width is most narrow.

2. **Space Self-phase Modulation**

The space self-phase modulation is the self-phase modulation generated on the cross section of light beam. For the Gaussian light beam, $\Delta\phi(r)$ along radial direction is showed a Gaussian distribution. Light at center $r = 0$ has a maximum intensity, where $\Delta\phi$ is maximum. If $|\Delta\phi(r)|_{max}$ is much larger than 2π, then on the transverse outputted power spectrum at the location with equal r appears center symmetric peaks and valleys, so that on the far-field projection occurs bright-dark ring structure, as Fig. 5.12. This is the result of interference by same inclination and different radius (different phase) light rings. The number of bright ring is the same as the number of dark ring. This number depends on the integer near $|\Delta\phi|_{max}/\pi$. The radius of outermost ring is formed by interference of light waves at the inflection points (at maximum slope) of Gaussian-type $\Delta\phi(r)$ curve. In the liquid crystal thin film has

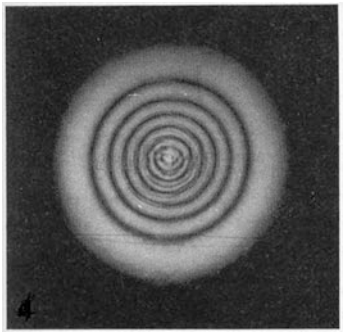

Fig. 5.12 A far-field photo of self-phase modulation space ring

been observed about 100 interference rings [14]. Figure 5.12 is a self-defocusing space light ring photograph by author's experiments using an nonlinear organic solution. Author also theoretically analyzed the ring formation mechanism [15].

5.3 Z-scan Measurement of Nonlinear Optical Parameter

The measurement of third-order nonlinear susceptibility of nonlinear material $\chi^{(3)}$ is very important in nonlinear optics. There are many measure methods, for example, nonlinear elliptical polarization method [1], interference method [16], third harmonic method [17], three-wave frequency mixing [18], degenerated four-wave mixing method [19], optical Kerr gate method [20], wavefront analysis method [21] etc. In which the degenerated four-wave mixing method has been introduced in Chap. 4 of this book. Most of above measurement methods have to use more than two light beams and cannot directly measure the real part and the imaginary part of the susceptibility. In the end of the eighties of 20 century people found a Z-scan method based on the self-focusing [22], not only this method can use a single light beam to accomplish the measurement, but also can measure out the real part and the imaginary part of susceptibility respectively, it can be used to measure the value and sign of the nonlinear refractive index and the nonlinear absorption coefficient by using one experimental setup. Using this method, the people can quickly judge the characteristic of measured nonlinear material: its nonlinear refraction is belong to self-focusing or self-defocusing, or its nonlinear absorption is belong to saturable absorption or reverse saturable absorption (or two-photon absorption).

5.3.1 Experimental Method of Z-scan Measurement

The principle of Z-scan measurement is shown in Fig. 5.13. A single mode Gaussian-type laser beam with intensity $I(z, r)$ is focused into a sample of nonlinear

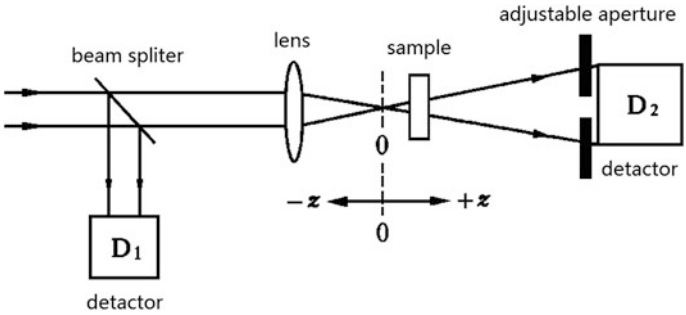

Fig. 5.13 Experimental setup for Z-scan measurement

material by a convergent lens. The sample is located near the focal point, and it can be removed relatively to the focal point along the axis of the light beam. The sample's moving is for change the location of focal point on the sample. The detector D_2 is used to measure the light intensity after the focal point at the far-field location. The detector D_1 is used to measure the relative light intensity before the focal point. There is an center hole adjustable aperture at the front of the detector D_2, the size of the hole is important for the measured result: the nonlinear refractive-index measurement has to use the small hole (close hole), because the refractive-index change is most sensitive to the small hole; however nonlinear absorption measurement needs use a large hole (open hole), because it requires the whole energy of light beam passing through the hole and entering into the detector D_2.

In the experiment, at first we move out the sample, and measure the output light power to get the input power date P_I, after that we place a thin film sample in the location near the focal point at $z = 0$. The incident light induces the self-focusing effect or the self-defocusing effect in the sample material, the strength of effect depend on the location of focal point on the sample. If we move the sample toward right and left along z coordinate near the focal point, we can change of the light energy passing through the hole of aperture. After measuring the transmitted light powers corresponding every locations of sample P_T, we can calculate the normalized transmittances $T(z) = P_T/P_I$. From the shape of the curve $T(z)$, we can judge the nonlinear characteristic of sample material and obtain the values of the nonlinear refraction coefficient and the nonlinear absorption coefficient.

In the Z-scan device, the refractive index of nonlinear medium at the some point of light propagation z-direction is

$$n(z, r) = n_0 + n_2 I(z, r), \tag{5.3.1}$$

where n_0 is linear refractive index of medium, n_2 is nonlinear refraction coefficient. If $n_2 > 0$, the medium shows self-focusing; if $n_2 < 0$, the medium shows self-defocusing. When the sample moves toward +z direction from left to right, the transmittance curve $T(z)$ measured in the close hole case, for $n_2 > 0$ sample,

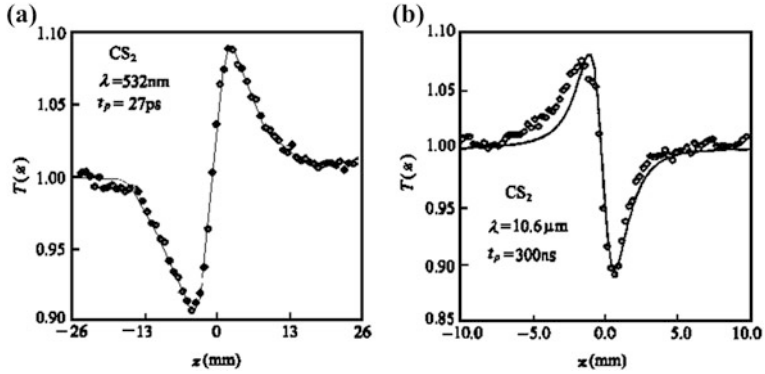

Fig. 5.14 Curves of normalized transmittance variation with z coordinate in close hole case for measurement of nonlinear refractive index of sample CS_2: **a** the self-focusing ($n_2 > 0$); **b** the self-defocusing ($n_2 < 0$)

the light intensity passing focal point is gradually decreased, so it is formed a valley-peak curve, on the contrary, for $n_2 < 0$ sample, the light intensity passing focal point is gradually increased, so it is formed a peak-valley curve.

Figure 5.14 gives two transmittance curves of $T(z)$ obtained from the z-scan measurement using a liquid sample CS_2 filling in a liquid cell with thickness of 1 mm. Figure 5.14a is a light Kerr effect self-focusing curve using a pulse laser with wavelength of 532 nm, pulsewidth of 27 ps and light power density of $2.6\,\mathrm{GW/cm^2}$ as the light source. The measured refractive-index change was $\Delta n = 5.6 \times 10^{-5}$. Figure 5.14b is a thermal effect induced self-defocusing curve using a pulse laser with wavelength of 10.6 μm, pulsewidth of 300 ns, single pulse energy of 0.85 mJ as the light source. The measured refractive-index change was $\Delta n = -1 \times 10^{-3}$. From figures we can see, the results of experiment (black point) and theory (thin solid line) are basically consistent.

In the Z-scan device, at some z point in light propagation direction the nonlinear absorption of medium is

$$\alpha(z, r) = \alpha_0 + \beta I(z, r), \tag{5.3.2}$$

where α_0 is linear absorption coefficient, β is nonlinear absorption coefficient. When $\beta < 0$, it is saturable absorption; when $\beta > 0$, it is reverse saturable absorption or two photon absorption (see Chap. 7). For the saturable absorption sample, the measured transmittance curve is a symmetrical peak curve with the center of the focal point position;for the reverse saturable absorption or two photon absorption, the measured transmittance curve is a symmetrical valley curve with the center of the focal point position, as shown in Fig. 5.15.

Figure 5.15b shows the two-photon absorption measured curve using the 2.7 mm-thickness sample ZnSe and the laser pulse source at wavelength 532 nm, with pulsewidth 27 ps and peak intensity 0.21 $\mathrm{GW/cm^2}$. The theoretical curve is

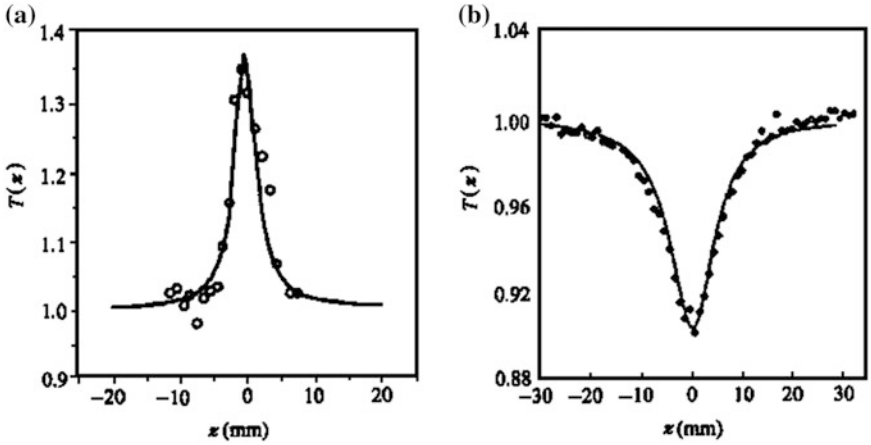

Fig. 5.15 Curves of normalized transmittance variation with z coordinate in open hole case for measurement of nonlinear absorption: **a** the saturable absorption ($\beta < 0$); **b** the reverse saturable absorption or two-photon absorption ($\beta > 0$)

also consistent with the experimental curve. From calculation of measured curve the β = 5.8 cm/GW was obtained.

If the material has nonlinear refraction and nonlinear absorption two effects in the same time, refractive-index curve in Fig. 5.14 will be deformation. we should from the measured results by small hole method minus the measured results by open hole method, than we can obtain the accurate nonlinear refractive-index measurement results.

5.3.2 Theoretical Calculation of Z-scan Measurement [23]

1. **Close Hole Z-scan Method for Measuring Nonlinear Refraction Coefficient**

How to quantitatively calculate the imaginary part (refractive index) and the real part (absorption coefficient) values of nonlinear polarization according to the measured experimental curves?

Set a Gaussian beam with a waist radius w_0 propagating along +z direction, the radius of light beam at point z is $w(z)$, the optical field amplitude $E(z, r, t)$ can be expressed as

$$E(z, r, t) = E_0(t)\frac{w_0}{w(z)}\exp\left(-\frac{r^2}{w^2(z)} - \frac{ikr^2}{2R(z)}\right)e^{-i\phi(z,t)}, \tag{5.3.3}$$

where $w^2(z) = w_0^2(1 + z^2/z_0^2)$, $R(z)=z(1 + z_0^2/z^2)$ is the curvature radius of wavefront at z, $z_0 = kw_0^2n/2$ is the diffraction length of light beam, $k = 2\pi/\lambda$ is the

wave vector, $E_0(t)$ is the light electric amplitude at focal point, it contains the time envelope of light pulse.

Assuming the thickness of sample L is much smaller than the diffraction length of the Gaussian light beam, i.e., $L \ll z_0$, so when light beam passes through the sample, the variation of beam radius can be neglected, and the nonlinear absorption of sample is also neglected, in this condition, because the light beam passing though the sample induces the refractive-index change Δn, the wavefront change will be

$$\Delta\phi(z,r,t) = \frac{\Delta\phi_0(t)}{1+z^2/z_0^2} e^{-\frac{2r^2}{w^2(z)}}, \tag{5.3.4}$$

where $\Delta\phi_0(t)$ is the wavefront change in the sample at focal point (z = 0), that is

$$\Delta\phi_0(t) = k\Delta n_0(t) L_{eff} = k n_2 I_0(t) L_{eff}, \tag{5.3.5}$$

where L_{eff} is the equivalence thickness of the sample:

$$L_{\text{eff}} = (1 - e^{-\alpha L})/\alpha. \tag{5.3.6}$$

Here α denotes the linear absorption coefficient of the sample.

Equation (5.3.5) shows that from the wavefront change in the sample we can find the nonlinear refractive index of medium Δn_0 and the nonlinear refraction coefficient n_2. In order to know wavefront change in the sample, we need to know the light electrical field distribution at the sample.

The light electrical field complex amplitude at the plane e where the light outputs from the sample is

$$E_{\text{e}}(z,r,t) = E_{\text{o}}(z,r,t) e^{-\frac{\alpha L}{2}} \cdot e^{i\Delta\phi(z,r,t)}. \tag{5.3.7}$$

This is not a simple Gaussian light beam, it can be divided the superposition of a series of Gaussian light beams with different beam waists. So we should take the Taylor series expansion to $e^{\text{i}\Delta\phi(z,r,t)}$ in Eq. (5.3.7), namely

$$e^{i\Delta\phi(z,r,t)} = \sum_{m=0}^{\infty} \frac{[i\ \Delta\phi_0(z,t)]^m}{m!} e^{-\frac{2mr^2}{w^2(z)}}. \tag{5.3.8}$$

According to Huygens principle, every sub Gaussian beam may passes the small hole of aperture respectively, then recombination together at aperture outputted plane a. Finally, by using Eqs. (5.3.3) and (5.3.8), we find the far field distribution of light on the small hole screen at the plane a:

$$E_a(z,r,t) = E(z,0,t) e^{-\frac{\alpha L}{2}} \sum_{m=0}^{\infty} \frac{[i\ \Delta\phi_0(z,t)]^m}{m!} \frac{w_{m_0}}{w_m} e^{-\frac{r^2}{w_m^2} - \frac{ikr^2}{2Rm} + i\theta}. \tag{5.3.9}$$

To define d is the space distance between the sample and the small hole plane, and setting $g = 1 + d/R(z)$ (for the parallel light, $R \to \infty$, $g = 1$), then each parameter in Eq. (5.3.9) is:

$$\begin{aligned} w_{m_0}^2 &= \frac{w^2(z)}{2m+1} \\ w_m^2 &= w_{m_0}^2 \left[g^2 + \frac{d^2}{d_m^2} \right] \\ d_m &= \frac{k w_{m_0}^2}{2} \\ R_m &= d \left[1 - \frac{g}{g^2 + d^2/d_m^2} \right]^{-1} \\ \theta_m &= \tan^{-1} \left[\frac{d/d_m}{g} \right] \end{aligned} \tag{5.3.10}$$

To integral the square of above complex number light field on the cross section of the small hole, the light power passing through the small hole can be obtained, which is

$$P_{\mathrm{T}}(z, \Delta\phi_0(t)) = c\varepsilon_0 n_0 \pi \int_0^{r_a} |E_a(z, r, t)|^2 r dr. \tag{5.3.11}$$

Considering the variation of light pulse power with time, the normalized transmittance of Z-scan is

$$T(z) = \frac{\int_{-\infty}^{\infty} P_{\mathrm{T}}(z, \Delta\phi(t)) dt}{S \int_{-\infty}^{\infty} P_{\mathrm{I}}(t) dt}, \tag{5.3.12}$$

where $P_{\mathrm{I}}(t)$ is the light power incident into the sample and S is the linear transmittance of the aperture, namely

$$P_{\mathrm{I}}(t) = \pi w_0^2 I_0(t); \tag{5.3.13}$$

$$S = 1 - e^{-\frac{2r_a}{w_a}}, \tag{5.3.14}$$

where r_a is the radius of the small hole, w_a is the radius of light beam. $S = 0$ and $S = 1$ are corresponding to the completed close hole case and the open hole case, respectively.

If taking $\Delta\phi_0 = \pm 0.25$ and $S = 0.01$, the sample moves from –z to +z, using Eq. (5.3.12), we can pass the numerical calculation to obtain the curves $T(z)$–z as shown in Fig. 5.16. These are the symmetrical z-scan curves for valley-peak ($\Delta n > 0$) and for peak-valley ($\Delta n < 0$).

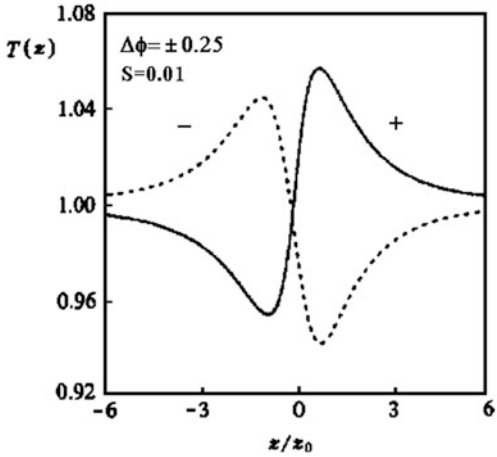

Fig. 5.16 *T* (*z*)-Z *curves* calculated by Z-scan theory when taking $n_2 > 0$ and $n_2 < 0$

In the practical calculation, transmittance Eq. (5.3.12) can be expressed approximately. If setting $r = 0$, $\Delta\phi(t) \ll 1$, and satisfying the far filed condition $d \gg z_0$, in Eq. (5.3.9) we only remain two items, then give an approximate normalized transmittance formula:

$$T(z, \Delta\phi_0) = 1 - \frac{4\Delta\phi_0(t)x}{(x^2+9)(x^2+1)}, \tag{5.3.15}$$

where $\Delta\phi_0(t) = k\Delta n L_{eff}$ is nonlinear phase change at focal point, $x = z/z_0$ is the ratio of sample located z coordinate and the diffraction length.

Theory proved that in practice measurement only require measuring difference value ΔT between peak and valley of experimental curve $T(z)$, then can calculate to get nonlinear refractive index Δn. When hole is very small, i.e., $S \approx 0$, from Eq. (5.3.15) we can calculate to get

$$\Delta T \approx 0.406|\Delta\phi_0|. \tag{5.3.16}$$

Using Eq. (5.3.5), can approximately obtain the nonlinear refractive index:

$$\Delta n \approx \frac{\Delta T}{0.406 k L_{eff}}. \tag{5.3.17}$$

When hole is larger, but phase change at focal point $|\Delta\phi_0| \leq \pi$,

$$\Delta T \approx 0.406(1-S)^{0.25}|\Delta\phi_0|. \tag{5.3.18}$$

In this case the nonlinear refractive index formula is

$$\Delta n = \frac{\Delta T}{0.406(1-S)^{0.25} k L_{eff}}. \tag{5.3.19}$$

2. **Open Hole Z-scan Method for Measuring Nonlinear Absorption Coefficient**

For nonlinear absorption material, the absorption coefficient of sample is

$$\alpha(I) = \alpha_0 + \Delta\alpha = \alpha_0 + \beta I, \tag{5.3.20}$$

where α_0 is the linear absorption coefficient, β is the nonlinear absorption coefficient. The light intensity distribution of outputted surface of sample and the phase shift can be expressed as

$$I_e(r, z, t) = \frac{I_0(r, z, t)\exp[-\alpha(I)l]}{1 + q(r, z, t)}, \tag{5.3.21}$$

and

$$\Delta\phi = \frac{kn_2}{\beta}\ln[1 + q(r, z, t)], \tag{5.3.22}$$

where

$$q(r, z, t) = \beta I(r, z, t)L_{\text{eff}}. \tag{5.3.23}$$

The complex field amplitude on outputted surface of sample can be expressed as

$$E_e = E(z, r, t)e^{-\alpha L/2}(1 + q)^{\left(i\frac{kn_2}{\beta} - \frac{1}{2}\right)}. \tag{5.3.24}$$

where kn_2/β is the ratio of real part and imaginary part of third-order susceptibility $\chi^{(3)}$, so we can see that the nonlinear refractive index and nonlinear absorption coefficient all have contribution to the far-field wavefront variation and transmittance. But in the open hole (S = 1) condition, the transmittance is not sensitive to the wavefront distortion induced by refractive-index change, which is only a function of nonlinear absorption. Therefore the transmitted power can be obtained by integral of the space cross section, don't need consider the process of propagation in the free space. At the location z, by integral of Eq. (5.3.21), the transmitted power is obtained:

$$P(z, t) = P_1(t)\mathrm{e}^{-\alpha L}\frac{\ln[1 + q_0(z, t)]}{q_0(z, t)}, \tag{5.3.25}$$

where

$$q_0(z, t) = \beta I_0(t)L_{\text{eff}}/(1 + z^2/z_0^2). \tag{5.3.26}$$

$P_1(t)$ is the input power, it determines by Eq. (5.3.13).

For Gaussian-type light pulse, the normalized energy transmittance can be obtained by time integral of Eq. (5.3.25), that is given by

$$T(z) = \frac{1}{\sqrt{\pi} q_0(z,0)} \int_{-\infty}^{\infty} \ln\left[1 + q_0(z,0) e^{-\tau^2}\right] \mathrm{d}\tau \,. \tag{5.3.27}$$

When the nonlinear absorption is smaller, to satisfy the condition of $|q_0| < 1$, the transmittance can be indicated as a summation of peak intensity, namely

$$T(z) = \sum_{m=0}^{\infty} \frac{[-q_0(z,0)]^m}{(m+1)^{3/2}}, \quad (\text{when } q_0 < 1). \tag{5.3.27}$$

where

$$q_0(z,0) = \beta I_0(0) L_{\text{eff}} / (1 + z^2/z_0^2), \tag{5.3.28}$$

where $I(0)$ is light intensity at $z = 0$. From Eqs. (5.3.27) to (5.3.28) the β value can be calculated.

Figure 5.17 is the curve of variation of normalized transmittance with time under different β value obtained by numerical calculation method

When open hole ($S = 1$), the transmittance takes first-order approximation of Eq. (5.3.27), the transmittance formula can be simplified to be

$$T(z) = 1 - \frac{q_0(z,0)}{2\sqrt{2}}, \tag{5.3.29}$$

where $q_0(z,0)$ is denoted by Eq. (5.3.28).

From Eqs. (5.3.29) and (5.3.28), setting $z = 0$, we obtain the nonlinear absorption coefficient approximation expression:

$$\beta = \frac{2^{\frac{3}{2}}[1 - T(0)]}{I(0) L_{eff}}, \tag{5.3.30}$$

where $T(0)$ is open-hole transmittance for $S = 1$ at $z = 0$.

5.3.3 Other Z-scan Technologies

After E.W. Van Stryland et al. invented Z-scan method for measuring parameters of nonlinear optical materials scientists also developed some new Z-scan technologies. Here we will take three examples to introduce.

1. **Reflecting Z-scan Technique** [24]

This is a method for measurement of nonlinear characteristics on the surface of high absorption medium. The experimental setup is shown in Fig. 5.18. In this

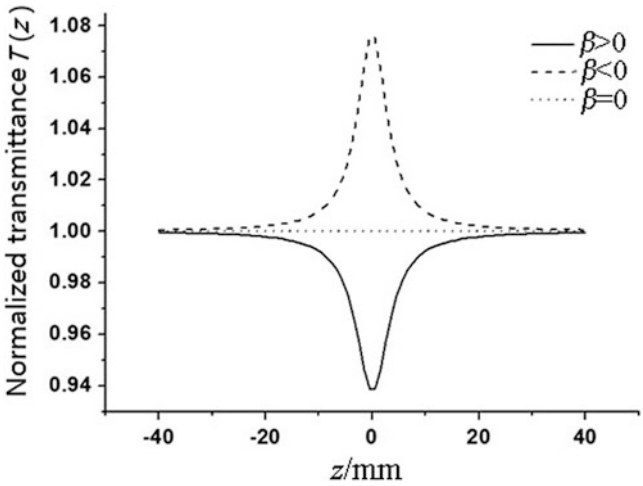

Fig. 5.17 Using Z-scan theory calculated $T(z)$–z *curves* when taking β as positive, negative and zero

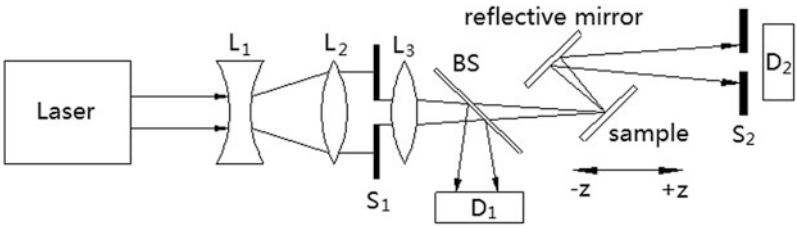

Fig. 5.18 The experimental setup of reflecting-type Z-scan technique

Z-scan device, if one can adjust the angle between the propagation direction of light beam and the normal direction of sample surface to be Brewster angle, it is useful to enhance the measurement accuracy.

2. **Bicolor Z-scan Technique** [25]

In the general Z-scan device, it only uses a laser beam with single wavelength. However in the bicolor Z-scan device it uses two laser beams with different wavelengths to form a hybrid light beam inputting the medium. In which one beam is a strong pump light at frequency ω_P, the other beam is a weak probe beam at frequency ω. In general using a fundamental frequency light and a double frequency light to form a hybrid light beam. It is just using pump-probe method to measure the nonlinear refraction coefficient n_2 and two-photon absorption coefficient β.

If adding a time delay device in one beam path of bicolor lights, then we can use for time resolution dynamic measurement of nonlinear optics characteristics of material [26].

3. **White Light Z-scan Technique** [27]

The experimental setup of white light Z-scan technique is shown in Fig. 5.19.

On the top left corner has a Ti sapphire laser, it produces a pulse laser at wavelength of 775 nm, with pulsewidth of 150 fs, it is divided into two beams by a beam splitter: one beam is used for pump a tunable optical parameter amplifier as a pump light; the other beam is inputted into an sample cell containing the distilled water to produce the continues white light, further use a lowpass filter to remove the pump light and the infrared spectrum part of the continues white light. white light is a broad-band probe light, it with the pump light outputted from the parameter amplifier together input the measured sample as the bicolor Z-scan light source to use directly measuring the light spectra of nonlinear absorption including the saturable absorption, revers saturable absorption, or two-photo absorption.

Review Questions of Chapter 5

1. What is optical Kerr effect? What difference between self-phase modulation (SPM) optical Kerr effect and cross-phase modulation (XPM) optical Kerr effect? Write down their nonlinear polarization expressions.
2. In self-phase modulation optical Kerr effect, there are two nonlinear refraction coefficients $\bar{n}_2$ and n_2, please explain what is their different meaning and expressions?
3. What is the relationship between two nonlinear refraction coefficients n_2 and $n_2^{(\text{cross})}$ for SPM and XPM two optical Kerr effects? What is difference of phase modulation to the signal light by these two Kerr effects?
4. What is optical-Kerr-effect induced birefringence? To describe the principle of the signal light and pump light orthogonal polarization-type optical Kerr box all-optical switch.

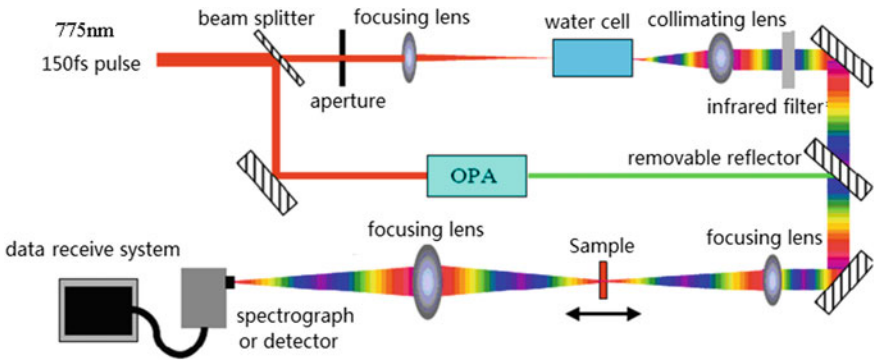

Fig. 5.19 The experimental setup of white light Z-scan technique

5. What are self-focusing and self-defocusing of light beam? What is difference between they and the optical diffraction? Under what condition the optical self-tripping can occur? Discuss the law of light beam radius variation with propagation distance under different incidence case in the self-focusing.
6. Under quasi steady state condition of self-focusing, the focal point how to move with time in the medium? Under transient state condition of self-focusing, how to explain the light pulse propagation forming the horn-shape wavefront in the medium?
7. To explain the phenomenon of self-focusing induced time self-phase modulation (frequency spectrum broaden) and space self-phase modulation (space ring).
8. How to use Z-scan technique to measure the nonlinear refractive index and the nonlinear absorption coefficient of the medium? How to judge the characteristic of nonlinear medium is belong to self-focusing or self-defocusing; saturable absorption or reverse saturable absorption from the Z-scan transmittance curve?

References

1. P.D. Maker, R.W. Terhune, C.M. Savage, Intensity-dependent changes in the refractive index of liquids. Phys. Rev. Lett. **12**(18), 507–509 (1964)
2. Y.R. Shen, Electrostriction, optical Kerr effect and self-focusing of laser beams. Phys. Lett. **20** (4), 378–380 (1966)
3. A. Owyoung, R.W. Hellwarth, N. George, Origin of the nonlinear refractive index of liquid ccl_4. Phys. Rev. A **4**(6), 2342–2347 (1971)
4. G.K.L. Wong, Y.R. Shen, Study of pretransitional behavior of laser-field-induced molecular alignment in isotropic nematic substances. Phys. Rev. A **10**(4), 1277–1284 (1974)
5. D. Heiman, R.W. Hellwarth et al., Raman-induced Kerr effect. Phys. Rev. Lett. **36**(4), 189–192 (1976)
6. E.G. Hanson, Y.R. Shen, G.K.L. Wong, Optical-field-induced refractive indices and orientational relaxation times in a homologous series of isotropic nematic substances. Phys. Rev. A **14**(3), 1281–1289 (1976)
7. R.W. Boyd, *Nonlinear Optics*, 3rd edn. (Elsevier Inc, USA, 2008)
8. P.L. Kelley, Self-focusing of optical beams. Phys. Rev. Lett. **15**(26), 1005–1008 (1965)
9. M.M.T. Loy, Y.R. Shen, Study of self-focusing and small-scale filaments of light in nonlinear media. IEEE J. Quant. Electr. **9**(3), 409–422 (1973)
10. Y.R. Shen, Self-focusing: experimental. Prog. Quantum Electron. **4**(1), 1–34 (1975)
11. N. Bloembergen, P. Lallemand, Complex intensity-dependent index of refraction, frequency broadening of stimulated Raman lines, and stimulated Rayleigh scattering. Phys. Rev. Lett. **16** (3), 81–84 (1966)
12. Y.R. Shen, M.M.T. Loy, Theoretical interpretation of small-scale filaments of light originating from moving focal spots. Phys. Rev. A **3**(6), 2099–2105 (1971)
13. Y.R. Shen, *The Principles of Nonlinear Optics* (Wiley, New York, 1984)
14. S.D. Durbin, S.M. Arakelian, Y.R. Shen, Laser-induced diffraction rings from a nematic-liquid-crystal film. Opt. Lett. **6**(9), 411–413 (1981)
15. C. Li, P. Zhou, in *Optical Bistability III*, eds. by H.M. Gibbs, P. Mandel, N. Peyghambarian, S.D. Smith (Springer-Verlag, 1986), p. 260
16. A.P. Veduta, B.P. Kirsanoy, Variation of the refractive index of liquids and glasses in a high intensity field of a ruby laser. J. Exp. Theor. Phys. **27**(5), 736–738 (1968)

17. B. Buchalter, G.R. Meredith, Third-order optical susceptibility of glasses determined by third harmonic generation. Appl. Opt. **21**(17), 3221–3224 (1982)
18. R. Adair, L.L. Chase, S.A. Payne, Nonlinear refractive-index measurements of glasses using three-wave frequency mixing. J. Opt. Soc. Am. B **4**(6), 875–881 (1987)
19. C.K. Wu et al., Measurement of third-order susceptibility by using degenerated four-wave mixing. Chin. J. Phys. **29**(4), 508–510 (1980)
20. C.V. Shank, E.P. Ippen, Anisotropic absorption saturation with picosecond pulses. Appl. Phys. Lett. **26**(2), 62–63 (1975)
21. D. Rativa, R.E. de Araujo, A.S.L. Gomes, B. Vohnsen, Hartmann-Shack wavefront sensing for nonlinear materials characterization. Opt. Express **17**(24), 22047–22053 (2009)
22. M. Sheik-bahae, A.A. Said, E.W. Van Stryland, High-sensitivity, single-beam n_2 measurements. Opt. Lett. **14**(17), 955–957 (1989)
23. M. Sheik-bahae, A.A. Said, T. Wei et al., Sensitive measurement of optical nonlinearities using a single beam. IEEE J. Quant. Electr. **26**(4), 760–769 (1990)
24. D.V. Petrov, A.S.L. Gomes et al., Reflection Z-scan technique for measurements of optical properties of surfaces. Appl. Phys. Lett. **65**(9), 1067–1069 (1994)
25. M. Sheik-bahae, J. Wang, R. DeSalvo et al., Measurement of nondegenerate nonlinearities using a two-color Z scan. Opt. Lett. **17**(4), 258–260 (1992)
26. J. Wang, M. Sheik-bahae, A.A. Said et al., Time-resolved Z-scan measurements of optical nonlinearities. J. Opt. Soc. Am. B **11**(6), 1009–1017 (1994)
27. M.J. Balu, D.J. Hales, E.W. Hagan, Van Stryland, White-light continuum Z-scan technique for nonlinear materials characterization. Opt. Express **12**(16), 3820–3826 (2004)

Chapter 6
Nonlinear Stimulated Scattering

In this chapter, the first section reviews the various kinds of light scattering phenomena in the nature and points out the difference between stimulated scattering (nonlinear scattering) and spontaneous scattering (linear scattering). The stimulated scattering is belonging to the third-order nonlinear optics effects. The second and third sections will study two stimulated scattering phenomena respectively: the stimulated Raman scattering and the stimulated Brillouin scattering. We will introduce their classical theoretical models, and finally give their related experimental methods.

6.1 Introduction to Light Scattering

6.1.1 Classification of Light Scattering

Light scattering is a phenomenon that when the light passes through the medium, the part of the light energy deviate the original propagation direction to occur the light energy redistribution. The light energy can be described us the product of photon energy $\hbar\omega$ and photon number N, i.e., $\varepsilon = \hbar\omega N$. That means the light scattering not only change the space distribution of the photon number, but also can produce the new lights at the frequency different with the frequency of original light. Therefore, we can also say that the light scattering is a phenomenon of the light redistribution on the frequency spectrum.

Light scattering is arising from the inhomogeneous distribution of medium properties (mainly the refractive index of medium), namely there exists the so called "scattering centers". According to the different reasons inducing the heterogeneity of medium, the light scattering can be divided into different categories.

If the medium is consisted of the pure matter with the same component (such as same molecules and atoms), according to the different reason to form the scattering

© Shanghai Jiao Tong University Press,
Shanghai and Springer Nature Singapore Pte Ltd., 2017

C. Li, *Nonlinear Optics*, DOI 10.1007/978-981-10-1488-8_6

center, the scattering can be divided into several kinds. In addition, there also exist other kinds of light scatterings produced by doping external particles or due to structure defects. Below we adopt the classical concept that the electric dipoles induce the secondary radiation under the action of the external light electric field to introduce several light scatterings with different mechanism in the nature.

1. **Rayleigh Scattering**

The medium is composed with the identical molecules and atoms, but the density of molecules or atoms has the random fluctuation in the space scale far less than the light wavelength. Under the action of the external light electric field, the fluctuation can be regarded as the forced oscillation of the electric dipoles, which produce the secondary radiation with a non-uniform space distribution, it is called Rayleigh scattering. The property of this light scattering is that: the frequency of scattering light is the same as that of input light; the relation between the scattering-light intensity and the input-light wavelength is $I_{scatt} \propto 1/\lambda^4$. From this formula we can see, the wavelength shorter, the scattering-light intensity stronger. The blue color of the sunny sky is just due to this reason.

2. **Rayleigh-wing Scattering**

Some organic liquids are composed with the anisotropic molecules (for example carbon disulfide, nitrobenzene, benzene etc.), because the orientation fluctuation of anisotropic molecules and the intermolecular thermal collision, in the scattering spectrum, accept Rayleigh scattering at the wavelength coincident with the wavelength of input light, it also exists the continuous spectrum broadening on the two sides of the center wavelength, i.e. it occurs the continuous frequency shift phenomenon, this light scattering is called the Rayleigh-wing scattering.

3. **Raman Scattering**

This kind scattering mainly happens in the molecular component medium. When an external light field at certain frequency inputs the medium, it will induce the forced oscillation of molecular electrical dipole. Because the molecular vibration (or rotation) frequency modulates the forced oscillation frequency of molecular electrical dipole, the frequency of electrical dipole generated second radiation light (scattering light) has a certain movement relative to the frequency of input light. The scattering light with the rad shift of frequency is called Stokes scattering light; and the scattering light with the blue shift of frequency is called Anti-stokes scattering light.

4. **Brillouin Scattering**

In the pure mediums, there are always the thermal motion, to lead the fluctuate variation of the medium density (or refractive index). Under the action of light electric field, via the electrostriction effect, to lead the periodic variation of medium density (or refractive index); it is equivalent to exist an acoustic wave field that can scatter the incident light. The frequency shift quantity of scattering light is equal to the phonon frequency; its magnitude is related with scattering angle, the frequency

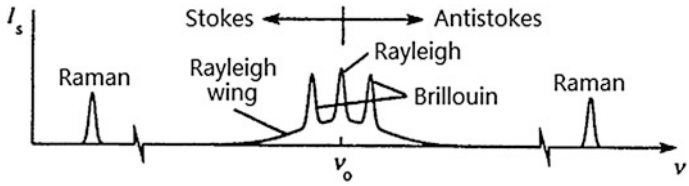

Fig. 6.1 Several spectrums of light scattering in the pure medium

of incident photon and the velocity of acoustic wave field. The Brillouin scattering also has the Stokes and Anti-stokes two kinds of scattering lights.

Figure 6.1 gives several spectrums of light scattering in the pure medium.

5. **Tyndall Scattering and Mie Scattering**

Above introduced are several light scatterings in pure medium consisted of molecules or atoms.

In addition, there are the extraneous impurities, particles, etc. in the medium and the structure defects of the medium all can cause the light scattering. For example, the impurities, stones, bubbles, stripes, dislocations etc. in solid glass and crystal can form the scattering centers. The everyday scattering behavior of suspended impurities, dusts and aerosols in air and liquid are also belong to this kind phenomenon. In these phenomena, the frequency of the scattering light is same as the frequency of the incident light. The relationship between the scattered light intensity and the light wavelength is $I_s \propto \lambda^{\eta}$, in which η is relative to $\lambda/a_0, a_0$ is the radius of the scattering particle. There are three kinds of cases:

When $a_0 >> \lambda, \eta \to 0$, the scattering light intensity is independent of the incident light wavelength, this kind scattering is called Tyndall scattering. The white cloud in the sky is just the result of this scattering.

When $a_0 \approx \lambda$, i.e., the size of a_0 is in the order of magnitude of λ, the η takes the oscillating value with change of λ/a_0. This scattering is called as Mie scattering.

When $a_0 << \lambda$, then $\eta \to -4, I_s \propto \lambda^{-4}$, this is the case of Rayleigh scattering.

6.1.2 Stimulated Radiation Light Scattering Characteristics

Spontaneous radiation light scattering is caused by interaction of the spontaneous radiation light (nature light) with the medium. Because the intensity of nature light is too weak, when it acts with the medium, do not change the optical properties of the medium, so the scattering light is still the spontaneous radiation light. However, the stimulated radiation light scattering is caused by interaction of the stimulated radiation light (laser) with the medium, the intensity of laser is very high, it can changes the optical properties of the medium (such as refractive index), the scattering light is still a stimulated light. The stimulated radiation light scattering has several kinds, including the stimulated Raman scattering (SRS), the stimulated

Brillouin scattering (SBS), the stimulated Rayleigh-wing scattering, and the stimulated Kerr scattering, etc. The stimulated radiation light scattering is one of third-order nonlinear optics effects.

The stimulated radiation light scattering in comparison with the spontaneous radiation light scattering has the following new properties:

(1) **High Gain**
The stimulated scattering outputted light intensity is possible to reach the same order of magnitude of the incident light intensity, even more strong. Because it has a high amplification ability, the stimulated scattering light could use up the incident light energy.

(2) **High Directionality**
The divergence angle of forward and backward stimulated scattering light can reach the same of divergence angle of incident laser, for example to reach milliradian, even to reach the diffraction limitation.

(3) **High Monochromaticity**
The width of scattered spectrum is obvious narrow down. It can produce the monochromatic light with the spectrum width as same as the spectrum width of incident laser or narrower.

(4) **Pulsewidth Compression**
The pulsewidth of stimulated radiation scattering light pulse can reach the date much smaller than the pulsewidth of incident laser pulse.

(5) **Threshold Value**
When the intensity of incident laser is larger than a threshold intensity, the coherence, directivity and intensity will be obvious enhanced.

(6) **High Order Scattering**
When increasing the input intensity or the medium length, the more high-order Stokes and anti-Stokes scattering lights will occur.

(7) **Phase Conjugation**
The phase of the backward stimulated scattering light has a conjugation relation with the phase of the incident light, the backward scattering can be used to generate phase conjugation wave. It has a higher nonlinear reflectivity; it does not need to consider the phase match.

6.2 Stimulated Raman Scattering

6.2.1 Physical Picture of Stimulated Raman Scattering

1. Spectral Characteristic of Stimulated Raman Scattering

In 1928 Raman discovered the spontaneous Raman scattering. In the scattering spectrum, except the original frequency component ω_a, it also appears the new frequency component ω_s (Stokes lane) and ω_a (anti-Stokes lane), and $\omega_s < \omega_0 < \omega_a$;

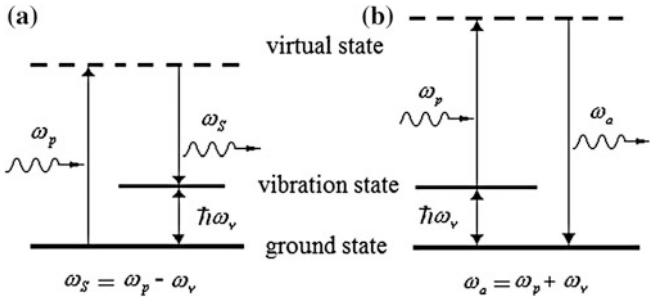

Fig. 6.2 Energy-level diagrams for explaining Raman scattering **a** Stokes scattering; **b** Anti-Stokes scattering

In general, the anti-Stokes lane is weaker than the Stokes lane in several orders of magnitude. We can use the energy-level diagram Fig. 6.2 to explain the formation process of Raman scattering.

The process of Raman scattering is: the molecule in the ground state absorbs the photon of pump light at frequency ω_p jumping to a virtual state, and then transits from that virtual state to the vibration (or rotation) state of the molecule, at same time launching a Stokes photon at frequency ω_s, as shown in Fig. 6.2a. On the other hand, the molecule located at the vibration (or rotation) state absorbs a photon of pump light at ω_p jumping to another virtual state, then transits from that virtual state to the ground state, at same time launching an anti-Stokes photon at frequency ω_a as shown in Fig. 6.2b. Because in the thermal equilibrium case, the molecular number in the ground state is much greater than the molecular number in the vibration state, so the number of the photon at frequency ω_s is much greater than the number of the photon at frequency ω_a, therefore the Stokes scattering light intensity is much stronger than the anti-Stokes scattering light intensity.

The stimulated Raman scattering spectrogram has different characteristic in comparison with the spontaneous Raman scattering spectrogram: the spontaneous Raman scattering spectrogram only has two first-order scattering spectral lines, but on the stimulated Raman scattering spectrogram, there are many high order scattering spectral lines, as shown in Fig. 6.3.

2. Classical Oscillator Picture of Stimulated Raman Scattering

Now we give a classical oscillator picture for explaining the formation of stimulated Raman scattering, as shown in Fig. 6.4.

Figure 6.4a shows that when a pump light at frequency ω_p inputs into the medium consisted of the molecules at the intrinsic vibration frequency ω_v, it induces the molecular polarization to form an electrical dipole, and generates the forced oscillation at frequency ω_p, which induces the secondary radiation, the frequency of radiation light is modulated by molecular vibration frequency, so that it occurs the frequency shift, to produce a Stokes scattering light at the frequency of $\omega_s = \omega_P - \omega_v$ and an anti-Stokes scattering light at the frequency of $\omega_a = \omega_P + \omega_v$.

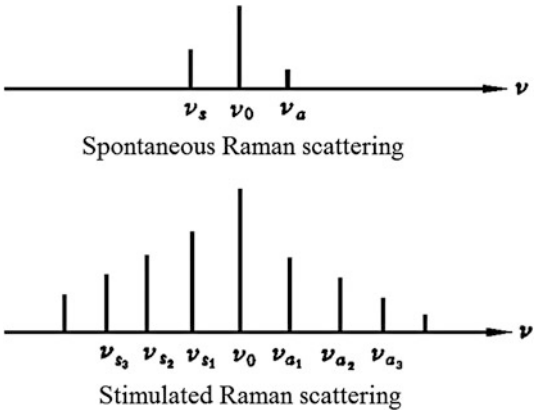

Fig. 6.3 Comparison of spectrograms of the spontaneous Raman scattering and the stimulated Raman scattering

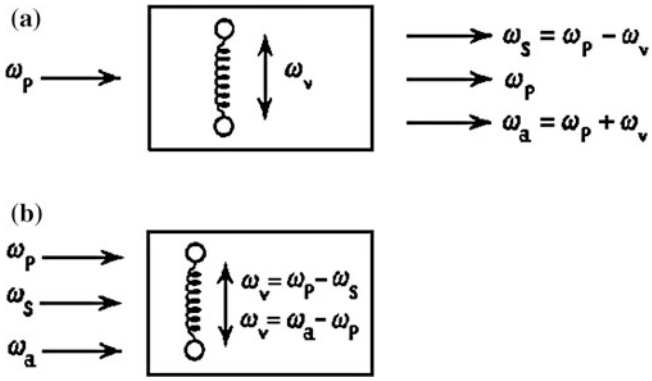

Fig. 6.4 Classical oscillator picture for explaining the formation of stimulated Raman scattering: **a** the frequency of electrical-dipole secondary radiation is modulated by the frequency of medium molecular vibration to generate the Stokes scattering light; **b** the difference frequency between the pump light and the Stokes light further intensifies the medium molecular vibration to increase the Stokes light

Figure 6.4b shows that the original pump light and Stokes light (anti-Stokes light) together input the medium to form the light at the difference frequency of $\omega_v = \omega_p - \omega_s$ (or $\omega_v = \omega_p - \omega_a$), the difference frequency light intensifies the molecular vibration of medium, thereby further generate the Stokes light at frequency ω_s (or the anti-Stokes light at frequency ω_a), this positive feedback action similar to avalanche makes the Stokes light (or the anti-Stokes light) further increases.

3. **Photon Picture of Stimulated Raman Scattering**

Using the frequency and the wave vector to represent the incident photon $(\omega_p, \boldsymbol{k}_p)$, the Stoke scattering photon $(\omega_s, \boldsymbol{k}_s)$, the anti-Stokes photon $(\omega_a, \boldsymbol{k}_a)$ and the Raman vibration of medium $(\omega_v, \boldsymbol{k}_v)$, the Stokes light and the anti-Stokes light of first-order stimulated Raman scattering must obey the following energy and momentum conservation relationships:

$$\begin{aligned} \omega_s &= \omega_p - \omega_v \\ \omega_a &= \omega_p + \omega_v, \end{aligned} \tag{6.2.1}$$

$$\begin{aligned} \boldsymbol{k}_s &= \boldsymbol{k}_p - \boldsymbol{k}_v \\ \boldsymbol{k}_a &= \boldsymbol{k}_p + \boldsymbol{k}_v. \end{aligned} \tag{6.2.2}$$

The stimulated Stokes scattering light and the stimulated anti-Stokes scattering light are concurrence, but two scattering lights in general are non-collinear. In the phase matching condition, their propagation directions satisfy the vector relationship, as shown in Fig. 6.5.

That is to say, the first-order anti-Stokes scattering light is generated by interaction between the pump light and the first-order Stokes scattering light in the third-order nonlinear process. Three of them satisfy the following wave-vector matching condition:

$$\Delta \boldsymbol{k} = 2\boldsymbol{k}_p - \boldsymbol{k}_s - \boldsymbol{k}_a = 0. \tag{6.2.3}$$

According to wave-vector relation showed in Fig. 6.5 we have

$$k_s \cos\theta_s + k_a \cos\theta_a = 2k_p. \tag{6.2.4}$$

The refractive indexes of the Stokes scattering light and the anti-Stokes scattering light can be denoted as the sum of the linear refractive index and the nonlinear refractive index, respectively:

$$n_\mathrm{s} = n_\mathrm{p} + \Delta n_\mathrm{s}, \tag{6.2.5}$$

$$n_\mathrm{a} = n_\mathrm{p} + \Delta n_\mathrm{a}. \tag{6.2.6}$$

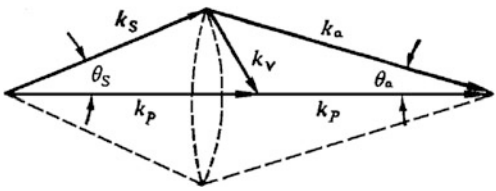

Fig. 6.5 Vector diagram of the propagation directions of stimulated Raman scattering lights

Because $\cos\theta \approx 1 - \frac{\theta^2}{2}, k = \frac{\omega}{c}n$, from Eqs. (6.2.4) to (6.2.6), we obtain

$$\left(1 + \frac{\Delta n_s}{n_p}\right)\left(1 - \frac{\theta_s^2}{2}\right)\omega_s + \left(1 + \frac{\Delta n_a}{n_p}\right)\left(1 - \frac{\theta_a^2}{2}\right)\omega_a = 2\omega_p. \tag{6.2.7}$$

On the other hand, the three light frequencies have to satisfy the energy conservation condition:

$$\omega_s + \omega_a = 2\omega_p. \tag{6.2.8}$$

Let Eqs. (6.2.7) minus (6.2.8), assuming $\theta_s^2 \approx \theta_a^2 = \theta^2$, and $2(\Delta n_s\omega_s + \Delta n_a\omega_a)\theta^2$ can be neglected because it is much smaller than $n_p(\omega_s + \omega_a)\theta^2$, so we obtain the divergence angle of the first-order anti-Stokes scattering light:

$$\theta^2 \cong \frac{2(\Delta n_s\omega_s + \Delta n_a\omega_a)}{n_p(\omega_s + \omega_a)}. \tag{6.2.9}$$

Visible,both the first-order Raman scattering Stokes light and the anti-Stokes light are outputted along a same cone angle θ, which is the intersection angle between the scattering light and the incident pump light. In the same way, we can understand the different high-order Raman scattering lights will output along the different cone angles.

An experiment showed that when a Ruby laser beam focuses into a Nitrobenzene sample, on the output screen in the far field of scattering light can see a ring-shape transverse structure, as shown in Fig. 6.6. The each-order Raman scattering lights (including Stokes and anti-Stokes lights) respectively start from the focal point and output in different cone angle to form the rings with different radius on the screen. The first-order Raman scattering light has maximum intensity located at the center of rings. The high-order Raman scattering light is corresponding to the larger and weaker rings.

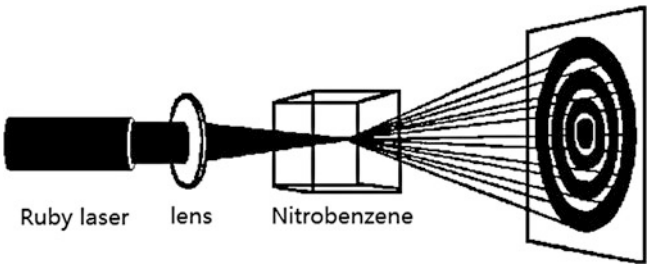

Fig. 6.6 Experiment for observing the angle distribution of stimulated Raman scattering lights

The stimulated Raman scattering has many important applications, for example, it can be used for frequency shift of laser outputted light for broadening the output frequency region; it can be used for the Raman amplifier and the wavelength division multiplexing device in fiber communication. Using backward stimulated scattering can obtain the phase conjugation light to realize the high efficient image aberration self-compensating; in addition, one can use silicon ring waveguide to make a Raman scattering laser to output the Stokes laser beam etc.

6.2.2 Classical Theory of Stimulated Raman Scattering

1. **Gain Factor of Stokes Scattering Light Field**

Now we introduce the classical theory of stimulated Raman scattering [1–5]. At first we use nonlinear coupled equations to analyze the stimulated Raman scattering process. In the isotropic medium, a pump light field $\boldsymbol{E}_P(\omega_P)$ at frequency ω_p inputs the medium, which interacts with the medium to produce the Stokes scattering light field $\boldsymbol{E}_s(\omega_s)$ at frequency ω_s, these two lights propagate all along z-direction. Under the phase matching condition, the nonlinear coupled equation for $\boldsymbol{E}_s(z, \omega_s)$ is

$$\frac{d\boldsymbol{E}_s(z)}{dz} = \frac{i\omega_s}{2\varepsilon_0 c n_s}\boldsymbol{P}^{(3)}(\mathrm{z}). \tag{6.2.10}$$

The photon's energy and momentum conservation relationships for Stokes Raman scattering are

$$\omega_s = \omega_p - \omega_p + \omega_s,$$
$$\boldsymbol{k}_s = \boldsymbol{k}_p - \boldsymbol{k}_p + \boldsymbol{k}_s.$$

The nonlinear polarization is given by

$$\boldsymbol{P}^{(3)}(z) = 6\varepsilon_0\chi_R^{(3)}(\omega_s; \omega_p, -\omega_p, \omega_s)\left|\boldsymbol{E}_p\right|^2\boldsymbol{E}_s(z). \tag{6.2.11}$$

where $\chi_R^{(3)}(\omega_s; \omega_p, -\omega_p, \omega_s)$ is the susceptibility for Stokes Raman scattering light, it is simply expressed as $\chi_R^{(3)}(\omega_s)$, which can be divided into the real and imaginary two parts:

$$\chi_R^{(3)}(\omega_s) = \chi_R^{(3)}(\omega_s)' + i\chi_R^{(3)\prime\prime}(\omega_s). \tag{6.2.12}$$

The real part reflects the refractive-index change (phase change), the imaginary part reflects the absorption coefficient change (energy change). Because we only study the energy exchange relation in the scattering process, in following discuss we only maintain the imaginary part items.

Substituting Eq. (6.2.11) into Eq. (6.2.10), and taking the imaginary part of susceptibility $i\chi_R^{(3)\prime\prime}(\omega_s)$, we obtain

$$\frac{d\boldsymbol{E}_s(z)}{dz} = -\frac{3\omega_s}{cn_s}\chi_R^{(3)\prime\prime}(\omega_s)\left|\boldsymbol{E}_p\right|^2\boldsymbol{E}_s(z). \tag{6.2.13}$$

Using $I_p = \frac{1}{2}\varepsilon_0 c n_P\left|\boldsymbol{E}_p\right|^2$ to replace $\left|\boldsymbol{E}_p\right|^2$ by the light intensity I_p, we solve Eq. (6.2.13) to obtain

$$\boldsymbol{E}_s(z) = \boldsymbol{E}_{s0}\exp\left[-\frac{6\omega_s}{\varepsilon_0 c^2 n_p n_s}\chi_R''(\omega_s)I_p z\right] = \boldsymbol{E}_{s0}e^{\frac{1}{2}gI_p z}, \tag{6.2.14}$$

where g factor is

$$g = -\frac{12\omega_s}{\varepsilon_0 c^2 n_p n_s}\chi_R''(\omega_s). \tag{6.2.15}$$

We can see that if $\chi_R'' < 0$ g is a gain factor. Below we will see that χ_R'' indeed is smaller than zero, so the Stokes scattering light field is exponential increase along z-direction.

2. Formula Derivation of Susceptibility for Stimulated Raman Scattering

Now we start derivate the expression of $\chi_R^{(3)}$ in detail. We suppose that the medium is consisted of molecules (or atoms), each molecule (atom) is similar to an electrical dipole, and there are N non-interactional electrical dipoles in per unit volume of the medium. When an additional light field $\boldsymbol{E}(z,t)$ inputs the medium, and interacts with electrical dipoles to lead them forced oscillation. The length of electrical dipole is denoted by $q(t)$, when forced oscillation of electrical dipole, the length of electrical dipole is changed with time respect to its equilibrium-state length q_0. So $q(t)$ is a function of time, as shown in Fig. 6.7.

The classical motion equation for describing the forced oscillation of molecular electrical dipole is

$$\frac{\partial^2 \mathrm{q}(t)}{\partial t^2} + 2\gamma\frac{\partial \mathrm{q}(t)}{\partial t} + \omega_v^2\mathrm{q}(t) = \frac{\mathrm{F}(z,t)}{m}, \tag{6.2.16}$$

where ω_v is the resonance frequency of electrical dipole, γ is the relaxation rate (attenuation constant) of electrical dipole, $\boldsymbol{F}(z,t)$ is the acting force of external electrical field, m is the mass of electrical dipole molecule.

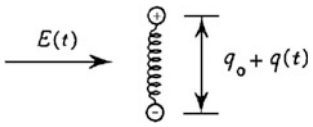

Fig. 6.7 Molecular electrical dipole model for describing the stimulated Raman scattering

Under the action of light field, the polarization of electrical dipole is

$$p(z,t) = \varepsilon \boldsymbol{E}(z,t). \tag{6.2.17}$$

The relationship of the dielectric coefficient ε and the electrical-dipole susceptibility α is

$$\varepsilon = \varepsilon_0(1+\alpha), \tag{6.2.18}$$

The electrical-dipole susceptibility α is a function of the time:

$$\alpha(t) = \alpha_0 + \left(\frac{\partial \alpha}{\partial q}\right)_0 q(t), \tag{6.2.19}$$

where the first item α_0 is the linear susceptibility of electrical dipole in the equilibrium state, the second item is the nonlinear susceptibility of electrical dipole. Considering Eqs. (6.2.17) and (6.2.18), the static electricity energy of electrical dipole is

$$W = \frac{1}{2}[\mathrm{p}(z,t)\cdot \boldsymbol{E}(z,t)] = \frac{1}{2}\varepsilon_0(1+\alpha)\left\langle \boldsymbol{E}^2(z,t)\right\rangle, \tag{6.2.20}$$

where $\langle\rangle$ denotes the time average value of total light field intensity in an optical period (it is possible containing several frequency components).

The electrical field force induced in external field is the derivative of electrostatic energy to the length change of electrical dipole. Utilizing Eqs. (6.2.20) and (6.3.19), we obtain

$$F(z,t) = \frac{dW}{dq} = \frac{\varepsilon_0}{2}\left(\frac{\partial \alpha}{\partial q}\right)_0 \left\langle \boldsymbol{E}^2(z,t)\right\rangle. \tag{6.2.21}$$

In order to find the average value of field intensity, assuming the total light field in medium is the sum of pump light field and Stokes light field:

$$\boldsymbol{E}(z,t) = \boldsymbol{E}_p e^{i(k_p z - \omega_p t)} + \boldsymbol{E}_s e^{i(k_s z - \omega_s t)} + c.c. \tag{6.2.22}$$

Because the total light field has two light fields at different frequencies, so in $\left\langle E^2(z,t)\right\rangle$ there are several items with different frequencies, we omit high frequency items containing $2\omega_p, 2\omega_s$ and $\omega_p + \omega_s$ etc., only maintain the low frequency items containing $\omega_p - \omega_s$, than we have

$$\left\langle E^2(z,t)\right\rangle \approx 2\boldsymbol{E}_p \boldsymbol{E}_s^* e^{i(Kz - \Omega t)} + c.c., \tag{6.2.23}$$

where $\boldsymbol{K}$ and Ω are defined as respectively:

$$K = \boldsymbol{k}_p - \boldsymbol{k}_s, \Omega = \omega_p - \omega_s. \tag{6.2.24}$$

From Eq. (6.2.21), the dipole received force is

$$F(z,t) = \varepsilon_0 \left(\frac{\partial \alpha}{\partial q}\right)_0 [\boldsymbol{E}_p \boldsymbol{E}_s^* e^{i(Kz-\Omega t)} + c.c.]. \tag{6.2.25}$$

In order to solve dipole motion Eq. (6.2.16), we can used a testing solution:

$$\boldsymbol{q}(t) = \boldsymbol{q}(\Omega) e^{i(Kz-\Omega t)} + c.c. \tag{6.2.26}$$

Substituting Eqs. (6.2.26) and (6.2.25) into Eq. (6.2.16), we obtain

$$-\Omega^2 \mathrm{q}(\Omega) - 2i\Omega\gamma \mathrm{q}(\Omega) + \omega_v^2 \mathrm{q}(\Omega) = \frac{\varepsilon_0}{m} \left(\frac{\partial \alpha}{\partial q}\right)_0 \mathrm{E}_p \mathrm{E}_s^*. \tag{6.2.27}$$

Thus we obtain the electrical dipole vibration amplitude:

$$q(\Omega) = \frac{(\varepsilon_0/m)(\partial\alpha/\partial q)_0 \mathrm{E}_p \mathrm{E}_s^*}{\omega_v^2 - \Omega^2 - 2i\Omega\gamma}. \tag{6.2.28}$$

Now we are going to find the third-order polarization and susceptibility. According to Eqs. (6.2.18) and (6.2.19), the total polarization of medium is

$$\begin{aligned} \boldsymbol{P}(z,t) &= N\boldsymbol{p}(z,t) = \varepsilon_0 N(1+\alpha)\boldsymbol{E}(z,t) \\ &= \varepsilon_0 N[1 + \alpha_0 + \left(\frac{\partial \alpha}{\partial q}\right)_0 \boldsymbol{q}(z,t)]\boldsymbol{E}(z,t). \end{aligned} \tag{6.2.29}$$

Equation (6.2.29) includes the first-order polarization (linear polarization) and the third-order polarization of medium. In which the first-order polarization is

$$\boldsymbol{P}^{(1)} = \varepsilon_0 N(1+\alpha_0)\boldsymbol{E}(z,t). \tag{6.2.30}$$

According to Eqs. (6.2.29), (6.2.26) and (6.2.22), the third-order polarization is

$$\boldsymbol{P}^{(3)}(z,t) = \varepsilon_0 N \left(\frac{\partial \alpha}{\partial q}\right)_0 [\boldsymbol{q}(\Omega) e^{i(Kz-\Omega t)} + c.c.] \times [\boldsymbol{E}_p e^{i(k_P z - \omega_P t)} + \boldsymbol{E}_s e^{i(k_s z - \omega_s t)} + c.c.]. \tag{6.2.31}$$

So the nonlinear polarization contains several different frequency difference components, in which the Stokes light at frequency ω_s induced nonlinear polarization of medium can be expressed as

$$\boldsymbol{P}_s^{(3)}(z,t) = \boldsymbol{P}^{(3)}(\omega_s)e^{i(k_s z-\omega_s t)}. \tag{6.2.32}$$

If only taking the items containing phase $e^{i(k_s z-\omega_s t)}$ in the various products of Eq. (6.2.31), (utilize $\boldsymbol{k}_s = \boldsymbol{k}_p - \mathrm{K}$ and $\omega_s = \omega_p - \Omega$), the third-order nonlinear polarization amplitude for Stokes light is given by

$$\boldsymbol{P}^{(3)}(\omega_s) = \varepsilon_0 N\left(\frac{\partial\alpha}{\partial q}\right)_0 \boldsymbol{q}^*(\Omega)\boldsymbol{E}_p. \tag{6.2.33}$$

Taking conjugated complex of electrical dipole amplitude Eq. (6.2.28), and then substituting it into Eq. (6.2.33), we obtain

$$\boldsymbol{P}^{(3)}(\omega_s) = \frac{\varepsilon_0^2(N/m)(\partial\alpha/\partial q)_0^2\left|\boldsymbol{E}_p\right|^2}{\omega_v^2 - \Omega^2 + 2i\Omega\gamma}\boldsymbol{E}_s(\omega). \tag{6.2.34}$$

Substituting Eq. (6.2.34) into Eq. (6.2.32), and utilizing $\boldsymbol{E}_s(z,t) = E_s(\omega)e^{i(k_s z-\omega_s t)}$, the time-domain Stokes polarization is given by

$$\boldsymbol{P}_s^{(3)}(z,t) = \frac{\varepsilon_0^2(N/m)(\partial\alpha/\partial q)_0^2\left|\boldsymbol{E}_p\right|^2}{\omega_v^2 - \Omega^2 + 2i\Omega\gamma}\boldsymbol{E}_s(\mathrm{z},t). \tag{6.2.35}$$

Now comparing Eq. (6.2.35) with third-order nonlinear polarization definition Eq. (6.2.11) we obtain the third-order nonlinear susceptibility formula:

$$\chi_R^{(3)}(\omega_s) = \frac{\varepsilon_0(N/6\,\mathrm{m})(\partial\alpha/\partial q)_0^2}{\omega_v^2 - (\omega_p - \omega_s)^2 + 2i(\omega_p - \omega_s)\gamma}. \tag{6.2.36}$$

Considering the near resonance condition $\Omega = \omega_P - \omega_S \approx \omega_v$, then Eq. (6.2.36) also can be expressed as

$$\chi_R^{(3)}(\omega_s) \cong \frac{\varepsilon_0(N/12\,\mathrm{m}\omega_v)(\partial\alpha/\partial q)_0^2}{(\omega_s - \omega_p + \omega_v) + i\gamma}. \tag{6.2.37}$$

According to the definition $\chi_R^{(3)}(\omega_s) = \chi_R'(\omega_s) + i\chi_R''(\omega_s)$, the above third-order nonlinear susceptibility can be divided into the real part and the imaginary part, respectively:

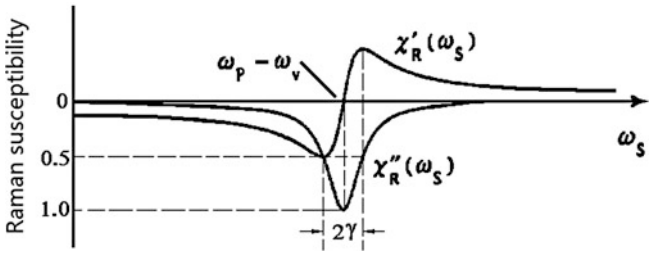

Fig. 6.8 Curves of real part and imaginary part of the nonlinear susceptibility induced by the stimulated Raman scattering light

$$\chi'_R(\omega_s) \cong \frac{\varepsilon_0 N(\partial\alpha/\partial q)_0^2(\omega_v - \omega_p + \omega_p)}{12\,\mathrm{m}\omega_v[(\omega_s - \omega_p + \omega_v)^2 + \gamma^2]}, \tag{6.2.38}$$

$$\chi''_R(\omega_s) \cong \frac{-\varepsilon_0 N(\partial\alpha/\partial q)_0^2\gamma}{12\,\mathrm{m}\omega_v[(\omega_s - \omega_p + \omega_v)^2 + \gamma^2]}. \tag{6.2.39}$$

Figure 6.8 draws the curves of real part and imaginary part of the nonlinear susceptibility induced by the stimulated Raman scattering light.

We can see that Raman scattering Stokes light induced nonlinear susceptibility imaginary part is a negative value, according to Eq. (6.2.15), the Stokes field at ω_s has a positive gain factor g, which is given by

$$g = \frac{\omega_s N(\partial\alpha/\partial q)_0^2\gamma}{c^2 n_p n_s m\omega_v[(\omega_s - \omega_p + \omega_v)^2 + \gamma^2]}. \tag{6.2.40}$$

Therefore stimulated Raman scattering Stokes light field is continues increased in propagation process along z-direction.

In same way we can analyze the propagation law of anti-Stokes light field, as long as replacing ω_s by ω_a in Eq. (6.2.36). So the anti-Stokes light induced nonlinear susceptibility is given by

$$\chi_R^{(3)}(\omega_a) = \frac{\varepsilon_0(N/6\,\mathrm{m})(\partial\alpha/\partial q)_0^2}{\omega_v^2 - (\omega_p - \omega_a)^2 + 2i(\omega_p - \omega_a)\gamma}. \tag{6.2.41}$$

Because the anti-Stokes Raman scattering has following energy and momentum conservation relationships:

$$\omega_a = \omega_p + \omega_p - \omega_s,$$
$$\boldsymbol{k}_a = \boldsymbol{k}_p + \boldsymbol{k}_p - \boldsymbol{k}_s.$$

Then we have

$$\omega_p - \omega_s = -(\omega_p - \omega_a), \tag{6.2.42}$$

namely

$$\chi_R^{(3)}(\omega_a) = \chi_R^{(3)}(\omega_s)^*. \tag{6.2.43}$$

Under near resonance condition, Eq. (6.2.41) becomes

$$\chi_R^{(3)}(\omega_a) \cong -\frac{\varepsilon_0(N/12\,\mathrm{m}\omega_v)(\partial\alpha/\partial q)_0^2}{(\omega_a - \omega_p - \omega_v) + i\gamma}. \tag{6.2.44}$$

The real part and the imaginary part are expressed respectively as

$$\chi_R'(\omega_a) \cong \frac{-\varepsilon_0 N(\partial\alpha/\partial q)_0^2(\omega_a - \omega_p - \omega_v)}{12\,\mathrm{m}\omega_v[(\omega_a - \omega_p - \omega_v)^2 + \gamma^2]}, \tag{6.2.45}$$

and

$$\chi_R''(\omega_a) \cong \frac{\varepsilon_0 N(\partial\alpha/\partial q)_0^2\gamma}{12\,\mathrm{m}\omega_v[(\omega_a - \omega_P - \omega_v)^2 + \gamma^2]}. \tag{6.2.46}$$

Similar to Eq. (6.2.15), the anti-Stokes field amplitude is

$$E_a(z) = E_{a0}\exp\left(\frac{1}{2}gI_p z\right). \tag{6.2.47}$$

where

$$g = -\frac{\omega_a N(\partial\alpha/\partial q)_0^2\gamma}{c^2 n_P n_a m\omega_v[(\omega_a - \omega_P - \omega_v)^2 + \gamma^2]}. \tag{6.2.48}$$

Because this g factor is negative value, the anti-Stokes field is attenuated with increase of z.

Figure 6.9 draws the relation between Stokes and Anti-stokes stimulated Raman scattering nonlinear susceptibility frequency spectrums.

6.2.3 Experiments of Stimulated Raman Scattering

People have been observed the stimulated Raman scattering (SRS) effect in many materials, including the liquid (for example benzene, CS_2, CCI_4, acetone, etc.),

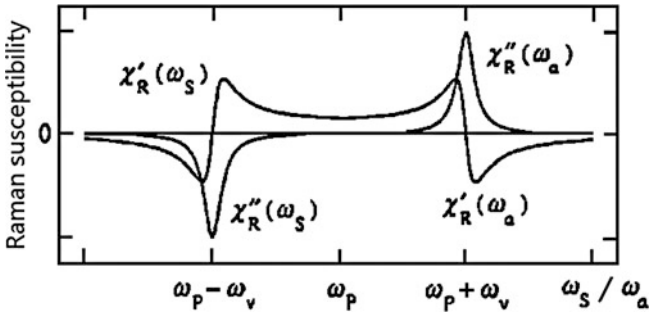

Fig. 6.9 Relation between Stokes and anti-Stokes stimulated Raman scattering nonlinear susceptibility frequency spectrums

solid (for example diamond, calcite, lithium niobate, nitrate barium, etc.), gas (H_2, D_2, N_2, CH_4, SF_6, etc.), semiconductor (such as InSb, etc. spin inversion Raman scattering). The basic requirements of working mediums for generating SRS: ① high transparency to SRS light and pump light; ② with larger scattering cross section; ③ it can sustain the stronger incident pump light intensity.

According to the different working medium, application requirement and experimental condition, one can adopt three kinds of different experimental setups to generate SRS, as shown in Fig. 6.10. The first setup is that, the incident laser via focus lens one-way passing through the Raman medium. When the focused pump light beam and the scattering light beam form a tenuous effective gain area in the medium, it can observe the forward and backward scattering lights. Second setup is that, the Raman medium is placed alone in a resonant cavity outside the pump laser cavity, the SRS light back and forth oscillation in the cavity. When the total gain of SRS achieves greater than the various losses, it can output a stable SRS light beam. The third setup is that, the Raman medium is placed within the pump laser cavity, the shared resonant cavity offers the feedback for laser and SBS light; and let them output to outside the cavity.

6.3 Stimulated Brillouin Scattering

6.3.1 Physical Picture of Stimulated Brillouin Scattering

The Brillouin scattering originates from the interaction between the light electric field and the acoustic wave field in molecular medium or solid medium, namely the interaction between photons and phonons. It is different with the spontaneous Brillouin scattering, the produce process of stimulated Brillouin scattering is: under the action of laser electric field, through the electrostriction effect to lead the periodic change of medium density (and the refractive index), to induce an acoustic wave field (similar to the motion grating). When the incident light passes through

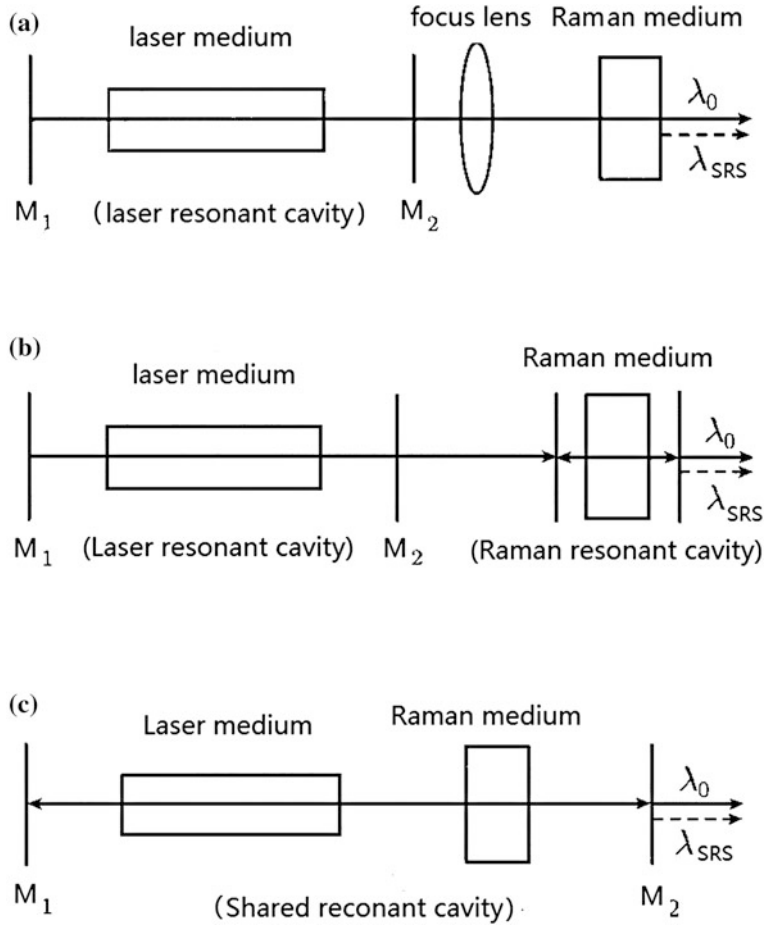

Fig. 6.10 Experimental setups for producing the stimulated Raman scattering: **a** One-way traveling wave amplification type; **b** Raman resonant cavity type; **c** Laser and Raman shared resonant cavity type

the acoustic wave field, it generates a maximum of diffraction with a frequency shift in a certain direction, i.e. the scattering light. The frequency shift quantity of scattering light is related with the motion velocity of acoustic wave field in the medium and the propagation direction of scattering light.

If denoting the photons and the phonon by frequency and wave vector: the incident pump photon $(\omega_p, \boldsymbol{k}_p)$, the Stokes scattering photon $(\omega_s, \boldsymbol{k}_s)$, the anti-Stokes photon $(\omega_a, \boldsymbol{k}_a)$ and the induced phonon $(\omega_b, \boldsymbol{k}_b)$, the Stokes scattering light and anti-Stokes scattering light of first-order stimulated Brillouin scattering must satisfy the energy and momentum conservation conditions respectively, i.e.,

For the Stokes scattering:

$$\begin{aligned} \omega_p &= \omega_s + \omega_b \\ \boldsymbol{k}_p &= \boldsymbol{k}_\mathrm{s} + \boldsymbol{k}_b, \end{aligned} \tag{6.3.1}$$

For the anti-Stokes scattering:

$$\begin{aligned} \omega_\mathrm{a} &= \omega_p + \omega_b \\ \boldsymbol{k}_a &= \boldsymbol{k}_p + \boldsymbol{k}_b. \end{aligned} \tag{6.3.2}$$

In the Stokes scattering case, from Eq. (6.3.1) we can see, there is a part of incident-light- field energy translating into induced acoustic-wave-field energy in the medium. Stokes scattering can be divided into two kinds of the forward scattering and the backward scattering. Their wave vector relations for momentum conservation are shown in Fig. 6.11.

The relationship between the wave vector k_b and the frequency ω_b of acoustic wave is $\omega_b = k_b v_b$, v_b is the velocity of acoustic wave. Because acoustic velocity v_b is smaller than light velocities v_p and v_s in several orders of magnitude, i.e., $v_b << v_p, v_s$, so we can regard $v_s \approx v_p$ and $k_s \approx k_p$, and then from Fig. 6.11 can see

$$\frac{1}{2} k_b \approx k_p \sin\frac{\theta}{2}, \tag{6.3.3}$$

where $k_b = \frac{\omega_b}{v_b}, k_P = \frac{\omega_p n_p}{c}$, then using Eq. (6.3.1), we have

$$\omega_p - \omega_s = \omega_b = \frac{2\omega_p n_p v_b}{c} \sin\frac{\theta}{2}, \tag{6.3.4}$$

where θ is the intersection angle between wave vector of scattering light $\boldsymbol{k}_s$ and the wave vector of incident light $\boldsymbol{k}_p$. When $\theta = 0, \omega_b = 0$, so $\omega_p = \omega_s$, i.e., without Brillouin frequency shift; when $\theta = \pi$, the Brillouin frequency shift takes a maximum $\omega_{b\max}$, i.e.,

$$\omega_p - \omega_s = \omega_{b\max} = \frac{2\omega_p n_p v_b}{c}. \tag{6.3.5}$$

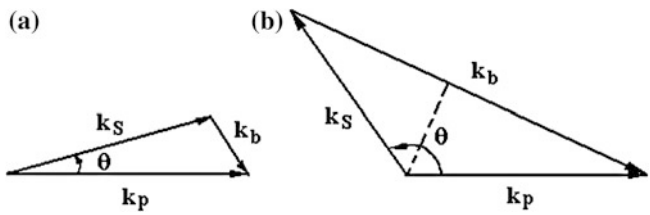

Fig. 6.11 Wave vector relations for momentum conservation of the stimulated Brillouin stokes scattering: **a** Forward scattering; **b** Backward scattering

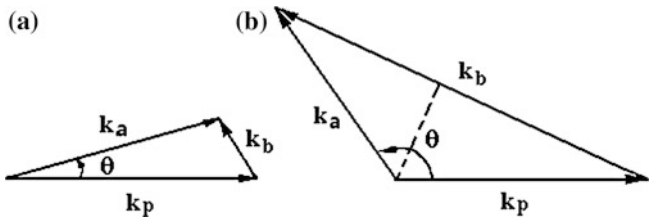

Fig. 6.12 Wave vector relations for momentum conservation of the stimulated Brillouin anti-stokes scattering: **a** forward scattering; **b** backward scattering

We can see that the backward Brillouin Stokes scattering has maximum frequency shift. In this case the direction of acoustic wave field is the same as the direction of incident light field, but the direction of scattering light field is the reverse direction of the incident light field, these three fields are collinear. When we measure out the backward Brillouin scattering frequency shift $\omega_p - \omega_s$, using Eq. (6.3.5) we can calculate the acoustic velocity of the medium.

In the anti-Stokes scattering case, the wave vector relation for momentum conservation is shown in Fig. 6.12.

The frequency shift value of anti-Stokes light respect to the incident light is also

$$\omega_a - \omega_p = \omega_b = \frac{2\omega_p n_p v_b}{c} \sin\frac{\theta}{2}. \tag{6.3.6}$$

Visible,when $\theta = \pi$, the frequency shift value of backward Brillouin anti-Stokes scattering is a maximum, but the direction of the acoustic wave field in medium is reverse to the direction of the incident light.

6.3.2 *Classical Theory of Stimulated Brillouin Scattering*

This section theoretically analyzes the backward stimulated Brillouin scattering process as shown in Fig. 6.13 [6–8]. The pump light propagates along z-direction in the medium, the propagation direction of Stokes scattering light is reversed with the

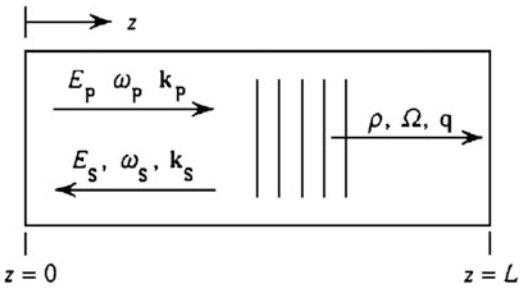

Fig. 6.13 Schematic diagram of the backward stimulated Brillouin stokes scattering process. The propagation directions of the pump light field (E_p, ω_p, k_p), the Brillouin scattering Stokes wave field (E_s, ω_s, k_s) and the acoustic wave field (ρ, Ω, q) are collinear

direction of pump light. The pump light field (E_p, ω_p, k_p) interacts with the acoustic wave field (ρ, Ω, q), generating stimulated Brillouin scattering Stokes wave field (E_s, ω_s, k_s), where ρ is the density of medium, the frequency and the wave vector of phonon are $\Omega = \omega_p - \omega_s$ and $q = 2k_P$ respectively.

The material density changed with time is given by

$$\boldsymbol{\rho}(z,t) = \boldsymbol{\rho}_0 + \Delta\boldsymbol{\rho} = \boldsymbol{\rho}_0 + [\tilde{\boldsymbol{\rho}}(z,t)e^{i(qz-\Omega t)} + c.c.]. \tag{6.3.7}$$

where $\boldsymbol{\rho}_0$ is the average material density; the second item in right side of equation is density change with time; $\tilde{\boldsymbol{\rho}}(z,t)$ is the amplitude of acoustic wave.

The total light field in Brillouin medium is expressed as

$$\boldsymbol{E}(z,t) = \boldsymbol{E}_p(z,t) + \boldsymbol{E}_s(z,t), \tag{6.3.8}$$

where

$$E_p(z,t) = \boldsymbol{A}_p(z,t)e^{i(k_p z-\omega_p t)} + c.c., \tag{6.3.9}$$

$$E_s(z,t) = \boldsymbol{A}_s(z,t)e^{i(-k_s z-\omega_s t)} + c.c.. \tag{6.3.10}$$

The material density change is satisfied the acoustic wave equation:

$$\frac{\partial^2\boldsymbol{\rho}}{\partial t^2} - \Gamma\nabla^2\frac{\partial\boldsymbol{\rho}}{\partial t} - v_b^2\nabla^2\boldsymbol{\rho} = -\nabla\cdot\boldsymbol{F}, \tag{6.3.11}$$

where v_b is the acoustic velocity; Γ is the damping parameter; $\boldsymbol{F}$ is electric field force (it is origin from the electrostriction stress).

The electrostriction coefficient is defined as

$$\gamma_e = \rho\frac{\partial\varepsilon}{\partial\rho}. \tag{6.3.12}$$

The light field energy density is

$$W = \frac{1}{2}(P\cdot E) = \frac{1}{2}\varepsilon\langle\boldsymbol{E}^2\rangle, \tag{6.3.13}$$

where $\langle E^2\rangle$ denotes the average value of light intensity in an optical period.

The light field energy density change is due to the density compress induced change of dielectric coefficient:

$$\Delta W = \frac{1}{2}\Delta\varepsilon\langle\boldsymbol{E}^2\rangle = \frac{1}{2}\left(\frac{\partial\varepsilon}{\partial\rho}\Delta\rho\right)\langle\boldsymbol{E}^2\rangle = \frac{1}{2}\gamma_e\frac{\Delta\rho}{\rho}\langle\boldsymbol{E}^2\rangle. \tag{6.3.14}$$

The light field energy density change is equal to that the electrostriction pressure p_e compresses the material to do the work in unit volume:

$$\Delta W = p_e \frac{\Delta V}{V} = -p_e \frac{\Delta \rho}{\rho}. \tag{6.3.15}$$

In Eq. (6.3.15) the minus sign is because that the compression of material volume leads increase of density of material.

To compare Eqs. (6.3.14) and (6.3.15) we can get the pressure:

$$p_e = -\frac{1}{2}\gamma_e \langle \boldsymbol{E}^2 \rangle. \tag{6.3.16}$$

Then the electric field force $\boldsymbol{F}$ is

$$\boldsymbol{F} = -\nabla p_e = \frac{1}{2}\gamma_e \nabla \langle \boldsymbol{E}^2 \rangle. \tag{6.3.17}$$

Substituting the field expression Eq. (6.3.8) into Eq. (6.3.17), taking the item at low frequency $\Omega = \omega_p - \omega_s$, we obtain the divergence of external force:

$$\nabla \cdot \boldsymbol{F} = -\gamma_e q^2 [\boldsymbol{A}_p \boldsymbol{A}_s^* e^{i(qz-\Omega t)} + c.c]. \tag{6.3.18}$$

To substitute Eqs. (6.3.7) and (6.3.18) into the acoustic Eq. (6.3.11), considering the acoustic wave amplitude in space and time slow-variation-amplitude approximation, neglecting the items containing the space and time second derivative to ρ, and eliminating the phase factor of field, we obtain

$$(\Omega_B^2 - \Omega^2 - i\Omega\Gamma_B)\tilde{\boldsymbol{\rho}} - 2i\Omega \frac{\partial \tilde{\boldsymbol{\rho}}}{\partial t} - 2iqv_b^2 \frac{\partial \tilde{\boldsymbol{\rho}}}{\partial z} = \gamma_e q^2 \boldsymbol{A}_p \boldsymbol{A}_s^*, \tag{6.3.19}$$

where

$$\Gamma_B = q^2 \Gamma \tag{6.3.20}$$

is the Brillouin line width, $\Gamma_B = 1/\tau_b$, τ_b is the lifetime of phonon. $\Omega = \omega_p - \omega_s$ is the frequency of phonon; $\Omega_B = |\boldsymbol{q}| v_b$ is Brillouin frequency, where $q = k_b \approx 2k_p$. Because of the strong damping, the propagation distance of phonon is very short. The item containing $\partial\rho/\partial z$ can be neglected. Considering the steady state case, the item containing $\partial\rho/\partial t$ is zero, thus the acoustic wave amplitude is given by

$$\tilde{\boldsymbol{\rho}}(z,t) = \gamma_e q^2 \frac{\boldsymbol{A}_p \boldsymbol{A}_s^*}{\Omega_B^2 - \Omega^2 - i\Omega\Gamma_B}. \tag{6.3.21}$$

For nonlinear light field wave equation, we can also adopt the slowly-varying-amplitude approximation and the steady state condition, and satisfy the phase matching condition, and then the wave equations for the incident light field amplitude and the Stokes scattering light field amplitude are given by respectively:

$$\frac{dE_p}{dz} = \frac{i\omega_p}{2\varepsilon_0 c n_p} P_p^{(3)}(z), \tag{6.3.22}$$

$$\frac{dE_s}{dz} = -\frac{i\omega_s}{2\varepsilon_0 c n_s} P_s^{(3)}(z). \tag{6.3.23}$$

Because the total polarization is

$$\boldsymbol{P} = \varepsilon \boldsymbol{E} = (\varepsilon_L + \Delta\varepsilon)\boldsymbol{E} = \boldsymbol{P}_L + \boldsymbol{P}_{NL}, \tag{6.3.24}$$

where the nonlinear polarization is

$$\boldsymbol{P}_{\mathrm{NL}} = \boldsymbol{P}^{(3)} = \Delta\varepsilon \boldsymbol{E}. \tag{6.3.25}$$

According to Eqs. (6.3.25) and (6.3.12), and $|\Delta\rho| = \tilde{\rho}$, then we have

$$\boldsymbol{P}^{(3)} = \Delta\varepsilon \boldsymbol{E} = \frac{\partial\varepsilon}{\partial\rho}\Delta\rho \boldsymbol{E} = \frac{\gamma_e}{\rho_0}\tilde{\rho}\boldsymbol{E}. \tag{6.3.26}$$

The incident pump light and the Stokes scattering light induced nonlinear polarizations can be expressed as respectively

$$P_p^{(3)} = \boldsymbol{p}_p^{(3)} e^{i(k_p z - \omega_p t)} + c.c., \tag{6.3.27}$$

$$P_s^{(3)} = \boldsymbol{p}_s^{(3)} e^{i(-k_s z - \omega_s t)} + c.c. \tag{6.3.28}$$

Form Eqs. (6.3.26) to (6.3.21), the polarization wave amplitude is

$$\boldsymbol{p}_p^{(3)} = \frac{\gamma_e}{\rho_0}\tilde{\rho}\boldsymbol{A}_s = \frac{q^2\gamma_e^2}{\rho_0}\frac{|\boldsymbol{A}_s|^2\boldsymbol{A}_p}{\Omega_B^2 - \Omega^2 - i\Omega\Gamma_B}, \tag{6.3.29}$$

$$\boldsymbol{p}_s^{(3)} = \frac{\gamma_e}{\rho_0}\tilde{\rho}^*\boldsymbol{A}_p = \frac{q^2\gamma_e^2}{\rho_0}\frac{|\boldsymbol{A}_p|^2\boldsymbol{A}_s}{\Omega_B^2 - \Omega^2 + i\Omega\Gamma_B}. \tag{6.3.30}$$

Substituting the field expressions (6.3.9) and (6.3.10), the polarization wave amplitude expressions (6.3.29) and (6.3.30) into field Eqs. (6.3.22) and (6.3.23);

using Eq. (6.3.26); and setting $\omega_p \approx \omega_s \approx \omega$ and $n_p \approx n_s \approx n$, we can obtain a group of field amplitude coupled equations:

$$\frac{d\boldsymbol{A}_p}{dz} = \frac{i\omega q^2 \gamma_e^2}{2\varepsilon_0 c n \rho_0} \frac{|\boldsymbol{A}_s|^2 \boldsymbol{A}_p}{\Omega_B^2 - \Omega^2 - i\Omega\Gamma_B}, \tag{6.3.31}$$

$$\frac{d\boldsymbol{A}_s}{dz} = -\frac{i\omega q^2 \gamma_e^2}{2\varepsilon_0 c n \rho_0} \frac{|\boldsymbol{A}_p|^2 \boldsymbol{A}_s}{\Omega_B^2 - \Omega^2 + i\Omega\Gamma_B}. \tag{6.3.32}$$

Using the relationship of light intensity and field amplitude:

$$I_p(z) = \frac{1}{2}\varepsilon_0 c n |\boldsymbol{A}_p|^2, \tag{6.3.33}$$

$$I_s(z) = \frac{1}{2}\varepsilon_0 c n |\boldsymbol{A}_s|^2, \tag{6.3.34}$$

From Eqs. (6.3.31) to (6.3.32) we can obtain

$$\frac{dI_p}{dz} = -gI_pI_s, \tag{6.3.35}$$

$$\frac{dI_s}{dz} = -gI_pI_s. \tag{6.3.36}$$

where g is the gain factor of Brillouin scattering. Setting $\Omega_B + \Omega \approx 2\Omega$ and $\Omega_B - \Omega \approx 0$, g can be approximately expressed as

$$g = g_0 \frac{(\Gamma_B/2)^2}{(\Omega_B - \Omega)^2 + (\Gamma_B/2)^2}. \tag{6.3.37}$$

When $\Omega = \Omega_B, g = g_0, g_0$ is the gain factor at canter of spectrum line:

$$g_0 = \frac{\omega q^2 \gamma_e^2}{\varepsilon_0^2 n^2 c^2 \rho_0 \Omega \Gamma_B}. \tag{6.2.38}$$

Because $\Omega = \Omega_B = qv_b, q = 2k_P$, so

$$g_0 = \frac{4\gamma_e^2 \omega^2}{\varepsilon_0^2 n v_b c^3 \rho_0 \Gamma_B}. \tag{6.3.39}$$

According to the Boundary condition in Fig. 6.13, assuming the pump light intensity is a constant, i.e., $I_p =$ constant, the solution of Eq. (6.3.36) is

$$I_s(z) = I_s(L)e^{gI_p(L-z)}. \tag{6.3.40}$$

We can see that the Brillouin scattering Stokes wave in the medium is reverse propagation and exponential increase.

6.3.3 Experiments of Stimulated Brillouin Scattering

The requirements to the working medium of stimulated Brillouin scattering are: ① high transparency in pump light frequency area; ② with higher mass density and larger electrostriction coefficient; ③ it can sustain the higher focused laser power do not be damage. Actually, almost all common optical medium can be used for generating the SBS light, including the solid medium (crystalline quartz, fused quartz, optical grass, optical fiber, organic crystal, polymer material etc.), the liquid medium (carbon disulfide, benzene, acetone, carbon tetrachloride, glycerin, water, etc.),the gas medium (H_2, N_2, CH_4, CO_2 etc.), in general these gases is in high pressure state for increasing the density of gas. Because the frequency range of Brillouin scattering is very small (smaller than 1 cm^{-1} order of magnitude), the pump light source for generating SBS usually is used the pulsed laser with spectral width less than 1 cm^{-1}.

Figure 6.14 shows the several experimental setups for realizing SBS. Figure 6.14a is a common setup. The pump light via a lens focuses into the medium and one-way passes through it to produce a backward Brillouin scattering. In order to prevent the backward SBS return to laser to affect the normal work, an optical isolator consisted of a polarizing prism and a $\lambda/4$ wave plate is placed between the laser and the scattering medium. After the polarization plane of backward SBS light rotates 90°, it outputs from the polarizing prism. In the setup in Fig. 6.14b, a SBS medium is placed into an optical resonant cavity. The axis of cavity deflects a small angle respect to the pump light, it can generate a SBS light near the reverse direction ($\theta \approx \pi$). The feedback of light cavity can decrease the threshold of pump light; it also can realize the tuning of frequency shift through adjusting the angle. Figure 6.14c is placing the scattering medium into a light cavity, its axis is perpendicular to the direction of pump light, a thicker pump light via a cylindrical lens from edgewise focuses into scattering medium, and produces SBS light with angle $\theta = \pi/2$. In Fig. 6.14d, the backward SBS light produced by the scattering medium is amplified via a laser amplifier and then outputs from a polarization lens with 90°-rotated polarization. This setup is frequently used for the experiment that uses a backward SBS to produce the phase conjugation light.

In comparison with the stimulated Raman scattering, the stimulated Brillouin scattering has smaller frequency shift, in order to measure it, except using the high resolution spectrograph, it usually uses an F–P etalon to process the spectrum

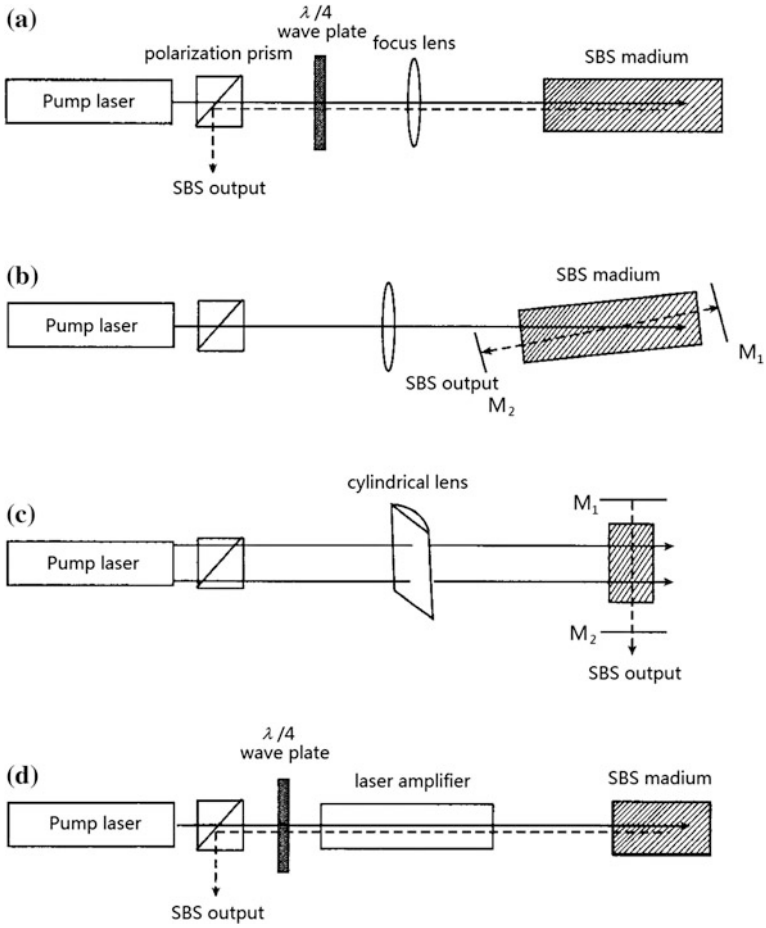

Fig. 6.14 Experimental setups for the stimulated Raman scattering: **a** the pump light one-way passes through medium to generate a backward SBS that outputs from the side of a polarization lens; **b** the medium placed in a resonant cavity generating a near backward SBS output; **c** the medium placed in resonant cavity generating SBS outputted along 90° direction; **d** the backward SBS passes through a laser amplifier and outputs from side of polarization lens

photograph analysis. Figure 6.15 shows an experimental setup for measuring the frequency shift of the backward SBS light respect to the pump light by using an F–P etalon. Using a planar beam splitter with part reflectivity to make a backward SBS light beam and a half of pump light beam sampling from another plane reflector together pass through a concave lens, interference imaging on the F–P etalon respectively, to form interference ring with double ring structure. In which a group of complete ring is formed by the SBS light; another group of half ring is formed by the pump light. If know the free spectral region of the etalon, then the frequency shift of SBS can be determined from the interval between two groups of rings.

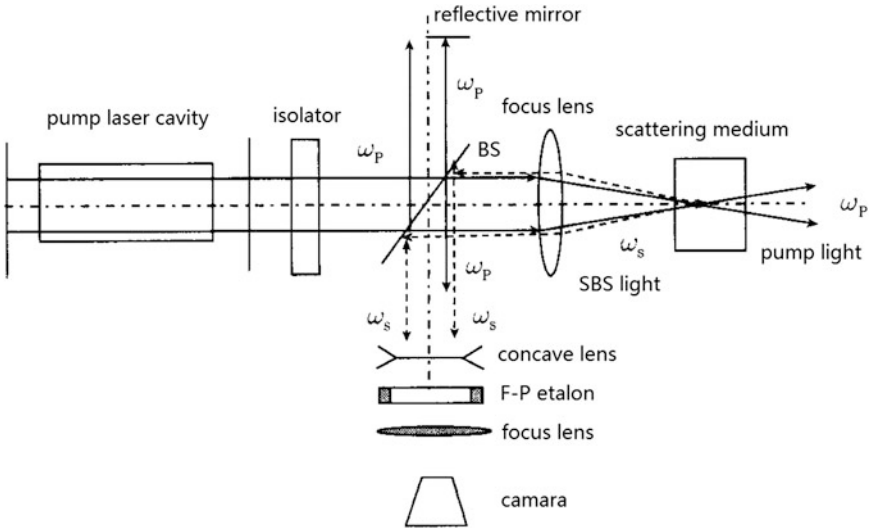

Fig. 6.15 Experimental setup for measuring the frequency shift of backward SBS using an F–P etalon

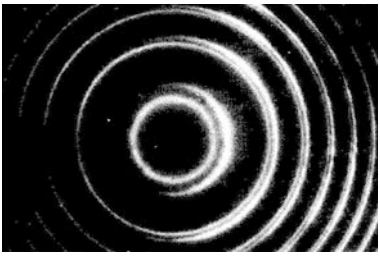

Fig. 6.16 The photo of the interference ring of the dimethyl-sulfoxide backward SBS light (whole ring) and the interference ring of 532 nm-pump light (half ring) taken by an F–P etalon. From the interval of two interference rings can determine the frequency shift of SBS

Figure 6.16 shows a ring-shape interference photo of the backward SBS light of the dimethyl sulfoxide liquid (whole ring) and the 532 nm-pump laser (half ring) taken on a 3 mm-thick quartz glass etalon.

Review Questions of Chapter 6

1. Which types do light scattering has? What are origins and characteristics of these light scatterings?
2. What is the difference between the stimulated radiation scattering and the spontaneous radiation scattering?
3. Please describe the classical physical picture of the stimulated Raman scattering generation. How to determine the propagation directions of Stokes scattering

light and anti-Stokes scattering light? How to experimentally demonstrate the stimulated Raman scattering?

4. Using classical theory method to derive the formula of stimulated Raman scattering nonlinear susceptibility. Please show the frequency spectrum characteristics of the real part and imaginary part of susceptibility for Stokes scattering and anti-Stokes scattering respectively.
5. Please describe the classical physical picture of the stimulated Brillouin scattering generation. Please discuss the propagation law of the pump light, the scattering light and the acoustic wave. How to experimentally demonstrate the stimulated Brillouin scattering?
6. Using classical theory method to derive the nonlinear polarization formulae of the stimulated Brillouin Stokes scattering and anti-Stokes scattering. Please discuss their propagation directions and gains.
7. From point of view of energy and momentum conservation to discuss: what are different physical mechanisms and properties of SRS and SBS?

References

1. G. Eckhardt, R.W. Hellwarth et al., Stimulated Raman scattering from organic liquids. Phys. Rev. Lett. **9**(11), 455–457 (1962)
2. E. Garmire, E. Pandarese, C.H. Townes, Coherently driven molecular vibrations and light modulation. Phys. Rev. Lett. **11**(4), 160–163 (1963)
3. N. Bloembergen, Y.R. Shen, Coupling between vibrations and light waves in Raman laser media. Phys. Rev. Lett. **12**(18), 504–507 (1964)
4. Y.R. Shen, N. Bloembergen, Theory of stimulated Brillouin and Raman scattering. Phys. Rev. **137**(6A), A1786–A1805 (1965)
5. R.W. Boyd, *Nonlinear Optics* (Academic Press, 1992)
6. R.Y. Chiao, C.H. Townes, B.P. Stoicheff, Stimulated Brillouin scattering and coherent generation of intense hypersonic waves. Phys. Rev. Lett. **12**(21), 592–595 (1964)
7. C.L. Tang, Saturation and spectral characteristics of the Stokes emission in the stimulated Brillouin process. J. Appl. Phys. **37**(8), 2945–2956 (1966)
8. M. Maier, Quasisteady state in the stimulated Brillouin scattering of liquids. Phys. Rev. **166**(1), 113–119 (1968)

Chapter 7
Nonlinear Absorption and Refraction of Light

Nonlinear light absorption is a basic phenomenon of the interaction between the light and the matter. The nonlinear absorption can be described as the absorption coefficient of the medium being a function of the light intensity. Firstly this chapter studies the single-photon absorption (SPA) and the two-photon absorption (TPA) based on the light-matter interaction under the condition of far away the resonance. Secondly this chapter studies the saturable absorption (SA) and the reverse saturable absorption (RSA) based on the light-matter interaction under the condition of close to the resonance. In addition, the applications of these nonlinear absorptions are also introduced, such as the application of TPA in the semiconductor all-optical switches and the application of RSA in the all-optical limiters. In this chapter, according to the K–K relation, we also discuss the single-photon refraction (SPR) related to the single-photon absorption (SPA); the saturable refraction (SR) and the reverse saturable refraction (RSR) related to the SA and the RSA, respectively.

7.1 Single-Photon Absorption and Two-Photon Absorption

7.1.1 Light-Intensity Transmission Equations

1. Light-Intensity Transmission Equations for SPA and/or TPA

When a laser beam propagates in a medium, if the interaction between light and matter is far away from the resonance, it may exists two kinds of absorptions in the medium at the same time: the single-photon absorption and the two-photon absorption. We denote the total absorption coefficient of medium as α_T:

$$\alpha_T = \alpha + \beta I. \tag{7.1.1}$$

© Shanghai Jiao Tong University Press,
Shanghai and Springer Nature Singapore Pte Ltd., 2017

C. Li, *Nonlinear Optics*, DOI 10.1007/978-981-10-1488-8_7

where α is the single-photon absorption coefficient, I is the light intensity, and β is a ratio coefficient, it is called the two-photon absorption coefficient.

Suppose a laser beam with intensity I and at frequency ω propagates along z-axis direction in the medium. Because of the existence of light absorption, the light intensity decreases with the increase of the transmission distance. The light-intensity transmission equation can be expressed as

$$\frac{dI}{dz} = -\alpha_{\mathrm{T}} I = -(\alpha + \beta I)I. \tag{7.1.2}$$

The numerical value of β is generally very small. When the light intensity is not very strong, i.e., $\alpha >> \beta I$, the TPA can be neglected, so the Eq. (7.1.2) can be written as

$$\frac{dI}{dz} = -\alpha I. \tag{7.1.3}$$

This is the light-intensity transmission equation for the single-photon absorption in $\alpha >> \beta I$ case.

However, if the light intensity I being strong enough to lead $\beta I >> \alpha$, the single-photon absorption coefficient can be neglected, i.e., $\alpha \approx 0$, Eq. (7.1.2) can be written as

$$\frac{dI}{dz} = -\beta I^2. \tag{7.1.4}$$

This is the light-intensity transmission equation for two-photon absorption process in $\beta I >> \alpha$ case.

As we know that the medium is composed by atoms or molecules. Supposing the energy-level structure of the atom or molecule is a two-level system, and denoting the lower energy level as E_1 and the upper energy level as E_2, when a light inputs the medium, the atoms or molecules could absorb the incident photons to make the energy-level transition in the certain condition. If the photon energy $\hbar\omega$ is near the energy difference between two levels, i.e., $\hbar\omega = E_2 - E_1$, in this case the SPA is dominator. However, if the photon energy $\hbar\omega$ is near a half of the energy difference between two levels, i.e., $\hbar\omega = (E_2 - E_1)/2$, in this case the TPA is dominator. It can be seen that the light absorption of medium is whether SPA or TPA depends on the frequency of the incident light and the energy-level structure of medium.

From the light-intensity transmission Eq. (7.1.2) we can see that the light absorption is whether SPA or TPA also depends on the light intensity I: in weak light intensity case the absorption is appeared SPA; but in strong light intensity case the absorption is appeared TPA. As we know that the light intensity is $I = (N\hbar\omega)/\Delta S\Delta t$, where N$\hbar\omega$ is the total light energy ($\hbar\omega$ is the energy of photon, N is total photon number), ΔS is the cross sectional area of passing light and Δt is the time of passing light (near the pulsewidth of light). So the intensity I is inversely

proportional to the pulsewidth of light Δt, For example, the pulsewidth of femtosecond laser is shorter than that of picosecond laser in1000 times, so the intensity of the femtosecond laser is larger than that of picosecond laser in 1000 times. Therefore, under the action of the picosecond (or wider) pulsed laser, the absorption performance of the medium belongs to the SPA. Nevertheless under the action of femtosecond laser, the medium shows the TPA effect. In short, the light absorption performance of the medium also relies on the pulsewidth of the incident light.

2. **Light-Intensity Transmission Equations in Third-Order Nonlinear and Linear Case**

If we only consider the third-order nonlinear optics effect in off-resonance case, the single-photon absorption coefficient can be expressed as

$$\alpha = \alpha_0 + \Delta\alpha = \alpha_0 + \alpha_2 I, \tag{7.1.5}$$

where α_0 is the linear absorption coefficient, $\Delta\alpha$ denotes the third-order nonlinear absorption in SPA process, which is proportional to the light intensity I, α_2 is a ratio coefficient, it is called the nonlinear absorption coefficient. In the next section we will show that $\Delta\alpha$ is negative, i.e., $\alpha_2 < 0$, so the single-photon absorption coefficient α can be expressed as

$$\alpha = \alpha_0 - |\alpha_2| I. \tag{7.1.6}$$

Equation (7.1.6) shows that the absorption coefficient α is a linear function of the light intensity I, and the single-photon absorption coefficient decreases with the increase of the intensity.

As we mention before, the two-photon absorption βI is proportional to the light intensity I, same as the third-order nonlinear absorption $\alpha_2 I$ in SPA, so TPA is also a kind of third-order-nonlinear effects. But the sign symbols of both ratio coefficients are different: $\beta > 0$ and $\alpha_2 < 0$. The total nonlinear absorption can be written as

$$\alpha_T = \alpha + \beta I = \alpha_0 - |\alpha_2| I + \beta I. \tag{7.1.7}$$

Substituting Eq. (7.1.7) into Eq. (7.1.2), then we obtain:

$$\frac{dI}{dt} = -\alpha_0 I - (\beta - |\alpha_2|) I^2. \tag{7.1.8}$$

This is the light-intensity transmission equation when considering the third-order nonlinear effects of SPA and TPA.

Actually, in general $|\alpha_2|$ is much smaller than β, i.e., $\beta >> |\alpha_2|$, so that the light-intensity transmission equation can be approximately written as

$$\frac{dI}{dz} = -\alpha_0 I - \beta I^2. \tag{7.1.9}$$

This is the light-intensity transmission equation when omitting the single-photon nonlinear absorption.

Equation (7.1.9) shows that when the incident-light intensity is very small, all of the nonlinear effects can be ignored, thus Eq. (7.1.9) becomes

$$\frac{dI}{dz} = -\alpha_0 I. \tag{7.1.10}$$

This is the light-intensity transmission equation for the single-photon absorption in low-intensity case.

7.1.2 Single-Photon Nonlinear Absorption and Refraction

1. **Single-Photon Nonlinear Absorption**

If a monochromatic light at frequency ω is inputted into an isotropic medium with thickness of L, and it propagates along the z-coordinate direction, denoting the light-field amplitude at z point as $\boldsymbol{E}(z, \omega)$, the light intensity at that point as $I(z, \omega)$, the inputted field amplitude as $\boldsymbol{E}(0, \omega)$ and the outputted field amplitude as $\boldsymbol{E}(L, \omega)$, consequently the third-order nonlinear single-photon absorption process is shown in Fig. 7.1, where the total absorption coefficient of medium α can be divided into two parts: the linear absorption α_0 and the nonlinear absorption $\Delta\alpha$.

As we know that the steady-state nonlinear wave equation in the isotropic medium under the slowly-varying-amplitude approximation is

$$\frac{d\boldsymbol{E}(z, \omega)}{dz} = \frac{i\omega}{2\varepsilon_0 c n_0} \boldsymbol{P}(z, \omega). \tag{7.1.11}$$

We only consider the first- and third-order nonlinear polarization processes, the total polarization is given by

$$\boldsymbol{P}(z, \omega) = \boldsymbol{P}^{(1)}(z, \omega) + \boldsymbol{P}^{(3)}(z, \omega). \tag{7.1.12}$$

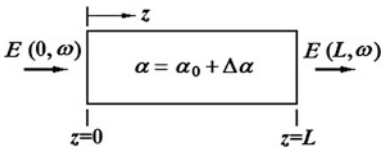

Fig. 7.1 Schematic diagram of the third-order nonlinear single-photon absorption process

Because we just discussed the light absorption, only taking the imaginary part of susceptibility $i\chi''$, the first-order linear polarization is

$$\boldsymbol{P}^{(1)}(z,\omega) = i\varepsilon_0\chi^{(1)''}(\omega)\boldsymbol{E}(z,\omega). \tag{7.1.13}$$

And the third-order nonlinear polarization is

$$\boldsymbol{P}^{(3)}(z,\omega) = 3i\varepsilon_0\chi^{(3)''}(\omega;\omega,-\omega,\omega)|\boldsymbol{E}|^2\boldsymbol{E}(z,\omega). \tag{7.1.14}$$

Substituting Eqs. (7.1.12)–(7.1.14) into Eq. (7.1.11), we will obtain

$$\frac{d\boldsymbol{E}(z,\omega)}{dz} = -\frac{1}{2}\left[\frac{\omega}{cn_0}\chi^{(1)''}(\omega) + \frac{3\omega}{cn_0}\chi^{(3)''}(\omega;\omega,-\omega,\omega)|\boldsymbol{E}|^2\right]\boldsymbol{E}(z,\omega). \tag{7.1.15}$$

Using $I = \frac{1}{2}\varepsilon_0 cn_0|\boldsymbol{E}|^2(\omega)$, Eq. (7.1.15) becomes

$$\frac{d\boldsymbol{E}(z,\omega)}{dz} = -\frac{1}{2}\left[\frac{\omega}{cn_0}\chi^{(1)''}(\omega) + \frac{6\omega}{\varepsilon_0 c^2 n_0^2}\chi^{(3)''}(\omega)I\right]\boldsymbol{E}(z,\omega). \tag{7.1.16}$$

We express the first item of the right side of Eq. (7.1.16) as the linear absorption coefficient α_0:

$$\alpha_0 = \frac{\omega}{cn_0}\chi^{(1)''}(\omega), \tag{7.1.17}$$

and the second item is the nonlinear absorption coefficient $\Delta\alpha$:

$$\Delta\alpha = \frac{6\omega}{\varepsilon_0 c^2 n_0^2}\chi^{(3)''}(\omega)I, \tag{7.1.18}$$

the total absorption coefficient α is then

$$\alpha = \alpha_0 + \Delta\alpha. \tag{7.1.19}$$

To replace the bracket in Eq. (7.1.16) with Eq. (7.1.19), then we will obtain the integral solution of the field amplitude at z point:

$$\boldsymbol{E}(z,\omega) = \boldsymbol{E}(0,\omega)e^{-\frac{\alpha}{2}z}. \tag{7.1.20}$$

Therefore, the relationship between the input intensity and the output intensity is

$$I(z) = I(0)e^{-\alpha z}. \tag{7.1.21}$$

This means that for a certain input intensity $I(0)$ and medium absorption coefficient α, the output intensity presents an exponential decay with the increase of z.

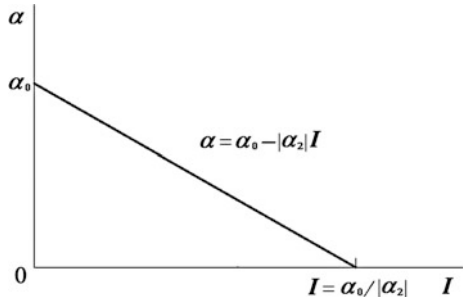

Fig. 7.2 The absorption coefficient of medium as a function of the intensity in the case of third-order nonlinear polarization for the single-photon absorption

According to Eqs. (7.1.19) and (7.1.18), the absorption coefficient α in Eq. (7.1.21) can be expressed as

$$\alpha = \alpha_0 + \Delta\alpha = \alpha_0 + \alpha_2 I. \tag{7.1.22}$$

where α_2 is the nonlinear absorption coefficient, which can be written as

$$\alpha_2 = \frac{6\omega}{\varepsilon_0 c^2 n_0^2}\chi^{(3)\prime\prime}(\omega). \tag{7.1.23}$$

Obviously, α_2 is proportional to the imaginary part of the third-order susceptibility. It can be proved that $\chi^{(3)\prime\prime}(\omega) < 0$, so $\alpha_2 < 0$, Eq. (7.1.22) can be written as

$$\alpha = \alpha_0 - |\alpha_2| I. \tag{7.1.24}$$

Equation (7.1.24) means that the absorption coefficient linearly decreases with the increase of light intensity. When $I = \alpha_0/|\alpha_2|, \alpha = 0$, the curve of α verses the I is shown in Fig. 7.2.

Assuming the length of the medium is L, the transmittance of medium can be expressed as

$$T = \frac{I(L)}{I(0)} = e^{-\alpha L} = e^{-(\alpha_0 - |\alpha_2| I)L}. \tag{7.1.25}$$

In this case the transmittance of medium increases with the increase of intensity. When $I \to \alpha_0/|\alpha_2|, T = 1$. That means in the high-power case the medium becomes transparency without absorption.

2. Single-Photon Nonlinear Refraction

According to the K–K relation [see Eq. (2.3.32)], there is a relationship between the refractive-index change and the absorption coefficient change, which is

$$\Delta n(\omega) = \frac{c}{\pi} P \cdot V \cdot \int_0^\infty \frac{\Delta\alpha(\omega')}{\omega'^2 - \omega^2} d\omega'. \tag{7.1.26}$$

One can conduct an experiment to test the $\Delta\alpha = \alpha - \alpha_0$ for different frequency to get a $\Delta\alpha(\omega')$ spectrum, and calculate by using Eq. (7.1.26) to get $\Delta n = n - n_0$ for a certain ω, where n_0 is the linear absorption coefficient. Therefore the nonlinear refractive index of medium n for a certain ω can be obtained.

As we know that when an incident laser at ω and with I inputs into the medium, the Kerr effect will happen:

$$n = n_0 + \Delta n = n_0 + n_2 I. \tag{7.1.27}$$

where n_2 is the nonlinear absorption coefficient. Equation (7.1.27) tells us that the refractive index of medium n is a function of the intensity I, this is just the third-order nonlinear refraction in the single photon case.

We have learnt from Chaps. 2 to 5 that the n_2 is proportional to the real part of the third-order susceptibility:

$$n_2 = \frac{3}{\varepsilon_0 c n_0^2} \chi^{(3)\prime}(\omega). \tag{7.1.28}$$

We can see that Eqs. (7.1.27) and (7.1.28) for describing the nonlinear refraction are corresponding to Eqs. (7.1.22) and (7.1.23) for describing the nonlinear absorption. Both effects belong to the third-order nonlinear optical phenomenon in the single-photon process.

7.1.3 General Theory of Two-Photon Absorption

When two light beams at different frequencies ω_1 and ω_2 pass through the nonlinear medium simultaneously, if the sum of two photon energies is close to an energy difference of two energy levels of the medium, i.e., $\hbar\omega_1 + \hbar\omega_2 = E_2 - E_1$, one may find the two light beams at ω_1 and ω_2 simultaneously decay due to the absorption of the medium. Such phenomenon is called two-photon absorption (TPA) [1]. Figure 7.3 shows a schematic diagram of the two-photon resonance absorption. The feature of this effect is that there is a virtual energy level between two real energy levels.

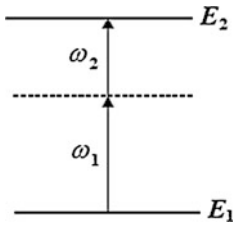

Fig. 7.3 Schematic diagram of two-photon resonance absorption

The two-photon absorption is a kind of third-order nonlinear optical effects, which can be described by a slowly-varying-amplitude-approximation nonlinear wave equation, which is

$$\frac{\partial \boldsymbol{E}(z,\omega_{\mathrm{i}})}{\partial z} = \frac{i\omega_{\mathrm{i}}}{2\varepsilon_0 cn}\boldsymbol{P}^{(3)}(z,\omega_{\mathrm{i}}) \cdot \omega_{\mathrm{i}} = 1,2 \tag{7.1.29}$$

Assuming there are two light waves with frequencies of ω_1 and ω_2 propagating along z direction, the field amplitudes of two lights can be written as

$$\boldsymbol{E}(z,\omega_1) = \boldsymbol{E}_0(z,\omega_1)e^{i(kz-\omega_1 t)} + c.c. \tag{7.1.30}$$

$$\boldsymbol{E}(z,\omega_2) = \boldsymbol{E}_0(z,\omega_2)e^{i(kz-\omega_2 t)} + c.c. \tag{7.1.31}$$

The nonlinear polarizations induced by these two fields are respectively

$$\boldsymbol{P}^{(3)}(\omega_1) = 6\varepsilon_0\chi^{(3)}(\omega_1;\omega_2,-\omega_2,\omega_1)\boldsymbol{E}(\omega_2)\boldsymbol{E}^*(\omega_2)\boldsymbol{E}(\omega_1), \tag{7.1.32}$$

$$\boldsymbol{P}^{(3)}(\omega_2) = 6\varepsilon_0\chi^{(3)}(\omega_2;\omega_1,-\omega_1,\omega_2)\boldsymbol{E}(\omega_1)\boldsymbol{E}^*(\omega_1)\boldsymbol{E}(\omega_2). \tag{7.1.33}$$

Because we only concern the absorption, taking the imaginary part of the susceptibility, and substituting Eqs. (7.1.32) and (7.1.33) into Eq. (7.1.29), then we obtain two nonlinear wave equations:

$$\frac{\partial \boldsymbol{E}(z,\omega_1)}{\partial z} = -\frac{3\omega_1}{cn_1}\chi^{(3)\prime\prime}(\omega_1;\omega_2,-\omega_2,\omega_1)\boldsymbol{E}(\omega_2)\boldsymbol{E}^*(\omega_2)\boldsymbol{E}(\omega_1), \tag{7.1.34}$$

$$\frac{\partial \boldsymbol{E}(z,\omega_2)}{\partial z} = -\frac{3\omega_2}{cn_2}\chi^{(3)\prime\prime}(\omega_2;\omega_1,-\omega_1,\omega_2)\boldsymbol{E}(\omega_1)\boldsymbol{E}^*(\omega_1)\boldsymbol{E}(\omega_2). \tag{7.1.35}$$

According to the symmetric rule of susceptibility, we have

$$\chi^{(3)\prime\prime}(\omega_1;\omega_2,-\omega_2,\omega_1) = \chi^{(3)\prime\prime}(\omega_2;\omega_1,-\omega_1,\omega_2). \tag{7.1.36}$$

Taking the procedure of Eq. (7.1.34) $\times\, \boldsymbol{E}^*(\omega_1)$- Eq. (7.1.35) $\times\, \boldsymbol{E}^*(\omega_2)$, we then get the following equation:

$$\frac{n_1}{\omega_1}\boldsymbol{E}^*(z,\omega_1)\frac{\partial \boldsymbol{E}(z,\omega_1)}{\partial z} - \frac{n_2}{\omega_2}\boldsymbol{E}^*(z,\omega_2)\frac{\partial \boldsymbol{E}(z,\omega_2)}{\partial z} = 0. \tag{7.1.37}$$

To integrate of z on both side of Eq. (7.1.33), we obtain

$$\frac{n_1}{\omega_1}|\boldsymbol{E}(z,\omega_1)|^2 - \frac{n_2}{\omega_2}|\boldsymbol{E}(z,\omega_2)|^2 = \text{constant}. \tag{7.1.38}$$

Using $I_i = \frac{1}{2}c\varepsilon_0 n_i |E_i|^2 (i = 1, 2)$, Eq. (7.1.38) becomes:

$$\frac{I_1(z, \omega_1)}{\hbar\omega_1} - \frac{I_2(z, \omega_2)}{\hbar\omega_2} = \text{constant}. \tag{7.1.39}$$

To rewrite Eq. (7.1.39) to be the photon-umber relationship:

$$N(z, \omega_1) - N(z, \omega_2) = N(0, \omega_1) - N(0, \omega_2), \tag{7.1.40}$$

or

$$N(z, \omega_1) - N(0, \omega_1) = N(z, \omega_2) - N(0, \omega_2). \tag{7.1.41}$$

It shows that the two light beams at ω_1 and ω_2 are absorbed and amplified by the medium at the same time in TPA process.

On the both sides of Eq. (7.1.34) times $\boldsymbol{E}^*(z, \omega_1)$ and on the both sides of Eq. (7.1.35) time $\boldsymbol{E}^*(z, \omega_2)$, respectively, therefore TPA process can be expressed by the following two coupled equations:

$$\frac{dI_1}{dz} = -\beta_1 I_1 I_2, \tag{7.1.42}$$

$$\frac{dI_2}{dz} = -\beta_2 I_1 I_2. \tag{7.1.43}$$

where β_1 and β_2 are two-photon absorption coefficients:

$$\beta_1 = \frac{6\omega_1}{\varepsilon_0 c^2 n_1 n_2} \chi^{(3)\prime\prime}, \tag{7.1.44}$$

$$\beta_2 = \frac{6\omega_2}{\varepsilon_0 c^2 n_1 n_2} \chi^{(3)\prime\prime}. \tag{7.1.45}$$

We can see that β_1 and β_2 are all proportional to the imaginary part of the third-order nonlinear susceptibility.

Specifically, when a single light beam at the frequency ω and with the intensity I propagates in the medium, it also can generate the two-photon effect. In this case, the two photons have the same frequency: $\omega_1 = \omega_2 = \omega$. And the related two light beams have $I_1 = I_2 = I$ and $\beta_1 = \beta_2 = \beta$. TPA process in this case can be expressed by one equation, that is

$$\frac{dI}{dz} = -\beta I^2, \tag{7.1.46}$$

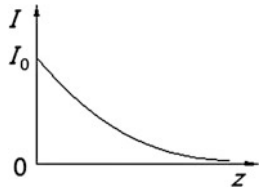

Fig. 7.4 The light intensity as a function of the propagation distant in TPA process of single light beam

where

$$\beta = \frac{6\omega}{\varepsilon_0 c^2 n^2} \chi^{(3)\prime\prime}. \tag{7.1.47}$$

If the intensity of light incident into the medium at $z = 0$ is $I(0) = I_0$, the solution of Eq. (7.1.46) will be

$$I(Z) = \frac{I_0}{1 + I_0 \beta z}. \tag{7.1.48}$$

The relation of the light intensity (I) versus the propagation distant (z) in TPA process is shown in Fig. 7.4.

7.1.4 Two-Photon Absorption and Refraction in Semiconductor

1. **Two-Photon Absorption and Free-Carrier Absorption in Semiconductor**

In the semiconductor, there are a conduction band and a valence band, these two-band structure is equivalent to a two energy-level system. The interval between the two bands is called the forbidden band (or the bandgap). When a light beam irradiates a semiconductor medium, the light absorption phenomenon is generated: the semiconductor absorbs a photon with energy near or exceed the bandgap, i.e., $\hbar\omega \geq E_g$, it will stimulate an electron from the valence band jumping to the conduction band to be a free electron. At the same time, a hole at valence band also becomes a free hole. Both of two free-carriers bind together to form a free electron-hole pair, as shown in Fig. 7.5.

A large number of photons stimulate the electrons to generate a quantity of free electron-hole pairs, and induces the change of the free-carrier concentration, therefore it results in the change of the absorption coefficient of semiconductor. That is the nonlinear absorption phenomenon of semiconductor in the single-photon case.

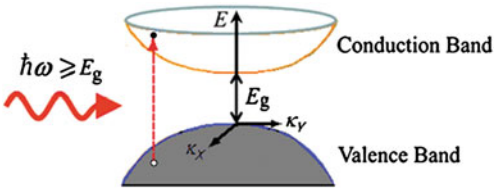

Fig. 7.5 Schematic diagram of light absorption in semiconductor

The experiment also shows that if the light frequency is ω', the photon energy equals to a half of the bandgap, i.e., $\hbar\omega' = E_g/2$, it also finds the light absorption: absorbing two photons at frequency ω' to stimulate two electron-hole pairs at the same time, then change the free-carrier concentration and the absorption coefficient. That is two-photon absorption phenomenon.

A laser beam propagates in the semiconductor along the z direction, as we presented in Sect. 1.7.1, the light-intensity transmission equation is

$$\frac{dI}{dz} = -\alpha I - \beta I^2. \tag{7.1.49}$$

where α is the single-photon absorption coefficient (here $\alpha \approx \alpha_0$); β is the two-photon absorption coefficient. How can we measure the α and β by using the experimental method?

We can solve the Eq. (7.1.49) to get the following formula [2]

$$I(z) = \frac{I(0)\alpha e^{-\alpha z}}{\alpha + \beta I(0)(1 - e^{-\alpha z})}. \tag{7.1.50}$$

Taking $z = L$, Eq. (7.1.50) can be written to

$$\frac{1}{I(L)} = \frac{1}{e^{-\alpha L} I(0)} + \frac{\beta(1 - e^{-\alpha L})}{\alpha e^{-\alpha L}}, \tag{7.1.51}$$

where $I(0)$ is the input light-intensity; $I(L)$ is the output-light intensity. and L is the length of material.

Setting $Y = 1/I(L), X = 1/I(0)$, and $B = \beta(1 - e^{-\alpha L})/\alpha e^{-\alpha L}$, Eq. (7.1.51) becomes

$$Y = \mathrm{e}^{\alpha L} X + B. \tag{7.1.52}$$

The common method of measuring nonlinear absorption coefficients is using the measured semiconductor material to make a slab waveguide with the length of L, inputting a short-pulse laser and continuously changing its power, then measuring the input intensity $I(0)$ and the output intensity $I(L)$, and taking their reciprocal values to record on a coordinate graphs of $Y - X = 1/I(L) - 1/I(0)$ as the experimental points. To connect the experimental points in a nearly straight line, as shown in Fig. 7.6. From the slope of the straight line $\mathrm{e}^{\alpha L}$, we can calculate to obtain

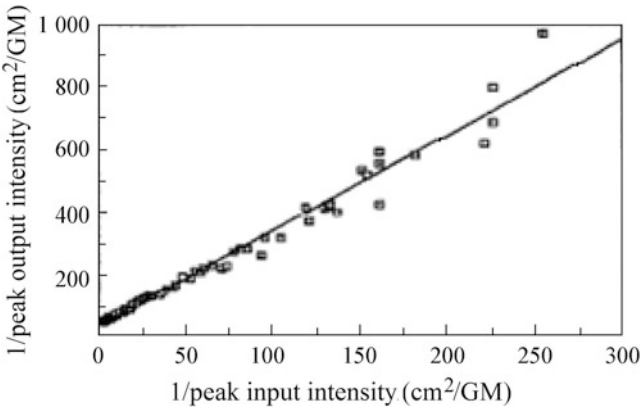

Fig. 7.6 The reciprocal input intensity as a function of the reciprocal output intensity. The experimental points obtained from an measurement form a straight line

the absorption coefficient α, and then from the intercept of the straight line on the vertical axis Y, i.e., $B = \beta(1 - e^{-\alpha L})/\alpha e^{-\alpha L}$, finally to find the value of β.

For example, a *GaAs*/*AlGaAs* MQW ridge waveguide with a dimension of long × high × wide = 1 cm × 0.8 μm × 1.5–5.5 μm, using a mold-lock YAG laser at the wavelength of 1.064μm and with the pulsewidth of 90 ps as the input laser, continuously changing the input intensity, to get an experimental curve (see Fig. 7.6). The measured results are: $\alpha = 112\text{m}^{-1}$ and $\beta = 2.0 \times 10^{-10}\text{m/W}$ for TM polarization mode; $\alpha = 90\text{m}^{-1}$ and $\beta = 2.7 \times 10^{-10}\text{m/W}$ for TM polarization mode.

It is worth noting that the light source used in the experiment is a pulsed laser, the measured intensity by photodetector is the average intensity. However, the calculated intensity by the theoretical formula is the peak intensity. How to transfer the average intensity to the peak power?

We assume that the incident laser is a Gaussian beam; its intensity is a Gaussian-type time function:

$$I(t) = I_0 \exp\left(\frac{-2t^2}{T^2}\right), \tag{7.1.53}$$

where I_0 is the peak intensity, T is the full width at half maximum amplitude (FWHM). Because we define the full width at $1/e$ of maximum intensity as $\sqrt{2}T$, the phase factor of Gaussian beam is written as $\exp(-2t^2/T^2)$, as shown in Fig. 7.7.

The Fig. 7.7 shows that the time original point is located at the maximum intensity, when $t = 0$, the phase factor is $e^0 = 1$, so $I(t) = I_0$; when $t = (\sqrt{2}/2)T = T/\sqrt{2}$, the phase factor is e^{-1}, so $I(t) = (1/e)I_0$. For the Gaussian pulse, the relationship between the peak intensity I_0 and the average intensity I_{avg} can be calculated to obtain:

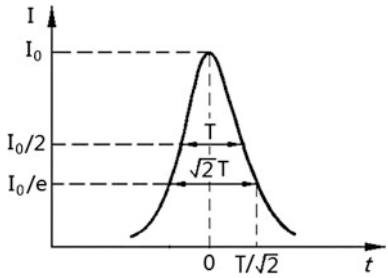

Fig. 7.7 Diagram for explaining the phase factor of Gaussian beam

$$\frac{I}{I_{avg}} = \frac{\sqrt{2t_p}}{\sqrt{\pi T}}, \tag{7.1.54}$$

where T is FWHM of the Gaussian pulse; t_p is the width of average intensity, which is the width of a square pulse, who's total energy equals to that of the Gaussian pulse. For example, in the above experiment, we used a YAG pulsed laser, the measured data are $T = 75\,ps$ and $t_p = 13\,ns$, so the ratio of the peak intensity and the average intensity is 138.

Now we substitute the measured data $\alpha = 100\,\mathrm{m}^{-1}$, $\beta = 2 \times 10^{-10}\,\mathrm{m/W}$, $t_p = 13\,\mathrm{ns}$, $T = 75\,\mathrm{ps}$ and $L = 0.01\,\mathrm{m}$ into Eq. (7.1.51), calculating to obtain the input-output intensity curve for two-photon absorption, i.e., the $I(L) - I(0)$ curve (1), as shown in Fig. 7.8. Obviously, with the increase of the input light intensity, the output light intensity has a saturation characteristic.

In fact, in the semiconductor, there is another nonlinear absorption mechanism—free carrier absorption (FCA). The FCA mainly derives from two-photon absorption (TPA): the medium absorbs two photon energy ($2\hbar\omega$), then stimulates the electronic transition to generate the electron-hole pairs, i.e., free carriers. When measuring the two-photon absorption coefficient β by using Eq. (7.1.51), people often cannot distinguish FCA from TPA. The curve (1) shown in Fig. 7.8 includes both effects.

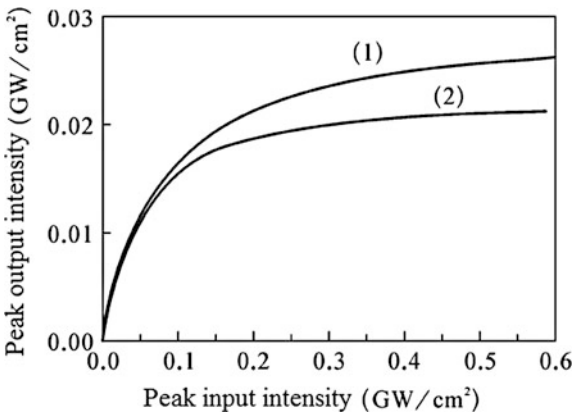

Fig. 7.8 The curve of output intensity versus input intensity for two-photon absorption obtained from the calculation. (1) without considering the effect of FCE to TPA, calculated by using Eq. (7.1.51); (2) considering the effect of FCE to TPA, calculated by using Eqs. (7.1.60) and (7.1.61)

In order to exclude FCA from the TPA measured data, we need modify Eq. (7.1.49), namely adding a new item in its right side for describing FCA [2]:

$$\frac{dI}{dz} = -\alpha I - \beta I^2 - \sigma_{\mathrm{ex}} \Delta N I. \tag{7.1.55}$$

where σ_{ex} is the total absorption cross section of free carriers; ΔN is the change of free-carrier number density, which comes from the two-photon absorption. Using Eq. (7.1.4), we have

$$\frac{dI}{dz} = \frac{d\varepsilon}{dt} = \frac{dN}{dt}(2\,h\nu) = \beta I^2, \tag{7.1.56}$$

where ε is the light-energy density; $h\nu$ is the single-photon energy, N is the free-carrier number density and β is the two-photon absorption coefficient. Thus the change of the free-carrier umber density with the time is

$$\frac{dN}{dt} = \frac{\beta I^2}{2h\nu}. \tag{7.1.57}$$

Assuming the incident light is a Gaussian-type pulse as shown in Eq. (7.1.53), the change of the free-carrier number density under a single pulse ΔN_{P} can be found from the following integral calculation:

$$\Delta N_{\mathrm{P}} = \frac{\beta}{2h\nu} \int_{-\infty}^{\infty} I_0^2 \exp\left(\frac{-4t^2}{T^2}\right) dt = \frac{\sqrt{\pi}\beta T I_0^2}{4h\nu}, \tag{7.1.58}$$

where T is FWHM of light; I_0 is the peak intensity of the light.

Actually no carrier is produced by one light pulse. If the recombination time of the carrier is τ, before this time the other pulses also have contribution to the production of the carrier. Suppose the pulse duration of the laser pulse is t_{p}, thus the change of total free-carrier number density is

$$\begin{aligned}\Delta N &= \Delta N_{\mathrm{P}}\left[1 + \exp\left(\frac{-t_{\mathrm{p}}}{\tau}\right) + \exp\left(\frac{-2t_{\mathrm{p}}}{\tau}\right) + \exp\left(\frac{-3t_{\mathrm{p}}}{\tau}\right) + \cdots\right] \\ &= \frac{\Delta N_{\mathrm{P}}}{\left[1 - \exp(-t_{\mathrm{p}}/\tau)\right]}.\end{aligned} \tag{7.1.59}$$

Substituting Eq. (7.1.59) into Eq. (7.1.55), and giving a definition of the free-carrier absorption coefficient γ, which is a physical quantity independent from the intensity:

$$\gamma = \frac{\sigma_{ex}\Delta N}{I_0^2} = \frac{\sqrt{\pi}\sigma_{ex}\beta T}{4h\nu[1 - \exp(-t_{\mathrm{P}}/\tau)]}, \tag{7.1.60}$$

and setting $I_0^2 = I^2$, we then obtain

$$\frac{dI}{dz} = -\alpha I - \beta I^2 - \gamma I^3. \tag{7.1.61}$$

This is the light-intensity transmission equation including the free-carrier absorption for semiconductors.

Therefore, the total absorption coefficient of semiconductor is

$$\alpha_T = \alpha + \beta I + \gamma I^2. \tag{7.1.62}$$

The Eq. (7.1.61) can find its analytical solutions [2].

Taking the following data measured in experiments: $\alpha = 100\,\mathrm{m}^{-1}, \beta = 2 \times 10^{-10}\,\mathrm{m/W}$, $t_p = 13\,\mathrm{ns}$, $T = 75\,\mathrm{ps}$, $\tau = 30\,\mathrm{ns}$, $L = 00.01\,\mathrm{m}$, $h\nu = 1.167\,\mathrm{eV}$, and $\sigma_{ex} = 5 \times 10^{-22}\,\mathrm{m}^2$, we calculated by Eq. (7.1.60) to get $\gamma = 5.1 \times 10^{-23} m^3/W^2$, and further calculated using Eq. (7.1.61) to obtain the output-input characteristic curve, as shown in the curve (2) of Fig. 7.8.

When eliminating the action of FCE, we can see that the TPA output-input curve (2) has stronger saturation feature compared with the curve (1), and the value of β becomes smaller. The calculation showed that the value of β reduced from $2.0 \times 10^{-10}\,\mathrm{m/W}$ to $1.5 \times 10^{-10}\,\mathrm{m/W}$ for TM polarization mode; and from $2.7 \times 10^{-10}\,\mathrm{m/W}$ to $2.0 \times 10^{-10}\,\mathrm{m/W}$ for TE polarization mode.

Therefore, it can be seen that although the influence of FCE to TPA is not very big, this effect cannot be ignored.

2. Two-Photon Absorption Induced Refractive-Index Variation in Silicon

In this section we will discuss the interaction between the femtosecond laser at the wavelength of 1.55 μm and the silicon material. The laser induces the two-photon absorption effect, and produces the refractive-index variation of material. In the TPA process, the two photons are absorbed by the semiconductor material to produce two electron-hole pairs. The absorption of two photons at the same time causes the free electron-density change ΔN_e and the free hole-density change ΔN_h in the semiconductor. The change of the carrier density can induce the refractive-index variation Δn and the absorption-coefficient variation $\Delta\alpha$ of the semiconductor. The calculation according to the Drude model obtains the following two equations [3]:

$$\Delta n = -\frac{e^2\lambda^2}{8\pi^2 c^2 \varepsilon_0 n}\left(\frac{\Delta N_e}{m_{ce}^*} + \frac{\Delta N_h}{m_{ch}^*}\right), \tag{7.1.63}$$

$$\Delta\alpha = \frac{e^2\lambda^3}{4\pi^2 c^3 \varepsilon_0 n}\left(\frac{\Delta N_e}{\mu_e\left(m_{ce}^*\right)^2} + \frac{\Delta N_h}{\mu_h\left(m_{ch}^*\right)^2}\right), \tag{7.1.64}$$

where e is electron charge, ε_0 is dielectric constant in free space; n is linear refractive index of material; c is light velocity; m_0 is electron mass; m_{ce}^* is electron conductivity effective mass, $m_{ce}^* = 0.26m_0$; m_{ch}^* is hole conductivity effective mass, $m_{ch}^* = 0.39m_0$; μ_e is electron mobility; μ_h is hole mobility; ΔN_e is electron-number change in every cube centimeter; ΔN_h is hole-number change in every cube centimeter.

According to the absorption spectrum obtained from experiments and calculation using the K–K relation, the relationship between the refractive-index change and the carrier-number-density change at the wavelength of 1.55 μm in silicon can be obtained [3]:

$$\Delta n = \Delta n_e + \Delta n_h = -\left[8.8 \times 10^{-22}\Delta N_e + 8.5 \times 10^{-22}(\Delta N_h)^{0.8}\right], \tag{7.1.65}$$

where Δn_e represents the refractive-index change induced by electron-number-density change ΔN_e; Δn_h represents the refractive-index change induced by hole-number-density change ΔN_h. The minus symbol in Eq. (7.1.65) shows that the increase of the free-carrier density results in the decrease of the refractive index of material.

Assuming the electron-number-density change equals to the hole-number-density change, i.e., $\Delta N_e = \Delta N_h = \Delta N$, and the incident light is a Gaussian-type pulse, the free-carrier–number- density change due to the two-photon absorption is expressed by Eq. (7.1.58), that is

$$\Delta N = \frac{\sqrt{\pi}\beta T_0^2}{4\,h\nu} = \frac{\sqrt{\pi}\beta T P^2}{4\,h\nu S^2}. \tag{7.1.66}$$

where β is the two-photon absorption coefficient; $h\nu$ is a photon energy; T is the FWHM of the Gaussian pulse; P is the peak power of the light; S is the cross section of the silicon waveguide. In addition, according to Eq. (7.1.54), the ratio between the peak power P and the average power P_{avg} is given by

$$\frac{P}{P_{avg}} = \frac{\sqrt{2}t_p}{\sqrt{\pi}T}. \tag{7.1.67}$$

Substituting Eqs. (7.1.66) and (7.1.66) into Eq. (7.1.65), we obtain the refractive-index change as a function of the average power of pump light for silicon materials, that is

$$\begin{aligned}\Delta n &= \Delta n_e + \Delta n_h \\ &= -\left[8.8 \times 10^{-22}\frac{\beta t_\mathrm{p}^2}{2\,h\nu\sqrt{\pi}TS^2}P_{avg}^2 + 8.5 \times 10^{-22}\left(\frac{\beta t_p^2}{2\,h\nu\sqrt{\pi}TS^2}P_{avg}^2\right)^{0.8}\right].\end{aligned} \tag{7.1.68}$$

It is clear that in the case of two-photon absorption under the action of a femtosecond pulse laser, the refractive-index change is approximately proportional to the square of the average power ($\Delta n \propto P_{avg}^2$). However in the case of single-photon absorption under the action of CW laser or wide-width pulsed laser (up to the picosecond) being proportional to the light peak power ($\Delta n \propto P$), i.e., the Kerr effect. That is to say, in silicon materials, the optical nonlinearity based on the TPA is much stronger than that based on the Kerr effect.

In Chap. 10 we will introduce the all-optical switches in a silicon ridge nanowaveguide microring, which is based on TPA effect. The device is bumped by a femtosecond laser. The switching power of the device is lower about 10 mW, which is reduced in 1000 time compared with the Kerr effect based all-optical switches.

However, TPA effect in silicon induces the FCA effect, which reduces the switching time of devices due to the long free-carrier recombination time (~ 1 ns). The switching time of the TPA based all-optical switches can only reach about 100 ps. In order to overcome the speed limitations due to the FCA effect, scientists suggest using a silicon–organic hybrid (SOH) approach, which is to replace the silicon ridge waveguide with a silicon slotted waveguide filled with a nonlinear organic molecular material. Therefore these all-optical switches have fast response time due to the Kerr effect, their switching time can be less than 10 ps.

7.2 Saturable Absorption and Reverse Saturable Absorption

Previous section discussed two kinds of nonlinear optical absorptions: the single-photon absorption and the two-photon absorption under the condition of the light-matter interaction away from resonance. We only studied the third-order nonlinear optical process. This section will discuss another two kinds of nonlinear optical absorptions: the saturable absorption and the reverse saturable absorption. Because they are under the condition of the light-matter interaction on the resonance, we should use the energy-level-transition model of molecules (or atoms) to describe. Actuary, the model implies the all different high order nonlinear optical processes.

7.2.1 Molecular-Energy-Level Model of Saturable Absorption

1. **Macroscopical Characteristics of Saturable Absorption**

Many experiments show that, when a laser irradiates some organic materials, the absorption coefficient of the material will decrease with the increase of light

intensity, until reaching a saturation value. This effect is known as the saturable absorption (RS). The relationship between the absorption coefficient $\alpha(I)$ and the light intensity I is expressed as [4]

$$\alpha(I) = \frac{\alpha_0}{1 + \frac{I}{I_c}}. \tag{7.2.1}$$

where α_0 is the linear absorption coefficient of the material; I_c is the saturation intensity, which depends on the property of material.

Figure 7.9 shows a curve of the absorption coefficient as a function of the light intensity. In the figure, the vertical axis denotes the absorption coefficient of $\alpha(I)$; the horizontal axis denotes the relative light intensity of I/I_c, here I_c is the saturation intensity, which determines the speed of absorption saturation with the increase of the light intensity. We can see that if I_c is smaller, the $\alpha(I)$ declines faster; when $I \approx 0, \alpha = \alpha_0$; when $I = I_c, \alpha = \alpha_0/2$; and when $I \to \infty, \alpha \to 0$.

Assuming the length of the medium is L, the incident light intensity is $I(0)$, and the transmitted light intensity is $I(L)$, in the case of the saturable absorption, the transmission of medium is

$$T = \frac{I(L)}{I(0)} = e^{-\alpha(I)L}. \tag{7.2.2}$$

According to Eqs. (7.2.2) and (7.2.1), the transmission of medium increase with the increase of the intensity until to $T = 1$ when $I \to \infty$. It means that the medium becomes transparent under a strong light intensity, this phenomenon is called as "bleaching".

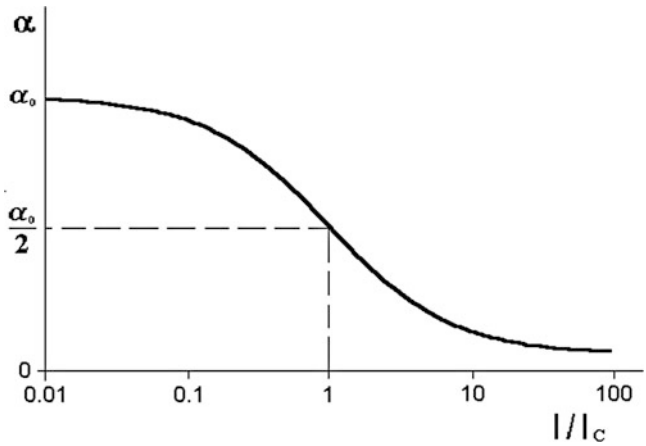

Fig. 7.9 Characteristic curve of the saturable absorption

In the 1970s the saturable absorption is widely applied in the laser-pulse compression techniques, such as Q-switching and mode locking [5]. In the 1980s, scientists studied the intrinsic optical bistable devices, which are based on the saturable absorption effect [6].

The saturable absorption cannot be described by the nonlinear polarization theory, but it can be simply explained by the energy-level transition model of microcosmic particle (molecule, ion or atom) system under the laser's action. When the particles in the ground state absorb the energy of photons of extraneous laser and jump to the first excited states, if the laser is strong enough, it will make the absorption of system to be saturation. This is the origin of the saturable absorption phenomenon. Here we are going to discuss the two-level and three-level model for the saturable absorption by using the rate equation theory [7].

2. **Two Energy-Level Model of Saturable Absorption**

Firstly we consider the saturable absorption in a simple two-level molecular model, which consists of the ground-state S_0 with energy ε_1 and molecular-number density n_1 and the first excited-state S_1 with energy ε_2 and molecular-number density n_2, as shown in Fig. 7.10.

Under the resonance interaction between the light at frequency ω, with intensity I and the two-level molecular medium, the photon energy equals to the difference of two-level energies, i.e., $\hbar\omega = \varepsilon_1 - \varepsilon_0$. The molecules on the ground-state absorb the photons jumping to the excited state as a stimulated transition with an absorption cross section (or a transition probability) of σ_0. Because the lifetime of molecule in the excited-state is very short, the molecules return to the ground-state from the excited-state through two ways: the most of molecules through the spontaneous radiation (or non-radiation) with a relaxation time τ_{21} (or a transition probability $1/\tau_{21}$); only a part of molecules come back to ground-state through the stimulated radiation with the same transition probability of σ_0.

Denoting the total molecule-number density as N, the change of n_2 with the time is described by the following rate equations:

$$\frac{\partial n_2}{\partial t} = \frac{\sigma_0}{\hbar\omega} I(n_1 - n_2) - \frac{n_2}{\tau_{21}}, \tag{7.2.3}$$

and

$$N = n_1 + n_2. \tag{7.2.4}$$

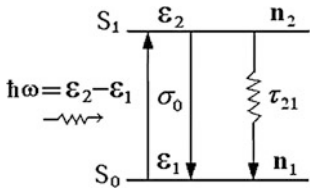

Fig. 7.10 Light-induced saturable absorption in a two-level molecular model

When the pulsewidth of laser is much larger than the molecule relaxation time, i.e., $\tau_L >> \tau_{21}$, it can be treated as meeting the steady-state condition, so $\partial/\partial t = 0$ in Eq. (7.2.3), then we obtain the difference of molecule-number density between the two energy levels, that is

$$\Delta n = n_1 - n_2 = \frac{N}{1 + \frac{I}{I_c}}, \tag{7.2.5}$$

where I_c is the saturation intensity defined as

$$I_c = \frac{\hbar\omega}{2\sigma_0\tau_{21}}. \tag{7.2.6}$$

When $I = 0$, the linear absorption coefficient is

$$\alpha_0 = N\sigma_0, \tag{7.2.7}$$

When $I \neq 0$, the nonlinear absorption coefficient is

$$\alpha(I) = \Delta n(I)\sigma_0. \tag{7.2.8}$$

Substituting Eqs. (7.2.7) and (7.2.8) into Eq. (7.2.5), then we obtain Eq. (7.2.1) for the saturable absorption:

$$\alpha(I) = \frac{\alpha_0}{1 + \frac{I}{I_c}}.$$

We can see that when $I \to \infty, \Delta n \to 0$, then $n_1 \approx n_2$. That is to say, under the action of a strong light, through the transition of molecules $S_0 \to S_1$ and $S_1 \to S_0$, the molecule-number density of the ground state equals to that of the excited state. It means that the molecular system achieves a balance state, the photons cannot be absorbed by the medium again, and the light will totally pass through the medium. This is the essence of the absorption saturation of a two-energy-level system.

The semiconductor material has two energy bands with different energy: the conduction band and the valence band. So we can regard the semiconductor as a two energy-level system. Figure 7.11 shows an experimental curve for a $GaAs/GaAlAs$ MQW material with a length of L [6]. The curve shows the exciton absorption $\alpha_{\text{ex}}L$ as a function of the light intensity I, i.e., a $\alpha_{ex}L - I$ curve. The wavelength of incident laser at 0.85μm is just at the peak of the exciton absorption spectrum.

From Fig. 7.11 we can see that when the light intensity $I \to \infty$, the exciton absorption coefficient α_{ex} does not go to zero, but tends to a value of $\alpha_{\text{ex}}L = 0.26$. It shows the existence of other absorption effects. Later we will point out that this effect mainly comes from the excited-states nonlinear absorption.

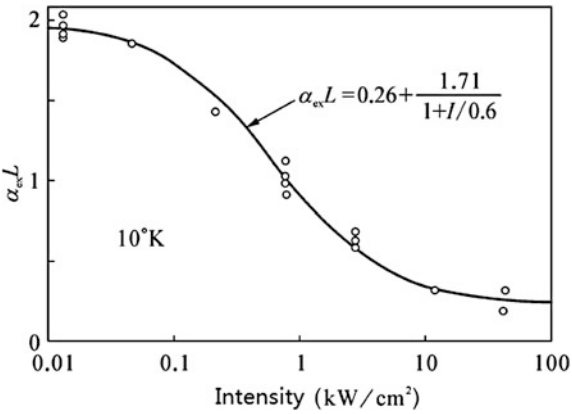

Fig. 7.11 Curve of the exciton absorption as a function of the light intensity in a *GaAs/GaAlAs* MQW material with a length of L under 10 K low temperature, the wavelength of laser is 0.85 μm

3. Three Energy-Level Model of Saturable Absorption

In dye-molecule materials, there are a singlet energy-level system and a triplet energy-level system; each of them can be regarded as a two-level system. The saturable absorption of dye molecules can be regarded as a three-level model with two excited-state level S_1, T_1 and a mutual ground-state level S_0, as shown in Fig. 7.12.

The molecules on the ground state S_0 absorb the extraneous photons, and jump to the singlet excited state S_1 with an absorption section σ_0. The molecules on the state S_1 transit to the triple excited state T_1 with a large probability of $1/\tau_{23}$. Only a small number of molecules on the state S_1 directly go back to the state S_0. Because of the probability of $1/\tau_{21}$ being very small, a large number of molecules accumulate in the state T_1. Under a strong incident light intensity, the number of molecules on the state T_1 will reach to a saturation value that equals to the total number of the molecular system.

The rate equations for describing the change of molecule number density n_1, n_3 and n_1 with the time for the three excited states S_1, T_1 and S_0 are expressed as respectively [7]

$$\frac{\partial n_2}{\partial t} = \frac{\sigma_0}{\hbar\omega} I(n_1 - n_2) - \frac{n_2}{\tau_{21}} - \frac{n_2}{\tau_{23}}, \tag{7.2.9}$$

$$\frac{\partial n_3}{\partial t} = \frac{n_2}{\tau_{23}} - \frac{n_3}{\tau_{31}}, \tag{7.2.10}$$

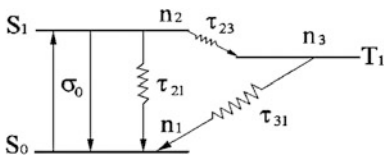

Fig. 7.12 Three-level model for explaining the saturable absorption in dye-molecule materials

$$n_1 + n_2 + n_3 = N, \tag{7.2.11}$$

where N is the total molecule number density of the system.

In the steady-state condition, we have $\partial/\partial t = 0$. Considering $\tau_{31}, \tau_{21} >> \tau_{23}$, the solutions of above three equations will be

$$n_1 = \frac{N}{1 + \frac{I}{I_c}}, \tag{7.2.12}$$

$$n_2 \approx 0, \tag{7.2.13}$$

$$n_3 = \frac{N}{1 + \frac{I_c}{I}}, \tag{7.2.14}$$

where I_c is the saturation intensity of the three-level system, which is

$$I_c = \frac{\hbar\omega}{\sigma_0 \tau_{31}}. \tag{7.2.15}$$

The linear and nonlinear absorption coefficients are respectively

$$\alpha_0 = N\sigma_0, \tag{7.2.16}$$

$$\alpha = \Delta n \sigma_0 \cong n_1 \sigma_0. \tag{7.2.17}$$

From Eqs. (7.2.16), (7.2.17) to (7.2.12), we obtain the absorption coefficient Formula (7.2.1) again. It is obviously, the law of the saturable absorption of the three-level model is the same as that of the two-level model. However, the physical conception of absorption saturation for both models is different. From Eqs. (7.2.12) to (7.2.14) we can see, when $I \to \infty$ and $n_1 \to \infty$, then $n_3 \to N$. It means that the all of molecules transfer from the ground-state to the triplet excited-state via the singlet excited-state under a strong incident light. As a result, the system cannot absorb photons again. This is the essence of the absorption saturation for the three-level system.

The saturable absorption phenomenon mainly occurs at the peak wavelength of the linear absorption spectrum (i.e., the resonance absorption region), where the absorption coefficient has very strong intensity-dependence, i.e., the system has a strong optical nonlinearity.

7.2.2 Relation Between Saturable Absorption and Three-Order Nonlinear Absorption

Formerly we pointed out that the relationship between the absorption coefficient and the light intensity in the case of the third-order nonlinear polarization is linear as shown in Fig. 7.2. However, based on what we have derived from the rate equations, the relationship between those two is saturable as shown in Fig. 7.9, which is not a line relationship. How to explain this difference? Our interpretation is that the saturated absorption is a nonlinear resonant absorption based on the energy-level transition process, implicating that the saturated absorption of the system includes the contributions of each order nonlinear polarization effects, not only the third-order nonlinear polarization effect. Here we want to prove that the third-order nonlinear absorption is only a linear approximation of the saturated absorption under the weak intensity.

Now we consider a two-level system bumped by a laser beam. The saturation intensity of this system I_c is expressed by Eq. (7.2.6). When the intensity in the medium I is very small then I_c, i.e., $I << I_c$, we take the Taylor series expansion for Eq. (7.2.1), and only keep the linear approximation item, the nonlinear absorption coefficient of the system will be

$$\alpha = \alpha_0 \left(1 + \frac{I}{I_c}\right)^{-1} \approx \alpha_0 \left(1 - \frac{I}{I_c}\right) = \alpha_0 - \frac{\alpha_0}{I_c} I. \tag{7.2.18}$$

In this case, the absorption coefficient is a linear function of the light intensity, as shown in Fig. 7.13.

In compare with Eq. (7.2.18): $\alpha = \alpha_0 - |\alpha_2| I$, we have

$$|\alpha_2| = \frac{\alpha_0}{I_c}, \tag{7.2.19}$$

In short, the third-order nonlinear absorption is a linear approximation of the saturated absorption under the condition of $I << I_c$.

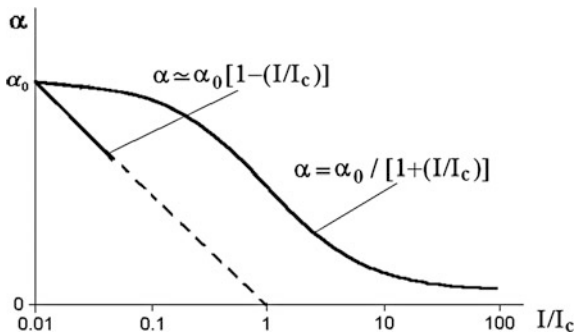

Fig. 7.13 The comparison of the saturable absorption and the third-order nonlinear absorption

7.2.3 Molecular-Energy-Level Mode of Reverse Saturable Absorption

1. **Five-Level Model of Reverse Saturable Absorption** [8]

An effect is called as the reverse saturable absorption (RSA) in which the absorption coefficient increases with the increase of the light intensity, as shown in Fig. 7.14. In the figure, α is the absorption coefficient of the medium; I is the light intensity in the medium; and α_0 is the linear absorption coefficient, i.e., low-intensity absorption coefficient of the medium.

RSA is a nonlinear optical absorption caused by the transitions between excited states under a strong light radiation. The large organic molecules have a large number of energy levels. Within the non-resonance wavelength area, the ground-state absorption is weak; but the excited-state nonlinear absorption may appear stronger, it is possible to generate the RSA.

In order to describe the reverse saturable absorption in the organic large molecules, a five-level model is used, which is consisted of the singlet and triplet two energy-level systems, as show in Fig. 7.15.

In Fig. 7.15, $0, 1, 2, 3, 4, \ldots$ denotes the lowest electronic energy-level; and $1', 2', 3', 4', \ldots$ denotes the upper vibration and rotation energy levels. S_0 is the ground-state level, S_1 and S_2 are the first and a higher excited-state levels in the singlet system. T_1 and T_2 are the first and the higher excited-state levels in the triplet system. When a laser beam at the frequency ω irradiates the molecule system, the molecules on electronic level 0,1,3 simultaneously absorb the photons at the frequency ω, and jump to the sublevels $1', 2', 4'$ with the absorption cross-section $\sigma_0, \sigma_S, \sigma_T$, respectively. Because the life time of the molecules in these sublevels is very short (shorter than a picosecond), the molecules jump down to the lower levels of 1, 2, 4 through a rapid relaxation, then down to the level 0, 1, 3 by the nonradioactive relaxation. At the room temperature, the stimulated emission of organic molecules is in a very small probability, it can be ignored. The lifetime of levels 1 and 3 are τ_S (about tens of nanoseconds) and τ_T (up to microseconds or more), respectively.

The inter-system relaxation time τ_{ST} in the transition between levels 1–3 is generally short (nanoseconds or sub-nanoseconds), namely $\tau_{ST} << \tau_{S0}$ and τ_{T0},

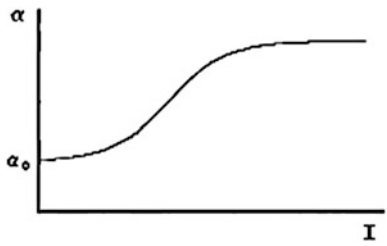

Fig. 7.14 Characteristic curve of the reverse saturable absorption

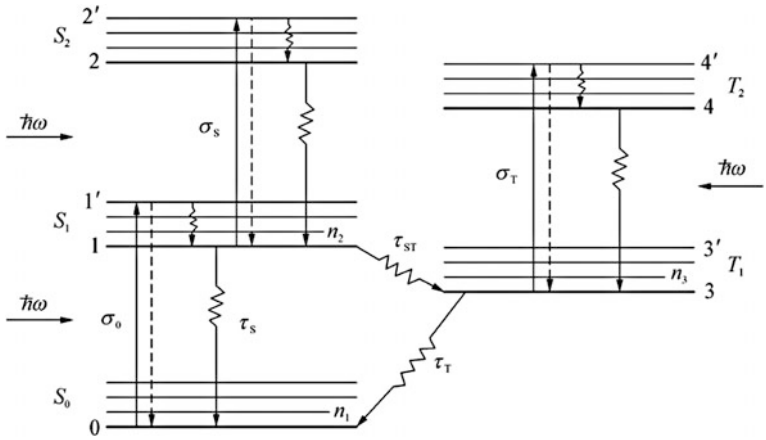

Fig. 7.15 Five-level model of organic large molecules for explaining the reverse saturable absorption

hence its transition probability is great. Because the probability from excited state T_1 to S_0 is very small, the most of molecules accumulate to the level 3.

Under the excitation of a laser, except the stimulated absorption from the electronic level 0, 1, 3 to the sublevels $1', 2', 4'$, existing also the stimulated absorption $S_1 \rightarrow S_2$ and $T_1 \rightarrow T_2$, they all contribute to the change of the total absorption coefficient. However the lifetimes of state S_2 and T_2 are very short ($\leq$ps), the probability for remaining in these states is very little, so molecule-number density in these two high energy levels can be ignored. We just consider the changes of molecule-number densities n_1, n_2 and n_3 at the energy levels S_0, S_1 and T_1 with the time.

In the large organic molecules with the central symmetry, there are a large number of energy levels and easy to generate the RSA, which is suitable to explain by using the above five-level model. For example, the metal phthalocyanine (MPc) molecules with two dimensional π-electronic mechanism and the C_{60} molecules with three dimensional π-electronic mechanism as shown in Fig. 7.16a, b respectively. There are many vibration and rotation levels near every electronic level, it makes a possibility that the molecules in ground-state and the excited-state of single or triple energy-level systems absorbing the photons with the same frequency at the same time. Figure 7.16c, d illustrates the linear absorption spectrum of MPc and C_{60}. It is visible that near the peak of linear absorption spectrum (in resonance region), the ground-state absorption is much greater than the excited-state absorption, i.e., $\sigma_0 >> \sigma_S$ and σ_T, the saturable absorption occurs only. However, near the wavelength of 500 nm at the valley of the ground-state absorption spectrum (in unresonance area), the excited-state absorption might be greater than the ground-state absorption, i.e., $\sigma_S > \sigma_0$ and $\sigma_T > \sigma_0$, so the reverse saturable absorption can be realized.

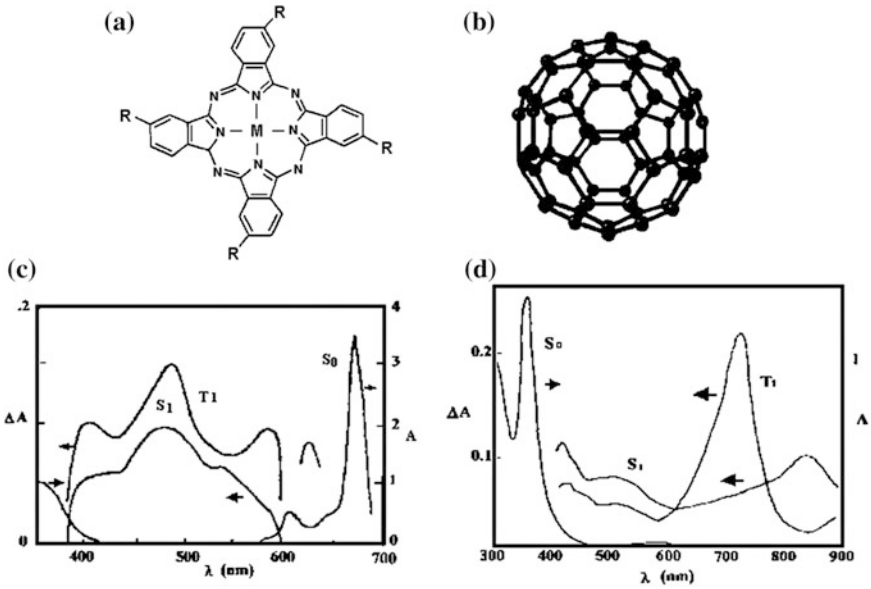

Fig. 7.16 The π-electron organic molecular structures: **a** MP_C; **b**C_{60}. The ground-state and the excited-state absorption spectra: **c** MP_C; **d**C_{60}

2. Dynamic Equation Solution of Reverse Saturable Absorption [9, 10]

In order to find the relationship between the absorption coefficient and the light intensity for RSA, we need build three rate-equations for molecule-number densities of n_1, n_2 and n_3, in addition, we also should build a light-intensity propagation equation. So the following four dynamic equations are established for solving the four unknowns: the molecule number densities $n_1(t), n_2(t), n_3(t)$ and the intensity $I(z,t)$:

$$\frac{\partial n_2}{\partial t} = \frac{\sigma_0 I n_1}{\hbar\omega} - \frac{n_2}{\tau_{S0}} - \frac{n_2}{\tau_{\mathrm{ST}}}, \tag{7.2.20}$$

$$\frac{\partial n_3}{\partial t} = \frac{n_2}{\tau_{ST}} - \frac{n_3}{\tau_{T0}}, \tag{7.2.21}$$

$$n_1 + n_2 + n_3 = N, \tag{7.2.22}$$

$$\frac{\partial I(z,t)}{\partial z} = -\alpha(I) I(z,t), \tag{7.2.23}$$

where

$$\alpha(I) = \sigma_0 n_1 + \sigma_{\mathrm{S}} n_2 + \sigma_{\mathrm{T}} n_3. \tag{7.2.24}$$

In Eq. (7.2.24), the $\sigma_0 n_1, \sigma_{\mathrm{S}} n_2$ and $\sigma_{\mathrm{T}} n_3$ are the contributors of levels S_0, S_1 and T_1 to the total absorption coefficient of the system respectively. In general, in

a molecular system, if the interaction among the molecules is relatively weak, the total absorption coefficient α equals to the sum of the every energy-level absorption coefficient $\alpha_i (i = 1, 2, 3, \ldots)$, and α_i is a product of the molecule-number density n_i and the absorption cross-section σ_i of the every electron energy level. If the molecular medium has m electron energy levels, the total absorption coefficient α is

$$\alpha = \sum_{i=1}^{m} \alpha_i = \sum_{i=1}^{m} \sigma_i n_i \cdot i = 1, 2, 3, \ldots, m \tag{7.2.25}$$

If the incident laser is assumed a Gaussian-type light pulse, its intensity at the position z and time t can be written as (see (7.1.53))

$$I(z, t) = I(z) e^{-2(t/\tau_L)^2}, \tag{7.2.26}$$

where $I(z)$ is the intensity at $t = 0$, τ_L is the full width at half maximum amplitude (FWHM) of the laser pulse. Actually, in the experiments with a pulsed laser source, the quantity measured by the photodetector is not the intensity $I(z, t)$, but the fluence $F(z)$, which is defined as

$$F(z) = \int_{-\infty}^{\infty} I(z, t) dt. \tag{7.2.27}$$

The dynamic Eqs. (7.2.20)–(7.2.24) and Eqs. (7.2.26) and (7.2.27) have the time and space variables. We should numerically solve these equations by using computer.

If we know the incident fluence $F(0)$ and the thickness of sample L, we can calculate to get the output fluence $F(L)$ and the transmittace $T = F(L)/F(0)$ as a function of $F(0)$, i.e., T–$F(0)$ cueve. Because $T = e^{-\alpha L}$, in terms of RSA, the absorption coefficient increases with the increase of the light intensity, it means that the transmittance will decrease with the increase of the light intensity.

We have done a experiment to prove above theoretical results. In the experiment, the RSA sample is a C_{60}-toluene solution with concentration of 7.2×10^{-4}M filled in a liquid cell with thickness of 5 mm. The RSA characteristic is described by a five-level model. The absorption cross sections of the C_{60}-toluene solution are $\sigma_0 = 2.87 \times 10^{-18}\text{cm}^2$, $\sigma_S = 1.57 \times 10^{-17}\text{cm}^2$ and $\sigma_T = 9.22 \times 10^{-18}\text{cm}^2$. The relaxation times are $\tau_{S0} = 30$ ns, $\tau_{T0} = 280$ μs and $\tau_{ST} = 1.2$ ns. The light source is a frequency-doubled YAG laser at wavelength of 532 nm. This laser can output respectively two kinds of light pulses with pulsewidth of 8 ns and 21 ps.

Under these two incident laser pulses, we obtained two experiment curves of T–$F(0)$ for RSA which is consistent with our theoretical calculation results in the range of $F(0) = 1 - 10^3\ \text{mJ/cm}^2$, as shown in Fig. 7.17.

We can see that the RSA effect in ps-pulse case is stronger than that in ns-pulse case. When the incident fluence is larger than 1 J/cm^2, the theoretical curve in ns

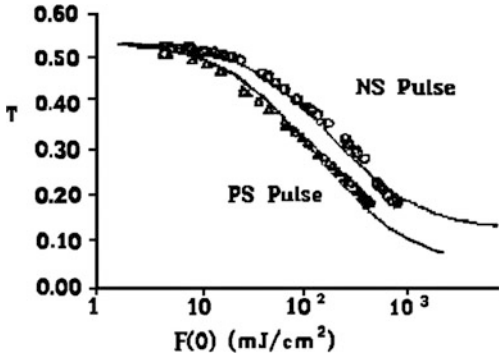

Fig. 7.17 Theoretical and experimental curves of the energy transmittance T versus the incident fluence $F(0)$ for the C_{60}-toluene solution under two lasers with pulsewidth of 8 ns and 21 ps

case is different from the experimental curve due to the other effects, such as thermal effect, diffraction, two-photon absorption, and light-induced material damage and so on.

RSA theory based on five-level molecular model shows that when the laser pulsewidth τ_L is greater than the singlet-triplet relaxation time, i.e., $\tau_L > \tau_{ST}$, for instance, the ns-light pulse inputs the molecular system with the inter-system relaxation time of ≤1 ns. In this case the molecules instantly pass through the singlet excited state to the triplet excited state, then the triplet excited-state absorption ($\alpha_3 = \sigma_T n_3$) plays a dominant role. The condition to realize RSA is $\sigma_T > \sigma_0$. Therefore, when incident light pulse with nanosecond pulsewidth, the five-level model can be simplified to be the three-level model (S_0-T_1-T_2), as shown in Fig. 7.18a.

However, when the laser pulsewidth is small than the singlet-triplet relaxation time, i.e., $\tau_L < \tau_{ST}$, for instance, the ps-light pulse inputs the molecular system with the inter-system relaxation time of ≤1 ns. In this case the molecules cannot transit to the triplet system from the singlet system, then the singlet excited-state absorption ($\alpha_2 = \sigma_S n_2$) plays a dominant role. In this case the condition to realize RSA is $\sigma_S > \sigma_0$. So the five-level model can be simplified to be the three-level model (S_0-S_1-S_2), as shown in Fig. 7.18b.

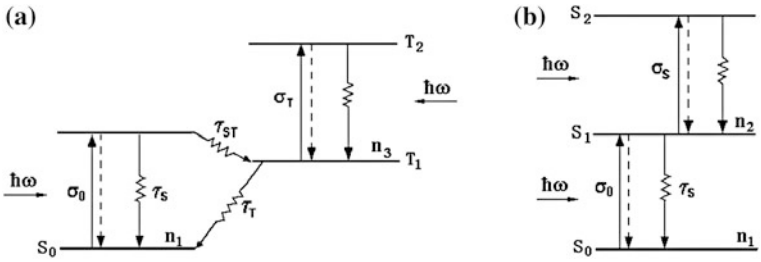

Fig. 7.18 Simplified RSA molecular models: **a** the three-level model (S_0-T_1-T_2) when inputting a ns light pulse: **b** the three-level model (S_0-S_1-S_2) when inputting the ps light pulse

3. **Steady-State Equation Solutions** [10]

When the pulsewidth of incident light pulse τ_L is much larger than the life times of all excited energy-levels, the nonlinear optical absorption process can deal with as a steady-state problem, namely $\partial/\partial t = 0$ in Eqs. (2.2.20) and (2.2.21). Assuming $\tau_{T0} > > \tau_{ST}$ and $\tau_{S0} > > \tau_{ST}$, the solutions of rate equations for n_1, n_2 and n_3 are

$$n_1 = \frac{N}{1 + \frac{I}{I_c}}, \tag{7.2.28}$$

$$n_2 \approx 0, \tag{7.2.29}$$

$$n_3 = \frac{N}{1 + \frac{I_c}{I}}, \tag{7.2.30}$$

where

$$I_c = \frac{\hbar\omega}{\sigma_0 \tau_{TO}}. \tag{7.2.31}$$

Considering

$$\alpha_0 = N\sigma_0, \tag{7.2.32}$$

$$\alpha = n_1\sigma_0 + n_3\sigma_T, \tag{7.2.33}$$

We obtain

$$\alpha = \alpha_0 \left[\frac{1 + \left(\frac{\sigma_T}{\sigma_0}\right)\frac{I}{I_c}}{1 + \frac{I}{I_c}} \right]. \tag{7.2.34}$$

The curves of the absorption coefficient α as a function of the intensity I for different σ_T/σ_0 is shown in Fig. 7.19, in which the saturation intensity is $I_c = 10^5$ W/cm^2. From the figure we can see when $\sigma_T < \sigma_0$ the curves belong to the saturable absorption; when $\sigma_T > \sigma_0$, the curves belong to the reveres saturable absorption; when $\sigma_T = \sigma_0, \alpha = \alpha_0$, the curve is a straight line; when $I \to \infty, \alpha \to \alpha_0(\sigma_T/\sigma_0)$; when $I = I_c$, $\alpha = (\alpha_0/2)[1 + (\sigma_T/\sigma_0)]$.

In addition using the rate-equation theory to study the RSA in five-energy-level molecular system; we also used the density matrix theory to study the RSA in multiple energy-level system [11]. We have found the conversion effects between RSA and SA [12, 13], as well as the conditions of the conversion between RSA and SA [14].

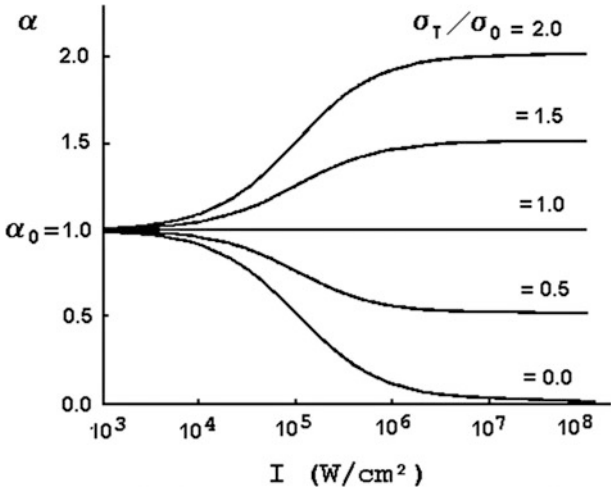

Fig. 7.19 Relationship between the absorption coefficient α and the intensity I under the different σ_T/σ_0 and $I_c = 10^5$ W/cm^2

7.2.4 Application of Reverse Saturable Absorption in All-Optical Limiting

Researches on the nonlinear optical absorption and related various excited-state nonlinear effects deepen the people's understanding to the interaction between light and matter. On this basis, it opens up a new field of an excited-state nonlinear optics.

Revers saturated absorption can be used as an kind of all-optical bistable devices, which is the enhanced-absorption-type mirrorless devices [6]. Another important application of RSA is for laser protection, made into a nonlinear optical limiters to protect the human eyes or photodetectors from laser weapon damage [15–18].

A characteristic curve of nonlinear optical limiters is shown in Fig. 7.20. In the figure, F_I is the incident fluence, F_0 is the outputted fluence, F_{IC} is the limiting threshold of incident fluence, F_{0C} is the limiting threshold of outputted fluence, F_{ID} is damage threshold of incident fluence, $F_{ID} - F_{IC}$ is the dynamic range for incident fluence, T_0 is the linear transmittance.

As an example of the nonlinear optical limiter, Fig. 7.21 shows the working principle of a grating-type optical limiter under a strong laser pulse. This nonlinear optical limiter is made up of two pieces of quartz gratings sandwiched with a nonlinear organic liquid film. The refractive index of the organic liquid is matched with the quartz (about $n_0 = 1.5$) in ordinary case without laser pulse, and then the incident light can pass through the device with a high transmittance. However, under a strong laser pulse to make the liquid vaporization, the refractive index of liquid will be changed about $\Delta n \approx 0.5$, and then the laser beam will be scattered by the gratings.

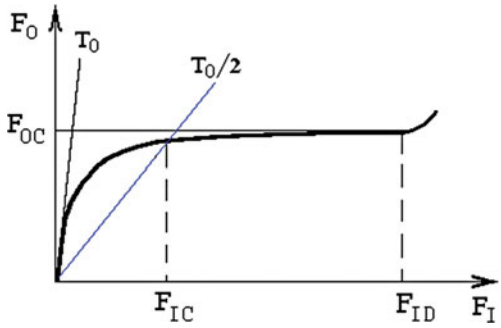

Fig. 7.20 A characteristic curve of nonlinear optical limiters

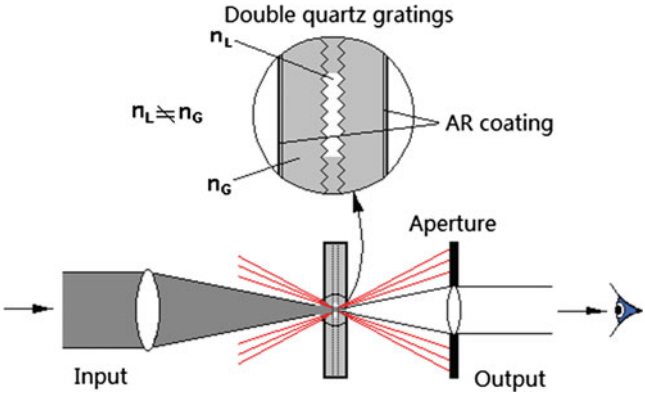

Fig. 7.21 Schematic diagram of a grating-type nonlinear optical limiter

Because of the grating is designed to be that the zero-order scattering intensity is zero, so the incident light is blocked by a small aperture in front of the eyes of observer, thus the optical limiter can protect human eyes from the laser damage.

The device performance parameters are: the linear transmittance >80 %; the output limiting threshold <0.5 mJ/cm^2 (just small than the eye-damage threshold); the dynamic range of $F_{ID} - F_{IC} > 10^4$; the response time of ns, the spectral range of 400–700 nm.

7.3 Saturable Refraction and Reverse Saturable Refraction

7.3.1 Description of Saturable Refraction and Reverse Saturable Refraction [19, 20]

We have mentioned before in the last section, if the interaction among molecules is weak, and the molecular system has *m* energy-levels, the system's absorption

coefficient α equals to the sum of the absorption coefficients contributed by individual energy level α_i, the α_i is proportional to the molecular-number density of the corresponding energy level N_i, the ratio is just the absorption cross-section σ_i as described by Eq. (7.2.25).

When the light irradiates a molecular system to make the energy-level transition of molecules, resulting in the absorption-coefficient change, according to K-K relation, the refractivity-index of system is also to be changed. We can regard that the total refractivity-index of molecular system n equals to the sum of the every energy-level contributed refractivity index n_i, but it should plus 1, because in the vacuum without molecule, the refractivity index is 1, it is not 0.

Similar to the absorption cross section σ with the area dimension, we define a new physical quantity η with the volume dimension to describe the refractive index. We call this quantity as the refraction volume. Therefore, in general speaking, for a molecular system with m electron energy-levels, if the interaction among molecules can be neglected; the total refractive index of the system n is a sum of the refractive index of every electron energy-level n_i plus 1. The refractive index of every electron energy-level n_i is proportional to the molecular number density N_i, the ratio coefficient is the refraction volume η_i of that electron energy-level. Thus the total refractive index of the molecular system can be expressed as

$$n = 1 + \sum_{i=1}^{m} n_i = 1 + \sum_{i=1}^{m} \eta_i N_i, \quad i = 1, 2, 3, \ldots m \tag{7.3.1}$$

where the molecular number density N_i is a function of the light intensity.

Using above five energy-level model in Fig. 7.15, the molecular number densities for the ground state, the singlet and triplet first excited states are denoted by N_1, N_2, and N_3 respectively, and the refraction volumes for the ground state, the singlet and triplet first excited states are denoted by η_0, η_S and η_T respectively, the total refractive index of the system n can be written as

$$n = 1 + \eta_0 N_1 + \eta_S N_2 + \eta_T N_3. \tag{7.3.2}$$

When the incident light is very weak, all of the molecules stay in the ground state, then $N_2 = N_3 = 0$ and $N_1 = N$, the Eq. (7.3.2) becomes

$$n_0 = 1 + \eta_0 N, \tag{7.3.3}$$

where n_0 is the linear refractive index of molecular system, N is the total molecular number density.

As above mentioned in last section, the change of molecular number density of each energy-level with changing the time can be described by the following rate equations:

$$\frac{\partial N_2}{\partial t} = \frac{\sigma_0 I N_1}{\hbar\omega} - \frac{N_2}{\tau_S} - \frac{N_2}{\tau_{ST}}, \tag{7.3.4}$$

$$\frac{\partial N_3}{\partial t} = \frac{N_2}{\tau_{ST}} - \frac{N_3}{\tau_T}, \tag{7.3.5}$$

$$N_1 + N_2 + N_3 = N, \tag{7.3.6}$$

If pulsewidth of the incident laser is much bigger than the all of the energy-level live times of the molecular system, we can regard that the interaction between light and molecular system as a steady-state process. It means $\partial/\partial t = 0$ in the above rate equations, and we don't need to consider the variation of the laser intensity, instead taking its peek intensity of I, we can solve the Eqs. (7.3.4)–(7.3.5) to get the following variables N_1, N_2 and N_3:

$$N_1 = \frac{N}{1 + (A + B)I'}, \tag{7.3.7}$$

$$N_2 = \frac{ANI'}{1 + (A + B)I'}, \tag{7.3.8}$$

$$N_3 = \frac{BNI'}{1 + (A + B)I'}, \tag{7.3.9}$$

where $I' \equiv \frac{I}{I_c}, I_c \equiv \frac{\hbar\omega}{\sigma_0 \tau_S}$ is the saturation intensity, and

$$A \equiv \frac{\tau_{\mathrm{ST}}}{\tau_{\mathrm{ST}} + \tau_{\mathrm{S}}}, \tag{7.3.10}$$

$$B \equiv \frac{\tau_{\mathrm{T}}}{\tau_{\mathrm{ST}} + \tau_{\mathrm{S}}}. \tag{7.3.11}$$

Substituting Eqs. (7.3.7)–(7.3.9) into Eqs. (7.2.3), the total refractive-index of the system can be written as

$$n = 1 + \frac{\eta_0 + (A\eta_{\mathrm{S}} + B\eta_{\mathrm{T}})I'}{1 + (A + B)I'} N. \tag{7.3.12}$$

From Eq. (7.3.12) we can see, when the light is strong enough, not only the ground-state, but also the excited-states in singlet and triplet systems, all have contributions to the total refractive -index of the system. However, when the light is very weak ($I << I_c$) i.e., $I' \to 0$, the total refractive -index then becomes a linear refractive-index, i.e., $n_0 = 1 + \eta_0 N$.

We should say that the contributions of the singlet excited-state and the triplet excited-states to the total refractive index are different. The size of their contribution

depends on the parameter values of A and B. From Eqs. (7.3.10) and (7.3.11) we can see, if $\tau_{ST} >> \tau_S$ and τ_T , then $A \approx 1$, and $B \approx 0$. In this case molecules cannot jump to the triplet-state from the singlet-state. The nonlinear refractive index of the system is mainly induced by the singlet first excited-state. The five-level model is degenerated to the three-level model, as shown in Fig. 7.18b. Thus Eq. (7.3.12) becomes

$$n = 1 + \frac{1 + (\eta_S/\eta_0)I'}{1 + I'}\eta_0 N, \tag{7.3.13}$$

where $I' \equiv \frac{I}{I_c}$ and $I_c \equiv \frac{\hbar\omega}{\sigma_0\tau_S}$.

If $\tau_{ST} << \tau_S$ and τ_T, then $A \approx 0$ and $B \approx \tau_T/\tau_S$. In this case, most of molecules transit to the triplet-state from the singlet-state. The nonlinear refractive index of the system is mainly induced by the triplet first excited-state. The five-level model is also degenerated to another three-level model, as shown in Fig. 7.18a. Thus Eq. (7.3.12) becomes

$$n = 1 + \frac{1 + (\eta_T/\eta_0)I''}{1 + I''}\eta_0 N, \tag{7.3.14}$$

where $I'' \equiv \frac{I}{I'_c}$ and $I'_c \equiv \frac{\hbar\omega}{\sigma_0\tau_T}$. This formula is suitable for the majority organic materials. We will discuss it below in detail.

Firstly, we discuss the dependent relation of the refractive index with the light intensity. If light is weak, we have $I << I'_c$, i.e., $I'' << 1$, the refractive index of the system is a linear refractive index: $n_0 = 1 + \eta_0 N$; if the light is very strong, we have $I >> I'_c$, i.e., $I'' >> 1$, the refractive index is a saturable constant: $n = 1 + \eta_T N$. For the middle saturation, the light intensity is $I = I'_c$, i.e. $I'' = 1$, thus $n = [2 + (\eta_0 + \eta_T)](N/2)$.

Secondly, we discuss that how the ratio (η_T/η_0) affects the refractive index of the system. If $\eta_T < \eta_0$, the system refractive index decreases with the increase of the light intensity, this is the case of the saturation refraction (SR). If $\eta_T > \eta_0$, the system refractive index increases with the increase of the light intensity, this is the reverse saturation refraction (RSR). If $\eta_T << \eta_0$, Eq. (7.3.14) for expressing the refractive index of the three-level system will be simplified into a saturation equation for expressing the refractive index of the two-level system, that is

$$n = 1 + \frac{\eta_0 N}{1 + \frac{I}{I_c}}. \tag{7.3.15}$$

We can see that the refractive index decreases with the increase of the light intensity.

As a sample, we investigate the C_{60} in toluene solution under the exposure by a laser at wavelength of 532 nm. The solvent toluene is a linear liquid, its refractive index is

$$n_{S0} = 1 + \eta_{S0} N_S, \tag{7.3.16}$$

where η_{S0} and N_S are the fundamental-state refraction volume and total molecular number density of the solution, respectively. Therefore, the linear refractive index of C_{60} in toluene solution under the weak light is

$$n_0 = 1 + \eta_{S0} N_S + \eta_0 N. \tag{7.3.17}$$

According to Eq. (7.3.14), the refractive-index formula of C_{60} in toluene solution is

$$n = n_{S0} + \frac{1 + (\eta_T/\eta_0) I''}{1 + I''} \eta_0 N. \tag{7.3.18}$$

We take the following data for C_{60} in toluene solution: $\sigma_0 = 2.87 \times 10^{-18}\,\mathrm{cm}^2$, $\sigma_S = 1.57 \times 10^{-17}\,\mathrm{cm}^2$, $\tau_S = 30\,\mathrm{ns}$, $\tau_T = 280\,\mu\mathrm{s}$, $\tau_{ST} = 1.2\,\mathrm{ns}$, $N = 1.68\times10^{18}/\mathrm{cm}^3$, $\eta_0 = 8.44 \times 10^{-22}\,\mathrm{cm}^3$, $I'_c = 460\,\mathrm{W/cm}^2$, to calculate and obtain $n_0 = 1.4984$.

Figure 7.22 presents a group of the curves of the refractive index of C_{60} in toluene solution as a function of the intensity. The curves of 1, 2, 3, 4, 5 are corresponding to $\eta_T = 12.66 \times 10^{-22}\,\mathrm{cm}^3$, $10.55 \times 10^{-22}\,\mathrm{cm}^3$, $8.44 \times 10^{-22}\,\mathrm{cm}^3$, $6.33 \times 10^{-22}\,\mathrm{cm}^3$, 4.22×10^{-22} cm or $(\eta_T/\eta_0) = 1.50, 1.25, 1.00, 0.75, 0.50$. Among these, Curves 1 and 2 belong to $\eta_T > \eta_0$, i.e., the reverse saturable refraction; Curves 4 and 5 belong to $\eta_T < \eta_0$, i.e., the saturable refraction; Curve 3 belongs to $\eta_T = \eta_0$, the refractive index is n_0, which does not change with the optical intensity.

7.3.2 *Physical Significance of Sign Symbol of Nonlinear Refraction Coefficient*

The refractive index of optical Kerr medium can be express as $n = n_0 + \Delta n = n_0 + n_2 I$, where n_2 is nonlinear refraction coefficient. The value of n_2 can be positive or negative for different materials. How to explain the sign symbol of nonlinear refraction coefficient n_2? Now we try to answer this question.

Because $n_0 = 1 + \eta_0 N$ and $n = n_0 + \Delta n$, using Eqs. (7.3.13) and (7.3.14) obtaining from the singlet and triplet models respectively, we can deduce to get the refractive-index change i.e., the nonlinear refractive index of a three-level system:

$$\Delta n = \frac{(\eta_s - \eta_0) N I'}{1 + I'}, \tag{7.3.19}$$

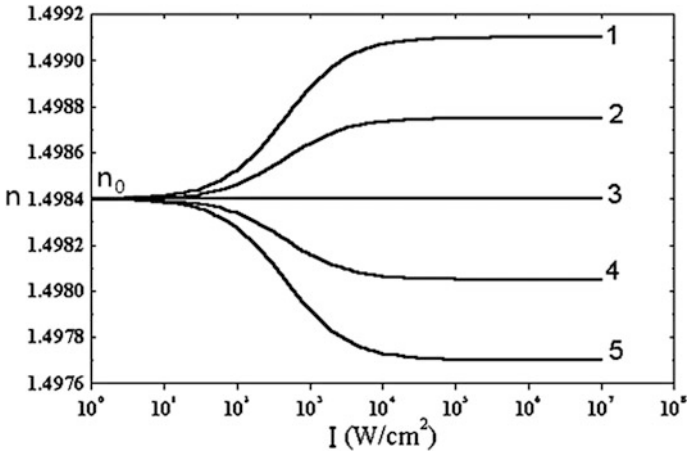

Fig. 7.22 The refractive index as a function of optical intensity for five energy-level of C_{60} in toluene solution, *Curves* of 1, 2, 3, 4, 5 are corresponding to (η_T/η_0) = 1.50, 1.25, 1.00, 0.75, 0.50

$$\Delta n = \frac{(\eta_T - \eta_0)NI''}{1 + I''}. \tag{7.3.20}$$

When $I \ll I_c$, i.e., $I' \ll 1$; or $I \ll I'_c$, i.e., $I'' \ll 1$. Taking Taylor series expansion for Eqs. (7.3.19) and (7.3.20) and only keeping the linear approximation item, the refractive-index change will be

$$\Delta n = \frac{(\eta_S - \eta_0)N}{I_c} I, \tag{7.3.21}$$

$$\Delta n = \frac{(\eta_T - \eta_0)N}{I'_c} I. \tag{7.3.22}$$

Equations (7.3.21) and (7.3.22) show the Kerr effect of the singlet and the triplet system respectively.

Now we obtain the microscopic expressions of nonlinear refraction coefficient n_2, for the singlet system with three-level model, which is

$$n_2 = \frac{(\eta_S - \eta_0)\sigma_0 \tau_S N}{\hbar\omega}; \tag{7.3.23}$$

for the triplet-system with three-level model, which is

$$n_2 = \frac{(\eta_T - \eta_0)\sigma_0 \tau_T N}{\hbar\omega}. \tag{7.3.24}$$

Equations (7.3.23) and (7.3.24) point out that the sign symbol of n_2 depends on the difference between the excited-state refraction volume η_S or η_T and the ground-state refraction volume η_0. If $\eta_S < \eta_0$ or $\eta_T < \eta_0$, namely the system is dominated in the saturable refraction, n_2 is negative; on the contrary, if $\eta_S > \eta_0$ or $\eta_T > \eta_0$, namely the system is dominated in the reverse saturable refraction, n_2 is positive. For example, most of liquid molecular systems far from the resonance belong to the reverse saturable refraction with the positive n_2; however, the compound semiconductors at the exciton-resonance area, such as GaAs, belong to the saturable refraction with the negative n_2. Apparently this judgment should be proved by more experimental results with multiple different materials.

Review Questions of Chapter 7

1. Please deduce the absorption coefficient formula for third-order nonlinear absorption, and explain the relationship between the absorption coefficient and the transmittance of light intensity.
2. What is the two-photon absorption? Please deduce the formula of relationship between two-photon absorption coefficient and the light intensity. How to measure the two-photon absorption coefficient of semiconductor? What is the influence of the free-carrier absorption in this measurement?
3. What is the difference between two nonlinear-refractive-index formulas under two-photon absorption and single-photon absorption (i.e. optical Kerr effect) for the semiconductor?
4. According to two-level and three-level models of molecular systems, to derive the absorption coefficient formulas of the saturated absorption, and explain the reason of absorption-saturation phenomenon in these two molecular models.
5. Why two absorption-coefficient formulas for saturated absorption and third-order nonlinear absorption are different? What the relationship between these two effects is?
6. What is the reverse-saturated absorption? Starting from the five-level model of molecule system to analysis the causes of the saturated absorption; and to deduce the absorption coefficient formula for reverse-saturated absorption under the steady-state condition. Under what conditions the contribution of singlet- or triplet-excited-state absorption is dominate?
7. What is the nonlinear grating-type optical limiter? Please explain the role of reverse-saturated absorption in this limiter.
8. What is the reverse-saturation refraction? Please write down the refractive-index formulas considering the transition between excited states and the linear approximation formula under weak light intensity. From these formulas to explain the physical meaning of the sign symbol of nonlinear refraction coefficient n_2.

References

1. W. Kaiser, C.G.B. Garrett, Two-photon excitation in $CaF_2 \cdot Eu^{3+}$. Phys. Rev. Lett. **7**(6), 229–231 (1961)
2. F.R. Laughton, J.H. Marsh, Intuitive model to include the effect of free-carries absorption in calculating the two-photon absorption coefficient. Appl. Phys. Lett. **60**, 166–168 (1992)
3. R.A. Soref, B.R. Bennett. Electro optical effects in silicon. IEEE. J Quant. Electron QE-**23**(1), 123–129 (1987)
4. A. Szoke, A. Javan, Isotope shift and saturation behavior of the 1.15−μ transition of Ne. Phys. Rev. Lett. **10**(12), 521–524 (1963)
5. M. Hereher, W. Chu, D.L. Stockman, An experimental study of saturable absorbers for ruby lasers. IEEE J. Quant. Electr. **4**(11), 954–968 (1968)
6. H.M. Gibbs, *Optical Bistability: Controlling Light with Light* (Academic Press, NY, 1985)
7. C. Li, R. Zhang, Research progress of nonlinear optical absorptions. Physics (in Chinese) **23** (12), 705–710 (1994)
8. L.W. Tutt, S.W. McCahon, Reverse saturable absorption in metal cluster compounds. Opt. Lett. **15**(12), 700–702 (1990)
9. C. Li, L. Zhang, R. Wang, Y. Song, Y. Wang, Dynamics of reverse saturable absorption and all-optical switching in C_{60}. J. Opt. Soc. B **11**(8), 1356–1360 (1994)
10. C. Li, L. Zhang, M. Yang, H. Wang, Y. Wang, Dynamic and steady-state behaviors of reverse saturable absorption in metallophthalocyanine. Phys. Rev. A **49**(2), 49–57 (1994)
11. C. Li, J. Si, M. Yang, R. Wang, L. Zhang, Excited-state nonlinear absorption in multi-energy-level molecular systems. Phys. Rev. A **51**(1), 569–575 (1995)
12. J. Si, M. Yang, Y. W, Lei Z, C. Li, Nonlinear absorption in metallo-porphyrin-like. Opt. Commun. **109**, 487–491 (1994)
13. J. Si, M. Yang, Y. Wang, C. Li, Nonlinear excited-state absorption in Cadmium Texaphyrin solution. Appl. Phys. Lett. **64**(23), 3083–3085 (1994)
14. X. Deng, X. Zhang, Y. Wang, Y. Song, S. Liu, C. Li, Intensity threshold in the conversion from reverse saturable absorption to saturable absorption and its application in optical limiting. Opt. Commum. **168**, 207–212 (1999)
15. C. Li, R. Wang, H.-K. Liu, Nonlinear optical limiters with grating sandwich structure for eye protection. J. Non. Opt. Phys. Mater. **9**(4), 413–422 (2000)
16. C. Li, Y. Wang, G. Fang et al., The wideband optical limiter in nonlinear liquid sandwiched between two gratings. Acta. Optica. Sinica. **19**(3), 407–413 (1999)
17. F. Li, X. Yang, Y. Song, S. Liu, C. Li, Optical Limiting and Excited-state nonlinear optical properties in Lead Phthalocyanine. Chin. J. Laser B **6**(5), 424–428 (1997)
18. Y. Song, G. Fang, Y. Wang, S. Liu, C. Li, Optical limiting properties of fullerene derivatives. Appl. Phys. Lett. **74**(3), 332–334 (1999)
19. C. Li, X. Deng, Y. Wang, Nonlinear absorption and refraction in multilevel organic molecular system. Chin. Phys. Lett. **17**(8), 574–576 (2000)
20. C. Li, Y. Wang, X. Zhang, Nonlinear refraction in multilevel molecular systems. Chin. Phys. **9** (3), 194–197 (2000)

Chapter 8
Optical Bistability and Its Instability

This chapter studies the property of the nonlinear optical system with feedback—optical bistability. We will discuss firstly the basic conception of optical bistability; secondly, the working principles of typical optical bistable devices (OBD) including two kinds of all-optical OBDs: nonlinear F–P etalons filled with the saturable absorption material and optical Kerr material, and three kinds of electro-optical hybrid OBDs: electro-optical F–P etalon, electro-optical M–Z interferometer, and electro-optical polarization modulation; finally, the theoretical analysis of stability problems of optical bistability, including the stability condition of optical bistability system, and two kinds of optical instability: the optical pulsation in the double feedback system and the optical chaos in the feedback delayed system.

8.1 Introduction to Optical Bistability

8.1.1 Basic Conception of Optical Bistability [1–4]

1. **Definition of Optical Bistability**

If an optical system under a given incident light intensity (I_{i0}) exists two possible transmitted light intensities (I_{t1} and I_{t2}), and a recoverable and fast switching conversion between these two intensity states can be realized, then we say that this system possesses optical bistability (OB), as shown in Fig. 8.1.

Figure 8.2 shows the characteristic curve for describing the relation of input intensity and output intensity ($I_t - I_i$ curve) of the optical bistability system. It is clear that the transmitted light intensity is a two-value (or multiple-value) function of the incident light intensity.

© Shanghai Jiao Tong University Press,
Shanghai and Springer Nature Singapore Pte Ltd., 2017

C. Li, *Nonlinear Optics*, DOI 10.1007/978-981-10-1488-8_8

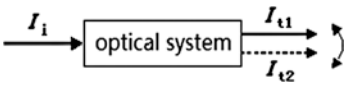

Fig. 8.1 Schematic diagram of the definition of optical bistability

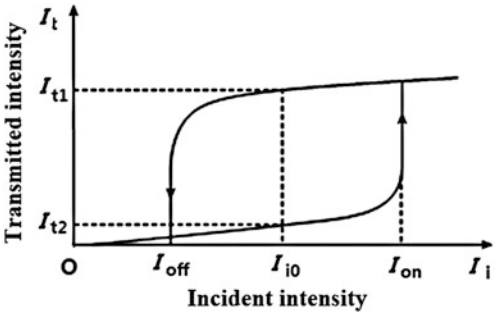

Fig. 8.2 Characteristic *curve* of optical bistability

The characteristic curve of optical bistability is a hysteresis loop similar to ferromagnetism loop or ferroelectricity loop. The characteristic curve of OB has following two properties:

(1) **Retardation**:
In the two intensity stable states, the transmitted light change always lags behind the incident light change. This retardation is arising from the negative feedback in the system; the negative feedback determines the bistability of system.

(2) **Mutability**:
The two stable states of transmitted light intensity can be rapid interconversion, this mutability is arising from the positive feedback of system; the positive feedback determines the fast switching characteristic of system.
In short, the feedback in optical bistability plays an important role. The optical bistability, in general, is the bistability of light intensity (or light power), sometimes this conception of bistability can be expand to other physical quantities, such as frequency etc.

2. **Composition of Optical Bistable Devices**

The optical device with optical bistability is called Optical Bistable Device (OBD). OBD is a kind of nonlinear optical devices, which are based on both factors: the nonlinear medium and the feedback mechanism, as shown in Fig. 8.3.

The typical OBD is an F–P etalon filled with the nonlinear medium, as shown in Fig. 8.4. The feedback is completed by two reflective mirrors of F–P cavity.

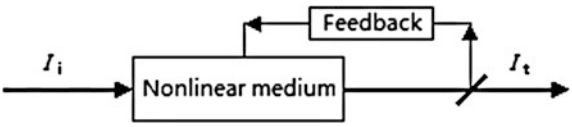

Fig. 8.3 Composition principle of optical bistable device

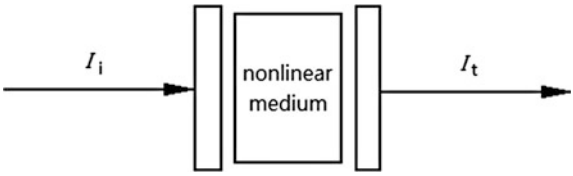

Fig. 8.4 Optical bistable device consisted of a nonlinear F–P etalon

Table 8.1 Comparison between OBD and laser

Similarities	Differentia	
	OBD	Laser
Cavity feedback	Negative/positive feedback	Positive feedback
Optical medium	Nonlinear medium (passive)	Gam medium (active)
Radiation characteristic	Superradiation	Stimulated radiation
Nonequilibrium phase transition	First class	Second class

The F–P type optical bistable device looks like a laser. As we known that the laser is consisted of three elements: the gain medium, the optical resonant cavity, and the pump energy source. The composition of OBD also has three elements: the nonlinear medium, the feedback system and the input energy.

A comparison between the optical bistable device and the laser is shown in Table 8.1. Both of them have some similarities and differentia. For example, both have an optical resonator to provide a feedback for enhancing the interaction between light and medium. But the medium placed in the cavity is different: for laser, it is an active medium with gain, but for OBD, it is a passive nonlinear medium; and the action of optical resonator is different: for laser, it only needs a positive feedback, to guarantee a stable laser oscillation output; but for OBD, it need a negative feedback to obtain two positive stable outputs, and also need a positive feedback to realize the fast switching between two states. In addition, both of them all produce the light radiation, but both of radiations are different, for laser, it is a stimulated radiation; for OBD, it is a superradiation; from physical point view, both of them are belong to the nonequilibrium phase-transition system, but the laser is a second-class nonequilibrium phase-transition system, and OBD is a first-class nonequilibrium phase-transition system.

8.1.2 Classification of Optical Bistable Device

Classified by feedback methods, the OBD is mainly divided into two kinds: the intrinsic optical bistable device and the hybrid optical bistable device.

1. **Intrinsic OBD**

The intrinsic OBD is based on the all-optical feedback; it is also called the all-optical OBD. The typical intrinsic OBD is a nonlinear F–P etalon, which is an

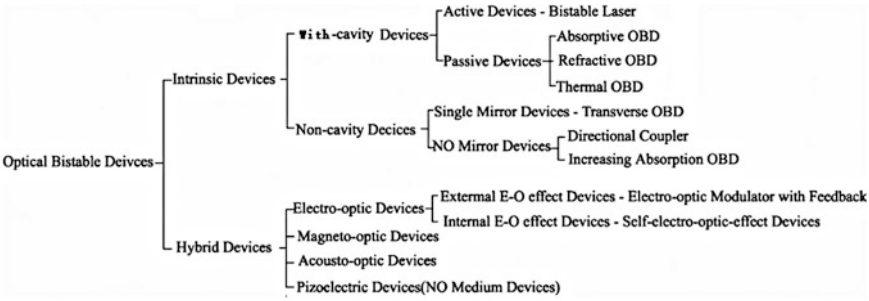

Fig. 8.5 Classification of optical bistable device

F–P etalon containing a nonlinear medium, as shown in Fig. 8.4. According to the different mechanism of nonlinear medium, the intrinsic OBD can be further divided into three types:

1. Absorption OBD, which is caused by the light-induced nonlinear absorption coefficient change, i.e., $\Delta\alpha(I)$.
2. Refraction OBD, which is caused by the light-induced nonlinear reflective-index change i.e., $\Delta\alpha(I)$, it also called the dispersion OBD.
3. Thermal OBD, which is caused by the thermal-induced nonlinear refractive-index change, it also can sum up as the refraction OBD.

2. **Hybrid OBD**

The hybrid OBD is based on a mixed feedback, which is a combination of optical feedback and another physical feedback mechanism, such as the electro-optic feedback, the magneto-optic feedback, acousto-optic feedback, etc. The typical electro-optic hybrid OBD is an electro-optic crystal modulator inside an interferometer (see Sect. 8.2.2).

Optical bistable device has a great variety, in addition to classify by feedback method and the nonlinear mechanism, the all-optical OBD can be divided into with-cavity and non-cavity. The with-cavity OBD includes active type and passive type, and the non-cavity OBD can be divided into single mirror device and without mirror device (due to internal feedback mechanism). The electro-optic hybrid OBD can be divided into the external electro-optic effect device and the internal electro-optic effect device. The classification of optical bistable device is shown in Fig. 8.5.

8.2 Optical Bistable Device

8.2.1 *Principle of F–P Etalon Intrinsic Optical Bistable Device*

1. **F–P Etalon Absorption Optical Bistable Device**

The typical absorption OBD is constituted by placing the saturable absorption medium (absorber) in the F–P resonant cavity, as shown in Fig. 8.6, where I_i and I_t are incident and transmitted light intensities, respectively, and I is the light intensity in the medium inside the cavity.

We have mentioned before the absorption coefficient of the saturable absorption medium is

$$\alpha = \frac{\alpha_0}{1 + (I/I_c)}, \tag{8.2.1}$$

where α_0 is the linear absorption coefficient; $\boldsymbol{I}$ is the light intensity in the medium; I_c is the saturable intensity. The Eq. (8.2.1) shows that the absorption coefficient α decreases with the increase of light intensity $\boldsymbol{I}$. When the $\boldsymbol{I}$ reaches $I_c, \alpha = \alpha_0/2$.

In 1969 Szöke et al. [5] gave a theoretical model of absorption OB, they analyzed the light electrical-field distribution in absorption F–P etalon OBD, as shown in Fig. 8.7.

The F–P cavity is filled with the absorption medium. The absorption coefficient of absorption medium is α (here do not consider the refraction and the dispersion). Assuming the interval between two mirrors of F–P cavity is L, the reflectivity and the transmittance of mirrors are R and T respectively, and the frequency of incident laser is equal to the resonant frequency of F–P cavity. To denote the incident,

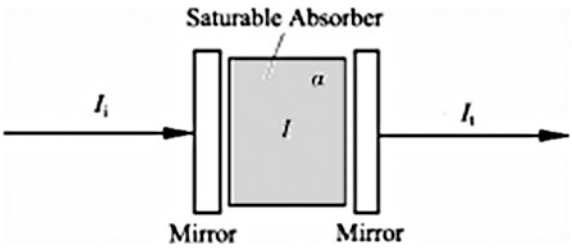

Fig. 8.6 F–P etalon absorption optical bistable device

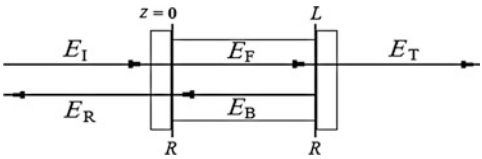

Fig. 8.7 Light electrical-field distribution in F–P etalon absorption OBD

reflection, forward, backward and transmitted electric-field amplitude as $E_{\mathrm{I}}, E_{\mathrm{R}}, E_{\mathrm{F}}, E_{\mathrm{B}}, E_{\mathrm{T}}$ respectively, then at $z = 0$, the relationship among these electric-field amplitudes can be expressed as

$$E_{\mathrm{F}}(0) = \sqrt{T}E_{\mathrm{I}} + Re^{-(\alpha/2)2L}E_{\mathrm{F}}(0) = \sqrt{T}E_{\mathrm{I}} + Re^{-\alpha L}E_{\mathrm{F}}(0) \tag{8.2.2}$$

Equation (8.2.2) can be written to

$$\frac{E_{\mathrm{F}}(0)}{E_{\mathrm{I}}} = \frac{\sqrt{T}}{1 - Re^{-\alpha L}}. \tag{8.2.3}$$

Because $\alpha L << 1, e^{-\alpha L} \approx 1 - \alpha L$ and $1 - R = T$, then Eq. (8.2.3) can be written to approximately:

$$\frac{E_{\mathrm{F}}(0)}{E_{\mathrm{I}}} \approx \frac{\sqrt{T}}{1 - R(1 - \alpha L)} = \frac{1}{\sqrt{T}(1 + k)}, \tag{8.2.4}$$

where

$$k \equiv \frac{R\alpha L}{1 - R}. \tag{8.2.5}$$

According to Eq. (8.2.1), we have

$$\alpha = \frac{\alpha_0}{1 + I_{\mathrm{F}}/I_c}. \tag{8.2.6}$$

Substituting Eq. (8.2.6) into Eq. (8.2.5), then we obtain

$$k = \frac{k_0}{1 + I_{\mathrm{F}}/I_{\mathrm{c}}}, \tag{8.2.7}$$

where

$$k_0 = \frac{R\alpha_0 L}{1 - R}. \tag{8.2.8}$$

At $z = L$, the relationship of electric-field amplitudes E_{T} and E_{F} is given by

$$E_{\mathrm{T}} = \sqrt{\mathrm{T}}E_{\mathrm{F}}(L) = \sqrt{T}e^{-\alpha L/2}E_{\mathrm{F}}(0) \approx \sqrt{T}E_{\mathrm{F}}(0). \tag{8.2.9}$$

Combing Eqs. (8.2.9) and (8.2.4), we obtain

$$\frac{E_{\mathrm{I}}}{E_{\mathrm{T}}} = 1 + k. \tag{8.2.10}$$

Using Eqs. (8.2.10) and (8.2.7), and $I_{\mathrm{T}} \propto |E_{\mathrm{T}}|^2, I_{\mathrm{I}} \propto |E_{\mathrm{I}}|^2$, we obtain

$$\frac{I_{\mathrm{I}}}{I_{\mathrm{T}}} = (1 + \mathrm{k})^2 = \left(1 + \frac{k_0}{1 + I_{\mathrm{T}}/TI_{\mathrm{c}}}\right)^2. \tag{8.2.11}$$

Defining the normalized incident light intensity $X \equiv I_{\mathrm{I}}/TI_{\mathrm{c}}$ and the normalized transmitted light intensity $Y \equiv I_{\mathrm{T}}/TI_{\mathrm{c}}$, Eq. (8.2.11) can be written as

$$X = Y\left(1 + \frac{k_0}{1 + Y}\right)^2. \tag{8.2.12}$$

This is a cubic curve of transmitted light intensity Y; it has the inflection point and the negative slope region, so the system could possess the optical bistability.

Taking different k_0, we can calculate to get a group of relationship curves between the normalized transmitted light intensity and the normalized incident light intensity, i.e., optical bistability curves, as shown in Fig. 8.8.

From Fig. 8.8 we can see, the condition for generating the optical bistability (or negative slop region) is

$$k_0 \equiv \frac{R\alpha_0 L}{1 - R} > 8. \tag{8.2.13}$$

Because $1 - R = T$ and $R \approx 1$, the threshold condition of absorption OB can be express as

$$\frac{\alpha_0 L}{T} > 8. \tag{8.2.14}$$

Here T is transmitted loss of reflective mirror. That is to say, the generation of optical bistability requires the single-trip linear absorption loss of medium in the

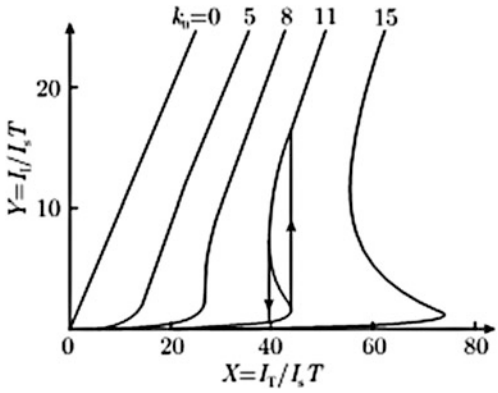

Fig. 8.8 Optical bistability *curves* of F–P etalon absorption OBD under different k_0

cavity greater than the transmittance of reflective mirror in eight times. Here mentioned linear absorption loss actually is nonlinear absorption loss under minimum low light intensity, because from Eq. (8.2.6) we can see that when $I_F \approx 0, \alpha \approx \alpha_0$; and the transmittance of reflective mirror is the cavity loss when without medium in cavity.

Because the finesse of F–P interferometer is

$$F = \frac{\pi\sqrt{R}}{T}, \tag{8.2.15}$$

The threshold condition of absorption OB also can be expressed as

$$(\alpha_0\sqrt{R}F/\pi) > 8. \tag{8.2.16}$$

Obvious, increasing the finesse of F–P interferometer, the reflectivity of cavity mirror and the linear absorption coefficient of material, it is benefit to satisfy the threshold condition of absorption OB.

In the beginning scientists observed the absorption OB according to above condition, they did not find the optical bistability, hence scientists guessed that maybe there is a kind of background absorption coefficient α_B to stop the generation of the optical bistability. This background absorption coefficient comes from the excited state absorption or the non-resonant absorption of other transition process. Because the action of $\alpha_B L$ can be regarded as a cavity own loss similar to the transmitted loss T. Considering the effect of background absorption, the Eq. (8.2.14) can be rewritten as

$$\frac{\alpha_0 L}{T + \alpha_B \mathrm{L}} > 8. \tag{8.2.17}$$

That is to say, for a certain linear absorption loss of medium in cavity, when decreasing the transmittance of cavity mirror and the background absorption of medium, it is advantageous to generate the absorption optical bistability.

2. **F–P Etalon Refraction Optical Bistable Device**

The typical refraction (dispersion) intrinsic OBD is an F–P etalon filled with an optical Kerr medium, as shown in Fig. 8.9. Setting the incident intensity is ***I*i,** the

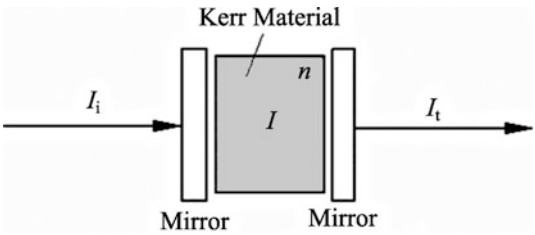

Fig. 8.9 F–P etalon refraction optical bistable device

transmitted intensity is ***I*t,** the intensity inside the medium in the cavity is I, the length of F–P cavity is L, and the reflectivity of each mirror is R.

For the optical Kerr medium, the refractive index of medium is a linear function of the light intensity:

$$n = n_0 + n_2 I, \tag{8.2.18}$$

where n_0 is the linear refractive index of medium, n_2 is the nonlinear refraction coefficient. I is light intensity inside the medium in F–P cavity, which can be approximately expressed as

$$I \approx \left(\frac{1+R}{1-R}\right) I_t, \tag{8.2.19}$$

where I_t is the transmitted light intensity of F–P cavity; R is the reflectivity of the reflective mirror of F–P cavity. Substituting Eq. (8.2.19) into Eq. (8.2.18), then we obtain

$$n = n_0 + n_2 \left(\frac{1+R}{1-R}\right) I_t. \tag{8.2.20}$$

Figure 8.10 plots the optical paths of F–P interferometer based on multi-beam interference.

Setting the cavity length of F–P interferometer is L, the phase difference between two adjacent transmitted lights, i.e., a round-trip phase shift, which is

$$\phi = \frac{2\pi}{\lambda} n(2L) = \frac{4\pi}{\lambda} nL. \tag{8.2.21}$$

Substituting Eq. (8.2.20) into Eq. (8.2.21), we obtain

$$\phi = \phi_0 + \phi_2 I_t, \tag{8.2.22}$$

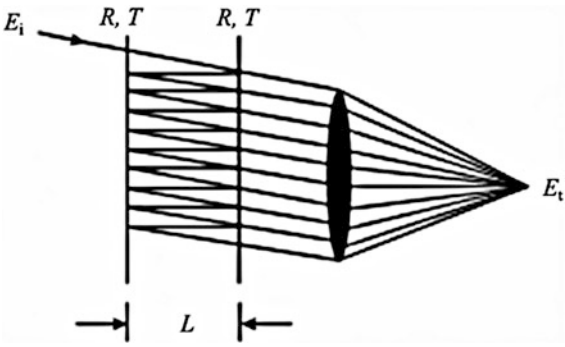

Fig. 8.10 Schematic diagram of the multi-beam interference for F–P interferometer

where ϕ_0 is the light phase shift for a round-trip in the cavity when $I_t \approx 0$ (or the initial phase shift):

$$\phi_0 = \frac{4\pi}{\lambda} n_0 L. \tag{8.2.23}$$

ϕ_2 is a constant related with the nonlinear refraction coefficient n_2:

$$\phi_2 = \frac{4\pi}{\lambda}\left(\frac{1+R}{1-R}\right) n_2 L. \tag{8.2.24}$$

From Eq. (8.2.22), the relationship between the transmittance of device τ and the phase shift of light ϕ is

$$\tau = \frac{I_t}{I_i} = \frac{\phi - \phi_0}{\phi_2 I_i}. \tag{8.2.25}$$

Here the relationship of τ and ϕ is a straight line,the slope of straight line is depended on the reciprocal of the incident light intensity. We call Eq. (8.2.25) the feedback relation of OB.

According to the characteristic of F–P interferometer, there is another period relationship between the transmittance τ and the phase shift ϕ:

$$\tau = \frac{I_t}{I_i} = \frac{1}{1 + \frac{4R}{T^2}\sin^2\frac{\phi}{2}}, \tag{8.2.26}$$

where R and T is the refractivity and transmittance of the reflective mirror, respectively. If ignoring the absorption, $R + T = 1$. We call Eq. (8.2.26) the modulation relation of OB.

The relationship curve of $\tau - \phi$ for the F–P interferometer is shown in Fig. 8.11. The spacing between two adjacent transmission peaks is 2π, the half peak width is $\delta\phi$, and the initial phase shift is ϕ_0.

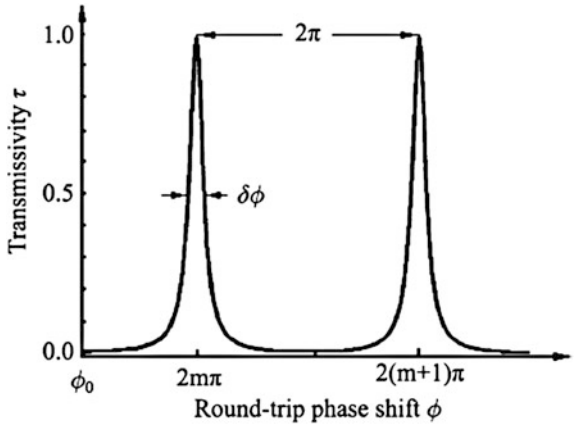

Fig. 8.11 Relationship *curve* of $\tau - \phi$ for the F–P interferometer

In order to solve the simultaneous Eqs. (8.2.25) and (8.2.26), we can use a graphing method to find the intersection points of two curves described by these two equations, as shown in Fig. 8.12. When we gradually increase the incident intensity, from Eq. (8.2.25) we can see, the slope of the line is gradually reduced, so that the intersection points are moving along $a - 1 - b - c$ in turn. Inversely, when we gradually decrease the incident intensity, the slope of the line is gradually increased. The intersection points are moving along $c - 3 - d - a$ in turn.

Corresponding to these operating points, we can plot a characteristic curve of the refraction OB, i.e., the transmitted intensity as a function of the incident intensity, as shown in Fig. 8.13.

Connecting the operating points of $a - 1 - b - 2 - d - 3 - c$, we can obtain an S-shape OB loop. We will proof that the S-shape curve $b - 2 - d$(dotted line) with the negative slope is unstable, so that at operating points b and d the device occurs switching on and switching off, respectively. The OBD operating range is between the straight lines of bc and ad. Within this range there are two possible transmitted intensities corresponding to one incident intensity, such as at the incident intensity I_{i0}, there are two transmitted intensities I_{t1} and I_{t3}.

Below we use an analytical method to study the characteristic of refraction OB [6]. At first we rewrite the Eq. (8.2.26) (it is a transcendental function) to be a linear algebraic equation. Because the optical bistability happens near the peak of the $\tau - \phi$ curve $\phi = 2m\pi(m = 0, 1, 2, \cdots)$, were the sinusoidal function can be approximately written as $\sin(\phi/2) \approx \phi/2$, then Eq. (8.2.26) becomes

$$I_i \approx \left(1 + \frac{R\phi^2}{T^2}\right) I_t. \tag{8.2.27}$$

Figure 8.14 shows the $\tau - \phi$ curve at the vicinity of the peak $\phi = 2m\pi(m = 0$ and 1). Because the coordinate origin is at the peak $m = 0$, ϕ and ϕ_0 are all negative, so Eq. (8.2.22) can be rewritten as

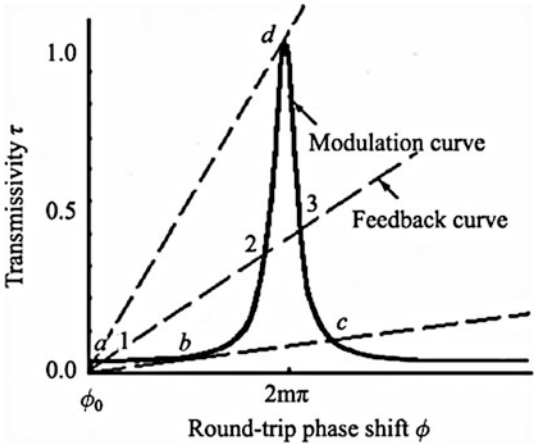

Fig. 8.12 Use of the graphing method to find the operating points of refraction OBD

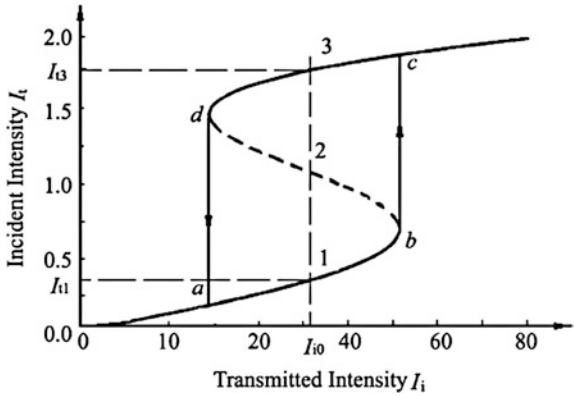

Fig. 8.13 Use of the graphing method to plot the characteristic curve of the refraction OB

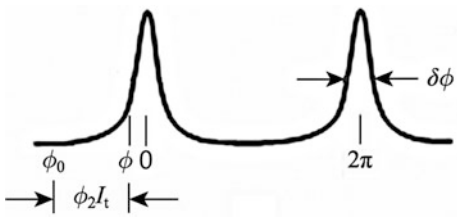

Fig. 8.14 $\tau - \phi$ *curve* at the vicinity of the peak at $\phi = 2m\pi$ (m = 0 and 1)

$$\phi = \phi_0 - \phi_2 I_t. \tag{8.2.28}$$

Substituting Eq. (8.2.28) into Eq. (8.2.27), then we obtain

$$I_i = [1 + \frac{R}{T^2}(\phi_0 - \phi_2 I_t)^2] I_t. \tag{8.2.29}$$

Setting $I_I = \frac{\phi_2}{\phi_0} I_i, I_T = \frac{\phi_2}{\phi_0} I_t$ and $k = \frac{R\phi_0^2}{T^2}$, Eq. (8.2.29) becomes

$$I_I = kI_T^3 - 2kI_T^2 + (1+k)I_T. \tag{8.2.30}$$

This is a cubic equation of I_T. For the different initial phase shift ϕ_0 (i.e., the different $\boldsymbol{k}$) there are different refraction OB curves, as shown in Fig. 8.15 for the reflectivity of cavity mirror R = 0.9. In the figure, ϕ_0 = 0.183 corresponds to the critical OB curve.

In general speaking, the slope of $\frac{dI_T}{dI_I}$ on the each point of optical bistability curve depends on the characteristic of system at that point:

When $0 < \frac{dI_T}{dI_I} \leq 1$, no gain and OB;
When $1 < \frac{dI_T}{dI_I} \leq \infty$, differential gain;
When $-\infty < \frac{dI_T}{dI_I} < 0$, optical bistability.

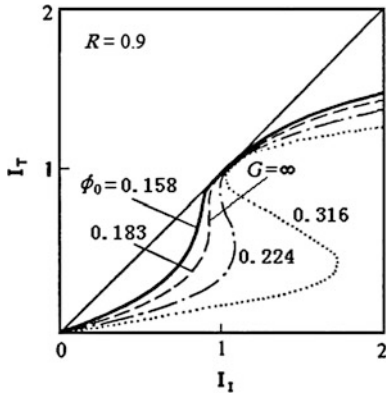

Fig. 8.15 Different refraction OB *curves* (I_t as a function of I_i) for different ϕ_0

So the optical bistability only occurs in the negative slope region of OB curve.

In order to find the threshold conditions for OB, we should take the second derivative: $\frac{d^2 I_I}{dI_T^2} = 0$ to find the inflection point of the OB curve, which is cut-off point between differential gain and optical bistability, were the slope is

$$G = \frac{dI_t}{dI_i} = \infty. \tag{8.2.31}$$

The second derivative to Eq. (8.2.30) is

$$\frac{dI_I}{dI_T} = 3kI_T^2 - 4kI_T + 1 + K$$
$$\frac{d^2 I_I}{dI_T^2} = 6kI_T - 4k = 0$$

Then we obtain the transmitted intensity at the inflection point: $I_T = \frac{2}{3}$. Substituting this value into Eq. (8.2.31):

$$G = \frac{dI_T}{dI_I} = \left(\frac{dI_I}{dI_T}\right)^{-1} = [3kI_T^2 - 4kI_T + 1 + k]^{-1}\Big|_{I_T=\frac{2}{3}} = (1 - \frac{k}{3})^{-1} = \infty$$

We obtain the k value corresponding to the critical OB curve: $k = 3$.

From the definition of $k : k = \frac{R\phi_0^2}{T^2} = 3$, to get the initial phase shift:$|\phi_0| = \frac{\sqrt{3}T}{\sqrt{R}}$. Using the finesse formula of F−P etalon (8.2.15): $F = \frac{\pi\sqrt{R}}{T}$, the initial phase shift for generating OB should be

$$|\phi_0| > \frac{\sqrt{3}\pi}{F}. \tag{8.2.32}$$

Further using the definition of F−P finesse

$$F = \frac{2\pi}{\delta\phi}, \tag{8.2.33}$$

the threshold condition for optical bistability is given by

$$|\phi_0| > \frac{\sqrt{3}\pi}{F} \cong \frac{2\pi}{F} = \delta\phi. \tag{8.2.34}$$

It is clear that in order to realize the refraction OB, we must select the initial phase shift ϕ_0 larger than the half of width of transmitted peak of τ-ϕ curve.

Substituting $I_T = \frac{2}{3}$ and $k = 3$ into Eq. (8.2.28), to obtain $I_I = \frac{8}{9}$, so the transmitted intensity and the incident intensity at the inflection point of OB curve are given by

$$\left.\begin{aligned} I_{tc} &= \tfrac{2}{3}\tfrac{\phi_0}{\phi_2} = \tfrac{2}{3}\tfrac{\sqrt{3}\pi}{\phi_2 F} \\ I_{ic} &= \tfrac{8}{9}\tfrac{\phi_0}{\phi_2} = \tfrac{8}{9}\tfrac{\sqrt{3}\pi}{\phi_2 F} \end{aligned}\right\}. \tag{8.2.35}$$

In conclusion, in order to obtain the bester F–P etalon refraction OB, the following conditions are required:

1. Appropriate choice of the initial phase shift for reducing the threshold intensity;
2. The high F–P finesse is required for reducing the total phase shift;
3. The strong enough incident light intensity is needed for meeting the threshold conditions;
4. The material with large nonlinear refraction coefficient is needed for reducing the threshold intensity.

In 1982 Gibbs et al. presented a first room temperature MQW F–P etalon OBD, as shown in Fig. 8.16 [6]. The MQW etalon consists of 61 periods, each period containing a 34.6 nm-thick GaAs layer and a 40.1 nm-thick $Al_{0.27}Ga_{0.73}As$ layer. The total thickness of GaAs is only 2 μm. The GaAs/AlGaA*s* MQW sample with dielectric coatings on both surfaces is supported by the GaAs substrate. On the top of substrate has an etched hole with 1–2 mm-diameter for laser beam access.

They used a tunable dye laser pumped by a krypton ion laser with wavelength region of 700–870 nm, and chose a light at GaAs exciton absorption peak wavelength as the incident light. The intensity of incident light was modulated by an acousto-optic modulator to be a triangle waveform. The measuring results were displayed by a 500 MHz oscilloscope. The triangle waveform of incident light, the lagging waveform of transmitted light and the output-input OB loop are shown in Fig. 8.17. The switching power density of this switching device was 1 $mW/\mu m^2$ and the switching time of this switching device was 20–40 ns.

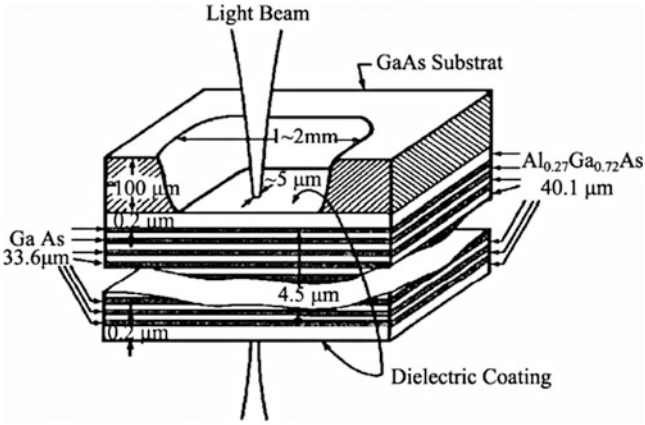

Fig. 8.16 Structure of room-temperature GaAs/AlGaAs MQW etalon OBD

8.2.2 Principle of Electro-Optical Hybrid Optical Bistable Device

In general the electro-optical hybrid OBD is placed an electro-optical modulator into an interferometer to provide the electro-optical mixing feedback. The E–O hybrid OBD has two types: the multi-beam interference type (such as F–P interferometer) and two-beam interference type (such as M–Z interferometer).

1. **Electro-Optical F–P Interferometer OBD** [7]

The experimental setup of electro-optical F–P etalon OBD is shown in Fig. 8.18. A electro-optical crystal modulator with two coated electrodes on two side surfaces is placed into an F–P cavity. The part of transmitted light is converted into the electrical signal by a photodetector. This electrical signal is amplified by an amplifier, and then applies on the electrodes of crystal to modulate the phase of light passing through the E–O crystal. One can use a He – Ne laser beam as the

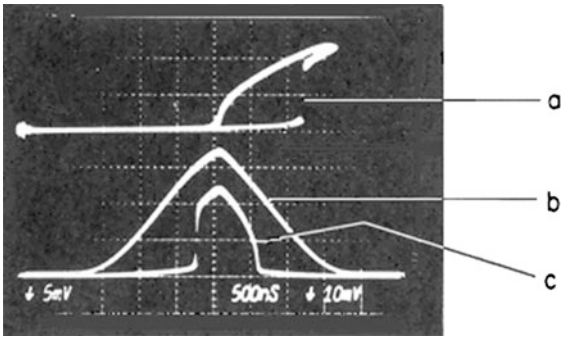

Fig. 8.17 The characteristic curves of GaAs-AlGaAs MQW etalon OBD: **a** OB loop; **b** incident light waveform; **c** outputted light waveform

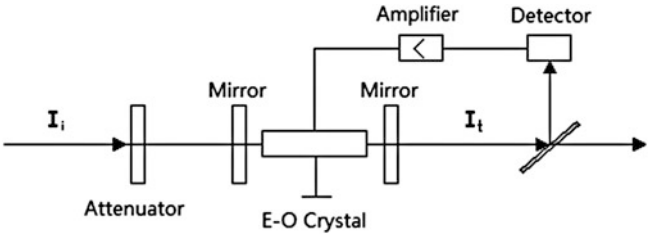

Fig. 8.18 Experimental setup of electro-optical F–P interferometer OBD

incident light, and via an adjustable attenuator to periodically vary the incident light intensity, and use two detectors to receive the input and output light signals respectively, and then convert to be the electrical signals, sending to the oscilloscope for demonstrating the OB characteristic curve.

Considering the loss of crystal, the transmittance of F–P interferometer is given by

$$\tau = \frac{\tau_m}{1 + K\sin^2\frac{\phi}{2}}, \tag{8.2.36}$$

where

$$\tau_m = \left(\frac{1-R}{1-RA}\right)^2 A, \quad K = \frac{4AR}{(1-RA)^2}, \tag{8.2.37}$$

where τ is the transmittance of devise; ϕ is the phase shift of light in a round trip of the cavity; A is the single-pass loss of light propagating in the crystal; R is the refractivity of F–P cavity refractive mirror. Equation (8.2.36) is modulation relation of OB.

If the detector and amplifier are working in the linear region, the output light intensity of device is proportional to the electrical voltage outputted from amplifier, i.e., $I_t \propto V$. This electrical voltage applies on the crystal to generate the Kerr electro-optical effect, inducing the refractive-index change of crystal, so $\Delta n \propto E = V/d$ (d is the thickness of crystal), and the refractive-index change makes the light round-trip phase change: $\Delta\phi = \frac{4\pi}{\lambda}\Delta nL$. Therefore in the whole feedback process, we have $I_t \propto V \propto \Delta\phi$. It can be written to

$$\Delta\phi = \phi - \phi_0 = kI_t. \tag{8.2.38}$$

So $\Delta\phi$ is proportional to the outputted light intensity, k is a ratio coefficient. Then we obtain another $\tau - \phi$ relation:

$$\tau = \frac{I_t}{I_i} = \frac{\phi - \phi_0}{kI_i}. \tag{8.2.39}$$

This $\tau - \phi$ linear relation is the feedback relation of OB.

From Eqs. (8.2.36) and (8.2.39), using the graphing method we can obtain the OB curve, as shown in Fig. 8.13.

2. **Electro-Optical M–Z Interferometer OBD** [8]

Figure 8.19 shows an experimental facility of a fiber type electro-optical M–Z interferometer OBD. Such device is based on the two-light beam interference principle. A $LiNbO_3$ stab waveguide electro-optical modulator is inserted in one of arms of M–Z interferometer, which is used for controlling the phase difference between two light beams on two arms. The realization of the optoelectrical feedback is through the photodetector D_2 and an electrical amplifier. The output electrical voltage adds on the electrodes of the electro-optical crystal modulator. The input light source is a semiconductor laser, which is controlled by an electrical modulation to form an input light with periodic changing intensity. The outputted light intensity and the incident light intensity of device are measured by photodetectors D_1 and D_2 respectively, converted into electrical signals, and sending to the terminals X and Y of oscilloscope. The optical bistability curve ($I_t - \mathrm{I_i}$ curve) is displayed on the screen of the oscilloscope.

The incident light with intensity I_i is divided by coupler C_1 into two lights with intensities I_1 and $I_2, I_1 \approx I_2 = I_\mathrm{i}/2$. Two lights propagate respectively along the two arms of M–Z interferometer, one of them is changed the phase by the electro-optical modulator. Two lights are interference in the coupler C_2, the total transmitted light intensity is given by

$$I_t = \frac{1}{2} I_i \alpha (1 + M \cos \phi), \tag{8.2.40}$$

where ϕ is the phase difference of two lights with intensities of I_1 and I_2; I_i is the incident light intensity; α is a constant depended on the insertion loss of coupler; M is the contrast defined by

$$M = 2\sqrt{I_1 I_2}/(I_1 + I_2). \tag{8.2.41}$$

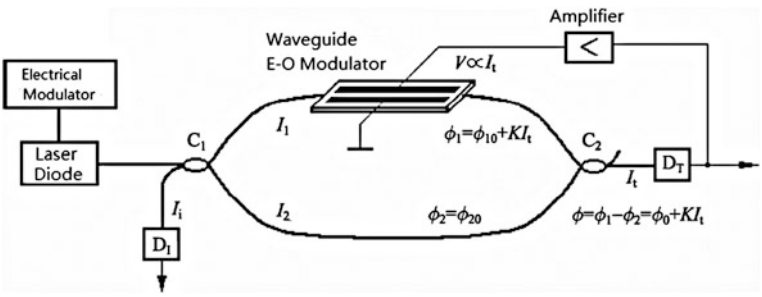

Fig. 8.19 Experimental facility of fiber-type electro-optical M–Z interferometer OBD

The transmittance of this OBD is

$$\tau = \frac{I_t}{I_i} = \frac{\alpha}{2}(1 + M\cos\phi). \tag{8.2.42}$$

Equation (8.2.42) shows the transmittance of device is a function of the phase difference between two lights ϕ, this $\tau - \phi$ relationship is the modulation relation of OBD.

Assuming the initial phase difference is ϕ_0, the outputted light intensity I_t is converted to the electrical voltage signal V by the photodetector D_2, the electrical voltage V is applied on the electrodes of electro-optical modulator to induce the phase difference change:

$$\Delta\phi = \phi - \phi_0 = \pi\left(\frac{V}{V_{1/2}}\right), \tag{8.2.43}$$

where $V_{1/2}$ the half-wave voltage of E–O modulator, its value depends on the length and thick of crystal and electro-optical coefficient of crystal.

Because $V \propto I_t$, so we obtain

$$\phi - \phi_0 = kI_t, \tag{8.2.44}$$

Thus there is a linear relation between transmittance τ and phase difference ϕ:

$$\tau = \frac{I_t}{I_i} = \frac{\phi - \phi_0}{kI_i}, \tag{8.2.45}$$

where k is a constant depended on the detector D_2, amplifier, and parameters of E–O crystal. Equation (8.2.45) described $\tau - \phi$ relationship is the feedback relation of OBD.

Figure 8.20a draws out two $\tau - \phi$ relation curves, from the intersection values of two curves one can obtain $I_t - \mathrm{I_i}$ optical bistability curve, as shown in Fig. 8.20b.

Suppose that the applied voltage of above E–O modulator is high enough, it can let the feedback straight line to reach the second peak of cosine modulation curve, thus it is possible to occur the three intensity stable states, as shown in Fig. 8.21 (Points 1, 2, 3). Of course, if the E–O crystal can sustain higher light intensity, the higher electrical voltage could induce larger phase change, then more number stable intensities appear, i.e., the optical multi-stability.

The OBD based on two light-beam interference principle has other forms, for example, Michelson interferometer OBD [9], in this device, the incident light is divided into two beams by beam splitter (or fiber coupler), and propagate along two orthogonal paths, then reflected back along original paths by two reflective mirrors respectively, they interfere at the beam splitter, the output light signal is converted to electrical voltage signal by a detector, adding the electrical voltage signal on the

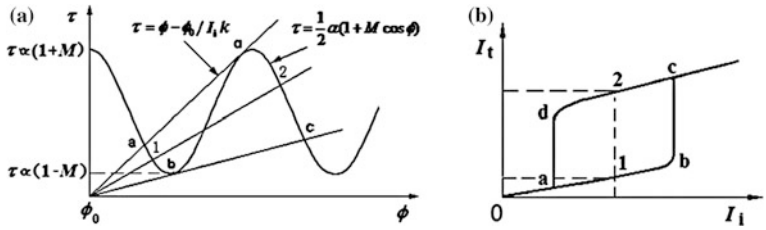

Fig. 8.20 Using graphing method to find OB characteristic curve of O–E hybrid M–Z interferometer OBD: **a** two kinds of $\tau - \varphi$ relationship curves; **b** optical bistability loop

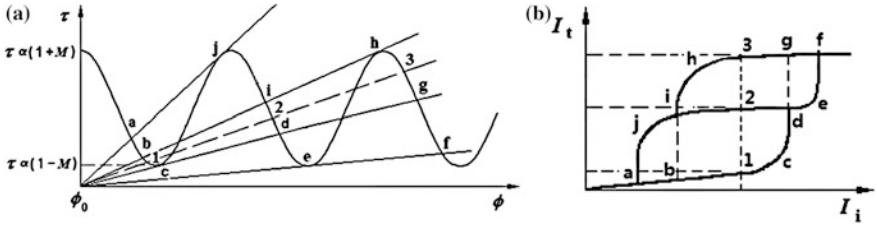

Fig. 8.21 Plotting explain of electro-optical hybrid optical three-stability: **a** $\tau - \phi$ modulation *curve* and feedback *curve*; **b** optical three-stability *curve*

electrodes of E–O crystal that is inserted in one of light path, to change the phase shift between two light beams.

3. **Electro-Optical Polarization Modulation OBD** [10]

Here we introduce a two beam interfere OBD with simplest structure, which only has one light path, do not need interferometer. It is based on the electricity-induced birefringence effect of E–O crystal. When the light beam passes through the E–O crystal, it is divided into two light beams with orthogonal polarization directions, i.e., o-light and e-light, each of them has different refractive index in the crystal. Mutual interference of two beams generates phase difference; this phase difference is modulated by the feedback electrical voltage, which is proportional to the output light intensity. The experimental facility is shown in Fig. 8.22.

The light intensity modulator is constituted by placing an E–O crystal phase modulator between two orthogonal polarizers P_2 and P_3. The detector D_2 receives outputted light signal and converts into the electrical voltage signal, a part of it is sent to the input terminal y of oscilloscope, another part passes through the amplifier A to be amplified, the output voltage signal V is proportional to the output light signal intensity. And via a DC bias V_B (for adjusting the working point) together applied on the electrode of E–O crystal. The input light comes from a He - Ne laser, its intensity signal is received by the detector D_1 and converted into electrical voltage signal sending to the input terminal x of the oscilloscope. Using a continuously rotated

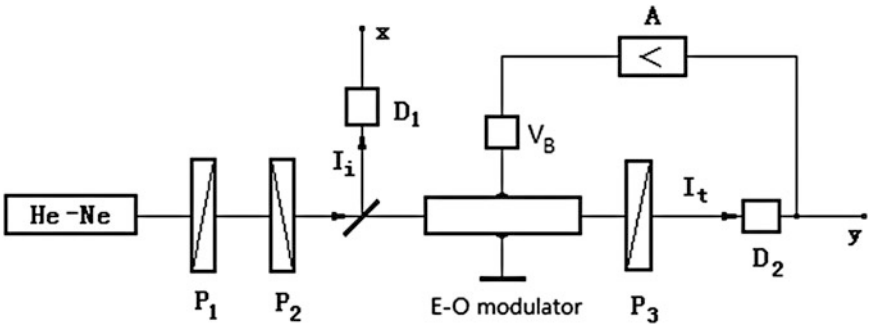

Fig. 8.22 Experimental facility for the electro-optical polarization modulator OBD

polarizer P_1 to make the input light intensity sine-type periodic change, then we can observe the optical bistability curve on the screen of the oscilloscope.

The total voltage applied on the electrode of E–O crystal is

$$\mathrm{V} = k\mathrm{I_t} + V_B. \tag{8.2.46}$$

The transmittance of device is

$$\tau = \frac{I_t}{I_i} = \frac{V - V_\mathrm{B}}{kI_i}. \tag{8.2.47}$$

This is $\tau - V$ feedback relation of OBD.

On the other hand, the relationship of transmittance of E–O modulator τ and the phase difference between two lights ϕ is

$$\tau = \frac{I_t}{I_i} = \frac{1}{2}[1 - \cos\phi]. \tag{8.2.48}$$

In the E–O crystal applied the electrical voltage, o-light and e-light mutual interferes, the phase difference of ϕ is proportional to the modulated voltage V, namely

$$\phi = \pi\frac{V}{V_{1/2}} \tag{8.2.49}$$

where $V_{1/2}$ is the half-wave electrical voltage of E–O crystal.

Substituting Eqs. (8.2.49) into (8.2.48), we obtain

$$\tau = \frac{1}{2}\left[1 - \cos\left(\frac{\pi}{V_{1/2}}V\right)\right], \tag{8.2.50}$$

This is $\tau - V$ modulation relation of OBD.

To combine Eqs. (8.2.48) and (8.2.50), using graphing method, we can obtain optical bistability curve as shown in Fig. 8.23.

Above introduced E–O polarization modulation OBD, because using a lineal simplifier, its feedback curve is a straight line, so the top line of OB loop is not flat. When we used a silicon controlled rectifier to make the amplifier, which has a nonlinear output characteristic, we obtained a nice optical bistability loop, similar to a rectangular loop with a flat output characteristic [10].

8.2.3 Application of Optical Bistable Devices

Optical bistable device has many applications, at first it is used for all-optical switches, which will be the basic device for future all-optical systems, for example, all-optical communication and all-optical computer. In addition, using the stabilization of optical bistability, OBD also can be made the light power stabilizer outside the laser cavity; using the instability of optical bistability, OBD can be made the period controllable light pulse generator, etc.

The more matured application of OBD is used to optical flip flop for optical data storage. Optical flip flop is an intensity-time type switching, its characteristics of the input intensity and the output intensity versus time are shown in Fig. 8.24. The device is working on the high and low power states. In order to switch between two states, it needs two light pulses for switching-on and switching-off of the device.

The working principle of optical flip flop based on optical bistability is shown in Fig. 8.25.

Figure 8.25a is characteristic curve of optical bistability (input power P_t versus output power P_i). Firstly, we need an input light with power P_0 in the center of bistable region P_{off}–P_{on}, to keep the device working in the two output power states: P_H (high state) and P_L (low state). This input power is called the maintaining light. Secondly, in order to switch the device between two output power states, we need another two input light pulses: switch-on pulse and switch-off pulse. At moment t_{on}, we send the switch-on pulse with positive peak power larger than P_{on}–P_o. After staying on high state for a period time, at the moment t_{off}, we send a switch-off

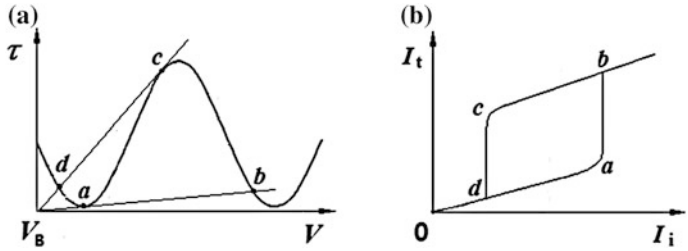

Fig. 8.23 Use of graphing method to find optical bistability curve of E–O polarization modulation OBD: **a** Two kinds of $\tau - V$ curves; **b** Optical bistability *curve*

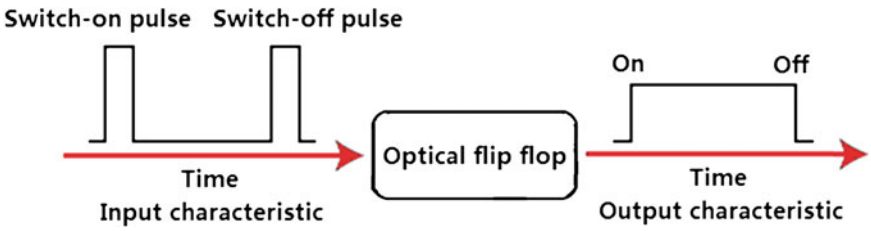

Fig. 8.24 Input and output characteristics of optical flip flop

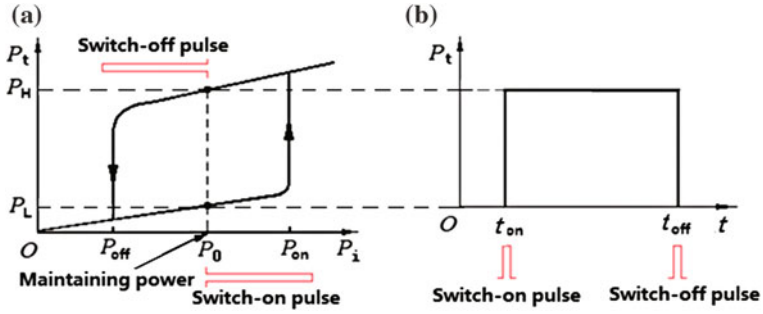

Fig. 8.25 Principle of optical flip flop based on optical bistability: **a** P_t–P_i optical bistability *curve*; **b** P_t–t characteristic curve

pulse with negative peak power larger than P_0–$P_{off,}$ the device will return to the low state.

Previous introduced F–P cavity type WQM semiconductor OBD can be used for optical flip flop, but the manufacturing technique of the device is complex. In 2000 Agrawal et al. proposed a semiconductor integrated waveguide OBD used for optical flip flop, that device had a Bragg grating distributed feedback structure, as shown in Fig. 8.26 [11].

On the InP substrate they fabricated the InGaAsP waveguide layer with thickness of 500 nm, then made a InP layer on it with thickness of 100 nm, and then through the etching to form a Bragg grating with grating period of 233 nm, the deepness of 50 nm and the grating length of 3 mm. The nonlinear refraction coefficient is $n_2 = -45 \times 10^{-12}$ cm^2/W. The grating wavelength is 1430 nm at the center of grating bandgap. They input a holding light into the grating waveguide, the holding light has a wavelength of 1560 μm close to the grating wavelength and within forbidden band, so the device has a low transmittance, the outputted power is at off-state. The wavelength of two control lights is selected at 1.55 μm. The pulsewidth of both control pulses is 8 ns. When the switch-on light pulse inputs the waveguide to produce Kerr effect and the waveguide refractive-index change, it induces the shift of grating transmittance spectrum, until the wavelength of holding light moving to outside of the bandgap, in this case the device achieves the on-state;

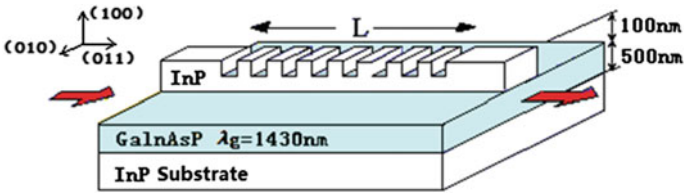

Fig. 8.26 Configuration of optical flip-flop in InGaAsP distributed feedback grating integrated waveguide

in reverse, the negative switch-off pulse will lead the device return to the off-state. Figure 8.27 shows the shift of transmittance spectrum under the switch-on pulse to switch on the device. In this device the switch-on light power is 27 mW, and the switch-off light power is 10 mW. The switching time of the device can be short to 1 ps or less.

Figure 8.28 shows the characteristic curves of input power and output power as a function of time for this InGaAsP grating waveguide optical flip-flop.

8.3 Optical Instability of Optical Bistability

8.3.1 Stability Analysis of Optical Bistability

As we discussed before, the all-optical OBDs consist of the nonlinear medium and all-optical feedback, as shown in Fig. 8.29a; and most of the hybrid OBDs consist of the electric-optical modulator and the electric-optical feedback, as shown in Fig. 8.29b.

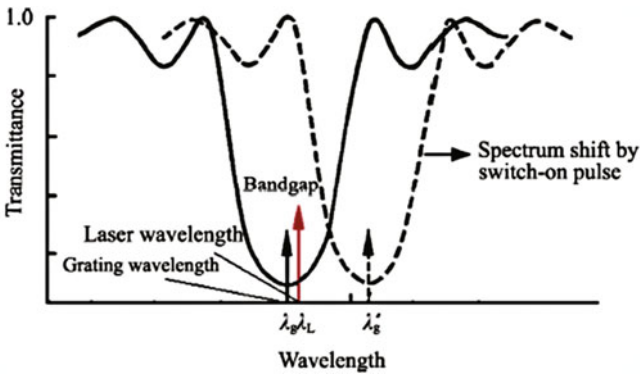

Fig. 8.27 Sketch map of transmittance spectrum shift due to switch-on pulse in grating waveguide optical flip flop. λ_g is the grating wavelength, λ'_g is its shifted value; λ_L is the wavelength of the holding light

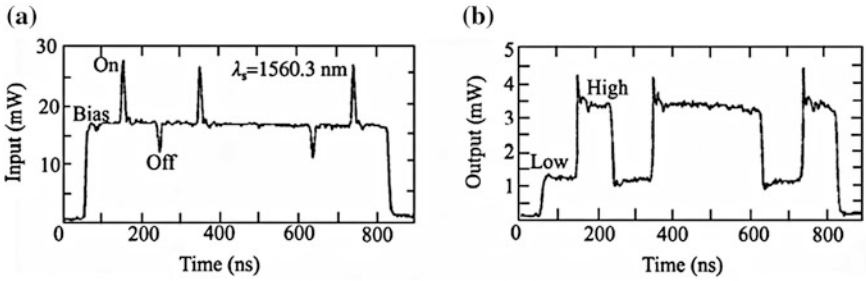

Fig. 8.28 Input and output power as a function of time for InGaAsP grating waveguide optical flip-flop: **a** Input power waveform; **b** Output power waveform

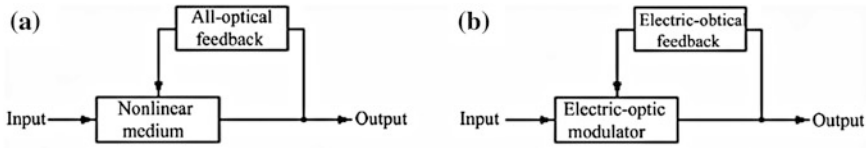

Fig. 8.29 Principles of two kinds of optical bistable devices: **a** All-optical OBD; **b** Electric-optic hybrid OBD

Under steady-state condition, the modulation and the feedback equations can be written as respectively:

$$I_t = I_i T(\phi), \tag{8.3.1}$$

$$\phi = \phi_0 + kI_t. \tag{8.3.2}$$

where I_i and I_t is the incident and the transmitted light intensities. $T(\phi)$ is the transmittance of device, ϕ is the phase shift, ϕ_0 is the initial phase shift, k is the ratio constant.

According to Eqs. (8.3.1) and (8.3.2), the transmittance T is a linear function of the phase shift ϕ.

$$T(\phi) = \frac{\phi - \phi_0}{kI_i}. \tag{8.3.3}$$

This $T - \phi$ equation is the feedback relation of OBD. On the other hand, there is another $T - \phi$ equation, namely the modulation relation of OBD, which is depended on the type of the interferometer constituted OBD as follows.

(1) Multiple-beam-interfered F–P interferometer:

$$T(\phi) = \frac{1}{1 + K\sin^2\frac{\phi}{2}}. \tag{8.3.4}$$

(2) Double-beam-interfered M–Z interferometer

$$T(\phi) = \frac{\alpha}{2}(1 + M\cos\phi). \tag{8.3.5}$$

As discussed above, Eqs. (8.3.3) and (8.3.4) or (8.3.5) can be simultaneously solved by using graphing method to get optical bistability characteristic curve ($I_t - I_i$ curve). In previous section we have mentioned that the working point on the $I_t - I_i$ curve has different stability, it depends on the slope of $I_t - I_i$ curve at that point: if the slope is positive, i.e., $\frac{dI_t}{dI_i} > 0$, that point is stable; but if the slope is negative, i.e., $\frac{dI_t}{dI_i} < 0$, that point is unstable. Now we are going to prove this conclusion.

For this purpose we should consider the dynamic behavior of OBD. We assume both quantities I_t and ϕ are functions of the time, and add an item containing the rate of change with time for I_t and ϕ respectively in Eqs. (8.3.1) and (8.3.2), hence we obtain the following dynamic coupling equations:

$$\tau_M \dot{I}_t = -I_t + T(\phi)I_i, \tag{8.3.6}$$

$$\tau_F \dot{\phi} = -\phi + \phi_0 + kI_t, \tag{8.3.7}$$

where τ_M and τ_F are time constants for modulation system and feedback system respectively. Setting $kI_t = u$ and $kI_i = v$, the coupling Eqs. (8.3.6) and (8.3.7) are simplified as

$$\tau_M \dot{u} = -u + T(\phi)v, \tag{8.3.8}$$

$$\tau_F \dot{\phi} = -\phi + \phi_0 + u. \tag{8.3.9}$$

Making Taylor series expansion for $T(\phi)$ near the balance point ϕ_s, and then taking the linear approximation, (i.e., taking the first two terms), we obtain

$$\begin{aligned} T(\phi) &= T(\phi_s) + T'(\phi_s)\Delta\phi + \frac{1}{2}T''(\phi_s)\Delta\phi^2 + \ldots \\ &\approx T(\phi_s) + T'(\phi_s)\Delta\phi. \end{aligned}$$

Assuming that

$$u = u_s + \Delta u, \tag{8.3.10}$$

$$\phi = \phi_s + \Delta\phi, \tag{8.3.11}$$

where u_s and ϕ_s are values at balance points, which satisfy Eqs. (8.3.1) and (8.3.2). Substituting Eqs. (8.3.10) and (8.3.11) into Eqs. (8.3.8) and (8.3.9), and using

Eqs. (8.3.1) and (8.3.2), then we obtain the following two constant-coefficient differential equations

$$\Delta\dot{u} = -\frac{1}{\tau_M}\Delta u + \frac{1}{\tau_M}T'(\phi_s)v\Delta\phi, \tag{8.3.12}$$

$$\Delta\dot{\phi} = \frac{1}{\tau_F}\Delta u - \frac{1}{\tau_F}\Delta\phi. \tag{8.3.13}$$

In order to solve the above constant-coefficient differential equations, we must find in advance the characteristic roots of the following secular equation:

$$\begin{vmatrix} -\frac{1}{\tau_M} - \lambda & \frac{1}{\tau_M}T'(\phi_s)v \\ \frac{1}{\tau_F} & -\frac{1}{\tau_F} - \lambda \end{vmatrix} = 0, \tag{8.3.14}$$

Then we obtain

$$\tau_M\tau_F\lambda^2 + (\tau_M + \tau_F)\lambda + (1 - T'(\phi_s)v = 0. \tag{8.3.15}$$

There are two characteristic roots, which are

$$\lambda_{1,2} = \frac{1}{2\tau_M\tau_F}[-(\tau_M + \tau_F) \pm \sqrt{(\tau_M + \tau_F)^2 - 4(\tau_M\tau_F)(1 - T'v)}]. \tag{8.3.16}$$

According to the stability mathematical theory for constant-coefficient differential equations, from the properties of roots one can judge the solution is whether stable or unstable. For example, the general constant-coefficient differential equations are

$$\frac{dx}{dt} = a_{11}x + a_{12}y$$
$$\frac{dy}{dt} = a_{21}x + a_{22}y$$

The secular equation is

$$\begin{vmatrix} a_{11} - \lambda & a_{12} \\ a_{21} & a_{22} - \lambda \end{vmatrix} = 0$$

If the characteristic roots λ_1 and λ_2 are real number, and $\lambda_1 \neq \lambda_2$, there are general solutions:

$$x = c_1\alpha_1 e^{\lambda_1 t} + c_2\beta_1 e^{\lambda_2 t}$$
$$y = c_1\alpha_2 e^{\lambda_1 t} + c_2\beta_2 e^{\lambda_2 t}$$

When $\lambda_1 < 0$ and $\lambda_2 < 0$, the solution is stable (convergence). However, when $\lambda_1 > 0$ and/or $\lambda_2 > 0$, the solution is unstable (divergence).

For Eq. (8.3.16), we have two roots $\lambda_1 = \lambda_+$ and $\lambda_2 = \lambda_-$. If $1 - T'(\phi_s)v < 0$, then $\lambda_1 = \lambda_+ > 0$, it is unstable. In order to know the meaning of unstable condition $1 - T'(\phi_s)v < 0$, we rewrite Eq. (8.3.1) to be $u = T(\phi)v$, and substitute it into Eq. (8.3.2), then obtain

$$\phi = \phi_0 + T(\phi)v. \tag{8.3.17}$$

To take differential of two sides in above equation, we get

$$d\phi = T'(\phi)v d\phi + T(\phi)dv, \tag{8.3.18}$$

Note that $T'(\phi) \approx T'(\phi_s)$, namely

$$d\phi = du = \frac{T(\phi)}{1 - T'(\phi_s)v} dv. \tag{8.3.19}$$

So the unstable condition becomes

$$\frac{du}{dv} = \frac{dI_t}{dI_i} = \frac{T(\phi)}{1 - T'(\phi_s)v} < 0. \tag{8.3.20}$$

As a result, the unstable condition is $\frac{dI_t}{dI_i} < 0$.

If in Eq. (8.3.16),$1 - T'(\phi_s)v > 0$, the two roots are negative, i.e., $\lambda_1 = \lambda_+ < 0$ and $\lambda_2 = \lambda_- < 0$, the device is stability.

$$\frac{du}{dv} = \frac{dI_t}{dI_i} = \frac{T(\phi)}{1 - T'(\phi_s)v} > 0. \tag{8.3.21}$$

As a result, the stable condition is $\frac{dI_t}{dI_i} > 0$.

To summarize the above analysis, the optical bistability curve is unstable in the negative-slope region, but stable in the positive-slope region.

In 1984, Li and Chen [12] gave a definition of stability degree S used to describe the stability at any working point on the optical bistability curve, which is the ratio of the input relative intensity to the output relative intensity at that point, i.e.,

$$S = \lim \left[\frac{\Delta I_i}{I_i} / \frac{\Delta I_t}{I_t} \right]_{\Delta I_i \to 0} = T(\phi_s) / \frac{dI_t}{dI_i}. \tag{8.3.22}$$

Using Eq. (8.3.20), S can be written as

$$S = 1 - T'(\phi_s)v. \tag{8.3.23}$$

Therefore, when we examine the stability of any point on the OB curve, if at that point $S > 0$, it is stable; if at that point $S < 0$, it is unstable. In other word, the positive-slope region on the OB curve is stable and the negative-slope region is unstable, as shown in Fig. 8.30.

8.3.2 *Instability of Optical Bistability*

The optical instability of OBD is a dynamic phenomenon, which is that under the fixed incident intensity, the OBD working in the positive-slope region (S > 0) appears the unstable variations of the output intensity, such as regeneration pulsations, self-pulsing, periodic oscillation, chaos and so on.

The instability of OBD is mainly classified into the following two types:

McCall Instability—Regeneration pulsations, it is arising from the corporate action of two nonlinear mechanisms with opposing and unequal response times. The McCall instability can also be called double feedback instability.

Ikeda Instability—Periodic oscillation, period-doubling, bifurcation and optical chaos, they originate from the time-delay feedback. The Ikeda instability can also be called time-delay feedback instability.

Below we will discuss these two instability phenomena, which can be demonstrated by hybrid OBDs.

1. **McCall Instability–Double Feedback Instability** [13]

In 1978, McCall mathematically proved that if an optical bistable system has two kinds of nonlinear mechanisms with two opposing signs and unequal time constants, under a fixed incident light intensity, the relaxation oscillation of output light intensity can be generated. In 1981, Okada demonstrated the double feedback instability by using an electro-optic hybrid OBD. The experimental setup is shown in Fig. 8.31.

In the experiment, an E-O crystal modulator is placed between two orthogonal polarizers. The incident light comes from a CW He–Ne laser. There are two feedback circuits: one consists of detector D_1, resistance r_1, and capacitance c_1, and

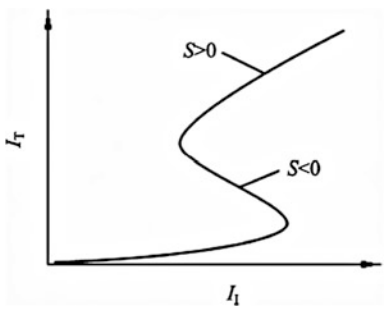

Fig. 8.30 The stability of optical bistability depends on the stability degree S: $S > 0$ in positive-slope region is stable; $S < 0$ in negative-slope region is unstable

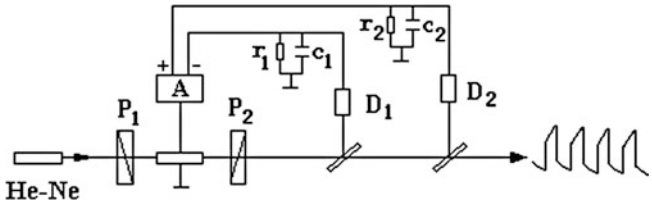

Fig. 8.31 Experimental setup for demonstrating the double feedback instability using an optoelectrical hybrid OBD

the other one consists of D_2, r_2 and c_2. Through adjusting capacitances c_1 and c_2, the feedback time constants τ_1 and τ_2 can be changed; and through controlling the gain of amplifier a and the optic-electric transform factor k, the feedback quantity can be changed. Assuming the response speed of medium is much faster than the feedback speed, the two dynamic equations can be written as

$$\tau_1\dot{\phi}_1 = \phi_{01} - \phi_1 + aI_t, \tag{8.3.24}$$

$$\tau_2\dot{\phi}_2 = \phi_{02} - \phi_2 + akI_t. \tag{8.3.25}$$

Using the definitions $aI_t \equiv U, aI_i \equiv V$, and $\psi = \phi_1 + \phi_2$; the $I_t = T(\psi)I_i$ can be written as $U = T(\psi)V$. Therefore, the two dynamic equations become

$$\tau_1\dot{\phi}_1 = \phi_{01} - \phi_1 + T(\psi)V, \tag{8.3.26}$$

$$\tau_2\dot{\phi}_2 = \phi_{02} - \phi_2 + kT(\psi)V. \tag{8.3.27}$$

Considering $\phi_1 = \phi_{1s} + \Delta\phi_1, \phi_2 = \phi_{2s} + \Delta\phi_2, \psi = \psi_s + \Delta\psi$, and $T(\psi) = T(\psi_s) + T'(\psi_s)(\Delta\phi_1 + \Delta\phi_2)$, substituting them into the above two equations, and on both sides of Eqs. (8.3.26) and (8.3.27) for differential, we obtain

$$\Delta\dot{\phi}_1 = \frac{1}{\tau_1}(-1 + T'(\psi_s)V)\Delta\phi_1 + \frac{1}{\tau_1}T'(\psi_s)V\Delta\phi_2, \tag{8.3.28}$$

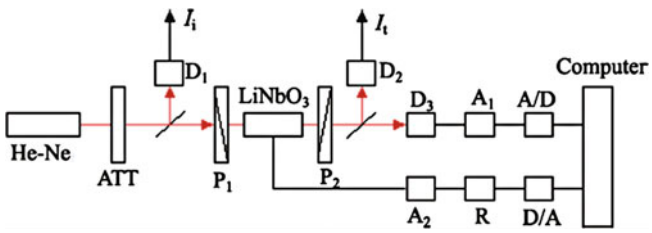

Fig. 8.32 Experimental setup for demonstrating the time-delay instability using a hybrid OBD system

$$\Delta\dot{\phi}_2 = \frac{1}{\tau_2}kT'(\psi_s)V\Delta\phi_1 + \frac{1}{\tau_2}(-1 + kT'(\psi_s)V)\Delta\phi_2. \tag{8.3.29}$$

Using the definitions of

$$\boldsymbol{P} = \begin{pmatrix} \Delta\phi_1 \\ \Delta\phi_2 \end{pmatrix},$$

and

$$\boldsymbol{A} = \begin{pmatrix} \frac{1}{\tau_1}(-1 + T'V) & \frac{1}{\tau_1}T'V \\ \frac{1}{\tau_2}kT'V & \frac{1}{\tau_2}(-1 + kT'V) \end{pmatrix} = \begin{bmatrix} a & b \\ c & d \end{bmatrix}, \tag{8.3.30}$$

then the Eqs. (8.3.28) and (8.3.29) can be expressed as the following matrix equation:

$$\dot{\boldsymbol{P}} = \boldsymbol{AP}. \tag{8.3.31}$$

In order to find solutions, we have to solve the following secular equation:

$$\begin{vmatrix} a - \lambda & b \\ c & d - \lambda \end{vmatrix} = 0, \tag{8.3.32}$$

and the characteristic equation

$$\lambda^2 - (a + d)\lambda + (ad - bc) = 0. \tag{8.3.33}$$

The characteristic root is a complex number $\lambda = \alpha \pm i\beta$, where

$$\begin{aligned} \alpha &= \frac{1}{2}(a + d) \\ \beta &= \frac{1}{2}[4(ad - bc) - (a + d)^2]^{\frac{1}{2}} \end{aligned} \tag{8.3.34}$$

When $\alpha = 0$, i.e., $a + d = 0$, we have $\lambda = \pm i\beta(\beta \neq 0)$, the system appears a stable oscillation, in this case $\beta = (ad - bc)^{1/2} > 0$, so β is a real number, Actually, it is an oscillating angular frequency, i.e., $\beta = \omega$.

Combining two equations $\omega = (ad - bc)^{1/2}$ and $a + d = 0$, and setting $r = \frac{\tau_1}{\tau_2}$, the oscillating angular frequency is given by

$$\omega = \frac{1}{\tau_2}\sqrt{-\frac{1 + \frac{k}{r}}{1 + kr}}. \tag{8.3.35}$$

Clearly, the angular frequency ω changes along with changing of k and r.

Because ω is a real number, to require $\frac{1+\frac{k}{r}}{1+kr} < 0$.

If $1+\frac{k}{r} > 0$, i.e., $k > -r$, and $1+kr < 0$, i.e., $k < -\frac{1}{r}$, so that $-r < k < -\frac{1}{r}$ and $r > 1$. If $1+\frac{k}{r} < 0$, i.e., $k < -r$, and $1+kr > 0$, i.e., $k > -\frac{1}{r}$, so that $-\frac{1}{r} < k < -r$ and $r < 1$.

When $\tau_1 > \tau_2 (r > 1)$, the oscillation condition is

$$-\frac{\tau_1}{\tau_2} < k < -\frac{\tau_2}{\tau_1}. \tag{8.3.36}$$

When $\tau_1 < \tau_2, (r < 1)$, the oscillation condition is

$$-\frac{\tau_2}{\tau_1} < k < -\frac{\tau_1}{\tau_2}. \tag{8.3.37}$$

In conclusion, we obtain the following results for double feedback instability of OB:

1. The one request is $k < 0$, that means the outputs of two feedback circuits must be opposite in phase.
2. The other request is $\tau_1 \neq \tau_2$, because if $\tau_1 = \tau_2$, or $r = 1, \omega$ is an imaginary number, namely without oscillation. Therefore, the different time constants are required.
3. When $k = 0$, it means having single feedback only, according to Eq. (8.3.35), the frequency ω is an imaginary number, namely without oscillation.
4. When $k = -1$, two feedbacks are counteracted, but the oscillation still occurs, with the frequency of $\omega = \frac{1}{\sqrt{\tau_1 \tau_2}}$. The case of $\tau_1 = \tau_2 = \tau$ and $\omega = \frac{1}{\tau}$ is allowed.
5. The value range for r is $0 \to \infty$, for k is $-\infty \to 0$ and for ω is $0 \to \infty$.

The McCall instability can be explained as follows: the two feedback mechanisms of the device provide two different feedbacks: one is positive and the other is negative. Due to their different time constants, at different moment, only one feedback plays a dominant role, and the periodic alternant, results in the fluctuation of output-light intensity, i.e., the regeneration pulsation phenomenon.

2. **Ikeda Instability-Time-Delay Feedback Instability [14]**

In 1978, Ikada pointed out that in certain time-delay feedback condition, even in the differential gain region of high and low branches in optical bistability loop could be unstable; the transmitted light appeared periodic oscillation until going to chaos. The time-delay instability can be demonstrated by using the hybrid OBD, as shown in Fig. 8.9.

The experimental setup consists of a hybrid OBD and a computer controlled time-delay system. In the figure, D_1–D_3 are photodetectors, A_1 and A_2 are amplifies, A/D is an analog to digital converter and D/A is a digital to analog converter, R is a time-delay adjustor.

The response time of system τ is adjusted by R, the adjusted range is $\tau = 1 - 3\,\text{ms}$. The time delay of computer is t_R, the selected sampling period is 160 μs.

Suppose ϕ_0 is the initial phase (without feedback signal), k is the optic-electric conversion coefficient, $\phi = (\pi/V_{1/2})V$ is the phase shift, M is the modulation degree, α is the peak transmittance, then the dynamic equations are

$$\tau\frac{d\phi(t)}{dt} + \phi(t) - \phi_0 = kI_t(t - t_R), \tag{8.3.38}$$

$$I_t(t) = I_i T(\varphi(t)) = I_i\frac{\alpha}{2}(1 + M\cos\phi). \tag{8.3.39}$$

The experimental results are: When $t_R << \tau$, for example $t_R = 160\,\mu\text{s}, \tau = 1\,\text{ms}$, the regular optical bistability can be obtained; When $t_R >> \tau$, for example $t_R = 40\,\text{ms}, \tau = 1\,\text{ms}$, in high branch of OB curve appears the oscillation with period of

$$2^{N+1}t_R = 2t_R, 4t_R, 8, \ldots (N = 0, 1, 2, \ldots) \tag{8.3.40}$$

that is period doubling and bifurcation. Finally the chaos occurs. We also can see that there are some periodic windows inside the chaos.

In order to understand the origin of periodic oscillations, Gibbs et al. used an iterative method to get the graphical solution [15]. Following the same method we can start from Eqs. (8.3.38) and (8.3.39). Because $t_R >> \tau$, two equations can be combined into one equation, which is

$$\phi(t) = \phi_0 + kI_i\frac{\alpha}{2}[1 + M\cos\phi(t - t_R)]. \tag{8.3.41}$$

Assuming $\mu = kI_i\frac{\alpha}{2}, \phi_0 = 0, \phi_n = \phi(t - t_R), \phi_{n+1} = \phi(t)$, we obtain the following an iterative equation:

$$\phi_{n+1} = \mu[1 + M\cos\phi_n] = f(\phi_n). \tag{8.2.42}$$

According to Eq. (8.3.41), because $\phi_0 = 0$, we have $\phi(t) \propto I_t$, so following the variation trail of ϕ in the iterative process, then we can find the law of output intensity change. Since $\mu \propto I_i$, taking different μ means change different incident intensity. When taking $\mu = \mu_1, \mu = \mu_2$ and $\mu = \mu_3$ respectively, i.e., gradually

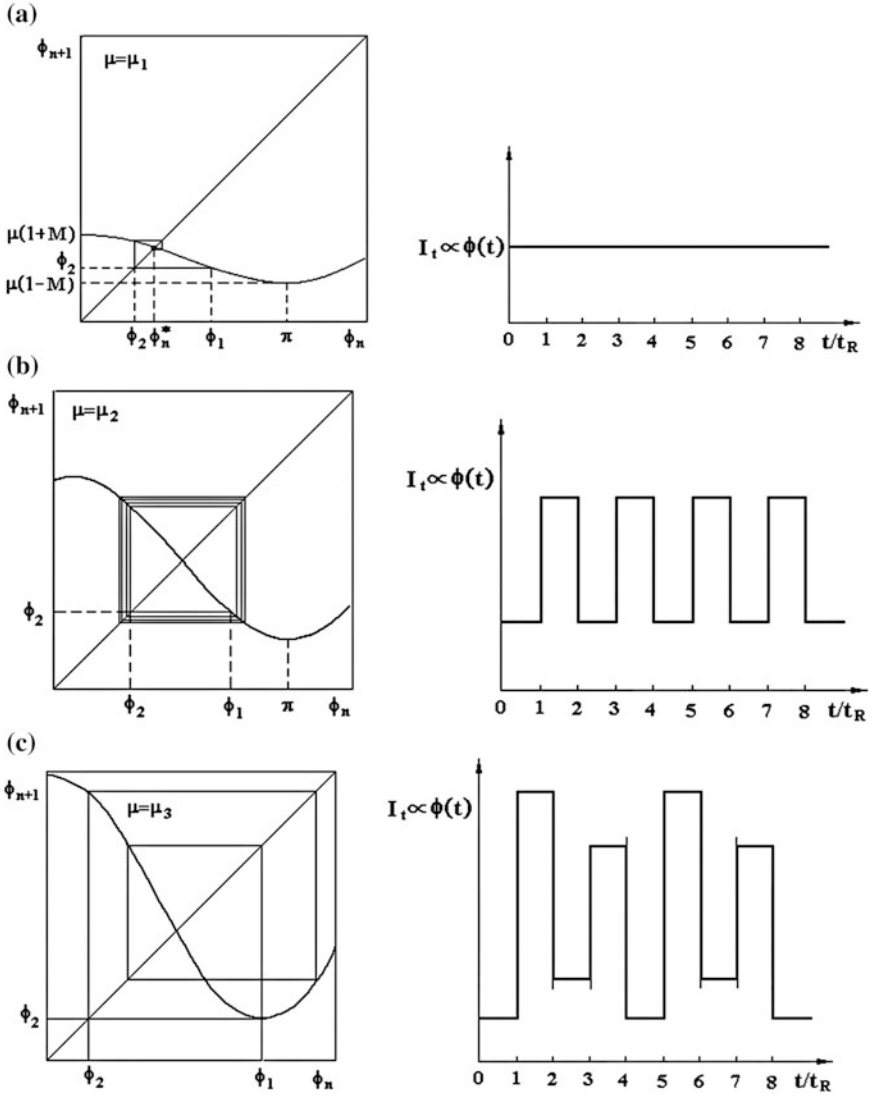

Fig. 8.33 Use of iterative method to draw periodic doubling waveforms: **a** CW; **b** period two; **c** period four

increase the incident intensity, we can draw the periodic doubling of outputted intensity, as shown in Fig. 8.33, to display the waveforms of (a) continuous, (b) period two, (c) period four and so on.

In 1983, Chunfei Li and Lixue Chen used an E–O polarization modulation type hybrid OBD, as shown in Fig. 8.32, under the time-delay feedback controlled by a computer, experimentally demonstrated the instability of optical bistability [16], to obtain the following experimental photons.

Figure 8.34 shows two photos of period doubling for optical bistability.

When changing the incident light intensity and the feedback gain, we can change the optical bistability to appear the process from continuous to oscillation bifurcation (period doubling), until to chaos starting from high branch or low branch or both on OB curve. Figure 8.35 shows the different paths to chaos from steady state of optical bistability in different conditions.

The significances of the optical chaos are as follows:

1. The optical chaos not only appears in OBDs, but also in lasers. The chaotic phenomenon is common existing in the nature. Research on instability of OBDs can enrich human understanding to chaotic phenomenon. In addition, the optical chaos is a good means to study the non-equilibrium statistical physics
2. The study of optical instability may help people to understand the difference between noise and chaos in laser and other photonic and electronic devices. That is useful for designing photonic devices to utilize or avoid the optical chaos.
3. Optical chaos can be used to change the continuous light into the pulsed light, or to compress the pulsewidth of laser, and can be used to make new optical oscillation generators. In addition, the chaos synchronization can be used in chaotic secure communication

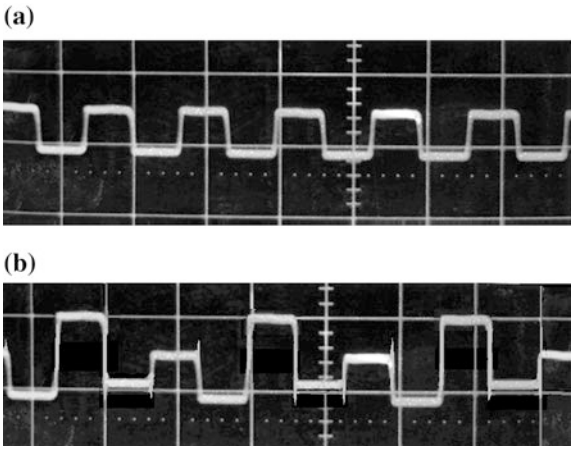

Fig. 8.34 Experimental photos of periodic doubling of OB **a** $T = 2t_R$; **b** $T = 4t_R$

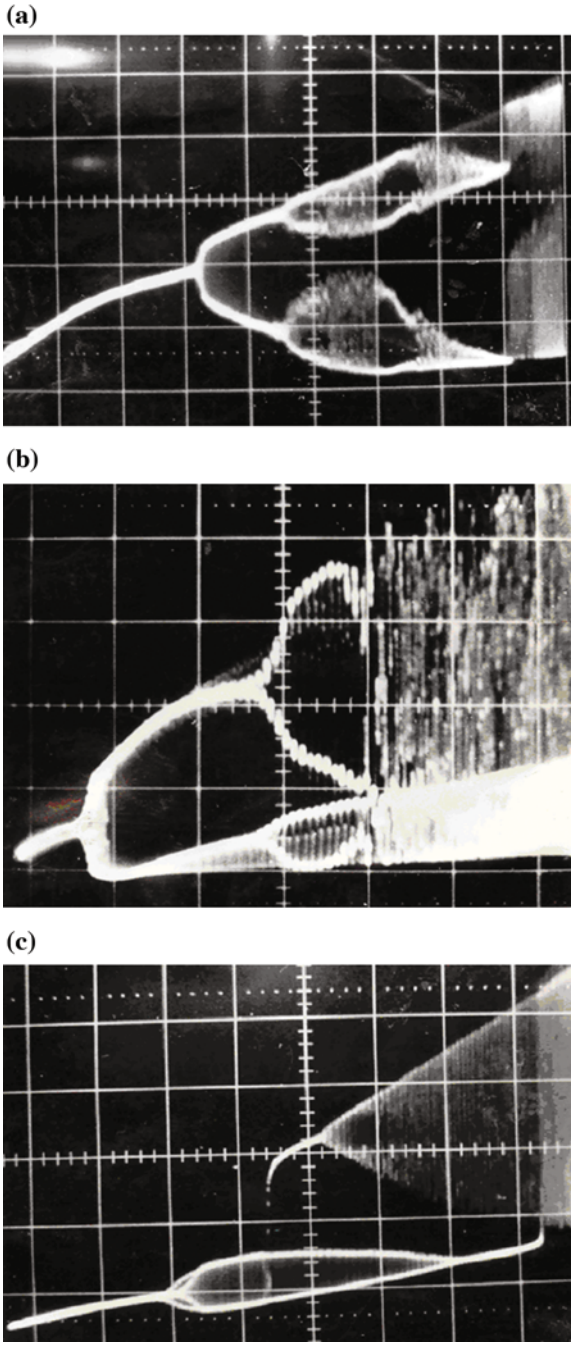

Fig. 8.35 Experimental photos for different path to chaos from OB *curve* **a** from the stable high branch to chaos; **b** from the stable low branch to chaos; **c** from high and low stable branches simultaneously to chaos

Review Questions of Chapter 8

1. What is optical bistability? What are basic elements of optical bistable device? What are similarities and differences between OBD and laser? Which types do OBD has?
2. Discuss the principle of absorption F–P etalon optical bistable device.
3. Discuss the principle of refraction F–P etalon optical bistable device.
4. Review the principle of O–E hybrid OBD including E–O F–P interferometer OBD, E–O M–Z interferometer OBD and E–O polarization modulation OBD.
5. What are applications of OBD? What is optical flip flop? Please illustrate.
6. What is stability condition of optical bistability? How to prove it?
7. What is double feedback optical instability? Discuss its generated condition.
8. What is time-delay feedback optical instability? Discuss its generated condition.

References

1. C. Li, Optical bistable devices and its application. Prog. Phys. (Nanjing) **6**(4), 427 (1986)
2. C. Li, Optics bistability studies for 20 years. Physics (Beijing) **25**(5), 267–272 (1996)
3. P. Ye, in *Nonlinear Optics*, ed. by C.F. Li. Chapter IV: Optical Bistable Devices (Chinese Science and Technology Press, Beijing, 1999)
4. H.M. Gibbs, *Optical Bistability: Controlling Light with Light* (Academic Press Inc., 1985)
5. A. Szöke, V. Daneu, J. Goldhar, et al. Bistable optical element and its applications. Appl. Phys. Lett. **15**(11), 376–379 (1969)
6. H.M. Gibbs, S.S. Tarng, J.L. Jewell et al. Room-temperature excitonic optical bistability in a GaAs-GaAlAs superlattice etalon. Appl. Phys. Lett. **41**, 221–222 (1982)
7. P.W. Smith, Hybrid bistable optical devices. Opt. Eng. **19**, 456–462 (1980)
8. C. Li, F. Zhou, K. Yang, High accuracy optical bistable interferometer fiber sensors. J. Non. Opt. Phys. Mater. **11**(2), 125–130 (2002)
9. C. Li, J. Ji, Demonstration of optical bistability using a Michelson interferometer. IEEE JQE QE-**17**(8), 1317–1320 (1981)
10. C. Li, Optical bistable device with nonlinear feedback. Physics **9**(2), 99–101 (1980)
11. K. Nakatsuhara, T. Mizumoto, R. Munakata et al., All-optical set-reset operation in a distributed feedback GaInAsP waveguide. IEEE Photonics Technol. Lett. **10**, 78–80 (1998)
12. C. Li, L. Chen, Stability degree of optical bistability and light intensity stabilizer. Acta Opt. Sini. **4**, 907–912 (1984)
13. S.L. McCall, Instability and regenerative pulsation phenomena in Fabry Perot nonlinear optic media devices. Appl. Phys. Lett. **32**(5), 284 (1978)
14. K. Ikeda, Optical chaos due to a competition between multiple oscillations. J. Opt. Soc. Am. **B** (1), 487 (1982)
15. H.M. Gibbs, F.A. Hopf, D.L. Kplan, R.L. Shoemaker, Periodic oscillation and chaos in optical bistability; possible guided-wave all-optical square-wave oscillators. Proc. SPIE **317**, 297–304 (1982)
16. L. Chen, C. Li, J. Hong, Periodic and chaotic behaviors in optical bistability. Chin. Phys. Lett. **1**(2), 884–885 (1984)

Chapter 9
Propagation of Light Pulse in Fiber and Optical Soliton

This chapter studies the phenomenon of nonlinear interaction between the laser pulse and the propagation fiber. At first, we will deduce the nonlinear Schrodinger equation for describing the propagation of light pulse in the fiber. Under this foundation, we will analyze the two effects of dispersion and self-phase modulation how to affect the propagation of light pulse in the fiber and how to form the time optical soliton in both combined action. And we will give the time optical soliton equation, the fundamental wave solution and the characteristic of the time optical soliton. Finally, we will briefly introduce the basic conception and characteristic of the space optical soliton.

9.1 Nonlinear Schrodinger Equation [1]

Most nonlinear effects in fiber are related with that the light pulses with pulsewidth in the range of 10 ns $\sim$ 10 fs propagate in the fiber. In the propagation process, both the dispersion and the nonlinearity all affect the shape and spectrum of light pulse. For describing the propagation of light pulses in the nonlinear fiber we need use the time-domain nonlinear Schrodinger equation. We will deduce this equation taking following four steps:

① Reforming the general nonlinear time-domain wave equation to be the time-domain wave equation in the isotopic medium;
② Through Fourier transform to deduce the frequency-domain wave equation for describing the propagation of monochromic light in isotopic medium, namely Helmholtz equation;
③ In the single mode fiber condition solving Helmholtz equation, to deduce the frequency-domain wave equation for describing the propagation of monochromic light in single mode fiber;

© Shanghai Jiao Tong University Press,
Shanghai and Springer Nature Singapore Pte Ltd., 2017

C. Li, *Nonlinear Optics*, DOI 10.1007/978-981-10-1488-8_9

④ Through revers Fourier transform to deduce the time-domain nonlinear Schrodinger equation, which describes that when the light pulse propagate in the fiber to generate the dispersion, absorption, and Kerr effect.

9.1.1 Helmholtz Equation

If the medium is without absorption loss ($\sigma = 0$), according to Eq. (2.1.17), the general wave equation can be written to

$$\nabla \times \nabla \times \boldsymbol{E} + \mu_0 \frac{\partial^2 \boldsymbol{\varepsilon} \cdot \boldsymbol{E}}{\partial t^2} = -\mu_0 \frac{\partial^2 \boldsymbol{P}_{NL}}{\partial t^2}. \tag{9.1.1}$$

Assuming the fiber medium is isotopic, we have $\nabla \cdot \boldsymbol{E} = 0$, so that $\nabla \times \nabla \times \boldsymbol{E} = \nabla(\nabla \cdot \boldsymbol{E}) - \nabla^2 \boldsymbol{E} = -\nabla^2 \boldsymbol{E}$. Because dielectric coefficient is $\varepsilon = \varepsilon_0(1 + \chi^{(1)})$, where $\boldsymbol{\chi}^{(1)}$ linear susceptibility, and linear polarization is $\mathrm{P}_L = \varepsilon_0 \boldsymbol{\chi}^{(1)} \cdot \mathrm{E}$, using $c = 1/\sqrt{\mu_0 \varepsilon_0}$, Eq. (9.1.1) can be rewritten to

$$\nabla^2 \boldsymbol{E} - \frac{1}{c^2} \frac{\partial^2 \boldsymbol{E}}{\partial t^2} = \frac{1}{\varepsilon_0 c^2} \frac{\partial^2 \boldsymbol{P}_L}{\partial t^2} + \frac{1}{\varepsilon_0 c^2} \frac{\partial^2 \boldsymbol{P}_{NL}}{\partial t^2}. \tag{9.1.2}$$

The total polarization of medium is

$$\boldsymbol{P}(\boldsymbol{r}, t) = \boldsymbol{P}_L(\boldsymbol{r}, t) + \boldsymbol{P}_{NL}(\boldsymbol{r}, t). \tag{9.1.3}$$

In the following discussion we assume: ① the medium is isotopic, non-absorption, far from resonance; ② $\boldsymbol{P}_{NL}$ can be regarded as the perturbation of $\boldsymbol{P}$, because in general the nonlinear variation of refractive index $< 10^{-6}$; ③ when the light propagates along the fiber length direction, its polarization keeps no change, so we can treatment by using scalar method; ④ the light wave is quasi-monochromic, namely $\Delta\omega/\omega_0 << 1$ is satisfied, because the center frequency of light wave is about $\omega_0 \approx 10^{15}$ Hz, and spectrum wide of light pulse is $\Delta\omega < 0.1\mathrm{ps} = 10^{13}\mathrm{Hz}$.

We suppose the light wave propagates in fiber along z-direction, the polarization is along x-direction, so we have

$$\boldsymbol{E}(\boldsymbol{r}, t) = \hat{\boldsymbol{x}}[E(\boldsymbol{r}, t) \exp(-i\omega_0 t) + c.c.], \tag{9.1.4}$$

$$\boldsymbol{P}_L(\boldsymbol{r}, t) = \hat{\boldsymbol{x}}[P_L(\boldsymbol{r}, t) \exp(-i\omega_0 t) + c.c.], \tag{9.1.5}$$

$$\boldsymbol{P}_{NL}(\boldsymbol{r},t) = \hat{\boldsymbol{x}}[P_{NL}(\boldsymbol{r},t)\exp(-i\omega_0 t) + c.c.], \tag{9.1.6}$$

where $\hat{\boldsymbol{x}}$ is the unit vector for polarization along x-direction. Substituting Eqs. (9.1.4)–(9.1.6) into Eq. (9.1.2), in the same time using the Fourier transform to $\boldsymbol{E}(\boldsymbol{r},t)$, the electrical field intensity is denoted as the frequency-domain form:

$$\tilde{\boldsymbol{E}}(\mathbf{r},\omega-\omega_0) = \int_{-\infty}^{\infty} \boldsymbol{E}(\boldsymbol{r},t)\exp[i(\omega-\omega_0)t]dt. \tag{9.1.7}$$

Therefore we deduce out the Helmholtz equation, which is satisfied by the monochromic wave in the isotopic medium:

$$\nabla^2\tilde{\boldsymbol{E}} + \varepsilon(\omega)k_0^2\tilde{\boldsymbol{E}} = 0, \tag{9.1.8}$$

where $k_0 = \omega/c$ is the wave vector in vacuum; $\varepsilon(\omega)$ is the complex dielectric coefficient. Now we investigate the physical mining of $\varepsilon(\omega)$.

If we only consider the linear effect and the three-order nonlinear effect, the polarization can be written as

$$\boldsymbol{P} = \boldsymbol{P}^{(1)} + \boldsymbol{P}^{(3)} = \varepsilon_0\chi^{(1)}\boldsymbol{E} + 3\varepsilon_0\chi^{(3)}|\boldsymbol{E}|^2\boldsymbol{E}. \tag{9.1.9}$$

According to the definition of electric induction intensity and using Eq. (9.1.9), we have

$$\boldsymbol{D} = \varepsilon_0\boldsymbol{E} + \boldsymbol{P} = \varepsilon_0\boldsymbol{E} + \varepsilon_0\chi^{(1)}\boldsymbol{E} + 3\varepsilon_0\chi^{(3)}|\boldsymbol{E}|^2\boldsymbol{E} = \varepsilon(\omega)\boldsymbol{E}. \tag{9.1.10}$$

So the dielectric coefficient $\varepsilon(\omega)$ is given by

$$\varepsilon(\omega) = \varepsilon_0\left(1 + \chi^{(1)}(\omega) + 3\chi^{(3)}|\boldsymbol{E}(\omega)|^2\right). \tag{9.1.11}$$

In general $\varepsilon(\omega)$ is a complex umber, the real part is corresponding to the refractive index $\tilde{n}$, and the imaginary part is corresponding to the absorption coefficient $\tilde{\alpha}$, so $\varepsilon(\omega)$ can be defined as

$$\varepsilon(\omega) = (\boldsymbol{n} + \boldsymbol{i\alpha}/\boldsymbol{2k_0})^2. \tag{9.1.12}$$

And the refractive index and the absorption coefficient can be divided into linear and nonlinear two parts:

$$\tilde{n} = n + \Delta n, \tag{9.1.13}$$

$$\tilde{\alpha} = \alpha + \Delta\alpha. \tag{9.1.14}$$

where n and α are linear refractive index and linear absorption (as same as n_0 and α_0 in previous chapter); the relations of Δn and $\Delta\alpha$ with the light intensity I have been given in second chapter:

$$\Delta n = \frac{3}{\varepsilon_0 c n^2}\chi^{(3)\prime}(\omega)I,$$
$$\Delta\alpha = \frac{6\omega}{\varepsilon_0 c^2 n^2}\chi^{(3)\prime\prime}(\omega)I,$$

Using formula $I = \frac{1}{2}\varepsilon_0 c n|\boldsymbol{E}|^2$, Eqs. (9.1.13) and (9.1.14) become:

$$\tilde{n} = n + \bar{n}_2|\boldsymbol{E}|^2, \tag{9.1.15}$$

$$\tilde{\alpha} = \alpha + \bar{\alpha}_2|\boldsymbol{E}|^2, \tag{9.1.16}$$

where

$$\bar{n}_2 = \frac{3}{2n}\chi^{(3)\prime}, \tag{9.1.17}$$

$$\bar{\alpha}_2 = \frac{3\omega}{cn}\chi^{(3)\prime\prime}. \tag{9.1.18}$$

$\bar{n}_2$ is nonlinear refraction coefficient; $\bar{\alpha}_2$ can be called two-photon absorption coefficient (or write as β), for silica fiber the absorption coefficient $\tilde{\alpha}$ is very small, it can be neglected, so the dielectric coefficient can be approximately written as $\varepsilon \approx \tilde{n}^2$.

Using Eqs. (9.1.12) and (9.1.13), omitting the items containing $(\Delta n)^2$, $(i\tilde{\alpha}/2k_0)^2$, and $\Delta n(i\tilde{\alpha}/2k_0)$, and using Eq. (9.1.15), the dielectric coefficient $\varepsilon(\omega)$ can be approximately written as

$$\varepsilon(\omega) = \left(\tilde{n} + \frac{i\tilde{\alpha}}{2k_0}\right)^2 \approx \left[n^2 + 2n\left(\bar{n}_2|E|^2 + \frac{i\tilde{\alpha}}{2k_0}\right)\right]. \tag{9.1.19}$$

To define the complex number nonlinear refractive index $\boldsymbol{\Delta n}$ as

$$\boldsymbol{\Delta n} = \bar{n}_2|E|^2 + \frac{i\tilde{\alpha}}{2k_0}. \tag{9.1.20}$$

Then Eq. (9.1.19) can be approximately expressed as

$$\varepsilon(\omega) \approx n^2 + 2n\boldsymbol{\Delta n}. \tag{9.1.21}$$

Visible, $\boldsymbol{\Delta n}$ can be regarded the first perturbation of the dielectric coefficient $\varepsilon(\omega)$, which includes the nonlinearity and the absorption loss of fiber

If in Eq. (9.1.20) we replace $\bar{n}_2$ by n_2, replace $|E|^2$ by $I = P/S_{\text{eff}}$, and approximately replace $\tilde{\alpha}$ by α, Eq. (9.1.20) can be written as

$$\Delta \boldsymbol{n} \approx n_2 \frac{P}{S_{eff}} + \frac{i\alpha}{2k_0}, \tag{9.1.22}$$

where the unit of nonlinear refraction coefficient n_2 is m^2/W; the unit of power P is W, the unit of efficient cross-section of fiber core S_{eff} is m^2.

9.1.2 Derivation of Frequency-Domain Wave Equation in Fiber

Helmholtz Eq. (9.1.8) can be solved by using method of separation of variables. Assuming that the solution form is

$$\tilde{E}(r, \omega - \omega_0) = F(x, y)\tilde{A}(z, \omega - \omega_0)\exp(i\beta_0 z), \tag{9.1.23}$$

where $F(x, y)$ is transverse-mode distribution function of light pulse in the fiber; $\tilde{A}(z, \omega)$ is light electrical filed amplitude; $\exp(i\beta_0 z)$ is the phase factor, in which $\beta_0 = \beta(\omega_0)$ is the wave number for central wavelength.

Substituting the trying solution (9.1.23) into Eq. (9.1.8), which can be divided into two equations related to $F(x, y)$ and $\tilde{A}(z, \omega)$ respectively:

$$\frac{\partial^2 F}{\partial x^2} + \frac{\partial^2 F}{\partial y^2} + [\varepsilon(\omega)k_0^2 - \tilde{\beta}^2]F = 0, \tag{9.1.24}$$

$$2i\beta_0 \frac{\partial \tilde{A}}{\partial z} + (\tilde{\beta}^2 - \beta_0^2)\tilde{A} = 0. \tag{9.1.25}$$

In the process of deduction of Eq. (9.1.25), because $\tilde{A}(z, \omega)$ is a slow-variation function of z, we have neglected the item containing $\partial^2\tilde{A}/\partial z^2$.

$\tilde{\beta}$ in Eqs. (9.1.24) and (9.1.25) can be expressed to be linear and nonlinear two parts:

$$\tilde{\beta} = \beta(\omega) + \Delta\beta(\omega). \tag{9.1.26}$$

$\tilde{\beta}^2$ in Eq. (9.1.24) can be written to $\tilde{\beta}^2 \approx \beta(\omega)^2 + 2\beta(\omega)\Delta\beta(\omega)$, using Eq. (9.1.21), then Eq. (9.1.24) can be rewritten to

$$\frac{\partial^2 F}{\partial x^2} + \frac{\partial^2 F}{\partial y^2} + 2[n(\omega)\Delta\boldsymbol{n}(\omega/c)^2 - \beta(\omega)\Delta\beta(\omega)]F = 0. \tag{9.1.27}$$

Taking double integral of x and y to function $F(x,y)$, $\Delta\beta(\omega)$ can be regard a constant, moving it to outside of the integral sign, from Eq. (9.1.27) we obtain

$$\Delta\beta(\omega) = \frac{\omega^2 n(\omega)}{c^2\beta(\omega)} \frac{\int\int_{-\infty}^{\infty} \Delta\boldsymbol{n}(\omega)|F(x,y)|^2 dxdy}{\int\int_{-\infty}^{\infty} |F(x,y)|^2 dxdy}. \tag{9.1.28}$$

The physical meaning of this formula is: in the envelop of the light pulse propagated in the fiber, the wave number change of a monochromatic light $\Delta\beta(\omega)$ comes from light induced complex number refractive-index change $\Delta\boldsymbol{n}$, which is the first perturbation of $\varepsilon(\omega)$; and $\Delta\beta(\omega)$ can be regarded as the first perturbation of $\tilde{\beta}$.

Using Eq. (9.1.26) and approximate relation $\tilde{\beta}^2 - \beta_0^2 \approx 2\beta_0(\tilde{\beta} - \beta_0)$, the Eq. (9.1.25) becomes

$$\frac{\partial\tilde{A}}{\partial z} = i[\beta(\omega) + \Delta\beta(\omega) - \beta_0]\tilde{A}. \tag{9.1.29}$$

In order to obtain the exact expression and meaning of $\beta(\omega)$ in above equation, we expend $\beta(\omega)$ to be Taylor series nearby the central frequency ω_0:

$$\beta(\omega) = \beta_0 + (\omega - \omega_0)\beta_1 + \frac{1}{2}(\omega - \omega_0)^2\beta_2 + \frac{1}{6}(\omega - \omega_0)^3\beta_3 + \ldots. \tag{9.1.30}$$

In which β_n is

$$\beta_n = \left(\frac{d^n\beta}{d\omega^n}\right)_{\omega=\omega_0} \quad (n = 0, 1, 2, \ldots). \tag{9.1.31}$$

β_0 is the wave number of central frequency; β_1 is the wave number of wave packet, which is related with the group velocity v_g and the refractive index of group velocity n_g, β_2; denotes the dispersion of group velocity (GVD), which is related with frequency broaden of light pulse. β_1 and β_2 are respectively defined as

$$\beta_1 = \frac{d\beta}{d\omega} = \frac{1}{v_g} = \frac{n_g}{c} = \frac{1}{c}\left(n + \omega\frac{dn}{d\omega}\right), \tag{9.1.32}$$

$$\beta_2 = \frac{d^2\beta}{d\omega^2} = \frac{d\beta_1}{d\omega} = \frac{1}{c}\left(2\frac{dn}{d\omega} + \omega\frac{d^2n}{d\omega^2}\right). \tag{9.1.33}$$

We have assumed spectrum width $\Delta\omega << \omega_0$, so in expansion Eq. (9.1.30), the high-order (higher than three-order) items can be neglected (only for the specific frequency, such as near zero dispersion waveguide of fiber, $\beta_2 \approx 0$, than we consider β_3 in the three-order item), therefore we only take preceding three items in Eq. (9.1.30), i.e.,

$$\Delta\beta(\omega) = \beta_0 + (\omega - \omega_0)\Delta\beta_1 + \frac{1}{2}(\omega - \omega_0)^2\Delta\beta_2. \tag{9.1.34}$$

Substituting Eq. (9.1.34) into Eq. (9.1.29), we obtain

$$\frac{\partial\tilde{A}}{\partial z} = i[(\omega - \omega_0)\Delta\beta_1 + \frac{1}{2}(\omega - \omega_0)^2\Delta\beta_2 + \Delta\beta(\omega)]\tilde{A}. \tag{9.1.35}$$

9.1.3 Derivation of Nonlinear Schrodinger Equation

At first, using Eqs. (9.1.4) and (9.1.23), the time-domain light electrical filed intensity expression can be written as:

$$\mathbf{E}(\boldsymbol{r}, t) = \hat{\boldsymbol{x}}[E(x, y)A(z, t)\exp\ i(\beta_0 z - \omega_0 t) + c.c.], \tag{9.1.36}$$

where $A(z, t)$ is time-domain slow-variation electrical filed amplitude, which can be obtained from the reverse Fourier transform of frequency electrical filed amplitude $\tilde{A}(z, \omega - \omega_0)$:

$$A(z, t) = \frac{1}{2\pi}\int_{-\infty}^{\infty} \tilde{A}(z, \omega - \omega_0)\exp[i(\omega - \omega_0)t]d\omega. \tag{9.1.37}$$

After than through reverse Fourier transform, we transfer the frequency-domain amplitude Eq. (9.1.35) to be time-domain amplitude equation. In the reverse Fourier transform, we can use the operator $i(\partial/\partial t)$ to instead of $\omega - \omega_0$ in Eq. (9.1.35), the time-domain form of that equation is given by

$$\frac{\partial A}{\partial z} + \beta_1\frac{\partial A}{\partial t} + \frac{i\beta_2}{2}\frac{\partial^2 A}{\partial t^2} = i\Delta\beta(\omega)A. \tag{9.1.38}$$

$\Delta\beta(\omega)$ in the right side of Eq. (9.1.38) includes the fiber loss (α) and the nonlinearity ($\Delta\boldsymbol{n}$).

Now we use Eq. (9.1.28) to find $\Delta\beta(\omega)$. Under first-class perturbation, we suppose $\Delta\boldsymbol{n}$ does not affect the model-filed distribution $F(x, y)$ in the pulsewidth range, so we can pull out $\Delta\boldsymbol{n}$ to outside the integral, further use expression (9.1.22) of $\Delta\boldsymbol{n}$, and setting $\beta(\omega) \approx n(\omega)\frac{\omega}{c}$, under condition of $\Delta\omega << \omega_0$, we can approximately use $\Delta\beta_0$ instead of $\Delta\beta(\omega)$, therefore the $\Delta\beta(\omega)$ in Eq. (9.1.38) can be written as

$$\Delta\beta(\omega) = \Delta\beta_0 \approx \frac{n_2(\omega_0)\omega_0}{cS_{\text{eff}}}|A|^2 + \frac{i\alpha}{2}, \tag{9.1.39}$$

here we used $P = |A|^2$, because the amplitude A is normalized. $|A|^2$ represents power (the unit is W). Substituting the Eq. (9.1.39) into Eq. (9.1.38), the time-domain amplitude Eq. (9.1.38) becomes the following form:

$$\frac{\partial A}{\partial z} + \beta_1 \frac{\partial A}{\partial t} + \frac{i\beta_2}{2}\frac{\partial^2 A}{\partial t^2} + \frac{\alpha}{2}A = i\gamma(\omega_0)|A|^2 A, \tag{9.1.40}$$

where γ is the nonlinear coefficient, its definition is

$$\gamma(\omega_0) = \frac{n_2(\omega_0)\omega_0}{cS_{eff}}. \tag{9.1.41}$$

The unit of $\gamma|A|^2$ is m^{-1}. S_{eff} is the effective cross-section of fiber core, which is defined as

$$S_{eff} = \frac{\left(\int\int_{-\infty}^{\infty} |F(x,y)|^2 dxdy\right)^2}{\int\int_{-\infty}^{\infty} |F(x,y)|^4 dxdy}, \tag{9.1.42}$$

where $F(x, y)$ is distribution function of fundamental mode light filed of fiber. For single-mode fiber, its fundamental mode can expressed as a Gaussian distribution, i.e.,

$$F(x, y) = \exp[-(x^2 + y^2)/w^2]. \tag{9.1.43}$$

The effective cross-section of fiber core is

$$S_{eff} = \pi w^2. \tag{9.1.44}$$

For the fiber at near the normalized cut-off frequency $V = 2$, the parameter w is equal to the radius of fiber core, i.e., $w \approx a$, and $S_{eff} = \pi a^2$. When wavelength at vicinity of 1.5 μm, the general cross-section of fiber core is $S_{eff} = 20 - 100\,\mu\text{m}^2$. If taking $n_2 \approx 2.6 \times 10^{-20}\text{m}^2/\text{W}$, the range of nonlinear coefficient is $\gamma = 1 \sim 10\,\text{W}^{-1}/\text{km}$.

Equation (9.1.40) describes the propagation law of picosecond light pulse in single-mode fiber. The equation is called Nonlinear Schrödinger (NLS) Equation. In which α denotes absorption loss, γ denotes nonlinearity effect, the moving group velocity of pulse waveform is $v_g \equiv 1/\beta_1$, the group velocity dispersion (GVD) effect is depended on the parameter β_2. The plus or minus of β_2 is depended on whether greater or smaller than zero-dispersion wavelength 1.31 μm, please see following appendix.

Appendix: Dispersion of Fiber

Dispersion of single-mode fiber is usually used the dispersion coefficient D_{m} to describe, the relationship between D_{m} and β_2 is

$$D_m = \frac{d\beta_1}{d\lambda} = -\frac{2\pi c}{\lambda^2}\beta_2 \approx -\frac{\lambda}{c}\frac{d^2 n}{d\lambda^2}. \tag{9.1.45}$$

This is the material dispersion. The wave number of wave packet $\beta_1 = 1/v_g$ is the time delay due to that the wave packet propagated with group velocity passes through a unit distance, its unit is ps/km; the dispersion coefficient D_{m} is the time delay induced by unit spectrum width, its unit is ps/(km · nm); and the unit of group-velocity dispersion parameter β_2 is $\mathrm{ps}^2/\mathrm{km}$.

Figure 9.1 gives the relation of variation of group-velocity dispersion parameter of single-mode silica fiber β_2 with the wavelength. We can see that β_2 tends to zero in the vicinity of wavelength 1.31 μm, for even longer wavelength it becomes negative value, for example, when $\lambda \approx 1.55\,\mu\mathrm{m}$, $\beta_2 \approx -25\mathrm{ps}^2/\mathrm{km}$. The wavelength at $\beta_2 = 0$ is called zero-dispersion wavelength λ_D.

The material dispersion D_{m} is related with the fiber doping situation, for different doping, the law of refractive-index variation with the wavelength is different, i.e., the characteristic of dispersion is different. There is also a dispersion, which relies on the waveguide structure of fiber, it is called waveguide dispersion D_w. For different fiber waveguide structure, in which the refractive index of efficient mode is different with the material refractive index, therefore dispersion characteristic is different. The main action is change the location of zero-dispersion wavelength λ_D, to lead it shifts along long wavelength direction.

The total dispersion of single mode fiber D is a sum of material dispersion and waveguide dispersion: $D = D_m + D_w$.

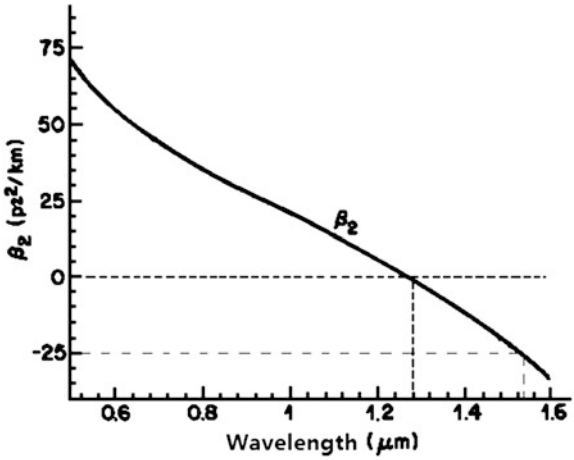

Fig. 9.1 Relation between the group velocity dispersion β_2 and the wavelength for single mode silica fiber

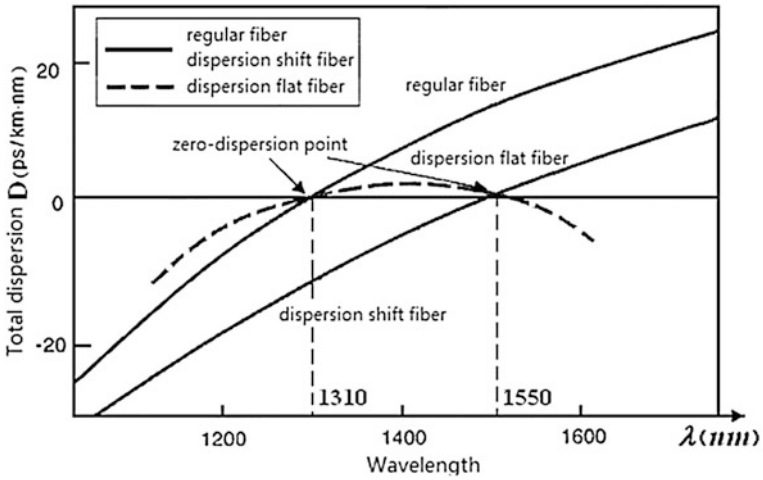

Fig. 9.2 Dispersion–wavelength curves for three kinds of single-mode fibers: the regular fiber, the dispersion shift fiber and the dispersion flat fiber

There are common three kinds of single-mode fibers: the regular fiber (λ_D = 1.31 μm),the dispersion shift fiber (λ_D = 1.55 μm) and the dispersion flat fiber (λ_D = 1.31 μm and 1.55 μm), their dispersion-wavelength characteristic curves are shown in Fig. 9.2.

9.2 Group Velocity Dispersion and Self-phase Modulation [1]

In two sides of Eq. (9.1.40) multiply by i, then we obtain

$$i\frac{\partial A}{\partial z} + i\beta_1\frac{\partial A}{\partial t} = -\frac{i\alpha}{2}A + \frac{\beta_2}{2}\frac{\partial^2 A}{\partial t^2} - \gamma|A|^2 A. \tag{9.2.1}$$

If we use the time coordinate of motion reference system with group velocity v_g (the space coordinate is no change),

$$T = t - z/v_g = t - \beta_1 z, \tag{9.2.2}$$

and using the derivation formula for the function of functions, we obtain

$$\begin{aligned}\frac{\partial A(z,T)}{\partial z} &= \frac{\partial}{\partial z}A(z, t = T + \frac{z}{v_g}) = \frac{\partial A(z,t)}{\partial z} + \frac{\partial A(z,t)}{\partial t}\cdot\frac{\partial t}{\partial z} \\ &= \frac{\partial A(z,t)}{\partial z} + \frac{\partial A(z,t)}{\partial t}\cdot\frac{1}{v_g} = \frac{\partial A(z,t)}{\partial z} + \beta_1\frac{\partial A(z,t)}{\partial t}.\end{aligned}$$

Equation (9.2.1) becomes

$$i\frac{\partial A}{\partial z} = -\frac{i\alpha}{2}A + \frac{\beta_2}{2}\frac{\partial^2 A}{\partial T^2} - \gamma|A|^2 A. \tag{9.2.3}$$

This is NLS equation for describing the propagation of light pulse in the fiber. $A(z, T)$ is the amplitude of pulse envelop. The first item of right side describes the absorption of light pulse in the fiber, the second item describes the group velocity dispersion (GVD) of light pulse, the third item describes self-phase modulation (SPM) of light pulse (the nonlinear optics effect). Actually, this equation is neglected the high-order nonlinear effects. This equation is suitable to use for describing the propagation of light pulse with initial pulsewidth $T_0 > 5ps$ in the fiber.

When the light pulse propagates in the fiber for a certain length L, in order to estimate which effect: the dispersion effect or the self-phase modulation, plays main role, we respectively introduce two physical quantities: the dispersion length L_D and the nonlinear length L_{NL}, according to the comparison of the length of L_D or L_{NL} relative to fiber length L, to determine which effect has more important contribution.

For realizing the normalization of the equation, we introduce a normalized time τ, which is relative to the initial pulsewidth T_0:

$$\tau = \frac{T}{T_0} = \frac{t - z/v_g}{T_0}. \tag{9.2.4}$$

In the same time, we introduce a normalized light filed amplitude $U(z, \tau)$, which is proportional to the amplitude $A(z, \tau)$, the proportionality coefficient includes the input light power and the absorption loss related with propagation distance:

$$A(z, \tau) = \sqrt{P_0}\exp(-\alpha z/2)U(z, \tau), \tag{9.2.5}$$

where P_0 is the peak power of input light pulse; the exponent factor is for measuring the fiber loss. So the Eq. (9.2.3) is rewritten to

$$i\frac{\partial U}{\partial z} = \frac{\mathrm{sgn}(\beta_2)}{2L_D}\frac{\partial^2 U}{\partial \tau^2} - \frac{\exp(-\alpha z)}{L_{NL}}|U|^2 U, \tag{9.2.6}$$

where $\mathrm{sgn}(\beta_2) = \pm 1$ is determined by the symbol of GVD parameter β_2; L_D is dispersion length, which is defined as

$$L_D = \frac{T_0^2}{|\beta_2|}; \tag{9.2.7}$$

L_{NL} is nonlinear length, which is defined as

$$L_{NL} = \frac{1}{\gamma P_0}. \tag{9.2.8}$$

We can see that L_D is related with the fiber group velocity dispersion parameter β_2 and the initial width of input light pulse T_0; and L_{NL} is related with the nonlinear parameter of fiber γ and the peak power of input light pulse P_0. Namely β_2 and T_0 determine the group velocity dispersion GVD. And γ and P_0 determine the self-phase modulation SPM. According to comparison of L_D and L_{NL} with the actual length of fiber L in numerical relative size, we can put the light pulse propagation in optical fiber into four cases. Below we start from Eq. (9.2.6) to study these four cases respectively.

9.2.1 Pulse Propagation Excluding Dispersion and Nonlinearity

When the length of fiber is very short, i.e., $L << L_D$ and $L << L_{NL}$, whether dispersion or nonlinearity both not play important role. In Eq. (9.2.6), two items of right side are all equal to zero, i.e., $\frac{\partial U(z,\tau)}{\partial z} = 0$, then $U(z,\tau) = U(0,\tau)$, namely in propagation process the shape of light pulse keeps no change (except the absorption induces slightly decrease of power). This case is favorable to the optical communication.

For example, for the standard fiber at wavelength $\lambda = 1.55\,\mu\text{m}$, $|\beta_2| \approx 20\,\text{ps}^2/\text{km}$, and $\gamma \approx 2\,\text{W}^{-1}\text{km}^{-1}$, if the light pulse with $T_0 \geq 100\,\text{ps}$ and $P_0 \leq 1\,\text{mW}$, in this case L_D and $L_{NL} \geq 500\,\text{km}$, for the fiber with length of $L \leq 50\,\text{km}$, the dispersion and the nonlinearity all can be neglected. But when the pulsewidth of incident pulse is narrow down, and the power of incident pulse increase, L_D and L_{NL} become smaller, such as $T_0 \approx 1\,\text{ps}$ and $P_0 \approx 1\,\text{W}$, then L_D and $L_{NL} \approx 100\,\text{m}$, for this fiber, when its length exceeds 10 m, we should consider the influences of the dispersion effect and the nonlinearity effect in the same time.

9.2.2 Influence of Dispersion to Pulse Propagation

If $L << L_{NL}$, but $L \approx L_D$, the second item of right side of Eq. (9.2.6) can be neglected, the pulse variation mainly depends on the group velocity dispersion (GVD). In this case L_D is much smaller than L_{NL}:

$$\frac{L_D}{L_{NL}} = \frac{\gamma P_0 T_0^2}{|\beta_2|} << 1. \tag{9.2.9}$$

Roughly estimating, for the standard fiber at $\lambda = 1.55\,\mu\text{m}$, taking the typical values of γ and $|\beta_2|$, this case is suitable to the light pulse with power of $P_0 << 1\,\text{W}$ and pulsewidth of 1 ps.

Below we will discuss the influence of group velocity dispersion to the light pulse. Assuming in Eq. (9.2.3), $\gamma = 0$, using the normalized amplitude defined by Eq. (9.2.5) $U(z, T)$, then $U(z, T)$ is satisfied the following linear partial differential equation:

$$i\frac{\partial U}{\partial z} = \frac{\beta_2}{2}\frac{\partial^2 U}{\partial T^2}. \tag{9.2.10}$$

This equation is easy to solve by using Fourier transformation method. Suppose $\tilde{U}(z, \omega)$ is the Fourier transformation of $U(z, T)$, namely

$$U(z, T) = \frac{1}{2\pi}\int_{-\infty}^{\infty} \tilde{U}(z, \omega)\exp(-i\omega T)d\omega, \tag{9.2.11}$$

Then it satisfies the ordinary differential equation

$$i\frac{\partial \tilde{U}}{\partial z} = -\frac{1}{2}\beta_2\omega^2\tilde{U}. \tag{9.2.12}$$

The solution is

$$\tilde{U}(z, \omega) = \tilde{U}(0, \omega)\exp(\frac{i}{2}\beta_2\omega^2 z). \tag{9.2.13}$$

Equation (9.2.13) shows that GVD changes the phase of each frequency spectrum component in the pulse, the size of change is different according to the different frequency ω and the transmission distance z. Substituting Eq. (9.2.13) into Eq. (9.2.11), we can obtain the general solution of Eq. (9.2.10):

$$U(z, T) = \frac{1}{2\pi}\int_{-\infty}^{\infty} \tilde{U}(0, \omega)\exp(\frac{i}{2}\beta_2\omega^2 z - i\omega T)dT, \tag{9.2.14}$$

where $\tilde{U}(0, \omega)$ is the Fourier transformation of incident light filed at $z = 0$, namely

$$\tilde{U}(0, \omega) = \int_{-\infty}^{\infty} U(0, T)\exp(i\omega T)dT. \tag{9.2.15}$$

Equations (9.2.14) and (9.2.15) are suitable to the arbitrary shape incident pulse. If the incident pulse is a Gaussian pulse (as shown in Fig. 9.3):

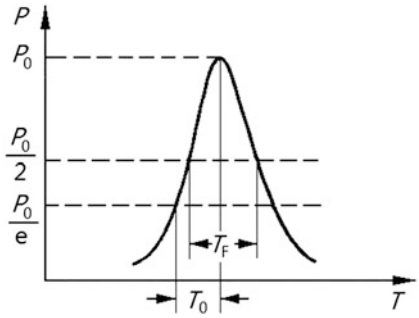

Fig. 9.3 Gaussian pulse waveform and the relation of T_0 and T_{FWHM}

$$U(0,T) = \exp\left(-\frac{T^2}{2T_0^2}\right), \tag{9.2.16}$$

where T_0 is the same as the pulsewidth of light pulse introduced by Eq. (9.2.4), its strict definition is the half width of the light pulse at $1/e$ of peek value. Actually in common use, T_0 is replaced by full width at half maximum T_{FWHM}. For Gaussian light pulse, the relationship between T_{FWHM} and T_0 is

$$T_{\mathrm{FWHM}} = 2(\ln 2)^{1/2} T_0 \approx 1.665 T_0. \tag{9.2.17}$$

Using Eqs. (9.2.14)–(9.2.16), and to integral, we obtain the amplitude at any point z along the fiber:

$$U(z,T) = \frac{T_0}{(T_0^2 - i\beta_2 z)^{1/2}} \exp\left(-\frac{T^2}{2(T_0^2 - i\beta_2 z)}\right). \tag{9.2.18}$$

So the light pulse in the propagation keeps its Gaussian shape, but its pulsewidth T_1 is increased with increasing of z as follows:

$$T_1(z) = T_0[1 + (z/L_D)^2]^{1/2}. \tag{9.2.19}$$

Equation (9.2.19) shows that except the broaden factor T_1/T_0 is related with z, it also depends on the dispersion length $L_D = T_0^2/|\beta_2|$. For a certain fiber length, if the pulsewidth T_0 is shorter and dispersion $|\beta_2|$ is lager, the dispersion length L_D is shorter, than the pulse broaden is larger at $z = L_D$, the broaden of Gaussian pulse is $\sqrt{2}$ times of that of the incident pulse. Figure 9.4 shows the broaden situations of Gaussian pulse $|U(z,T)|^2 - T/T_0$ curves at $z/L_D = 0, 2$, and 4 induced by dispersion. It is clear that propagation distance is longer, the pulse broaden is larger.

To comparison Eqs. (9.2.16) and (9.2.18) we can see, although incident pulse is not chirped (the frequency is not modulated), the transmitted pulse becomes chirped (the frequency is modulated). For clear, we rewrite the Eq. (9.2.18) to be following form:

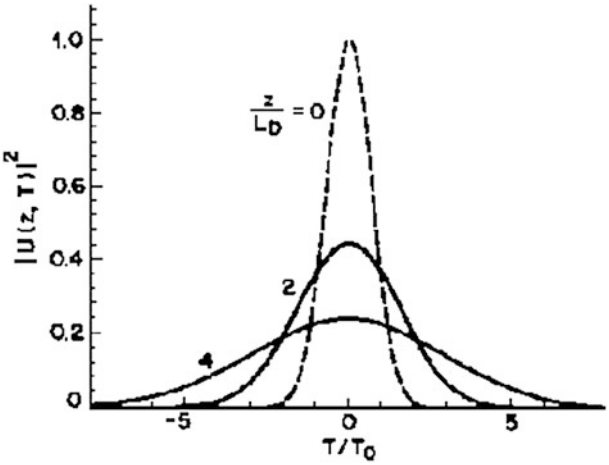

Fig. 9.4 Broadening of Gaussian pulse due to dispersion effect at $z = 2L_D, 4L_D$. The vertical coordinate is the normalized light intensity, the transverse coordinate is the normalized time, and the imaginary line denotes the incident pulse waveform at $z = 0$

$$U(z,T) = |U(z,T)| \exp[i\phi(z,T)], \tag{9.2.20}$$

where

$$\phi(z,T) = -\frac{\mathrm{sgn}(\beta_2)(z/L_D)}{1+(z/L_D)^2}\frac{T^2}{T_0^2} + \frac{1}{2}\tan^{-1}\left(\frac{z}{L_D}\right). \tag{9.2.21}$$

It is dispersion induced phase variation (phase shift) of light pulse with time. It means that in the two sides of center frequency ω_0, there are different frequency difference between the frequency at each moment ω and the center frequency ω_0, namely $\delta\omega = \omega - \omega_0$, this frequency difference is equal to a negative number of the time derivative of phase shift, i.e., $\delta\omega(T) = -\partial\phi/\partial T$ [the negative sign is due to selection of factor $\exp(-i\omega_0 t)$ in the light-filed expression (9.1.4)]:

$$\delta\omega(T) = -\frac{\partial\phi}{\partial T} = \frac{\mathrm{sgn}(\beta_2)(2z/L_D)}{1+(z/L_D)^2}\frac{T}{T_0^2}. \tag{9.2.22}$$

It means that the fiber dispersion applies a time-dependent frequency to the light pulse, that frequency variation with time is frequency chirp. Because the relation between the chirp and the time is a linear relation, it is called linear frequency chirp. The plus or minus of chirp $\delta\omega$ depends on the sign of β_2, in the normal dispersion region ($\beta_2 > 0$), in the pulse leading edge ($T < 0$), $\delta\omega$ is minus (red shift), but in the pulse tailing edge ($T > 0$), $\delta\omega$ is plus (blue shift), i.e., red head and violet tail; in the anomalous dispersion region ($\beta_2 < 0$), the contrary is the case, $\delta\omega$ of the pulse leading edge is plus (blue shift), and $\delta\omega$ of the pulse tailing edge is

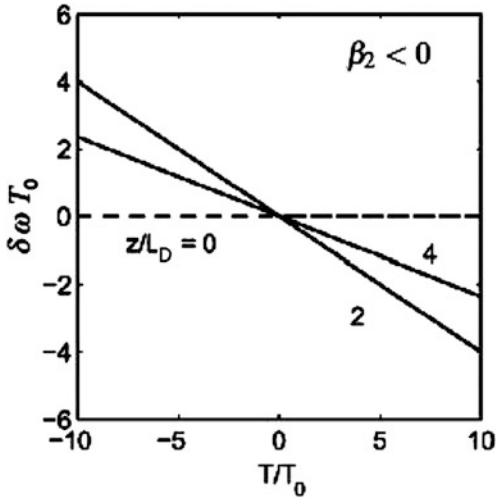

Fig. 9.5 Normalized frequency chirp of Gaussian light pulse $\delta\omega T_0$ as a function of T/T_0 (*straight line* relation) at $z = 2L_D, 4L_D$, the imaginary line denotes that the incident pulse at $z = 0$ is no chirp

minus (red shift), i.e., violet head and red tail. The curves of $\delta\omega T_0 - (T/T_0)$ is shown in Fig. 9.5. Form the figure we can see, when $z = 0$, the Gaussian light pulse has no chirp $\delta\omega$; the chirp becomes larger with increase of propagation distance of light pulse; when $z = L_D$, the chirp is maximum, after that the chirp gradually becomes smaller, until disappears.

We can understand the dispersion induced light-pulse broadening in this way: because of GVD effect, the different frequency component has different propagation velocity in the fiber. In the normal dispersion region ($\beta_2 > 0$), the red light component is going faster than the blue light component, but in the anomalous dispersion region ($\beta_2 < 0$), the blue light component is going faster than red light component. Any relative decay of different frequency component all leads the pulse broadening. Only when all frequency components arrive at the same time, the pulsewidth is possible to keep no change.

9.2.3 *Influence of Self-phase Modulation to Pulse Propagation*

If $L << L_D$, but $L \approx L_{NL}$, The first item of left of Eq. (9.2.6) can be neglected, the pulse change mainly depends on the self-phase modulation (SPM). In this case L_{NL} is much smaller than L_D:

$$\frac{L_D}{L_{NL}} = \frac{\gamma P_0 T_0^2}{|\beta_2|} \gg 1. \tag{9.2.23}$$

This condition is suitable the light pulse with more wide pulsewidth $T_0 > 100\,\text{ps}$ and power $P_0 \approx 1\,\text{W}$ propagates in the regular fiber at $\lambda = 1.55\,\mu\text{m}$. Omitting the dispersion item, Eq. (9.2.6) becomes

$$\frac{\partial U}{\partial z} = \frac{ie^{-\alpha z}}{L_{NL}}|U|^2 U, \tag{9.2.24}$$

where α is the loss of fiber; $L_{NL} = (\gamma P_0)^{-1}$; $\gamma = n_2\omega_0/cS_{eff}$.

Setting the trying solution of Eq. (9.2.24) is

$$U = V\,\exp(i\phi_{NL}), \tag{9.2.25}$$

Substituting Eq. (9.2.25) into Eq. (9.2.24), than divided it into the real part (amplitude) and imaginary part (nonlinear phase shift) two equations:

$$\frac{\partial V}{\partial z} = 0, \tag{9.2.26}$$

$$\frac{\partial \phi_{NL}}{\partial z} = \frac{e^{-\alpha z}}{L_{NL}} V^2. \tag{9.2.27}$$

Because from Eq. (9.2.26) we can know that the amplitude V is without change with z, we can directly integral to Eq. (9.2.27), than obtain the general solution:

$$U(L,T) = U(0,T)\exp[i\phi_{NL}(L,T)], \tag{9.2.28}$$

where $U(0,T)$ is the light filed amplitude at $z = 0$, the nonlinear phase shift $\phi_{NL}(L,T)$ is:

$$\phi_{NL}(L,T) = |U(0,T)|^2(L_{eff}/L_{NL}), \tag{9.2.29}$$

where L_{eff} is the effective length related with the absorption loss:

$$L_{eff} = [1 - \exp(-\alpha L)]/\alpha. \tag{9.2.30}$$

From Eq. (9.2.29) one can see, SPM induced nonlinear phase shift is proportional to the intensity of incident light in every moment, so the law of the phase-shift variation with time is the same as the law of the incident-light-pulse intensity variation with time, from Eq. (9.2.30) one can see, the increase of phase shift with increasing of fiber length. Due to the absorption loss of fiber, the efficient length L_{eff} is smaller than the length of fiber L. But when without loss, i.e., $\alpha = 0$, than $L_{eff} = L$. Because U is normalized, $U(0,0) = 1$ is maximum value, therefore the maximum phase shift $\phi_{\max}$ appears at $T = 0$ of the center of pulse. From Eq. (9.2.29), we obtain

$$\phi_{\max} = L_{eff}/L_{NL} = \gamma P_0 L_{eff}. \tag{9.2.31}$$

Equation (9.2.31) shows the physical meaning of nonlinear length is the efficient propagation length under $\phi_{\max} = 1$. If taking the typical nonlinear parameter $\gamma = 2\,\mathrm{W}^{-1}\mathrm{km}^{-1}$ for fiber at $\lambda = 1.55\,\mu\mathrm{m}$, when $P_0 = 10\,\mathrm{mW}$, we have $L_{NL} = 50\,\mathrm{km}$. L_{NL} will shorten with increase of P_0.

SPM induced frequency-spectrum broadening is coming from the variation of $\phi_{NL}(L, T)$ with time, it means that there are different frequency difference between the instantaneous frequency at two sides of center frequency in every moment and the center frequency. Using Eq. (9.2.29), we can calculate to get the frequency difference:

$$\delta\omega(T) = -\frac{\partial\phi_{NL}}{\partial T} = -\left(\frac{L_{eff}}{L_{NL}}\right)\frac{\partial}{\partial T}|U(0,T)|^2. \tag{9.2.32}$$

The variation of $\delta\omega$ with time is called the frequency chirp. This SPM induced chirp is increased with increasing of the propagation distance. In other word, as the light pulse propagation in optical fiber, the new frequency components produced continuously, cause frequency spectrum broadening continuously.

From Eq. (9.2.32) one can see, the frequency chirp is related with the pulse waveform. If the light pulse is Gaussian type, than SPM induced chirp is

$$\delta\omega(T) = 2\frac{L_{eff}}{L_{NL}}\frac{T}{T_0^2}\exp\left[-\frac{T^2}{T_0}\right]. \tag{9.2.33}$$

Figure 9.6 shows when $L_{eff} = L_{NL}$, the action of self-phase modulation to the Gaussian-pulse propagation produced characteristic curves: the nonlinear phase shift ϕ_{NL} change with time (above) and the frequency chirp $\delta\omega$ change with time (below). According to Eq. (9.2.29), the curve of ϕ_{NL} change with time in the figure above is the same as the curve of pulse-intensity change with time. From the figure below we can see, the curve of frequency chirp $\delta\omega$ change with time has following characteristic: at the pulse leading edge, $\delta\omega$ is negative (red shift); to reach the pulse tailing edge, $\delta\omega$ becomes positive (blue shift), i.e., it appears red head and violet tail phenomenon; in the wide range of the pulse center region the chirp is linear and upward (up chirp); at the steepest inflection point of pulse leading edge and pulse tailing edge, there is maximum chirp value.

9.2.4 Combined Action of Dispersion and Self-phase Modulation

When $L \geq L_D$ and $L \geq L_{NL}$, GVD and SPM combined action to the light pulse. The interaction between both generates entirely different influence to the behavior of light pulse. In the fiber anomalous dispersion region ($\beta_2 < 0$), the actions of GVD

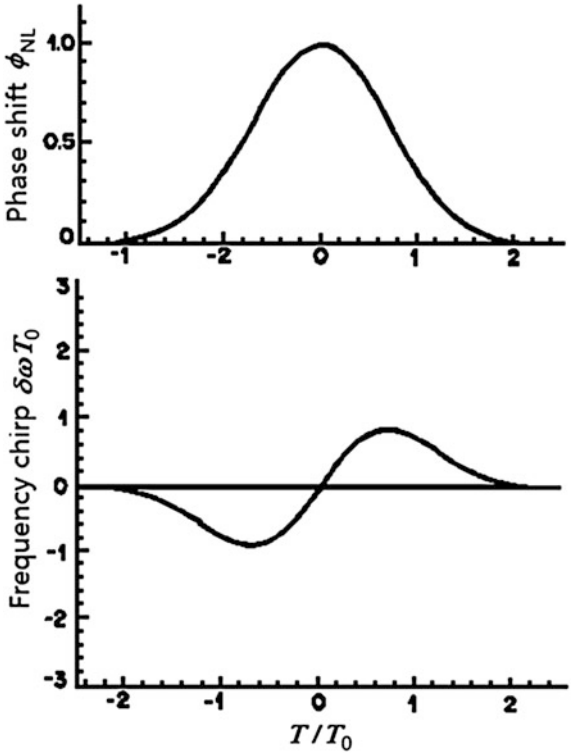

Fig. 9.6 Curves of phase shift ϕ_{NL} (*power*) and frequency chirp $\delta\omega$ as a function of time for Gaussian pulse propagation characteristic produced by self-phase modulation

and SPM are opposite: GVD generates violet head and red trail chirp; but SPM generates red head and violet trail chirp. When both reach the balance, it can eliminate the chirp in the optical fiber, the pulse shape will remain unchanged, thus the optical soliton will be produced.

Now we rewrite the nonlinear Schrodinger Eq. (9.2.6) into following normalized form:

$$i\frac{\partial U}{\partial \xi} = \mathrm{sgn}(\beta_2)\frac{1}{2}\frac{\partial^2 U}{\partial \tau^2} - N^2 e^{-\alpha z}|U|^2 U, \tag{9.2.34}$$

where ξ and τ denote the normalized variables distance and time respectively, which are defined as

$$\xi = z/L_D, \quad \tau = T/T_0. \tag{9.2.35}$$

The definition of parameter N is

$$N^2 = \frac{L_D}{L_{NL}} \equiv \frac{\gamma P_0 T_0^2}{|\beta_2|}. \tag{9.2.36}$$

In Eq. (9.2.34), $\mathrm{sgn}(\beta_2) = \pm$ depend on that the GVD is in normal dispersion region $(\beta_2 > 0)$ or in anomalous dispersion region $(\beta_2 > 0)$. The integer value N depends on the relative strength of SPM and GVD in the evolution process of light pulse in the fiber. When $N \ll 1$, the action of GVD is dominating; and when $N \gg 1$, the action of SPM is dominating, but when $N \approx 1$, the two actions of SPM and GVD are equal.

For a specific N, there are many practical groups of pulsewidth and power suitable Eq. (9.2.36), for example, if $N = 1$, one can select: $T_0 = 1\,\mathrm{ps}$ and $P_0 = 1\,\mathrm{W}$; $T_0 = 10\,\mathrm{ps}$ and $P_0 = 10\,\mathrm{mW}$; $T_0 = 0.1\,\mathrm{ps}$ and $P_0 = 100\,\mathrm{W}$, etc.

NLS Eq. (9.2.34) is a nonlinear partial differential equation. In general it cannot obtain the analytical solution. In order to obtain the numerical solution of the NLS equation, one can employ the split-step Fourier method, namely use of different differential operator to denote the linear and nonlinear effects of dispersion and absorption respectively, applied to the different segment of fiber, replacing the differential operator by the Fourier frequency, using finite Fourier transform (FFT) algorithm to numerical calculation.

Figure 9.7 draws the evolution process of pulsewidth and frequency spectrum for an non-initial chirp Gaussian pulse propagating in the fiber with length of $z = 5L_D$ in fiber normal dispersion region $(\beta_2 > 0)$, and in the condition of $N = 1$ and $\alpha = 0$. Because in the normal dispersion region SPM makes the pulse leading

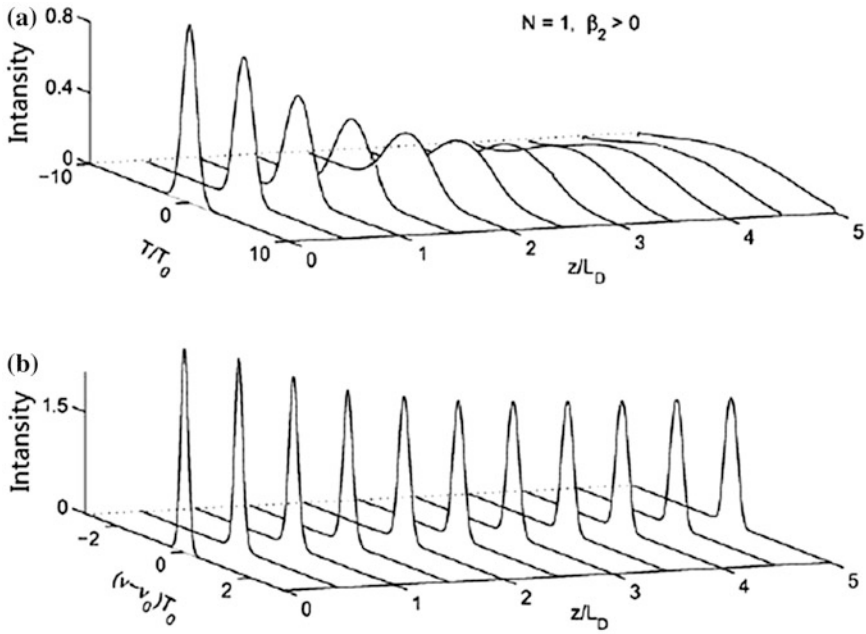

Fig. 9.7 When a Gaussian pulse without initial chirp propagates in a fiber with length of $z = 5L_D$, in the fiber normal dispersion region $(\beta_2 > 0)$ and condition of $N = 1$ and $\alpha = 0$, the curves of **a** pulse shape versus distance; **b** frequency spectrum versus distance

edge to red shift and pulse trailing edge to blue shift, its action is the same as the GVD, therefore SPM induced pulse broadening speed is faster than the case only has the action of GVD.

In the anomalous dispersion region ($\beta_2 > 0$), the evolution process of pulse-width and frequency spectrum of Gaussian pulse under other same condition ($N = 1$ and $\alpha = 0$) is shown in Fig. 9.8. In the beginning, the speed of pulse broadening is slower than the speed in the case without SPM (it only has GVD), until when $z > 4L_D$, than basically achieve the unchanged state. But the frequency spectrum width is much narrower than the width in the case without SPM (it only has GVD). It is not hard to understand, according to Eq. (9.2.32), SPM generated chirp is possible; but according to Eq. (9.2.22), GVD generated chirp in $\beta_2 < 0$ region is negative. When $N = 1$, the actions of two chirps in the nearby the center of Gaussian pulse cancel each other out. In the pulse propagation process, though the combined action of GVD and SPM, self-regulation of the pulse shape, as far as possible entirely offset these two inverse chirps, to maintain non-chirped pulse propagation. The generation process of optical soliton is similar to this situation: in the beginning the Gaussian pulse inputs, it is not fundamental-state soliton, so it has a certain broadening. However the combined action of GVD and SPM leads the pulse shaping, finally the pulse evolves into a hyperbolic secant type fundamental-state optical soliton, as shown in Fig. 9.8.

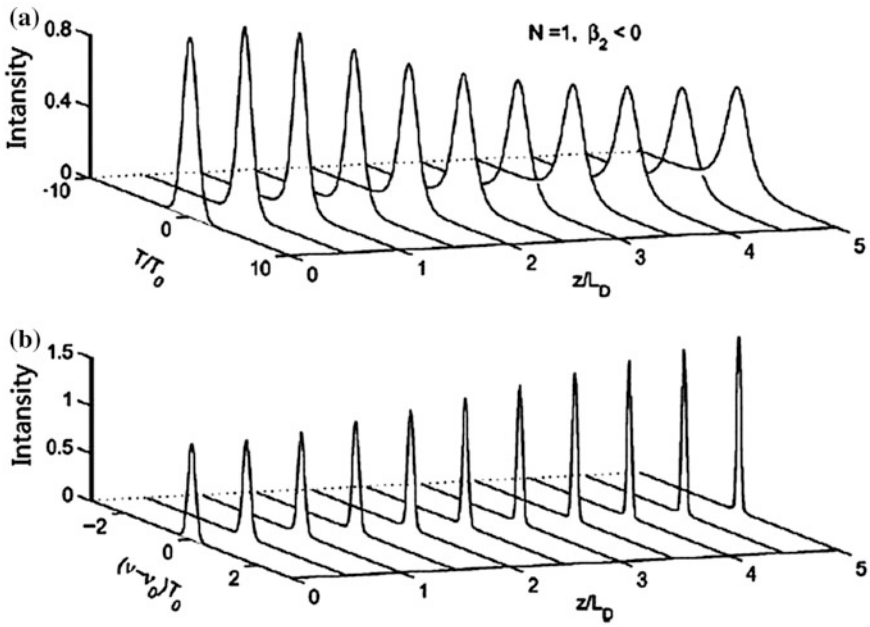

Fig. 9.8 Non-chirp Gaussian pulse propagation curves: **a** pulse shape and **b** frequency spectrum in anomalous dispersion region ($\beta_2 > 0$), and in condition of $N = 1$ and $\alpha = 0$

Actually, although many lasers launched laser pulses are all Gaussian type, only some specially-made mode-locked laser generates the hyperbolic secant type optical soliton, namely

$$U(0,T) = \sec\mathrm{h}\left(\frac{T}{T_0}\right)\exp\left(-\frac{iCT^2}{2T_0^2}\right), \tag{9.2.37}$$

where C is the chirp parameter, it depends on the initial chirp of pulse. T_0 is the half width at 1/e of peak intensity, for hyperbolic secant type optical pulse, the relation between T_0 and the full width at half maximum intensity T_{FWHM} is

$$T_{FWHM} = 2\ln(1+\sqrt{2})T_0 \approx 1.763T_0. \tag{9.2.38}$$

In comparison with Eq. (9.2.17), we can see that the difference of T_{FWHM} between the hyperbolic secant type light pulse and the Gaussian type light pulse is not too big, but the hyperbolic secant type light pulsewidth is narrower than the Gaussian type light pulsewidth.

If light pulse is non-chirp pulse, $C = 0$, i.e., it is the fundamental wave optical soliton. In the propagation process, its waveform and optical spectrum all keep no change. If the incident light pulse deviate the hyperbolic secant pulse waveform, the combined action of GVD and SPM can make the light pulse to evolve to be hyperbolic secant pulse.

9.3 Time Soliton and Space Soliton

Optical soliton can be interpreted as a matter state when both of linear effect and nonlinear effect achieve a balance in the propagation of light wave. Optical soliton in general is classified into the time optical soliton and the space optical soliton. The time soliton is a balance state of light pulse when two opposite chirp effects induced by the dispersion and the nonlinear self-phase modulation achieve a balance. The space soliton is a balance state of light pulse when the diffraction and the nonlinear self-focusing achieve a balance.

9.3.1 Time Soliton

In 1834 S. Russell, a shipbuilder of the United Kingdom observed a circular smooth wave peak of water wave in a narrow river channel, this phenomenon is called solitary wave or soliton by later generations. In 1895, Korteweg and De Vries proposed KDV equation to explain it. Until the 70s of 20th century the development of fiber communication, the optical soliton study brought to attention.

In 1971 Zeldovich and Sobelman at the first time proposed the theory of compressing light pulse with SPM by using GVD effect [2]; in 1972 Zakharov and Shabat based on analysis of nonlinear wave equation, obtained the conclusion of existence of time soliton wave solution with hyperbolic secant form [3]. In 1973, Bell Labs A. Hasegawa and F. Tappert firstly propose the idea for application of optical soliton in the optical fiber communication [4]. Because the formation of stable optical soliton requires very high technology, until to1980, Mollenauer et al. firstly observed optical soliton in Bell laboratory [5]. In 1984 Mollenauer et al. successfully developed the color center soliton laser [6], in 1991, Smith et al. successfully developed all-fiber integrated erbium-doped fiber soliton laser [7], in 1999, P. Andrekson et al. completed several field investigations of soliton propagation in fiber [8].

Time soliton can be described by nonlinear Schrodinger Eq. (9.2.3). If neglecting the absorption loss, the nonlinear Schrodinger Equation can be simplified as

$$i\frac{\partial A}{\partial z} = \frac{\beta_2}{2}\frac{\partial^2 A}{\partial T^2} - \gamma|A|^2 A, \tag{9.3.1}$$

where $A = A(z, T)$ is amplitude of pulse envelop (wave packet); β_2 is GVD parameter; γ is SPM nonlinear parameter.

In order to normalize Eq. (9.3.1), we introduce three dimensionless variables:

$$U = \frac{A}{\sqrt{P_0}},\ \xi = \frac{z}{L_D},\ \tau = \frac{T}{T_0}. \tag{9.3.2}$$

Then the equation becomes

$$i\frac{\partial U}{\partial \xi} = \mathrm{sgn}(\beta_2)\frac{1}{2}\frac{\partial^2 U}{\partial \tau^2} - N^2|U|^2 U, \tag{9.3.3}$$

where P_0 is the pulse peak power; T_0 is the incident pulsewidth; Parameter N is defined as

$$N^2 = \frac{L_D}{L_{NL}} = \frac{\gamma P_0 T_0^2}{|\beta_2|}. \tag{9.3.4}$$

Through the definition of

$$u = NU = \sqrt{\gamma L_D} A, \tag{9.3.5}$$

The parameter N can be eliminated from Eq. (9.3.3). Considering in anomalous dispersion GVD case, we take $\mathrm{sgn}(\beta_2) = -1$, the equation becomes following standard form of nonlinear Schrodinger (NLS) Equation:

$$i\frac{\partial u}{\partial \xi} + \frac{1}{2}\frac{\partial^2 u}{\partial \tau^2} + |u|^2 u = 0. \tag{9.3.6}$$

Equation (9.3.6) can be solved by using inverse scattering method. Actually, it is a method similar to Fourier transform. This method is using the incident filed at $z = 0$ to obtain the initial scattering data, than through solving lineal scattering problem to obtain the change of propagation field along z, than from the changed scattering data to rebuild the new propagation field. The process of this method is too complicate; here we just introduce a simpler method to solve the fundamental state soliton.

Suppose NLS Equation has a solution maintaining a no-changed shape, namely

$$u(\xi, \tau) = V(\tau)\exp[i\phi(\xi, \tau)], \tag{9.3.7}$$

where V is independent with ξ, Eq. (9.3.7) denotes the fundamental state soliton with no-changed shape in propagation process. The phase ϕ is a function of ξ and τ.

Substituting Eq. (9.3.7) into Eq. (9.3.6), and then separating into real part and imaginary part, one can obtained the two equations related with amplitude V and phase ϕ, respectively. The phase equation shows that ϕ should adopt the form of $\phi(\xi, \tau) = K\xi - \delta\tau$, in which K and δ are constant. If taking $\delta = 0$ (without frequency shift), then V should satisfy

$$\frac{d^2 V}{d\tau^2} = 2V(K - V^2). \tag{9.3.8}$$

In the two sides of Eq. (9.3.8) multiply by $2(dV/d\tau)$, and integral to τ, we can obtain

$$(dV/d\tau)^2 = 2KV^2 - V^4 + C, \tag{9.3.9}$$

where C is integration constant. Using boundary condition, namely when $|\tau| \to \infty$, V and $dV/d\tau$ are equal to zero, so $C = 0$. Constant K is depended on the condition that at soliton peak value, $V = 1$ and $dV/d\tau = 0$. And assuming the peak value appears at $\tau = 0$, thus we can get $K = 1/2$, then $\phi = \xi/2$. Simple integral to the equation, to obtain $V(\tau) = \operatorname{sec}\mathrm{h}\,\tau$, from this we can obtain the following soliton solution:

$$u(\xi, \tau) = \operatorname{sec}\mathrm{h}(\tau)\exp(i\xi/2). \tag{9.3.10}$$

This is a standard form of fundamental state soliton. Equation (9.3.10) indicates that if light pulse is a hyperbolic secant pulse with pulsewidth T_0, peak power P_0 satisfied Eq. (9.3.4) with $N = 1$. If this pulse inputs into a lossless idea fiber, the pulse will be non-distortion propagation, never change its shape in any distance. Setting $N = 1$ in Eq. (9.3.4), we can obtain the peak power required for propagating fundamental state soliton, i.e.,

$$P_0 = \frac{|\beta_2|}{\gamma T_0^2} \approx \frac{3.11|\beta_2|}{\gamma T_{FWHM}^2}, \tag{9.3.11}$$

where the relation of $T_{FWHM} \approx 1.76T_0$ is used.

For the dispersion shift fiber at 1.55 μm, the typical values are $\beta_2 = -1\,\mathrm{ps}^2/\mathrm{km}$ and $\gamma = 3\,\mathrm{W}^{-1}/\mathrm{km}$. When $T_0 = 1\,\mathrm{ps}$, P_0 is about 1 W; when $T_0 = 10\,\mathrm{ps}$, P_0 is reduced to 10 mW. Therefore even for 20 Gb/s high bit rate transmission system, it can be reached by semiconductor laser at this power level, also can form the fundamental state soliton in the fiber.

The solution satisfied NLS Eq. (9.3.10) is not only above described so called "bright soliton" solution, but also having many other solutions. For example the "dark soliton" is also a solution. Its intensity profile is a caving on the uniform background. We only change the symbol of time-differential item in Eq. (9.3.6), the NLS equation for describing the dark soliton can be obtained:

$$i\frac{\partial u}{\partial \xi} - \frac{1}{2}\frac{\partial^2 u}{\partial \tau^2} + |u|^2 u = 0. \tag{9.3.12}$$

We can assume the form of solution is

$$u(\xi, \tau) = V(\tau)\exp[i\phi(\xi, \tau)]. \tag{9.3.13}$$

Then substrate it into V and ϕ satisfied differential equations, thus we can obtain the solution of dark soliton. The difference compared with the bright soliton is: when $|\tau| \to \infty$, $V(\tau)$ becomes a non-zero constant, its general solution can be written as

$$|V(\xi, \tau)| = V(\tau) = \eta\{1 - B^2 \operatorname{sech}^2[\eta B(\tau - \tau_s)]\}^{1/2}. \tag{9.3.14}$$

The phase is

$$\phi(\xi, \tau) = \frac{1}{2}\eta^2(3 - B^2)\xi + \eta\sqrt{1 - B^2}\tau + \arctan\left[\frac{B\tanh(\eta B\tau)}{\sqrt{1 - B^2}}\right], \tag{9.3.15}$$

where parameters η and τ_s are denoted the amplitude of soliton and the location of caving, respectively. B is denoted the deep of caving ($|B| \le 1$). For $|B| = 1$, the intensity of caving center drops to zero; for other value of B, caving not tends to zero. So the dark soliton for $|B| < 1$ is called gray soliton. The parameter B determines the dark degree of gray soliton. The gray soliton for $|B| = 1$ is called dark soliton. In Eq. (9.3.14), to set $\eta = 1$ and $B = 1$, we can obtain the standard form of dark soliton:

$$u(\xi, \tau) = \tanh(\tau)\exp(i\xi). \tag{9.3.16}$$

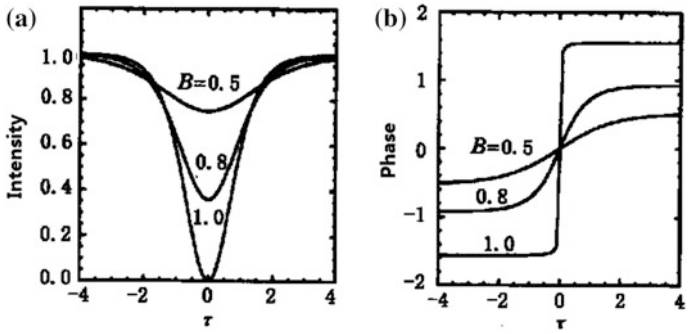

Fig. 9.9 Characteristic curves of dark soliton for different parameter B: **a** the intensity versus the time; **b** the phase versus the time

Therefore the dark soliton has the hyperbolic tangent type amplitude. The dark soliton is a hyperbolic tangent pulse with a sunk at the center, it keeps no change when propagation in normal dispersion region.

Figure 9.9 gives the intensity-time curve and the phase-time curve for dark soliton when Btakes different values. At $\tau = 0$, the dark soliton is a hyperbolic tangent pulse with a center sink, the sink of black soliton is maximum, $|B|$ is smaller, the sink is smaller; at $\tau = 0$, also has a phase break, the phase break of black soliton is $\pi.|B|$ is smaller, the phase break is smaller, and change slower.

9.3.2 Space Soliton

In comparison with time soliton, the conception of space soliton is proposed later. So called space soliton is that the light pulse propagates in nonlinear medium, when the linear diffraction and the nonlinear self-focusing effect both reach a balance, the pulse propagation forwards ahead with a stable space form. The study related to space soliton should date back to 1964, Chiao et al. [9] started to study the self-focusing, they proposed the description of light beam "self-trapping" effect. But until 1972 Zakharov and Shabat [10] given the soliton theory by using classical nonlinear Schrodinger equation, after that people gradually aware the self-focusing filament is just a kind of space bright optical soliton.

In the situation of neglecting the medium loss, the propagation of space soliton can be described by using following NLS equation:

$$i\frac{\partial q}{\partial \xi} + \frac{\partial^2 q}{\partial \zeta^2} - 2|q|^2 q = 0. \tag{9.3.17}$$

where $q = E/E_0$ is normalized filed amplitude; $\xi = z/z_0$ is the normalized vertical coordinate; $\zeta = x/x_0$ is the normalized transverse coordinate. Here E_0 is maximum amplitude of filed, $z_0 = 2n_0/(\beta n_2|E_0|^2)$ is the characteristic scale of space soliton propagation, $x_0 = \sqrt{n_0}/(\beta\sqrt{n_2}|E_0|^2)$ is the characteristic scale of space soliton width. Here n_0 is linear refractive index, β is light propagation constant in the medium.

The space optical soliton also can be divided into two kinds of the bright soliton and the dark soliton. In 1985 A. Barthelemy et al. in the first experimentally proved that in the Kerr medium, the diffraction effect and the nonlinear self-focusing effect reach a balance to form a space bright soliton. Actually, any medium with self-focusing effect all can observe the space bright soliton, the materials including various three-order nonlinear optical medium, two-order nonlinear crystal, liquid crystal composed with anisotropic molecules, and photorefractive materials.

In 1987, P.A. Belanger and P. Mathieu, at the first time, started from NLS equation to prove that the existence of the space dark soliton in self-focusing Kerr medium is possible. In 1988, Maneuf et al. [11] observed the change from fundamental soliton to three–order soliton in KDP crystal. After that people observed space dark optical soliton in different mediums, and tried to apply the space dark soliton in design of controllable flexibility optical waveguide, X and Y-type directional couplers, and all-optical switches, etc. in 1996, Li's [12] research group experimentally proved the existence of space dark soliton in C_{60} solution and demonstrated the space dark soliton induced flexibility optical waveguide. In 1997 they also experimentally demonstrated the thermal induced space dark soliton in chlorophyll-acetone solution [13].

In general, the experimental studies of space dark soliton are used the material with minus nonlinear refractive index $(\Delta n < 0)$, including various isotopic three-order nonlinear medium, and the wavelength of incident laser are selected nearby the single photon and two-photon resonant frequency; in addition the anisotropic two-order nonlinear crystal and photorefractive materials, etc. can also produce the refractive index change $\Delta n < 0$, to demonstrate the space dark soliton.

Review Questions of Chapter 9

1. There are which steps to deduce the Nonlinear Schrodinger Eq. (9.1.38) for describing the propagation of picosecond light pulse in the single mode fiber; what physical meaning in that equation?
2. Illustrate the source, meaning, significance and application of following forms of NLS equations: (1) Eq. (9.2.3) using group-velocity motion time coordinate; (2) Eq. (9.2.6) containing normalized time, dispersion length and nonlinear length; (3) Eq. (9.2.34) containing normalized time, normalized distance and parameter N; (4) Standard Eq. (9.3.6) using normalized time, distance, and amplitude.
3. Please deduce the material dispersion formula (9.1.43). What are regular fiber, dispersion shift fiber and dispersion flat fiber? Draw the dispersion-wavelength

characteristic curves. What is normal dispersion and anomalous dispersion? In which kind fiber for generation of optical soliton?

4. Discuss the propagation of light pulse in following four cases: (1) excluding dispersion and nonlinearity; (2) consider the influence of dispersion; (3) consider the influence of self-phase modulation; (4) consider the combined action of dispersion and self-phase modulation. Explain the formation of time optical soliton.
5. From NLS Eq. (9.3.6) to find the solution of fundamental wave time optical soliton. Write down dark soliton equation and its fundamental state solution. What is the characteristic of dark soliton, what is difference between bright soliton and dark soliton?
6. What is space optical soliton? Illustrate its generation mechanism. What is nonlinear Schrodinger equation for describing space optical soliton?

References

1. G.P. Agrawal, *Nonlinear Fiber Optics*, 4th edn. (Academic Press, New York, 2006)
2. B. Zeldovich, I.I. Sobelman, Possibility of shortening light pulses in alkali-metal vapor. JETP **13**(3), 129–131 (1971)
3. V.E. Zekharov, A.B. Shabat, Exact theory of two-dimensional self-focusing and one-dimensional self-modulation of wave in nonlinear media. JETP **34**(1), 62–65 (1972)
4. A. Hasegawa, F. Tappert, Transmission of stationary nonlinear optical pulses in dispersive dielectric fibers. I. Anomalous dispersion. Appl. Phys. Lett. **23**(3), 142–144 (1973)
5. L.F. Mollenauer, R.H. Stolen, J.P. Dorden, Experimental observation of picosecond pulse narrowing and solitons in optical fibers. Phys. Rev. Lett. **45**(13), 1095–1098 (1980)
6. L.F. Mollenauer, R.H. Stolen, The soliton laser. Opt. Lett. **9**(1), 13–15 (1984)
7. K. Smith. E.J. Greer, R. Wyatt, et. al., Totally integrated erbium fibre soliton laser pumped by laser diode. Electron Lett. **27**(3), 244–246 (1991)
8. P.A. Andrekson, Laser focus world. Feature Article **35**(5), 145–153 (1999)
9. R.Y. Chiao, E. Garmire, C.H. Townes, Self-trapping of optical beams. Phys. Rev. Lett. **13**(15), 479–482 (1964)
10. V.E. Zakharov, A.B. Shabat, Exact theory of two-dimensional self-focusing and one-dimensional self-modulation of wave in nonlinear media. Sovi. Phys. JETP **34**(1), 62–69 (1972)
11. S. Maneuf, R. Desailly, C. Froehly, Stable self-trapping of laser beams: observation in a nonlinear planar waveguide. Opt. Commun. **65**(3), 193–198 (1988)
12. C. Li, T. Hong, Space dark soliton and its induced feasible optical waveguide in C_{60} solution. Acta Phys. Sini. **45**(10), 1671–1975 (1996)
13. L. Hong, X. Jiandong, S. Liu, C. Li, J. Hong, Experiments of thermal induced space dark soliton in chlorophyll-acetone solution. Acta Optica Sinica **18**(1), 37–40 (1998)

Chapter 10
All-Optical Switch Based on Nonlinear Optics

In this chapter, the first section gives the reviews of all-optical switch (AOS), including the significance, basic principle, classification method, application requirement, recent problem, and development direction. The following sections discuss the six classes of all-optical switches, including optical coupler AOS, Sagnac interferometer AOS, M–Z interferometer AOS, ring resonator AOS, fiber grating AOS, and nanoscale AOS. We will respectively introduce the working principle of these AOSs, and estimate the switching power and the switching time of these AOSs. The working principles of these AOSs are based on various nonlinear optical effects including single photon or two-photon induced nonlinear refractive index change, or nonlinear absorption coefficient change, etc. Up to now, the all-optical switch research is in the stage of fundamental study, it can not reach the technology indexes required by practice device with low power, high speed, and low loss properties. In order to realize these technology indexes, we need shrink the space scale of devices, seek high nonlinearity and low absorption materials, design reasonable nano-structure devices, adopt the probe laser at optical communication wavelength and the pump laser with ultrashort pulsewidth, and use mature opto-electronic integrated technique. Exploration of the practical nano-scale AOSs is present main research direction of all-optical switch.

10.1 Summarization of All-Optical Switch

10.1.1 Research Direction of All-Optical Switch [1]

1. **Significance of All-Optical Switch**

In the early 1960s the invention of laser marks that the optics started development from "Traditional Optics" to "Modern Optics". So called "Modern Optics" is the optics that use laser as optical source. And the laser is consisted of coherence

© Shanghai Jiao Tong University Press,
Shanghai and Springer Nature Singapore Pte Ltd., 2017

C. Li, *Nonlinear Optics*, DOI 10.1007/978-981-10-1488-8_10

photons, so "Modern Optics" is just "Photonis". Nowadays the Photonics already developed to "Optoelectronics" stage or "Micrometer photonics" state, the characteristic of this stage is "controlling light with electricity" and "opto-electronic hybrid", the devises used in this stage, such as semiconductor laser, optical modulator, optical amplifier, photodetector, and electricity controlled optical switch, etc. All of them are "controlling light with electricity" devices and with micrometer scale. The application systems in this stage, such as the optical communication system, the computer system and the optical sensing system are all opto-electricity hybrid systems. For present optical communication system, signal transmission is all-optical, but the signal switching is still used the electronic technology. For precent computer, although the external input and output equipment and storage and display equipment have been changed to photonic technology, but the data process chips are still using the electronic technology. For present sensing system, the sensing device have already used the optical grating sensor, however the signal processing (demodulation technology) still use the electronic method. In today's "optoelectronics stage", the photonic technology has been widely used, many electronic technology have been replaced by photonic technology. But the respect of core technology—information processing technology, the photonics is far behind the electronics. Today's electronic information processing is digitalized, because the electronics has the transistor—an "electricity controlling with electricity" device. However up to now we have no "optical transistor"—"light controlling with light" device that just is all-optical switch. So today's optical information technology is only analog, not digital.

The next stage of photonics will be the stage of "all-optical photonics" or "nanophotonics". In this stage, the nanoscale photonic device will develop to "light controlling with light" or all-optical device. The digital optical information processing will be realized, the computer chip will adopt the all-optical logic elements, the optical communication will use all-optical switching technology; all these all-optical technologies are based on the all-optical switches. Therefore, the all-optical switch is a key technology of future photonic technology.

2. Working Principle of All-Optical Switch

The development of electronics is based on the transistor. The fundamental device in electronic computer is switching transistor; it is a device in which the strong electrical signal is controlled by a weak electrical signal. The laser has been invented for half a of century, why up to now people can not make a practical optical switching transistor based on "light controlling with light", namely all-optical switch? The primary cause is the electrically neutral of photon, among photons without strong electromagnetic interaction, so no way to directly realize "light controlling with light". The only way is using the indirect method—nonlinear optics method to drive the optical switch, i.e., using a pump light changes the transmission medium of signal light, to realize the switching of signal light.

In order to understand the working principle of all-optical switch, as an example, we discuss a space type all-optical switch based on the M–Z nonlinear waveguide

interferometer, as shown in Fig. 10.1. The two arms of M–Z interferometer have same length L and different materials: one is made by nonlinear material (doped silica) with the nonlinear refraction coefficient n_2, another one is linear material (pure silica). A signal light with a low power inputs the interferometer from port 1, and divides into two beams travelling in the two arms. Because the M–Z interferometer is symmetric, the signal light will output from Port 2. When a pump light with a strong power P inputs the interferometer from port 1, and divides into two beams going to two arms, each beam has power $P/2$. Due to Kerr effect the pump light induces refractive-index change Δn in the nonlinear arm, $\Delta n = n_2 P/2S$ (S is the cross sectional area of waveguide). When the signal light beam passes through the nonlinear arm of interferometer, the phase shift in the nonlinear arm will be $\Delta\phi = (2\pi/\lambda)\Delta nL = \pi n_2 LP/\lambda S$, which is just the difference between two phase shifts of signal light beams in two arms. We can prove that the intensities of outputted signal light at two output ports are depended on the phase difference $\Delta\phi$. When the power P is strong enough to make $\Delta\phi = \pi$, the signal light will be totally switched from Port 2 to Port 3. When removing the pump light, the outputted signal light will return to Port 2.

3. Technology Index of Practical All-Optical Switch

The practical all-optical switches are required to achieve technology indexes mainly in the following three aspects: switching power, switching time and optical loss of device:

(1) Low switching power: the switching power ≤ 10 mW (milliwatt magnitude), like the signal power of fiber communication;
(2) High switching speed: the switching time ≤ 10 ps (picosecond magnitude), like the maximum switching speed of electronic switches.
(3) Low optical loss: the insertion loss ≤ 0.5 dB (sub-decibel magnitude), near the transmission loss of fiber, easy to cascade of devices.

But so far existing all-optical switches are difficult to achieve above three technology indexes at the same time.

4. Problem of All-Optical Switch Study

Since the invention of laser people began to study all-optical switch, already spent half a century, expend a lot of research funding, published a mass of research papers, but so far the practical all-optical switching devices are not available in the market. That is why? Because the research of all-optical switch based on nonlinear

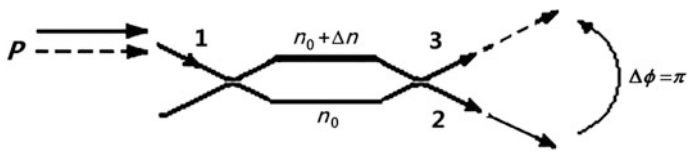

Fig. 10.1 Working principle of nonlinear M–Z interferometer all-optical switch, when pump power is strong enough to make $\Delta\phi = \pi$, the outputted signal light will switch from Port 2 to Port 3

optics has been faced with following three contradiction problems, which are hard to overcome until now:

(1) The contradiction between the switching power and the absorption loss. The all-optical switch usually is based on three-order nonlinear optics effect, it requires high power of pump laser; the pump power is much higher than the controlled signal light power. The high power makes a strong thermal effect, to lead the device unstable. In order to reduce switching power, one need enhance the nonlinearity of material, for this purpose one may select the pump laser at wavelength of resonance absorption area. So that greatly increase of the absorption loss of material, to make the optical switches cannot cascading operation. For example, the semiconductor at wavelength of exciton absorption peak has very strong optical nonlinearity, but its absorption loss is very big; the quartz material has low optical absorption loss, but its optical nonlinearity is too bad, required the switching power is much high.

(2) The contradiction between switching power and switching time (switching speed). For example, the all-optical switch using the liquid crystal material has high optical nonlinearity and low switching power, but its optical switching relays on the molecular rotation, the switching time is long; the all-optical switch using quartz material has high switching speed and low absorption loss, but the molecule of quartz has high symmetry, so its optical nonlinearity is very low. In order to decrease the switching power of quartz all-optical switching, people may adopt the ring resonator structure to increase the optical nonlinearity. But the photon lifetime of ring cavity (nanosecond) limits the switching speed of the device. People also can use two-photon absorption effect to enhance the refractive index change, and than to decrease the switching power (to 10 mW), however, the two-photon absorption accompanies the free carrier absorption to limit the switching time (100 ps only).

(3) The contradiction between switch-on time and switch-off time. In general the switch-on time of all-optical switch depends on the pulsewidth of pump light, if the pump light used picosecond or femtosecond light, the switch-on time can reach picosecond; however, because the limitation of the carrier recombination time, or the molecular moving speed etc., the switch-off time often is longer than the switch-on time in two order of magnitudes (greater than nanosecond). For example, the switch-on time of semiconductor all-optical switch can achieve picosecond, but the carrier recombination time needs dozens of nanosecond. One may adopt ultrathin interface or nonuniform medium, etc. methods to enhance the speed of carrier recombination, but the nonuniformity of medium may increase the optical absorption of medium.

5. Approaches to the Problem

The past research of all-optical switch mainly focus on the seeking of the nonlinear materials with high n_2, less concentrate efforts on device structure and new physical

mechanism, so that up to now no way to solve the problem of practical all-optical switch. In order to solve the problem of practical all-optical switch, the scientists have carried out the following research works:

(1) Form the refractive index change formula of Kerr effect $\Delta n = n_2 I = n_2(P/S)$ we can see that Δn is not only related to n_2 of material, but also related to the waveguide cross-section area. For the certain n_2, the pump power P is proportional to the cross-section area S, hence compression of transverse dimension, use of the nanoscale optical waveguide and nanomaterial (photonic crystal and surface plasmon polariton), can effectively reduce the switching power.

(2) From light induced phase change formula $\Delta\phi = (2\pi/\lambda)\Delta nL = 2\pi n_0 LP/\lambda S$ we can see that, for a certain phase change $\Delta\phi$ (such as $\Delta\phi = \pi$), S and n_2, the pump power P is revers proportional to the device length L, so the increase of L is beneficial to reduction of pump power, but the increase of L will make the device dimension too big, and the switching time is increased. So scientists suggest using ring cavity structure, equivalently infinity increase of the length L. In the same time, to make decrease of the diameter of ring waveguide, the switching speed of device will be increased.

(3) In order to reduce the absorption loss, the optical switch can use silicon, silica or quartz materials, but the nonlinearity of these materials are very low, so the high switching power is required. Scientists suggest adopt micro resonant cavity structure (micro ring or micro F–P cavity), it can be used for accumulating the nonlinearity, to reduce the switching power.

(4) The Kerr effect belongs to single photon effect, the pump light induced refractive index change is proportional to the pump power, i.e., $\Delta n \propto P$. In order to enhance the refractive index change, we can use two-photon effect (TPA). Because its refractive index change is proportional to the square of average power of pump light, i.e., $\Delta n \propto \overline{P}^2$, thus the switching power can be reduced in 3 order of magnitude.

(5) The carrier recombination time of semiconductor greatly limits the switch-off time of all-optical switching. The carrier recombination time of semiconductor depends on grow, deposition, and the size of the device, from dozens of nanosecond to hundreds of picosecond. For example, the compound semiconductor (such as GaAs), the carrier recombination time is about 10 ns; for silicon material, the optical Kerr effect induced carrier recombination time <1 ns, but the two-photon absorption (TPA) under the femtosecond laser action, often accompanieds the free carrier absorption (FCA), the carrier recombination time is about 1 ns. In order to reduce the free carrier absorption, one may doping the oxygen ion O^+ into the silicon, to form the capture center of carrier, in this way the carrier recombination time can be reduced to 3 order of magnitude, to reach 1 ps. The ion-implanted silicon is called II-Si.

(6) In the aspect of nonlinear mechanism, except optical Kerr effect and two-photon effect, we can also explore other physical mechanism, for example, the photon induced band gap shift of photon crystal, the nonlinear

absorption of photon crystal waveguide, nonlinear transmission of coupling grating, or photo-induced solid-liquid phase transition or photo-induced molecule isomerism in the two side of interface of material. Under the nanoscale condition, these new mechanisms are possible to obtain the low switching power and fast switching speed of all-optical switches.

In conclusion, on the foundation of developing nano-photonics and ultrafast-photonics, to compress the device space dimension and the pulsewidth of driving laser, to adopt various nano-structures and new physical mechanisms, in the same time, to enhance the nonlinearity, response time, and transparency of material, finally the practical all-optical switches are possible to realize.

10.1.2 Classification of All-Optical Switch [1]

Different kinds of all-optical switches based different working principles have different characteristics, functions, and application in different occasions. When we discuss the classification of all-optical switch, we will further explain the working principles of all-optical switches.

1. **Classification According to Application Characteristic**

According to application characteristic we can classify the all-optical switch into three categories: the regular optical switch, the optical limiting switch and the optical bistable switch. Their output-input characteristics (P_t–P_i curve) are shown in Fig. 10.2.

The characteristic curves of the regular optical switch and the optical limiting switch are single valued, their switch-on power P_{on} and switch-off power P_{off} are coincided, and it is easy disturbed by the noise, the device is not very stable; the characteristic curve of optical bistable switch is a closed rectangular loop, the switch-on power P_{on} and the switch-off power P_{off} are located on the two side edges of the bistable region. Any input power P_0 in the bistable region is corresponding to two possible output powers P_t' and P_t'', when the action range of noise is smaller than bistable region, the device is very stable.

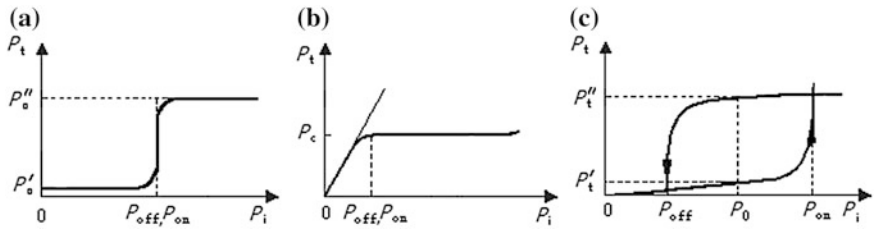

Fig. 10.2 Classification of all-optical switch according to application characteristic: **a** the regular optical switch; **b** the optical limiting switch; **c** the optical bistable switch

The difference between the optical limiting switch and the regular optical switch is that, when the input light power is smaller than the switch-on power, the regular optical switch is in the off-state, and the working characteristic of optical limiting switch likes a linear device: the output power is proportional to the input power. When the input light power of optical limiting switch is greater than the switch-on power, the outputted power is clamp down a low power (P_c) level. The characteristic of optical limiting switch likes that of an electronic voltage-stabilizing diode. So the optical limiting switch is called optical limiter.

The optical switches have a wide application. The regular optical switch can be used in optical communication network for optical switching components, automatic protection and monitoring, detection of batch optical devices, etc.; the optical bistable switch can be used in optical communication, optical computing and optical information processing, such as the optical flip-flop, optical memory, optical switching and optical logical elements; the optical limiting switch can be used in the militarily for making optical limiter to against the laser blind weapon.

2. **Classification According to Switching Function**

According to switching function the all-optical switch can be classified to four categories: the intensity switch, the space switch, the time switch and the waveguide switch, as shown in Fig. 10.3. The intensity switch is used to control some signal light channel on and off, such as the grating-type all-optical switch; the space switch is used to control signal light transforming between different channels, such as the interferometer-type all-optical switch; the time switch can control the time of

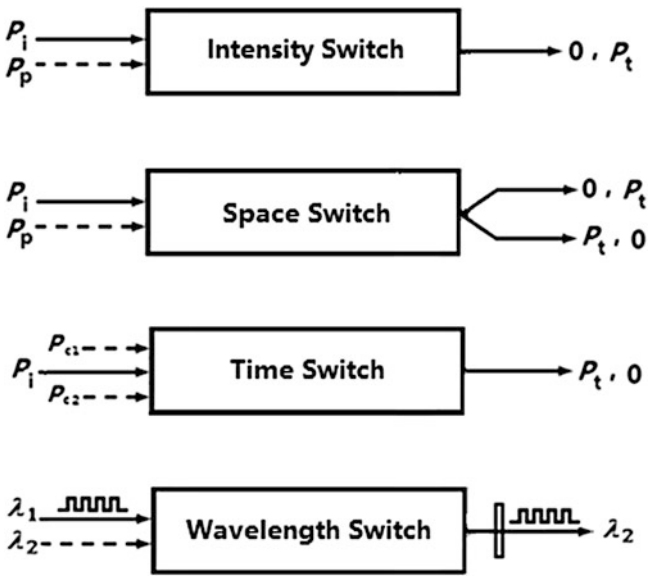

Fig. 10.3 Schematic diagrams of all-optical switches: the intensity switch, the space switch, the time switch and the waveguide switch

switch-on and switch-off of optical switch, such as the optical flip-flop; the wavelength switch can transfer the wavelength of signal carrier wave, such as the wavelength transverter. In Fig. 10.3, the solid line with arrows denotes signal light; the imaginary line with arrows denotes pump light.

3. **Classification According to Controlling Method**

According to the method of controlling signal-light intensity the all-optical switch can be classified into two categories: the cross-pump all-optical switch and the self-pump all-optical switch. As an example we use the following intensity-type all-optical switch to illustrate, as shown in Fig. 10.4.

A signal light beam with low power (P_i) inputs a intensity type all-optical switch in order to realize the switching of outputted signal light power, we can use two optical controlling method: one is using another pump light with high power (P_p), to change the optical parameter of medium (such as refractive index), to lead the phase change of the signal light, and further change its outputted power: transferring between low and high powers. When removing the pump light, the medium is no change, the outputted signal light power return to the original case, as shown in Fig. 10.4a. This is the method to realize the all-optical switch by using two light beams, which is called cross-pump method.

Another method is using incident signal light itself as the pump light to change the refractive index and to change the phase of the signal light. This way looks simpler, but it requires signal light power strong enough, and the power is adjustable. When incident signal power is weak (P_i), the medium without change, the outputted power at low state; when incident signal power becomes strong (P_i'), to induce the refractive index change, the power of output power switches to high state, as shown in Fig. 10.4b, this method to realize the all-optical switch by using one light beam only, which is called self-pump method.

Figure 10.5 shows how to realize the switching under the action of control pulse for an intensity-type all-optical switch. For cross-pump method, the control pulse comes from the pump light; for self-pump method, the control pulse comes from the

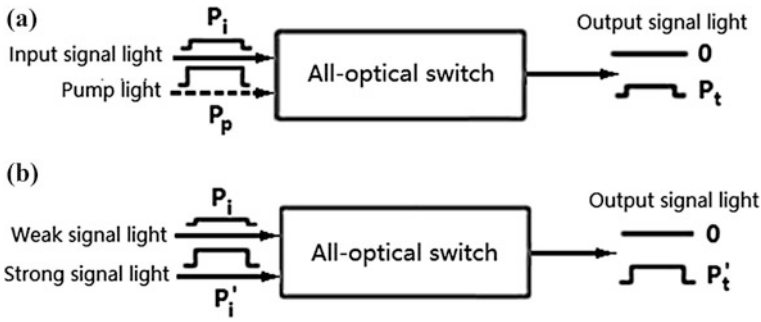

Fig. 10.4 Two kinds of switching methods for intensity-type all-optical switch: **a** the cross-pump method; **b** the self-pump method

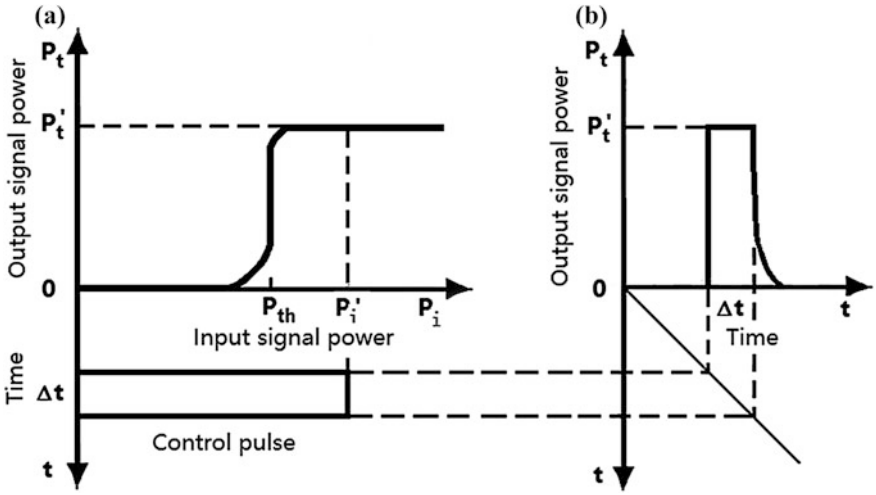

Fig. 10.5 Switching characteristic and output characteristic: **a** the output power versus the input power; **b** the output power versus the time

signal light itself. Figure 10.5a gives the switching characteristic of device (the output power versus the input power); Fig. 10.5b gives the output characteristic (the output power versus the time). Here we assume the controlling light pulse is a rectangular wave pulse with pulsewidth Δt and peek power P_i', $P_i' > P_{th}$. When the leading edge of pulse is not coming, the output signal power is zero, the device is in off-state; when the leading edge of pulse is coming, the device is in off-state, i.e., the output signal-light power becomes P_t'. From Fig. 10.5b we can see that the device keeps the output power P_t' inside the pulsewidth time (Δt), but the speed of switch-off is slower than the speed of switch-on, it appears an obvious trailing.

4. **Classification According to Nonlinear Mechanism**

Already studied all-optical switches based on nonlinear optics have different nonlinear mechanisms and working principles, which have used various nonlinear optical effects of materials: the nonlinear refraction, the nonlinear absorption, the nonlinear reflection, the nonlinear polarization, the nonlinear frequency change and the nonlinear phase transition etc. or used various nonlinear optical devices: the nonlinear interferometer, the nonlinear coupler, the nonlinear grating, the nonlinear amplifier etc., as shown in Table 10.1.

5. **Classification According to Nonlinear Material**

The performance of all-optical switch not only depends on the structure of device, but also the quality of material. For all-optical switch based on Kerr effect, the nonlinear refraction coefficient n_2, the nonlinear response time τ and the linear absorption α_0 are three most important optical parameters. So the quality factor of all-optical switch can be defined as

Table 10.1 Nonlinear mechanism and working principle of all-optical switch

	Nonlinear mechanism	Working principle
1	Nonlinear refraction	Optical Kerr effect, self-focusing and self-defocusing, two-photo refraction effect
2	Nonlinear absorption	Saturable absorption, reverse saturable absorption, two-photon absorption, photochromism effect
3	Nonlinear reflection	Interface between linear and nonlinear materials, nonlinear liquid sandwiched between two prisms or two gratings
4	Nonlinear polarization	Light induced nonlinear rotation in liquid crystal and chirality material
5	Frequency conversion	Frequency doubling, sum frequency, difference frequency, parameter process, four wave mixing, stimulated Rama scattering
6	Phase transition	Light induced material phase transition, to lead refractive index change or absorption coefficient change
7	Nonlinear interferometer	Light induced refractive index change in interferometer to lead the π phase difference between two beams
8	Nonlinear coupler	Light inputs an asymmetrical optical coupler to induce $\sqrt{3\pi}$ phase difference between two beams in coupler
9	Nonlinear grating	Single nonlinear grating, grating pair connected with a nonlinear fiber
10	Nonlinear amplifier	EDFA or SOA, or inserting the optical amplifier into an interferometer

Table 10.2 Property parameters of typical nonlinear optical materials

Material type	Typic material	Nonlinear mechanism	n_2 (cm^2/W)	α_0 (cm^{-1})	τ (s)	Q ($cm^3/\tau W$)
Liquid crystal	Nematic LC	Molecular orientation	10^{-3}	10^3	1	10^{-6}
Direct bandgap semiconductor	GaAs	Free exciton nonlinearity	10^{-6}	10^4	10^{-8}	10^{-2}
Organic material	CS_2	Molecular orientation	10^{-13}	10^{-1}	10^{-12}	10^1
Indirect bandgap semiconductor	Si	Electronic polarization	10^{-14}	10^{-5}	10^{-14}	10^5

$$Q = \frac{n_2}{\alpha_0 \tau}. \tag{10.1.1}$$

Table 10.2 lists property parameters of four typical nonlinear materials [2, 3] including the nonlinear refraction coefficient n_2, the nonlinear response time τ, the linear absorption α_0 and the quality factor Q. The four typical nonlinear materials are (1) liquid crystal (such as nematic liquid crystal) is based on molecular orientation nonlinear mechanism; (2) direct band-gap semiconductor (such as GaAs) is

based on free exciton nonlinear mechanism; (3) organic material (such as CS_2) is based on molecular orientation nonlinear mechanism; (4) indirect bandgap semiconductor (such as Si) is based on electronic polarization nonlinear mechanism.

From Table 10.2 we can see that, for these four materials from top to down, the numerical value of n_2, α_0 and τ are all reducing down (from large to small); but on the contrary, the numerical value of Q is growing up (from small to large). In these four materials, the liquid crystal has strongest nonlinearity, but the switching time is longest, it is not suitable to make fast optical switch. The direct band-gap semiconductor has stronger nonlinearity, but its linear absorption loss too large; it is unfavourable for cascading operation of optical switch. The quality factors of above two materials are not high. The organic material has better optical nonlinearity and switching speed, and absorption loss is not too large, so the quality factor is ok, but the physical and chemical stability of this material is not good, so it is not best material. The indirect bandgap semiconductor (such as Si) has shortest response time, smallest linear absorption coefficient, so it has best quality factor. In addition Si also has good heat conducting property (easy for integration), low price of material and mature processing technique, these advantages are favourable to all-optical switch. The only problem for Si material is low nonlinearity, later we will talk about that it is possible to use the nanoscale ring cavity structure to accumulate nonlinearity; and also can use two-photon absorption effect to enhance the nonlinear refractive index Δn, and than to decrease the switching power. Therefore, Si might be best material for making practical all-optical switch.

10.2 Nonlinear Optical Coupler All-Optical Switch

Starting from this section, the following five sections will study various interferometer type all-optical switches based on the optical Kerr effect. Firstly, we study the nonlinear optical coupler based all-optical switches. The optical coupler is a basic element of the optical interferometers, which is used for connecting the various optical components in the interferometer, and coupling the light into or out the interferometer. The optical coupler itself also can be regarded as an interferometer based on the two-beam interference principle.

The optical coupler (or called optical directional coupler) is consisted of two parallel single-mode straight waveguides (waveguide I and waveguide II), and two waveguides in coupling region (with length l) are closed proximity to each other (micrometer distance only), the device has four ports as shown in Fig. 10.6. In the coupling region the light can permeate from one waveguide to another one through the evanescent field. The optical

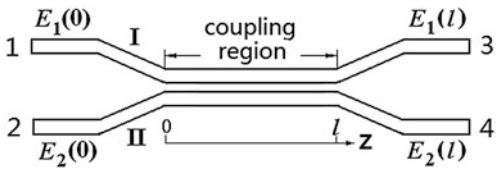

Fig. 10.6 Structure of optical directional coupler

waveguide pair can be silica fiber waveguides made by fused biconical taper technology; also can be strip-type plane waveguides of silicon, lithium niobate, semiconductor or organic materials made by plane integration technology.

We assume the incident light is a monochromatic plane wave, its electrical field amplitude can be denoted as $\boldsymbol{E}(z,t)e^{-(\omega t-\beta z)}$, where $\boldsymbol{E}(\mathsf{z},t)$ is slow-variation complex number electrical amplitude propagated with coordinate z; in the latter phase factor, ω is frequency, β is propagation constant. After the incident light inputs in the coupler from Port I, it is divided into two beams, which propagate along waveguide I and waveguide II respectively, two waveguide are parallel with z direction, two beams have field amplitudes $\boldsymbol{E}_1(\mathsf{z},t)$ and $\boldsymbol{E}_2(\mathsf{z},t)$ respectively. If the coupling between two waveguides is very weak, and light absorption can be neglected, according to optical waveguide coupling mode theory, the variation of $\boldsymbol{E}_1(\mathsf{z},t)$ and $\boldsymbol{E}_2(\mathsf{z},t)$ in space and time, in general, can be described by following coupled-mode equations (similar to NLS equations) [4]:

$$\frac{\partial \boldsymbol{E}_1}{\partial z}+\beta_1\frac{\partial \boldsymbol{E}_1}{\partial t}+\frac{i\beta_2}{2}\frac{\partial^2 \boldsymbol{E}_1}{\partial t^2}=i\kappa_{12}\boldsymbol{E}_2+i\delta\boldsymbol{E}_1+i\left(\gamma_1|\boldsymbol{E}_1|^2+\boldsymbol{C}_{12}|\boldsymbol{E}_2|^2\right)\boldsymbol{E}_1, \quad (10.2.1)$$

$$\frac{\partial \boldsymbol{E}_2}{\partial z}+\beta_1\frac{\partial \boldsymbol{E}_2}{\partial t}+\frac{i\beta_2}{2}\frac{\partial^2 \boldsymbol{E}_2}{\partial t^2}=i\kappa_{21}\boldsymbol{E}_1-i\delta\boldsymbol{E}_2+i\left(\gamma_2|\boldsymbol{E}_2|^2+\boldsymbol{C}_{21}|\boldsymbol{E}_1|^2\right)\boldsymbol{E}_2, \quad (10.2.2)$$

where $\beta_1 \equiv 1/v_g$, v_g is the group velocity; β_2 is the group velocity dispersion (GVD) parameter; κ_{12} and κ_{21} are the coupling coefficient of two waveguides; γ_1 and γ_2 are the self-phase modulation (SPM) parameters; $\boldsymbol{C}_{12}$ and $\boldsymbol{C}_{21}$ are the parameter for describing the cross-phase modulation (XPM); δ is the asymmetrical degree of two waveguides, which is defined as

$$\delta=\frac{1}{2}(\beta_{01}-\beta_{02}), \quad (10.2.3)$$

where β_{01} and β_{02} are propagation constants in waveguide I and waveguide II respectively.

10.2.1 Symmetric Coupler Under Low Incident Power

So called symmetric optical coupler is the coupler consisted of totally same two waveguides: the geometry structures of two waveguides are the same, i.e., $\kappa_{12} = \kappa_{21} = \kappa$; and the refractive indexes of two waveguides are same, i.e., $\beta_{01} = \beta_{02}$, or $\delta_a = 0$. When the incident light is continuous and low power, the nonlinear effect in the coupler don't need to consider. i.e., the refractive index of coupler is not change with the light power. In this case the parameters of Eqs. (10.2.1) and (10.2.2) γ_1, γ_2, $\boldsymbol{C}_{12}$ and $\boldsymbol{C}_{21}$ = 0, we can omit the items related with time and nonlinearity, thus the coupled-mode equations for symmetric coupler are

$$\frac{dE_1(z)}{dz} = i\kappa E_2(z), \tag{10.2.4}$$

$$\frac{dE_2(z)}{dz} = i\kappa E_1(z). \tag{10.2.5}$$

The solutions of Eqs. (10.2.4) and (10.2.5) are

$$E_1(z) = \cos(\kappa z)E_1(0) + i\sin(\kappa z)E_2(0), \tag{10.2.6}$$

$$E_2(z) = i\ \sin(\kappa z)E_1(0) + \cos(\kappa z)E_2(0). \tag{10.2.7}$$

Equations (10.2.6) and (10.2.7) can be written to the matrix form:

$$\begin{bmatrix} E_1(z) \\ E_2(z) \end{bmatrix} = \begin{bmatrix} \cos(\kappa z) & i\sin(\kappa z) \\ i\sin(\kappa z) & \cos(\kappa z) \end{bmatrix} \begin{bmatrix} E_1(0) \\ E_2(0) \end{bmatrix}. \tag{10.2.8}$$

To define the coupler reflectivity and the coupler transmittance respectively:

$$r = \cos(\kappa z), \tag{10.2.9}$$

$$t = \sin(\kappa z). \tag{10.2.10}$$

r and t are reflectivity and transmittance for light field amplitude, and r^2 and t^2 are reflectivity and transmittance for light power, if neglecting the absorption, both satisfy the following relationship:

$$r^2 + t^2 = 1. \tag{10.2.11}$$

Actually, $r^2 = C_r$ and $t^2 = C_t$ indicate the splitting ratios of output powers for waveguide I and waveguide II, respectively.

Using Eqs. (10.2.9) and (10.2.10), the Eqs. (10.2.6) and (10.2.7) can be written as

$$E_1(z) = rE_1(0) + itE_2(0), \tag{10.2.12}$$

$$E_2(z) = itE_1(0) + rE_2(0). \tag{10.2.13}$$

The matrix Eq. (10.2.8) also can be expressed to

$$\begin{bmatrix} E_1(z) \\ E_2(z) \end{bmatrix} = \begin{bmatrix} r & it \\ it & r \end{bmatrix} \begin{bmatrix} E_1(0) \\ E_2(0) \end{bmatrix}. \tag{10.2.14}$$

If incident light inputs coupler from Port 1, so $E_1(0) \neq 0$ and $E_2(0) = 0$. Assuming the length of coupling region is l, the output light amplitudes from waveguide I at Port 3 and waveguide II at Port 4 are respectively:

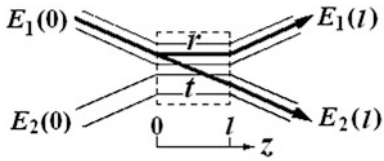

Fig. 10.7 Reflected path (r) (*bar path*) and transmitted path (t) (*cross path*) inside the optical coupler

$$E_1(l) = rE_1(0), \tag{10.2.15}$$

$$E_2(l) = itE_1(0). \tag{10.2.16}$$

There are two light paths inside the coupler, as shown in Fig. 10.7. We call the reflected path (r) as bar path, and call the transmitted path (t) as cross path, respectively. From Eqs. (10.2.15) to (10.2.16) we can see, the light passes through the direct arm without phase change, but passes through the cross arm with phase difference $\pi/2$, because $i = e^{i(\pi/2)}$.

Now we find out the output powers from Port 3 and Port 4 of the coupler. As we know that the relation between power and field amplitude is $P \propto |E|^2$, because the following discussion just concerns the relative relation between the output and input powers in two channels, for convenience, we assume $P = |E|^2$. In above symmetric coupler, setting $P_1(0) = |E_1(0)|^2 = P_{in}$, $P_2(0) = |E_2(0)|^2 = 0$, $P_1(l) = |E_1(l)|^2$ and $P_2(l) = |E_2(l)|^2$, In the two sides of Eqs. (10.2.15) and (10.2.16) multiply by conjugate complex number of electrical field amplitude, than we obtain the output powers from waveguide I and waveguide II of coupler respectively:

$$P_1(l) = P_{in}\cos^2(\kappa l), \tag{10.2.17}$$

$$P_2(l) = P_{in}\sin^2(\kappa l). \tag{10.2.18}$$

Obviously, the ratio of output and input powers from two waveguides only depends on the product of coupling coefficient and coupling region length κl, for a certain coupling coefficient κ, the relations between the output power $P_1(l)$ or $P_2(l)$ and the coupling region length l is shown in Fig. 10.8.

If taking coupling region length with $l = L_C = \pi/2\kappa$, from Eqs. (10.2.17) to (10.2.18) we can see, the light power totally outputs from waveguide II; if taking

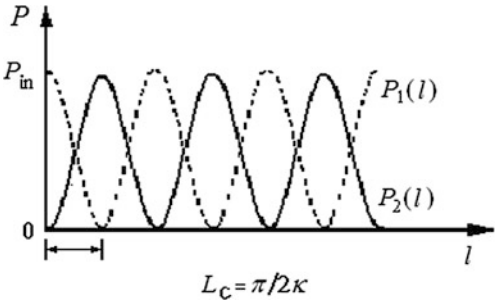

Fig. 10.8 Output light powers from waveguide I and waveguide II of the coupler as a function of coupling region length

$l = 2L_C = \pi/\kappa$, light power totally output from waveguide I; if taking $l = L_C/2 = \pi/4\pi$, the output powers of two waveguides are equal, to be $P_{in}/2$, this coupler is called 3 dB coupler (3 dB = 50 %). L_C is called the coupling length of the optical coupler.

From above discussion we can see, under low power of incident light, the output power ratios from two output ports of symmetrical coupler are not variation with the incident light power, so it can not to make all-optical switch. However, we will introduce below that under high power incidence, the two output power ratios of coupler will change with input light power, the all-optical switch can be realized by using the self-phase modulation and the cross-phase modulation two methods, respectively.

10.2.2 Symmetric Coupler All-Optical Switch in Self-phase Modulation

A quasi-continuous, high power and power adjustable signal light inputs a symmetric coupler with $l = L_c$ in self-phase modulation way. We denote the input power by P_0, there exists a critical power P_c, if the input power is much smaller than the critical power, i.e., $P_0 \ll P_c$, due to $l = L_c$, whole signal will output from waveguide II; if the input power grater than the critical power, i.e., $P_0 > P_c$, the optical Kerr effect is generated in two arms of the coupler. Because the powers in two arms are different, so the induced nonlinear refractive indexes are different, this leads the phase shifts of light beams in two arms are different. When the difference between two phase shifts reaches a certain value, the signal light will totally output from the waveguide I, as shown in Fig. 10.9.

We start from Eqs. (10.2.1) to (10.2.2), assume the input light is a wide pulse, it can be approximately regarded a continuous light; and do not consider the dispersion effect, so in the equations the items related with time and dispersion can be neglected; because the coupler is symmetric, i.e., $\kappa_{12} = \kappa_{21} \equiv \kappa$, $\delta = 0$; assuming the self-phase modulation and cross-phase modulation Kerr effect in two arms are symmetric, i.e., $\gamma_1 = \gamma_2 \equiv \gamma$ and $C_{12} = C_{21} \equiv \gamma\sigma$, thus Eqs. (10.2.1) and (10.2.2) can be simplified as [4]

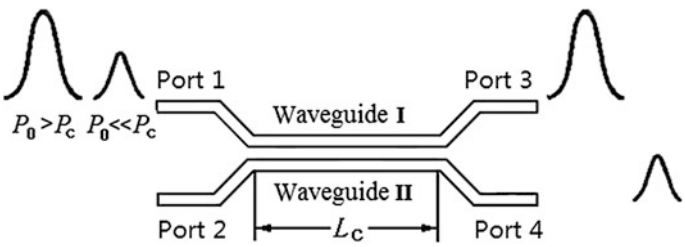

Fig. 10.9 Schematic diagram of all-optical switch based on a symmetric coupler working in self-phase modulation way

$$\frac{\partial \boldsymbol{E}_1}{\partial z} = i\kappa \boldsymbol{E}_2 + i\gamma\left(|\boldsymbol{E}_1|^2 + \sigma|\boldsymbol{E}_2|^2\right)\boldsymbol{E}_1, \tag{10.2.19}$$

$$\frac{\partial \boldsymbol{E}_2}{\partial z} = i\kappa \boldsymbol{E}_1 + i\gamma\left(|\boldsymbol{E}_2|^2 + \sigma|\boldsymbol{E}_1|^2\right)\boldsymbol{E}_2, \tag{10.2.20}$$

where the nonlinear parameter γ is

$$\gamma = \frac{k_0 n_2}{S}, \tag{10.2.21}$$

where n_2 is the nonlinear refraction coefficient, k_0 is the wave vector in vacuum; S is the effective cross-section of light field in waveguides.

Denoting the power and phase of light field in two arms by P_i and $\phi_i (i = 1, 2)$ respectively, than the light field amplitudes in two arms can be expressed as

$$E_i = \sqrt{P_i} e^{i\phi_i}. \quad (i = 1, 2) \tag{10.2.22}$$

Substituting Eq. (10.2.22) into Eqs. (10.2.19) and (10.2.20), and setting the phase-shit difference of two arms is $\phi = \phi_1 - \phi_2$, than we can obtain following three equations:

$$\frac{dP_1}{dz} = 2\kappa\sqrt{P_1 P_2}\sin\phi, \tag{10.2.23}$$

$$\frac{dP_2}{dz} = -2\kappa\sqrt{P_1 P_2}\sin\phi, \tag{10.2.24}$$

$$\frac{d\phi}{dz} = \frac{P_2 - P_1}{\sqrt{P_1 P_2}}\kappa con\phi + \frac{4\kappa}{P_c}(P_1 - P_2), \tag{10.2.25}$$

where P_c is the critical power, which is defined as

$$P_c = \frac{4\kappa}{\gamma(1-\sigma)}. \tag{10.2.26}$$

If we do not consider the action of cross-phase conduction between two arms, we have $\sigma = 0$, using Eq. (10.2.21), $k_0 = 2\pi/\lambda_0$ and $L_c = \pi/2\kappa$, Eq. (10.2.26) can rewrite to

$$P_c = \frac{4\kappa}{\gamma} = \frac{\lambda S}{n_2 \mathrm{L}_c}. \tag{10.2.27}$$

Equation (10.2.27) shows that for certain wavelength of input light and coupling length, the critical power decreases with the increase of the nonlinear refraction coefficient of waveguide material and with the decrease of the cross-section of waveguide.

Equations (10.2.23)–(10.2.25) can be solved analytically in terms of the elliptic function. For the case that the input power P_0 is initially launched into waveguide I of the coupler, the powers in waveguides I and II at point z are given by

$$P_1(z) = |E_1(z)|^2 = \frac{1}{2}P_0[1 + \mathrm{cn}(2\kappa|\tau)], \tag{10.2.28}$$

$$P_2(z) = P_0 - P_1(z), \tag{10.2.29}$$

where P_0 is the input power, $\mathrm{cn}(\mathrm{x}|\tau)$ is a Jacobi elliptic function, in which the coefficient $\tau = (P_0/P_c)^2$.

Under low input power, $P_0 \ll P_c(\tau \ll 1)$, Eq. (10.2.28) is simplified to be $P_1(z) = P_0 \cos^2(\kappa z)$; when $P_0 < P_c(\tau < 1)$, start happen the frequency conversion between two waveguides; when P_0 close to P_c, the variation period increases with increase of power; when $P_0 = P_c(\tau = 1)$, the period becomes infinite, Eq. (10.2.28) is simplified as $P_1(z) = \frac{1}{2}P_0[1 + \mathrm{sec\,h}(2\kappa z)]$, in the case the half power of waveguide II has transferred to the waveguide I; Finally, when $P_0 > P_c(\tau > 1)$, the solution once again becomes periodic and the power in waveguide I only has smaller and smaller fluctuation, until it becomes negligible for $P_0 \gg P_c$.

Figure 10.10 shows the all-optical switching for the quasi-CW beam in a symmetric fiber coupler with $l = L_c$, where the curves of the relative output powers $P_i(L_c)/P_0(i = 1, 2)$ for the core I (dashed line) and the core II (solid line) as a function of the relative input power $P_1(0)/P_c$ are presented.

It is worth noting that at $P_{0C} = 1.25P_c$ the whole power conversion occurs, so the threshold switching power of device is

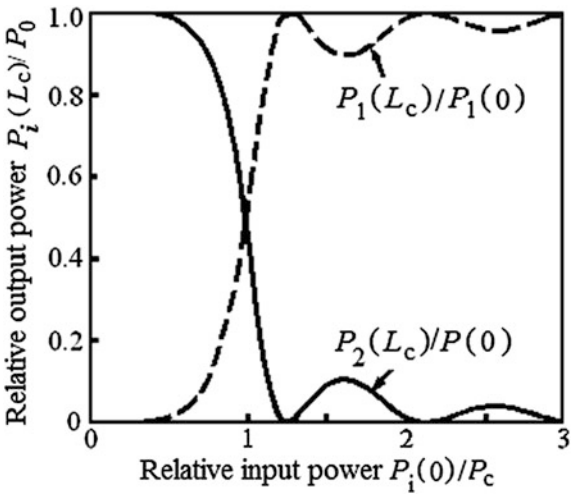

Fig. 10.10 Relative output powers at two output ports $P_i(L_c)/P_0$ $(i = 1, 2)$ as a function of relative input power $P_1(0)/P_c$ for an AOS in symmetric fiber coupler with $l = L_c$ working in SPM mode and quasi-CW incident light

$$P_{0c} = 1.25P_c = 1.25\frac{\lambda S}{n_2 L_c} = 2.5\frac{\kappa\lambda S}{\pi n_2}. \tag{10.2.30}$$

For example, consider a silica fiber coupler has nonlinear refraction coefficient $n_2 = 2.6 \times 10^{-20}\,\mathrm{m^2/W}$, effective cross-section of $S = 28.3\,\mu\mathrm{m}^2$ (for 3 μm-fiber radius) and coupling coefficient of $\kappa = 1\,\mathrm{cm}^{-1}$. When it is irradiated by a CW-incident light at $\lambda_0 = 1550\,\mathrm{nm}$, and assuming the power for a complete switching is 1.25 P_c, we calculate the switching power according to Eq. (10.2.30) to be P_c = 134 kW. This power is too strong and may damage the silica fibers.

A possible solution is to use a rare-earth-doped fiber coupler instead. For example, using a coupler made of the erbium-doped fiber $\left(n_2 = 3 \times 10^{-15}\,\mathrm{m^2/W}\right)$, the switching power can be reduced to 1.16 W. However, this power is still higher than the milliwatts-signal power in the fiber optical communication.

10.2.3 Asymmetric Coupler All-Optical Switch in Cross-Phase Modulation

Let us consider a waveguide coupler working in XPM mode as shown in Fig. 10.11. The signal beam at wavelength of 1550 nm is a low-power CW light with power P_{in}; and the pump beam at wavelength of 980 nm is a strong power light with power P_p, both of them input the coupler from same port (Port 1) through a WDM. Assuming the coupler is symmetric for the signal beam at 1550 nm, and the coupling length is L_c. If without the pump beam, all of the signal power will output from Port 4 according to the discussion in Sect. 10.2.1. However, the coupler for the pump beam at 980 nm is asymmetric. When the pump beam inputs into the coupler, it will induce the unequal reflective-index change in two waveguides. In this case the signal beam looks the coupler as an asymmetric coupler. So that we start to study an all-optical switch, in which a low-power CW signal beam is incident into an asymmetric coupler. The asymmetry of the coupler is induced by the power of the pump beam.

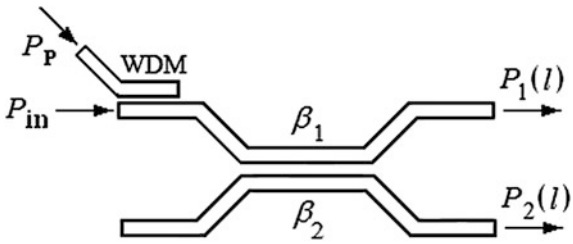

Fig. 10.11 Schematic diagram of AOS in an asymmetric coupler in XPM mode with a low-power CW signal light and a strong-power pump light, the coupling length is L_c

Now we start from Eqs. (10.2.1) to (10.2.2) to deduce the coupled-mode equations for signal light. Because the signal light is a low power, quasi-continuous light; it can not generate optical nonlinearity in the coupler, the items related with time and nonlinearity can be neglected; because the two waveguides of the coupler has same material and geometry structure, the coupling coefficients κ_{12} and κ_{21} are equal, i.e., $\kappa_{12} = \kappa_{21} = \kappa$. But the coupler for pump light with different frequency is asymmetric, so the power in the two arms are different, the refractive-index changes induced by Kerr effect are different too, thus propagation constants of signal lights in two arms are different, i.e., $\beta_{01} \neq \beta_{02}$, i.e., $\delta \neq 0$, therefore the coupled-mode equations can be written as [4]

$$\frac{dE_1}{dz} = i\kappa E_2 + i\delta E_1, \tag{10.2.31}$$

$$\frac{dE_2}{dz} = i\kappa E_1 - i\delta E_2, \tag{10.2.32}$$

where E_1 and E_2 are light field amplitudes in waveguide I and waveguide II, respectively, δ is defined by Eq. (10.2.3).

Taking derivative of Eqs. (10.2.31) and (10.2.32) with respect to z, we obtain

$$\frac{d^2E_1}{dz^2} = i\kappa\frac{dE_2}{dz} + i\delta\frac{dE_1}{dz}, \tag{10.2.33}$$

$$\frac{d^2E_2}{dz^2} = i\kappa\frac{dE_1}{dz} - i\delta\frac{dE_2}{dz}. \tag{10.2.34}$$

Making $(10.2.31) \times \delta + (10.2.32) \times \kappa$ to acquire

$$\kappa\frac{dE_2}{dz} = -\delta\frac{dE_1}{dz} + i\left(\delta^2 + \kappa^2\right)E_1 = -\delta\frac{dE_1}{dz} + i\kappa_e^2 E_1. \tag{10.2.35}$$

Substituting Eq. (10.2.35) into Eq. (10.2.33), we obtain

$$\frac{d^2E_1}{dz^2} + \kappa_e^2 E_1 = 0. \tag{10.2.36}$$

In same way, making $(10.2.31) \times \kappa - (10.2.32) \times \delta$ to acquire

$$\kappa\frac{dE_1}{dz} = \delta\frac{dE_2}{dz} + i\left(\delta^2 + \kappa^2\right)E_2 = \delta\frac{dE_2}{dz} + i\kappa_e^2 E_2. \tag{10.2.37}$$

Substituting Eq. (10.2.37) into Eq. (10.2.34), we obtain

$$\frac{d^2E_2}{dz^2} + \kappa_e^2 E_2 = 0. \tag{10.2.38}$$

In Eqs. (10.2.36) and (10.2.38), κ_e is

$$\kappa_e = \sqrt{\kappa^2 + \delta^2}. \tag{10.2.39}$$

According to initial value condition: $E_1(0) = E_{10}$ and $E_2(0) = E_{20}$, to solve differential Eqs. (10.2.36) and (10.2.38), the result is

$$\begin{bmatrix} E_1 \\ E_2 \end{bmatrix} = \begin{bmatrix} r' & it' \\ it' & r'* \end{bmatrix} \begin{bmatrix} E_{10} \\ E_{20} \end{bmatrix}, \tag{10.2.40}$$

where

$$r' = \cos(\kappa_e z) + i(\delta/\kappa_e)\sin(\kappa_e z) \tag{10.2.41}$$

$$t' = (\kappa/\kappa_e)\sin(\kappa_e z). \tag{10.2.42}$$

Because $|r'|^2$ and $|t'|^2$ are the power splitting ratios of the bar path and the cross path, respectively, according to the energy conservation principle, $|r'|^2 + |t'|^2 = 1$.

For the special situation of symmetric coupler under the low input power, we have $\delta = 0$, $\kappa_e = \kappa$, $r' = \cos(\kappa z)$, $r' = \sin(\kappa z)$, then we obtain the solution as same as Eq. (10.2.8), it shows the correction of Eq. (10.2.40).

By using the boundary conditions $\mathrm{E}_1(0) = \mathrm{E}_{\mathbf{in}}$ and $\boldsymbol{E}_2(0) = 0$ for a CW beam incident on Port 1, the solutions of Eqs. (10.2.33) and (10.2.34) are

$$E_1(l) = [\cos(\kappa_e l) + i(\delta/\kappa_e)\sin(\kappa_e l)]E_{\text{in}}, \tag{10.2.43}$$

$$E_2(l) = i(\kappa/\kappa_e)\sin(\kappa_e l)E_{\text{in}}, \tag{10.2.44}$$

where l is the coupling region length of the coupler.

Setting input power $P_{\text{in}} = |E_{\text{in}}|^2$, and output powers of two waveguides $P_1(l) = |E_1(l)|^2$ and $P_2(l) = |E_2(l)|^2$ respectively, from Eqs. (10.2.43) to (10.2.44), we obtain

$$P_1(l) = \left[\cos^2(\kappa_e l) + (\delta/\kappa_e)^2\sin^2(\kappa_e l)\right]P_{\text{in}}, \tag{10.2.45}$$

$$P_2(l) = \left[(\kappa/\kappa_e)^2\sin^2(\kappa_e l)\right]P_{\text{in}}. \tag{10.2.46}$$

So $P_{\text{in}} = P_1(l) + P_2(l)$ is existence. For low power symmetric coupler, $\delta = 0$, $\kappa = \kappa_e$, Eqs. (10.2.45) and (10.2.46) become Eqs. (10.2.15) and (10.2.16).

For the coupler with $l = L_c = \pi/2\kappa$, The phase difference of signal lights in two waveguides is $\Delta\phi = \Delta\beta L_c = \Delta\beta\pi/2\kappa$, so $\Delta\beta = 2\kappa\Delta\phi/\pi$, according to this relationship and Eq. (10.2.39), to get the relationships between $\kappa_e L_c$, κ/κ_e and $\Delta\phi$. Substituting these relationships into Eq. (10.2.46), finally we obtain the output signal power from waveguide II, which is

$$P_2(L_c) = P_{in}\left(\frac{\pi}{2}\right)^2 \sin c^2\left[\frac{\pi}{2}\sqrt{1+\left(\frac{\Delta\phi}{\pi}\right)^2}\right]. \tag{10.2.47}$$

Figure 10.12 exhibits the plot of the relative output power $P_2(L_c)/P_{in}$ as a function of the phase difference $\Delta\phi$. One can see that the threshold condition for a complete optical switching in the coupler with $l = L_c$ is $\Delta\phi = \sqrt{3}\pi$.

If we use the pump light to change the refractive-index difference Δn, thus change the phase difference of two arm signal lights $\Delta\phi$, when $\Delta\phi = \sqrt{3}\pi$, than we realize the switching of output signal power from waveduide II to waveguide I.

Assuming C_{rp} is the splitting ratio of the pump light on waveguide I, the incident pump light with power P_p is divided into two lights in two waveguides by the coupler, the two lights with following powers, respectively:

$$P_1 = C_{rp}P_p, \tag{10.2.48}$$

$$P_2 = |1 - C_{rp}|P_p. \tag{10.2.49}$$

These two powers produce the cross-phase modulation Kerr effect, to induce the refractive-index changes in waveguide I and waveguide II, respectively:

$$\Delta n_1 = 2n_2\frac{C_{rp}P_p}{S}, \tag{10.2.50}$$

$$\Delta n_2 = 2n_2\frac{|1 - C_{rp}|P_p}{S}, \tag{10.2.51}$$

where n_2 is nonlinear refraction coefficient, for CPM Kerr effect should be $n_2 \times 2$; S is efficient cross-section.

The difference between two refractive-index changes in two waveguides is

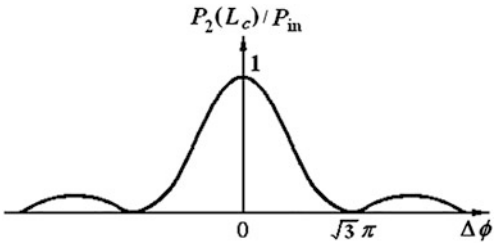

Fig. 10.12 Plot of the relative output power $P_2(L_c)/P_{in}$ as a function of the phase difference $\Delta\phi$. The threshold phase difference for a complete switching is $\sqrt{3}\pi$

$$\Delta n = \Delta n_2 - \Delta n_1 = \frac{n_2}{S} 2\left(1 - 2C_{rp}\right) P_p. \tag{10.2.52}$$

Therefore the phase difference between two signal lights in two waveguides is

$$\Delta\phi = \Delta\beta l = k_0 \Delta n l = \frac{4\pi n_2 l}{\lambda S} \left|1 - 2C_{rp}\right| P_p. \tag{10.2.53}$$

Using the switching threshold condition $\Delta\phi = \sqrt{3}\pi$ and $l = L_c$, from Eq. (10.2.53) we obtain the threshold switching power of pump light:

$$P_{pc} = \frac{\lambda S}{n_2 L_c} \cdot \frac{\sqrt{3}}{4\left|1 - 2C_{rp}\right|} \quad \left(C_{rp} \neq 1/2\right). \tag{10.2.54}$$

C_{rp}=1/2 is the case of 3 dB symmetric coupler, Obviously it can not produce the optical switching. If using $L_c = \pi/2\kappa$, than the threshold switching power of pump light can be written to

$$P_{pc} = \frac{\sqrt{3}\kappa\lambda S}{2\pi n_2} \cdot \frac{1}{\left|1 - 2C_{rp}\right|} \quad \left(C_{rp} \neq 1/2\right). \tag{10.2.55}$$

For example, considering a fiber coupler, we assume the signal light wavelength $\lambda = 1550\,\text{nm}$, for quartz material $n_2 = 2.6 \times 10^{-20}\,\text{m}^2/\text{W}$, effective cross-section $S = 28.3\,\mu\text{m}^2$ (radius of fiber core is 3 μm), $\kappa = 1\,\text{cm}^{-1}$, $C_{rp} \approx 1$, and calculate by using Eq. (10.2.55), to obtain the switching power P_{pc} = 46.5 kW. This switching power of CPM coupler all-optical switch is smaller than that of SPM coupler all-optical switch in 3 times, but the value is still too large, it is not suitable to use in optical communication.

10.3 Nonlinear Sagnac Interferometer All-Optical Switch

10.3.1 Symmetric Sagnac Interferometer in Low Incident Power

Sagnac interferometer (SI) is one of interferometers based on two-beam interference principle, which is consisted of a waveguide optical coupler connected with a waveguide loop. In this section, we focus on the optical fiber SIs. The research results are appropriate for the optical planar waveguide SIs.

At first we discuss the fiber symmetric SI, it consists of a 3 dB fiber coupler and a fiber loop, as shown in Fig. 10.13.

Sagnac interferometer has two output ports: reflected port (Port 1) and transmitted port (Port 2). The circulator in the figure is used for separating the reflected

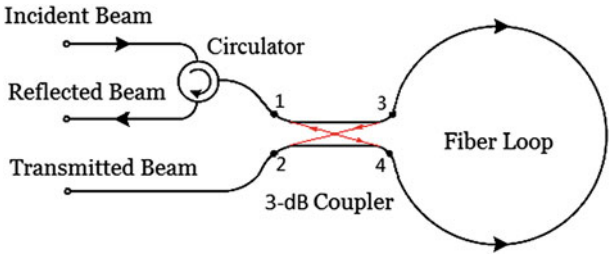

Fig. 10.13 A fiber symmetric Sagnac Interferometer consisted of a 3 dB fiber coupler and a fiber loop

light and incident light to avoid reflected light disturbs the light source. If the loop material of SI has optical nonlinearity, we call nonlinear Sagnac interferometer; if the coupler of SI is a 3 dB linear symmetric coupler, and the counter-propagated two lights in the loop are equal, than we call symmetric Sagnac interferometer, otherwise it is asymmetric Sagnac interferometer.

Now we through a simple analysis to point out that under the low-power incident light, the symmetric Sagnac interferometer can not make the all-optical switch.

The incident light inputs into the 3 dB coupler from Port 1, and separates into two light beams with a same power $P_{in}/2$ by the coupler. The two beams pass through bar path and cross path, and enter the fiber loop from Port 3 or Port 4 respectively. After one-cycle trip in the loop along opposite direction, the two beams returning to Port 4 and Port 3 have the same linear phase shift, without an additional phase difference between these beams. Each of two beams secondly separates into two lights by the cooper, than they pass through bar path and cross path again and output from Prot 1 and Port 2 of coupler. At each of the output port, there are two arriving beams, the resultant output powers depend on the phase difference of two coming beams. If two beams have zero phase difference (or $2m\pi$), it is the constructive interference, the two Bram powers are additive each other; if two lights have π phase difference (or $(2m+1)\pi$), it is the destructive interference, the two beam powers are subtract each other.

As we know that a beam passes through the cross path each time to induce a phase shift of $\pi/2$; but the beam passes through the bar path without phase shift. In our case, two beams along the paths 1-3-4-1 and 1-4-3-1 have the same phase shift of $\pi/2$, so the phase difference between them is zero, and the resultant power at Port 1 is P_{in}. However, the other two beams along the paths 1-3-4-2 and 1-4-3-2 have the phase shift of zero and π respectively, so the phase difference at Port 2 is π, and the resultant power of two beams at this port is zero. As a result, the all incident beam is always outputted from Port 1, without any transmitted beam at Port 2.

Therefore, the symmetric SI looks like a “fiber reflector” or “optical loop mirror” [5]. Such symmetric SI cannot be used to make the all-optical switch. In order to make the SI-type OBDs, the only way is breaking the symmetry of SI.

This conclusion can be strictly proved by using coupled-mode equation theory. If the Sagnac interferometer is consisted of a symmetric coupler with coupling region length l and coupling coefficient κ and a nonlinear loop with loop length L, from coupled-mode Eqs. (10.2.4) and (10.2.5) we find the solutions, which are [similar to Eqs. (10.2.6) and (10.2.7)]:

$$E_1(l) = \cos(\kappa l)E_1(0) + i\ \sin(\kappa l)E_2(0), \tag{10.3.1}$$

$$E_2(l) = \cos(\kappa l)E_2(0) + i\ \sin(\kappa l)E_1(0). \tag{10.3.2}$$

If a signal light with power P_{in} and at wavelength λ inputs from Port 1, the boundary condition is

$$E_1(0) = \sqrt{P_{\text{in}}}, \tag{10.3.3}$$

$$E_2(0) = 0. \tag{10.3.4}$$

The signal light is divided into two beams by the coupler, and the two beams output from Port 3 and Port 4, respectively. From Eqs. (10.3.1) to (10.3.4) to obtain their field amplitudes:

$$E_1(l) = \sqrt{P_{in}}\cos(\kappa l), \tag{10.3.5}$$

$$E_2(l) = i\sqrt{P_{in}}\sin(\kappa l). \tag{10.3.6}$$

These two beams enter the fiber loop and propagate along reverse directions: clockwise direction and anti-clockwise direction. Assuming the refractive indexes of loop medium for two beams are n_c and n_a respectively, after a circle trip the phase shifts are $\varphi_c = (2\pi/\lambda)n_cL$ and $\varphi_a = (2\pi/\lambda)n_aL$ respectively. When they enter coupler again, the field amplitudes at Port 3 and Port 4 are respectively:

$$E_1' = E_2(l)e^{i\phi_a} = i\sqrt{P_{in}}\sin(\kappa l)\mathrm{e}^{i2\pi n_aL/\lambda} \tag{10.3.7}$$

$$E_2' = E_1(l)e^{i\phi_c} = \sqrt{P_{in}}\cos(\kappa l)\mathrm{e}^{i2\pi n_cL/\lambda}. \tag{10.3.8}$$

Each of these beams divides again into two beams by the coupler, these four beams pass though coupler to arrive at Port 1 and 2, every port has two beams arriving. The field amplitudes of two beams passing through bar path and cross path respectively to reach Port 1 are

$$E_{r1} = i\sqrt{P_{in}}\sin(\kappa l)\cos(\kappa l)e^{i2\pi n_aL/\lambda}, \tag{10.3.9}$$

$$E_{t1} = i\sqrt{P_{in}}\cos(\kappa l)\sin(\kappa l)e^{i2\pi n_cL/\lambda}. \tag{10.3.10}$$

The total field amplitude at Port 1 is the superposition of these two field amplitudes, i.e., $E_r = E_{r1} + E_{t1}$. The total output power from Port 1 is

$$P_r = E_r \cdot E_r^* = (E_{r1} + E_{t1})(E_{r1} + E_{t1})^*. \tag{10.3.11}$$

We define the reflectivity R and the transmittance T of Sagnac interferometer as follows:

$$R = \frac{P_r}{P_{in}} = \frac{E_r \cdot E_r^*}{P_{in}}, \tag{10.3.12}$$

$$T = \frac{P_t}{P_{in}} = \frac{P_{in} - P_r}{P_{in}} = 1 - R. \tag{10.3.13}$$

Disregard loss, we have $P_{\text{in}} = P_r + P_t$.

Substitute Eqs. (10.3.9) and (10.3.10) into (10.3.11), then using (10.3.12) and (10.3.13), and trigonometric formula $2\sin\alpha \cdot \text{con}\alpha = \sin(2\alpha)$, $e^{i\alpha} + e^{-i\alpha} = 2\text{con}\alpha$ and $1 + \cos\alpha = 2\text{con}^2(\alpha/2)$, we obtain the reflectivity and the transmittance of Sagnac interferometer respectively:

$$R = \sin^2(2\kappa l)\cos^2\left(\frac{\pi\Delta nL}{\lambda}\right) = \sin^2(2\kappa l)\cos^2\left(\frac{\Delta\phi}{2}\right), \tag{10.3.14}$$

$$T = 1 - \sin^2(2\kappa l)\cos^2\left(\frac{\pi\Delta nL}{\lambda}\right) = 1 - \sin^2(2\kappa l)\cos^2\left(\frac{\Delta\phi}{2}\right), \tag{10.3.15}$$

where $\Delta n = n_a - n_c$ is the difference of refractive index induced by two reverse-direction propagated light beams in the loop, $\Delta\phi$ is the phase difference between these two light beams, which is $\Delta\phi = (2\pi/\lambda)\Delta nL$, where L is loop length.

If the power of input signal light is very weak, the refractive index of loop medium will not be changed, i.e., $n_c = n_a = n_0$, $\Delta n = 0$, thus $\Delta\phi = 0$. In this case, the the reflectivity and the transmittance of Sagnac interferometer become:

$$R = \sin^2(2\kappa l), \tag{10.3.16}$$

$$T = 1 - \sin^2(2\kappa l). \tag{10.3.17}$$

We can see that in weak input light case the output power of Sagnac interferometer only related with κl of the coupler, it has nothing to do with the input optical power. Figure 10.14 shows the curves of reflectivity and transmittance of Sagnac interferometer versus κl when changing of κl from 0 to $\pi/2$ in the low power case.

It is thus clear that, when $\kappa l = \pi/4$, namely the coupler is a 3 dB coupler, $R = 1$, $T = 0$, whole signal light will output from the reflected port; when $\kappa l = \pi/2$, $R = 0$, $T = 1$, whole signal light will output from the transmitted port; and when κl takes other value, the output power of signal light will has a certain ratio between

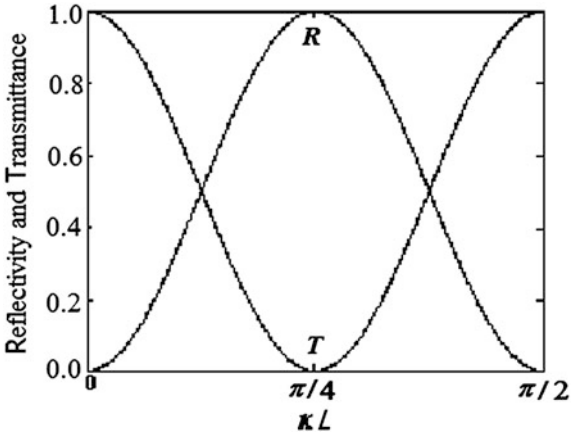

Fig. 10.14 Curves of reflectivity and transmittance of versus κl for Sagnac interferometer in low input power case

the reflected port and the transmitted port. In short, in low power incidence case, the output power of symmetric Sagnac interferometer not change with input power, so it can not to make an all-optical switch.

If backpropagated two beams in the loop have strong power, they can induce material to general refractive index change, but the two powers are not same, after one circle trip, the induced refractive index difference is not zero, i.e., $\Delta n = n_c - n_a \neq 0$, so that the phase difference between two light $\Delta\phi \neq 0$. When the power difference enough produce $\Delta\phi = \pi$, from Eqs. (10.3.14) to (10.3.15) can see, the output light will occur the switching conversion. According to $\Delta\phi = (2\pi/\lambda)\Delta nL$, the switching condition $\Delta\phi = \pi$ requires the refractive index difference is to reach

$$\Delta n = \frac{\lambda}{2L}. \tag{10.3.18}$$

Therefore in order to realize the nonlinear Sagnac interferometer all-optical switch, the Sagnac interferometer should has an asymmetric structure, and the power difference of backpropagation two beams in the loop can induce the phase difference to reach $\Delta\phi = \pi$. For this purpose we can adopt following method: (1) under the self-phase modulation (SPM), use of the non-3 dB coupler instead of non-3 dB coupler, to lead the incident signal light divided into two light beams with different power; (2) under the cross-phase modulation (CPM), the frequency of pump light has a large difference with the frequency of signal light, to lead the incident pump light divide into two beams with different power; (3) the optical loop can be asymmetric, for example inserting a optical amplifier into the loop, put it close to one of the two ports, to lead increase of the power difference between the backpropagated two beams. Below we will discuss three kinds of nonlinear Sagnac interferometer all-optical switches based on these three principles.

10.3.2 Sagnac Interferometer All-Optical Switch with a Non-3 dB Coupler

We use a non-3 dB coupler connecting with a nonlinear fiber loop to form an asymmetric Sagnac interferometer as shown in Fig. 10.15 [6]. A signal light input the non-3 dB coupler, the two beams output from Port 3 and Port 4 with different power, enter the loop taking counterpropagation, after one circle trip, two lights produces different nonlinear phase shift, if the input power is strong enough, can get the π phase difference. When the two beams return to the input ports of coupler and interfere each other, then can realize the switching from the refracted output port to the transmitted output port. If the power splitting ratio of two output ports is larger and the nonlinearity of loop material is stronger, then the required switching power is lower.

The incident beam with power P_{in} inputs the interferometer from the Input Port (Port 1), and divided into two beams by coupler, the two beams pass though the bar path and the cross path of the coupler respectively, and then both enter the fiber loop, propagating along reverse direction. Assuming the splitting ratio of coupler for bar path is C_r, the powers of the clockwise beam and the anticlockwise beam can be expressed as respectively

$$P_c = C_r P_{\text{in}}, \tag{10.3.19}$$

$$P_a = (1 - C_r)P_{in}, \tag{10.3.20}$$

where $C_r = r^2 = \cos^2(\kappa l)$, $1 - C_r = t^2 = \sin^2(\kappa l)$. If the incident power is very strong, we have to consider both the self-phase modulation Kerr effect (n_2) and the cross-phase modulation Kerr effect between two beams $(2n_2)$. Therefore, the refractive indexes in the loop material for these two beams are

$$n_a = n_0 + n_2 \frac{P_a + 2P_c}{S}, \tag{10.3.21}$$

$$n_c = n_0 + n_2 \frac{P_c + 2P_a}{S}. \tag{10.3.22}$$

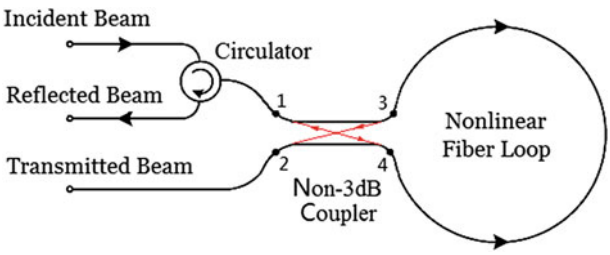

Fig. 10.15 All-optical switch in nonlinear Sagnac interferometer with a non-3 dB coupler working in SPM mode

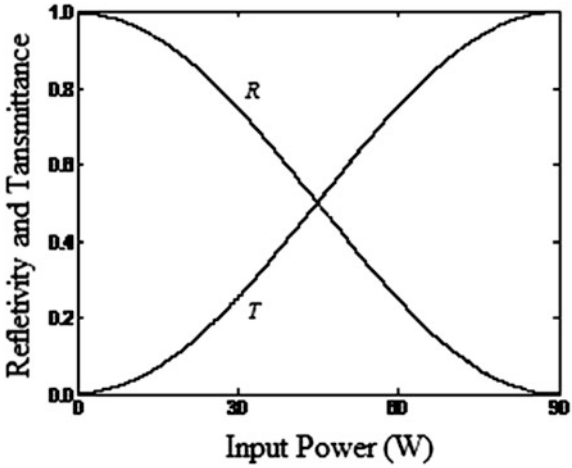

Fig. 10.16 Curves of the reflectivity and the transmittance of SI versus the incident power when the power ratio is $C_r = 0.47$ for an all-optical switch in a SI with a non-3 dB coupler in SPM mode

Substituting Eqs. (10.3.19) and (10.3.20) into Eqs. (10.3.21) and (10.3.22), we obtain the difference of two refractive indexes:

$$\Delta n = n_a - n_c = (2C_r - 1)\frac{n_2 P_{in}}{S}. \tag{10.3.23}$$

In the 3 dB coupler case, $C_r = 1/2$, according to Eq. (10.3.23), $\Delta n = 0$ From Eqs. (10.3.14) to (10.3.15), we obtain $R = 1$ and $T = 0$, that means the all power outputs from the reflected port. But when C_r takes other value, the two beams in the loop have different powers, so produced refractive-index difference is not zero, i.e., $\Delta n \neq 0$, thus the phase difference between two light $\Delta\phi \neq 0$. There are part light outputted from the transmitted port. In order to realize a complete optical switching, the condition is $\Delta n = \lambda/2L$, from Eq. (10.3.23) we obtain the expression of threshold switching power of device, that is

$$P_{inc} = \frac{\lambda S}{n_2 L} \cdot \frac{1}{2|2C_r - 1|}. \quad (C_r \neq 1/2) \tag{10.3.24}$$

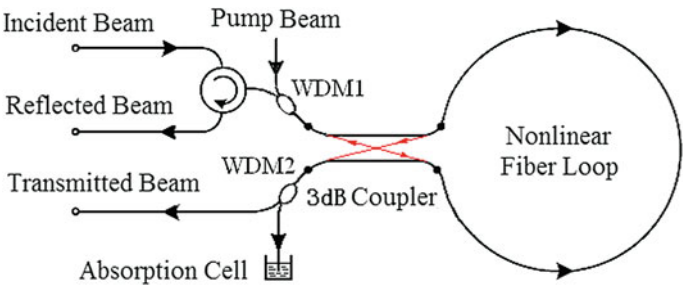

Fig. 10.17 All-optical switch in nonlinear Sagnac interferometer working in XPM mode, the frequency of pump light is different with that of the signal light

From Eq. (10.3.24) we can see, the switching power of device is related with splitting ratio, but in order to realize the all-optical switch, the coupler must be non-3 dB coupler, i.e., $C_r \neq 1/2$.

For example, for a fiber Sagnac interferometer with loop length L = 100 m, the wavelength of incident light is $\lambda = 1550\,\text{nm}$, taking the following data for the fiber coupler: $n_2 = 2.6 \times 10^{-20}\,\text{m}^2/\text{W}$, $S = 18.1\,\mu\text{m}^2$ (fiber core radius is $a = 2.4\,\mu\text{m}$), $\kappa = 1\,\text{cm}^{-1}$, $C_r = 0.47$, using Eqs. (10.3.14), (10.3.15) and (10.3.23), we draw out curves of the reflectivity R and the transmittance T versus the input power P_{in}, as shown in Fig. 10.16. Obviously, when input power increases to reach until 90 W, the output signal power totally switches from reflected port to transmitted port. This switching power is lower than that of single coupler optical switch, but for optical communication, it is still too large.

10.3.3 Sagnac Interferometer All-Optical Switch in Cross-Phase Modulation

The nonlinear fiber Sagnac interferometer with a 3 dB coupler (for signal light) is working in XPM mode. The wavelength of the pump beam is different with that of the signal beam, for example, the signal beam at 1550 nm and the pump beam at 980 nm. The pump beam and the signal beam together pass through a wavelength division multiplexer WDM1 input the device. The structure of this device is shown in Fig. 10.18 [7]. Because the frequency difference between the pump light and the signal light is very large, for the pump light the coupler is not a 3 dB coupler. The pump light passing the coupler separates into two beams with different power, when they enter the loop to propagate in reverse direction. Because the Kerr effect, they induce different nonlinear refractive index, to lead the two backpropagation signal

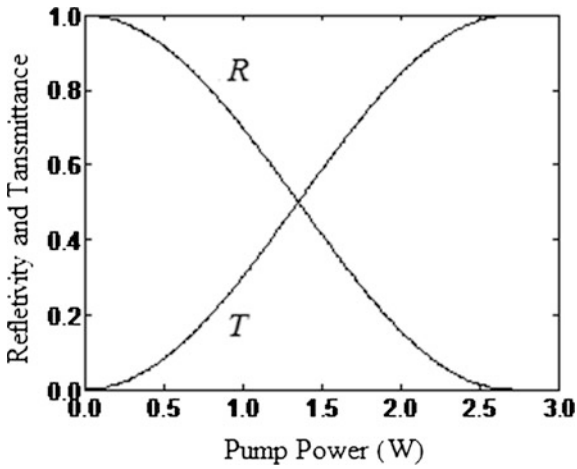

Fig. 10.18 The curves of reflectivity and transmittance versus pump power for the all-optical switch in SI using a pump wavelength different from the signal wavelength

beams with different phase shift. When the pump light is strong enough, the phase difference of two signal lights to reach π, the output signal power will be switching from Port 1 to Port 2. The remainder pump light will pass through the WDM2 going out to absorption cell.

Assuming incident pump light with power P_p, which is divided by coupler into two beams passing through the bar path and cross path, the splitting ratio of the bar path is C_{pr}. Two beams enter the fiber loop and propagate along reverse direction. The clockwise propagated pump light power is P_{pc}; the anticlockwise propagated pump light power is P_{pa}. The relationships of P_{pc} and P_{pa} with P_p are respectively:

$$P_{pc} = C_{pr}P_p, \tag{10.3.25}$$

$$P_{pa} = \left(1 - C_{pr}\right)P_p. \tag{10.3.26}$$

If the power of pump light is very strong, each of pump beams interacts with the loop material to induce a SPM Kerr effect, and the interaction of this pump beam with other pump beam induces a XPM Kerr effect. In addition, the interaction of this pump beam with the corresponding signal beam also induces a XPM Kerr effect, so the total power inducing the optical Kerr effect is $2\left(P_{pc} + 2P_{pa}\right)$, the refractive indexes receptive by two backpropagation signal lights are respectively:

$$n_a = n_0 + n_2\frac{2\left(P_{pa} + 2P_{pc}\right)}{S}, \tag{10.3.27}$$

$$n_c = n_0 + n_2\frac{2\left(P_{pc} + 2P_{pa}\right)}{S}. \tag{10.3.28}$$

Substituting Eqs. (10.3.25) and (10.3.26) into Eqs. (10.3.27) and (10.3.28), we obtain the difference of refractive index for the two signal beams, that is

$$\Delta n = n_a - n_c = \left(2C_{pr} - 1\right)\frac{n_2\left(2P_p\right)}{S}. \tag{10.3.29}$$

To substitute the difference of refractive index required for optical switching $\Delta n = \lambda/2L$ into Eq. (10.3.29), we obtain the threshold switching power:

$$P_{pc} = \frac{\lambda S}{n_2 L}\cdot\frac{1}{4\left|2C_{pr} - 1\right|}. \quad \left(C_{pr} \neq 1/2\right) \tag{10.3.30}$$

From Eq. (10.3.30) we can see that the switching power depends on the splitting ratio of the pump beam. Because the splitting ratio of pump light is related with the wavelength of pump light: if the pump wavelength is far from the signal wavelength, C_{pr} will be much different from 1/2, hence the switching power will be reduced intensively.

Taking data used for Fig. 10.16, we calculate by using Eqs. (10.3.14), (10.3.15), and (10.3.29) to obtain the curves of the refractivity and the transmittance as a function of the pump power as shown in Fig. 10.18. We can see that when the pump power increases to 2.7 W, the output signal power will be switched from Port 1 to Port 2. The switching power for XPM SI all-optical switch is small than that for SPM SI all-optical switch in 3 times, but it is still large for optical communication.

10.3.4 Sagnac Interferometer All-Optical Switch with a Optical Amplifier

Inserting a bidirectional erbium-doped fiber amplifier (EDFA) into the loop of SI, and the optical amplifier is located near one of the output ports of coupler [8] as shown in Fig. 10.19. The two beams travelling in the loop along reverse direction, their magnified beams by the optical amplifier travel different distance in the loop. Therefore, the phase shifts of two beams are different. When the phase-shift difference between two beams achieves to π, the switching can be accomplished. It is obviously, if the gain of the amplifier is larger, the nonlinearity of loop is stronger, and than the switching power will be lower.

If we put an amplifier near the end of the bar path of the coupler, and the gain of the optical amplifier is G, in the fiber loop, the power of the clockwise beam is amplified in G time. But the power of the anticlockwise beam is almost not amplified. Therefore, the powers of two signal beams are

$$P_c = GC_rP_{in} \tag{10.3.31}$$

$$P_a \approx (1 - C_r)P_{in}, \tag{10.3.32}$$

where P_{in} is input power, C_r is the splitting ratio for bar path of the coupler.

Because the optical Kerr effect, the two refractive indexes induced by two beams in the loop are

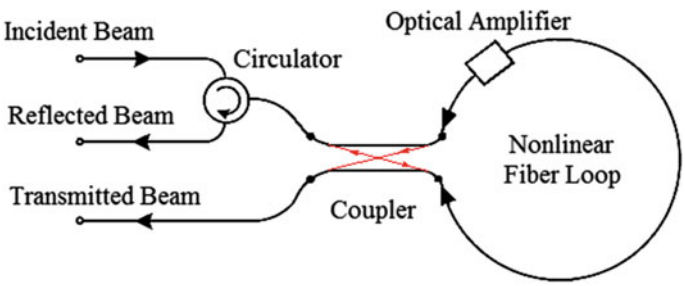

Fig. 10.19 All-optical switch in SI containing an asymmetrically placed optical amplifier in the loop

$$n_a = n_0 + n_2 \frac{P_a + 2P_c}{S}, \tag{10.3.33}$$

$$n_c = n_0 + n_2 \frac{P_c + 2P_a}{S}. \tag{10.3.34}$$

Substituting Eqs. (10.3.33) and (10.3.34) into Eqs. (10.3.31) and (10.3.32), we obtain the difference of refractive index:

$$\Delta n = n_a - n_c = \frac{C_r(1+G) - 1}{S} n_2 P_{\text{in}}. \tag{10.3.35}$$

Considering the optical switching requires $\Delta n = \lambda/2L$, then we obtain the threshold switching power of the device:

$$P_{inc} = \frac{\lambda S}{n_2 L} \cdot \frac{1}{2|C_r(1+G) - 1|}. \tag{10.3.36}$$

When $G = 1$, Eq. (10.3.36) becomes Eq. (10.3.24), it is the formula for Sagnac interferometer all-optical switch containing a non-3 dB coupler.

When $C_r = 1/2$, Eq. (10.3.36) becomes

$$P_{inc} = \frac{\lambda S}{n_2 L} \cdot \frac{1}{|G - 1|}. \quad (G \neq 1) \tag{10.3.37}$$

This is the formula for Sagnac interferometer all-optical switch containing a 3 dB coupler. In this case $G \neq 1$, otherwise it has no switching function. For reducing the switching power, it has to increase the magnification times G.

To compare three switching power formulas for Sagnac interferometer all-optical switch, i.e., Eqs. (10.3.25), (10.3.30) and (10.3.37), we can see they all have a same factor of $\lambda S/n_2 L$, this factor illustrates that the switching power of this kind optical switch is proportional to the cross sectional area of waveguide S, and reverse proportional to the nonlinear refraction coefficient of loop material n_2 and loop length L. In order to reduce the switching time, we may using the rare earth doping fiber or nonlinear waveguide for increasing n_2, but it will increase the absorption loss; also we can increase L, but it is not favourable to the minimization of device; the best way is reduce the cross sectional area of waveguide to use the nanoscale waveguide.

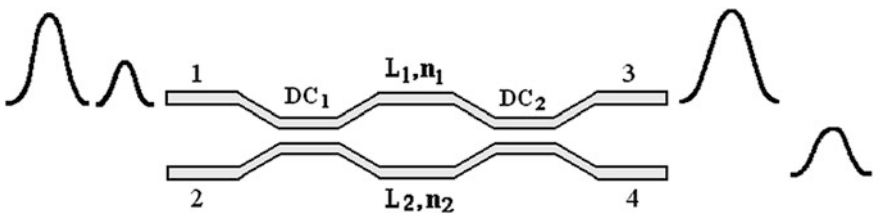

Fig. 10.20 Working principle of nonlinear M–Z interferometer all-optical switch

10.4 Nonlinear M–Z Interferometer All-Optical Switch

M–Z interferometer is an interferometer based on two-beam interference principle, which is consisted of two 3 dB couplers DC_1 and DC_2 connected with two straight waveguides I and II (Arm I and Arm II), the device has 4 ports, as shown in Fig. 10.20. There are two types of M–Z interferometer, which made by the optical fiber and the coplanar waveguide.

The working principle of self-pump M–Z nonlinear interferometer all-optical switch is described as follows. The two waveguides of M–Z interferometer are asymmetric: or made by different materials with different refractive index n_1 and n_2 or two waveguide have different length L_1 and L_2. When the signal light inputs from Port 1, and divides by coupler DC_1 into two beams with same intensity propagating in the waveguide I and waveguide II, respectively. Because two waveguides are asymmetric, when the two lights arrive at DC_2, they have different phase shift ϕ_1 and ϕ_2, two beams interfere in DC_2, and then output from Port 3 and Port 4. The output power distribution ratio between these two ports is depended on the difference of two phase shift: $\phi = \phi_1 - \phi_2$. We can prove that for the weak input power, the light outputs from Port 4, but when the input power strong enough, the phase-shift difference reaches to $\phi = \pi$, then the output light changes from Port 4 to Port 3 to realize all-optical switching.

However, if the two arms of M–Z interferometer are symmetric, the phase-shift difference of two arms $\phi = 0$, it can not make the optical switch.

10.4.1 M–Z Interferometer All-Optical Switch with Different Arm Materials

If lengths of two arms of M–Z interferometer are the equal, i.e., $L_1 = L_2 = L$; but the nonlinear refraction coefficient of two arms are different, i.e., $n_{12} \neq n_{22}$, under the action of a input light with power P_{in}, the optical-Kerr-effect induced refractive-index change on two arms is different, i.e., $\Delta n_1 \neq \Delta n_2$, and the phase shifts of two beams in the two arms are different, i.e., $\phi_1 \neq \phi_2$, where $\phi_1 = k_0 \Delta n_1 Ls$, $\phi_2 = k_0 \Delta n_2 L$ (k_0 is wave vector in vacuum). So the phase difference between two arms is not zero, i.e., $\phi = \phi_2 - \phi_1 \neq 0$. Now we are going to prove that when $\phi = 0 - \pi$, the switching of output light power from port 4 to port 3 will general.

Setting the signal light input the device from port 1, the input light field amplitude is E_1, the output light field amplitudes from Port 3 and port 4 are E_3 and E_4, we use the transmission matrix of symmetric coupler and optical waveguide, to write out the transmission matrix of M–Z interferometer:

$$\begin{bmatrix} E_3 \\ E_4 \end{bmatrix} = \begin{bmatrix} r & it \\ it & r \end{bmatrix} \begin{bmatrix} e^{-ik_0 n_1 L_1} & 0 \\ 0 & e^{-ik_0 n_2 L_2} \end{bmatrix} \begin{bmatrix} r & it \\ it & r \end{bmatrix} \begin{bmatrix} E_1 \\ 0 \end{bmatrix}, \tag{10.4.1}$$

where $r = \cos \kappa z$, $t = \sin \kappa z$, κ is coupling coefficient of two symmetric couplers, k_0 is wave vector in vacuum.

Because we use 3 dB coupler, so $\kappa z = \pi/4$, $r = t = \sqrt{2}/2$, then from Eq. (10.4.1) we can obtain:

$$E_3 = \frac{1}{2}\left[e^{-i\phi_1} - e^{-i\phi_2}\right]E_1, \tag{10.4.2}$$

$$E_4 = i\frac{1}{2}\left[e^{-i\phi_1} + e^{-i\phi_2}\right]E_1. \tag{10.4.3}$$

Assuming the input light power from Port 1 is $P_1 = |E_1|^2 = P_{in}$; the output light powers from Port 3 and Port 4 are $P_3 = |E_3|^2$ and $P_4 = |E_4|^2$, from Eqs. (10.4.2) to (10.4.3) we deduce to the output powers from Port 3 and Port 4, respectively:

$$P_3 = P_{in} \sin^2 \frac{\phi}{2}, \tag{10.4.4}$$

$$P_4 = P_{in} \cos^2 \frac{\phi}{2}. \tag{10.4.5}$$

From above two equations we can see, under the weak light $\phi = 0$, $P_3 = 0$ and $P_4 = P_{in}$, the light power inputted from Port 1 P_{in} will totally output from Port 4. If input power is strong enough to lead $\phi = \pi$, then $P_4 = 0$ and $P_3 = P_{in}$, P_{in} will totally output from Port 3. That is to say the condition for switching is that the phase-shift difference of two arm lights is π.

Assuming the linear refractive index of two arms of M–Z interferometer are approximately equal, $n_{01} \approx n_{02}$, but the nonlinear refraction coefficient is different, $n_{21} \neq n_{22}$, for example one arm is made by a common silica fiber, another one is mede by rear earth doped silica fiber. When the each of two arms accept the action of a strong light with power of $P_{in}/2$, the optical Kerr effect induces the nonlinear refractive index: $\Delta n_1 = n_{21}P_{in}/2S$ and $\Delta n_2 = n_{22}P_{in}/2S$, where S is the cross sectional area. The phase shifts of light beams in two arms are $\phi_1 = k_0\Delta n_1 L = k_0 n_{21} L P_{in}/2S$ and $\phi_2 = k_0\Delta n_2 L = k_0 n_{22} L P_{in}/2$ respectively, the phase-shift difference of two beams is

$$\phi = \phi_1 - \phi_2 = k_0 L(n_{21} - n_{22})\frac{P_{in}}{2S}. \tag{10.4.6}$$

Setting $n_{21} \gg n_{22}$, $n_{21} - n_{12} \approx n_{21}$, and using $k_0 = 2\pi/\lambda_0$ (λ_0 is the wavelength in vacuum), then the phase shift difference can be written as

$$\phi \approx \frac{\pi n_{21} L}{\lambda_0 S} P_{in}. \tag{10.4.7}$$

Because the condition for realizing the optical switching is $\phi = \pi$, therefore the threshold switching power is

$$P_{inc} \approx \frac{\lambda_0 S}{n_{21} L}. \tag{10.4.8}$$

From Eq. (10.4.8) we can see, for M–Z interferometer all-optical switch with two different nonlinear arms, in order to reduce the switching power, we can increase the difference of nonlinear refraction coefficient between two arms $n_{21} - n_{12}$, also can decrease the cross sectional area of waveguide S.

For example, we consider a fiber-type M–Z interferometer, its arm I is made by erbium-doped fiber, $n_{21} = 3 \times 10^{-15}\,\mathrm{m^2/W}$, and arm II is a regular fiber, $n_{22} = 2.6 \times 10^{-20}\,\mathrm{m^2/W}$, so $n_{21} \gg n_{22}$. The wavelength of signal light is $\lambda_0 = 1.55 \times 10^{-6}\,\mathrm{m}$, the length of two arm are $L = 10\,\mathrm{cm}$, the radius of two fibers is $r = 3\,\mu\mathrm{m}$, the cross sectional area is $S = \pi r^2 = 2.83 \times 10^{-11}\,\mathrm{m^2}$. We calculate using Eq. (10.4.8) to obtain the switching power $P_{inc} = 146\,\mathrm{mW}$. If changing the fiber radius to be 300 nm, $S = 2.83 \times 10^{-13}\,\mathrm{m^2}$, we find the switching power is decreased in 100 times, it is $P_{inc} = 1.46\,\mathrm{mW}$ only.

10.4.2 M–Z Interferometer All-Optical Switch with Different Arm Lengths

Now we set the two arms of M–Z interferometer have same nonlinear refraction coefficient, i.e., $n_1 = n_2 = n$, for example it is made by common silica fiber; but the lengths of two arms are different, i.e., $L_1 \neq L_2$, and assume $L_1 \gg L_2$, so $\Delta L = L_1 - L_2 \approx L_1$. This kind M–Z interferometer is shown in Fig. 10.21.

The light powers in two arms are the same, it is $P_{in}/2$, the phase shifts of two light beam in two arms are $\phi_1 = k_0 n_2 L_1 P_{in}/2S$ and $\phi_2 = k_0 n_2 L_2 P_{in}/2S$ respectively. The phase-shift difference is

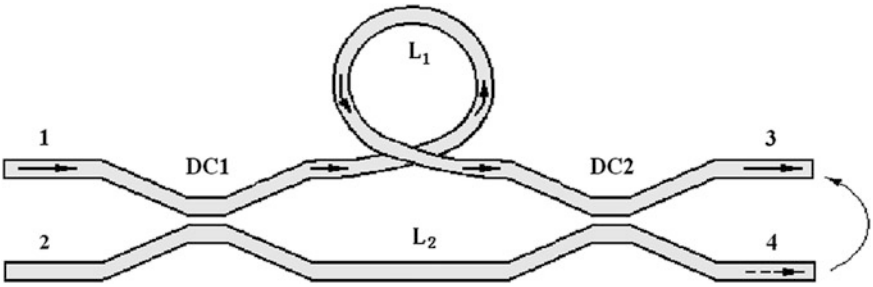

Fig. 10.21 M–Z interferometer all-optical switch with different arm length and same arm material

$$\phi = \phi_1 - \phi_2 = \frac{2\pi}{\lambda_0} n_2 \Delta L \frac{P_0}{2S} \approx \frac{\pi n_2 L_1 P_{in}}{\lambda_0 S}. \tag{10.4.9}$$

The condition for optical switching is $\phi = \pi$, thus the threshold switching power is

$$P_{inc} \approx \frac{\lambda_0 S}{n_2 L_1}. \tag{10.4.10}$$

Obviously, for the M–Z interferometer all-optical switch with different lengths of two arms, if the length difference of two arms is larger, and the cross sectional area is smaller, the required switching power will be smaller.

Considering a M–Z interferometer made with a common silica fiber and different arm length, the data of device are $n_2 = 2.6 \times 10^{-20}\,\mathrm{m^2/W}$, $L_1 - L_2 \approx L_1 = 10\,\mathrm{m}$, and $S = 2.83 \times 10^{-11}\,\mathrm{m^2}$. We calculate using Eq. (10.4.10) to obtain the switching power $P_{inc} = 169\,\mathrm{W}$. It is not suitable to the optical communication. In next section, we will point out that if we replace the long fiber arm to be a 10 m-long fiber ring, then we can reduce the switching power from hundred watts down to milliwatts.

10.5 Nonlinear Ring Resonator All-Optical Switch

The ring resonator (RR) is an interferometer based on the multiple-bean interference principle, which is similar to the FP interferometer, as shown in Fig. 10.22. The difference between FP and RR is that the FP is based on the standing-wave interference and the RR is based on the traveling-wave interference, the former is light in FP cavity making multiple back and forth trips and the latter is light in the ring cavity making multiple circle trips. The action of couplers C_2 and C_1 in the ring cavity is similar to the reflecting mirrors M_2 and M_1 in FP cavity, they except provide the feed back of light, also provide the input and output of the light. The

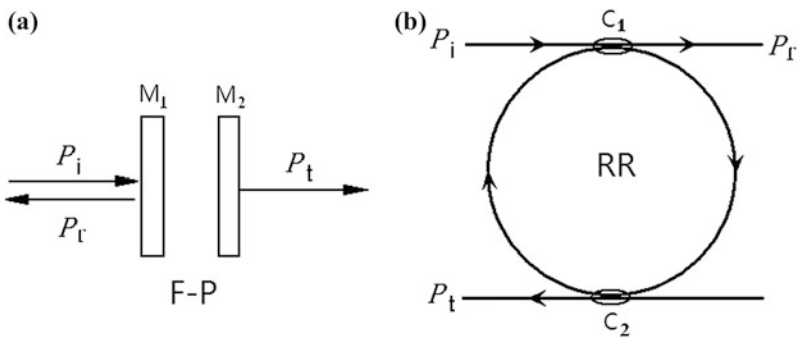

Fig. 10.22 Two kinds of multiple-bean interference: **a** FP resonant cavity; **b** ring resonator

light with power P_i inputs into device through C_1 or M_1; and outputs from C_2 or M_2 called transmitted output (with power P_t), and outputs from C_1 or M_1 called reflected output (with power P_r).

In PF resonant cavity or ring resonator, if the phase shift in single a round trip is φ, the transmittance of resonant cavity is $T = P_t/P_i$, the relationship curve between T and φ (for transmitted output) is shown in Fig. 10.23.

The structure of ring resonator has two kinds: one is the ring through two couplers coupling with two straight waveguides, as sown in Fig. 10.22b; another one is the ring through single coupler coupling with one straight waveguide, we can regard this ring resonator is that its second coupler with 100 % reflectivity. The single coupler RR (SCRR) all-optical switch is a 1 × 1 optical switch; the double coupler RR (DCRR) all-optical switch is a 1 × 2 optical switch.

10.5.1 All-Optical Switch in a M–Z Interferometer Coupled with a SCRR

In order to decrease the switching power of M–Z interferometer all-optical switch, 1999 Heebner and Boyd [9] proposed a new all-optical switch coupling a single coupler ring resonator with one of the arms of fiber M–Z interferometer, that equivalently infinite extends this arm, as shown in Fig. 10.24. The signal light travels in the ring for many times and accumulates the nonlinear phase shift, when the phase-shift difference achieves $\phi = \pi$, then can realize the switching conversion from Port 4 to Port 3 of M–Z interferometer. The switching power can be decreased in 4 orders of magnitude.

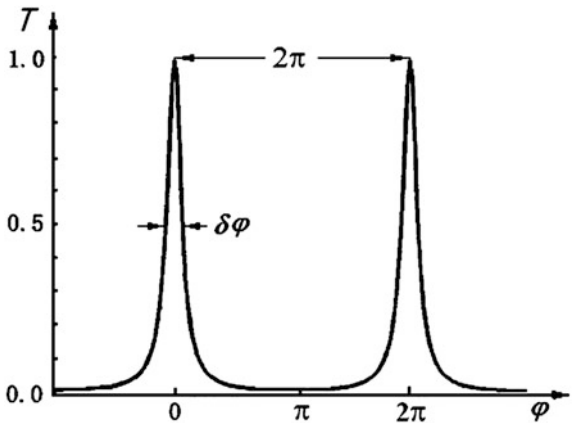

Fig. 10.23 The relationship curve of transmittance (*T*) and phase shift (φ) for FP or RR resonant cavity with transmitted output

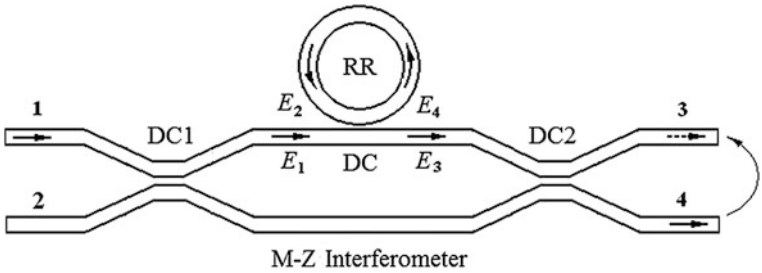

Fig. 10.24 Structure chart of all-optical switch in M–Z interferometer cooped with a ring cavity

At first we study the structure of a single coupler ring resonator (SCRR), which is coupling a ring resonator with a straight waveguide through a coupler DC, as shown in upper part of Fig. 10.24. Let E_1 is the field amplitude of signal light at the Input Port 1 of the coupler where the light inputs into the coupler from the straight waveguide; E_4 is the light field amplitude at the Output Port 4 of the coupler where the light inputs into the ring cavity from the coupler; E_2 is the light field amplitude at the Input Port 2 of the coupler where the light finishes a circle trip in the ring and inputs the coupler again. E_3 is the light field amplitude at Output Port 3 of the coupler where the light outputs from the coupler to the straight waveguide again. Actually, E_3 includes two parts: one is the amplitude of rE_1, which is that E_1 reflects to the straight waveguide passing through the bar path of coupler, and another one is the amplitude of itE_2, which is that E_2 transmits to the straight waveguide passing through the cross path of coupler; E_4 also includes two parts: one is the amplitude of itE_1, which is that E_1 transmits to the ring cavity passing through the cross path of the coupler, and another one is the amplitude of rE_2, which is that E_2 reflects to the ring cavity passing through the bar path of coupler; E_4 transforms to E_2, not only it has a fiber absorption loss α, but also has a phase shift φ. In addition, E_1 transforms to E_3, it has a phase change $\phi = \phi_3 - \phi_1$. Therefore, the relationships among the field amplitudes at every port are

$$E_3 = rE_1 + itE_2, \tag{10.5.1}$$

$$E_4 = itE_1 + rE_2, \tag{10.5.2}$$

$$E_3 = e^{i\phi}E_1, \tag{10.5.3}$$

$$E_2 = ae^{i\varphi}E_4 = e^{-\alpha l/2}e^{i\varphi}E_4, \tag{10.5.4}$$

where r and t is the reflectivity and the transmittance of coupler respectively, φ is the phase shift of the light for one circle trip in the ring; α is the absorption coefficient, $a = e^{-\alpha l/2}$ is the loss rate for one circle trip; l is the perimeter of the ring; $\phi = \phi_3 - \phi_1$ is the phase difference between the phase at Input Port 1 and the

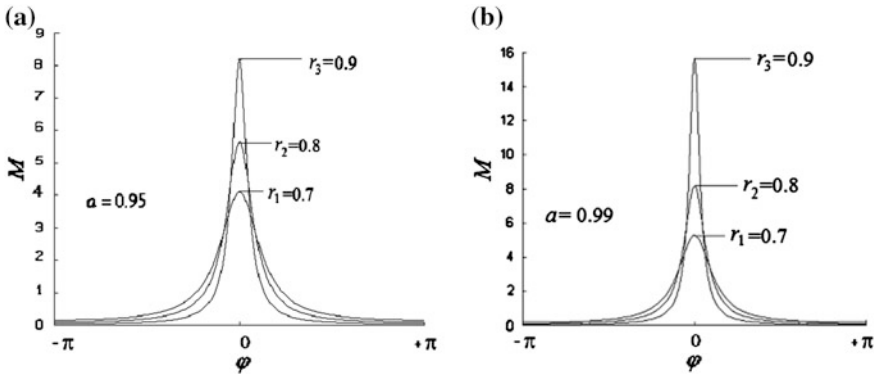

Fig. 10.25 Spectra of the ring amplification coefficient versus the one-circle phase shift under different coupler reflectivity: **a** a = 0.95; **b** a = 0.99

phase at Output Port 3, it is also the phase difference between two lights on two arms of M–Z interferometer.

From above Equations we obtain following relationship:

$$\frac{E_2}{E_1} = \frac{itae^{i\varphi}}{1 - rae^{i\varphi}}, \tag{10.5.5}$$

$$\frac{E_3}{E_1} = \frac{r - ae^{i\varphi}}{1 - rae^{i\varphi}}. \tag{10.5.6}$$

We define the amplification coefficient of ring cavity for light power is

$$M = \frac{P_2}{P_1} = \frac{|E_2|^2}{|E_1|^2} = \frac{(1 - r^2)a^2}{1 - 2ra\cos\varphi + r^2a^2}. \tag{10.5.7}$$

According to Eq. (10.5.7), the curves of M versus φ are drawn in Fig. 10.25. One can see that when $a \to 1$ (i.e., neglecting the ring loss), $r \to 1$ (i.e., keeping most power in the ring), the full width at half maximum (FWHM) of $\delta\varphi$ becomes smaller, and the peak of M becomes higher.

In Fig. 10.28a, b we can see that the peak value for $a = 0.99$ is twice of the peak value for $a = 0.95$; but the width $\delta\varphi$ of the former is much small then that of the latter. In the case of $a = 0.95$, the peak value for $r = 0.9$ is twice of the peak value for $r = 0.7$ and in the case of $a = 0.99$, the peak value for $r = 0.9$ is triple of the peak value for $r = 0.7$. In both case the width $\delta\varphi$ is remarkable increase with decrease of r.

From Eq. (10.5.7) we can see, if $a \to 1$, $r \to 1$, and in resonant case i.e., $\varphi = 2m\pi(m = 0, 1, 2\ldots)$, we can obtain maximum amplification coefficient:

$$M_{\max} \approx \frac{2}{1-r}. \tag{10.5.8}$$

In other hand, from the definition of the finesse of ring cavity F, we obtain

$$F = \frac{2\pi}{\delta\varphi} = \pi\left[2\sin^{-1}\left(\frac{1-ar}{2\sqrt{ar}}\right)\right]^{-1}. \tag{10.5.9}$$

In the condition of $a \to 1$, $r \to 1$ and $\varphi = 2\ m\pi$, we can get the maximum finesse and the relationship between the maximum finesse and the maximum amplification coefficient:

$$F_{\max} \approx \frac{\pi}{1-r} = \frac{\pi}{2}M_{\max}. \tag{10.5.10}$$

It means that $F_{\max}$ is proportional to $M_{\max}$. The curves of the finesse F as a function of a and r are drawn in Fig. 10.26 according to Eq. (10.5.9). It is obvious that if $a \to 1$, $r \to 1$, F increases dramatically.

Because ϕ is defined as $\phi = \phi_3 - \phi_1$, using Eqs. (10.5.3) and (10.5.6) we obtain

$$\phi = \arg\left[\frac{r - a\ \exp(i\varphi)}{1 - ra\ \exp(i\varphi)}\right]. \tag{10.5.11}$$

To calculate the first derivative of ϕ with respect to φ, and assuming $a \to 1$, $r \to 1$ and $\varphi = 2\ m\pi$, we obtain

$$\frac{d\phi}{d\varphi} \approx \frac{(1-r^2)a^2}{1 - 2ra\ \cos\phi + r^2a^2} \approx M_{\max}. \tag{10.5.12}$$

Using Eq. (10.5.6), the transmittance of ring cavity can be expressed as

$$T = \frac{|E_3|^2}{|E_1|^2} = \frac{r^2 - 2ar\mathrm{con}\varphi + a^2}{1 - 2ar\mathrm{con}\varphi + a^2r^2}. \tag{10.5.13}$$

The relation curve of the transmittance of ring as a function of the phase shift in one circle ($T - \varphi$ curve) is shown in Fig. 10.27. Actually, here $|E_3|^2/|(E_1|^2 = P_3/P_1$ is a reflectivity of single coupler ring resonator, i.e., $R = P_r/P_i$, so the curve in Fig. 10.27 is reverse to the curve in Fig. 10.23.

According to $\varphi = (2\pi/\lambda)nl$, for a certain l and n (for a low power), φ is reverse proportional to λ, so we can draw the curve of transmittance as a function of the wavelength ($T - \lambda$ curve), this is the transmittance spectrum of ring cavity. The

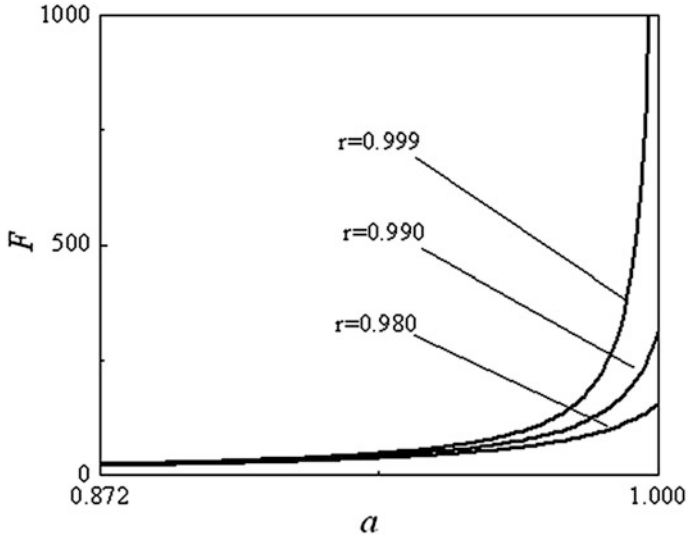

Fig. 10.26 The finesse of the ring as a function of the loss rate and the coupler refractivity

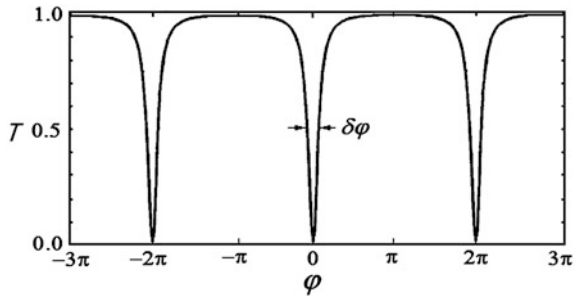

Fig. 10.27 The curve of the transmittance T versus the phase shift φ in the single-coupler ring resonator

$T-\lambda$ curve also can be obtained by experimental method. For example when a signal light at wavelength 1.550 **μ**m inputs in a micro ring, the measured $T-\lambda$ transmittance spectrum is shown in Fig. 10.28, which transmitted valley at $\lambda_V = 1.556\,\mu$m (the resonant wavelength).

In order to realize an all-optical switch, we can use a low-power signal light at resonant wavelength of ring cavity $\lambda_V = 1.55\,\mu$m incident into the ring, to satisfy the resonance condition, i.e., $\varphi = (2\pi/\lambda_V)nl = 2m\pi$, in this case $\lambda_V \propto n$. If in the same time, we send a pump light with power $\boldsymbol{P}$ to irradiate the ring material, according to Kerr effect, the change of refractive index will be induced, i.e., $\Delta n \propto P$, so we get $\Delta\lambda_V \propto \Delta n \propto P$. If we increase the pump power to lead the transmitted spectrum shift to a half of the peak width, the transmittance of device change from valley to the top, than the optical switching is accomplished.

Now we deduce the threshold switching power of the device. The light propagates for the one circle of the ring with length of l, the Kerr effect induced nonlinear

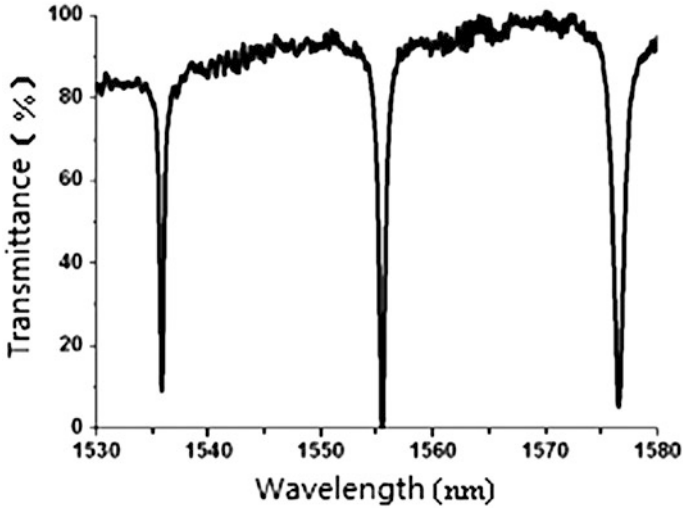

Fig. 10.28 Measured $T - \lambda$ transmittance spectrum of ring cavity, the input signal wavelength is 1.550 μm, the minimum transmittance valley at wavelength of 1.556 μm

phase shift φ is proportional to the light power P_2, and than the nonlinear phase-shift change $d\varphi$ induced by unit power P_2 is

$$\frac{d\varphi}{dP_2} = \frac{d}{dP_2}\left(\varphi_0 + \frac{2\pi}{\lambda_0} ln_2 \frac{P_2}{S}\right) = \frac{2\pi ln_2}{\lambda_0 S}. \tag{10.5.14}$$

Using Eqs. (10.5.13), (10.5.14) and $dP_2/dP_1 = P_2/P_1 = M_{\max}$, we can find unit power P_1 induced phase-shift difference of two arm lights in M–Z interferometer is given by

$$\frac{d\phi}{dP_1} = \frac{d\phi}{d\varphi}\frac{d\varphi}{dP_2}\frac{dP_2}{dP_1} = \frac{2\pi ln_2}{\lambda_0 S} M_{\max}^2. \tag{10.5.15}$$

Let us make a definite integral on both sides of the Eq. (10.5.15) with the up limits of π and P_{1c} for ϕ and P_1 respectively, i.e.,

$$\int_0^{\pi} d\phi = \frac{2\pi ln_2}{\lambda_0 S} M_{\max}^2 \int_0^{P_{1c}} dP_1. \tag{10.5.16}$$

Thus the total threshold switching power $P_{\text{inc}} = 2P_{1c}$ can be found as

$$P_{\text{inc}} = \frac{\lambda_0 S}{n_2 l} \cdot \frac{1}{M_{\max}^2}. \tag{10.5.17}$$

Using Eq. (10.5.10), we obtain

$$P_{\text{inc}} = \frac{\lambda_0 S}{n_2 l} \cdot \left(\frac{\pi}{2}\right)^2 \cdot \frac{1}{F_{\max}^2}. \tag{10.5.18}$$

To compare Eq. (10.5.17) with Eq. (10.4.10), we find the switching power P_{inc} is reduced in $M_{\max}^2$ times, it means that the switching power of the symmetric MZI coupled with a ring is much lower than that of MZI with different arm length in the condition that the ring length l is equal to the arm-length difference L. As an example, we take the data of $l = L_1 = 10\,\text{m}$, $r = 0.99$, $a = 1$, and $M_{\max}^2 \approx 4/(1-r)^2 = 40000$, using Eq. (10.5.17) we get the switching power $P_{\text{inc}} = 4.23\,\text{mW}$. However, the device with ring length 10 m is not suitable for application, we can reduce the length of the ring to be 1 *cm*, but the switching power becomes 42.3 W. The best way for reducing the switching power is reduction of cross sectional area of the waveguide to be nanoscale.

Equation (10.5.18) shows that the switching power is reverse proportional to the square of the finesse. In order to reduce the switching power we must enhance the finesse, there are two ways according to Eq. (10.5.9): one is decrease of cavity loss ($a \to 1$), another is increase of the coupler reflectivity ($r \to 1$).

10.5.2 All-Optical Switch in a DCRR

Figure 10.29 shows a ring resonator all-optical switch with two couplers coupled with two straight waveguides. In general the reflectivities of two couplers r_1 and r_2 are selected very large ($\to 1$) for keeping a high light energy density in the cavity. We will prove that if the signal light inputs cavity from left port of waveguide I,

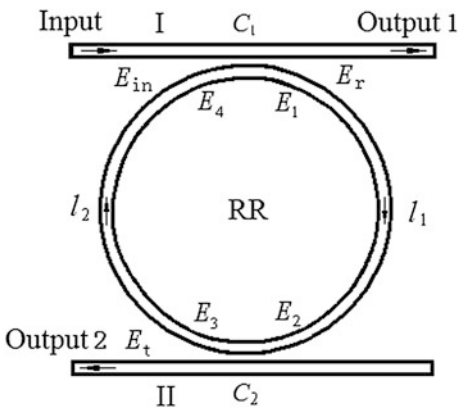

Fig. 10.29 Double-coupler-ring-resonator all-optical switch with one Input Port and two Output Ports

when the light power is weak, the light will output from the left of waveguide II (transmitted output Port 2); when the light power increases enough, after one circle trip, the phase shift of light reaches to $\varphi = \pi$, the output light will be changed to the right port of the waveguide I (reflected output Port 1).

Assuming the light inputs the ring cavity from Input Port and outputs from Output Port 1 and Output Port 2, the every field amplitude is satisfied the following transmission equations:

$$E_r = r_1 E_{in} + it_1 E_4, \tag{10.5.19}$$

$$E_1 = it_1 E_{in} + r_1 E_4, \tag{10.5.20}$$

$$E_2 = \exp(-\alpha_1 l_1/2)\exp(i\varphi_1)E_1, \tag{10.5.21}$$

$$E_3 = r_2 E_2, \tag{10.5.22}$$

$$E_t = it_2 E_2, \tag{10.5.23}$$

$$E_4 = \exp(-\alpha_2 l_2/2)\exp(i\varphi_2)E_3, \tag{10.5.24}$$

where r_i and t_i are the reflectivity and transmittance of two couplers, $i = 1, 2$ means for Coupler 1 and Coupler 2 respectively. If we used comer marks 1 and 2 denote the parameters of right and left half ring respectively, $a_1 = \exp(-\alpha_1 l_1/2)$ and $a_2 = \exp(-\alpha_2 l_2/2)$ are loss rates in the half rings, in which α_1 and α_2 are absorption coefficients, l_1 and l_2 are the lengths of half ring, $l = l_1 + l_2$ is the length of whole ring; $a = a_1 + a_2$ is the loss rate of whole ring; φ_1 and φ_2 are phase shifts in half rings, $\varphi = \varphi_1 + \varphi_2$ is phase shift for the whole ring.

Using Eqs. (10.5.19)–(10.5.24), we can deduce to obtain the expressions of the reflectivity and the transmittance of the DCRR all-optical switch:

$$R = \frac{P_r}{P_{in}} = \frac{|\boldsymbol{E}_r|^2}{|\boldsymbol{E}_{in}|^2} = \frac{r_1^2 - 2ar_1r_2\cos\varphi + a^2r_2^2}{1 - 2ar_1r_2\cos\varphi + a^2r_1^2r_2^2}, \tag{10.5.25}$$

$$T = \frac{P_t}{P_{in}} = \frac{|\boldsymbol{E}_t|^2}{|\boldsymbol{E}_{in}|^2} = \frac{a^2}{a_2}\cdot\frac{\left(1 - r_1^2\right)\left(1 - r_2^2\right)}{1 - 2ar_1r_2\cos\varphi + a^2r_1^2r_2^2}. \tag{10.5.26}$$

If the absorption loss can be neglected, i.e., $a_2 \approx a \approx 1$, and setting $r_1 = r_2 = r$, then Eqs. (10.5.25) and (10.5.26) can be written to

$$R = \frac{2r^2(1 - \cos\varphi)}{1 - 2r^2\cos\varphi + r^4} \tag{10.5.27}$$

$$T = \frac{(1 - r^2)^2}{1 - 2r^2\cos\varphi + r^4} \tag{10.5.28}$$

The reflectivity and transmittance of DCRR all-optical switch as a function of the phase shift for a ring trip are shown in Fig. 10.30.

Assuming the reflectivity of coupler $r \to 1$, when without the pump light, the phase shift for a ring trip is equal to linear value $\varphi = \varphi_0$, if $\varphi = \varphi_0 = 2m\pi\,(m = 0, 1, 2\ldots)$, from Eqs. (10.5.27) to (10.5.28) we can obtain $R = 0$ and $T = 1$. When adding a pump light, the Kerr effect will induce the nonlinear part of phase shift: $\varphi = \varphi_0 + \Delta\varphi$, if $\Delta\varphi = \pi$, i.e., $\varphi = (2m+1)\pi$, from Eqs. (10.5.27) to (10.5.28) we can obtain $R = 1$ and $T = 0$. Therefore, under the action of the pump light, the all-optical switching of device happens: $R = 0 \to 1$ and $T = 1 \to 0$, namely the light output changes from Port 2 to Port 1.

We define the power amplification coefficient is

$$M = \left|\frac{E_4}{E_{in}}\right|^2 = \frac{r_2^2\left(1 - a^2 r_1^2\right)}{1 - 2ar_1r_2\cos\varphi + a^2 r_1^2 r_2^2}, \tag{10.5.29}$$

When $r_1 = r_2 = r \to 1$, $a \to 1$, $\varphi = 2m\pi$, the maximum amplification coefficient is

$$M_{\max} \approx \frac{1}{1 - r^2}. \tag{10.5.30}$$

According to the definition of finesse of RR, we obtain

$$F = \frac{2\pi}{\delta\varphi} = \pi\left[2\arcsin\frac{1 - ar_1r_2}{2\sqrt{ar_1r_2}}\right]^{-1}.. \tag{10.5.31}$$

Setting $r = r_1 = r_2$, and $r \to 1$, $a \to 1$, the maximum finesse of RR is

$$F_{\max} \approx \frac{\pi}{1 - r^2} = \pi M_{\max}. \tag{10.5.32}$$

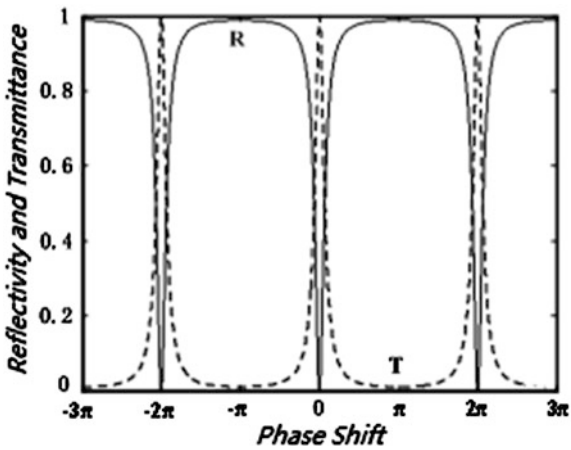

Fig. 10.30 Reflectivity and transmittance of DCRR all-optical switch as a function of the phase shift for a ring trip

Considering the optical Kerr effect, and the length of half ring is $l_1 = l_2 = l/2$, phase shift for one circle trip of light is

$$\varphi = \varphi_0 + \frac{\pi n_2 l}{\lambda S}\left(|E_2|^2 + |E_4|^2\right), \tag{10.5.33}$$

where S is cross sectional area of waveguide. In the condition of $a \to 1$ and $\phi = 2m\pi$, substituting

$$\frac{|E_2|^2}{|E_{in}|^2} = \frac{t_1^2}{1 - 2ar_1r_2\cos\varphi + a^2r_1^2r_2^2} \approx \frac{1 - r_1^2}{(1 - r_1r_2)^2}, \tag{10.5.34}$$

$$\frac{|E_4|^2}{|E_{in}|^2} = \frac{r_2^2t_1^2}{1 - 2ar_1r_2\cos\varphi + a^2r_1^2r_2^2} \approx \frac{r_2^2\left(1 - r_1^2\right)}{(1 - r_1r_2)^2}, \tag{10.5.35}$$

into Eq. (10.5.33), and setting input power $P_{in} = |E_{in}|^2$ and $r = r_1 = r_2$, we obtain

$$\varphi = \varphi_0 + \frac{\pi n_2 l}{\lambda_0 S}\left(|E_2|^2 + |E_4|^2\right) = \varphi_0 + \frac{\pi n_2 l}{\lambda_0 S}\cdot\frac{1 + r^2}{1 - r^2}P_{in}. \tag{10.5.36}$$

Making derivation of phase shift in the ring to the input power, and setting $r \to 1$, we obtain

$$\frac{d\varphi}{dP_{in}} = \frac{\pi n_2 l}{\lambda_0 S}\cdot\frac{1 + r^2}{1 - r^2} \approx \frac{2n_2 l}{\lambda_0 S}\cdot\frac{\pi}{1 - r^2}. \tag{10.5.37}$$

Using Eqs. (10.5.33), (10.5.37) can be written as

$$\frac{d\varphi}{dP_{in}} = \frac{2n_2 l}{\lambda_0 S}F_{\max}. \tag{10.5.38}$$

Making integration of above equation, and using the switching condition of $\phi = \pi$, we obtain the threshold switching power of DCRR all-optical switch, which is

$$P_{inc} = \frac{\lambda_0 S}{n_2 l}\cdot\frac{\pi}{2}\cdot\frac{1}{F_{\max}}. \tag{10.5.39}$$

To compare the Eqs. (10.5.39) and (10.5.18), the switching power of DCRR all-optical switch is larger than that of all-optical switch in M–Z interferometer coupled with a SCRR in $(2/\pi)F_{\max}$ times. From Eq. (10.5.39) we can see that in order to decrease switching power, we should increase the finesse of the ring cavity or decrease the cross sectional area of ring waveguide.

Except the switching power, the RR all-optical switch also has another important property index, which is switching time. The switching time τ of the ring resonator

depends on the two factors: the photon life time of ring cavity τ_c and the nonlinear response time of material τ_f, namely

$$\tau = \tau_c + \tau_f. \tag{10.5.40}$$

The life time of the ring τ_c depends on the frequency bandwidth Δv or the half width of resonance peak $\Delta\varphi$. From formulas $\tau_c = 1/\Delta v$, $\Delta\varphi = 2\pi nl\Delta v/c$, and $F = 2\pi/\Delta\varphi$, we obtain

$$\tau_c = \frac{nlF}{c}. \tag{10.5.41}$$

For example, setting $n = 1.5$, $l = 2\,\text{cm}$, $F = 10$, $c = 3 \times 10^{10}\,\text{cm/s}$, the result of calculation is that $\tau_c = 1\,\text{ns}$. If we use the silicon material, the Kerr response time is about 0.1 ns. So the switching time of the RR all-optical switch is limited by the life time of ring cavity in order of magnitude of nanosecond.

From Eq. (10.5.41) we can see, the cavity life time τ_c is proportional to the finesse F. But Eq. (10.5.39) shows that, the switching power P_{inc} is reverse proportional to the finesse F. Therefore, if we want to optimize the two parameters of switching power and the switching time in the same time, we have to make a trade off in selection of finesse. However, the reduction of the device size (including l and S) is beneficial to improving the quality of all-optical switches.

10.6 Nonlinear Fiber Grating All-Optical Switch

Although studied all-optical switches had many categories over the years, almost no macroscale all-optical switch can satisfy the practical requirements, only the all-optical switch based on the fiber grating is promising. Because the optical fiber grating has many advantages including low insertion loss, small size, simple structure and easy to match with the fiber system, so the fiber grating all-optical switches caused people's attention. There are many kinds of fiber gratings used to make all-optical switches, for example Bragg grating (FBG), long period fiber grating (LPFG), phase shift fiber grating, chirp fiber grating, etc. In this section we will introduce several nonlinear fiber grating all-optical switches with application prospect, which made by nonlinear doped quartz FBG and LPFG or nonlinear fiber connected FBG pair and LPFG pair.

According to different grating constant (grating period), we can divide the fiber grating into two categories:

(1) Fiber Bragg grating (FBG), the grating constant is $\Lambda_B < 1\,\mu\text{m}$, in 0.1 μm order of magnitude. Its mode coupling method is the interference between the forward-propagating mode and backward-propagating mode in reverse

direction, to form a reflected spectrum band with a nano bandwidth (such as 0.2 nm), and the grating wavelength is at the center of band. This is reflection–type optical grating.

(2) Long period fiber grating (LPFG). The grating constant is $\Lambda_L > 100\,\mu m$, for example 300 μm. Its mode coupling method is the interference between the fiber core mode and the cladding mode propagating in same direction, to form a transmitted spectrum band with a broad bandwidth, which is broader than the bandwidth of FBD in a hundred time (such as 20 nm). The grating waveguide is also at the center of band. This is transmission-type optical grating.

Figure 10.31 shows the mode coupling methods of two fiber gratings, and their outputted reflected spectrum and transmitted spectrum under a broad band incident signal light.

10.6.1 Single Nonlinear FBG All-Optical Switch

1. **Description of Fiber Bragg Grating**

If a narrow-band signal light inputs a fiber Bragg grating (FBG), its wavelength λ_i is equal to the grating wavelength (resonant wavelength) λ_B, i.e., $\lambda_i = \lambda_B$, this means that the Bragg condition is satisfied. According to principle of conservation of energy, the incident-light energy equals to the reflected-light energy, i.e.,

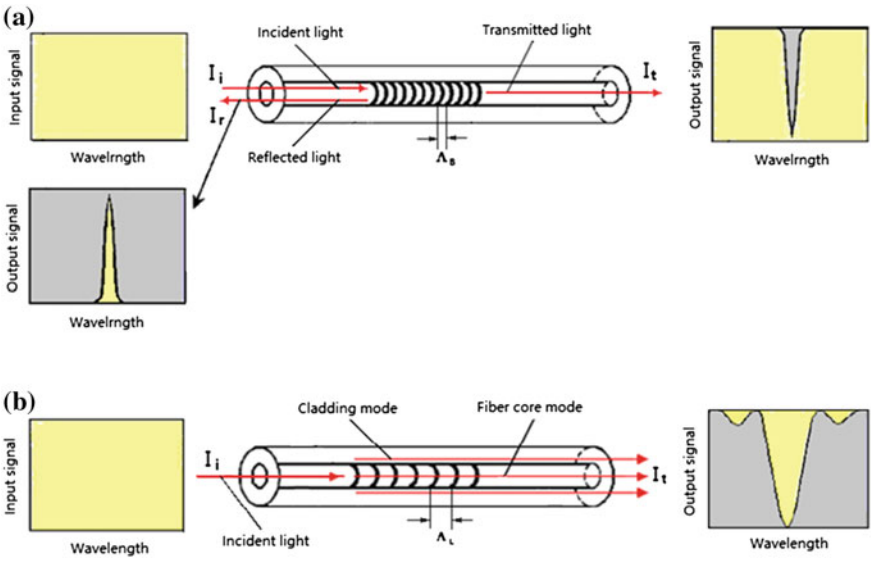

Fig. 10.31 Mode interference and output spectrums of two kinds of fiber gratings: **a** fiber Bragg grating (FBG); **b** long period fiber grating (LPFG)

$\hbar\omega_i = \hbar\omega_f$, then $\lambda_i = \lambda_f = \lambda_B$. In this case the reflected light spectrum is the same as the incident light spectrum, as shown in Fig. 10.32.

Further according to principle of conservation of momentum, the relationship of propagation constants is

$$\boldsymbol{\beta}_i - \boldsymbol{\beta}_f = \boldsymbol{\beta}, \tag{10.6.1}$$

where $\boldsymbol{\beta}_i$ and $\boldsymbol{\beta}_f$ are propagation constants (wave factors) of incident light and reflected light respectively, the numerical value of $\boldsymbol{\beta}_i$ and $\boldsymbol{\beta}_f$ are $\beta_i = \frac{2\pi n_{eff}}{\lambda_i}$ and $\beta_f = \frac{2\pi n_{eff}}{\lambda_f}$ respectively. Under Bragg condition and energy conservation principle, i.e., $\lambda_i = \lambda_f = \lambda_B$, so the numerical value of $\boldsymbol{\beta}_i$ or $\boldsymbol{\beta}_f$ are:

$$\beta_i = \beta_f = \frac{2\pi n_{eff}}{\lambda_B}, \tag{10.6.2}$$

where n_{eff} is effective refractive index of fiber. $\boldsymbol{\beta}$ is the propagation constant of grating, which is defined as

$$\beta = \frac{2\pi}{\Lambda_B}. \tag{10.6.3}$$

where Λ_B is the grating constant of FBG.

Because directions of propagation constants $\boldsymbol{\beta}_i$ and $\boldsymbol{\beta}_f$ are reverse, namely

$$\boldsymbol{\beta}_f = -\boldsymbol{\beta}_i, \tag{10.6.4}$$

According to Eq. (10.6.1), we have

$$2\beta_i = \beta. \tag{10.6.5}$$

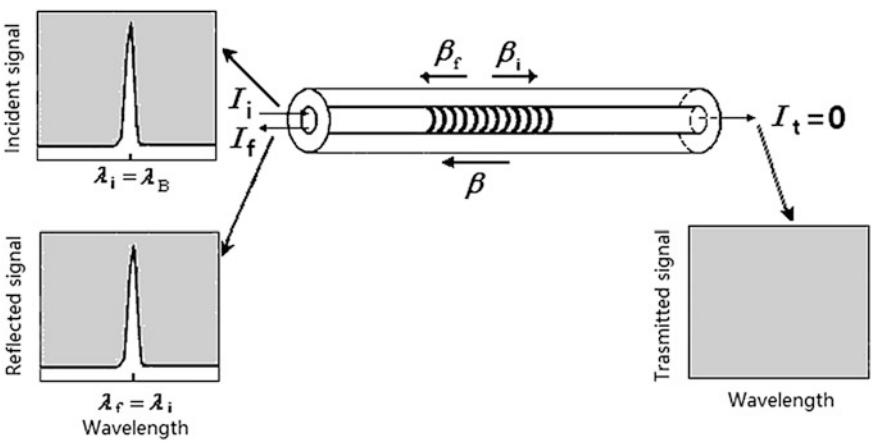

Fig. 10.32 When a narrow-band signal light at wavelength of grating wavelength inputs FBG, the energy and momentum conservation relations between the incident light and the reflected light

Substituting Eqs. (10.6.2) and (10.6.3) into (10.6.5), then we obtain

$$\lambda_B = 2n_{eff}\Lambda_B. \tag{10.6.6}$$

This is the expression of the grating wavelength of FBG.

The refractive index of uniform fiber Bragg grating can be expressed as

$$n(z) = n_{eff} + \overline{\delta n}_{eff}\cos\left(\frac{2\pi}{\Lambda}z\right), \tag{10.6.7}$$

where z is the displacement along axis direction of fiber, $\overline{\delta n}_{eff}$ is the modulation amplitude of average effective refractive index of grating, for short is modulation amplitude of grating.

Setting slow-variation electrical field amplitudes of light field propagated to forward direction and backward direction are respectively

$$A^+(z) = A(z)\exp(i\delta z - \phi/2), \tag{10.6.8}$$

$$B^+(z) = B(z)\exp(-i\delta z + \phi/2), \tag{10.6.9}$$

where δ is detuning parameter, which is defined the difference of incident wave vector respect to the grating wave vector:

$$\delta = 2\pi n_{eff}\left(\frac{1}{\lambda} - \frac{1}{\lambda_B}\right). \tag{10.6.10}$$

If $\delta = 0$, then we obtain $\lambda = \lambda_B$.

In steady state condition, the coupling mode equations of FBG are

$$\frac{\partial A^+}{\partial z} = i\delta A^+ + i\kappa B^+, \tag{10.6.11}$$

$$\frac{\partial B^+}{\partial z} = -i\delta B^+ - i\kappa A^+, \tag{10.6.12}$$

where A^+ and B^+ are the forward wave amplitude and the backward wave amplitude; κ is coupling coefficient, which is defined as

$$\kappa = \kappa* = \frac{\pi}{\lambda}s\overline{\delta n}_{eff}, \tag{10.6.13}$$

where S is the contrast ratio of refractive index modulation. The coupling coefficient is proportional to the modulation amplitude of grating.

Assuming the length of grating is L, the amplitude reflectivity of grating can be solved from Eqs. (10.6.11) to (10.6.12), it is given by

$$|r| = \frac{\kappa \sinh\left(\sqrt{\kappa^2 - \delta^2}L\right)}{\sqrt{(\kappa^2 - \delta^2)\cosh^2\left(\sqrt{\kappa^2 - \delta^2}L\right) + \delta^2 \sinh^2\left(\sqrt{\kappa^2 - \delta^2}L\right)}}. \tag{10.6.14}$$

So the energy reflectivity of grating $R = |r|^2$ can be expressed as

$$R = \frac{\kappa^2 \sinh^2 \sqrt{(\kappa L)^2 - (\delta L)^2}}{\kappa^2 \cosh^2 \sqrt{(\kappa L)^2 - (\delta L)^2} - \delta^2}. \tag{10.6.15}$$

Setting the parameter of FBG are $\Lambda_B = 534.986\,\text{nm}$, $L = 4$ mm, $\lambda_B = 1553.59$ nm, from Eq. (10.6.15) we can obtain the reflected spectrum of grating, as shown in Fig. 10.33.

According to (10.6.15), when $\delta = 0$, FBG has a maximum reflectivity at $\lambda = \lambda_B$, which is

$$R_{\max} = \tanh^2(\kappa L). \tag{10.6.16}$$

The reflected spectrum bandwidth of FBG $\Delta\lambda_0$ can be defined as the interval between two wavelengths where the reflectivity firstly becomes zero in both sides of grating wavelength, which can be obtain from Eq. (10.6.15), and set $\lambda = \lambda_B$ [10]:

$$\Delta\lambda_0 = \frac{\lambda_B^2}{n_{\text{eff}}L}\sqrt{1 + \left(\frac{\kappa L}{\pi}\right)^2}. \tag{10.6.17}$$

For weak coupling FBG (the modulation amplitude of grating is small), $\kappa L \ll \pi$, from Eq. (10.6.18), the reflected spectrum bandwidth is

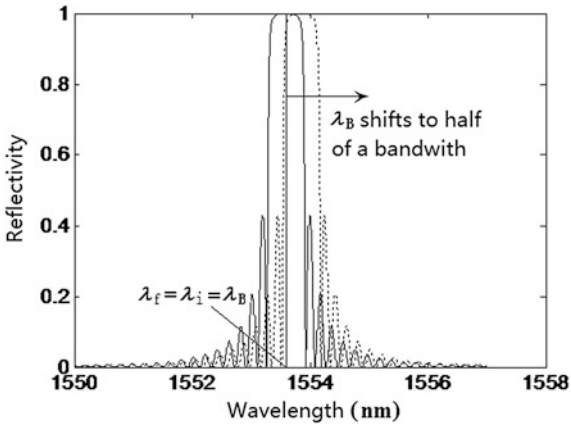

Fig. 10.33 Principle of FBG all-optical switch: the input power induced FBG reflected spectrum moving over the half of a bandwidth, the reflected light changes from maximum value to minimum value

$$\Delta\lambda_0 \approx \frac{\lambda_B^2}{n_{eff}L}. \tag{10.6.18}$$

Using Eq. (10.6.6), we obtain

$$\Delta\lambda_0 \approx \frac{2\lambda_B\Lambda_B}{L} = \frac{2\lambda_B}{N}, \tag{10.6.19}$$

where N is the total number of grating period, which is defined as

$$N = \frac{L}{\Lambda_B}. \tag{10.6.20}$$

Obviously, the reflected spectrum bandwidth of FBG is depended on the total number of grating period.

2. **Single FBG All-Optical Switch**

The signal light inputs FBG, and induces optical Kerr effect under self-phase modulation, to lead the change of refractive index of the fiber, which is

$$n_{eff} = n_0 + n_2\frac{P}{S}, \tag{10.6.21}$$

where n_0 is the linear refractive index of fiber; n_2 is the nonlinear refraction coefficient; P is the input light power; S is the effective sectional area of the fiber. Using Eqs. (10.6.6) and (10.6.21) we obtain the relationship between the change of grating wavelength and the input light power, which is

$$\Delta\lambda_B = 2\Delta n_{eff}\Lambda_B = 2\Lambda_B n_2\frac{P}{S}. \tag{10.6.22}$$

Obviously, the grating-wavelength change is proportional to the input power.

Figure 10.33 shows the shift of reflected spectrum of FBG with the increase of light power. In the beginning the wavelength of input light λ_i is the same as the wavelength of grating λ_B, which is located at the center of the reflected spectrum, were the reflectivity is a maximum value. With the increase of the input light power, the grating wavelength together with reflected spectrum moves to the long wavelength direction. When the moving to the half a bandwidth of the original reflected spectrum, the reflectivity of signal light to reach a minimum value. In this case the reflected light of FBG is accomplished a switching process.

Because under the action of the input power, the necessary condition for realizing the switching process is the shift of grating wavelength to half a bandwidth, i.e.,

$$\Delta\lambda_B = \frac{\Delta\lambda_0}{2}. \tag{10.6.23}$$

Using Eq. (10.6.19), for a weak coupling FBG, the shift of grating wavelength is

$$\Delta\lambda_{\mathrm{B}}=\frac{\Delta\lambda_0}{2}=\frac{\lambda_{\mathrm{B}}\Lambda_B}{\mathrm{L}}.. \tag{10.6.24}$$

To use Eqs. (10.6.22) and (10.6.24), the threshold switching power for FBG all-optical switch is given by

$$P_c=\frac{1}{2}\left(\frac{\lambda_{\mathrm{B}}S}{n_2L}\right). \tag{10.6.25}$$

Obviously, the switching power of FBG all-optical switch mainly depends on the nonlinear refraction coefficient n_2, but for common FBG made by quartz material, n_2 is very small, so the switching power is very high.

3. **Experiments for FBG All-Optical Switch**

(1) **FBG All-Optical Switch in Cross-phase Modulation Mode**

In 1990 Larochelle et al. firstly reported the FBG all-optical switching effect [11]. In their experiment the FBG with grating wavelength $\lambda_{\mathrm{B}}=514.5$ nm, the length of grating $L=3.5$ cm, the diameter of fiber core 4.4 μm; the signal light is a continuous Ar^+ laser at wavelength of 514.5 nm; the pump light is a Q switched and mode locked YAG pulse laser at wavelength of 1064 nm with the repetition frequency 1 kHz and the pulsewidth 100 ps. The signal light and the pump light are counterpropagation, and their polarization directions are orthogonal. Two silicon photoelectric diodes with the resting time 1 ns were used to detect the transmittance of the signal light. Under the cross-phase modulation, they demonstrated the optical switching with contrast ratio of 55 %. Figure 10.34 gives a variation curve of the

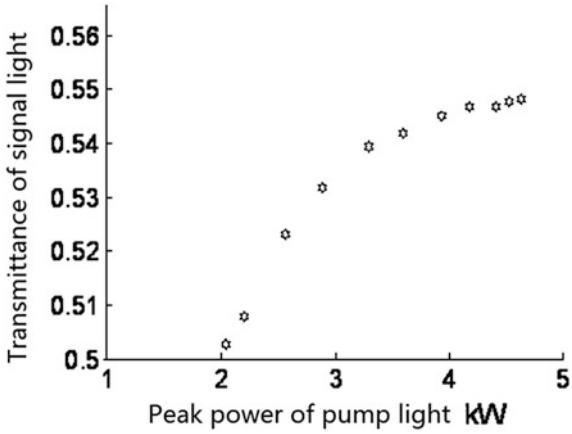

Fig. 10.34 The transmittance of signal light passing through FBG versus the peak power of pump light

transmittance of signal light versus the peak power of pump light. The switching peak power is about 4.5 kW.

(2) **FBG All-Optical Switching in Self-phase Modulation Mode**

In 1998 Broderick [12] and Taverner [13] et al. reported the research results of FBG all-optical switches. In their experimental setup there are two distributed feedback semiconductor light sources (DFB laser diode), as shown in Fig. 10.35. The setup can be used for SPM mode optical switch by using one light source and for CPM mode optical switch by using two light sources.

Light source 1 and light source 2 emit mutually orthogonal polarization lights, which are sent into the FBG through a polarization beam splitter (PBS). The output pump light is absorbed by a narrow band filter 2, and the signal light is transmitted and tested by the photodetector D_2. The reflected light from front end face of FBG is sent into photodetector D_1 via a circulator. Two photodetectors have fast response time with time resolution of 50 ps. The electrical signals outputted from two photodetectors are sent to a fast sampling oscilloscope.

In the experiment, the high power light pulse source used for SPM mode or CPM mode is consisted of a wavelength and power tunable DFB laser and an erbium-doped fiber amplifier (EDFA), with the power greater than 20 kW and the repetition frequency of 4 kHz. The signal light source is a low-power, narrow linewidth, continuous DFB laser with power of 1 mW, its linewidth is smaller than 10 MHz. The measured fiber grating is placed in a capillary tube. The grating has the resonant wavelength of 1535.93 nm, length of 8 cm, and two end sides are coating film for limiting the cladding mode.

In the SPM experiment, the wavelength of high power pulse light is in grating band gap deviated with the grating resonant wavelength about 0.007 nm (at high frequency side). The transmittance of grating as a function of the peak power is shown in Fig. 10.36. We can see that the increase of transmittance with increasing

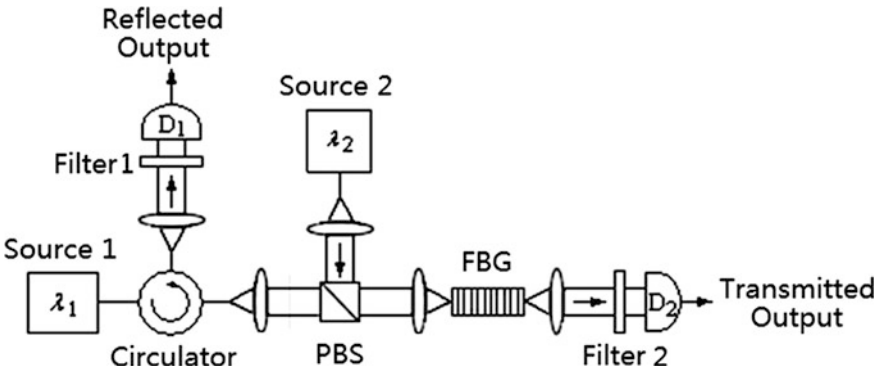

Fig. 10.35 Experimental setup for FBG all-optical switching with two DFB laser diodes and a polarization beam splitter (PBS)

of pulse peak power from 3 to 40 %. That means the optical switch has contrast ratio of 40 %. The threshold switching power is about 4 kW.

(3) **High Nonlinear FBG All-Optical Switching**

The above two examples are FBG all-optical switches based on the ordinary silica fiber. Because the nonlinear refraction coefficient of silica is very small, $n_2 = 2.6 \times 10^{-16}$ cm^2/W [14], the required switching power for these AOSs are generally in the range of 4.0–4.5 kW. From Eq. (10.6.25) we can see, if selecting the materials of fiber granting with large n_2, it is advantageous in reducing the switching power. Here we give two examples as follows.

In 1997, Janos et al. made an Yb^{3+}-doped silica FBG with length of 30 mm [15]. They used a CW laser diode at wavelength 1550 nm as a signal light source to detect the response of the grating; and a laser diode at wavelength 980 nm with rectangular-pulse output as a pump light. The light beam and the signal light together launched into the grating. Since the Yb^{3+}-doped silica fiber had high nonlinearity refraction coefficient, $n_2 = 6.2 \times 10^{-12}$ cm^2/W [18], when the pump power reached 20mW (with 1 Hz- repetition rate), it resulted in the all-optical switching, with switching contrast 63 %, corresponding to the grating effective-refractive-index change $\Delta n_{\text{eff}} = 1.6 \times 10^{-3}$. According to their analysis, the optical switching was based on thermal and electronic two effects, where the thermal effect contributes about 53 %, with the response time of 150 ms; the electronic effect contributes about 10 %, with the response time of 1 ms.

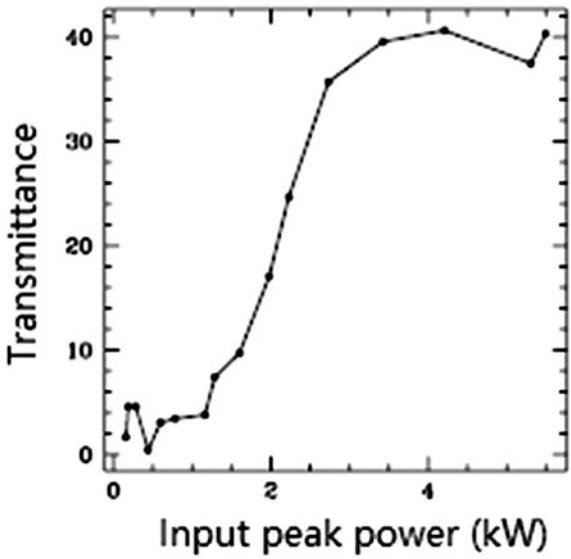

Fig. 10.36 Transmission characteristics of FBG all-optical switching in self-phase modulation mode. The transmittance increases from 2 to 40 %; the switching power is about 4 kW

In 2003, Guan et al. used the high-concentration Er^{3+}-doped fiber to make the FBG all-optical switch [16]. The Er^{3+}-doped fiber has the nonlinearity refraction coefficient of $n_2 = 3 \times 10^{-11} cm^2/W$ [19], and there is the peak-value absorption of 300 dB/m at wavelength of 1530 nm (the grating wavelength). They used a power-tunable laser at wavelength of 1480 nm as an incident light working in SPM mode. When the laser power was 20 mW and 50 Hz, they obtained the optical switching with switching contrast of 56 %. However, when the light power increased to 300 mW, the switching contrast achieved to 90, 70 and 37 %, corresponding to the modulation frequency of 50, 500 and 5 kHz, respectively.

Table 10.3 lists the nonlinear refraction coefficients and the response time τ for different fiber materials.

FBGs made by materials with large n_2 have low threshold switching power. The nonlinear refraction coefficient of the chalcogenide glass fiber is double-order of magnitude in comparison with that of the purity quartz fiber [17]. The FBG optical switches made by chalcogenide glass fiber have a much lower switching power. In addition, such chalcogenide glass material, compared with the rare earth-doped quartz material, has smaller absorption and higher optical transparency. The nonlinear refraction coefficient of erbium-doped silica fiber is higher than that of the ordinary silica fiber in about 5 orders of magnitude [19]. If the FBG optical switch is made by the erbium-doped silica fiber, the switching power can be greatly reduced, but the light absorption is stronger and the response time is longer (about 10 ms).

Here we should note that the nonlinear refraction coefficient n_2 is related with the doped concentration, the pump wavelength and the nonlinear mechanism. Due to these differences, the measured values of nonlinear refraction coefficients recorded in the references are different. Sometimes the measured value could be different in one order of magnitude or more.

10.6.2 Single Nonlinear LPFG All-Optical Switch

1. **Description of Long Period Fiber Grating**

In 1996 Erdogan analyzed the spectral characteristic of LPFG based on the mode coupling theory [20]. Figure 10.37 gives LPFG's transmission spectrum for the

Table 10.3 Nonlinear refraction coefficients and the response times for different fiber materials

Fiber materials	n_2 (cm^2/W)	Wavelength (nm)	Response time	References
Pure silica fiber	2.6×10^{-16}	1550	<1 ps	[14]
Sm-doped-silica fiber	3.0×10^{-15}	1064	<5 ns	[19]
Chalcogenide glass fiber	6.8×10^{-14}	700	2 ns	[17]
Yb-doped-silica fiber	6.2×10^{-12}	1310	750 μs	[18]
Er-doped-silica fiber	3.0×10^{-11}	514.5	10 ms	[19]
Nd-doped-silica fiber	4.7×10^{-11}	823	390 μs	[19]

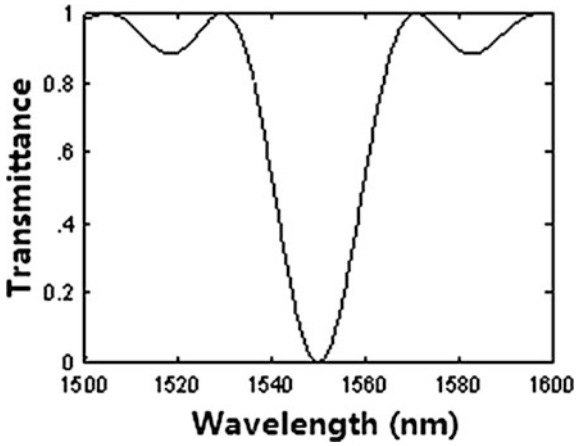

Fig. 10.37 Transmission spectrum of LPFG

average refractive-index modulation depth of $\overline{\delta n}_{\mathrm{eff}} = 6.45 \times 10^{-5}$ and the grating length of $L = 10\,\mathrm{mm}$. It shows that the LPFG's spectral width is approximately 20 nm, which is several hundred times of the FBG's spectral width.

When the light propagates in LPFG, we have to consider the mode coupling between the core mode and the cladding mode. If we only consider the coupling between the fundamental core mode LP_{01} and the m-order cladding mode $LP_{0\mathrm{m}}$, and denoting their propagation constants as β_{co} and β_{cl} respectively, then the momentum-conservation relation can be expressed as

$$\beta_{\mathrm{co}} - \beta_{\mathrm{cl}} = \beta_g = \frac{2\pi}{\Lambda_L}. \tag{10.6.26}$$

where β_g is the propagation constant of fiber grating, Λ_L is the grating constant of LPFG.

In addition, according to the definition of the propagation constants of core and cladding we obtain

$$\beta_{\mathrm{co}} - \beta_{\mathrm{cl}} = \frac{2\pi}{\lambda_{\mathrm{L}}}(\mathrm{n}_{\mathrm{co}} - n_{\mathrm{cl}}) = \frac{2\pi}{\lambda_{\mathrm{L}}}\Delta n_{\mathrm{g}}. \tag{10.6.27}$$

Using Eqs. (10.6.26) and (10.6.27), we obtain

$$\lambda_{\mathrm{L}} = \Lambda_{\mathrm{L}}\Delta \mathrm{n}_{\mathrm{g}}, \tag{10.6.28}$$

where λ_{L} is the grating wavelength of LPFG; Δn_{g} is the effective refractive-index difference between fundamental mode and cladding mode of fiber, i.e.,

$$\Delta n_g = n_{co} - n_{cl}. \tag{10.6.29}$$

Similar to FBG, the detuning of LPFG can be defined as

$$\delta = \frac{1}{2}\left[(\beta_{co} - \beta_{cl}) - \frac{2\pi}{\Lambda_L}\right] = \pi\Delta n_g\left(\frac{1}{\lambda} - \frac{1}{\lambda_L}\right); \tag{10.6.30}$$

and the coupling coefficient between two modes for LPFG is defined as

$$\kappa = \frac{\pi\overline{\delta n}_{eff}}{\lambda}. \tag{10.6.31}$$

where $\overline{\delta n}_{eff}$ is the average refractive-index modulation amplitude of LPFG.

The bandwidth $\Delta\lambda_0$ denoted by the interval between two first zero-transmittance points in two sides of transmission spectrum is [21]

$$\Delta\lambda_0 = \frac{2\lambda_L^2}{\Delta n_g L}\sqrt{1 - \left(\frac{\kappa L}{\pi}\right)^2}, \tag{10.6.32}$$

where L is the length of LPFG., assuming $\lambda = \lambda_L$.

For weak coupling LPFG, $\kappa L \ll \pi$, the bandwidth can be approximately expressed as

$$\Delta\lambda_0 = \frac{2\lambda_L^2}{\Delta n_g L} = \frac{2\lambda_L\Lambda_L}{L} = \frac{2\lambda_L}{N}, \tag{10.6.33}$$

where N is the total period number, which is defined as

$$N = \frac{L}{\Lambda_L}. \tag{10.6.34}$$

2. **Single LPFG All-Optical Switch**

The principle of all-optical switch based on LPFG is shown in Fig. 10.38.

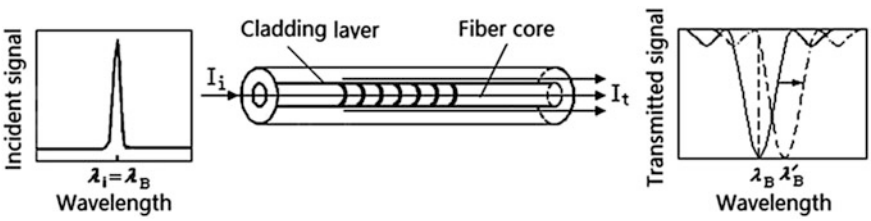

Fig. 10.38 Principle of LPFG all-optical switch

In self-phase modulation mode, when the wavelength of incident light is equal to the grating wavelength, the transmittance of grating is minimum value. With increase of signal power, optical Kerr effect induces the transmission spectrum moving to the long wavelength direction. When the grating wavelength moves to the half of a bandwidth, the transmittance arrives to maximum value, so transmitted light power switches from minimum to maximum.

The signal light power induces the Kerr effect and results in the change of refractive index of fiber core, i.e., $\Delta n_{\mathrm{co}} = n_2(P/S)$, the change of refractive index of cladding can be neglected, i.e., $\Delta n_{\mathrm{cl}} = 0$. Therefore,

$$\Delta\left(\Delta n_g\right) = \Delta n_{co} - \Delta n_{cl} \approx n_2(P/S). \tag{10.6.35}$$

Using Eq. (10.6.28), we obtain

$$\Delta\lambda_{\mathrm{L}} = \Delta\left(\Delta n_g\right)\Lambda_{\mathrm{L}} = n_2\Lambda_{\mathrm{L}}\frac{P}{S}. \tag{10.6.36}$$

Obviously, the shift of grating wavelength is proportional to the input power.

For accomplishing the optical switching, it requires $\Delta\lambda_{\mathrm{L}}=\Delta\lambda_0/2$, using Eqs. (10.6.33) and (10.6.28), for weak coupling LPFG, it requires the shift of grating wavelength:

$$\Delta\lambda_{\mathrm{L}} = \frac{\Delta\lambda_0}{2} = \frac{\lambda_{\mathrm{L}}\Lambda_{\mathrm{L}}}{\mathrm{L}}. \tag{10.6.37}$$

To compare Eqs. (10.6.36) and (10.6.37), we obtain the threshold switching power of LPFG:

$$P_c = \frac{\lambda_{\mathrm{L}}\mathrm{S}}{n_2\mathrm{L}}. \tag{10.6.38}$$

3. **The Experiment for LPFG All-Optical Switch**

In 1997, Eggleton et al. fabricated a LPFG by exposure of hydrogen-loaded germane silicate fibers to an ultraviolet (l – 248 nm) light through an amplitude mask made of chrome-plated silica [22]. The parameters of grating are: the length of grating is $d = 55\,\mathrm{mm}$, $\Lambda_{\mathrm{L}} = 320\,\mu\mathrm{m}$, $\Delta n_{\mathrm{g}} = 0.003$, and $\mathrm{n}_2 = 2.6 \times 10^{-16}\,\mathrm{cm}^2/\mathrm{W}$.

A schematic diagram of the experimental apparatus for testing the optical switching is shown in Fig. 10.39. A 100-ps pulsed light generated by a mode-locked, Q-switched YLF laser with a repetition rate of 500 Hz is coupled into the grating. The central wavelength of the YLF laser is 1052.8 nm, which is approximately coincident with the resonant wavelength of grating. The peak intensity of the pulses coupled into the fiber could be varied between 0 and 20 GW/cm^2. A spatial filter is used to remove the light guided by the cladding mode. Finally, the transmitted intensity is detected with a fast photodiode (resolution 20 ps).

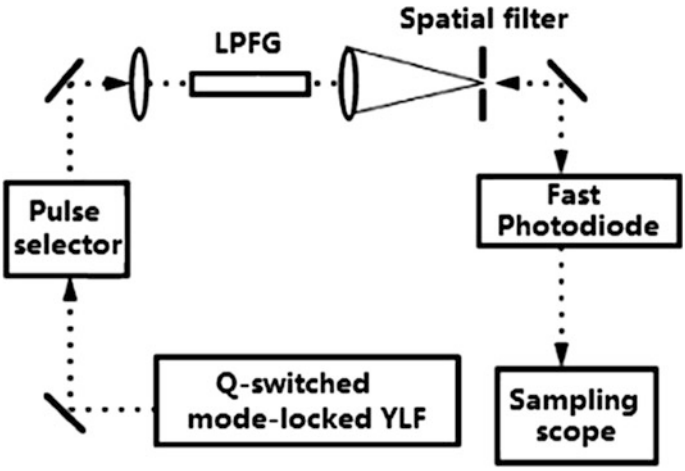

Fig. 10.39 Schematic diagrams of the experimental apparatus for LPFG all-optical switch

Figure 10.40 gives the transmittance variation with the increase of incident intensity at temperature of 40 °C, we can see that the switching threshold starts from the incident intensity greater than 5 GW/cm^2 (corresponding to the switching contrast about 40 %), since then the switching characteristic becomes nonlinear, when the incident intensity reaches 15 GW/cm^2, the switching characteristic begins

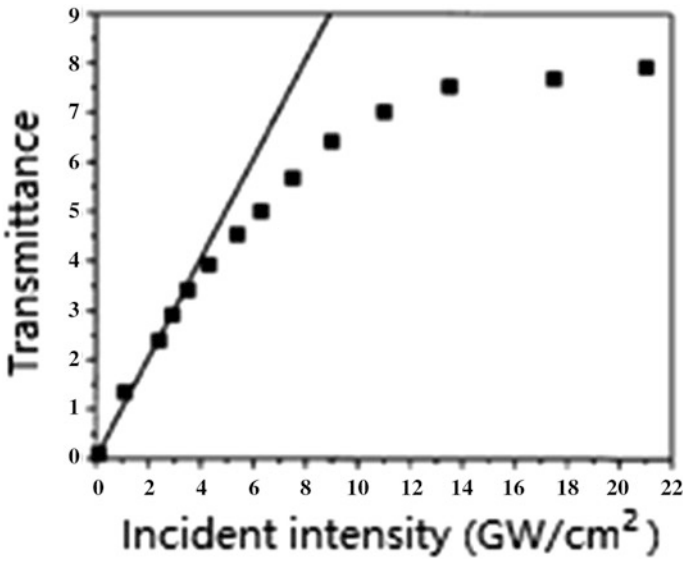

Fig. 10.40 Variation of transmitted power with the the increase of input intensity at temperature of 40 °C

saturation, to realize the optical switching with contrast of 80 %. If the sectional area is 30 μm^2 (the core diameter of 6 μm), the switching power is 4.5 kW.

10.6.3 Nonlinear Fiber Connected LPFG-Pair All-Optical Switch

1. **Usual Fiber Connected LPFG-pair All-Optical Switch**

In 2000, Yoochan et al. demonstrated a low intensity-operated all-optical switching working in XPM mode using a cascade of twin LPFGs with length L = 3 cm. The two LPFGs are connected by a usual fiber with a length of D = 60 cm [23]. The experimental apparatus is shown in Fig. 10.41.

The signal light source is a tunable laser diode at 1565 nm; the pump light source is a Q-switched Nd:YAG laser at 1064 nm. The signal light and pump light together launch to the cascaded twin LPFGs through a 3 dB coupler, the polarizations of the signal light and the pump light are adjusted to be parallel using a polarization controller (PC) in order to maximize the efficiency of nonlinear interaction. The output light passes through a collimator and then separates into two paths of the signal and pump lights by means of a prism. They are detected by PD 1 and PD 2, respectively, and then sent to an oscilloscope. The pump light measured by PD 3 is sent to the oscilloscope as a trigger signal.

The LPFG used has the grating wavelength of λ = 1565 nm. The measured transmission spectrum of LPFG-pair is shown in Fig. 10.42. The total width of transmission spectrum is 17 nm and the width of single peak is 0.5 nm. A pit in the center of spectrum will explain in next paragraph. The imaginary line is the transmission spectrum of single LPFG.

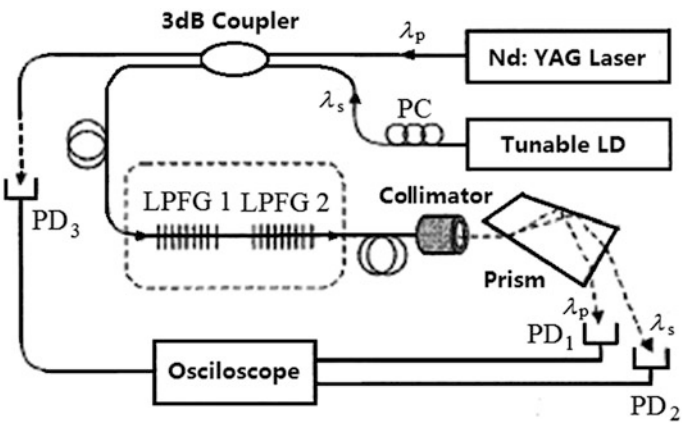

Fig. 10.41 Experimental setup of a regular fiber connected LPFG-pair all-optical switch

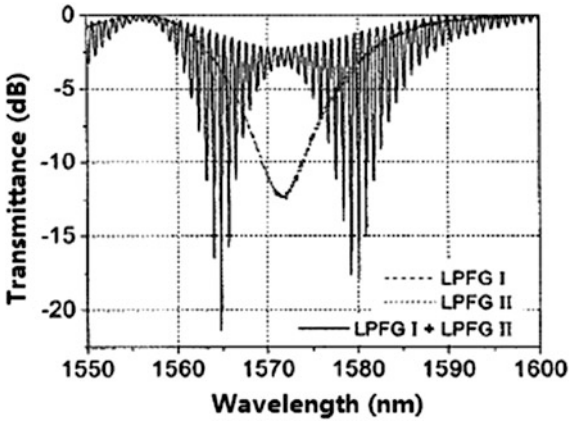

Fig. 10.42 Transmission spectrum of fiber connected LPFG-pair

The experimental results are shown in Fig. 10.43. Figure 10.43 (a) is the transmission spectrum for a single peak. The wavelength of transmittance maximal Point I is $\lambda_{s1} = 1565.2$ nm; The wavelength of transmittance minimal Point II is $\lambda_{s2} = 1564.8$ nm. Figure 10.43b shows the transmittance variational curves of two extreme points with the pump intensity: the transmittance of Point I (square point) is going down with increase of pump power; the transmittance of Point II (round point) is going up with increase of pump power. The switching contrast is about 20 %; the switching intensity is about 1 GW/cm^2, to set $S = 30$ μm^2, then the switching power is about 300 W, which is less than that of the optical switch for single fiber grating.

Chunfei Li's group in 2008 [24] and 2010 [25] have given a theoretical explanation to above experimental result. In the fiber connected LPFG pair, the two LPFGs can be regarded as two 3 dB optical couplers. The first LPFG separates the incident light into the fiber core mode and the cladding mode, both of them propagate in the fiber along same direction until arrive to the second LPFG, where

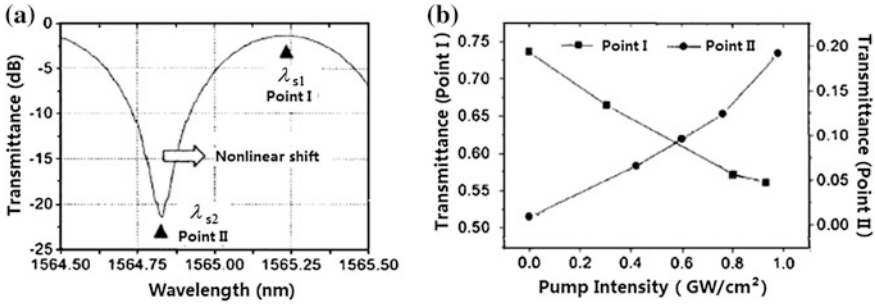

Fig. 10.43 LPFG-pair transmission spectrum for a single peak: **a** the transmission spectrum near wavelength at 1565.2 nm (Point I) and wavelength at 1567.8 (Point II) **b** the transmittance at Point I and Point II versus pump intensity

two modes interfere and output. Therefore, the fiber connected LPFG pair likes an M–Z interferometer, the two arms of which are the fiber core and the cladding layer, as Fig. 10.44.

Because in the fiber medium the average refractive index of fiber core and the average refractive index of cladding are different: n_{co} and n_{cl} respectively, the propagation constants of two mode are different: $\beta_1 = (2\pi/\lambda)n_{co}$ and $\beta_2 = (2\pi/\lambda)n_{cl}$ respectively. Assuming the field amplitudes of fiber core mode and cladding mode are denoted with $E_1(z)$ and $E_2(z)$ respectively, the initial condition are $E_1(0) = 1$, $E_2(0) = 0$, the grating length and the fiber length (interval of two LPFGs) are L and D respectively, and D ≪ L. The two LPFGs are equivalent to two 3 dB couplers, so the light amplitudes of transmitted signal light passing through the device can be expressed by the following transmission matrix:

$$\begin{pmatrix} E_1(D+2L) \\ E_2(D+2L) \end{pmatrix} = e^{i(\beta_1+\beta_2)L} \begin{pmatrix} e^{i\frac{KL}{2}} & 0 \\ 0 & e^{-i\frac{KL}{2}} \end{pmatrix} \begin{pmatrix} t & r \\ r & t^* \end{pmatrix} \begin{pmatrix} e^{i\beta_1 D} & 0 \\ 0 & e^{i\beta_2 D} \end{pmatrix} \begin{pmatrix} e^{-\alpha_1 D} & 0 \\ 0 & e^{-\alpha_2 D} \end{pmatrix} \times \begin{pmatrix} e^{i\frac{KL}{2}} & 0 \\ 0 & e^{-i\frac{KL}{2}} \end{pmatrix} \begin{pmatrix} t & r \\ r & t^* \end{pmatrix} \begin{pmatrix} 1 \\ 0 \end{pmatrix} \tag{10.6.39}$$

where K is the grating wave vector, i.e., $K = 2\pi/\Lambda$, Λ is the grating constant; α_1 and α_2 are absorption coefficient of fiber core and cladding respectively: the definitions of κ and δ are by Eqs. (10.6.31) and (10.6.30), respectively; r and t are the transmittance and the reflectivity of single LPFG respectively, which can find from coupling equations:

$$t = \cos\left(\sqrt{\kappa^2+\delta^2}L\right) + i\frac{\delta}{\sqrt{\kappa^2+\delta^2}}\sin\left(\sqrt{\kappa^2+\delta^2}L\right), \tag{10.6.40}$$

$$r = i\frac{\kappa}{\sqrt{\kappa^2+\delta^2}}\sin\left(\sqrt{\kappa^2+\delta^2}L\right). \tag{10.6.41}$$

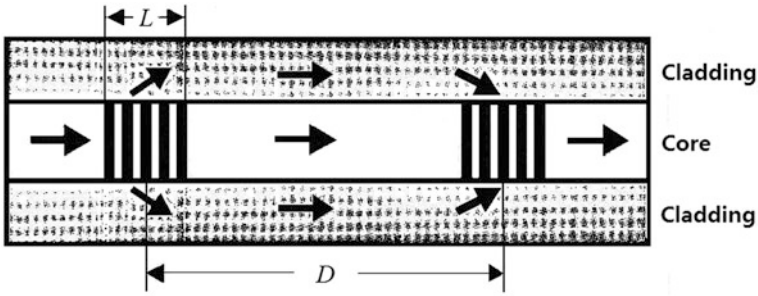

Fig. 10.44 Interference of the fiber core mode and the cladding mode in LPFG-pair based on M–Z interferometer

The transmittance for the incident light passing through the LPFG pair is given by [26]

$$T_{pair} = |T\ \exp(i\Delta\phi) - \gamma R|^2 = T^2 + \gamma^2 R^2 - 2\gamma TR\cos\Delta\phi, \tag{10.6.42}$$

where $T = |t|^2$ and $R = |r|^2$; γ is the loss coefficient of light in the fiber, which is

$$\gamma = \exp[-\alpha L] = \exp[-(\alpha_{\mathrm{co}} + \alpha_{\mathrm{cl}})]L \approx \exp[-\alpha_{\mathrm{cl}} L]. \tag{10.6.43}$$

Here the absorption coefficient of cladding mode is much larger than that of core mode, i.e., $\alpha_{\mathrm{cl}} \gg \alpha_{\mathrm{co}}$.

If without pump light, $\Delta\phi = \phi_0$, ϕ_0 is phase difference between core mode and cladding mode when two modes passing through the fiber length D, and D $\gg$ L, ϕ_0 can be written as

$$\phi_0 = \frac{2\pi D}{\lambda}\Delta n_{\mathrm{g}}, \tag{10.6.44}$$

where λ is the wavelength of incident signal light. Obviously, ϕ_0 is a function of wavelength λ.

Taking the data of Λ_{L} = 300 μm, $\Delta n_{\mathrm{g}} = 5 \times 10^{-3}$, $\lambda_{\mathrm{L}} = 1550\,\mathrm{nm}$, γ = 0.8, D = 60 cm, $\overline{\delta n}_{\mathrm{eff}} = 0.75 \times 10^{-5}$, $\kappa = \pi\overline{\delta n}_{\mathrm{eff}}/\lambda$, from Eqs. (10.6.40) to (10.6.44), changing wavelength (for the center with 1550 nm), we can calculate to get the transmission spectrum of fiber connected LPFG-pair, as shown in Fig. 10.45. in the figure we can see that the transmission spectrum of LPFG-pair (solid curve) is a group of interference fringes with periodic modulated, cosine-shape, narrow bandwidth and equal spacing, and formed inside the envelope of transmission spectrum for the individual LPFG (dashed curve).

Because the spacing of interference peak d is corresponding to the wavelength change when $\Delta\phi_0 = 2\pi$, namely

$$d = \Delta\lambda\frac{2\pi}{|\Delta\phi_0|}. \tag{10.6.45}$$

Using Eq. (10.6.44), then $\Delta\phi_0 = \frac{d\phi_0}{d\lambda}\Delta\lambda = -\frac{2\pi D}{\lambda^2}\Delta n_{\mathrm{g}}\Delta\lambda$, substituting into Eq. (10.6.45), we find the spacing between the vicinity interference peaks [27]:

$$d = \frac{\lambda^2}{\Delta n_{\mathrm{g}} D}. \tag{10.6.46}$$

Obviously, the spacing of interference peak is inverse proportional to the efficient refractive-index difference and the spacing between two gratings.

The average refractive-index modulation amplitude of grating $\overline{\delta n}_{\mathrm{eff}}$ has a larger effect on the shape of the transmission spectrum of LPFG pair, using $\overline{\delta n}_{\mathrm{eff}} = 0.75 \times 10^{-5}$, 0.96×10^{-5}, 1.11×10^{-5} and 1.25×10^{-5}, the resonance

wavelength of 1550 nm and the other parameter as same as the data used by Fig. 10.45, we obtain the different transmission spectra of LPFG pair as shown in Fig. 10.46. We can see that with increasing of $\overline{\delta n}_{\text{eff}}$, the interference peaks near the wavelength of 1550 nm decrease gradually. Finally the transmission spectrum splits to be a double-peak structure; it appears a pit in the central part, as shown in Fig. 10.46d, which is the same as Fig. 10.43.

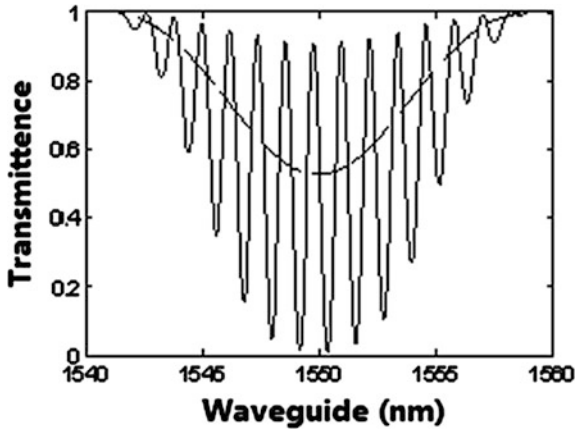

Fig. 10.45 Transmission spectra for an LPFG-pair (*solid curve*) in comparison with the transmission spectra for a single LPFG (*dashed curve*) when the grating wavelength is λ_D = 1550 nm

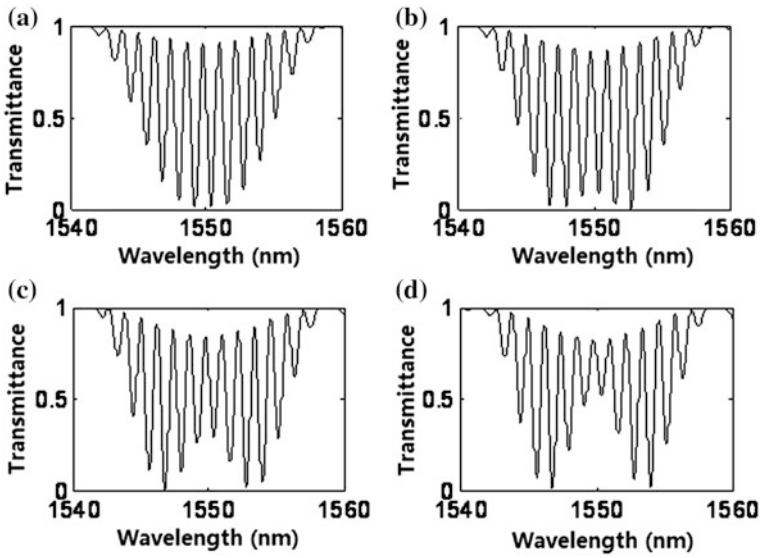

Fig. 10.46 Influence of grating's average refractive-index modulation amplitude $\overline{\delta n}_{\text{eff}}$ to the transmission spectra of LPFG-pair for $\overline{\delta n}_{\text{eff}}$ = **a** 0.75×10^{-5}; **b** 0.96×10^{-5}; **c** 1.11×10^{-5}; **d** 1.25×10^{-5}

We assume that the two LPFGs are linear; the pump power induces only the refractive-index change in the silica fiber due to the Kerr effect under XPM. The variation of the refractive index at the point z in the fiber is

$$\Delta n(z) = 2n_2 \frac{P(z)}{S} = 2n_2 \frac{P(0)\mathrm{e}^{-\alpha z}}{S}, \tag{10.6.47}$$

where $P(0)$ is the pump power at the point $z = 0$, α is the absorption coefficient, S is the effective cross sectional area in the usual silica fiber, n_2 the nonlinear refractive index, for the usual fiber it is $n_2 = 2.6 \times 10^{-16}\mathrm{cm}^2/\mathrm{W}$.

After the signal light with wavelength λ passes through the fiber with length D (assume $D \gg L$, the variation of nonlinear phase of the signal light is therefore

$$\Delta\phi = \Delta\phi_{\mathrm{NL}} = \int_0^D \frac{2\pi}{\lambda} \Delta n(z)\mathrm{d}z = \frac{4\pi n_2 P(0)}{\alpha\lambda S}\left(1 - \mathrm{e}^{-\alpha D}\right) \approx \frac{4\pi n_2 D P(0)}{\lambda S}, \tag{10.6.48}$$

where $P(0)$ is the pump power at the point $z = 0$. Obviously, the variation of nonlinear phase is proportional to the pump power.

Because the necessary condition for realizing switching is

$$\Delta\phi = \pi. \tag{10.6.49}$$

Substituting Eq. (10.6.49) into Eq. (10.6.48), we obtain the switching power for pump light, which is

$$P_{\mathrm{c}}(0) = \frac{\lambda S}{4n_2 D}. \tag{10.6.50}$$

Taking the data $\lambda = 1550$ nm, $n_2 = 2.6 \times 10^{-16}$ cm^2/W, $S = 30$ μm^2, using Eq. (10.6.50), we find that the switching power of the AOS in the silica fiber connected LPFG-pair P_{c} (0) = 745 W, the calculated data closes to the experimental data of 500 W measured by Jeong et al.

From Eq. (10.6.50), it can be seen that the threshold switching power is reverse-proportional to the nonlinear refraction coefficient. In order to reduce the switching power, we suggest using an EDF to replace the usual silica fiber connected with two LPFGs.

2. Nonlinear Fiber Connected LPFG-Pair All-Optical Switch

2008 Li et al. proposed a scheme of nonlinear fiber connected LPFG-pair all-optical switch [25]. The nonlinear fiber is a rare earth doped fiber, such as erbium doped fiber. The experimental setup they suggested is shown in Fig. 10.47. Using cross-phase modulation mode, the signal light and the pump light from two laser diodes together input a LPFG-pair through a wavelength division multiplexer. The pump light is a pulsed light at wavelength of 980 nm; signal light is continuous

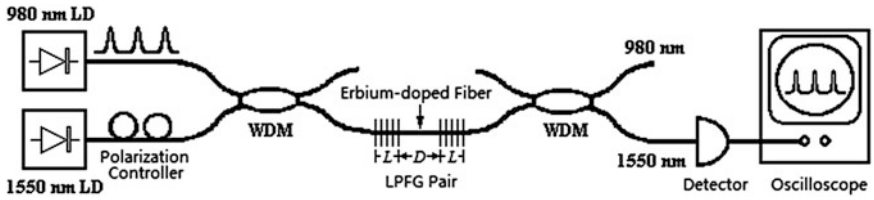

Fig. 10.47 Experimental setup for the nonlinear fiber connected LPFG-pair all-optical switch

light at wavelength at 1550 nm. The second WDM is for separating the signal light and the pump light. The optical switching characteristic of the signal light is measured by an oscilloscope.

The 1550 nm signal light passes through a Er^{3+}-doped fiber (EDF) pumped by 980 nm light, we should consider not only the refractive-index change, but also the optical amplification effect. In other words we have to use the resonant nonlinearity theory to deal with [28], which is based on the three-level model of Er^{3+} ions, as shown in Fig. 10.48.

The pump light propagates in the Er^{3+}-doped fiber along z direction, the pump power at z point is

$$P_{\mathrm{p}}(z) = P_{\mathrm{p0}} \exp\left(-\alpha_{\mathrm{p}} z\right), \tag{10.6.51}$$

where α_{p} is the absorption coefficient of EDF core, $\alpha_p = \sigma_{\mathrm{p}}\mathrm{N}$, σ_{P} is absorption cross section, N is the total ion number density.

Rate equations of energy level 2 and energy level 1 are respectively

$$\frac{\partial N_2}{\partial t} = \frac{\sigma_{\mathrm{p}} P_{\mathrm{p}}}{h v_{\mathrm{p}} S} N_1 - \frac{N_2}{\tau}, \tag{10.6.52}$$

$$N = N_1 + N_2, \tag{10.6.53}$$

where v_{p} is the frequency of pump light; S is effective cross section of EDF, N_1 and N_2 are the ion number densities of energy level 1 and energy level 2, they can solved from Eqs. (10.6.52) to (10.6.53):

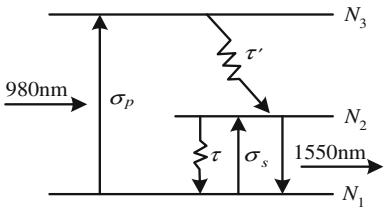

Fig. 10.48 Three-level model of Er^{3+} ions

$$N_1(z) = \frac{N}{1 + P_p(z)/P_c}, \tag{10.6.54}$$

$$N_2(z) = \frac{N}{1 + P_c/P_p(z)}, \tag{10.6.55}$$

where P_c is the saturation power:

$$P_c = \frac{h\nu_p S}{\sigma_p \tau}. \tag{10.6.56}$$

The plane wave signal light at wavelength of 1550 nm also propagates along z direction, its amplitude is

$$E(z, \omega) = E_0(z, \omega)e^{i(\beta z - \omega t)}, \tag{10.6.57}$$

where β is the complex number propagation constant, its real part is related with the refractive index; the imaginary part is related with gain coefficient:

$$\beta = \beta' + i\beta'' = k_0 n + i\frac{g}{2}, \tag{10.6.58}$$

where k_0 is the wave vector of signal light. The pump light induced the change of propagation constant is

$$\Delta\beta = k_0 \Delta n + i\frac{\Delta g}{2}. \tag{10.6.59}$$

The pump light induced refractive-index change of EDF is [28]:

$$\Delta n(\lambda) = \frac{\Gamma_s}{2nL}\int_0^D \left[\chi_p'(\lambda, z) - \chi_0'(\lambda, z)\right]dz, \tag{10.6.60}$$

where D is the length of EDF; n is the linear refractive index of EDF; Γ_s is is a filling factor of the finite overlap between the pump light field and the Er^{3+}concentration profile, χ_p' and χ_0' are the real parts of the complex susceptibility with and without the pump light respectively, which are calculated by the following formula [28]:

$$\chi_i'(\lambda, z) = -\frac{\lambda^3}{16\pi^2 n\tau_2}[N_1(z) - N_2(z)]\beta\xi_{12}(\upsilon - \upsilon_0), \tag{10.6.61}$$

where $i = p$, 0; $\xi_{12}(\upsilon - \upsilon_0)$ is the line shape function for the ion transition; τ_2 is the lifetime of level 2; and $N1$ and $N2$ are the populations at level 1 and level 2 respectively.

Using Eqs. (10.6.60) and (10.6.61) and Eqs. (10.6.54) and (10.6.55) we obtain

$$\Delta n(\lambda, z) = \frac{\Gamma_s N \lambda^3 \xi}{16\pi^2 n^2 \tau_2 \alpha_p D} \ln \frac{P_{p0} + P_c}{P_{p0}\exp(-\alpha_p D) + P_c}. \tag{10.6.62}$$

On the other hand, the expression for the gain coefficient is

$$g(\lambda) = \sigma_e''(\lambda) N_2 - \sigma_a''(\lambda) N_1, \tag{10.6.63}$$

where $\sigma_e''(\lambda)$ and $\sigma_a''(\lambda)$ are the emission cross-section and the absorption cross-section respectively, and they are approximately equal. Using Eqs. (10.6.54) and (10.6.55), the gain coefficient can be written as

$$g(\lambda) = \frac{P_{p0}\exp\left(-\alpha_p D\right) - P_c}{P_{p0}\exp\left(-\alpha_p D\right) + P_c} \sigma_a'' N. \tag{10.6.64}$$

The change of gain coefficient $\Delta g = g(\lambda) - g_0(\lambda)$ is

$$\Delta g = \frac{2P_{p0}\exp\left(-\alpha_p D\right)}{P_{p0}\exp\left(-\alpha_p D\right) + P_c} \sigma_a'' N. \tag{10.6.65}$$

Substituting Eqs. (10.6.62) and (10.6.65) into Eq. (10.6.59) we obtain $\Delta\beta$, so the nonlinear phase shift at second LPFG is

$$\Delta\phi_{NL} = \int_0^D |\Delta\beta| dz. \tag{10.6.66}$$

Under the action of pump light, the phase change of the signal light is

$$\Delta\phi = \Delta\phi_{NL}. \tag{10.6.67}$$

Using Eqs. (10.6.42), (10.6.66) and (10.6.67), we can calculate to obtain the transmission spectrum of EDF-LPFG-pair all-optical switch in the range of 1548–1552 nm under different pump power, as shown in Fig. 10.49 [27]. The data we used are as follows: $\lambda = 1550\,\text{nm}$, $n_2 = 3 \times 10^{-11}\,\text{cm}^2/\text{W}$, $L = 50\,\text{mm}$, $D = 35\,\text{cm}$, $S = 30\,\mu\text{m}^2$, $N = 1.5 \times 10^{26}\text{m}^{-3}$, $\alpha_P = 0.012\,\text{cm}^{-1}$, $\overline{\delta n}_{\text{eff}} = 0.75 \times 10^{-5}$, $\Gamma_s = 1$, $\xi = 10^{-14}$, $\tau_2 = 10\,\text{ms}$, $P_c = 30.54\,\text{mW}$, $\sigma_p = 2.58 \times 10^{-25}\,\text{m}^2$, $\sigma_a'' = 3 \times 10^{-25}\,\text{m}^2$, and $\gamma = 0.8$.

From Fig. 10.49 we can see that, the under the increase of pump light power, the transmission spectrum moves to the long wavelength direction, the power from low to high: (a) 0 mW; (b) 5.26 mW; (c) 15.12 mW; (d) 25.38 mW; (e) 36.40 mW, the transmission spectrum form from a to e, moving half a spectrum width respect to incident wavelength (at imaginary line), the transmittance changes from the maximum value to the minimum value, to realize the optical switching. The switching

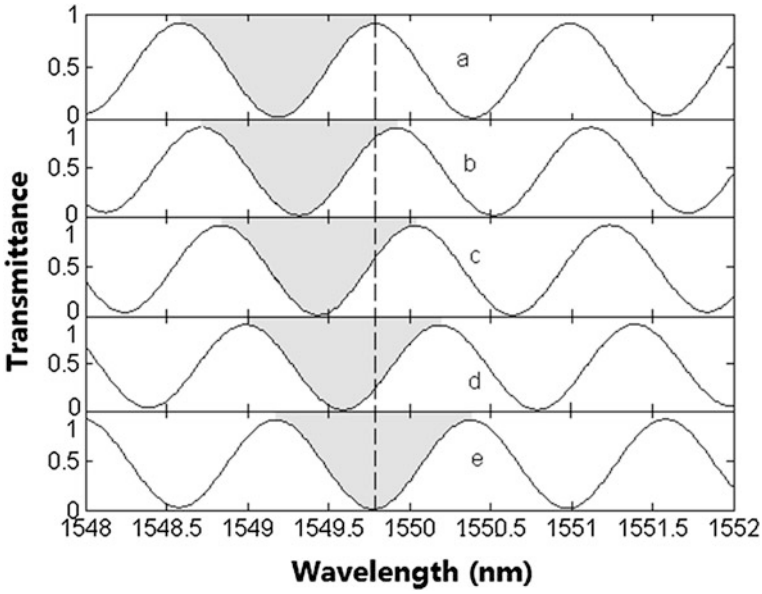

Fig. 10.49 Transmission spectra of the EDF-connected LPFG pair under different pump powers: **a** 0 mW, **b** 5.26 mW, **c** 15.12 mW, **d** 25.38 mW, **e** 36.40 mW

power is 36.40 mW. Obviously, the switching power of EDF-LPFG-pair all-optical switch is lower than that of usual fiber connected LPFG-pair all-optical switch in 4 orders of magnitude.

10.6.4 Nonlinear Fiber Connected FBG-Pair Optical Bistable Switch

Two symmetric fiber Bragg gratings (FBG) is connected by a rare-earth-doped nonlinear optical fiber, to form a nonlinear F–P interferometer, FBGs can be regarded as reflective mirrors, as shown in Fig. 10.50. The signal beam travels in the F–P cavity back and forth, forming the multiple-beam interference; at the same

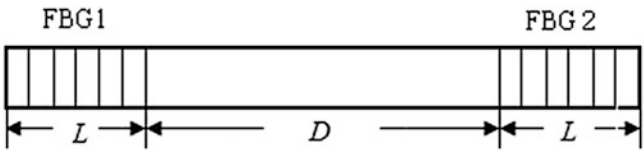

Fig. 10.50 Optical bistable switching device consisted of two same FBGs and a connected nonlinear fiber

time it interacts with the nonlinear media in the cavity to induce the refractive-index change and the round-trip-phase-shift change. In order to achieve the optical bistable switching operation in low switching power, we suggested using the Yb^{3+}-doped fiber with nonlinear refraction coefficient $n_2 = 6.2 \times 10^{-12}$ m^2/W. In contrast with the Er^{3+}-doped fiber, the ytterbium-doped fiber has a smaller absorption and a higher switching speed. Under SPM mode, the signal light can use a CW or pulsed light at 1550 nm.

1. **Transmission Matrix for Single FBG**

Let us first study the transmission characteristics in the individual FBG with length of L. As shown in Fig. 10.51, A_{in} and A_{out} denote the slow-variation amplitudes of the input and output light field propagating along forward direction; B_{in} and B_{out} denote the slow-variation amplitudes of the input and output light field propagating along backward direction respectively in a fiber Bragg grating.

When the low power continuous light inputs into FBG, the light field amplitudes can be found by solving the steady-state coupling mode Eqs. (10.6.11) and (10.6.12), namely

$$\frac{\partial A^+}{\partial z} = i\delta A^+ + i\kappa B^+, \tag{10.6.68}$$

$$\frac{\partial B^+}{\partial z} = -i\delta B^+ - i\kappa A^+, \tag{10.6.69}$$

where A^+ and B^+ are the slow-variation amplitudes of light field propagating along forward and backward directions, κ is coupling coefficient, δ is detuning parameter. The definitions of δ and κ are denoted by Eqs. (10.6.10) and (10.6.13).

Equations (10.6.68) and (10.6.69) can be rewritten as the follower transmission matrix form:

$$\begin{pmatrix} A_{in} \\ B_{out} \end{pmatrix} = \begin{pmatrix} s_{11} & s_{12} \\ s_{21} & s_{22} \end{pmatrix} \begin{pmatrix} A_{out} \\ B_{in} \end{pmatrix}. \tag{10.6.70}$$

Assuming the length of grating is L, the every elements of the above matrix are:

$$s_{11} = s_{22}^* = \cosh\left(\sqrt{\kappa^2 - \delta^2}L\right) - \frac{i\delta \sinh\left(\sqrt{\kappa^2 - \delta^2}L\right)}{\sqrt{\kappa^2 - \delta^2}L}, \tag{10.6.71}$$

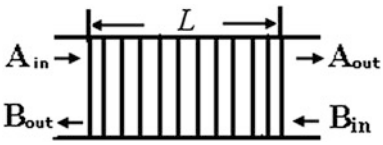

Fig. 10.51 Light transmission in an individual fiber Bragg grating

$$s_{21} = s_{12}^* = \frac{i\kappa \sinh\left(\sqrt{\kappa^2 - \delta^2}L\right)}{\sqrt{\kappa^2 - \delta^2}L}, \tag{10.6.72}$$

To define the transmittance coefficient and the reflectivity coefficient are respectively

$$t = \frac{1}{s_{11}} = |t| \exp(\varphi_t), \tag{10.6.73}$$

$$r = \frac{s_{21}}{s_{11}} = |r| \exp(\varphi_r), \tag{10.6.74}$$

where the amplitudes of the transmittance coefficient and the reflectivity coefficient are respectively:

$$|t| = \frac{\sqrt{\kappa^2 - \delta^2}}{\sqrt{\left(\kappa^2 - \delta^2\right)\cosh^2\left(\sqrt{\kappa^2 - \delta^2}L\right) + \delta^2 \sinh^2\left(\sqrt{\kappa^2 - \delta^2}L\right)}}, \tag{10.6.75}$$

$$|r| = \frac{\kappa \sinh\left(\sqrt{\kappa^2 - \delta^2}L\right)}{\sqrt{\left(\kappa^2 - \delta^2\right)\cosh^2\left(\sqrt{\kappa^2 - \delta^2}L\right) + \delta^2 \sinh^2\left(\sqrt{\kappa^2 - \delta^2}L\right)}}. \tag{10.6.76}$$

There is the relationship $|\mathrm{t}|^2 + |r|^2 = T + R = 1$ (the absorption is omitted), where T and R are transmittance and reflectivity of grating.

The phase of the transmittance coefficient is

$$\varphi_t = \arctan\left[\frac{\delta \sinh\left(\sqrt{\kappa^2 - \delta^2}L\right)}{\sqrt{\kappa^2 - \delta^2}\cosh\left(\sqrt{\kappa^2 - \delta^2}L\right)}\right], \tag{10.6.77}$$

The phase of reflectivity coefficient respect to the phase of the transmittance coefficient has a phase difference of $\pi/2$, i.e.,

$$\varphi_\mathrm{r} = \frac{\pi}{2} + \varphi_\mathrm{t}. \tag{10.6.78}$$

Therefore, the FBG's transmission matrix Eq. (10.6.70) can be rewritten to be

$$\begin{pmatrix} A_\mathrm{in} \\ A_\mathrm{out} \end{pmatrix} = \begin{pmatrix} 1/t & r^*/t^* \\ r/t & 1/t^* \end{pmatrix} \begin{pmatrix} A_\mathrm{out} \\ A_\mathrm{in} \end{pmatrix}. \tag{10.6.79}$$

2. Optical Bistability of Nonlinear-fiber Connected FBG-Pair

Now we study the optical bistability of the nonlinear-fiber connected FBG-pair system, which can be regard as an F–P resonant cavity, the two FBGs are reflected mirrors, as shown in Fig. 10.52.

Assuming the absorption coefficient of nonlinear fiber is α, the propagation constant is β, and the length of nonlinear fiber is D, the transmission matrix of nonlinear-fiber connected FBG-pair is

$$\begin{pmatrix} A_{\text{in1}} \\ B_{\text{out1}} \end{pmatrix} = \begin{pmatrix} 1/t & r^*/t^* \\ r/t & 1/t^* \end{pmatrix} \begin{pmatrix} \exp[(\alpha+i\beta)D] & 0 \\ 0 & \exp[-(\alpha+i\beta)D] \end{pmatrix} \begin{pmatrix} 1/t & r^*/t^* \\ r/t & 1/t^* \end{pmatrix} \begin{pmatrix} A_{\text{out2}} \\ B_{\text{in2}} \end{pmatrix}. \tag{10.6.80}$$

Equation (10.6.80) can be simplified as

$$\begin{pmatrix} A_{\text{in1}} \\ B_{\text{out1}} \end{pmatrix} = \begin{pmatrix} T_{11} & T_{12} \\ T_{21} & T_{22} \end{pmatrix} \begin{pmatrix} A_{\text{out2}} \\ B_{\text{in2}} \end{pmatrix}. \tag{10.6.81}$$

The matrix elements are

$$T_{11} = \frac{\exp[(\alpha - i\beta)D]}{t^2} + \frac{|r|^2 \exp[-(\alpha - i\beta)D]}{|t|^2}, \tag{10.6.82}$$

$$T_{12} = \frac{r^* \exp[(\alpha - i\beta)D]}{|t|^2} + \frac{r^* \exp[-(\alpha - i\beta)D]}{t^{*2}}, \tag{10.6.83}$$

$$T_{21} = \frac{r \exp[(\alpha - i\beta)D]}{t^2} + \frac{r \exp[-(\alpha - i\beta)D]}{|t|^2}, \tag{10.6.84}$$

$$T_{22} = \frac{|r|^2 \exp[(\alpha - i\beta)D]}{|t|^2} + \frac{\exp[-(\alpha - i\beta)D]}{t^{*2}}. \tag{10.6.85}$$

Considering the border conditions for signal light incident to OBG, $A_{\text{in1}}(0) = A_{\text{in1}}$ and $B_{\text{in2}}(D+2L) = 0$, we obtain the transmittance of nonlinear FBG-pair OBD system:

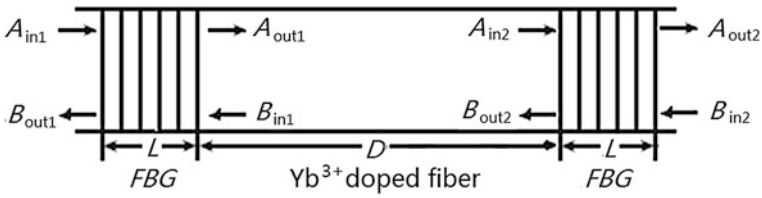

Fig. 10.52 Light propagation in the nonlinear FBG/F–P system

$$T_{\mathrm{F-P}} = \frac{P_{\mathrm{t}}}{P_{\mathrm{in}}} = \left|\frac{A_{\mathrm{out2}}}{A_{\mathrm{in1}}}\right|^2 = \left|\frac{1}{T_{11}}\right|^2 = \frac{(1-R)^2}{\exp(2\alpha D) - 2R + R^2\exp(-2\alpha D) + 4R\sin^2(\beta D + \varphi_{\mathrm{r}})}. \tag{10.6.86}$$

Equation (10.6.86) can be rewritten as

$$T_{\mathrm{F-P}} = \frac{P_t}{P_{in}} = \frac{H}{1 + F\sin^2(\phi/2)}. \tag{10.6.87}$$

This is modulation expression of nonlinear FBG-pair OBD system. In which, ϕ is a round-trip phase shift of light beam, $\phi/2$ is a single-path phase shift: $\phi/2 = \beta D + \varphi_{\mathrm{r}}$, the parameter H is maximum transmittance of nonlinear FBG-pair OBD, namely

$$H = \frac{(1-R)^2}{[R\exp(-\alpha D) - \exp(\alpha D)]^2}; \tag{10.6.88}$$

The parameter F is

$$F = \frac{4R_{\mathrm{e}}}{(1-R_{\mathrm{e}})^2}. \tag{10.6.89}$$

where R_{e} is called effective reflectivity, which is

$$R_{\mathrm{e}} = R\exp(-2\alpha D). \tag{10.6.90}$$

When the transmittance of nonlinear FBG-pair takes maximum value, the wavelength of incident light λ must satisfy the following resonance condition:

$$\beta D + \varphi_r = \frac{2\pi n_{eff}}{\lambda} D + \varphi_r = m\pi. \tag{10.6.91}$$

The incident-light wavelength at resonant wavelength $\lambda = \lambda_{\mathrm{B}}$ has maximum reflectivity, where $\phi_{\mathrm{f}} = \pi/2$. Using Eq. (10.6.91) and $\lambda_{\mathrm{B}} = 2n_{\mathrm{eff}}\Lambda$, D should satisfy the following condition for maximum transmittance of $T_{\mathrm{F\text{-}P}}$:

$$\mathrm{D} = \left(m - \frac{1}{2}\right)\Lambda. \tag{10.6.92}$$

Assume that the nonlinear fiber is putted along the z-axis direction, and the light amplitudes propagating along forward and backward directions at arbitrary point z are denoted as A_{f} and B_{b} respectively, then the matrix equation for expressing the relationship between field amplitudes $A_{\mathrm{f}}(\mathrm{z})$ and $B_{\mathrm{b}}(\mathrm{z})$ and the output field amplitudes A_{out2} and B_{in2}:

$$\begin{pmatrix} A_f \\ B_b \end{pmatrix} = \begin{pmatrix} \exp[-i\beta(D-z)] & 0 \\ 0 & \exp[i\beta(D-z)] \end{pmatrix} \begin{pmatrix} \exp[\alpha(D-z)] & 0 \\ 0 & \exp[-\alpha(D-z)] \end{pmatrix} \times \begin{pmatrix} 1/t & r^*/t^* \\ r/t & 1/t^* \end{pmatrix} \begin{pmatrix} A_{out2} \\ B_{in2} \end{pmatrix}. \tag{10.6.93}$$

From Eq. (10.6.93), the light intensity at arbitrary point z in nonlinear fiber can be found, which is

$$I_a(z) = |A_f + B_b|^2 = \frac{\exp[2\alpha(D-z) + Rexp[-2\alpha(D-z)]}{1-R} I_t. \tag{10.6.94}$$

Because the light power incident to the device is small (about 100 mw), we can only consider the nonlinear effects in the erbium-doped fiber, the nonlinear response of the fiber gratings is negligible. The refractive index of erbium-doped fiber, due to optical Kerr effect, is

$$n = n_0 + n_2 I_a(z). \tag{10.6.95}$$

The corresponding round-trip phase-shift variation is

$$\Delta\phi = \phi - \phi_0 = \frac{4\pi n D}{\lambda} - \frac{4\pi n_0 D}{\lambda} = n_2 \left(\frac{4\pi}{\lambda}\right) \int_0^D I_a(z) \mathrm{d}z = K I_t, \tag{10.6.96}$$

where I_a is intensity in the nonlinear fiber of FBG-pair, I_t is outputted intensity, n_2 is the nonlinear refraction coefficient of the nonlinear fiber, and the parameter K is

$$K = \frac{2\pi n_2[\exp(2\alpha D) - 1 + R - R\exp(-2\alpha D)]}{\alpha\lambda(1-R)}. \tag{10.6.97}$$

Using Eq. (10.6.96), we obtain the feedback expression of the nonlinear FBG-pair OBD:

$$T_{F-P} = \left|\frac{A_{out2}}{A_{in1}}\right|^2 = \frac{P_t}{P_{in}} = \frac{\phi - \phi_0}{K I_{in}}. \tag{10.6.98}$$

Equation (10.6.98) shows that for the certain incident intensity I_{in} the transmittance of device linearly changes with the phase shiftϕ.

Equations (10.6.87) and (10.6.98) for T-ϕ relation should meet simultaneously. We can use the drawing method, the solid lines correspond to Eq. (10.6.98) and the dotted lines correspond to Eq. (10.6.87). The intersection points of two curves are

operating points of the device, as shown in Fig. 10.53a. The obtained curve in Fig. 10.53b is the output power as a function of the input power, i.e., the optical bistability curve of device.

Now we use numerical simulation method to study the relation between the switching power and the nonlinear fiber length for EDF-pair OBD. The calculation used data are as follows: the wavelength of signal light $\lambda = 1550\,\text{nm}$, the absorption coefficient of Yb^{3+}-doped fiber $\alpha = 0.2\,\text{m}^{-1}$, the linear refractive index of fiber $n_0 = 1.452$, the nonlinear refraction coefficient of fiber $n_2 = 6.2 \times 10^{-12}\,\text{m}^2/\text{W}$, the effective cross sectional area $S = 50\,\mu\text{m}^2$, the average refractive-index modulation amplitude of grating $\overline{\delta n}_{\text{eff}} = 1.8 \times 10^{-4}$, the grating length L = 3 mm, and taking the lengths of nonlinear fiber D = 20, 30, 40, 50 cm. The optical bistability loops is shown in Fig. 10.54. Figure 10.54a is transmitted OB; Fig. 10.54b is reflected OB.

From Fig. 10.54 we can see, the length of nonlinear fiber is shorter, the switching power is higher, and the stable region of optical bistability is narrower. The lowest switching power is 50 mW.

We have systematically studied the fiber grating based all-optical switches, in structure aspect including single FBG and LPFG, and cascading FBG and LPFG pair; the nonlinear gratings have low switching power either single nonlinear grating or nonlinear fiber connected grating pair. Table 10.4 shows the comparison of switching powers for different fiber grating based AOSs working in different driving modes.

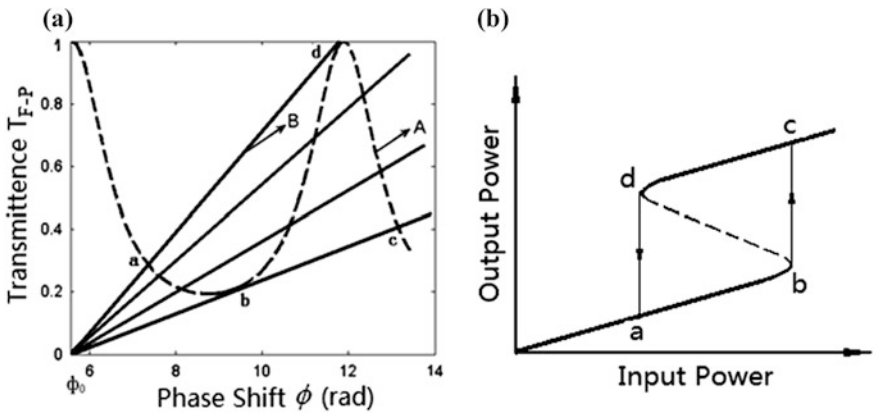

Fig. 10.53 Drawing method for optical bistability in nonlinear-fiber connected FBG-pair OBD: **a** curve A (*dotted line*) drawing from Eq. (10.6.87) and curve B (*solid line*) drawing from Eq. (10.6.98); **b** optical bistability loop

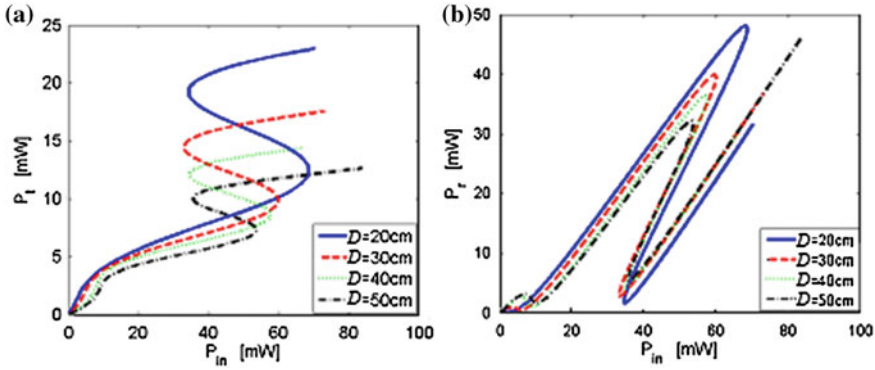

Fig. 10.54 Optical bistability characteristic of nonlinear-fiber connected FBG-pair when $\lambda = 1550$ nm, $\alpha = 0.2$ m^{-1}, $n_0 = 1.452$, $n_2 = 6.2 \times 10^{-12}$m^2/W, $L = 3$ mm, $\overline{\delta n}_{eff} = 1.8 \times 10^{-4}$, $S = 50$ μm^2, and $D = 20, 30, 40, 50$ cm: **a** transmitted OB; **b** reflected OB

Table 10.4 Comparisons of Switching Powers and Driving Mode for Different Fiber Grating AOSs

Type of fiber grating AOS	Driving mode	Switching power
Single silica FBG AOS	XPM	4500 W
Single silica FBG AOS	SPM	4000 W
Single silica LPFG AOS	SPM	4500 W
Single erbium-doped silica FBG AOS	SPM	20 mW
Single ytterbium-doped silica FBG AOS	XPM	20 mW
Common silica fiber connected FBG-pair AOS	XPM	500 W
Erbium-doped silica fiber connected LPFG-pair AOS	XPM	36 mW
Ytterbium-doped silica fiber connected FBG-pair OBD	SPM	50 mW

10.7 Nanoscale All-Optical Switches

In previous sections we systematically studied several kinds of nonlinear waveguide interferometer-type all-optical switches, and derived out their switching power formulas. Now we lest six typical switching device structures and switching power formulas as shown in Table 10.5 [29].

We use these formulas to calculate the switching powers for above fiber interferometer all-optical switches made with regular silica material, the obtained numerical values of switching power are from few watts to several kilowatts, which are much larger than milliwatt order of magnitude of the optical signal power used in optical communication, so such optical switches are clearly cannot be used in optical communication. How to reduce the switching power to make the practical all-optical switches?

Table 10.5 Structure diagrams and switching-power formulas for 6 kinds of typical interferometer AOSs

Optical switch type	Optical switch structure	Switching power formula
M–Z interferometer with different-index arms	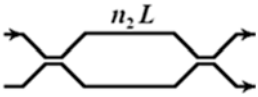	$P_{\text{inc}} = \frac{\lambda S}{n_2 L}$
Optical coupler	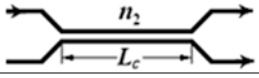	$P_{\text{inc}} = 1.25\frac{\lambda S}{n_2 L_c}$
Fiber bragg grating	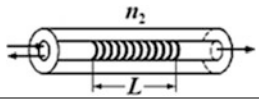	$P_{\text{inc}} = 0.5\frac{\lambda S}{n_2 L}$
Sagnac interferometer with asymmetric coupler	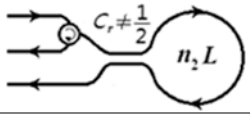	$P_{\text{inc}} = \frac{\lambda S}{n_2 L} \cdot \frac{1}{2\lvert 1-2C_r \rvert}$
Double coupler ring resonator	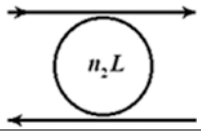	$P_{inc} = \frac{\lambda S}{n_2 L} \cdot \frac{\pi}{2}\frac{1}{F_{max}}$
M–Z interferometer coupled with a RR	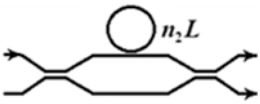	$P_{\text{inc}} = \frac{\lambda S}{n_2 L} \cdot \left(\frac{\pi}{2}\right)^2 \frac{1}{F_{\max}^2}$

We can see from above switching power formulas, there is a common factor, which is

$$P_{inc} = \frac{\lambda S}{n_2 L}$$

where λ is the wavelength of signal light; n_2 is the nonlinear refraction coefficient; S is the cross sectional area of the waveguide; L is nonlinear waveguide length. In addition, in the switching power formula of device with ring resonator, there is the ring fineness $F_{\max}$ in the denominator. According to the action of these parameters, we can through the analysis to propose the possible measures for reducing the switching power of optical switches. The measures are:

(1) To select waveguide materials with large nonlinear refraction coefficient n_2, such as rare earth-doped silica waveguide, the threshold switching power can be reduced. But the material doping may pay the price to increase the optical absorption, and to extend the switching time.

(2) To reduce the effective cross sectional area of waveguide S. If the S can be reduced from μm^2 to nm^2, the switching power can drop down from kW to mW. So we need using nanoscale waveguide to make all-optical switching device.
(3) To extend the waveguide length L, it is benefit for reducing switching power. But it will increase the overall size of device. We can use the microring structure. The ring structure can accumulate the nonlinearity, to offset the shortage of material with small n_2. Off course, the ring should have a high finesse F_{max}.

Therefore, using nanoscale materials and structures is an inevitable way for reducing switching power of all-optical switches. In addition, in order to enhance the switching speed, to reduce the size of device is also very important. The nanoscale all-optical switch is based on nanophotonics.

The main content of nanophotonics is studying on the interaction between nanoscale optical radiation and nanoscale materials or structures. The most important nano-materials are the materials with microcosmic periodicity, such as the quantum confinement materials (quantum wells, quantum wires and quantum dots, etc.) consisting of two semiconductor materials alternately with different bandgaps, and the photonic crystals materials consisting of two dielectric materials alternately with different refractive index; in addition the metallic nano-materials with a metal-dielectric nano-interface in which the interaction between the incident optical field and the periodic electromagnetic field to form a surface plasmon polariton (SPP) wave. The most important nano-structure for all-optical switch is nanoscale waveguide with nanometer cross section and the interferometers made by nano-waveguide, particularly, the nano-waveguide microring.

10.7.1 Nano-waveguide Interferometer All-Optical Switches

1. **AlGaAs Nano-waveguide Ring Coupled M–Z Interferometer AOS**

In 2004 J. Heebner et al. reported their research result for AlGaAs nano-waveguide ring coupled M–Z interferometer all-optical switch. The device is made by molecular beam epitaxy (MBE) and reactive ion etching (RIE) technology, growing three AlGaAs layers with different components on the GaAs substrate to form a ridge nano-waveguide with the structure of a ring coupled with an arm of M–Z interferometer, as shown in Figs. 10.55 and 10.56 [30].

The parameters of the device are: the ring waveguide and the straight waveguide with width 500 nm, the interval between ring and straight waveguide is 80 nm, the ring diameter is 10 μm, the length of ring is $l = 2\pi r \approx 30\,\mu m$, the finesse of ring is $F = 10$, the effective cross sectional area is $S = 0.5\,\mu m^2$, the nonlinear refraction coefficient of waveguide material is $n_2 = 10^{-17}\,m^2/W$. The device works in SPM mode, the wavelength of signal light is $\lambda_0 = 1.55\,\mu m$. Because the absorption loss of material is large, the switching power of device is higher, $P_{ic} \approx 64\,W$.

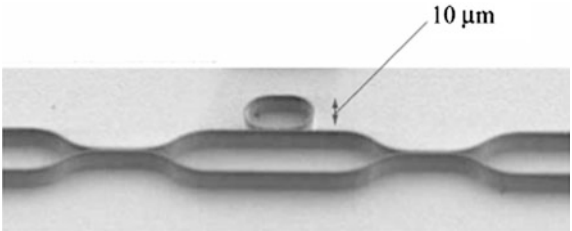

Fig. 10.55 AlGaAs nano-waveguide microring coupled M–Z interferometer all-optical switch

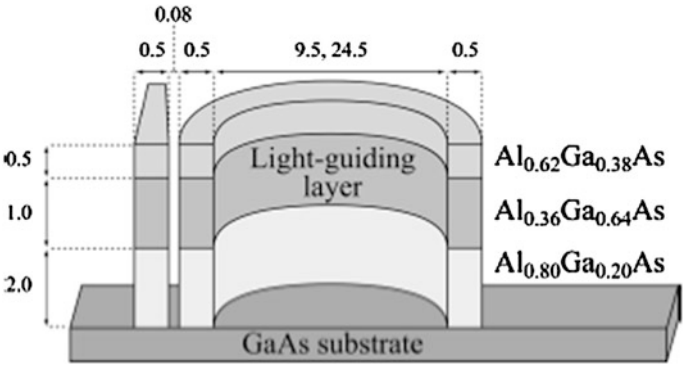

Fig. 10.56 Material and structure of AlGaAs ridge waveguide ring on the GaAs substrate

2. Silicon Ridged Nano-waveguides Ring Resonator AOS

2004 the Lipson' group firstly reported the experimental results about silicon based nano-waveguide ring resonator all-optical switch [31, 32]. The device is made with SOI (Silicon on insulator) wafer by Electron beam lithography and reaction ion beam etching technology to form a ridged nano-waveguide with cross-section

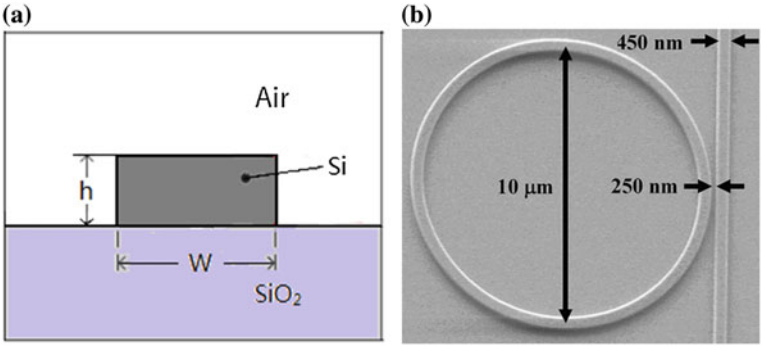

Fig. 10.57 Silicon nano-waveguide single-coupler ring cavity all-optical switch: **a** the cross section of waveguide; **b** the structure of ring device

dimension: W × h = 450 nm × 250 nm, as shown in Fig. 10.57a. Using this waveguide to make a ring with diameter of 10 μm, and the interval of ring and straight waveguide is 250 nm, as shown in Fig. 10.57b. The loss of device is smaller than 0.5 dB.

The optical switch is working on XPM mode. The probe (signal) light is a continuous laser diode with center wavelength at 1550 nm, coupling into the device from the end face of straight waveguide. The pump light comes from a Ti sapphire femtosecond laser with pulsewidth of 120 fs, single pulse energy of 1.5 nJ, repetition rate of 80 Hz and wavelength at 800 nm. The output laser converts by BBO crystal into the light pulses with wavelength at 400 nm, energy about 120 pJ. The pump light vertically irradiates the ring surface from the outside of device as shown in Fig. 10.58.

In resonant case ($\varphi = 2\ m\pi$) the periodic curve of transmittance of probe light versus wavelength of probe light is shown in Fig. 10.59. When without pump light, signal wavelength is at the of transmittance valley, corresponding to the off state of device; when adding the pump light on the device, the silicon material generates the two photon absorption effect, changes the concentrations of electron and hole carriers, induces the refractive-index change, the transmission spectrum will be moved from the transmittance valley to the transmittance peak, then the transmitted light of device realizes the switching from off to on, as shown in Fig. 10.59. In the process from wavelength at 1554.5 nm in transmittance peak to the wavelength of 1554.6 nm in transmittance valley, the wavelength change is only 0.1 nm, the corresponding refractive-index change is only 10^{-3}. The average switching power of the device is small than 10 mW, the switching time is about 70 ps.

3. Organic Molecular Filled Silicon Vertical Groove Nano-waveguide

In the two-photon absorption process of silicon material there is the free carrier absorption (FCA) effect. The carrier recombination time is about 1 ns. The FCA limits the nonlinear response time of above ridgid nano-waveguide, which is about 100 ps only, in other words, using this kind waveguide for optical information processing, the transmission speed cannot over 10 Gb/s. In order to enhance the nonlinear response time of silicon waveguide, scientists suggest using the groove-shape silicon nano-waveguide filled with high nonlinear organic molecular

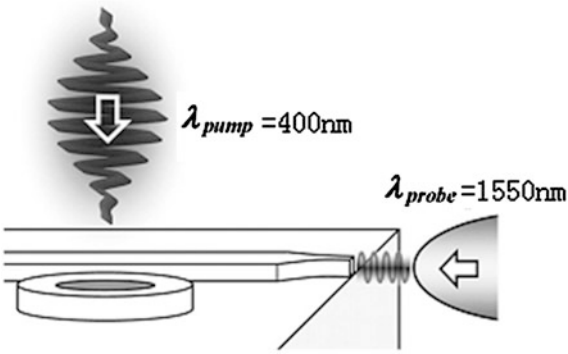

Fig. 10.58 Microring AOS irradiated by the pump beam and the probe beam with different patterns

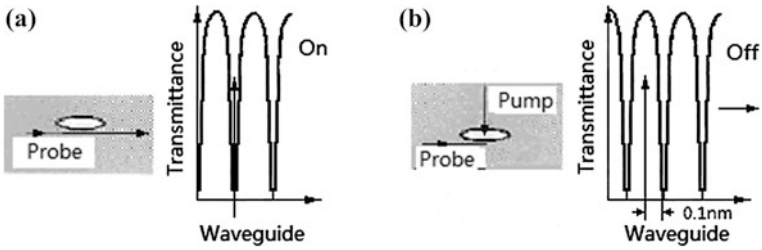

Fig. 10.59 Working principle of silicon nano-waveguide microring all-optical switch: **a** without pump light, the device is switching off; **b** adding pump light, the device is switching on

material, to form a silicon-organic hybrid (SOH) waveguide. The organic molecules can shorten the carrier recombination time, and its response time is only 1 ps, so nonlinear response time of SOH waveguide is 10 ps order of magnitude only, and the transmission speed can reach to 100 Gb/s.

In 2009 Koos et al. [33] published the research results of such SOH nano-waveguide and demonstrated an optical time-division-multiplexing (OTDM) experiment based on the four wave mixing (FWM) to prove its response time is small than 10 ps with 100 Gb/s all-optical information processing ability.

Their groove nano-waveguide is made on the SOI wafer by deep ultraviolet lithography and reactive ion etching technique, and then using molecular beam deposition method to uniformly fill with the high nonlinearity organic small molecules DDMEBT, as a waveguide cladding. The linear refractive index of DDMEBT is 1.8 (Si is 3.5), the nonlinear refraction coefficient is $n_2 = 1.7 \times 10^{-13}\text{cm}^2/\text{W}$ (wavelength at 1.5 nm). The molecular structure of DDMEBT is shown in Fig. 10.60.

The cross-section dimension of silicon groove nano-waveguide is shown in Fig. 10.61a: high h = 220 nm, width W = 212 nm, slit width W_{slot} = 205 nm, total length of waveguide L = 4 mm. the photo of atomic force microscope of waveguide is shown in Fig. 10.61b. Because the evanescent field effect of interface of

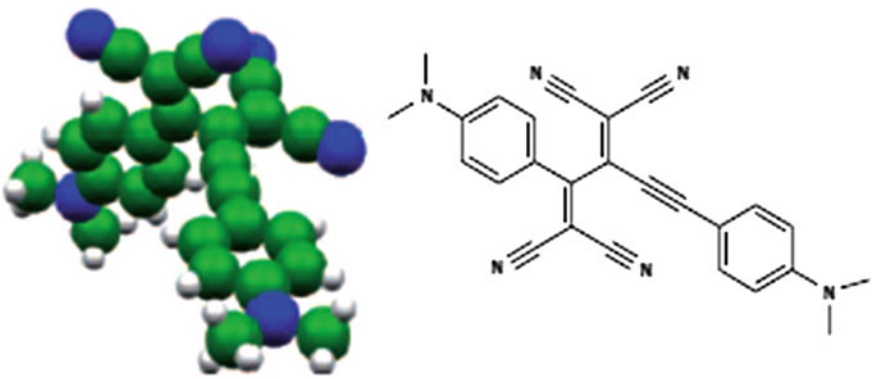

Fig. 10.60 Molecular structure of organic small molecule DDMEBT

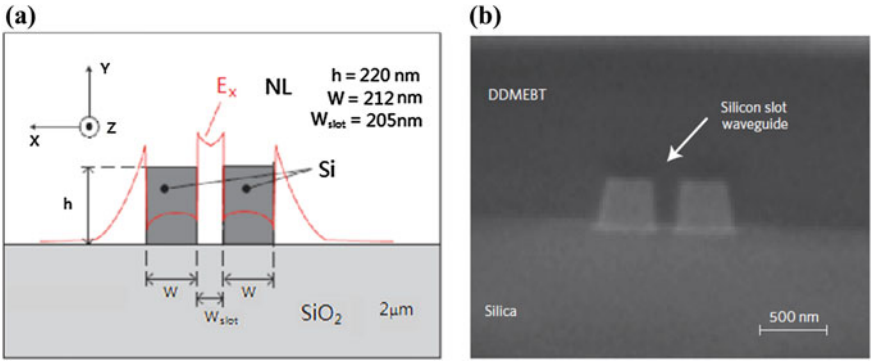

Fig. 10.61 Cross-section view of silicon vertical groove nano-waveguide filled with the organic small molecules, **a** structure dimension of SOH waveguide; **b** photo of atomic force microscope

silicon waveguide and the high nonlinearity of organic molecules, the horizontal light field E_x is very strong in the groove, to form a main channel of light transmission. This is a low refractive-index optical waveguide in the nanometer condition. The transmission loss of waveguide is 1.5 dB/mm; the coupling loss between fiber and waveguide is 4.1 dB.

4. Si-nc/SiO_2 Filled Silicon Cross Groove Nano-waveguide Ring AOS

In 2010 Martinez et al. [34] reported their new approach of silicon cross groove nano-waveguide ring resonator all-optical switch. They used complementary metal oxide semiconductors (CMOS) technology to make the cross groove nano-waveguide on SOI wafer, the cross-section view is shown in Fig. 10.62a. The substrate is SiO_2, the nether cladding of waveguide is crystal silicon (c-Si) with thickness of t_1 = 220 nm; the upper cladding is amorphous silicon (a-Si) with thickness of t_2 = 220 nm. In the groove (waveguide layer) using low pressure chemical vapor deposition (LPCVD) technology to deposit the nano-crystal silicon

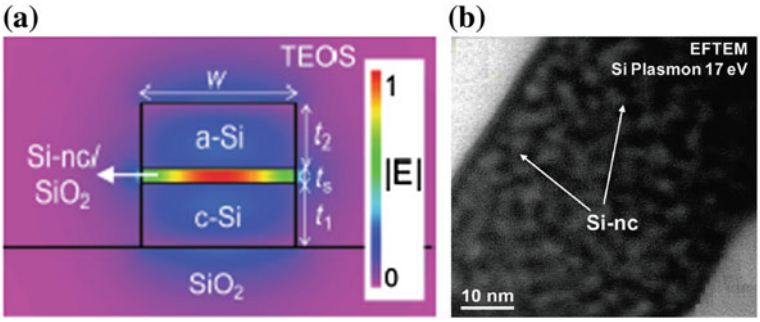

Fig. 10.62 Cross-section view of Si-nc/SiO_2 filled silicon cross groove nano-waveguide: **a** structure dimension of cross groove waveguide; **b** EFTEM photo of Si-nc/SiO_2 material in cross groove

embedded quartz: Si-nc/SiO_2 with thickness of t_s = 50 nm. The width of waveguide is W = 500 nm. The whole waveguide is covered by tetra-ethyl-ortho-silicate (TEOS). The electrical field is focus on the center of cross groove. Figure 10.62b gives a photo of the energy filtering transmitted electron microscopy (EFTEM) for Si-nc/SiO_2. The material has high optical nonlinearity, $n_2 = 2\times10^{-12}$ cm^2/W. The diameter of nano-crystal silicon is 2.4 nm, its nanoscale size offsets the limitation for switching time and absorption loss due to free carrier absorption (FCA) induced by two photon absorption (TPA) of silicon material. Hence the response time of materials is less than 10 ps. If Si-nc/SiO_2 deposited by LPCVD technology, the transmission loss of waveguide is about 20 dB/cm; if changed by PECVD (Plesma enhanced chemical vapor deposition) technology, the transmission loss of waveguide is 4 dB/cm only.

Figure 10.63a gives the electron microscope photo of ring resonator AOS with ring radius 20 μm, the interval between ring and straight waveguide is 250 nm, the total area of device is 500 μm^2.

The signal light and the pump light together input into device from left input port. The wavelength of continuous signal light near the ring resonant wavelength at 1544.5 nm; the pump light is a pulse light coming from a fiber laser with pulsewidth 1 ps and repetition frequency 10 GHz, the wavelength of pump light is selected at a neighbouring resonant wavelength 1557.5 nm. The measured transmission spectrums of ring resonator under different pump powers are shown in Fig. 10.63b. The linear transmitted spectrum (without pump) is the black line with the valley value of 17 dB. The quality factor of ring cavity is 1875; the corresponding photon lifetime is 1.54 ps. The pump power induces refractive index change in the ring; it is filtering by a filter at output port. When the pump power

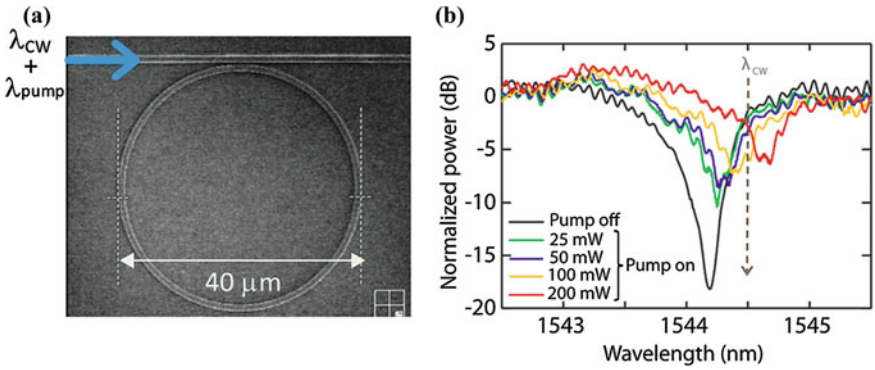

Fig. 10.63 Si-nc/SiO_2 filled cross groove silicon waveguide ring resonator all-optical switch: **a** electron microscope photo of waveguide ring resonator; **b** transmission spectrum under different pump powers. λ_{CW} is continuous incident signal light at 1.554.5 nm. The pump light power increases from 0 (*black line*) to 100mW (*yellow line*), realizing the all-optical switching with modulation depth of 50 %

increases from 0 to 200 mW, the transmitted spectrum generates a red shift as shown in Fig. 10.63b.

We can see that under the driving of pump light with 100 mW, the signal light realizes the optical switching with the modulation depth of 50 % (3 dB), measured switching time is 10 ps.

10.7.2 Photonic Crystal All-Optical Switch

Photonic crystal (PC) material is the periodic nanostructures composed of two dielectric materials with different refractive index, the spatial variation period is the same as the magnitude of the light wavelength, for visible light, the period is about hundreds of nanometers. In accordance with the structure classification, photonic crystals can be divided into one-dimensional, two-dimensional and three-dimensional materials, as shown in Fig. 10.64.

Similar to the semiconductor where the electrons within the atomic periodic potential have an energy-band structure, the photonic crystals also have an energy-band structure for photons. Figure 10.65 shows the energy-band structure of photonic crystal, which is light frequency ω versus state density $D(\omega)$. There is a bandgap (or forbidden band) between upper band and lower band.

The photons at wavelength in bandgap do not allow propagation in the specific direction of photonic crystal. The specific direction for 1-D photonic crystal is in the refractive-index periodic-change direction; for 2-D photonic crystal is in the cross plane of cyclical structure; for 3-D photonic crystal is in any direction.

The photons at wavelength in defect state will propagate inside the defect; but cannot propagate outside the defect. There are two kinds of defects in photonic crystal: line defect and point defect. In the line defect case, the light propagates along defect outspread direction, look likes a non-loss stripe-shaped optical waveguide; in the point defect case, it is equivalent to the existence of a high quality optical resonant cavity.

Utilizing the characteristics of energy band and defect state of photonic crystal we can make the intensity-type all-optical switches based on the pump light induced shifts of energy band or defect state and the space-type all-optical switches based on the nonlinear interferometers consisted of line defect state waveguide of photonic crystal.

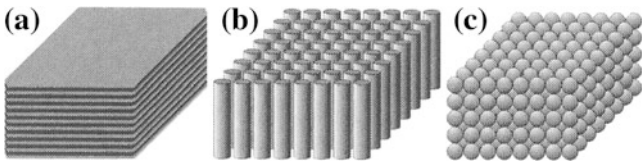

Fig. 10.64 Structure chart of photonic crystals with periodic structures: **a** 1-D; **b** 2-D; **c** 3-D

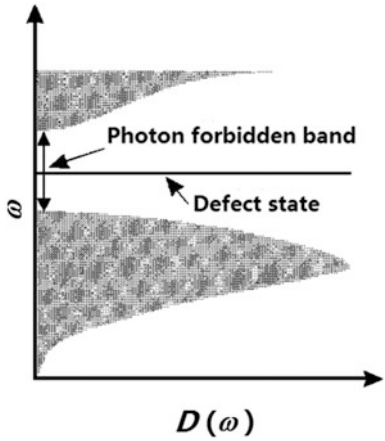

Fig. 10.65 Energy-band structure of photonic crystal: light frequency ω versus state density $D(\omega)$. There is a bandgap (forbidden band) between upper band and lower band, and a defect state in the bandgap

1. **2-D Photonic Crystal Defect Waveguide M–Z Interferometer AOS**

In 1993, Tajima [35] proposed a 2D photonic crystal defect waveguide M–Z interferometer AOS idea as shown in Fig. 10.66. In the photonic crystal MZI, there are quantum dots embedded into its two arms (only need a low bias voltage), which play a role of nonlinear phase shifter, In order to overcome the limitation of switching time by carrier recombination time (in order of magnitude of nanoseconds), he designed two controlling light pulses to control the switch-on and the switch-off of the signal light. Using the first pulse to lead the phase difference between two beams in two arms to reach π, the signal light then outputs (on state). The second pulse will eliminate the phase difference, then signal light cannot output (off state), in this way one can cut off the slow relaxation tail when the device switches off. The delay between two pulses can be realized by using the photonic crystal delayer. The switching time of this device is estimated lower than one picosecond, and the switching energy is smaller than 1pJ. The device is possible to be used in 40 Gb/s optical communication systems.

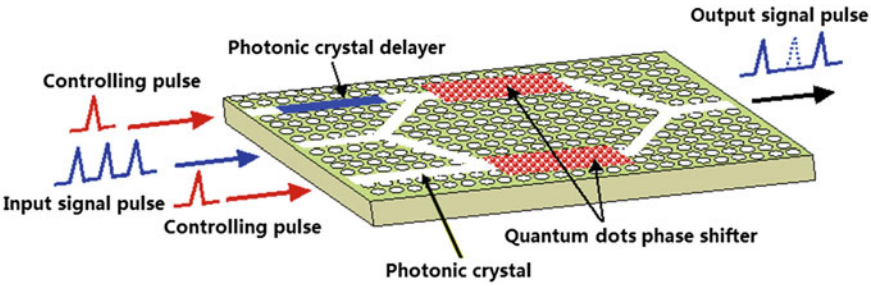

Fig. 10.66 2-D photonic crystal M–Z interferometer AOS with quantum dots phase shifter and two controlling light pulses

In 2002, Sugimoto et al. did a lot of works for the development of such a 2-D PC waveguide AOS [36]. The sample wafer was a 250 nm-thick GaAs waveguide core layer grown by MBE on top of a 2 μm-thick $Al_XGa_{1-X}As$ (X = 0.7–0.9) lower cladding layer on a GaAs substrate. The vertical structure of 2-D photonic crystal on the top of wafer is an air bridge-type slab fabricated by using the electron-beam lithography, reactive ion beam etching, and selective wet cutting. The 2-D photonic crystal slab has the thickness of 200–250 nm, with air hole diameter of 220 nm and lattice constant of 360–420 nm, designing for a single mode at a wavelength of ~1.3 μm. Figure 10.67a shows a plan-view diagram of the triangular lattice straight defect waveguide pattern on the 2-D photonic crystal slab.

In 2004 H. Nakamura et al. further reported their new MZI AOS device [37], as show in Fig. 10.67b. The total device length is 600 μm, in which InAs QD non-linear phase shifter with length of 500 μm. Under controlling pulse energy of 100fJ, the device obtains π-phase difference. The low switching energy obtained is due to adopt the quantum dots with low-saturation energy density $(13\ \mathrm{fJ} = \mu\mathrm{m}^2)$. The repetition-frequency signal pulses have the pulsewidth of 15 ps and the rise and fall time of 2 ps at wavelength of 1.3 μm. The device can be used in ultrafast time-resolved demultiplexer to lead the bit rate of 332 Gbit/s falling down to 42 Gb/s.

2. 2-D Photonic Crystal Ring resonator All-Optical Switch

In 2007, Qiang et al. [38] designed a 2-D photonic crystal ring resonator AOS using FDTD method, as shown in Fig. 10.68. The figure gives the designed square, hexagon and circular photonic crystal defect waveguides. In the corners of square-point-matrix dielectric-rod photonic crystal waveguide, they introduced four scatterers to yield a high sensitivity to wavelength. The theoretical value of efficiency of the spatial AOS at wavelength of 1567 nm achieved 98 %.

The structure of a single ring resonator AOS is shown in Fig. 10.69. The Input Port and Output Port are denoted by A and B, C, D respectively as shown in Fig. 10.69a. The normalized transmittance spectra are calculated by using FDTD method, as shown in Fig. 10.69b. The field distribution of this switch is shown in Fig. 10.72c, in which the upper diagram shows the reflection state at the

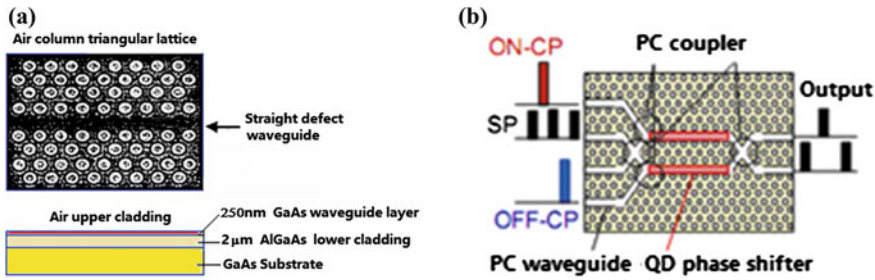

Fig. 10.67 2-D photonic crystal defect waveguide M–Z interferometer AOS: **a** triangular lattice straight defect waveguide; **b** configuration and working principle of device

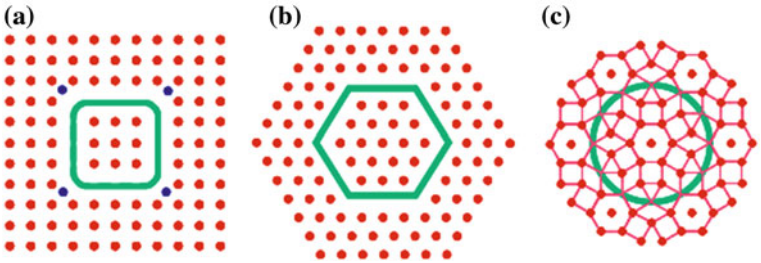

Fig. 10.68 Photonic crystal ring resonator structures: **a** the quasi-square ring in square point matrix; **b** the hexagon ring in triangle point matrix; **c** the circular ring in 12-fold symmetry quasi-photonic crystal structure

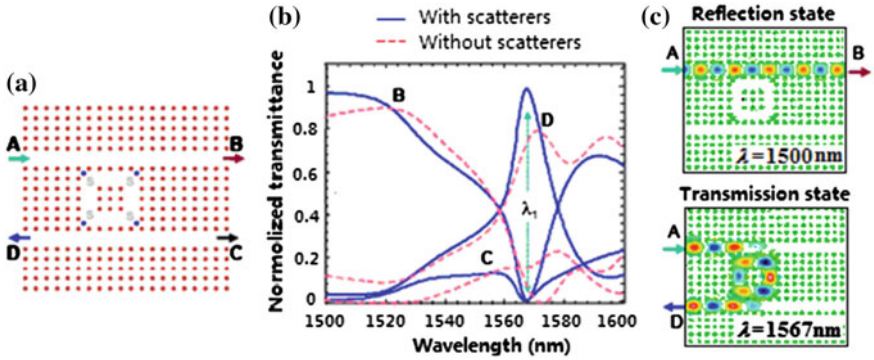

Fig. 10.69 Schematic diagram of single ring resonator photonic crystal AOS: **a** structure of single ring photonic crystal AOS; **b** normalized transmittance spectrum at Output Ports *B*, *C* and *D*. The full lines are with scatterers, the dotted lines are without scatterers; **c** optical field patterns of the reflection state and the transmission state

wavelength $\lambda_0 = 1500\,\text{nm}$ (on the resonance point); the lower diagram shows the transmission state at the wavelength $\lambda_0 = 1567\,\text{nm}$ (deviate from the resonance point).

3. 2-D Photonic Crystal Bandgap Shift and Defect-state Shift AOSs

2008–2009 Q. H. Gong's research group Hu et al. reported their experimental results of all-optical switches based on the photonic crystal bandgap shift and defect-state shift [39, 40]. The principles of these two AOSs are briefly described as follows: under the irradiation of pump light, it is possible to shift the bandgap of photonic crystal to lead the wavelength of signal light from outside of the bandgap to the inside the bandgap, i.e., signal light will be from transparent (switching on) to not transparent (switching off), as shown in Fig. 10.70a; the another possible is the pump light induce the shift of defect-state, to lead the wavelength of signal light changes from inside the defect state to outside the defect state, i.e., the signal light

from the transparent (switching on) to the not transparent (switching off), as shown in Fig. 10.70b. Figure 10.70c shows the optical switching process for both cases.

(1) **Nano-Ag Doped Polymer 2-D Photonic Crystal Bandgap Shift AOS**

For fabricating the PC sample, they doped the Ag nanoparticles with an average diameter of 15 nm into the solution of the polystyrene (PST), PST is a kind of polymer. The nano-Ag: PST had Ag-doped concentration of 5 %. The Ag nanoparticles formed the surface plasmon effect greatly enhances the optical non-linearity of the PST polymer. Then they used the spin coating method to make a thin film on the silicon dioxide substrate, and next used focused ion beam (FIB) etching technique to prepare the photonic crystal, which was comprised of square arrays of cylindrical air holes embedded in a nanocomposite slab to form a 2-D photonic crystal with the thickness, lattice constant and the air hole diameter of 300, 284 and 110 nm, respectively. The PC slab was connected directly with two access waveguides for input and output of the probe beam. The length and the width of each access waveguide were about 5 mm and 100 μm respectively, as shown in Fig. 10.71a.

Because the wavelength of transmission peek is 800 nm, so they selected the Ti: sapphire laser as signal light source at wavelength of 800 nm, with pulsewidth of 120 fs and repetition rate of 76 MHz; the wavelength of absorption peek of silver colloid is 420 nm, so they selected the frequency doubled by BBO crystal Ti: sapphire laser at wavelength of 400 nm as the pump light. The experimental setup for optical switching is shown in Fig. 10.71b. They obtained the switching properties: the switching intensity of 9 mW/μm^2, the switching time of 5 ps, and switching depth of 50 %.

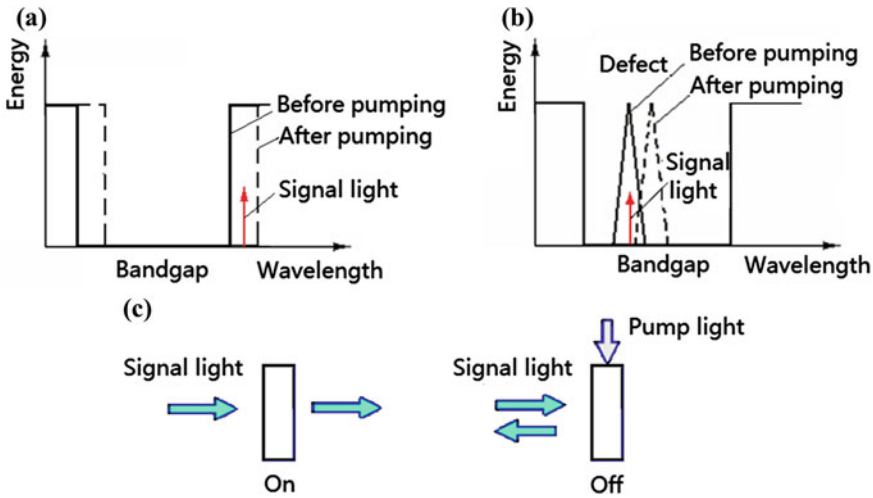

Fig. 10.70 Principles of photonic crystal bandgap and defect-state shift all-optical switches: **a** pump light induces the bandgap shift; **b** the pump light induces the defect-state shift; **c** optical switching for both processes

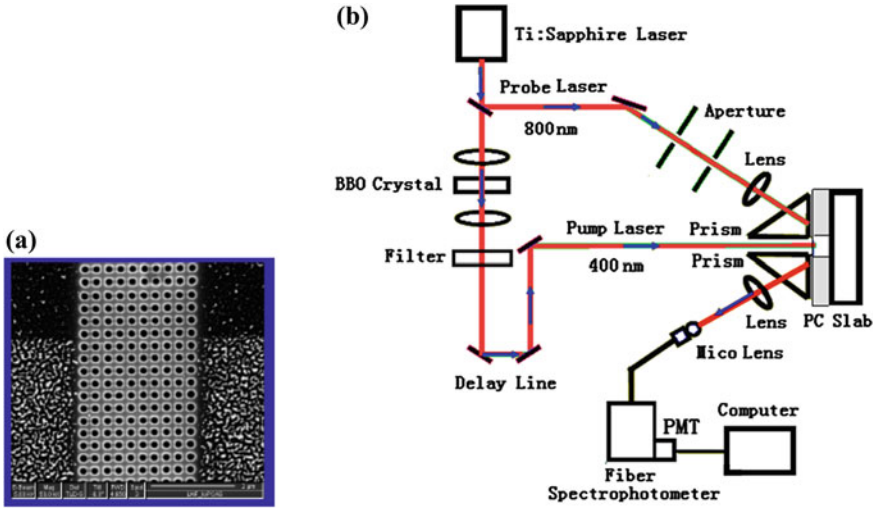

Fig. 10.71 Experiment of nano-Ag: PST 2-D photonic crystal bandgap-shift all-optical switch: **a** photonic crystal sampler; **b** experimental setup

(2) Coumarin-doped PST 2D Photonic Crystal Defect-state Shift AOS

They further studied the photonic crystal defect-state shift AOS by using organic dye-doped PST polymer. The dye they used is Coumarin 153 (C-153) with doping concentration 15 %. The sample of C-153 doped PST polymer with a line defect had film thickness 300 nm, lattice constant 320 nm, air hole radio 120 nm and defect width 440 nm, as shown in Fig. 10.72a.

The schema diagram and the energy-level map of nonlinearity enhancement in C-153 doped PST polymer is shown in Fig. 10.72b. The absorption peak of C-153 doped PST is at wavelength of 420 nm, thus the pump light at 400 nm and the probe light at 800 nm are used in pump-probe experiment. The experimental setup is same as the Fig. 10.71b. They obtained the optical switching properties: the switching intensity 0.1 MW/cm^2, the switching time 1.2 ps, and the switching depth 80 %.

4. Silicon/Air 2-D Photonic Crystal Waveguide F–P Cavity AOS

Previous introduced photonic crystal AOSs using organic polymer material, the stability in physics and chemistry is not good, and the working wavelength is not in optical communication band. In 2010 Michele Belott et al. proposed a new approach of AOS using silicon material. That is a Fabry-Perot cavity AOS made on a silicon/air photonic crystal ridge waveguide using SOI material [41]. The external structure of this device and a scanning electron micrograph (SEM) image of the PC F–P cavity with two reflected mirrors are shown in Fig. 10.73.

The samples were fabricated by using the electron beam lithography and reactive ion etching techniques on SOI wafers having a 260 nm thickness silicon core layer

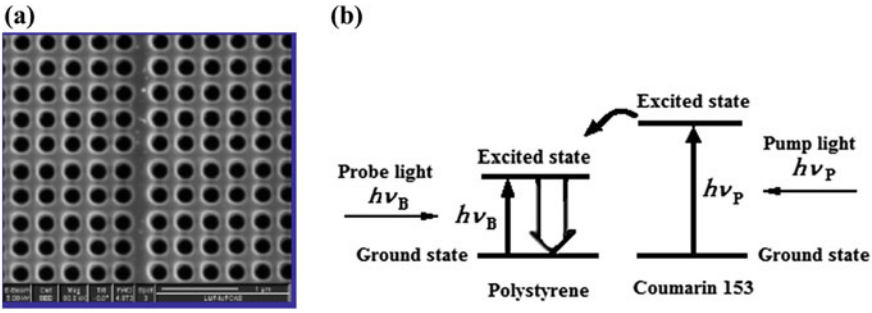

Fig. 10.72 Experiment of coumarin-doped PST 2D photonic crystal defect-state shift AOS: **a** photonic crystal sample; **b** principle of near resonance enhancement optical nonlinearity

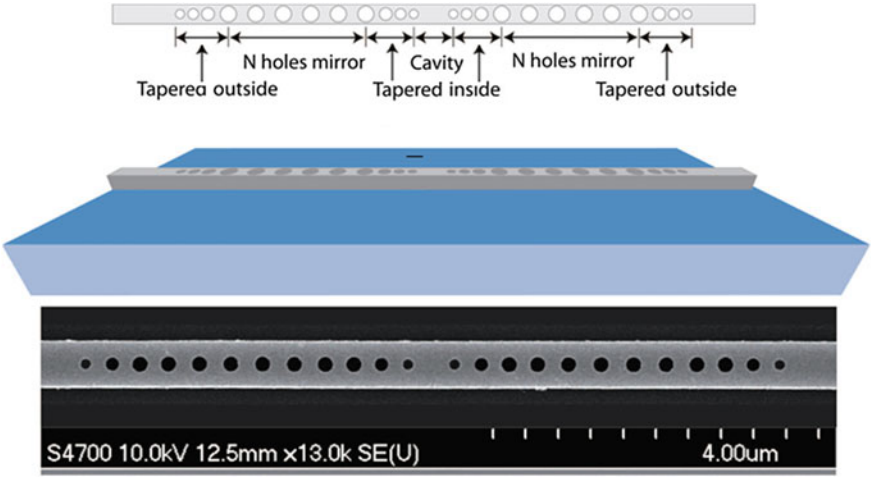

Fig. 10.73 External structure of PC F–P cavity embedded in a photonic crystal waveguide and a SEM image of the F–P cavity composed of two mirrors by periodically spaced holes and aperiodic taper region

supported by a 1 μm silica layer. At first they made a ridged nano-waveguide with thickness 260 nm, width 500 nm and length 10 μm, and then made a photonic crystal nanocavity on the waveguide consisting of a single row of circular air holes. The F–P cavity has 6 same holes in each reflected mirror with radius of 98 nm spaced by 350 nm. The PC mirror was designed to exhibit a large stop band center around 1550 nm for TE polarization. The regions in both sides of each mirror are tapered by means of 3 holes with different radii and aperiodic spacings (the spacing between adjacent holes are 300, 315, and 325 nm respectively. The corresponding hole radii are 65, 80, 85 nm), which makes it possible to reduce the mirror losses

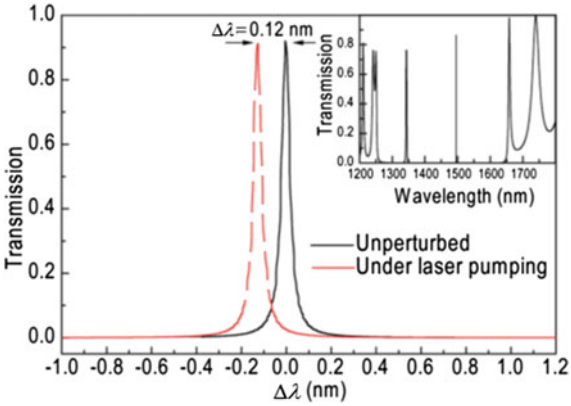

Fig. 10.74 Simulated transmission spectra of the device without (*solid curve*) and with (*imaginary curve*) the pump pulse. The simulated blue-shift is 0.12 nm. In the right inset, a broad-band spectrum is given, showing the cavity resonance wavelength at 1502.3 nm within the 1D photonic bandgap

due to out-of-plane scattering induced by optical impedance mismatch. So each mirror has a total of 12 holes. The interval between two mirrors (cavity length) is 425 nm. The whole structure is compact and the total device footprint to be 5 μm^2 (10 μm cavity length × 0.5 μm waveguide width).

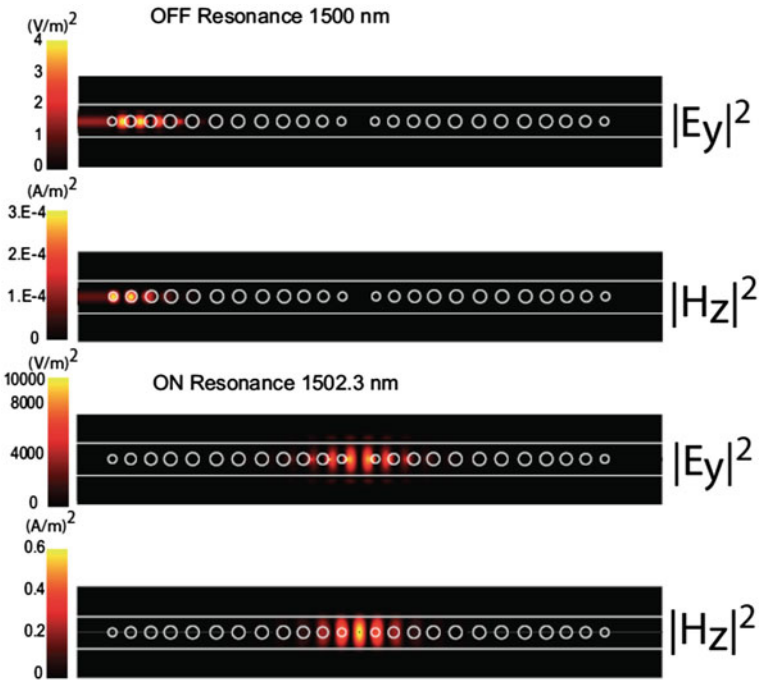

Fig. 10.75 Calculated field intensities at resonance (1502.3 nm) and off resonance (1500 nm) are shown for the $|E_y|^2$ and $|H_z|^2$ component, respectively. Notice the change in scales from off to on resonance

The simulated linear transmission spectra obtained by using a 2D finite difference time-domain (FDTD) method are shown in Fig. 10.74, which display a high-transmission ($\sim$90 %) resonance at 1502.3 nm for the unperturbed structure (solid line), it is switch-on state; and a 0.12 nm blue-shifted one for the pumped structure (imaginary line), at 1500 nm, which is switch-off state. In this process the refractive index of silicon reduced by 0.01 %. The calculated Q-factor of device can be estimated to approach 10^5. In the right inset, a broad-band spectrum is given, showing the cavity resonance wavelength at 1502.3 nm within the 1D photonic bandgap.

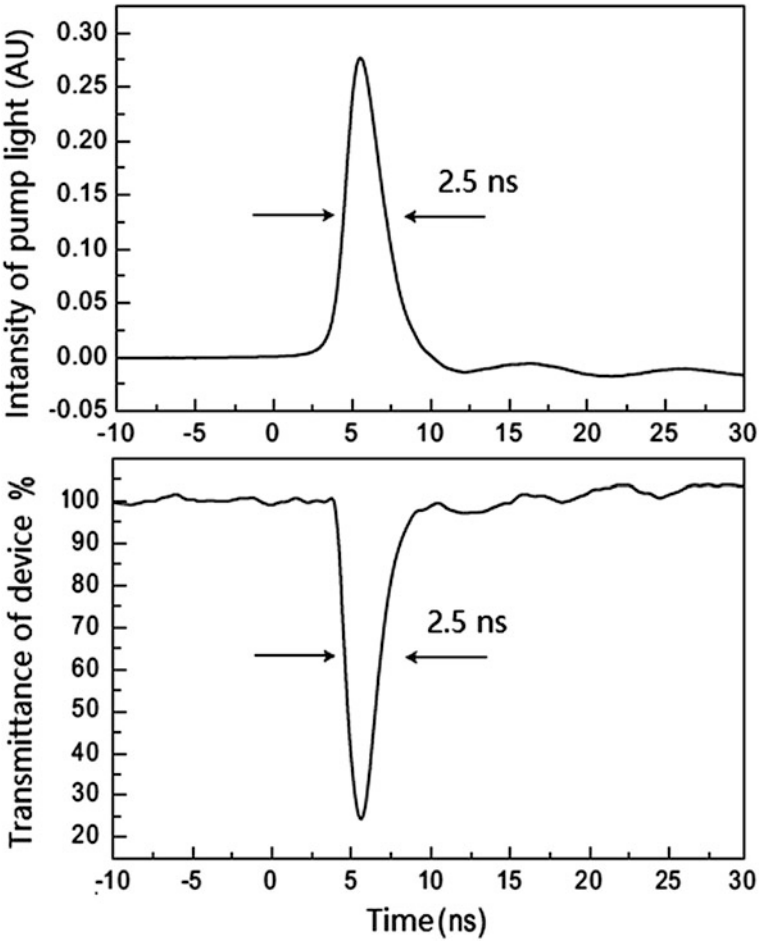

Fig. 10.76 Switching characteristic of silicon photonic crystal nan-waveguide F–P cavity AOS. The *upper figure* is the waveform of incident pump light; the *below figure* is the transmittance of device versus time measured by signal light at resonant wavelength

The field intensity for the $|E_y|^2$ and $|H_z|^2$ components is reported in Fig. 10.75 for off- and in- resonance case, respectively. Out of resonance at the wavelength of 1500 nm, the light traveling into the guide penetrates the first holes composing the mirror and it is completely reflected backwards. For the resonance case at 1502.3 nm, light passes through the mirror and the field is localized in the cavity region. Also the field intensities at resonance are enhanced by $\sim 10^4$ as compared to the off-resonance case, as it can be seen from the figure. The mode volume is very small and close to the diffraction limit, implying strong reduction of power density required for all-optical switching.

The optical switching experiment used pump light source is Q switched and frequency doubled Nd: YAG laser at wavelength 532 nm, with pulsewidth 2.5 ns and repetition frequency 11 kHz. The pump light is focused by microscopical object lens on the F–P cavity with the spot diameter about 5 μm. The pump light waveform is measured through an InGaAs avalanche diode, as shown in the upper of Fig. 10.76. Due to the Kerr effect, the pump light induces the refractive-index change in silicon material to lead the transmittance of signal light at resonant wavelength changing, as shown in the below of Fig. 10.76. We can see that when without pump light, the transmittance is maximum, the device is on; when the power of pump light reaches top value, the the transmittance is minimum, the device is off. The switching energy of device is lower than 120 fJ, and the switching amplitude larger than 10 dB, the switching time is limited by the pulsewidth of pump light, it shows only ns order of magnitude.

10.7.3 Surface Plasmon Polariton All-Optical Switch

In metal-dielectric interface, the resonant interaction between the incident light and the periodic electromagnetic field (surface plasmon) can generates a quantized optical wave, which is called surface plasmon polariton (SPP). According to the momentum conservation, the wavevector of SPP wave is determined by the following equation:

$$k_{sp} = k_0 n_d \sin\theta_{sp}, \tag{10.7.1}$$

where θ_{sp} is the incident angle corresponding to a dip reflectivity due to surface plasmon resonance (SPR) induced by resonance between the optical field (photons) and the electromagnetic field (electrons) in the metal-dielectric interface. k_0 is the wavevector of incident light in vacuum, n_d is the reflective index of the dielectric material. Equation 10.7.1 means that the wavevector of the SPP wave is equal to the wavevector component of incident light wave in the direction of the SPP wave propagation along the metal-dielectric interface.

Through solving the Maxwell Equation using the boundary conditions, it can be proved that the magnetic-field component of SPP-wave propagating in 2-D interface is parallel to the interface and perpendicular to the SPP wave propagation

direction, and there are two electrical field components of SPP-wave in the plane perpendicular to the interface. The electrical-field component perpendicular to the interface quickly decays exponentially. The decay distance in the dielectric is about 100 nm and in the metal is about 10 nm, as shown in Fig. 10.77.

Assuming the mediums in both sides of interface are isotopic materials, the dielectric coefficient of the dielectric ε_d is a positive rear number; the dielectric coefficient of the metal ε_m is a complex number depended on the light frequency ω (its real part is a negated number), and the incident light with a wavevector k_0 is a TM transverse-mode, the Maxwell electromagnetic-field equation and the boundary condition give the wavevector of SPP wave satisfied the following relation:

$$k_{sp} = k_0\sqrt{\frac{\varepsilon_d\varepsilon_m}{\varepsilon_d + \varepsilon_m}}. \tag{10.7.2}$$

In order to coupling the SPP wave in and out the nanoscale metal-dielectric interface, we can use the metal grating, nanoprobe; coupling prism, or taper coupler, as shown in Fig. 10.78.

In short, the SPP excitation by a laser beam should use the coupling devices, which has to close the metal-dielectric interface in nanoscale distance. One can adopt these SPP-excitation methods to make various kinds of nanoscale passive and active SPP devices, such as the couplers, beam splitters, optical sensors, lasers, detectors, amplifiers, modulators and all-optical switches. Based on this foundation, it is possible to develop the nanoscale photon and electron device joint integrated circuits.

Since the beginning of the 21th century scientists proposed a variety of principles of SPP nano all-optical switches. For example, the irradiation of pump light induces the nonlinear refractive index in the dielectric material or the phase transition of the material in one side of metal-dielectric interface to change the SPP propagation characteristic; the other example is making metal-dielectric-metal (MDM) nano-waveguide microring devices. The nanoscale SPP all-optical switches

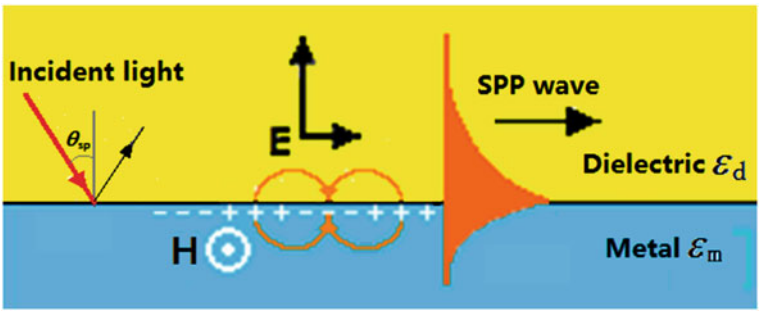

Fig. 10.77 The resonant interaction between incident light and the periodic electromagnetic field in metal-dielectric interface excites the SPP wave propagating along the interface

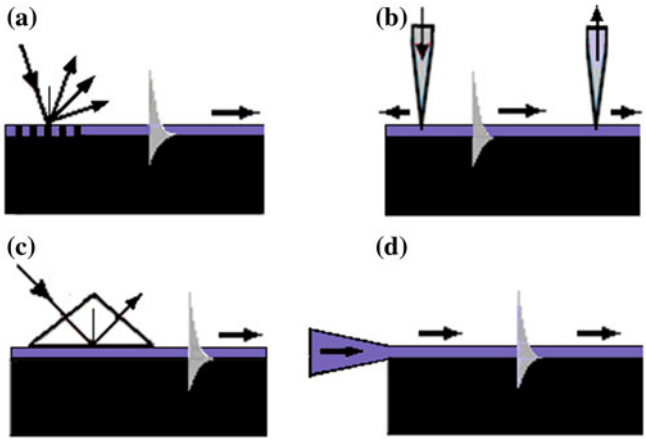

Fig. 10.78 Methods to coupling the SPP wave in or out the metal-dielectric interface: **a** metal grating; **b** nanoprobe; **c** coupling prism; **d** taper coupler

with low switching power and high switching speed are promising to use in the future applications.

1. **Nonlinear Nano-grating SPP Optical Bistable Switches**

In 2004 Porto et al. theoretically analyzed a 1-D metal grating filled with the nonlinear medium based on the F–P effect and SPP wave enhancement effect, the device appears optical bistability [42]. Figure 10.79a shows this metal nano-grating structure with the grating period $d = 0.75\,\mu\text{m}$, the slit width $a = 0.05\,\mu\text{m}$, and the grating thickness $h = 0.45\,\mu\text{m}$. Figure 10.79b shows the optical bistability curve of transmitted light intensity versus the incident light intensity for the nonlinear metal nano-grating. The incident light has the wavelength of $\lambda = 0.8\,\mu\text{m}$.

In 2008 Min et al. [43] designed an optical bistable switch with structure of a metal nano-grating coated with a Kerr optical nonlinear material by using finite-different-time-domain (FDTD) method, as shown in Fig. 10.80a. The material

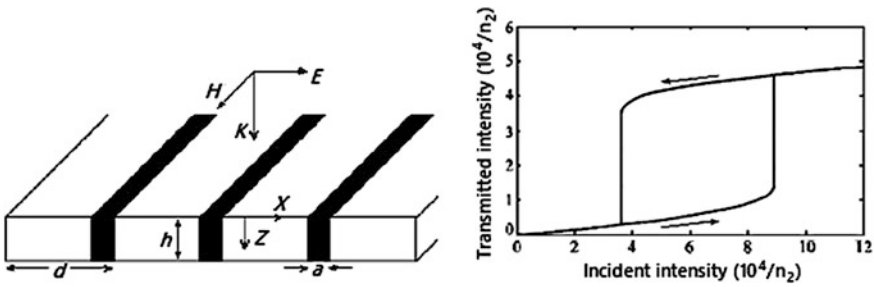

Fig. 10.79 Structure of 1-D metal nano-grating filled with a nonlinear medium: **a** the structure of grating; **b** optical bistability curve

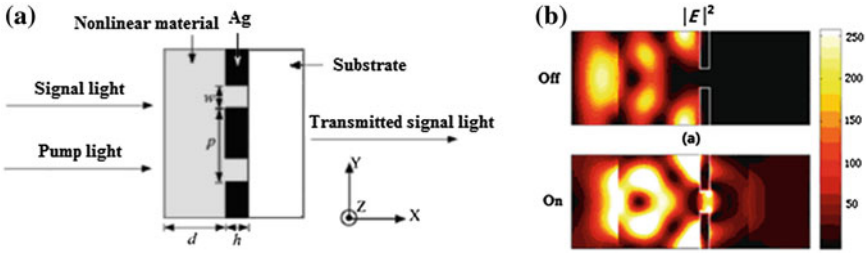

Fig. 10.80 Structure of nonlinear metal nano-grating optical bistable switch and field distribution: **a** structure of device; **b** distribution of signal-light electrical field $|E|^2$

of nano-granting is Ag, the thickness of Ag film is $h = 50\,\mu\text{m}$, the grating period is $p = 500\,\text{nm}$, the slit width is $w = 100\,\text{nm}$, the Kerr nonlinear material is Au:SiO_2 with 3-order polarizability $\chi^{(3)} = 1.7 \times 10^{-7}$esu and thickness $d = 430\,\text{nm}$, the substrate material is fuse silicon. The signal light at wavelength of 633 nm is a CW wave with TM-polarization. The pump light at 532 nm, with pulsewidth of 200 fs. Both the signal light and pump light together input granting structure from the left side of grating, when the incident pump light intensity reaches $12\,\text{MW/cm}^2$, the device is switching-on, the transmitted signal light outputs from the right side of grating.

Figure 10.80b gives the distribution of electrical filed intensity $|E|^2$ in switch-off and switch-on two cases. At the off state, the electric field is on the left of grating only; at the on state, there is the electric field in the slit and on the right side of the grating.

2. Metel or Dielectric Phase-Transition SPP All-Optical Switches

(1) Gallium Metel Phase-Transition SPP All-Optical Switches

In 2004, Krasavin et al. [44] proposed a SPP AOS based on the phase transition of metal gallium (Ga) coupled by optical grating, as shown in Fig. 10.81. The 1.55 μm-wavelength signal light inputs into the device from the left coupled grating to excite the SPP wave, which propagates along Au/Si interface with the length of 53 μm, and then outputs from the right decoupled grating. A Ga thin film with length of $L = 2.5\,\mu\text{m}$ is inserted in the propagation path.

When the control (pump) light has no irradiation, Ga is in solid state of α-Ga, which possesses the metal property, so SPP wave can effectively pass through the α-Ga and the Au/Si interface, and then output from the right decoupled grating; but when the control light irradiates the Ga/Si interface, because the Ga has a low melting point (29.8 °C), the surface layer of Ga is melted to be liquid phase of *m*-Ga, in which the metal and molecules coexist together, it has high anisotropic property, the propagation of SPP wave is stopped.

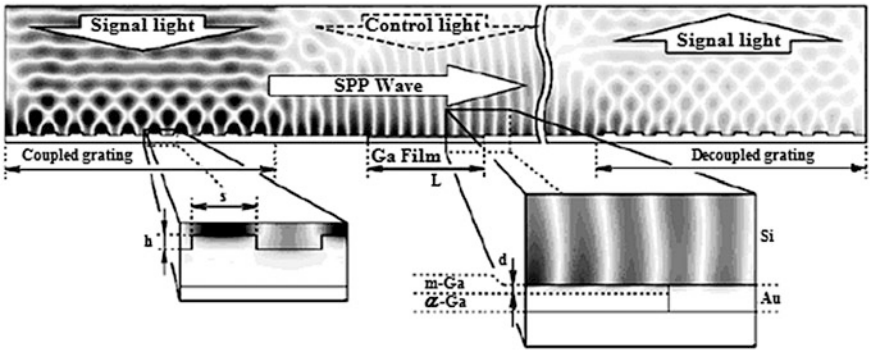

Fig. 10.81 Schematic diagram of Ga modulated grating coupled SPP all-optical switch

The calculation shows that this optical switch has modulation depth of 80% and the switching energy of 10 pJ for Ga area of 25 μm × 25 μm by using a fs-pump light. The switch-off time depends on the fusion time of *d*-thick liquid Ga about 2–4 ps and the switch-on time depends on the freezing time of Ga about the order of magnitude of ns to μs. Because the difficulties in grating manufacture etc., this switch was not realized in experiments.

In the same year Krasavin et al. [45] experimentally studied a prism-coupled Ga modulated SPP AOS, as shown in Fig. 10.82.

On the bottom of a BK7 grass prism coated with a layer of MgF_2 film with thickness of 158 nm, then a layer of Ga film, to form a metal-dielectric interface for excitation of SPP. If without the shine of controlling (pump) light, a *P*-polarization signal light at 780 nm is incident to MgF_2-Ga interface, at this time the Ga is in α-Ga at solid state. When the incident angle achieves the resonance angle $\beta = 66°$, the SPP wave is excited propagating in the MgF_2-Ga interface, so that reflected light decrease greatly; when the control light at 1064 nm inputs the interface, the

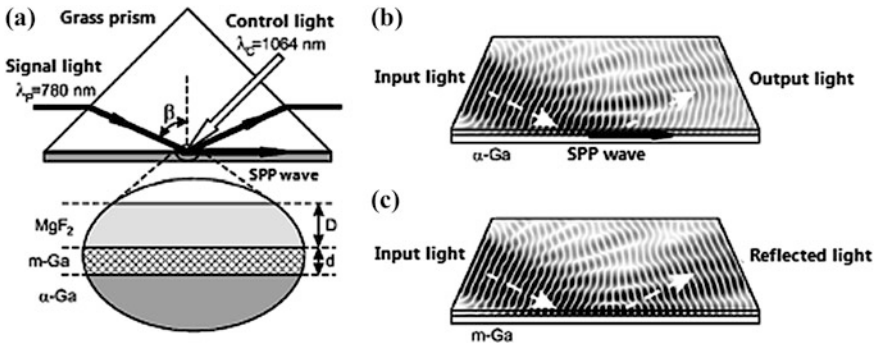

Fig. 10.82 Schematic diagram prism-structure Ga modulated SPP all-optical switch: **a** experimental setup; **b** field distribution in α-Ga phase; **c** field distribution in m-Ga phase

α-Ga solid phase transfers to the m-Ga liquid phase, the signal light cannot couple with SPP wave, thus the reflected light increases. The numeric calculation gets the Fig. 10.82b, c, in which the grey denotes the amplitude of the magnetic component (the deep color denotes the higher amplitude). The switch-on time of device is 4 ps and the switch-off time is 20 ns. When the energy density of the pump light reaches to 15 mJ/cm^2, the switching contrast is 94 %. This switch can effective modulate SPP signal in visible and inferred bands, the bandwidth can reach dozens of billion Hertz. However, the device is using a prism with big size, it is hard to integrate.

(2) **Photochromic Dielectric Phase-Transition SPP All-Optical Switches**

In 2008, Ragip et al. [46] proposed a SPP AOS based on the phase transition of dielectric material, which is photochromic material, as shown in Fig. 10.83a. The material manufacture method is that: firstly coating an aluminum thin film on the grass substrate, and make two gratings on it; secondly, doping the Spiropyran molecules into PMMA chlorobenzene solution, then coating it on the Al thin film to make a solid photochromic dielectric layer, and then a metal-dielectric interface is formed.

The signal light at wavelength of 632 nm is used for excitation of SPP in the metal-dielectric interface; the control (pump) light is an ultraviolet laser, whose vertically irradiation changes the molecular structure in photochromic layer, to transfer it from the transmission state to the absorption state, as shown in Fig. 10.83b, then the transmitted SPP wave occurs an optical switching from switch

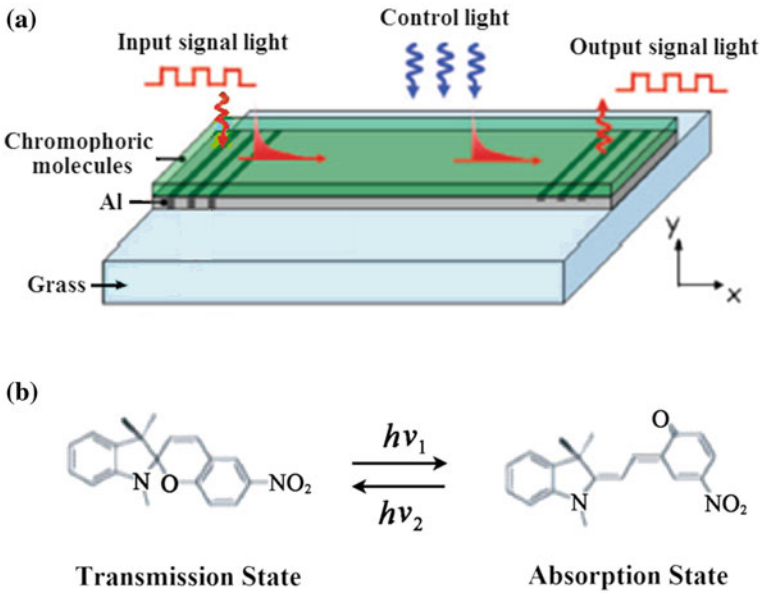

Fig. 10.83 SPP AOSs based on the phase transition of photochromic material: **a** structure of the device; **b** phase transition of photochromic molecules

on to switch off. The switching intensity of the device is 6.0 mW/cm^2, because the device area is 1.5 μm × 8 μm, so the switching power is 0.72 nW only.

3. Organic Polymer Waveguide Ring Resonator Phase-Transition SPP AOS

2011 Krasavin et al. [47] published the study results of nano ring cavity SPP all-optical switch based on the organic polymer phase transition. They firstly coated the 65 nm-thick gold film on the BK7 glass; secondly used the polymer PMMA and the disperse red (Dr1) (1 % weight ratio hybrid) to dissolve in the chlorobenzene solution and made it to be a 400 nm-thick solid thin film on the gold film by spin-coating method; finally using techniques of electron beam lithography and chemical etching to make a ring-cavity waveguide device with diameter of 10 μm, and the interval between ring and straight waveguide is about 185 nm. The Dr1/PMMA waveguide has width of 500 nm and high of 440 nm. The cross-section structure of waveguide is shown in Fig. 10.84a. In the waveguide, the fundamental mode of SPP light field is located on the gold film about 10 nm. Figure 10.84b shows an electronic microscope photo of the connection between the taper waveguide and ring waveguide. The fissure in the taper waveguide is used for coupling incident signal light, which is made by focused ion beam. Figure 10.84c shows the whole structure of the device. The signal light coming from a laser diode at the wavelength of 1550 nm focuses on the fissure of taper waveguide, coupling into the ring cavity to excite the SPP wave inside the ring. Another laser diode at wavelength of 532 nm as pump light from up side of device directly focus the ring

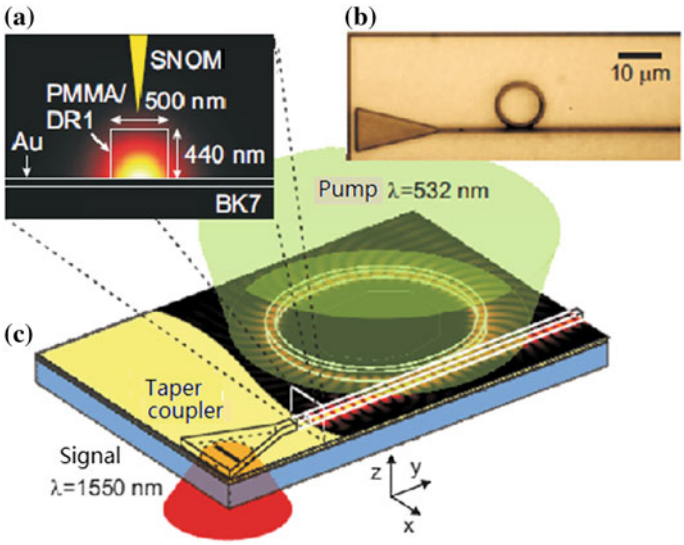

Fig. 10.84 Principle structure of Dr1/PMMA waveguide ring cavity all-optical switch: **a** electrical field distribution of cross-section of Dr1/PMMA waveguide; **b** electronic microscope photo of taper coupler with a fissure and ring resonator; **c** whole structure of ring device and the inputted signal and pump lights

upper face. Because light induced isomerization of Dr1 molecules (trans-cis transform), to change the refractive index $\Delta n = 4 \times 10^{-3}$, to lead the intensity change of SPP light, thus the SPP all-optical switching is realized.

In order to enhance the nonlinear coupling between ring waveguide and straight waveguide, the runway-shape ring resonator was designed, as shown in Fig. 10.85a. Setting $R = 5$ μm, $g = 500$ nm and $L_c = 1$ μm (or 2 μm). Figure 10.85b is scanning near-field optical microscope (SNOM) photo of runway-type ring resonator. Figure 10.85c shows the curve of the transmittance of device versus the power of pump light, which is measured by metal coated hollow fiber probe at A_2 (input point) and A_1 (output point). The insert figure is the curve of outputted intensity of SPP wave versus the pump power. As you see the switching power of device is about 100 mW. It is consistent with the result of simulation.

4. **MDM-SPP Silicon Waveguide Ring resonator All-Optical Switches**

In 2011 Sederberg et al. [48] proposed a numerical design of silicon based MDM-type SPP-waveguide nanoring all-optical switch. A schematic of the device is shown in Fig. 10.86. This device is fabricated by depositing a silver film with a thickness $t_{Ag} = 100$ nm (french grey) onto a SiO_2 substrate (watchet blue), then using the electron beam lithography, focused ion beam etching and deposition technology to make a Si nanoring waveguides (dark blue) with radius $r = 560$ nm, which corresponds to a footprint area of 1.00 μm^2. A straight Si waveguide for coupling the signal light at $\lambda = 1515$ nm into the ring is separated from the ring by a gap of $g_{Si} = 25$ nm. There is another SiO_2 waveguide (watchet blue) for coupling the ps pump light at $\lambda = 800$ nm into the ring, which is concentric to the ring resonator and offset from it by a gap of $g_{SiO2} = 20$ nm. The Si waveguide and SiO_2 waveguides have the same thickness of $t = 100$ nm and the width of $w_{Si} = w_{SiO2} = 100$ nm.

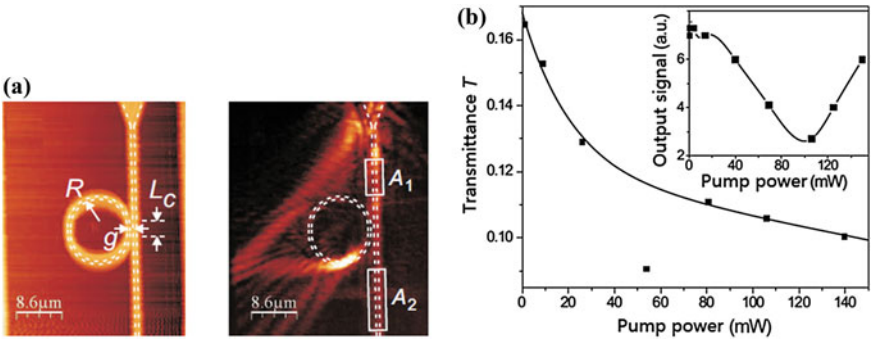

Fig. 10.85 Appearance of the runway-type ring resonator, measured field distribution and SPP transmission characteristic: **a** outline of ring cavity; **b** SNOM photo; **c** transmittance-pump power curve and outputted intensity-pump power curve

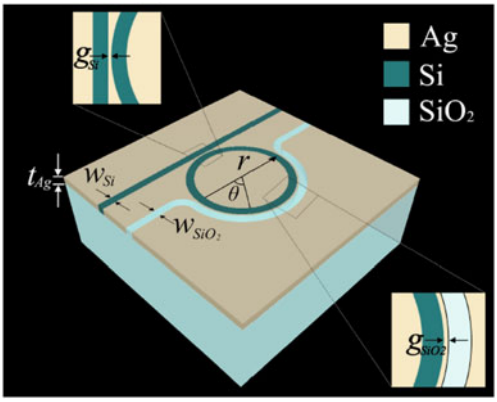

Fig. 10.86 Schematic depiction of MDM-type Si nano-waveguide ring resonator *S*PP all-optical switch

In order to enhance the switching speed of the device, the author suggested implanting O + ions into the Si to make the II-Si (ion-implanted Si) nanoring resonator, for introducing carrier trap centers in the Si and reducing the free carrier recombination time from ns down to 1 ps.

3-D FDTD simulations were used to model the behavior of the nanoring resonator. The Si ring waveguide was excited by a broadband pulse centered at $\lambda = 1550$ nm, FWHM = 390 nm, and the induced SPP mode profile shown in Fig. 10.87a. This mode has an effective refractive index of $n_{\mathrm{eff,Si}} = 3.382$ at $\lambda = 1515$ nm and undergoes a propagation loss of 4.371 dB/μm. By Fourier transforming the time domain signals, the broadband transmission spectrum is obtained as shown in Fig. 10.87b.

By iterative design of the nanoring resonator radius, r, and coupling gaps, g_{Si} and g_{SiO2}, a transmission minimum is obtained at a wavelength of $\lambda = 1515$ nm for a ring radius of $r = 560$ nm. The performance of the SiO_2 coupling plasmonic waveguide is investigated by exciting the SiO_2 waveguide with a broadband pulse centered at $\lambda = 800$ nm, FWHM = 94 nm, and the plasmonic mode profile shown in Fig. 10.87c. This mode has an effective index of $n_{\mathrm{eff,SiO2}} = 1.742$ at a pump wavelength at $\lambda = 800$ nm and undergoes a propagation loss of 2.292 dB/μm. The electric fields are recorded at ten ring angles in the range $0° \leq \theta \leq 135°$ and the power, P, coupled to the ring at each angle is normalized to the input power, as shown in Fig. 10.87d. It is important to note that the power is significantly reduced beyond $\theta = 135°$. For $0° \leq \theta \leq 35°$ the power coupled to the nanoring increases with θ due to the increasing coupling length between the SiO_2 waveguide and the Si nanoring. However, the above bandgap radiation undergoes substantial loss as it continues to propagate around the silicon nanoring and gradually decays by $\theta = 135°$. A majority of the free carriers are excited at $\theta \leq 60°$, where less dispersion will have accumulated.

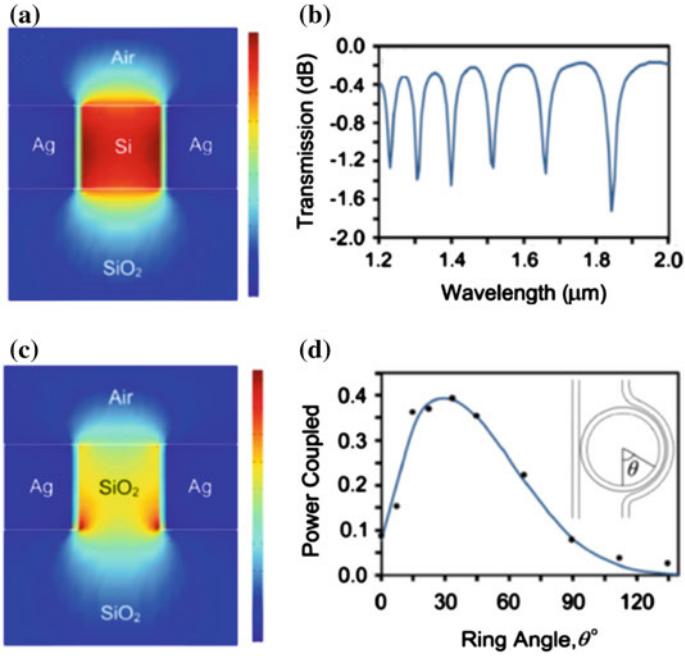

Fig. 10.87 Simulation of field distribution and propagation characteristic for Si ring waveguide and SiO_2 waveguide. **a** Electric field intensity distribution of signal light in Si waveguide. **b** Broadband transmission for nanoring resonator. **c** Electric field intensity distribution of pump light in SiO_2 waveguide. **d** Pump power coupled to nanoring versus nanoring angle θ (see *inset*)

In order to understand the dynamic behaviors of the switching device based on II-Si nanoring, the two simulated curves were given: the effect of the pumping strength on the position of the transmission spectrum as shown in Fig. 10.88a; and the effect of the pumping strength on the transmission-time curve as shown in Fig. 10.88b, in which the pumping strengths are denoted by n_o/n_c, where n_c is the carrier concentration without pump and n_o is pump-light induced carrier concentration that is proportional to the pump power.

The wavelength of the pump light is λ_p = 800 nm and with a duration of τ_p = 10 ps. If without pump light, the signal light has a transmission minimum, at wavelength of 1515 nm; when the pump light inputs the silicon SPP ring AOS, to increase the carrier concentration and decrease the refractive index of waveguide. It results in the blue shift of the transmission spectrum, the transmission minimum shifts from the wavelength of 1515 nm (n_0/n_c = 0) to 1500 nm (n_0/n_c = 0.22), then the device changes from off-state to the on-state as shown in Fig. 10.88a. Calculation shows that the switching energy is 0.88 pJ and the switching time is 3 ps as shown in Fig. 10.88b.

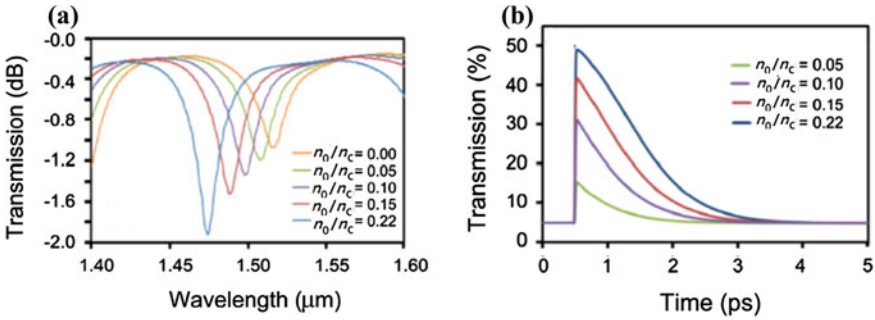

Fig. 10.88 Calculated transmittance change with wavelength and time under different pump power (denoted by n_0/n_c): **a** the blue shift of transmittance spectrum; **b** the time response of the transmittance

10.7.4 Silicon Nano-waveguide Resonant Cavity All-Optical Switch

Since 1975 H. M. Gibbs experimentally demonstrated the first all-optical bistable device based on the nonlinear refraction of medium within a Fabry-Perot etalon, the scientists have been studied on the all-optical switches for 40 years. During this period, the research of AOS has undergone the following three developmental stages: the all-optical bistable devices, the nonlinear interferometer all-optical switches and the nanoscale all-optical switches [1]. But the existing AOSs still not yet fully meet the technical requirements for practical application up to now. In the recent 10 years, the silicon based nano-waveguide microcavity all-optical switches, made with SOI (silicon on insulator) wafers, fabricated by CMOS (complementary metal-oxide-semiconductor) technology, using the signal light at the 1550 nm optical-communication wavelength and the pump light of ultrafast pulsed laser have become a research focus for the international scientific community, it greatly promotes the research on applicable all-optical switch.

There are many types of design scheme for silicon nanowaveguide cavity all-optical switches, we have discussed such AOS devices in previous three sections, including the device principles based on the nano-waveguide, the photonic crystal and the surface plasmon polariton; the silicon waveguide types of the ridge waveguide, the vertical groove waveguide and the cross groove waveguide; the silicon cavity devices based on ring cavity and FP cavity. Now we give a summary of 5 kinds of such AOS devices in Fig. 10.89. They are: (a) the silicon ridge nano-waveguide ring cavity AOS (see Sects. 10.7.1 and 10.7.2); (b) the silicon vertical groove nano-waveguide filled with organic molecule device (see Sects. 10.7.1 and 10.7.3); (c) the silicon cross groove nano-waveguide filled with Si-nc/SiO_2 ring cavity AOS (see Sects. 10.7.1 and 10.7.4); (d) the silicon ridge nano-waveguide photonic crystal F–P cavity AOS (see Sects. 10.7.2 and 10.7.4); (e) the silicon ridge nano-waveguide MDM-SPP ring cavity AOS (see Sects. 10.7.3 and 10.7.4).

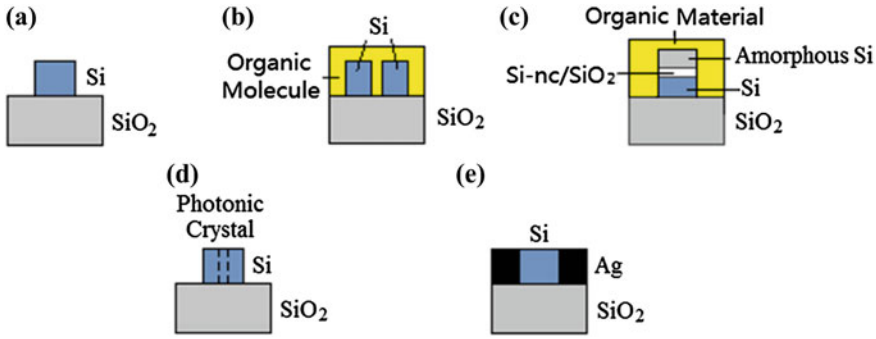

Fig. 10.89 Design schemes of integrated silicon based nano-waveguide cavity all-optical switches: **a** silicon ridge nano-waveguide ring cavity AOS; **b** silicon vertical groove nano-waveguide device **c** silicon cross groove nano-waveguide ring cavity AOS; **d** silicon ridge nano-waveguide photonic crystal F–P cavity AOS; **e** silicon ridge nano-waveguide MDM-SPP ring cavity AOS

The above 5 kinds of silicon nano-waveguide cavity AOSs have following characteristics:

(1) The signal light is a continuous wave at wavelength of 1550 nm for optical communication;
(2) The pump light is an ultrashort pulse laser (ps or ns laser) for reducing the switching time;
(3) The adopted material is the SOI wafer, in which the silicon is O^+ ion implanted Si (II-Si);
(4) The Si nanowaveguide can be made as the ridge, vertical groove and cross groove structures;
(5) The device structure is made as ring resonator or F–P cavity made by the nanowaveguide;
(6) The principle is based on nano-waveguide, photonic crystal or surface plasmon polariton;
(7) The manufacture of device is using the mature CMOS technology;
(8) The test of device is adopted the near-field-optics methods, such as SNOM and nano-probes.

In the near future, the silicon based all-optical switches could be integrated together with other silicon based nanophotonic devices, such as semiconductor lasers, optical amplifiers, optical modulators, optical detectors, etc. on the same piece of SOI wafer. This integration technology is promising to be used in the future all-optical logic operation for all-optical computer, and the all-optical switching for all-optical communication and so on.

Review Problem of Chapter 10

1. What is the significance of the study of optical switch? How to classify optical switch? What are the technical specifications of the practical all-optical switch?
2. Please describe the principles of coupler all-optical switches working in self-phase-modulation and cross-phase-modulation modes, and derive their switching power formulas.
3. Why Sagnac interferometer with 3 dB coupler can not make all-optical switch? What are the methods to achieve the Sagnac interferometer all-optical switches? Please derive their switching power formulas.
4. Why the symmetrical M–Z interferometer can not make all-optical switch? Please describe the principles of following two M–Z interferometer AOSs: two arms with different nonlinear refractive index and two arms with different lengths.
5. Why people want to use ring resonator all-optical switch? Please describe the principles of two kinds of ring resonator all-optical switches: the ring cavity with single coupler and with double couplers, and derive their switching power formulas.
6. Please describe the principles of the single FBG and LPFG AOSs and the nonlinear fiber connected LPFG pair and FBG pair AOSs, and compare their switching powers.
7. Compare switching power formulas of above nonlinear interferometer AOSs, what is the common law? What measures can reduce the switching power of AOS?
8. What methods and schemes can be used to achieve nanometer all-optical switches, what advantages and disadvantages they have?
9. What is the development trend of all-optical switch in the past decade? What are the types of silicon-based nano-waveguide resonant cavity AOSs? How to make these AOSs?

References

1. C. Li, *All-Optical Switches Based on Nonlinear Optics* (Science Press, Beijing, 2015)
2. H.M. Gibbs, *Optical Bistability: Controlling Light with Light* (Academic Press, New York, 1985)
3. R.W. Boyd, *Nonlinear Optics*, 3rd edn. (Academic Press, 2008)
4. G.P. Agrawal, *Application of Nonlinear Fiber Optics* (Academic Press, 2001)
5. N.J. Doran, D. Wood, Nonlinear optical loop mirror. Opt. Lett. **31**(1), 56–58 (1988)
6. M.G. Kane, W. Glesk, J.P. Sokoloff, P.R. Prucnal, Asymmetric optical loop mirror: analysis of all-optical switch. Appl. Opt. **33**(29), 6833–6841 (1994)
7. D.J. Richardson, R.L. Laming, D.N. Payne, Very low threshold Sagnac switch incorporating an Erbium doped fiber amplifier. Electron. Lett. **26**(21), 1779–1781 (1990)
8. M. Jinno, T. Matsumoto, Demonstration of laser-diode-pumped ultrafast all-optical switching in a nonlinear Sagnac interferometer. Electron. Lett. **27**(1), 75–76 (1991)
9. J.E. Heebner, R.W. Boyd, Enhanced all-optical switching by use of a nonlinear fiber ring resonator. Opt. Lett. **24**(12), 847–849 (1999)

10. T. Erdogan, Fiber grating spectra. IEEE J. Lightwave Technol. **15**(8), 1277–1294 (1997)
11. S. Larochelle, Y. Hibino, V. Mizrahi et al., All-optical switching of grating transmission using cross-phase modulation in optic all fibers. Electron. Lett. **26**(18), 1459–1460 (1990)
12. G.R. Broderick, D. Taverner, D.J. Richardson, Nonlinear switching in fiber Bragg gratings. Opt. Express **3**(11), 447–453 (1998)
13. D. Taverner, G.R. Broderick, D.J. Richardson et al., Nonlinear self-switching and multiple gap-soliton formation in a fiber Bragg grating. Opt. Lett. **23**(5), 328–538 (1998)
14. R.H. Stolen, W.A. Reed, K.S. Kim, et al., Measurement of the nonlinear refractive index of long dispersion-shifted fibers by self-phase modulation at 1.55 μm. J. Lightwave Technol. **16** (6), 1006–1012 (1998)
15. M. Janos, J. Arkwright, Z. Brodzeli, Low power nonlinear response of Yb^{3+}-doped optical fibre Bragg gratings. Electron. Lett. **33**(25), 2150–2151 (1997)
16. B. Guan, S. Liu, Erbium-doped fiber Bragg grating based all-optical switch. IEEE Proc. TH4A-(8)-7, 626 (2003)
17. H. Kobayashi, H. Kanbara, M. Kogaa, Third-order nonlinear optical properties of As_2S_3 chalcogenide glass. J. Appl. Phys. **74**(6), 3683–3687 (1993)
18. J.W. Arkwright, P. Elango, T.W. Whitbread et al., Low-power all-optical broad-band switching device using Ytterbium-doped fiber. IEEE Photon. Tech. Lett. **8**(3), 408–410 (1996)
19. P.L. Chu, Nonlinear effects in rare-earth-doped fibers and waveguide, Lasers and Electro-Optics Society Annual Meeting, LEOS '97 10th Annual Meeting. IEEE Conf. Proc. **1**(10–13), 371–372 (1997)
20. T. Erdogan, Cladding mode resonances in short and long-period fiber grating filters. J. Opt. Soc. Am. A **14**(8), 1760–1773 (1997)
21. L. Byeongh, J. Nishii, Dependence of fringe spacing on the grating separation in a long-period fiber grating pair. App. Opt. **38**(16), 1450–2459 (1999)
22. A.M. Vengsarkar, P.J. Lemaire, J.B. Judkins et al., Long-period fiber gratings as band-rejection filters. J Lightwave Tech. **14**(1), 58–65 (1996)
23. B.J. Eggleton, R.E. Slusher, J.B. Judkins et al., All-optical switching in long-period fiber gratings. Opt. Lett. **22**(12), 883–885 (1997)
24. C. Li, Z. Zhang, the optical switching in nonlinear fibre connected long period fiber grating pair. Chin. Laser **35**, 1–5 (2008)
25. B. Zhang, X. Wencheng, C. Li, Low-power all-optical switching in nonlinear M–Z interferometer made from a single-nonlinear-fiber-connected LPFG Pair. J. Nonlinear Opt. Phys. Mater. **19**(3), 415–425 (2010)
26. Y. Rao, Y. Wang, Z. Tao, *Principle and Application of Fiber Grating* (Science Press, Beijing, 2006)
27. J. Yoonchan, L. Byoungh, All-optical signal gating in cascaded long-period fiber gratings. IEEE Photon. Tech. Lett. **12**(9), 1216–1218 (2000)
28. C. Thirstrup, Y. Shi, B. Palsdottir, Pump-induced refractive index modulation and dispersion in Er^{3+}-doped fibers. J. Lightwave Technol. **14**(5), 732–740 (1996)
29. C. Li, Research prograss of nanophotonics all-optical switches. Physics **41**(1), 9–19 (2012)
30. J.E. Heebner, N.N. Lepeshkin, A. Schweinsberg, et al. Enhanced linear and nonlinear optical phase response of AlGaAs microring resonators. Opt. Lett. **29**(7), 69–771 (2004)
31. R. Vilson Almeida, A. Carlos, M. Lipson, All-optical control of light on a silicon chip. Nature **431**(28), 1081–1084 (2004)
32. M. Lipson, Overcoming the limitations of microelectronics using Si nanophotonics: solving the coupling, modulation and switching challenges. Nanotechnology **15**(10), S622–S627 (2004)
33. C. Koos, P. Vorreau, T. Vallaitis et al., All-optical high-speed signal processing with silicon–organic hybrid slot waveguides. Nat. Photon. **3**, 216–219 (2009)
34. A. Martınez, J. Blasco, P. Sanchis, et al., Ultrafast all-optical switching in a silicon-nanocrystal based silicon slot waveguide at telecom wavelengths. Nano Lett. 1506–1511 (2010)
35. K. Tajima, All-optical switch with switch-off time unrestricted by carrier lifetime. Jpn. J. Appl. Phys. **32**(12A), Ll746–Ll748 (1993)

36. K. Asakawa, Fabrication and characterization of photonic crystal slab waveguides and application to ultra-fast all-optical switching devices. IEEE ICTON **1**, 193–197 (2003)
37. H. Nakamura et al., Ultra-fast photonic crystal/quantum dot all optical switch for future photonic networks. Opt. Express **12**(26), 6606–6614 (2004)
38. Z. Qiang, W. Zhou, R.A. Soref, Optical add-drop filters based on photonic crystal ring resonators. Opt. Express **15**(4), 1823–1831 (2007)
39. X. Hu, P. Jiang, C. Ding et al., Picoseconds and low-power all-optical switching based on organic photonic band gap micro-cavity. Nat. Photon. **2**(3), 185–189 (2008)
40. X. Hu, P. Jiang, C. Xin, et al., Nano-Ag: polymeric composite material for ultrafast photonic crystal all-optical switching. Appl. Phys. Lett. **94**(3), 031103-1–031103-3 (2009)
41. B. Michele, G. Matteo, G. Dario et al., All-optical switching in silicon-on-insulator photonic wire nano–cavities. Opt. Express **18**(2), 1450–1461 (2010)
42. J.A. Porto, L. Martín-Moreno, F.J. García-Vidal, Optical bistability in subwavelength slit apertures containing nonlinear media. Phys. Rev. B **70**, 081402 (2004)
43. C. Min, P. Wang, C. Chen et al., All-optical switching in subwavelength metallic grating structure containing nonlinear optical materials. Opt. Lett. **33**(8), 869–871 (2008)
44. A.V. Krasavin, N.I. Zheludev, Active plasmonics: controlling signals in Au/Ga using nanoscale structural transformations. Appl. Phys. Lett. **84**(8), 1416–1417 (2004)
45. A.V. Krasavin, K.F. MacDonald, N.I. Zhelude, High-contrast moculation of light with light by control of suface plasmon polariton wave coupling. Appl. Phys. Lett. **85**, 3369 (2004)
46. A.P. Ragip, K.T. Shimizu, A. Nicholas et al., A nonvolatile plasmonic switch employing photochromic molecules. Nano Lett. **8**(5), 1506–1510 (2008)
47. A.V. Krasavin, S. Randhawa, J.-S. Bouillard, et al., Optically-programmable nonlinear photonic component for dielectric-loaded plasmonic circuitry. Opt. Express **19**(25), 25222–25229 (2011)
48. S. Sederberg, D. Driedger, M. Nielsen et al., Ultrafast all-optical switching in a silicon-based plasmonic nanoring resonator. Opt. Express **19**(23), 23494–23503 (2011)